ISBN 978-1-927797-45-7
ISSN 1198-273X

PICES SCIENTIFIC REPORT
No. 62, 2021

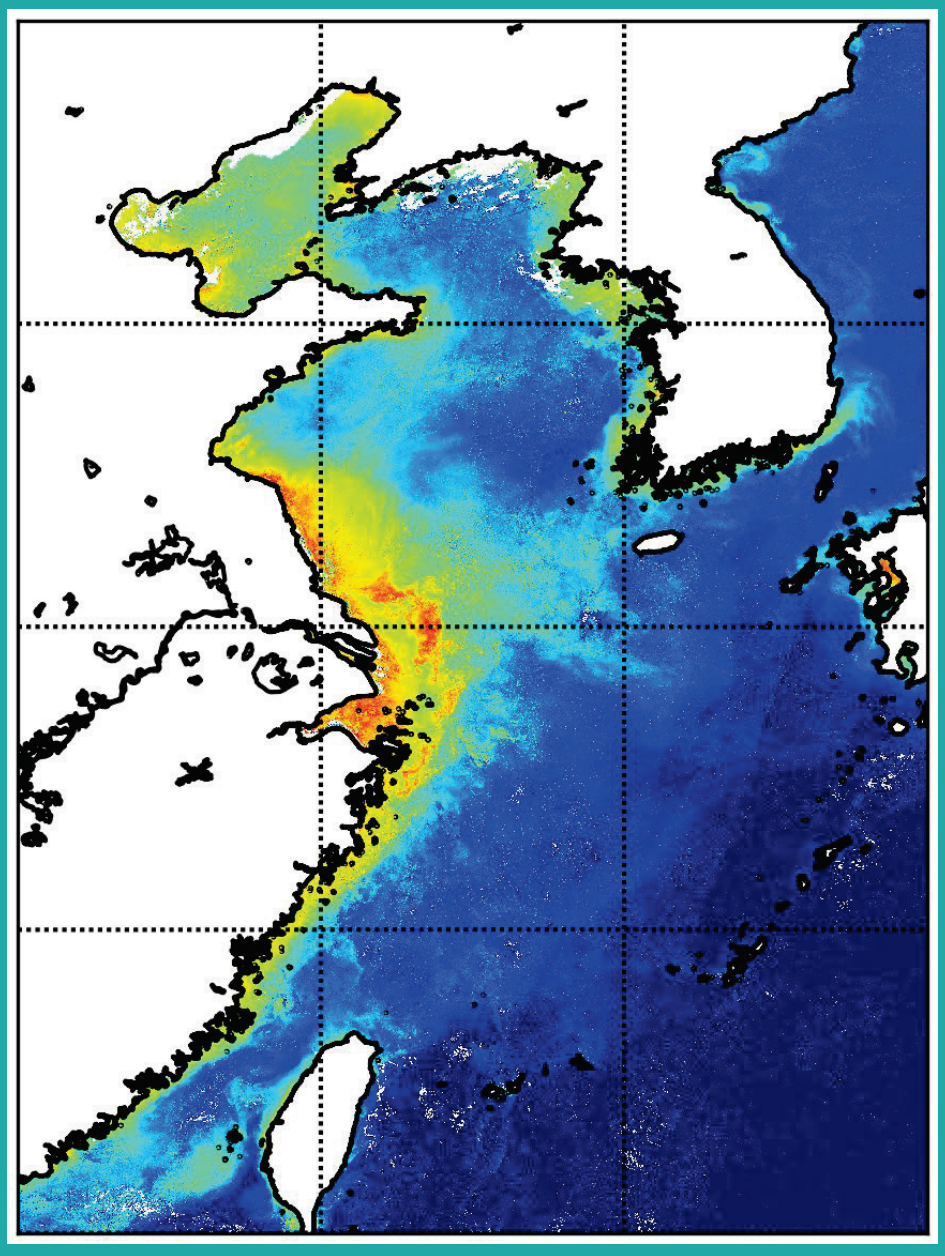

Oceanography of the Yellow Sea and East China Sea

NORTH PACIFIC MARINE SCIENCE ORGANIZATION

PICES

PICES Scientific Report No. 62
2021

Oceanography of the Yellow Sea and East China Sea

edited by
Joji Ishizaka, Guebuem Kim, Jae Hak Lee, Su Mei Liu, Fei Yu and Jing Zhang

September 2021

North Pacific Marine Science Organization (PICES)
P.O. Box 6000, Sidney, BC, V8L 4B2, Canada
www.pices.int

PICES Scientific Reports

Published since 1993, the PICES Scientific Report series includes final reports of PICES expert groups, proceedings of PICES workshops, data reports and reports of planning activities. Formal peer reviews of the scientific content of these publications are not generally conducted.

PICES Scientific Reports can be found at: https://meetings.pices.int/publications/scientific-reports

Front cover:
Satellite image of the Yellow Sea and East China Sea showing chlorophyll-a concentrations (red, the highest) during July 10 and 19, 2018. Derived from data from the Second-generation Global Imager (SGLI) of Global Change Observation Mission-Climate (GCOM-C) of Japan Aerospace Exploration Agency (JAXA).

This document should be cited as follows:

Ishizaka, J., Kim, G., Lee, J.H., Liu, S.M., Yu, F. and Zhang, J. (Eds.) 2021. Oceanography of the Yellow Sea and East China Sea. PICES Sci. Rep. No. 62. North Pacific Marine Science Organization, Sidney, BC, Canada, 298 pp.

Table of Contents

Contributing Authors

Physical Oceanography

Byoung-Ju Choi
Chonnam National University
Korea
bchoi@jnu.ac.kr

Xinyu Guo
Ehime University
Japan
guoxinyu@sci.ehime-u.ac.jp

Hailun He
Second Institute of Oceanography
Ministry of Natural Resources
China
hehailun@sio.org.cn

Atsuhiko Isobe
Research Institute for Applied Mechanics
Kyushu University
Japan
aisobe@riam.kyushu-u.ac.jp

Jae Hak Lee
Ocean Circulation and Climate Research Center
Korea Institute of Ocean Science and Technology
Korea
jhlee@kiost.ac.kr

Takeshi Matsuno
Research Institute for Applied Mechanics
Kyushu University
Japan
matsuno@riam.kyushu-u.ac.jp

SungHyun Nam
Seoul National University
Korea
namsh@snu.ac.kr

Fangli Qiao
First Institute of Oceanography
Ministry of Natural Resources
China
qiaofl@fio.org.cn

Chuanjie Wei
Research and Development Center of Marine Environmental Engineering and Technology
Institute of Oceanography
Chinese Academy of Sciences
China
weicj@qdio.ac.cn

Hao Wei
School of Marine Science and Technology
Tianjin University
China
weihao@ouc.edu.cn

Dongfeng Xu
Second Institute of Oceanography
Ministry of Natural Resources
China
xudongfengsio@sio.org.cn

Sang-Wook Yeh
Hanyang University, ERICA
Korea
swyeh@hanyang.ac.kr

Fei Yu
Institute of Oceanology
Chinese Academy of Sciences
China
yuf@qdio.ac.cn

Chemical Oceanography

Chun-Ok Jo
Reseach Institute of Oceanography, Anyang University
Korea
cojoo100@gmail.com

Guebuem Kim
Seoul National University
Korea
gkim@snu.ac.kr

Xianguo Li
College of Chemistry and Chemical Engineering/Key Laboratory of Marine Chemistry Theory and Technology
Ocean University of China
China
lixg@ouc.edu.cn

Yanbin Li
College of Chemistry and Chemical Engineering/Key Laboratory of Marine Chemistry Theory and Technology
Ocean University of China
China
liyanbin@ouc.edu.cn

Su Mei Liu[1,2]
[1] Key Laboratory of Marine Chemistry Theory and Technology Ministry of Education
Ocean University of China
[2] Laboratory for Marine Ecology and Environmental Science
Qingdao National Laboratory for Marine Science and Technology
China
sumeiliu@ouc.edu.cn

Sai-Chun Tan[1,2]
[1] State Key Laboratory of Numerical Modeling for Atmospheric Sciences and
Geophysical Fluid Dynamics Institute of Atmospheric Physics
Chinese Academy of Sciences
[2] Collaborative Innovation Center on Forecast and Evaluation of Meteorological Disasters
Nanjing University of Information Science and Technology
China
sctan@mail.iap.ac.cn

Yu Umezawa
Tokyo University of Agriculture and Technology
Japan
umezawa@me.tuat.ac.jp

Wang-Wang Ye
Key Laboratory of Marine Chemistry Theory and Technology
Ministry of Education
Ocean University of China
China
yezikasuo@126.com

Gui-Ling Zhang
Key Laboratory of Marine Chemistry Theory and Technology
Ministry of Education
Ocean University of China
China
guilingzhang@ouc.edu.cn

Jing Zhang
University of Toyama
Japan
jzhang@sci.u-toyama.ac.jp

Zhuoyi Zhu
Shanghai Jiao Tong University
China
zhu.zhuoyi@sjtu.edu.cn

Biological Oceanography

Chung Yeon Hwang
Seoul National University
Korea
chung.hwang@snu.ac.kr

Joij Ishizaka
Institute for Space-Earth Environmental Research
Nagoya University
Japan
jishizaka@nagoya-u.jp

Hiroshi Koshikawa
National Institute for Environmental Studies
Japan
koshikaw@nies.go.jp

Xinzheng Li
Institute of Oceanology, Chinese Academy of Sciences
China
lixzh@qdio.ac.cn

Cui Liang
China Institute of Oceaonology, Chinese Academy of Sciences
China
cui-liang@hotmail.com

Jae Hoon Noh
Korea Institute of Ocean Science and Technology
Korea
jhnoh@kiost.ac.kr

Weiwei Xian
Institute of Oceaonology, Chinese Academy of Sciences
China
wwxian@qdio.ac.cn

Yong Xu
Institute of Oceanology, Chinese Academy of Sciences
China
xuyong@qdio.ac.cn

Guang-Tao Zhang
Institute of Oceaonology, Chinese Academy of Sciences
China
gtzhang@qdio.ac.cn

Wuchang Zhang
Institute of Oceaonology, Chinese Academy of Sciences
China
wuchangzhang@qdio.ac.cn

Yuan Zhao
Institute of Oceaonology, Chinese Academy of Sciences
China
yuanzhao@qdio.ac.cn

Preface

The Advisory Panel for a Circulation Study of East Asian Marginal Seas (AP-CREAMS) of the North Pacific Marine Science Organization (PICES) has recognized a lack of an extensive review of the oceanography of the Yellow Sea and East China Sea. The Yellow Sea, including the Bohai Sea, and East China Sea are one of the most productive marine environments in the world, and they are also known to be facing rapid environmental changes in recent decades with possible eutrophication, climate change and other causes. It is also realized that there are many studies in this important area; however, there is almost no review which is internationally available. Thus, AP-CREAMS recommended to review the present conditions of the Yellow Sea and East China Sea and to prepare a report which could be widely used by the marine sciences community. Here, we have prepared "Oceanography of the Yellow Sea and East China Sea" for publication in the PICES Scientific Report series. Members of the editorial committee appreciate all the contributors of this report.

Joji Ishizaka, Guebuem Kim, Jae Hak Lee, SuMei Liu, Fei Yu, Jing Zhang
Editorial Committee

Physical Oceanography

Preface

This chapter summarizes the general understanding of physical oceanography in the Bohai, Yellow and East China seas based on published literature. The chapter consists of six sections: currents, tides and waves, water masses, ocean mixing, atmosphere–ocean interaction and long-term variations. The reviews generally indicate that the research trend had a turning period in the 1990s in its scope. Before the 1990s, research focused largely on tides and water masses, though work to understand the current system had been continuing for a long time. In the 1990s, the understanding of the current system improved significantly. Since the 2000s, observations of small-scale events, such as internal waves and frontal structures, have been growing and studies of ocean mixing, especially vertical mixing, has made considerable progress. Recently, research on processes in the atmosphere–ocean interface have been increasing. This includes the effect of waves, surface fluxes and tele-connections.

It is noted that the lack of time-series data and wintertime observations must be overcome to improve our understanding of these seas in the next generation. All sections made similar remarks that more *in-situ* observations need to be carried out to obtain long-term time series, and that regional numerical models, including various coupled models, need to be improved. A suggestion to see successful results for these demands in the future is collaboration of scientists from countries surrounding these seas under an international framework such as PICES.

Jae Hak Lee

1.1 Circulation

Xinyu Guo[1], Byoung-Ju Choi[2] and Fangli Qiao[3]

[1] Ehime University, Japan
[2] Chonnam National University, Korea
[3] First Institute of Oceanography, Ministry of Natural Resources, China

1.1.1 Introduction

The Bohai Sea, the Yellow Sea (YS) and the East China Sea (ECS) lie on the largest continental shelf in the northwestern Pacific Ocean (Fig. 1.1.1). The Bohai Sea and YS are separated by the Bohai Strait, while the YS and the ECS are separated by a line from the mouth of the Changjiang River to Jeju Island. With only one connection to the YS, the Bohai Sea becomes a semi-enclosed marginal sea with an average depth of 18 m (Xia *et al.*, 2019). The YS is also a semi-closed shelf sea connected to the Bohai Sea to the north and the ECS to the south; it has an area of 380,000 km^2 and extends from 31°40′N to 39°50′N and 119°10′E to 126°50′E. The YS has average and maximum water depths of 44 and 140 m, respectively.

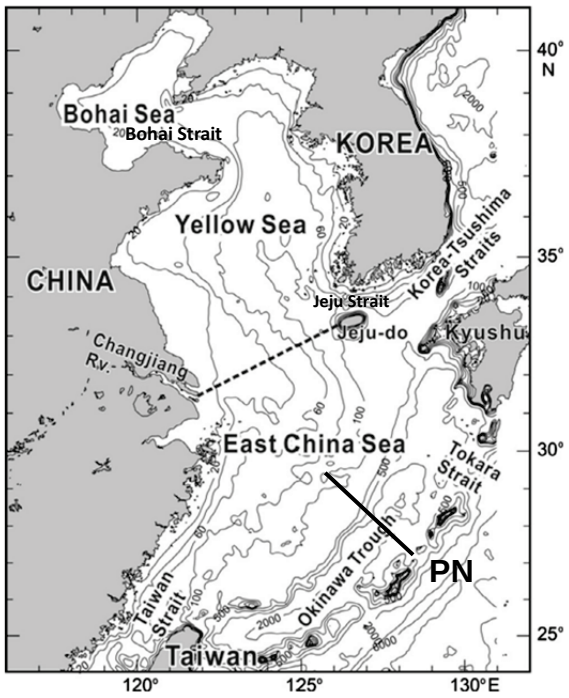

Fig. 1.1.1 Bathymetric map of the Bohai Sea, the Yellow Sea, and the East China Sea. Continuous lines denote isobaths in meters. Dashed line connecting the Changjiang River mouth and Jeju-do indicates the geographic boundary between the Yellow Sea and East China Sea. PN denotes a section observed regularly by the Japan Meteorological Agency. Modified from Lie and Cho (2016).

The ECS is connected to other marginal seas through the Tsushima Strait to the northeast and through the Taiwan Strait to the southwest and is open to the Pacific Ocean to the southeast; it has an area of 770,000 km^2 and extends from 21°54′N to 33°17′N and 117°05′E to 131°03′E. The ECS has both a shelf area and sharp slope and deep water areas with average and maximum water depths of 370 and 2940 m, respectively. Two-thirds of the ECS is on the continental shelf, and this part can be separated into an inner shelf, middle shelf, and outer shelf by the 50, 100, and 200 m isobaths, respectively, which largely run parallel to the coastline over the continental shelf. Immediately outside of the continental shelf is the Okinawa Trough with a depth of 600 to 2000 m.

As one of the most studied seas in the world, there have been already many review papers on the circulations in the Bohai Sea, YS and ECS (*e.g.*, Guan, 1994; Su, 1998; Lie, 1999; Su, 2001; Ichikawa and Beardsley, 2002; Lie and Cho, 2002; Isobe, 2008; Park *et al.* 2014, 2017). In this section, using a combination of review papers and newly published papers related to this topic, we present a comprehensive description on the circulation pattern in this area and its related dynamics. Finally, we present some outlooks on future works.

1.1.2 Bohai Sea and Yellow Sea circulation

Seasonal variation of circulation is prominent in the Bohai Sea and YS (Figs. 1.1.2, 1.1.3, and 1.1.4). Winter circulation is controlled mostly by topography and northerly wind bursts with northward flow in the middle and southward flow along both coastal boundaries of the basin. In summer, circulation is governed by topography, tidal mixing, and stratification with three-layer structure (Naimie *et al.*, 2001; Xia *et al.*, 2006; Lin *et al.*, 2011). A basin-scale cyclonic gyre is formed in the upper layer of the YS.

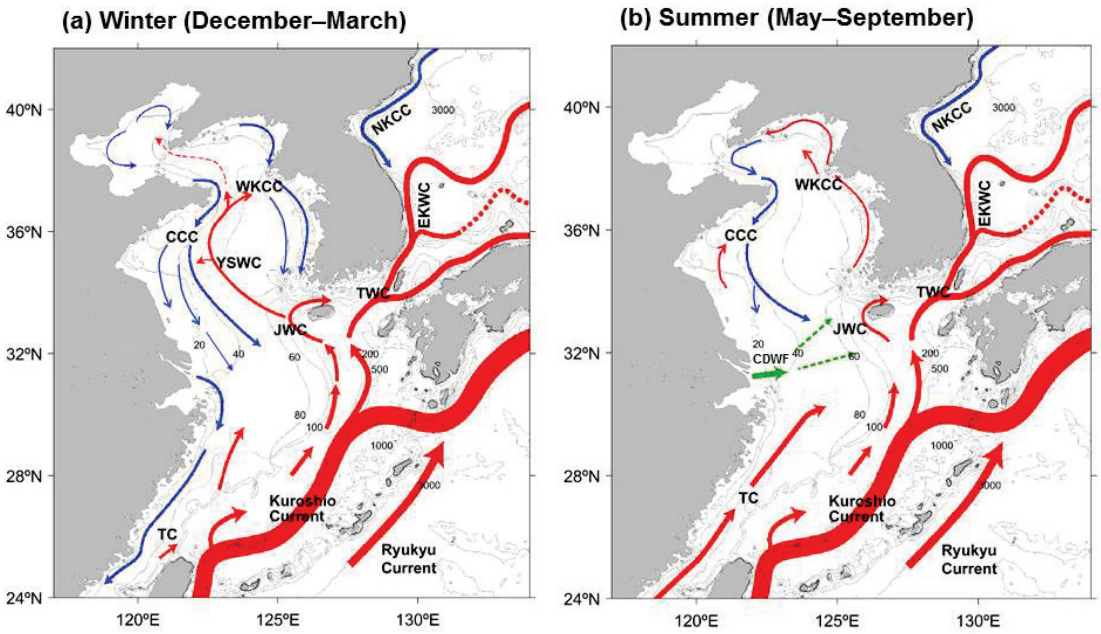

Fig. 1.1.2 Schematic pattern of circulation in the Bohai Sea, the YS and the ECS during (a) winter and (b) summer. JWC, YSWC, CCC, WKCC, and CDWF stand for Jeju Warm Current, Yellow Sea Warm Current, Chinese Coastal Current, and West Korea Coastal Current, Changjiang Diluted Water Flow, respectively. Modified from Park *et al.* (2017).

Seasonal circulation

Winter circulation

Northerly and northwesterly winds are dominant in winter (Hsueh, 1988; Teague and Jacobs, 2000; Lie and Cho, 2016). Northerly winds induce an anti-cyclonic gyre in the eastern half of the YS with the northward Yellow Sea Warm Current (YSWC) along the western side of the Yellow Sea Trough, the southward West Korea Coastal Current (WKCC) at the eastern part of the YS (Fig. 1.1.3a), and a cyclonic gyre in the western YS with the northward YSWC along the western side of Yellow Sea Trough and the southwestward and southeastward Chinese Coastal Current (CCC) over the western part of the YS (Fig. 1.1.2) (Le *et al*., 1993; Takahashi *et al*., 1995; Naimie *et al*., 2001; Ma *et al*., 2006; Lin and Yang, 2011).

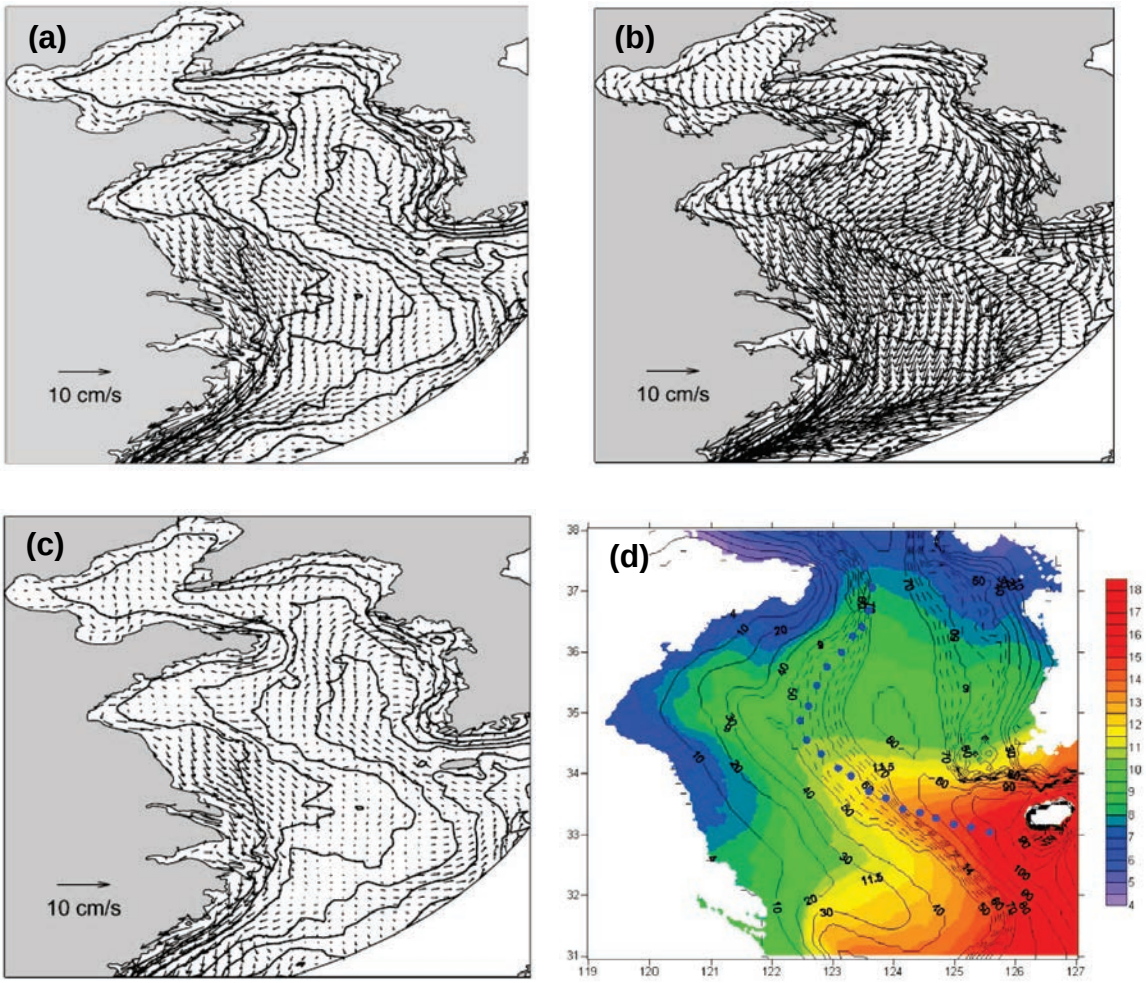

Fig. 1.1.3 Vertically (a) integrated circulation, (b) near surface current (z = 0.5 m), and (c) near bottom current (z = 0.5 m above bottom) in January from the three-dimensional simulation of Naimie *et al*. (2001). Reproduced with permission of Elsevier. (d) Mean SST (°C) in winter (DJF) from Advanced Very High Resolution Radiometer (AVHRR) observations from 1985 to 2009. Blue solid circles denote the axis of a warm water tongue as the pathway of the YSWC. Black lines are the bathymetry with the dashed lines representing 2.5-m intervals between 50 and 70 m. After Lin *et al*. (2011). Reproduced with permission of Wiley & Sons.

Although the interaction of topography, horizontal density gradient, and tidal mixing (tidal rectification) can induce a weak YSWC without wind forcing (Lee and Beardsley, 1999), northerly wind bursts accompanied by the propagating coastal shelf waves on the YSWC is the largest force influencing the northward current (Hsueh *et al*., 1986; Takahashi *et al*., 1995; Naimie *et al*., 2001; Ma *et al*., 2006; Qu *et al*., 2018). The YSWC is separated intermittently from only a portion of the Jeju Warm Current (JWC) to the west of Jeju Island during the northerly winds bursts. The JWC is the mean current flowing clockwise around Jeju Island in all seasons. The YSWC extension enters the Bohai Sea along the northern side of Bohai Strait and separates to form an anti-cyclonic gyre in the east and a cyclonic gyre in the west (Guan, 1994; Bian *et al*., 2016). Low salinity water flows out to the YS along the southern side of Bohai Strait.

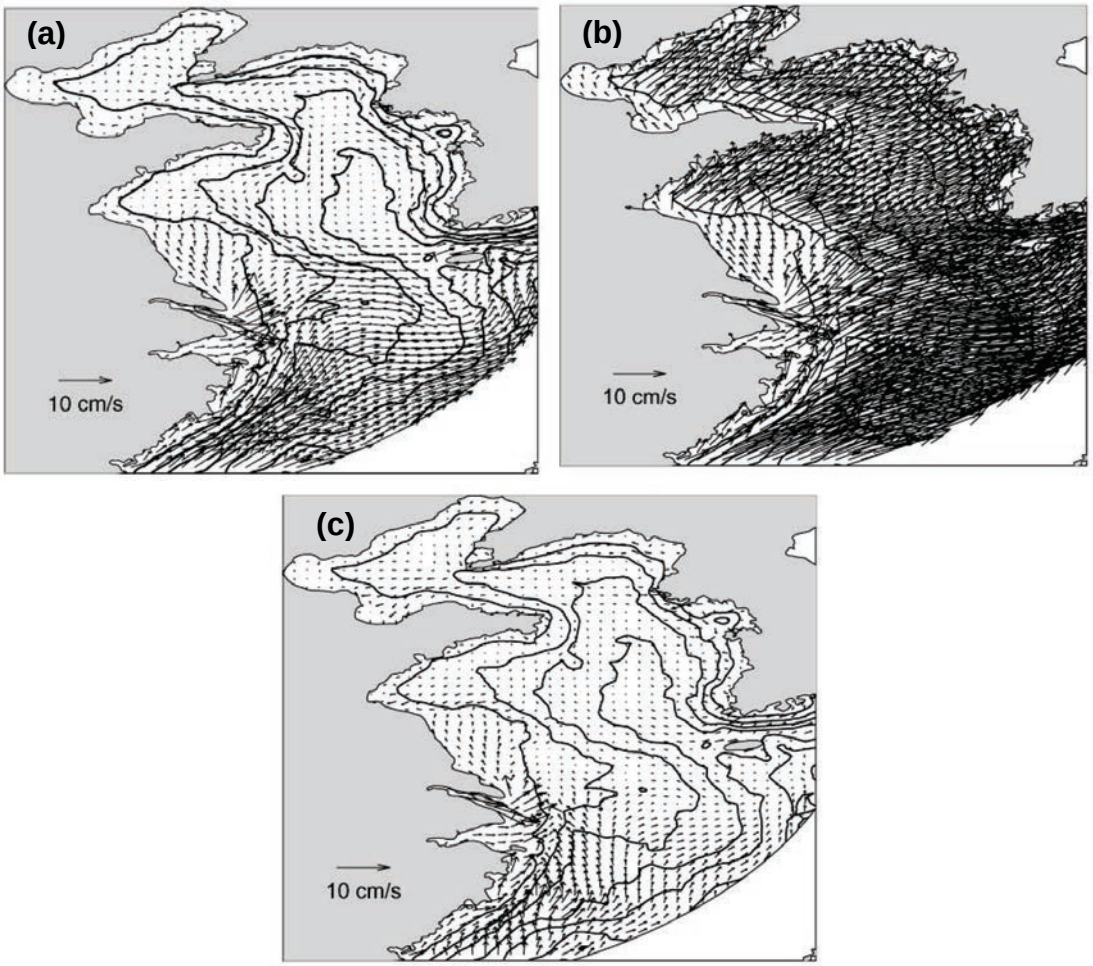

Fig. 1.1.4 Vertically (a) integrated circulation, (b) near surface current (z = 0.5 m), and (c) near bottom current (z = 0.5 m above bottom) in July from the three-dimensional simulation of Naimie *et al*. (2001).

Summer circulation

In summer, the water column of the YS is highly stratified offshore where the bottom depth (h) is deeper than about 60 m due to high solar radiation, while the water column remains relatively well mixed in shallow coastal regions (h < 40 m) due to strong tidal mixing. The tidal front and along-front jet form in the transition zone with depths between 30 and 60 m as a result of tidal rectification due to the interaction between tidal mixing and the stratified ocean (Lee and Beardsley, 1999; Naimie *et al*., 2001; Liu *et al*., 2003; Kwon *et al*., 2011; Yuan *et al*., 2013). The horizontal

circulation in the summer YS has a three-layer structure: in the surface layer (0–4 m), the prevailing current direction is northeastward; in the upper layer (4–40 m) it is dominated by a basin-scale cyclonic gyre; and in the bottom layer (below 40 m) the water diverges from the center area and there exists a weak southward current along the Yellow Sea Trough (Xia *et al*., 2006). Tidal mixing plays a dominant role in the formation of upwelling, and the relative importance of tidal mixing and wind forcing for upwelling has been further examined in numerical experiments. The southerly wind enhances the upwelling off the western coasts, but its overall influence on the whole YS upwelling is less important than that of the tidal mixing (Lü *et al*., 2010). The along-front jet produces a large, basin-wide cyclonic surface circulation along the 40- to 50-m isobaths in both the western and eastern YS, *i.e*., the CCC and WKCC, respectively (Fig. 1.1.2b).

Yellow Sea Warm Current

Average winter currents are northward on the western side of the Yellow Sea Trough (Isobe, 2008) (Figs. 1.1.2a, 1.1.3a, and 1.1.5). However, the YSWC is not a steady current but rather an intermittent (or episodic) current related to northerly wind bursts over the YS in winter (Hsueh, 1988; Ma *et al*., 2006; Isobe, 2008). The northerly wind fluctuates with a synoptic time scale (3–7 days) over the YS in winter (Hsueh, 1988; Teague and Jacobs, 2000) with bursts that produce a pressure gradient force to the north near the bottom of the ocean. As the northerly wind relaxes, the northward flowing YSWC gains strength along the Yellow Sea Trough, reaching a peak in northward speed 1 to 2 days later (Figs. 1.1.6 and 1.1.7). The YSWC has been thought to form at the end of October and remain in place until early March. During the weak northerly wind periods between two northerly wind bursts, a southward current flow appears at the upper and middle levels. Hence, the current does not continually flow toward the north throughout the winter in the middle of the Yellow Sea Trough.

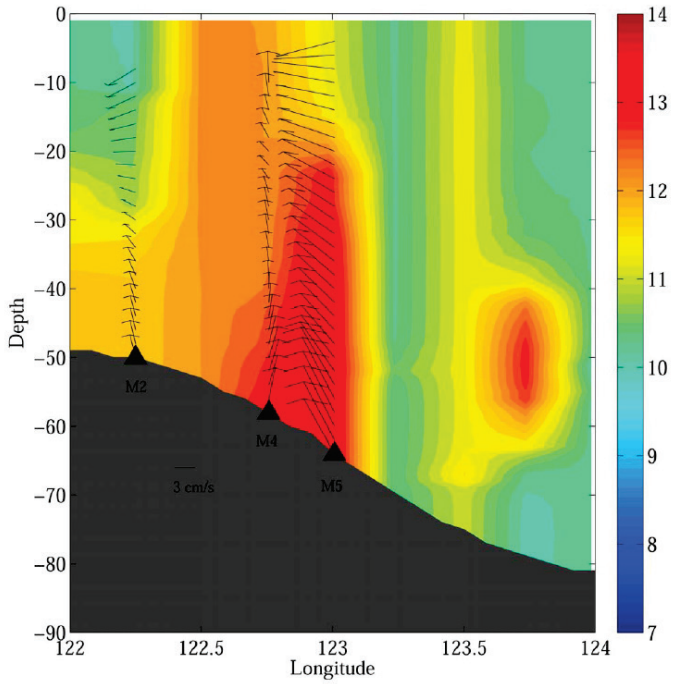

Fig. 1.1.5 Time-averaged currents at mooring stations M2 (122°15.06'E, 34°40.35'N), M4 (122°45.48'E, 34°40.21'N), and M5 (123°00.49'E, 34°40.01'N) with the background temperature (°C) along 34°40'N. Barotropic currents at M2, M4 and M5 are 2.40, 2.54, and 7.46 cm s^{-1}, respectively. After Lin *et al*. (2011). Reproduced with permission of Wiley & Sons.

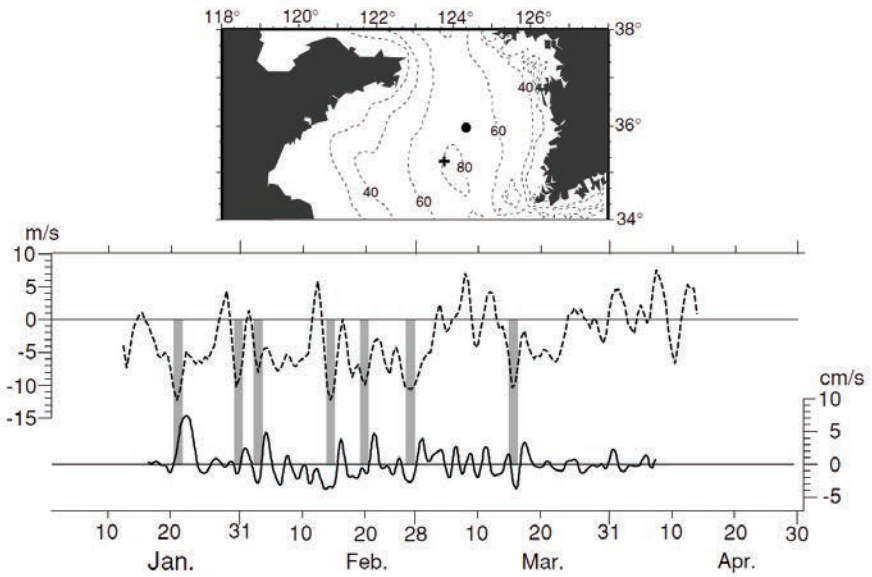

Fig. 1.1.6 Time series plot of the northward component of the mid-depth current (solid line in bottom panel) observed at the solid circle in the Yellow Sea in the upper panel from January to March 1986 (plot reproduced from Figure 6 in Hsueh, 1988). Broken line in the bottom panel is the northward component of the reanalysis wind at the cross in the upper panel. Grey bars are depicted to emphasize a correlation between southward winds and northward currents. Broken lines in upper panel indicate depth contours in meters. After Isobe (2008). Reproduced with permission of Springer Nature.

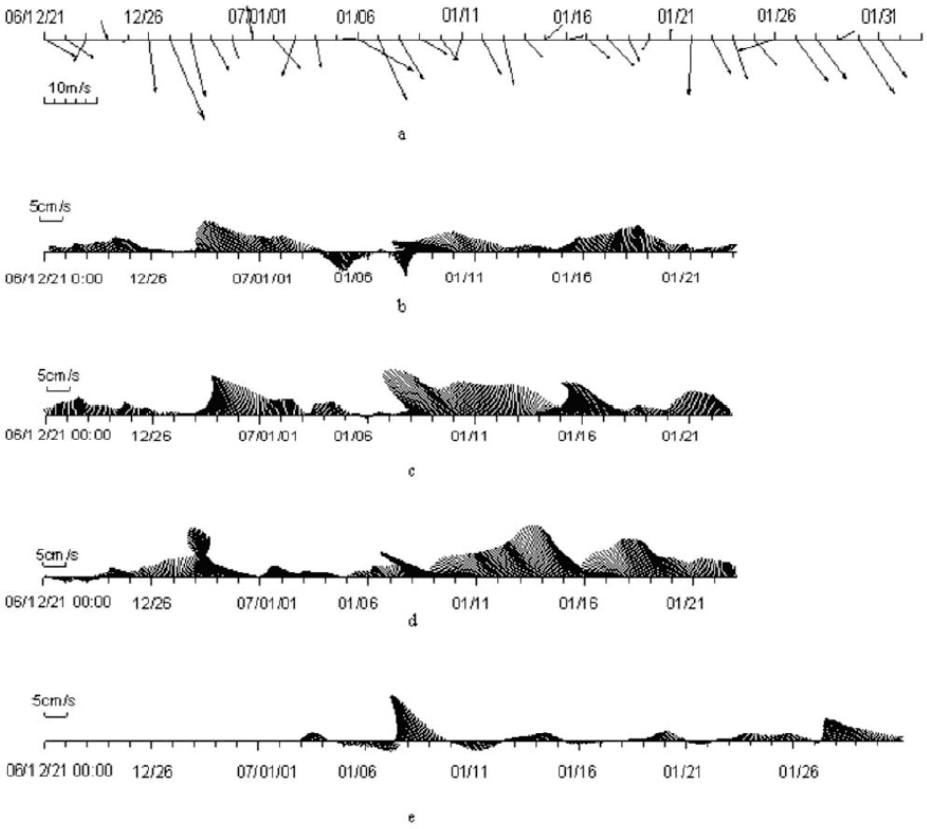

Fig. 1.1.7 The time series of observed daily wind in 2006–2007 winter in north Yellow Sea (averaged in the box from 34°N to 38°N, 122°E to 124°E) from (a) QuikSCAT data and near bottom residual current at stations (b) M2, (c) M4, (d) M5, and (e) M6. After Lin *et al*. (2011). Reproduced with permission of Wiley & Sons.

Direct current measurements

Hsueh (1988) found that the current was northward at the middle depth (38 m) and near the bottom (74 m) based on current meter mooring at the northern Yellow Sea Trough (124°E, 37°N) and bottom currents at 70 and 95 m depths were also northward based on a current meter positioned at the eastern side of Yellow Sea Trough (124.75°E, 35.25°N) in winter of 1986. Winds were mostly northerly from January to early March 1986. Teague and Jacobs (2000) monitored the YSWC using an acoustic Doppler current profiler (ADCP) in the middle of the Yellow Sea Trough (124.033°E, 35.967°N) from July 1995 to January 1996. Observations indicated that there was southward flow near the surface (14 m), northward and northeastward flow at the middle depth (44 m), and northward flow near the bottom (72 m) from the beginning of November 1 to January 15 in response to northerly wind pulses. From April 1996 to May 1998, Lie *et al*. (2001) conducted six Korea–China joint hydrographic surveys and four satellite-tracked drifter experiments in the YS. They analyzed the observational data and concluded that the SWC is not a persistent mean current and that Jeju Warm Current Water (JWCW) may be transported to the southwestern YS in winter by the intermittently generated northwestward currents on the western slope of the Yellow Sea Trough.

Because the YSWC was suggested to flow along the western slope of the Yellow Sea Trough based on hydrographic observation (Lie *et al*., 2001; Tang *et al*., 2001) and a numerical model (Takahashi *et al*., 1995), five ADCPs were deployed on the western side of the central Yellow Sea Trough from December 20, 2006 to January 23, 2007 (Yu *et al*., 2009; Lin *et al*., 2011). The YSWC was found to flow northwestward near the bottom with a speed of 4 to 10 cm s^{-1} on the western side of the Yellow Sea Trough (Fig. 1.1.5). The core of the YSWC was suggested to be near the bottom. The monthly mean flow of the current is northward from the surface to bottom on the western side of the Yellow Sea Trough with intensification following strong northerly wind bursts. The lag of the YSWC response to the northerly wind bursts was about 1 to 2 days (Lin *et al*., 2011). The YSWC was induced mainly by the barotropic current (Hsueh, 1988; Lin *et al*., 2011).

Hydrographic evidence

The YSWC had been thought to be present year-round with the main path lying along the central part of the Yellow Sea Trough (Nitani, 1972). However, the YSWC is prominent along the western slope of the Yellow Sea Trough only in winter (Zang *et al*., 2003). Hydrographic data in the 1980s (Lie, 1986; Park, 1986) did not show any evidence of the northward intrusion of saline water into the eastern YS in summer (Isobe, 2008). Mean surface salinity distribution from November to February showed the location of the main path of the YSWC along the western slope of the Yellow Sea Trough (Isobe, 2008). Vertical temperature and salinity profiles across zonal sections along 34°N, 35°N, and 36°N (Lie *et al*., 2009; Lin *et al*., 2011) revealed that a warm and saline core exits at the western side of Yellow Sea Trough. Climatological mean SST data and SST snapshots in winter from satellite observation also indicate the main path of the YSWC to be along the western slope of the Yellow Sea Trough (Lie *et al*., 2001; Lie *et al*., 2009; Yu *et al*., 2009; Lin *et al*., 2011; Wang *et al*., 2012; Park *et al*., 2017).

Theory and numerical modeling

Based on an early simple analytical model, a wind-induced pressure gradient in the lower layer along the Yellow Sea Trough was proposed to generate the YSWC (Park, 1986; Seung *et al*., 2012). When northwesterly winds blow over the YS in winter, the pressure gradient force dominates over the wind stress in deep waters along the Yellow Sea Trough where the local depth exceeds a critical depth (53 m), producing upwind northward flow in the lower layer along the Yellow Sea Trough.

The YSWC has been known to be accompanied by coastal shelf waves induced by northerly wind bursts in winter (Hsueh and Pang, 1989; Takahashi *et al*., 1995). In a two-dimensional numerical experiment, onset of a northerly wind in winter produced anti-cyclonic circulation in the eastern part of the YS and cyclonic circulation in the western part of the YS. However, only the anti-cyclonic circulation can be amplified with the northerly wind, which produces steady anti-cyclonic circulation in the YS, reaching equilibrium in about 2 days (Takahashi *et al*., 1995).

Three-dimensional modeling of wind-driven upwind flow in the YS showed that surface water was moved southward out of the Bohai Sea by northerly wind bursts, which decreased the sea level in the north relative to the sea level in the south (Riedlinger and Jacobs, 2000). The northward pressure gradient force induces a bottom flow to the north in the opposite direction of the northerly wind. This return flow is concentrated in the Yellow Sea Trough. Lin and Yang (2011) suggested that the YSWC was generated by trapped topographic waves in response to the northwesterly wind. Bottom friction was considered to be important for arresting the waves based on barotropic numerical modeling experiments. Three-dimensional simulation of the YS winter circulation with tidal forcing performed to examine the evolution of the YSWC showed that flow is northward at depths lower than 30 m along the western slope of the Yellow Sea Trough (Tak *et al*., 2016). Currents and winds varied on timescales of 12 and 20 days. One day after the northerly wind burst, an upwind current in the subsurface layer appeared in the center of the Yellow Sea Trough, while the downwind flow in the surface layer decreased significantly in the three-dimensional model. Two days later, the upwind flow in the subsurface layer shifted west of the Yellow Sea Trough due to cyclonic propagation of coastal shelf waves along the coast from the Korean coast to Chinese coast (Tak *et al*., 2016; Qu *et al*., 2018).

Jeju Warm Current

The JWC is the mean current that flows clockwise around Jeju Island and delivers warm and saline water (Jeju Warm Current Water; JWCW) around Jeju Island in all seasons (Chang *et al*., 1995; Lie *et al*., 1998, 2000; Pang *et al*., 2003). The YSWC is separated sporadically from only a portion of the JWC to the west of Jeju Island (124–125°E, 33.5–34°N) during strong northwesterly events in winter (Zang *et al*., 2003; Lie and Cho, 2016). Origins of the warm and saline water are not yet clearly known, but there are two possible origins. The first origin is the Kuroshio water which flows onto the shelf across isobaths and mixes with shelf waters (Nitani, 1972; Zang *et al*., 2003; Park *et al*., 2017); the other is a continuation of the Taiwan Strait Current mixing with shelf waters in the ECS (Lie *et al*., 2000).

Direct observation

Transport was estimated from current meters and ADCP measurements (Chang *et al*., 1995, 2000). Transport of the JWC reaches a maximum in summer and fall and a minimum in winter and spring. The strong core of the JWC moves away from Jeju Island to the middle of the strait during the summer and fall. In the summer and fall, the volume transport of the JWC is 0.51 to 0.66 Sv with a maximum speed of 30.0 cm s^{-1} in the middle of the Jeju Strait (Chang *et al*., 2000). In winter and spring, the volume transport of the JWC is 0.37 to 0.45 Sv and the maximum speed was 17.0 cm s^{-1} near Jeju Island.

Several drifters were deployed south of Jeju Island (126.3°E, 32.4°N and 126.1°E, 32.8°N) from 1991 to 1998. They floated clockwise around the west coast of Jeju Island and passed through the Jeju Strait, confirming the pathway of the JWC (Lie *et al*., 2000). The current speed was about 5 to 40 cm s^{-1} west of Jeju Island and in the Jeju Strait.

A current meter mooring was deployed just north of the strong frontal region (125.5°E, 34°N; northwest of Jeju Island), and the current velocity was measured from February to April 1986. From current meter observations, a relatively strong residual current with a speed of about 10 cm s^{-1} and a direction varying from northeast to southeast was identified, which indicates eastward flow of the current (Zang *et al*., 2003).

Hydrographic evidence

The JWC is a year-round current with seasonal variation (Lie *et al*., 2000). In winter, JWCW with relatively high salinity expands to the west and is bounded by a strong thermohaline front in the north. It reaches the southern mouth of the Yellow Sea Trough. In summer and autumn, the JWCW retreats to near Jeju Island and appears only in the lower layer. JWCW is affected by fresher water flowing eastward from the ECS in summer. The JWCW is defined as water with salinity greater than 34.0 and the modified JWCW as water with salinity of 33.5 to 34.0 (Lie *et al*., 2000).

Chinese coastal current

The coastal current flows year-round along the 40- to 50-m isobaths from the western side of the Bohai Strait to the mouth of the Changjiang River in the western YS (Su, 1998; Zang *et al*., 2003). It is also called the Yellow Sea Coastal Current (Su, 1998).

Direct current measurements

In winter, drift bottles and drift cards released along the Chinese coast showed that coastal currents flowed to the south along the 40- to 50-m isobaths in the western YS (Zhang *et al*., 1987). Most of the drift bottles and drift cards released at 35°N in May and June moved north, but those released along the slope of Changjiang Bank with bottom depths of 40- to 50-m moved to the south. Drift bottles and drift cards released at 36°N to 37°N in August moved to the south and arrived along the east coast of China from 36°N to 32°N. There were a comparatively large number of drifters deployed in summer, and the mean trajectory of the drifters revealed the summer circulation patterns in the YS (Lie and Cho, 2016). In summer, coastal currents are southeastward from 38°N to 37°N along the Chinese coast, flowing southwest from 37°N to 35°N and south from 35°N to 33°N along the 40- to 50-m isobaths (Beardsley *et al*., 1992; Lie and Cho, 2016). Over the Changjiang Bank, the surface current flows to the northeast toward Jeju Island while the subsurface (30–50 m) current flows east or southeast on the slope of the Changjiang Bank (Beardsley *et al*., 1992; Lie and Cho, 2016; Fig. 1.1.8b).

Theory and numerical modeling

In the deep region (h > 30 m) of the western YS, the water column is well mixed or vertically homogenous in winter. Tide residual currents flow to the southeast along the slope of the Changjiang Bank (40–50 m isobaths) and east from the Changjiang River with a speed of about 5 cm s^{-1} due to tide and topography interactions (Lee and Beardsley, 1999; Naimie *et al*., 2001).

There are few direct measurements of surface currents in the coastal regions (h < 40 m) of the western YS (120–122°E, 34–36°N) in winter and summer. In summer, both direct observation and numerical simulations indicate northwestward coastal currents in the shallow region (h < 40 m) (Fig. 1.1.4). Numerical models with realistic atmospheric forcing, topography, and coastline inputs identify a northwestward, along-coast surface current (32–35°N) in the western shallow part (h < 40 m) of the YS (Naimie *et al*., 2001; Kwon *et al*., 2011; Lee *et al*., 2011; Qiao *et al*., 2011). A

surface drifter also indicated a northward coastal current in summer along the 20- to 30-m isobaths (Yuan *et al*., 2013). The water column is stratified in the deep ocean (h > 60 m) in summer, and tide residual currents increase along the slope of the Changjiang Bank due to a southeastward jet along the tidal mixing front, which is generated by interactions between density stratification and tidal mixing (Lee and Beardsley, 1999; Naimie *et al*., 2001).

West Korea Coastal Current

The West Korea Coastal Current (WKCC) flows southward along the west coast of Korea in winter and northward in summer (Le *et al*., 1993; Guan, 1994; Park *et al*., 2017). It is also identified as the Korean Coastal Current (KCC) (Kwon *et al*., 2011; Park *et al*., 2017).

Direct current measurements

During winter, southward downwind currents have been observed, using a current meter mooring and satellite-tracked drifters in the eastern YS. Lie (1999) observed a residual current flowing mostly to the southwest with a speed of 7.6 and 6.1 cm s^{-1} at depths of 20 and 45 m, respectively, in the eastern YS (125.5°E, 36°N) in March 1984. Hsueh (1988) also observed a bottom (64 m) current flowing southward at 125.6°E, 36°N from January to April 1986. In the southeastern YS (125.5°E, 34.6°N), the residual current was toward the southeast for more than 40 days from March to April 1984 at depths of 20 and 45 m with a speed of about 3 and 2.6 cm s^{-1}, respectively (Lie, 1999).

A satellite-tracked drifter (No. 9605) deployed at the southeastern corner of the YS (125.22°E, 35.05°N) in April 1996 moved southward to 124.77°E, 34.10°N with a speed of 4 to 9 cm s^{-1} (Tang *et al*., 2001; Zang *et al*., 2003). Another satellite-tracked surface drifter (No. 27276) was deployed at a depth of 15 m in the coastal region in the southeastern corner of YS (125.51°E, 35.03°N) on February 21, 1997, and it moved southwestward for 18 days with mean speed of 4 cm s^{-1} (Lie *et al*., 2001). Zang *et al*. (2003) claimed that the WKCC flows toward the south approximately along the 40- to 50-m isobaths on the eastern side of the YS, turns to the east near 34°N, and enters the Jeju Strait along the northern edge of the thermohaline front. Subsurface currents were observed at the southeastern corner of the YS (124.1°E, 34.0°N) from a current meter mooring deployed from April 7 to 13, 1996 (Tang *et al*., 2001; Zang *et al*., 2003). The residual current at a depth of 40 m flowed to the northeast in the first two days and turned to the east from the third day of observation. The residual current at a depth of 80 m flowed to the northeast at the beginning of observations but quickly turned to the southeast after 1 day and where it remained (Zang *et al*., 2003).

In summer, a boundary current was observed along the tidal front in the southeastern corner of the YS (125.24°E, 35.22°N) from June 22, to August 7, 1983 with a current speed of about 9 to 10 cm s^{-1} along the front (Lie, 1986). Beardsley *et al*. (1992) identified the northward flow along the eastern boundary of YS from the trajectories of satellite-tracked drifting buoys (Fig. 1.1.8a). The Korea Hydrographic and Oceanic Administration (KHOA) observed northward or northwestward surface currents at 8 current meters deployed along the eastern boundary of the YS near the surface (5 m depth) in July and August 2007 (Fig. 1.1.8b) with a speed of about 10 cm s^{-1} (Kwon *et al*., 2011).

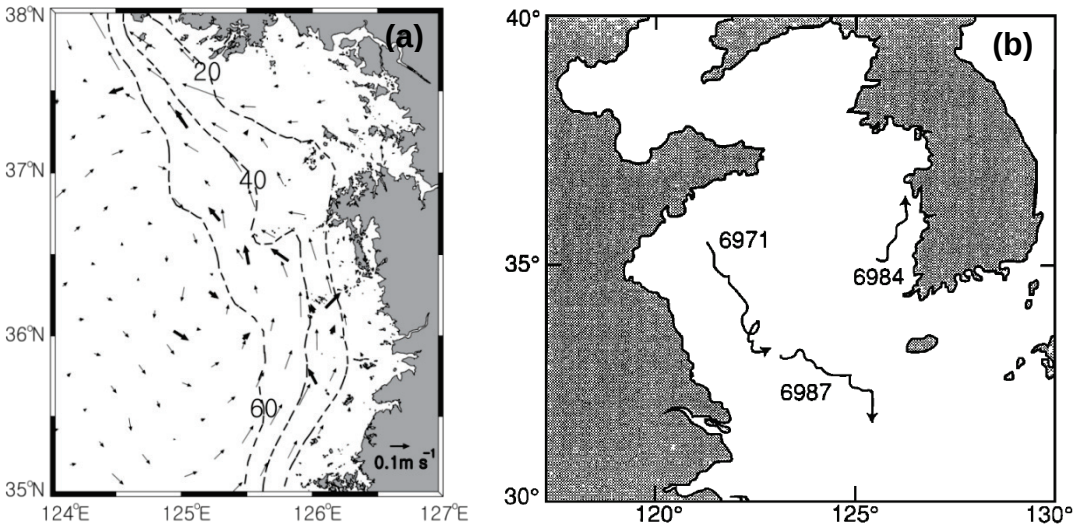

Fig. 1.1.8 (a) West Korea Coastal Current (WKCC) flowing northward or northwestward along the west coast of Korea at 5 m depth in summer. Solid vectors are observed by current meters in July and August 2007 and thin vectors are simulated mean currents in July by a three-dimensional model (Kwon *et al*., 2011). (b) Trajectories of near-surface drogue drifters tracked by satellite from July 1986 in the Yellow Sea and the East China Sea. Numbers indicate the drifter identification number. After Beardsley *et al*. (1992) and Lee and Beardsley (1999).

Hydrographic evidence

From winter to early spring, the WKCC transports coastal water toward the south along the 40- to 50-m isobaths in the eastern YS, and its velocity increases from north to south (Zang *et al*., 2003). The current turns toward the east or southeast near 34°N and enters into the Jeju Strait along the northern edge of thermohaline front.

In summer, cyclonic circulation forms in the upper layer of the YS along the tidal front which is generated by tidal mixing and vertical stratification due to solar radiation (Lie, 1986; Seung *et al*., 1990). However, the eastern boundary current, *i.e*., the WKCC in the YS is not a northward continuation of the saline JWC in summer (Lie, 1986).

Theory and numerical modeling

After relaxation of northerly winds during winter in the two-dimensional model simulation for the YS, coastally trapped waves travel counterclockwise around the YS and northward flow is enhanced along the Yellow Sea Trough (Hsueh *et al*., 1986). In a two-dimensional model with multi-year mean winter wind forcing and realistic bottom topography, a cyclonic gyre and an anti-cyclonic gyre were generated in the western and the eastern YS, respectively (Le *et al*., 1993). The basic features of the simulated circulation were northward flow along the western side of the Yellow Sea Trough and southward flows along the Chinese and Korean coasts. The southward coastal current off the west coast of Korea was the strongest in the model simulation. Trajectories of Lagrangian particles estimated from the simulated velocity demonstrated northward displacement of particles along the Yellow Sea Trough, which represents the YSWC, and southward drifting of particles along the eastern side of the Yellow Sea Trough, which represents the WKCC (Hsueh and Yuan, 1997; Riedlinger and Jacobs, 2000; Naimie *et al*., 2001).

Seung (1987) applied the geostrophic adjustment theory to the tidal front along the eastern boundary of the YS in summer and estimated the northward transport of the WKCC at 0.01 Sv, which is one order of magnitude smaller than 0.27 Sv estimated by the three-dimensional model of Kwon *et al.* (2011). Estimation of the YS surface circulation in summer by a diagnostic model using long-term temperature and salinity data (Yanagi and Takahashi, 1993) identified cyclonic circulation in the surface and middle layers. Satellite altimetry data and numerical modeling also confirmed the cyclonic surface circulation (Yanagi *et al.*, 1997). The Coriolis force is balanced against the pressure gradient across the front, which produces the WKCC flow northward along the tidal front (Naimie *et al.*, 2001; Xia *et al.*, 2006). Tidal stirring and surface wind mixing were found to be major factors that control the summertime boundary currents along the bottom tidal front (Kwon *et al.*, 2011). Tidal stirring was essential to generating the bottom temperature front and boundary current. Wind mixing made the boundary current wider and augmented its northward transport.

Bohai Sea coastal currents

The YSWC extension provides saline water to the Bohai Sea along the northern part of Bohai Strait in winter. When the YSWC extension reaches the northwestern coast of the Bohai Sea, it separates into a coastal current flowing westward along the west coast of Bohai Bay and a coastal current flowing northeastward along the west coast of Liaodong Bay (Fig. 1.1.9). In winter, circulation is generally cyclonic in Bohai Bay and anti-cyclonic in Liaodong Bay (Guan, 1994; Bian *et al.*, 2016). In summer, it is known that an anti-cyclonic circulation forms in Liaodong Bay. However, recent observation and numerical model simulation indicate more complicated circulation in the Bohai Sea (Hainbucher *et al.*, 2004; Xu *et al.*, 2006; Xia *et al.*, 2019).

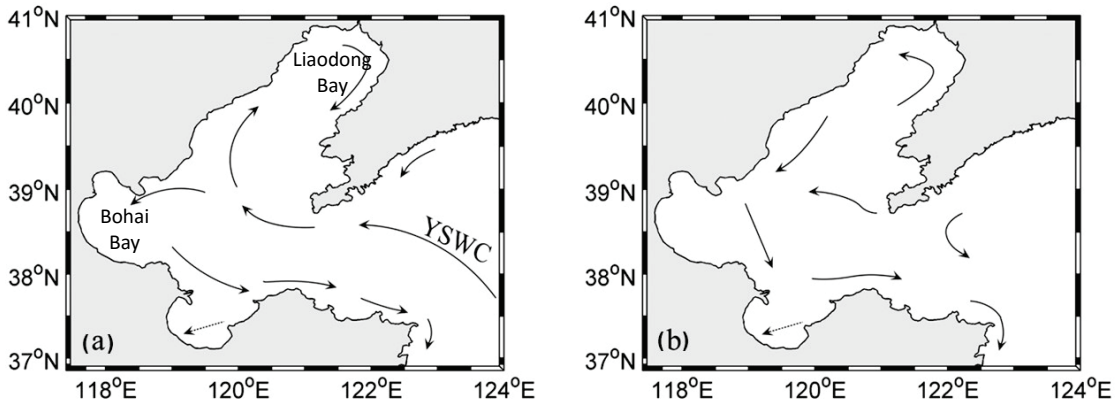

Fig. 1.1.9 General circulation in the Bohai Sea in (a) winter and (b) summer. After Guan (1994) and Bian *et al.* (2016).

1.1.3 East China Sea circulation

As with most ocean current systems, those in the ECS are mainly constrained by bathymetry and generally flow along isobaths. However, the currents flowing perpendicular to the isobaths also play an important role in the exchange of water and materials between the shelf seas and the Pacific Ocean. The vertical currents are weaker than horizontal ones by at least one order of magnitude but are significant for primary production because the upward currents can carry large amounts of nutrients from the lower to upper layers in the ocean. Schematics of the circulation pattern for the ECS are shown in Figure 1.1.10. The along-isobath currents out of the shelf are the northeastward

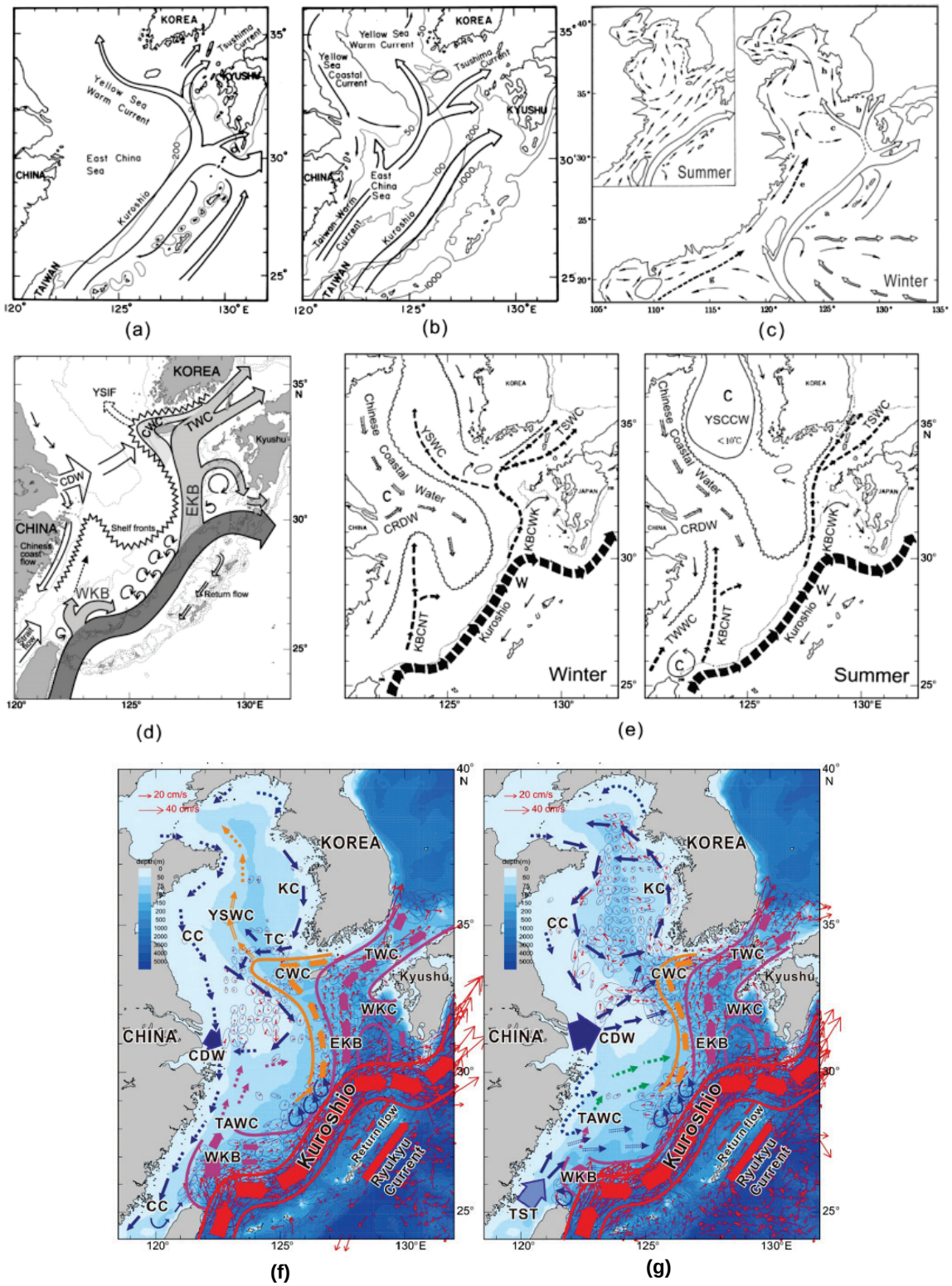

Fig. 1.1.10 Schematic circulation patterns of the Kuroshio and Kuroshio branch currents reproduced from Lie and Cho (2016) (upper panels) showing reproductions from (a) Nitani (1972), (b) Beardsley *et al*. (1985), (c) Guan (1994) for winter and summer; (d) Lie and Cho (2002), and (e) Kondo (1985) and Ichikawa and Beardsley (2002) and seasonal surface circulation in (f) winter (November–April) and (g) summer (May–October) in the YS and the ECS given by Lie and Cho (2016). Reproduced with permission of Elsevier, Springer Nature, and Wiley & Sons.

Kuroshio and the southwestward countercurrent between the Kuroshio and the Ryukyu Islands. The Kuroshio splits into two branches across the shelf break (Fig. 1.1.10e): the Kuroshio Branch Current north of Taiwan (KBCNT) and the Kuroshio Branch Current west of Kyushu (KBCWK). In the middle shelf of the ECS, the Taiwan Warm Current flows northeastward mainly along the isobaths with different origins in summer and winter. The Taiwan Strait Current is strong in summer but barely existent in winter. The Min-Zhe Coastal Current and Changjiang Diluted Water are located in the inner shelf, and both flow in totally different directions in summer and winter. Upwelling in the ECS mainly occurs northeast of Taiwan, along the southern coast of China, and off the Changjiang River Estuary.

Currents along isobaths

The Kuroshio, Taiwan Strait Current, Taiwan Warm Current, and Min-Zhe Coastal Current are constrained by bottom topography and flow generally along isobaths in the East China Sea.

Kuroshio

The Kuroshio is a strong western boundary current in the North Pacific Ocean. It originates from the North Equatorial Current and is characterized by high temperature and salinity. The Kuroshio enters the ECS from east of Taiwan, flows northeastward along the shelf break, and exits the ECS through the Tokara Strait. The observations on the Kuroshio in the ECS were concentrated east of Taiwan, the Tokara Strait and a section between them (PN line, Fig. 1.1.1).

The Kuroshio east of Taiwan has an impact of great significance to the downstream area. The Kuroshio maximum velocity in this area ranges from 0.7 to 1.4 m s^{-1} based on nine ship-based surveys conducted from 2012 to 2014 (Jan *et al*., 2015). The width of the Kuroshio is about 100 to 150 km (Liang *et al*., 2003; Hsin *et al*., 2008), and the thickness varies from 400 to 600 m (Jan *et al*., 2015). Based on observations from the moored current meter array PCM-1 in the World Ocean Circulation Experiment from 1994 to 1996, Johns *et al*. (2001) estimated the volume transport of the Kuroshio east of Taiwan to be 21.5 ± 2.5 Sv. This transport can be determined by the sea level difference between Taiwan and the southern Ryukyu Islands (Johns *et al*., 2001; Chang and Oey, 2011). Its variation has a dominant period of 100 days, which is related to the arrival of mesoscale eddies (Zhang *et al*., 2001). Chang and Oey (2011) demonstrated that the Kuroshio volume transport east of Taiwan is strong in fall and weak in spring, associated with the seasonal eddy activity of the Subtropical Counter Current. However, the Kuroshio volume transport shows a different seasonal pattern that is strong in summer and weak in winter based on other observations (Tang and Yang, 1993; Chuang and Liang, 1994; Hsin *et al*., 2011).

The Kuroshio across the PN line is often considered as an indicator of the Kuroshio in the ECS. Combining 23 months of inverted echo sounders and ADCP measurements, Andres *et al*. (2008) showed that the northeastward Kuroshio at the PN line was focused near the continental shelf and the maximum surface velocity is located 30 km offshore from the shelf break (Fig. 1.1.11). A dual-core and even multi-core distribution of velocities was separately observed at the surface and 210 dbar (Chen *et al*., 2009). Based on routine hydrographic measurements along the PN line conducted by the Japan Meteorological Agency since 1972, the mean transport from 1973 to 2000 was 25.8 Sv with a maximum of 27.0 Sv in summer and a minimum of 23.9 Sv in autumn (Ichikawa and Beardsley, 2002). Wei *et al*. (2013) extended this analysis to a period from 1955 to 2010 and reported an interannual variability of 2 to 5 years with an amplitude of 2.8 Sv. A model study by Kagimoto and Yamagata (1997) showed that transport across the PN line is strong in summer and weak in winter.

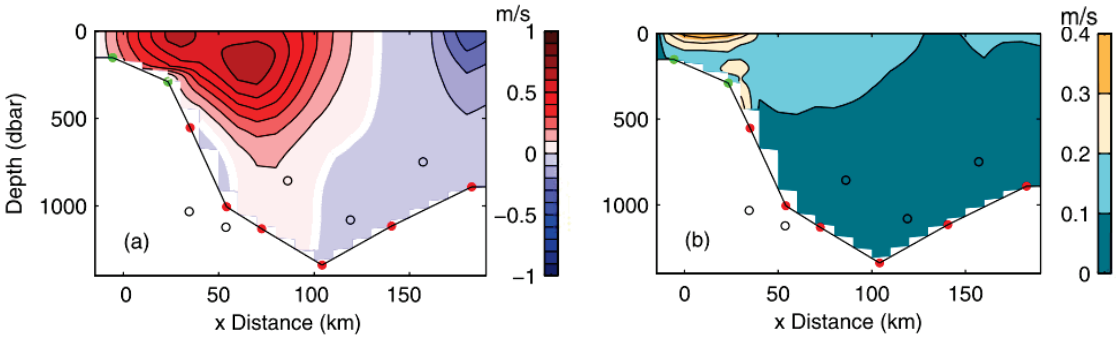

Fig. 1.1.11 (a) Mean and (b) standard deviation of Kuroshio velocity at the PN line as shown in Figure 1.1.1. Reproduced from Andres *et al*. (2008).

The Kuroshio in the Tokara Strait has little influence on the ECS but its current structure and volume transport are important to the Kuroshio south of Japan. Feng *et al*. (2000) analyzed four years of moored current meter data and reported a multicore structure in the Kuroshio in the Tokara Strait. The volume transport of the Kuroshio in the Tokara Strait is similar to that at the PN line (Wei *et al*., 2013). Using high resolution (an interval of 2 days in time and 2 km in space) ferryboat ADCP data from 2003 to 2011, Zhu *et al*. (2017) reported a mean volume transport of 23.03 Sv for the Kuroshio in the Tokara Strait, with a maximum volume transport (24.60 Sv) in July and a minimum (21.47 Sv) in November.

In addition to current velocity and transport, the position of the Kuroshio is also an important variable. The surface Kuroshio axis is located around the continental slope where the depth is 200 to 1000 m (Lie and Cho, 2016). The principal variations in the Kuroshio axis occur northeast of Taiwan where the axis shifts onshore in winter and offshore in summer (Sun and Su, 1994). The seasonal meridional migration of the Kuroshio axis southwest of Kyushu is also apparent (Sun and Su, 1994), which is explained by the joint effect of baroclinicity and bottom relief (Guo *et al*., 2003).

There are two southwestward currents within the Kuroshio region. One is the countercurrent beneath the Kuroshio (Ito *et al*., 1995; James *et al*., 1999) and the other is the countercurrent between the Kuroshio and the Ryukyu Islands (James *et al*., 1999; Oka and Kawabe, 2003; Hisaki and Imadu, 2009).

Taiwan Strait Current

The Taiwan Strait connects the ECS to the South China Sea (SCS). The Taiwan Strait Current flows through the Taiwan Strait and is a major source of the Taiwan Warm Current. Typically, there are three currents in the Taiwan Strait (Hu *et al*., 2010): the Chinese Coastal Current (CCC) and the Kuroshio branch are in the western and eastern Taiwan Strait, respectively, and the extension of the SCS water located in the western and central Taiwan Strait. The Taiwan Strait Current is stable and flows northeastward in summer but is weak and variable in winter (Chen *et al*., 2016).

There are several causes for the Taiwan Strait Current being weak and variable in winter. The CCC in winter flows southward along the Chinese coast and reaches the Taiwan Strait. Severe northeasterly winds in the winter may reverse the direction of the Taiwan Strait Current (Zhang *et al*., 2009; Chen *et al*., 2016). Liang *et al*. (2003) tracked the northward Kuroshio branch along the eastern side of the Taiwan Strait in both winter and summer using shipboard ADCP data from 1991 to 2000. Chen and Sheu (2006) demonstrated by satellite and *in situ* data that the northward Kuroshio branch and water from the SCS could reach only the southern Taiwan Strait in winter.

The mean transport through the Taiwan Strait is nearly zero or even southward in winter (Teague *et al*., 2003; Jan *et al*., 2006; Isobe, 2008; Chen *et al*., 2016). Qiu *et al*. (2011) analyzed the trajectories of about 100 satellite-tracked surface drifters from 1989 to 2007 and clarified that in winter the majority of them in the Taiwan Strait eventually turned southward. Thus, the Taiwan Strait Current, in regard to surface drifters, is not persistently northward in winter.

Taiwan Warm Current

The current off the Min-Zhe coast in the southern ECS has strong seasonality and is referred to as the Taiwan Warm Current. In summer, the Taiwan Warm Current flows northeastward off the coast at a velocity of about 20 to 40 cm s^{-1} (Katoh *et al*., 2000; Guan and Fang, 2006). Upon arriving at 28°N, it bifurcates into two branches: an onshore branch which flows northward and turns to the northeast off the mouth of the Changjiang River and an offshore branch which flows along the 100-m isobath and then joins the western side of the Kuroshio (Su and Pan, 1987). The Kuroshio surface water and the Taiwan Strait Current water constitute the surface water of the Taiwan Warm Current in summer (Weng and Wang, 1984; Su *et al*., 1994).

In winter, the Taiwan Warm Current flows in an upwind direction and reaches the Changjiang River Estuary (Lian *et al*., 2016). This phenomenon was often observed in snapshot surveys rather than in climatological hydrographic datasets, suggesting its episodic character in winter (Zhu *et al*., 2004). Taiwan Warm Current water originates mostly from the Kuroshio onshore intrusion northeast of Taiwan based on hydrographic and nutrient data, rather than from the weak wintertime Taiwan Strait Current (Liang and Su, 1994; Chen, 2003; Chen and Sheu, 2006). Lian *et al*. (2016) suggested that the Taiwan Warm Current originates farther from the mixing of the SCS water and Kuroshio branch water south of Taiwan (Fig. 1.1.12), which is supported by hydrographic observations and isotopic evidence (Liu *et al*., 2000; Jan *et al*., 2006; Chen, 2009).

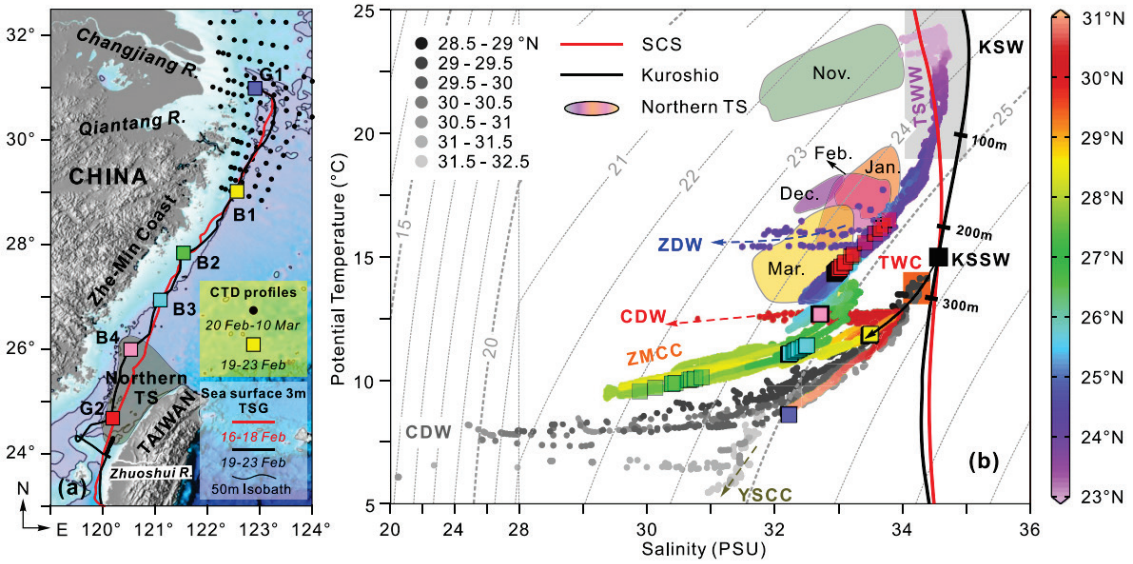

Fig. 1.1.12 (a) Schematic diagram of routine monitoring stations and (b) Temperature-Salinity diagram with reference historical curve of water masses of the South China Sea (SCS, red line), Kuroshio origin (black line) and historical data (1985–2003) in the northern Taiwan Strait in winter (shaded patches). See Lian *et al*. (2016) for more information on data distribution in (b).

Coastal current

The coastal current in the ECS is mainly the Min-Zhe Coastal Current that flows along the Min-Zhe coast southwestward in winter and northeastward in summer (Fig. 1.1.3). As the buoyant coastal current from the Changjiang River, the Min-Zhe Coastal Current is characterized by low salinity, low temperature, and high nutrient content (Lü *et al*., 2006; Qiao *et al*., 2006), and it plays an important role in transporting terrigenous materials to the open ocean.

From observations covering only one or a few sites (Guan, 1978; Zhu *et al*., 2004; Zhang *et al*., 2011; Zeng *et al*., 2012), it is difficult to estimate the transport of the Min-Zhe Coastal Current, which is modulated by strong tidal currents. Model results showed that the transport is 0.12 Sv and that 80% of the freshwater from the Changjiang River is transported by this current (Li and Rong, 2012). Based on a well-designed cruise survey, the subtidal characteristics of the Min-Zhe Coastal Current were comprehensively quantified (Wu *et al*., 2013). The Min-Zhe Coastal Current was confined within the 40-m isobath and had a maximum surface speed of ~50 cm s^{-1}. The lower salinity suggests the transport of Changjiang-diluted water. The Min-Zhe Coastal Current is estimated to have a volume transport of ~0.215 Sv, which is ten times larger than runoff of the Changjiang River, and it transports over 90% of the freshwater from the Changjiang (Wu *et al*., 2013). Primarily buoyancy and local winds drive the Min-Zhe Coastal Current, and the former accounts for ~0.128 Sv of the observed volume transport (Wu *et al*., 2013).

Circulation across isobaths

Kuroshio intrusion

The main stream of the Kuroshio flows northeastward along the shelf break while a portion escapes from the constraint of steep topography and intrudes onshore. Two main areas of intrusion are northeast of Taiwan and southwest of Kyushu.

The Kuroshio northeast of Taiwan intrudes onto the shelf after leaving the island (Chuang and Liang, 1994; Tang *et al*., 1999). The water intrusion is named the Kuroshio Branch Current north of Taiwan (KBCNT) (Ichikawa and Beardsley, 2002), which can reach as far as 26.5°N according to composite of trajectories of drifting buoys (Lie and Cho, 2016) and then turns right to the main stream due to bottom friction and the topographic beta effect (Qiu and Imasato, 1990; Su, 2001). The rest of the intruded water northeast of Taiwan goes farther onto the ECS shelf along the second route (Liu *et al*., 2014). The nearshore Kuroshio branch shows gradual upwelling from the shelf break to the continental shelf off the Changjiang River Estuary in summer as detected from *in situ* salinity data (Yang *et al*., 2011, 2012).

The Kuroshio onshore intrusion northeast of Taiwan is strong and extends farther onshore in winter (Tang *et al*., 2000; Hsin *et al*., 2013). Ichikawa *et al.* (2008) demonstrated that the Kuroshio main stream is strong and moves offshore in summer. Wu *et al.* (2014) showed a Hovmöller diagram of climatological monthly surface geostrophic velocity flowing perpendicular to the cross-shelf section northeast of Taiwan (Fig. 1.1.13). The western edge of the current indicates the variability of the intrusion as it gradually migrates seaward after winter and reaches the easternmost place in July when the Kuroshio main stream velocity reaches a peak (> 0.8 m s^{-1}).

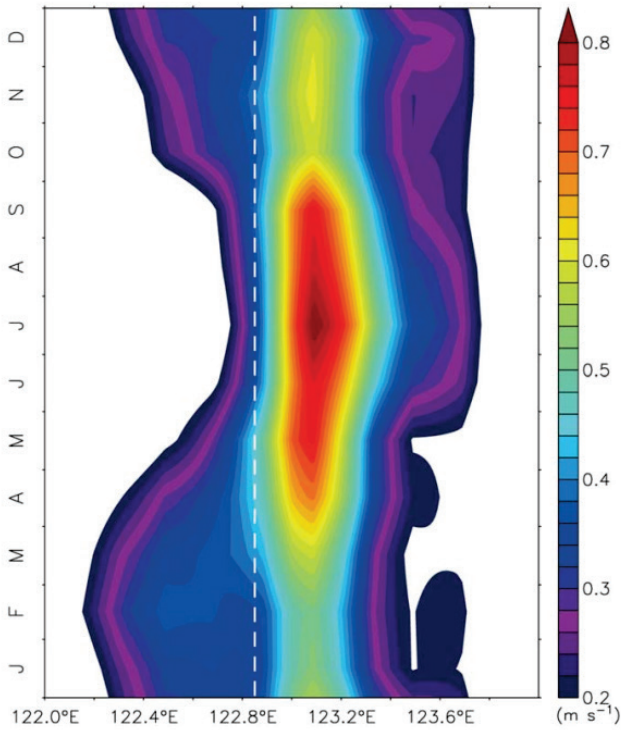

Fig. 1.1.13 Hovmöller diagram of monthly climatological surface geostrophic velocity of the Kuroshio derived from altimeter data in the northeast of Taiwan, 25–27°N. Reproduced from Wu *et al*. (2014).

From observations, Tang and Yang (1993) and Chuang and Liang (1994) found that the currents northeast of Taiwan in winter were not well correlated with local wind conditions. Oey *et al*. (2010) and Wu *et al*. (2014) proposed that, in winter, surface heat flux rather than local wind conditions is responsible for the Kuroshio intrusion northeast of Taiwan. The importance of the role of surface heat flux is consistent with dynamical analysis of model results indicating that the change in density field is a primary factor in the seasonal variability of the Kuroshio onshore flux at a fixed location along the shelf break (Guo *et al*., 2006).

When the Kuroshio main stream reaches southwest of Kyushu, it turns right to the east and exits the ECS through the Tokara Strait. As a result of conservation of potential vorticity, another Kuroshio Branch Current west of Kyushu (KBCWK) forms and intrudes over the outer shelf across the shelf break (Hsueh *et al*., 1996; Lie *et al*., 1998; Isobe, 2000). The KBCWK is traceable by its high salinity, and bifurcates into three branches in the outer shelf (Lie and Cho, 2002). It has smaller seasonal variability than the KBCNT (Lie and Cho, 2016).

In addition to the onshore intrusions at the two locations discussed above, the Kuroshio onshore intrusion across the entire shelf break of the ECS has received more attention recently. This onshore intrusion has strong seasonal variation, showing a maximum in autumn and a minimum in summer (Teague *et al*., 2003; Guo *et al*., 2006; Isobe, 2008), and shows distinct vertical variation that can be separated into the surface Ekman layer, bottom Ekman layer, and a middle layer between the two Ekman layers (Zhou *et al*., 2015; Ding *et al*., 2016; Wang and Oey, 2016; Zhang *et al*., 2018). Strong seasonal variation in the Kuroshio onshore transport across the entire shelf break is associated with the monsoon and changes in the density field (Chao, 1990; Guo *et al*., 2006), as well as volume transport through the Taiwan Strait and Kuroshio transport east of Taiwan (Lee and Matsuno, 2007).

Changjiang Diluted Water

The Changjiang River accounts for most of the freshwater discharge into the ECS. A major coastal water mass, the Changjiang Diluted Water (CDW), is found in the surface layer and has salinity less than 32 (Su and Weng, 1994).

The CDW flows offshore to the Kuroshio frontal area in spring (Chang and Isobe, 2003). Usually the CDW is confined to a thin surface layer with a thickness of 10 to 15 m. It extends farther offshore to the northeast over the western shelf of the northern ECS in summer (Lie *et al*., 2003; Hu *et al*., 2016), enters the Jeju Strait from the west (Beardsley *et al*., 1992), and goes through the western channel of the Tsushima Strait in August (Chang and Isobe, 2003). With the appearance of the northeasterly monsoon in autumn, the CDW retreats to the western YS and remains close to the Chinese coast in a narrow band. In winter, it reaches the Taiwan Strait against the Taiwan Warm Current (Hu, 1994; Chang and Isobe, 2003). Low salinity shelf water was observed in the Kuroshio subsurface layer (~100 m depth) around the shelf break of the ECS (Isobe *et al*., 2004), suggesting a possible discharge of the CDW to the open ocean.

Southwesterly or southerly winds cause the northeastward extension of the CDW in summer, while strong northeasterly winds cause the southwestward extension to the Taiwan Strait in winter (Chang and Isobe, 2003; Lie *et al*., 2003). The area of the CDW in summer over the continental shelf is associated with the Changjiang River discharge (Chen *et al*., 2009; Tseng *et al*., 2011). When the discharge in August is at a low level over years, its area is more strongly correlated with southwesterly winds (Bai *et al*., 2014).

A tracer experiment was carried out to assess the relative importance of outlets of the CDW (Chang and Isobe, 2003). About 68% of the Changjiang discharge likely passes through the Tsushima Strait, which is supported by hydrographic and ADCP observations at the Tsushima Strait (Isobe *et al*., 2002), and about 27% is transported through the Taiwan Strait in autumn and winter. An interesting influence of CDW is that it promotes sea surface warming (Park *et al*., 2011; Moon *et al*., 2019) that further likely affects precipitation over a large area, including Japan (Manda *et al*., 2014).

Vertical circulation

Upwelling is the upward movement of water that usually brings nutrient-rich water to the sunlit upper layer. Thus, the upwelling area is usually recognized as having a lower sea surface temperature (SST) and a higher chlorophyll *a* concentration than the surrounding water.

Upwelling northeast of Taiwan

The cold eddy northeast of Taiwan is characterized by low temperature and high salinity (Tseng *et al*., 2012). It appears as two or three cold cores in summer and autumn, and has large seasonal variations (Xiu *et al*., 2001). Observational data revealed that the upwelling below 100 m depth is strongest in summer. However, upwelling at about 30 m below the surface is stronger in winter than in summer (Chang *et al*., 2009). Model results showed the largest upwelling velocity to be on the order of 5×10^{-6} m s^{-1}, and the strong upwelling was related to the Kuroshio onshore intrusion northeast of Taiwan (*e.g*., Lee and Chao, 2003; Xiu and Huang, 2006).

The cold eddy northeast of Taiwan has also been recognized as a cold dome over the shelf northeast of Taiwan (Jan *et al*., 2011), and was confirmed by some high resolution numerical models (Gopalakrishnan *et al*., 2013). The cold dome is recognized as having a diameter of approximately 100 km and being centered around 25.625°N, 122.125°E when taking the temperature at a depth of

50 m as the reference. The monsoon-driven winter intrusion of the Kuroshio onshore promotes upwelling and transports more subsurface water to the cold dome than does the summer monsoon period. The cold dome is more easily detected at the sea surface in summer than in winter (Jan *et al*., 2001; Gopalakrishnan *et al*., 2013).

Coastal upwelling

The coastal upwelling phenomenon is observed off the Changjiang River Estuary with a center at about 31°30′N, 122°40′E and a spatial longitude–latitude scale of 1° × 1° (Zhao *et al*., 2001). During cruises in August 2000, sections off the mouth of the Changjiang River showed a temperature distribution of 20 to 23°C and salinity of about 34, suggesting the presence of upwelling (Zhu, 2003; Zhu *et a*l., 2003; Lü *et al*., 2006). Lü *et al.* (2006) suggested that tidal mixing plays a major role in inducing upwelling off the estuary in summer. Topography, the Changjiang River discharge, the Taiwan Warm Current, and wind are less important factors.

Along the Min-Zhe coast upwelling appears in June, becomes strongest in July and August, and wanes in late September (Lou *et al*., 2011). The SST of 24° to 27°C in summer in the upwelling region is about 2° to 4°C lower than in surrounding waters (Hu and Zhao, 2007; Lou *et al*., 2011). In addition, upwelling signals were detected as a high concentration of nutrients and low concentration of dissolved oxygen from observational data in January 1999, in which a doming structure was found (Qiao *et al*., 2006).

According to the classical Ekman transport theory, southwesterly winds prevail along the eastern Min-Zhe coast in summer, causing offshore transport of water in the upper layer, and thus inducing coastal upwelling along the coast. Therefore, wind-driven offshore Ekman transport has been regarded as the crucial mechanism for coastal upwelling in the ECS in summer. However, numerical experiments suggest tidal mixing plays a predominant role in inducing this upwelling. Strong tidal mixing results in a considerable horizontal density gradient across the tidal front, and upwelling is induced as a branch of the secondary circulation which is stimulated by the cross-frontal density gradient. The influence of wind on upwelling is small. In fact, wind forcing exerts negative influences on upwelling by weakening the encroachment of the Taiwan Warm Current onto the continental shelf, which is totally different from the classical Ekman pumping (Lü *et al*., 2006). Although the upwelling is maintained in winter, and the presence of a density (or salinity) front between the coastal water and the Taiwan Warm Current is the primary controlling factor responsible for upwelling in winter (Qiao *et al*., 2006), the wind, the Taiwan Warm Current, and the tidal mixing influence the extension and intensity of the density front in winter.

Three kinds of low-frequency waves, the Kelvin wave mode, the first shelf wave mode, and the second shelf wave mode, were identified from five mooring array observations in the coastal water of ECS in winter of 2007. The periods of the waves varied from 2 to 10 days. The remotely generated free Kelvin wave is a major factor to cause the sea level variation, while the Kelvin wave and the locally generated first shelf wave work together to control the downwind flow. The wave energy increases toward the direction of wave propagating and decreases to the offshore (Yin *et al*., 2014).

1.1.4 Summary and future work

The Bohai Sea, the YS and the ECS are marginal seas on the continental shelf of the northwestern Pacific Ocean. Currents in the YS have noticeable seasonal variation. In winter, northerly winds induce an anti-cyclonic gyre in the eastern YS and a cyclonic gyre in the western YS, both of which

are composed of the northward YSWC along the Yellow Sea Trough and the southward West Korea Coastal Current in the east and the southward Chinese Coastal Current in the west. The YSWC flows northwest near the bottom with a speed of 4 to 10 cm s^{-1} on the western side of the Yellow Sea Trough. The YSWC extension enters the Bohai Sea along the northern side of the Bohai Strait and forms an anti-cyclonic gyre in the east and a cyclonic gyre in the west of the Bohai Sea. The Jeju Warm Current is the mean current that flows clockwise around Jeju Island and delivers warm and saline water. The relaxation of northerly wind bursts accompanied by propagating coastal shelf waves sporadically induces the northward intrusion of the YSWC from the Jeju Warm Current to the west of Jeju Island. In summer, horizontal circulation in the YS has a three-layer structure: northeastward current in the surface layer (0–4 m), a basin-scale cyclonic circulation in the upper layer (4–40 m) with boundary currents along the tidal mixing fronts, and a weak southward flow along the Yellow Sea Trough in the bottom layer. The West Korea Coastal Current flows northward with a speed of about 10 cm s^{-1} along the tidal mixing front in the eastern YS and the Chinese Coastal Current flows to the south along the 40- to 50-m isobaths. Over the shallow (h < 40 m) western shelf of the YS, the surface current flows northeastward due to southerly winds.

In the ECS, the Kuroshio main stream flows northeastward along the shelf break over the continental slope where the bottom depth is 200–1000 m and its mean transport is about 25.8 Sv. An onshore intrusion of the Kuroshio occurs across the entire shelf break of the ECS and it is weaker in summer and stronger in autumn. Two main regions of the Kuroshio intrusion are to the northeast of Taiwan and southwest of Kyushu. The Taiwan Strait Current flows northeastward through the Taiwan Strait and is a major source of the Taiwan Warm Current. The Taiwan Warm Current flows northeastward off the Min-Zhe coast at a velocity of about 20 to 40 cm s^{-1} in summer. The Min-Zhe Coastal Current flows along the Min-Zhe coast northeastward in summer and southwestward in winter. It is confined within the 40-m isobath and transports the CDW. The CDW flows offshore to the Kuroshio frontal area in spring and to the northeast over the western shelf of the northern ECS in summer. It remains close to the Chinese coast in a narrow band in autumn and reaches the Taiwan Strait in winter. Strong upwelling northeast of Taiwan is related to the Kuroshio onshore intrusion. Upwelling off the Changjiang River Estuary in summer is induced by tidal mixing. At the Min-Zhe coast, subsurface water upwells due to a density gradient by a tidal mixing front in summer and a density front in winter.

In this review, we summarized the general understanding on the circulations in the Bohai Sea, YS and ECS from a view of steady state to seasonal variations with coverage of literature on observations, modeling, and processes. We did not include studies on the interannual variations and even longer-term variations of circulations in the YS and ECS although they are very important to the community. One reason for this choice is the lack of such studies, which inhibit summarization and generalizations on the subject. It is easy to imagine the difficulties to solve this issue. However, with the accumulation of observed data in past decades and more modeling work based on a new generation surface wave-tide-circulation coupled models in the future, we expect a rapid advance on this topic. The collaboration of scientists from countries surrounding the YS and ECS under an international framework such as PICES is absolutely necessary to accomplish this goal.

Acknowledgements

The authors thank PICES for providing us a chance for this review. X. Guo thanks support from Ms. Jing Zhang who helped him to finish the first draft of ECS part. X. Guo was supported by Grants-in-Aid for Scientific Research (MEXT KAKENHI grant numbers: JP15H05821/26287116). B.-J. Choi was supported by the Basic Science Research Program through the National Research Foundation of Korea (NRF) funded by the Ministry of Education (NRF-2016R1D1A1B03935246 and NRF-2016R1A6A1A03012647). F. Qiao was supported by the International Cooperation

Project of the Indo-Pacific Ocean Environment Variation and Air–Sea Interaction under Grant GASI-IPOVAI-05 and the Qingdao National Laboratory for Marine Science and Technology under Grant 2016ASKJ16.

1.1.5 References

Andres, M., Wimbush, M., Park, J.H., Chang, K.I., Lim, B.H., Watts, D.R., Ichikawa, H. and Teague W.J. 2008. Observations of Kuroshio flow variations in the East China Sea. *J. Geophys. Res. Oceans* **113**: C05013, doi:10.1029/2007JC004200.

Bai, Y., He, X., Pan, D., Chen, C.T.A., Kang, Y., Chen, X. and Cai, W.J. 2014. Summertime Changjiang River plume variation during 1998-2010, *J. Geophys. Res. Oceans* **119**: 6238–6257, doi:10.1002/2014JC009866.

Beardsley, R.C., Limeburner, R., Yu, H. and Cannon, G.A. 1985. Discharge of the Changjiang (Yangtze River) into the East China Sea. *Cont. Shelf Res*. **4**: 57–76, doi:10.1016/0278-4343(85)90022-6.

Beardsley, R.C., Limeburner, R., Kim, K. and Candela, J. 1992. Lagrangian flow observations in the East China, Yellow and Japan seas. *La mer* **30**: 297–314.

Bian, C.W., Jiang, W.S., Pohlmann, T. and Sündermann, J. 2016. Hydrography-physical description of the Bohai Sea. *J. Coast. Res*. **74**: 1–12, doi:10.2112/SI74-001.1.

Chang, K.-I., Kim, K., Lee, S.W. and Shim, T.B. 1995. Hydrography and sub-tidal current in the Cheju Strait in spring 1983. *J. Korean Soc. Oceanogr*. **20**: 203–215.

Chang, K.-I., Suk, M.-S., Pang, I.-C. and Teague, W.J. 2000. Observations of the Cheju current. *J. Korean Soc. Oceanogr*. **35**: 129–152.

Chang, P.-H. and Isobe, A. 2003. A numerical study on the Changjiang diluted water in the Yellow and East China Seas. *J. Geophys. Res*. **108**: 3299, doi:10.1029/2002JC001749.

Chang, Y.L. and Oey, L.Y. 2011. Interannual and seasonal variations of Kuroshio transport east of Taiwan inferred from 29 years of tide-gauge data. *Geophys. Res. Lett*. **38**: doi:10.1029/2011GL047062.

Chang, Y.L., Wu, C.R. and Oey, L.Y. 2009. Bimodal behavior of the seasonal upwelling off the northeastern coast of Taiwan. *J. Geophys. Res. Oceans* **114**: C03027, doi:10.1029/2008JC005131.

Chao, S.-Y. 1990. Circulation of the East China Sea, a numerical study. *J. Oceanogr*. **46**: 273–295, doi:10.1007/BF02123503.

Chen, C., Shiah, F., Chiang, K., Gong, G. and Kemp, W.M. 2009. Effects of the Changjiang (Yangtze) River discharge on planktonic community respiration in the East China Sea. *J. Geophys. Res. Oceans* **114**: doi:10.1029/2008JC004891.

Chen, C.-T.A. 2003. Rare northward flow in the Taiwan Strait in winter: a note. *Cont. Shelf Res*. **23**: 387–391, doi:10.1016/S0278-4343(02)00209-1.

Chen, C.-T.A. 2009. Chemical and physical fronts in the Bohai, Yellow and East China seas. *J. Mar. Syst*. **78**: 394–410, doi:10.1016/j.jmarsys.2008.11.016.

Chen, C.T.A. and Sheu, D.D. 2006. Does the Taiwan warm current originate in the Taiwan Strait in wintertime? *J. Geophys. Res. Oceans* **111**: C04005, doi:10.1029/2005JC003281.

Chen, H., Qiao, F., Ezer, T., Yuan, Y. and Hua, F. 2009. Multi-core structure of the Kuroshio in the East China Sea from long-term transect observations. *Ocean Dyn*. **59**: 477–488, doi:10.1007/s10236-009-0182-9.

Chen, H.-W., Liu, C.-T., Matsuno, T., Ichikawa, K., Fukudome, K., Yang, Y., Doong, D.-J. and Tsai, W.-L. 2016. Temporal variations of volume transport through the Taiwan Strait, as identified by three-year measurements. *Cont. Shelf Res*. **114**: 41–53, doi:10.1016/j.csr.2015.12.010.

Chuang, W.-S. and Liang, W.-D. 1994. Seasonal variability of intrusion of the Kuroshio water across the continental shelf northeast of Taiwan. *J. Oceanogr*. **50**: 531–542, doi:10.1007/BF02235422.

Ding, R., Huang, D., Xuan, J., Mayer, B., Zhou, F. and Pohlmann, T. 2016. Cross-shelf water exchange in the East China Sea as estimated by satellite altimetry and in situ hydrographic measurement, *J. Geophys. Res. Oceans* **121**: 7192–7211, doi:10.1002/2016JC011972.

Feng, M., Mitsudera, H. and Yoshikawa, Y. 2000. Structure and variability of the Kuroshio current in Tokara Strait. *J. Phys. Oceanogr*. **30**: 2257–2276, doi:10.1175/1520-0485(2000)030<2257:SAVOTK>2.0.CO;2.

Gopalakrishnan, G., Cornuelle, B.D., Gawarkiewicz, G. and McClean, J.L. 2013. Structure and evolution of the cold dome off northeastern Taiwan: A numerical study. *Oceanography* **26**: 66–79, doi:10.5670/oceanog.2013.06.

Guan, B. 1978. Characteristics of the East China Sea current system. *Essays East China Sea Shelf*. Institute of Oceanology, pp. 126–133 (in Chinese).

Guan, B. 1994. Patterns and structures of the currents in Bohai, Huanghai and East China Seas, pp. 17–26 *in:* Oceanology of China Seas, vol. 1 *edited by* D. Zhou, Y.-B. Liang and C.-K. Zeng (C.K.Tseng), Kluwer Academic, Dordrecht.

Guan, B. and Fang, G. 2006. Winter counter-wind currents off the southeastern China coast: A review. *J. Oceanogr*. **62**: 1–24, doi:10.1007/s10872-006-0028-8.

Guo, X., Hukuda, H., Miyazawa, Y. and Yamagata, T. 2003. A triply nested ocean model for simulating the Kuroshio—Roles of horizontal resolution on JEBAR. *J. Phys. Oceanogr*. **33**: 146–169, doi: 10.1175/1520-0485(2003)033<0146:ATNOMF>2.0.CO;2.

Guo, X., Miyazawa, Y. and Yamagata, T. 2006. The Kuroshio onshore intrusion along the shelf break of the East China Sea: The origin of the Tsushima Warm Current. *J. Phys. Oceanogr*. **36**: 2205–2231, doi:10.1175/jpo2976.1.

Hainbucher D., Hao, W., Pohlmann, T., Sündermann, J. and Feng, S. 2004. Variability of the Bohai Sea circulation based on model calculations. *J. Mar. Syst.* **44**: 153–174, doi:10.1016/j.jmarsys.2003.09.008.

Hisaki, Y. and Imadu, C. 2009. Southward recirculation of the East China Sea Kuroshio west of Okinawa Island. *J. Geophys. Res*. *Oceans* **114**: C06013, doi:10.1029/2008JC004943.

Hsin, Y.C., Wu, C.R. and Shaw, P.T. 2008. Spatial and temporal variations of the Kuroshio east of Taiwan 1982-2005: A numerical study. *J. Geophys. Res. Oceans* **113**: C04002, doi:10.1029/2007JC004485.

Hsin, Y., Chiang, T. and Wu, C. 2011. Fluctuations of the thermal fronts off northeastern Taiwan. *J. Geophys. Res. Oceans* **116**: C10005, doi:10.1029/2011JC007066.

Hsin, Y.-C., Qiu, B., Chiang, T.-L. and Wu, C.-R. 2013. Seasonal to interannual variations in the intensity and central position of the surface Kuroshio east of Taiwan. *J. Geophys. Res. Oceans* **118**: 4305–4316, doi:10.1002/jgrc.20323.

Hsueh, Y. 1988. Recent current observations in the eastern Yellow Sea. *J. Geophys. Res*. **93**: 6875–6884, doi:10.1029/JC093iC06p06875.

Hsueh, Y. and Pang, I.C. 1989. Coastally trapped long waves in the Yellow Sea. *J. Phys. Oceanogr*. **19**: 612–625, doi:10.1175/1520-0485(1989)019<0612:CTLWIT>2.0.CO;2.

Hsueh, Y. and Yuan, D. 1997. A numerical study of the currents, heat advection and sea level fluctuations in the Yellow Sea in winter 1986. *J. Phys. Oceanogr*. **27**: 2313–2326, doi:10.1175/1520-0485(1997)027<2313:ANSOCH>2.0.CO;2.

Hsueh, Y., Romea, R.D. and deWitt, P.W. 1986. Wintertime winds and sea-level fluctuations in the northeast China Sea. Part II: Numerical model. *J. Phys. Oceanogr*. **16**: 241–261, doi: 10.1175/1520-0485(1986)016<0241:WWACSL>2.0.CO;2.

Hsueh, Y., Lie, H.J. and Ichikawa, H. 1996. On the branching of the Kuroshio west of Kyushu, *J. Geophys. Res.* **101**: 3851–3857, doi:10.1029/95jc03754.

Hu, D.-X. 1994. Some striking features of circulation in Huanghai Sea and East China Sea, pp. 27–38 *in:* Oceanology of China Seas, vol. 1, edited by *edited by* D. Zhou, Y.B. Liang and C.-K. Tseng, Kluwer Academic, Norwell, Mass.

Hu, J., Kawamura, H., Li, C., Hong, H. and Jiang, Y. 2010. Review on current and seawater volume transport through the Taiwan Strait. *J. Oceanogr*. **66**: 591–610, doi:10.1007/s10872-010-0049-1.

Hu, M. and Zhao, C. 2007. Long-time observation of upwelling in the Zhoushan Islands and adjacent seas during the summer season. *Period. Ocean Univ. China* **S1**: 241–246 (in Chinese with English abstract).

Hu, Z., Wang, D., Pan, D., He, X., Miyazawa, Y., Bai, Y., Wang, D. and Gong, F. 2016. Mapping surface tidal currents and Changjiang plume in the East China sea from geostationary ocean color imager. *J. Geophys. Res. Oceans* **121**: 1563–1572, doi:10.1002/2015JC011469.

Ichikawa, H. and Beardsley, R.C. 2002. The current system in the Yellow and East China Seas. *J. Oceanogr*. **58**: 77–92, doi:10.1023/A:1015876701363.

Ichikawa, K., Tokeshi, R., Kashima, M., Sato, K., Matsuoka, T., Kojima, S. and Fujii, S. 2008. Kuroshio variations in the upstream region as seen by HF radar and satellite altimetry data. *Int. J. Remote Sens*. **29**: 6417–6426, doi:10.1080/01431160802175454.

Isobe, A. 2000. Two-layer model on the branching of the Kuroshio southwest of Kyushu, Japan. *J. Phys. Oceanogr*. **30**: 2461–2476, doi:10.1175/1520-0485(2000)030<2461:TLMOTB>2.0.CO;2.

Isobe, A. 2008. Recent advances in ocean-circulation research on the Yellow Sea and East China Sea shelves. *J. Oceanogr*. **64**: 569–584, doi:10.1007/s10872-008-0048-7.

Isobe, A., Ando, M., Watanabe, T., Senjyu, T., Sugihara, S. and Manda, A. 2002. Freshwater and temperature transports through the Tsushima-Korea Straits. *J. Geophys. Res. Oceans* **107**: 3065, doi:10.1029/2000JC000702.

Isobe, A., Fujiwara, E., Chang, P.-H., Sugimatsu, K., Shimizu, M., Matsuno, T. and Manda, A. 2004. Intrusion of less saline shelf water into the Kuroshio subsurface layer in the East China Sea. *J. Oceanogr*. **60**: 853–863, doi:10.1007/s10872-004-5778-6.

Ito, T., Kaneko, A., Furukawa, H., Gohda, N. and Koterayama, W. 1995. A structure of the Kuroshio and its related upwelling on the East China Sea shelf slope. *J. Oceanogr*. **51**: 267–278, doi:10.1007/BF02285165.

James, C., Wimbush, M., Ichikawa, H., James, C., Wimbush, M. and Ichikawa, H. 1999. Kuroshio meanders in the East China Sea. *J. Phys. Oceanogr*. **29**: 259–272, doi:10.1175/1520-0485(1999)029<0259:KMITEC>2.0.CO;2.

Jan, S., Sheu, D.D. and Kuo, H.M. 2006. Water mass and throughflow transport variability in the Taiwan Strait. *J. Geophys. Res. Oceans* **111**: C12012, doi:10.1029/2006JC003656.

Jan, S., Chen, C.-C., Tsai, Y.-L., Yang, Y.J., Wang, J., Chern, C.-S., Gawarkiewicz, G., Lien, R.-C., Centurioni, L. and Kuo, J.-Y. 2011. Mean structure and variability of the cold dome northeast of Taiwan. *Oceanogr*. **24**: 100–109, doi:10.5670/oceanog.2011.98.

Jan, S., Yang, Y.J., Wang, J., Mensah, V., Kuo, T.H., Chiou, M.D., Chern, C.S., Chang, M.H. and Chien, H. 2015. Large variability of the Kuroshio at 23.75°N east of Taiwan. *J. Geophys. Res. Oceans* **120**: 1825–1840, doi:10.1002/2014JC010614.

Johns, W.E., Lee, T.N., Zhang, D., Zantopp, R., Liu, C.-T. and Yang, Y. 2001. The Kuroshio east of Taiwan: Moored transport observations from the WOCE PCM-1 array. *J. Phys. Oceanogr*. **31**: 1031–1053, doi:10.1175/1520-0485(2001)031<1031:TKEOTM>2.0.CO;2.

Kagimoto, T. and Yamagata, T. 1997. Seasonal transport variations of the Kuroshio: An OGCM simulation. *J. Phys. Oceanogr*. **27**: 403–418, doi:10.1175/1520-0485(1997)027<0403:STVOTK>2.0.CO;2.

Katoh, O., Morinaga, K. and Nakagawa, N. 2000. Current distributions in the southern East China Sea in summer. *J. Geophys. Res. Oceans* **105**: 8565, doi:10.1029/1999JC900309.

Kondo, M. 1985. Oceanographic investigations of fishing grounds in the East China Sea and the Yellow Sea- I. Characteristics of the mean temperature and salinity distributions measured at 50 m and near the bottom. *Bull. Seikai Reg. Fish. Res. Lab*. **62**: 19–66 (in Japanese).

Kwon, K.M., Choi, B.-J., Lee, S.-H., Cho, Y.K. and Jang, C.J. 2011. Coastal current along the eastern boundary of the Yellow Sea in summer: Numerical simulations. *J. Korean Soc. Oceanogr*. **16**: 155–168, doi:10.7850/jkso.2011.16.4.155.

Le, K.-T., Feng, M. and Wang, Y. 1993. A numerical study of wintertime circulation in the Bohai and Huanghai Seas. *Chin. J. Oceanol. Limnol*. **11**: 149–160, doi:10.1007/BF02850822.

Lee, H.-J. and Chao, S.-Y. 2003. A climatological description of circulation in and around the East China Sea. *Deep Sea Res. II* **50**: 1065–1084, doi:10.1016/S0967-0645(03)00010-9.

Lee, J.H., Pang, I.-C., Moon, I.-J. and Ryu, J.-H. 2011. On physical factors that controlled the massive green tide occurrence along the southern coast of the Shandong Peninsula in 2008: A numerical study using a particle-tracking experiment. *J. Geophys. Res*. *Oceans* **116**: C12036, doi:10.1029/2011JC007512.

Lee, J.-S. and Matsuno, T. 2007. Intrusion of Kuroshio water onto the continental shelf of the East China Sea. *J. Oceanogr*. **63**: 309–325, doi:10.1007/s10872-007-0030-9.

Lee, S.H. and Beardsley, R.C. 1999. Infuence of stratification on residual tidal currents in the Yellow Sea. *J. Geophys. Res*. **104**: 15,679−15,701, doi:10.1029/1999JC900108.

Li, M. and Rong, Z. 2012. Effects of tides on freshwater and volume transports in the Changjiang River plume. *J. Geophys. Res. Oceans* **117**: doi:10.1029/2011JC007716.

Lian, E., Yang, S., Wu, H., Yang, C., Li, C. and Liu, J.T. 2016. Kuroshio subsurface water feeds the wintertime Taiwan Warm Current on the inner East China Sea shelf. *J. Geophys. Res. Oceans* **121**: 4790–4803, doi:10.1002/2016JC011869.

Liang, W.-D., Tang, T.Y., Yang, Y.J., Ko, M.T. and Chuang, W.-S. 2003. Upper-ocean currents around Taiwan. *Deep Sea Res. II* **50**: 1085–1105, doi:10.1016/S0967-0645(03)00011-0.

Liang, X.S. and Su, J.L. 1994. A two-layer model for the summer circulation of the East China Sea. *Acta Oceanol. Sin.* **13**: 325–344.

Lie, H.-J. 1986. Summertime hydrographic features in the southeastern Hwanghae. *Prog. Oceanogr*. **17**: 229–242, doi:10.1016/0079-6611(86)90046-7.

Lie, H.J. 1999. On the Huanghai (Yellow) Sea circulation: A review by current measurements. *Acta Oceanol. Sin.* **18**: 355–374.

Lie, H.-J. and Cho, C.-H. 2002. Recent advances in understanding the circulation and hydrography of the East China Sea. *Fish. Oceanogr*. **11**: 318–328, doi:10.1046/j.1365-2419.2002.00215.x.

Lie, H.-J. and Cho, C.-H. 2016. Seasonal circulation patterns of the Yellow and East China Seas derived from satellite-tracked drifter trajectories and hydrographic observations. *Prog. Oceanogr*. **146**: 121–141, doi:10.1016/j.pocean.2016.06.004.

Lie, H.-J., Cho, C.-H., Lee, J.-H., Niiler, P. and Hu, J.-H. 1998. Separation of the Kuroshio water and its penetration onto the continental shelf west of Kyushu. *J. Geophys. Res*. **103**: 2963–2976, doi: 10.1029/97JC03288.

Lie, H.-J., Cho, C.-H., Lee, J.-H., Lee, S. and Tang, Y. 2000. Seasonal variation of the Cheju Warm Current in the northern East China Sea. *J. Oceanogr*. **56**: 197–211, doi:10.1023/A:1011139313988.

Lie, H.-J., Cho, C.-H., Lee, J.-H., Lee, S., Tang, Y. and Zou, E. 2001. Does the Yellow Sea Warm Current really exist as a persistent mean flow? *J. Geophys. Res.* **106**: 22,199–22,210, doi:10.1029/2000JC000629.

Lie, H.-J., Cho, C., Lee, J. and Lee, S. 2003. Structure and eastward extension of the Changjiang River plume in the East China Sea. *J. Geophys. Res*. *Oceans* **108**: 3077, doi:10.1029/2001JC001194.

Lie, H.-J., Cho, C.-H. and Lee, S. 2009. Tongue-shaped frontal structure and warm water intrusion in the southern Yellow Sea in winter. *J. Geophys. Res. Oceans* **114**: C01003, doi:10.1029/2007JC004683.

Lin, X. and Yang, J. 2011. An asymmetric upwind flow, Yellow Sea Warm Current: 2. Arrested topographic waves in response to the northwesterly wind. *J. Geophys. Res*. *Oceans* **116**: C04027, doi: 10.1029/2010JC006514.

Lin, X., Yang, J., Guo, J., Zhang, Z., Yin, Y., Song, X. and Zhang, X. 2011. An asymmetric upwind flow, Yellow Sea Warm Current: 1. New observations in the western Yellow Sea. *J. Geophys. Res*. *Oceans* **116**: C04026, doi:10.1029/2010JC006513.

Liu, G., Wang, H., Sun, S. and Han, B. 2003. Numerical study on the velocity structure around tidal fronts in the Yellow Sea. *Adv. Atmos. Sci*. **20**: 453–460, doi:10.1007/BF02690803.

Liu, K.-K., Tang, T.Y., Gong, G.-C., Chen, L.-Y. and Shiah, F.-K. 2000. Cross-shelf and along-shelf nutrient fluxes derived from flow fields and chemical hydrography observed in the southern East China Sea off northern Taiwan. *Cont. Shelf Res*. **20**: 493–523, doi:10.1016/S0278-4343(99)00083-7.

Liu, X., Dong, C., Chen, D. and Su, J. 2014. The pattern and variability of winter Kuroshio intrusion northeast of Taiwan. *J. Geophys. Res. Oceans* **119**: 5380–5394, doi:10.1002/2014JC009879.

Lou, X., Shi, A., Xiao, Q. and Zhang, H. 2011. Satellite observation of the Zhejiang Coastal upwelling in the East China Sea during 2007-2009. Proc. of the SPIE, Vol. 8175, p. 81751M–1, doi:10.1117/12.898140.

Lü, X., Qiao, F., Xia, C., Zhu, J. and Yuan, Y. 2006. Upwelling off Yangtze River estuary in summer, *J. Geophys. Res. Oceans* **111**: C11S08, doi:10.1029/2005JC003250.

Lü, X., Qiao, F., Xia, C., Wang, G. and Yuan, Y. 2010. Upwelling and surface cold patches in the Yellow Sea in summer: Effects of tidal mixing on the vertical circulation. *Cont. Shelf Res*. **30**: 620–632, doi:10.1016/j.csr.2009.09.002.

Ma, J., Qiao, F., Xia, C. and Kim, C.S. 2006. Effects of the Yellow Sea Warm Current on the winter temperature distribution in a numerical model. *J. Geophys. Res. Oceans* **111**: C11S04, doi: 10.1029/2005JC003171.

Manda, A., Nakamura, H., Asano, N., Iizuka, S., Miyama, T., Moteki, Q., Yoshioka, M.K., Nishii, K. and Miyasaka, T. 2014. Impacts of a warming marginal sea on torrential rainfall organized under the Asian summer monsoon. *Sci. Rep*. **4**: doi:10.1038/srep05741.

Moon J.-H., Kim, T., Son, Y.B., Hong, J.-S., Lee, J.-H., Chang, P.-H. and Kim, S.-K. 2019. Contribution of low-salinity water to sea surface warming of the East China Sea in the summer of 2016. *Prog. Oceanogr*. **175**: 68–80, doi:10.1016/j.pocean.2019.03.012.

Naimie, C.E., Blain, C.A. and Lynch, D.R. 2001. Seasonal mean circulation in the Yellow Sea — a model-generated climatology. *Cont. Shelf Res*. **21**: 667−695, doi:10.1016/S0278-4343(00)00102-3.

Nitani, H. 1972. Beginning of the Kuroshio, pp. 353–369 *in:* Kuroshio—Its Physical Aspects *edited by* H. Stommel and K. Yoshida, University of Tokyo Press, Tokyo.

Oey, L.-Y., Hsin, Y.-C. and Wu, C.-R. 2010. Why does the Kuroshio northeast of Taiwan shift shelfward in winter? *Ocean Dyn*. **60**: 413–426, doi:10.1007/s10236-009-0259-5.

Oka, E. and Kawabe, M. 2003. Dynamic structure of the Kuroshio south of Kyushu in relation to the Kuroshio path variations. *J. Oceanogr*. **59**: 595–608, doi:10.1023/B:JOCE.0000009589.28241.93.

Pang, I.-C., Hong, C.-S., Chang, K.-I., Lee, J.C. and Kim, J.-T. 2003. Monthly variation of water mass distribution and current in the Cheju Strait. *J. Korean Soc. Oceanogr*. **38**: 87–100.

Park, K.-A., Park, J.-E., Choi, B.-J., Lee, S.-H., Lee, E., Byun, D.-S. and Kim, Y.-T. 2014. An analysis of oceanic current maps of the Yellow Sea and the East China Sea in secondary school science textbooks. *J. Korean Earth Sci. Soc*. **35**: 439−466, doi:10.5467/JKESS.2014.35.6.439.

Park, K.-A., Park, J.-E., Choi, B.-J., Lee, S.-H., Shin, H.-R., Lee, S.-R., Byun, D.-S., Kang, B. and Lee, E. 2017. Schematic maps of ocean currents in the Yellow Sea and the East China Sea for science textbooks based on scientific knowledge from oceanic measurements. *J. Korean Soc. Ocean*. **22**: 151−171, doi:10.7850/jkso.2017.22.4.151 (in Korean with English abstract).

Park, T., Jang, C.-J., Jungclaus, J.H., Haak, H., Park, W. and Oh, I.-S. 2011. Effects of the Changjiang river discharge on sea surface warming in the Yellow and East China Seas in summer. *Cont. Shelf Res*. **31**: 15–22, doi:10.1016/j.csr.2010.10.012.

Park, Y.H. 1986. Water characteristics and movements of the Yellow Sea Warm Current in summer. *Prog. Oceanogr*. **17**: 243–254, doi:10.1016/0079-6611(86)90047-9.

Qiao, F., Yang, Y., Lü, X., Xia, C., Chen, X., Wang, B. and Yuan, Y. 2006. Coastal upwelling in the East China Sea in winter. *J. Geophys. Res. Oceans* **111**: C11S06, doi:10.1029/2005JC003264.

Qiao, F., Wang, G., Lü, X. and Dia, D. 2011. Drift characteristics of green macroalgae in the Yellow Sea in 2008 and 2010. *Chin. Sci. Bull*. **56**: 2236–2242, doi:10.1007/s11434-011-4551-7.

Qiu, B. and Imasato, N. 1990. A numerical study on the formation of the Kuroshio counter current and the Kuroshio branch current in the East China Sea. *Cont. Shelf Res*. **10**: 165–184, doi:10.1016/0278-4343(90)90028-k.

Qiu, Y., Li, L., Chen, C.-T.A., Guo, X. and Jing, C. 2011. Currents in the Taiwan Strait as observed by surface drifters. *J. Oceanogr*. **67**: 395–404, doi:10.1007/s10872-011-0033-4.

Qu, L., Lin, X., Hetland, R.D. and Guo, J. 2018. The asymmetric continental shelf wave in response to the synoptic wind burst in a semienclosed double-shelf basin. *J. Geophys. Res. Oceans* **123**: 131–148, doi:10.1002/2017JC013025.

Riedlinger, S.K. and Jacobs, G.A. 2000. Study of the dynamic of wind driven transports into the Yellow Sea during winter. *J. Geophys. Res*. *Oceans* **105**: 28,695–28,708, doi:10.1029/2000JC900127.

Seung, Y.H. 1987. A summer circulation inferred from the density (temperature) distribution in the eastern Yellow Sea. *J. Ocean. Soc. of Korea* **22**: 63−70.

Seung, Y.H., Chung, J.H. and Park, Y.C. 1990. Oceanographic studies related to the tidal front in the mid-Yellow Sea off Korea: Physical aspect. *J. Oceanol. Soc. Korea* **25**: 84–95.

Seung, Y.H., Yoon, J.-H. and Lim, E.-P. 2012. Evidences of intermittent wind-induced flow in the Yellow Sea obtained from AVHRR SST data. *Ocean Polar Res.* **34**: 395–401, doi:10.4217/OPR.2012.34.4.395.

Su, J. 1998. Circulation dynamics of the China Seas north of 18°N, pp. 483–505 *in:* The Sea, vol. 11 *edited by* A.R. Robinson and K.H. Brink, John Wiley & Sons Inc., New York.

Su, J.L. 2001. A review of circulation dynamics of the coastal oceans near China. *Acta Oceanol. Sin.* **23**: 1–16 (in Chinese).

Su, J. and Pan, Y. 1987. On the shelf circulation north of Taiwan. *Acta Oceanol. Sin.* **6**(Suppl. 1): 1–20.

Su, J., Pan, Y. and Liang, X. 1994. Kuroshio intrusion and Taiwan Warm Current, pp. 59–70 *in:* Oceanology of China Seas *edited by* Y. Liang, T. Zhou and C.-K. Zeng, Springer, Dordrecht.

Su, Y. and Weng, X. 1994. Water masses in China Seas, pp. 3–26 *in:* Oceanology of China Seas, *edited by* Y. Liang, T. Zhou and C.-K. Zeng, Springer, Dordrecht.

Sun, X. and Su, Y. 1994. On the variation of Kuroshio in East China Sea, pp. 49–58 *in:* Oceanology of China Seas, *edited by* Y. Liang, T. Zhou and C.-K. Zeng, Springer, Dordrecht.

Tak, Y.-J., Cho, Y.-K., Seo, G.-H. and Choi, B.-J. 2016. Evolution of wind driven flows in the Yellow Sea during winter. *J. Geophys. Res. Oceans* **121**: 1970–1983, doi:10.1002/ 2016JC011622.

Takahashi, S., Isoda, Y. and Yanagi, T. 1995. A numerical study on the formation and variation of a clockwise-circulation during winter in the Yellow Sea. *J. Oceanogr*. **51**: 83–98, doi:10.1007/BF02235938.

Tang, T.Y. and Yang, Y.J. 1993. Low frequency current variability on the shelf break northeast of Taiwan. *J. Oceanogr*. **49**: 193–210, doi:10.1007/BF02237288.

Tang, T.-Y., Hsueh, Y., Yang, Y.J. and Ma, J.C. 1999. Continental slope flow northeast of Taiwan. *J. Phys. Oceanogr.* **29**: 1353–1362, doi:10.1175/1520-0485(1999)029<1353:CSFNOT>2.0.CO;2.

Tang, T.Y., Tai, J.H. and Yang, Y.J. 2000. The flow pattern north of Taiwan and the migration of the Kuroshio. *Cont. Shelf Res.* **20**: 349–371, doi:10.1016/S0278-4343(99)00076-X.

Tang, Y.X., Zou, E.M. and Lie, H.J. 2001. On the origin and path of the Huanghai Warm Current during winter and early spring. *Acta Oceanol. Sin.* **23**: 1–12 (in Chinese).

Teague, W. and Jacobs, G. 2000. Current observations on the development of the Yellow Sea Warm Current. *J. Geophys. Res. Oceans* **105**: 3401–3411, doi:10.1029/1999JC900301.

Teague, W.J., Jacobs, G.A., Ko, D.S., Tang, T.Y., Chang, K.I. and Suk, M.S. 2003. Connectivity of the Taiwan, Cheju, and Korea straits. *Cont. Shelf Res*. **23**: 63–77, doi:10.1016/s0278-4343(02)00150-4.

Tseng, C., Liu, K., Gong, G., Shen, P. and Cai, W. 2011. CO_2 uptake in the East China Sea relying on Changjiang runoff is prone to change. *Geophys. Res. Lett*. **38**: doi:10.1029/2011GL049774.

Tseng, Y.-H., Shen, M.-L., Jan, S., Dietrich, D.E. and Chiang, C.-P. 2012. Validation of the Kuroshio current system in the dual-domain Pacific Ocean model framework. *Prog. Oceanogr*. **105**: 102–124, doi:10.1016/j.pocean.2012.04.003.

Wang, F., Liu, C. and Meng, Q. 2012. Effect of the Yellow Sea warm current fronts on the westward shift of the Yellow Sea warm tongue in winter. *Cont. Shelf Res.* **45**: 98–107, doi:10.1016/j.csr.2012.06.005.

Wang, J. and Oey, L.Y. 2016. Seasonal exchanges of the Kuroshio and shelf waters and their impacts on the shelf currents of the East China Sea. *J. Phys. Oceanogr*. **46**: 1615–1632, doi:10.1175/JPO-D-15-0183.1.

Wei, Y.Z., Huang, D. and Zhu, X.H. 2013. Interannual to decadal variability of the Kuroshio Current in the East China Sea from 1955 to 2010 as indicated by in-situ hydrographic data. *J. Oceanogr*. **69**: 571–589, doi:10.1007/s10872-013-0193-5.

Weng, X.C. and Wang, C.M. 1984. A preliminary study on the T-S characteristics and the origin of Taiwan Warm Current water in summer. *Stud. Mar. Sin*. **21**: 113–133 (in Chinese).

Wu, C.-R., Hsin, Y.-C., Chiang, T.-L., Lin, Y.-F. and Tsui, I.F. 2014. Seasonal and interannual changes of the Kuroshio intrusion onto the East China Sea Shelf. *J. Geophys. Res. Oceans* **119**: 5039–5051, doi: 10.1002/2013jc009748.

Wu, H., Deng, B., Yuan, R., Hu, J., Gu, J., Shen, F., Zhu, J. and Zhang, J. 2013. Detiding measurement on transport of the Changjiang-derived buoyant coastal current. *J. Phys. Oceanogr*. **43**: 2388–2399, doi:10.1175/JPO-D-12-0158.1.

Xia, C., Qiao, F., Yang, Y., Ma, J. and Yuan, Y. 2006. Three-dimensional structure of the summertime circulation in the Yellow Sea from a wave-tide-circulation coupled model. *J. Geophys. Res. Oceans* **111**: C11S03, doi:10.1029/2005JC003218.

Xia, C., Guo, J., Wang, G., Chen, Z. and Kuang, X. 2019. The summertime circulation of the Bohai Sea simulated from a high-resolution wave-tide-circulation coupled model. *Acta Oceanol. Sin.* **38**: 32–37, doi:10.1007/s13131-018-1145-0.

Xiu, S., Wang, K. and Sun, P. 2001. Study on the information of remote sensing for cold eddies and its variations in the sea area northeast of Taiwan-I. The seasonal variations of the cold eddies. *J. Oceanogr. Huanghai Bohai Seas* **19**: 57–64 (in Chinese).

Xiu, S.M. and Huang, H.S. 2006. Study on numerical simulation for upwelling of winter off northeastern Taiwan. *J. Hydrodyn*. **21**: 331–338.

Xu, R., Zhao, B., Huang, J., Yang, Y. and Lei, F. 2006. The mean residual circulations in the Bohai Sea. *Mar. Sci*. **30**: 47–52 (in Chinese).

Yanagi, T. and Takahashi, S. 1993. Seasonal variation of circulations in the East China Sea and the Yellow Sea. *J. Oceanorg*. **49**: 503−520, doi:10.1007/BF02237458.

Yanagi, T. Morimoto, A. and Ichikawa, K. 1997. Seasonal variation in surface circulation of the East China Sea and the Yellow Sea derived from satellite altimetric data. *Cont. Shelf Res*. **17**: 655−644, doi:10.1016/S0278-4343(96)00054-4.

Yang, D., Yin, B., Liu, Z. and Feng, X. 2011. Numerical study of the ocean circulation on the East China Sea shelf and a Kuroshio bottom branch northeast of Taiwan in summer. *J. Geophys. Res. Oceans* **116**: C05015, doi:10.1029/2010JC006777.

Yang, D., Yin, B., Liu, Z., Bai, T., Qi, J. and Chen, H. 2012. Numerical study on the pattern and origins of Kuroshio branches in the bottom water of southern East China Sea in summer. *J. Geophys. Res. Oceans* **117**: 1–16, doi:10.1029/2011JC007528.

Yin, L., Qiao, F. and Zheng, Q. 2014. Coastal trapped-waves in the East China Sea observed by a mooring array in winter 2006. *J. Phys. Oceangr*. **44**: 576–590, doi:10.1175/JPO-D-13-07.1.

Yu, F., Zhang, Z., Diao, X. and Guo, J. 2009. Observational evidence of the Yellow Sea warm current. *Chin. J. Oceanol. Limnol*. **27**: 677–683, doi:10.1007/s00343-010-0006-2.

Yuan, D., Li, Y., Qiao, F. and Zhao, W. 2013. Temperature inversion in the Huanghai Sea bottom cold water in summer. *Acta Oceanol. Sin.* **32**: 42–47, doi:10.1007/s13131-013-0287-3.

Zang, J., Tang, Y., Zhou, E. and Lie, H.-J. 2003. Analysis of Yellow Sea circulation. *Chin. Sci. Bull*. **48**(Suppl.): 12–20, doi:10.1007/BF02900935.

Zeng, D., Ni, X. and Huang, D. 2012. Temporal and spatial variability of the ZheMing Coastal Current and the Taiwan Warm Current in winter in the southern Zhejiang coast sea. *Sci. China Series D: Earth Sci*. **42**: 1123–1134 (in Chinese).

Zhang, D., Lee, T.N., Johns, W.E., Liu, C.-T. and Zantopp, R. 2001. The Kuroshio east of Taiwan: Modes of variability and relationship to interior ocean mesoscale eddies. *J. Phys. Oceanogr*. **31**: 1054–1074, doi:10.1175/1520-0485(2001)031<1054:TKEOTM>2.0.CO;2.

Zhang, F.G., Mao, H.I. and Leng, Y.G. 1987. Analysis of drift bottle and drift card experiments in the Bohai and Yellow Sea (1975–1980). *Chin. J. Oceanol. Limnol*. **5**: 67–72, doi:10.1007/BF02848524.

Zhang, H., Du, P. and Zheng, X. 2011. Characteristics analysis of residual current of Zhejiang-Fujian water. *Mar. Sci. Bull*. **30**: 152–158 (in Chinese).

Zhang, J., Guo, X., Zhao, L., Miyazawa, Y. and Sun, Q. 2017. Water exchange across isobaths over the continental shelf of the East China Sea. *J. Phys. Oceanogr*. **47**: 1043–1060, doi:10.1175/JPO-D-16-0231.1.

Zhang, W.Z., Hong, H.S., Shang, S.P., Yan, X.H. and Chai, F. 2009. Strong southward transport events due to typhoons in the Taiwan Strait. *J. Geophys. Res. Oceans* **114**: C11013, doi:10.1029/2009JC005372.

Zhao, B.R., Ren, G.F., Cao, D.M. and Yang, Y.L. 2001. Characteristics of the ecological environment in upwelling area adjacent to the Changjiang River estuary. *Oceanol. Limnol. Sin.* **32**: 327–333 (in Chinese).

Zhou, F., Xue, H., Huang, D., Xuan, J., Ni, X., Xiu, P. and Hao, Q. 2015. Cross-shelf exchange in the shelf of the East China Sea. *J. Geophys. Res. Oceans* **120**: 1545–1572, doi:10.1002/2014JC010567.

Zhu, J. 2003. Dynamic mechanism of the upwelling on the west side of the submerged river valley off the Changjiang mouth in summertime. *Chinese Sci. Bull*. **48**: 2754–2758 (in Chinese).

Zhu, J., Ding, P. and Hu, D. 2003. Observation of the diluted water and plume front off the Changjiang River estuary during August 2000. *Oceanol. Limnol. Sin.* **34**: 249–255 (in Chinese).

Zhu, J., Chen, C., Ding, P., Li, C. and Lin, H. 2004. Does the Taiwan warm current exist in winter? *Geophys. Res. Lett*. **31**: doi:10.1029/2004GL019997.

Zhu, X.H., Nakamura, H., Dong, M., Nishina, A. and Yamashiro, T. 2017. Tidal currents and Kuroshio transport variations in the Tokara Strait estimated from ferryboat ADCP data. *J. Geophys. Res. Oceans* **122**: 2120–2142, doi:10.1002/2016JC012329.

1.2 Tides and Waves

Dongfeng Xu[1], SungHyun Nam[2] and Hailun He[1]

[1] Second Institute of Oceanography, Ministry of Natural Resources, China
[2] Seoul National University, Korea

1.2.1 Introduction

When we are facing the ocean, the distinct tide exists everywhere. Egbert and Ray (2000) estimated that 1 TW (terawatt), representing 25 to 30% of the total tidal dissipation occurs in the deep ocean, generally near areas of rough topography. This tidal dissipation slows the Earth's rotation (Lambeck, 1975) and causes the moon to retreat from the Earth (Kvale *et al.*, 1999). Besides the total tidal dissipation, Munk and Wunsch (1998) estimated that the wind provides the other 1.2 TW. These two powers maintain the global abyssal density distribution, which prevents the ocean from turning into a stagnant pool of cold salty water (Munk and Wunsch, 1998).

When tides interact with steep topography, internal waves usually can be generated by the interaction of the tidal current with the topography, which is similar to the phenominon of a Lee wave when winds interact with a high mountain. Generation of oceanic internal waves (IWs) at inertial to buoyancy frequencies often include those at tidal periods (hereafter referred as internal tides, ITs) can be an important sink of the energy provided from winds and tides, *i.e.*, sink of barotropic tidal energy or energy conversion from barotropic to baroclinic tides. The East China Sea (ECS) shelf slope is known to be one of the most important generation regions of ITs or surface tidal energy sinks with one of the strongest semidiurnal (M_2) ITs among the world's shelf slopes generated (Baines, 1982; Kuroda and Mitsudera, 1995; Niwa and Hibiya, 2004; Park *et al.*, 2006). In particular, 2nd-mode as well as more typical 1st-mode IT structures have been observed as generated at the shelf break in the central ECS during ebb tide periods (Kuroda and Mitsudera, 1995; Park *et al.*, 2006). Since the speed of barotropic tidal currents are often comparable or higher than the phase speed of the 2nd-mode ITs on the shelf or the northern ECS, ebb tides are optimal for the IT generation. Although the ECS ITs are poorly understood in spite of their importance in redistributing heat, energy, and materials, here we review generation and propagation of ITs in the ECS, based on a few observations and numerical models.

Surface wave studies are important in scientific and engineering communities from three aspects. First, surface waves change the roughness of the sea surface, participate in air–sea exchange, and then play an important role at the atmospheric and oceanic boundary layers (Song, 2009; He and Chen, 2011; Li *et al.*, 2013; He and Song, 2014; Song *et al.*, 2015; He *et al.*, 2018b). Second, the mean state and the extreme value of surface waves supply basic information for coastal and offshore design and also ship route design in the marginal sea (He *et al.*, 2009; Li and He, 2013). Third, the impact of surface waves on geomorphological phenomena are significant, and include coastal shoreline stability and longshore migration of sediment.

1.2.2 External tides

The Yellow Sea and East China Sea (YECS) tides have been extensively studied in recent decades (Fang, 1986), especially under the development of numerical modeling technology and the launch of the TOPEX/Poseidon altimetry satellite (Yanagi *et al*., 1997). Here we review some new progress in the study of the YECS, based on new observations and numerical models.

Egbert and Erofeeva (2002) assimilated TOPEX/Poseidon altimetric data into the generalized inverse (GI) modeling of barotropic ocean tides, which forms the basis for the Oregon State University (OSU) Tidal Inversion Software (OTIS). Here we present the M_2 Co-amplitude (red dash, in cm) and Co-phase lag line charts of the M_2 constituent (Fig. 1.2.1a). This result is similar to that of Fang (1986) which was inferred from observation and calculation (Fig. 1.2.1b). The M_2 semi-diurnal tidal ellipse (Fig. 1.2.2) is similar to that derived from observation (Chen, 1992). The new ocean color satellite sensor, Geostationary Ocean Color Imager (GOCI), can provide more tidal information on the YECS. Hu *et al*. (2016) used the GOCI data to derive surface M_2 tidal currents, which are validated with a comprehensive set of 28 surface drifters and four mooring observations (Fig. 1.2.3).

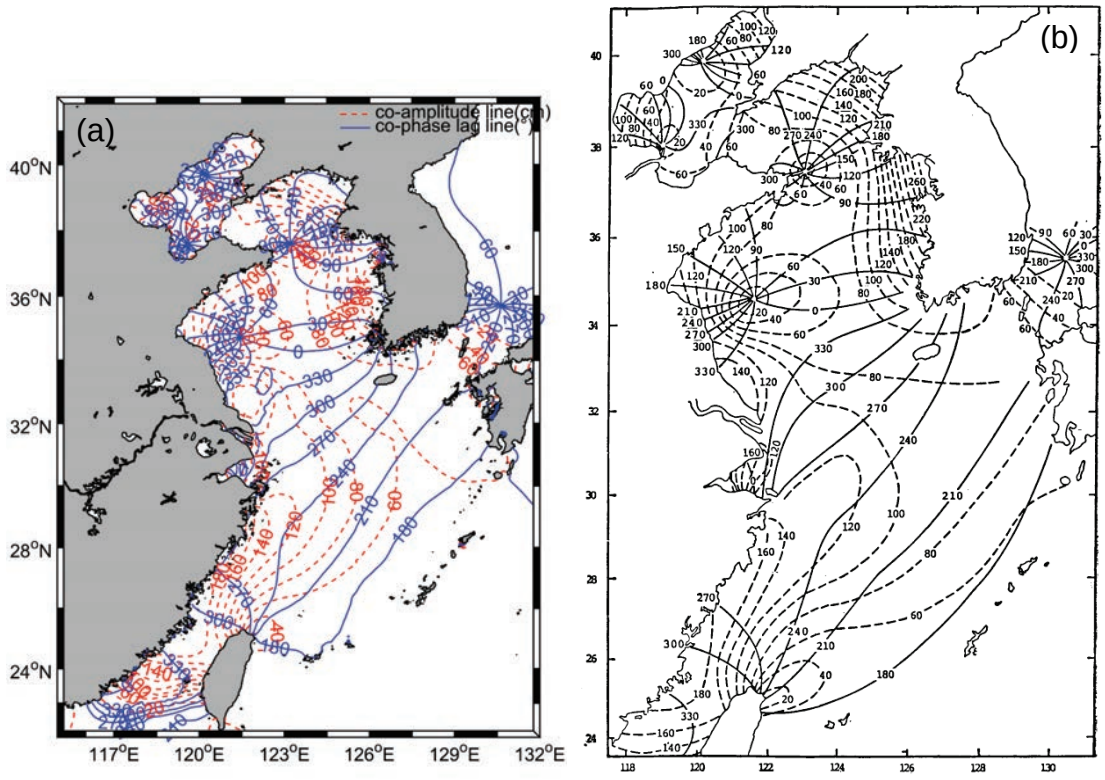

Fig. 1.2.1 (a) Co-amplitude (red dash, in cm) and Co-phase lag line (blue solid, in degrees referred to 120°E) charts of M_2 constituent for the YECS derived from the TPXO-8 of Oregon State University (OSU) high-resolution regional tidal model with a 1/30 degree resolution. (b) Distribution of M_2 tidal amplitude H (in cm) and phase lag g (in degrees and referred to 120°E) in the YECS. From Fang (1986).

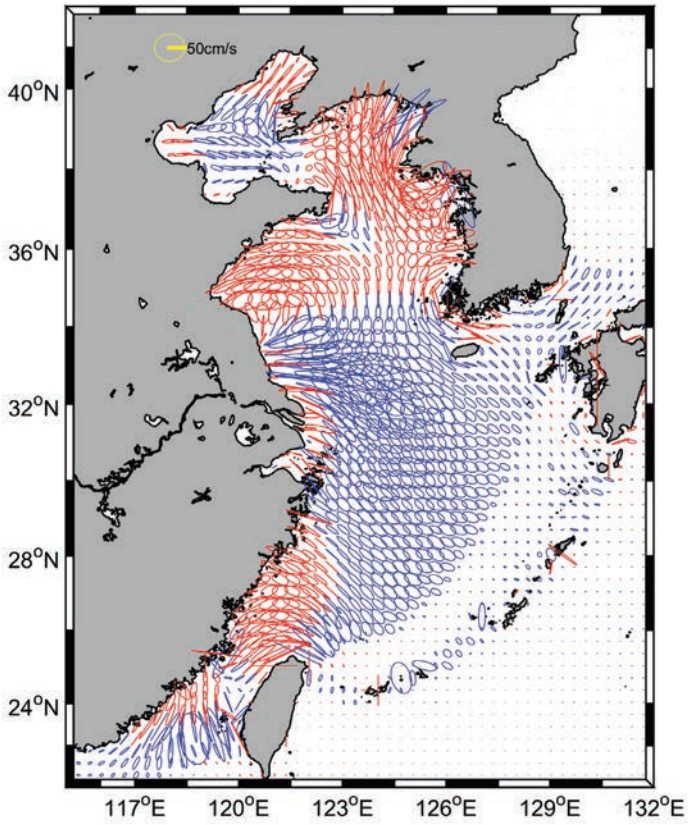

Fig. 1.2.2 M_2 semi-diurnal tidal ellipses for the YECS derived from the TPXO-8 of Oregon State University (OSU) high-resolution regional tidal model with a 1/30 degree resolution (red : anti-clockwise, blue: clockwise).

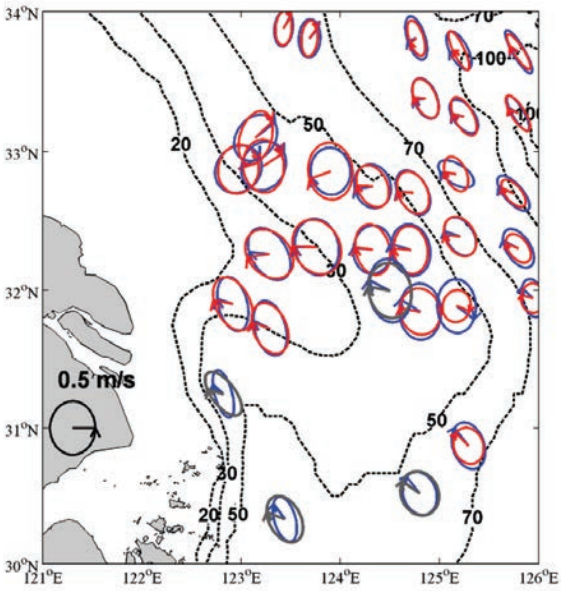

Fig. 1.2.3 Comparison of M_2 semidiurnal tidal ellipses between satellite (blue) and *in situ* observations from four moorings (gray) and 28 drifter locations (red). Arrows denote the tidal phase relative to GMT. From Hu *et al*. (2016). Reproduced with permission of Wiley & Sons.

The tide plays a significant role in mixing in the YECS area. With the help of a three-dimensional numerical model, the patch-like structure of low-salinity water detached from the Chanjiang diluted water (CDW) is demonstrated to be related with intense tide-induced vertical mixing during the spring tide (Moon *et al*., 2010). Yang *et al*. (2017) studied the tidal straining within two different stations which have different stratification environments in the ECS through field observation. Their results showed that the tidal straining induces a semi-diurnal switching between stable and unstable stratification at both stations. Near-bottom high-frequency velocity measurements further reveal that the dissipation rate of turbulent kinetic energy (TKE) is highly elevated during periods when unstable stratification occurs.

1.2.3 Surface waves

Measurement of surface waves comes from multiple platforms which include buoy, radar and satellite. Among them, wave buoy is the most reliable measurement platform. However, the number of wave buoys is very rare in the YECS (Ebuchi and Kawamura, 1994). Radar retrieving supplies fine grid resolution but limited spatial coverage (Chen *et al*., 2017; Shao *et al*., 2017). Then, satellite (TOPEX/Poseidon) data show significant wave heights (Ebuchi and Kawamura, 1994; Chen *et al*., 2004), but the cross-track resolutions are too coarse to match the demand for a marginal sea (Fig. 1.2.4). Therefore, due to the insufficiency of observations, numerical models are widely used in regional surface wave studies (Chen *et al*., 2013; He and Xu, 2016; He *et al*., 2018a). Benefiting from suitable parameterization of physical terms (or source terms; The Wamdi Group, 1988; Tolman *et al*., 2002), state-of-the-art wave models (third-generation wave models) have relatively good performance for regional scale (Cui *et al*., 2012; Chen *et al*., 2013; Xu *et al*., 2017). Furthermore, wave models assimilate satellite wave height and provide further reanalysis data for surface waves (Dee *et al*., 2011; Wang *et al*., 2016).

Recently, the results of long-term (1988 to 2002) simulations of surface waves in the northern Pacific, using a third-generation wave model, supplied several maps of surface waves in the YECS (He and Xu, 2016; He *et al*., 2018a). As far as a buoy station is concerned, the comparison validates the model results, where the relative errors of wave height keep below 11%, and relative errors of wave period are better than –22%. Similarly, when we compare satellite and model data, the high correlation reveals the consistency between the two datasets on monthly mean significant wave heights (H_s) (Fig. 1.2.4; He *et al*., 2018a).

The climatological results emphasize the seasonal variations of surface waves (Fig. 1.2.5). In winter and autumn, H_s in the ECS is generally greater than 1.5 m, and can reach more than 2.0 m on the east side of Taiwan Island and in the northwestern Pacific while in spring and summer, H_s is really weak and less than 1.5 m. The seasonal variances of H_s are closely related to the monsoon. In winter, the generation of high waves in the southeast of the ECS is not only the result of powerful winds from the north but also due to the large fetch length (fetch length is defined as the effect forcing distance between a local area with the coast along the direction of wind forcing). In summer, H_s is relative weak due to the low wind speed. On the other hand, the dependence of H_s on fetch of wind forcing also reveals the influence of topography, where the H_s pattern is similar to the bathymetry. As for mean wave period (T_m), it also decreases from southeast to northwest and from open ocean to the coastal area. There are some seasonal variations on T_m, in which T_m in autumn is longer than in other seasons (He and Xu, 2016; He *et al*., 2018a).

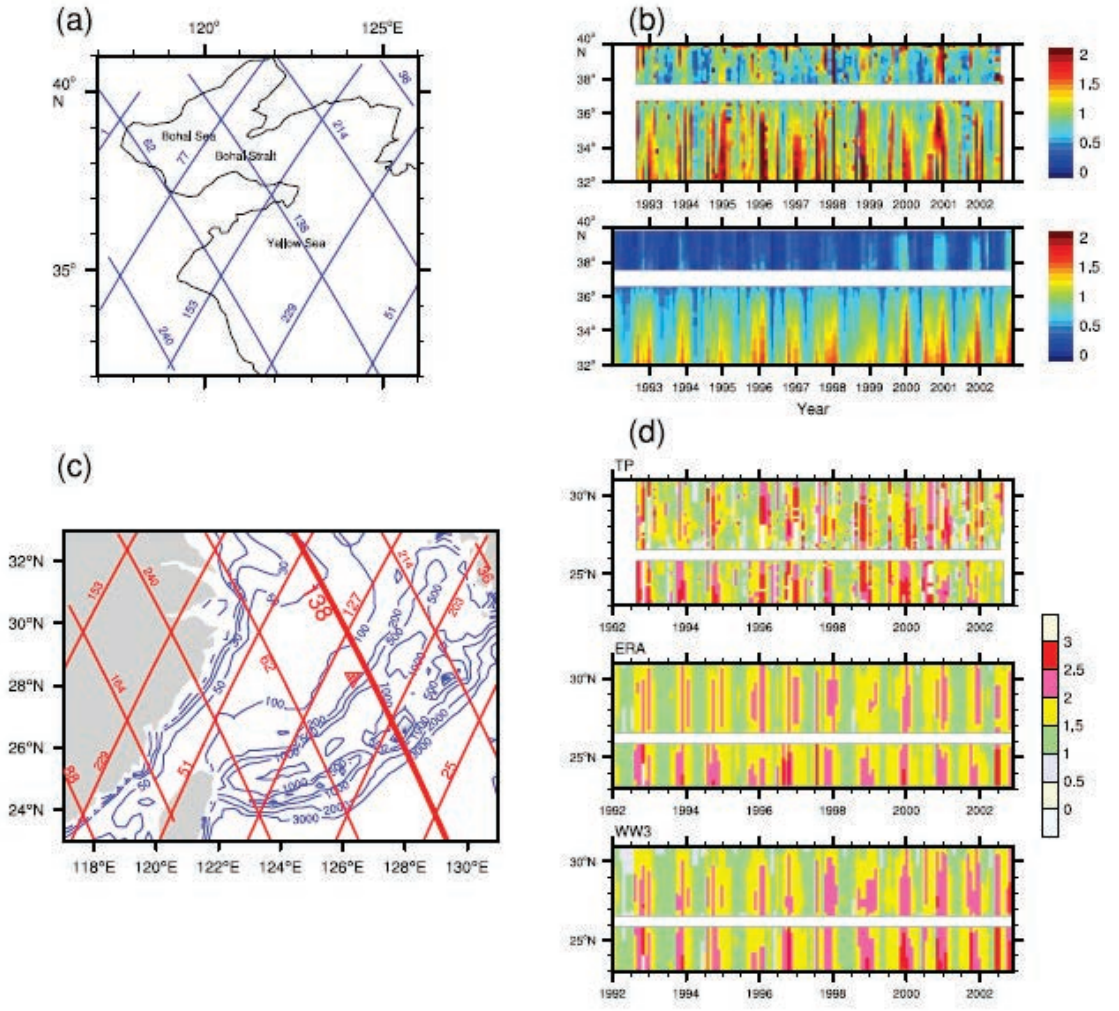

Fig. 1.2.4 (a) Satellite passes of TOPEX/Poseidon altimeter (TP) and (b) time–latitude Hovmöller plot of monthly mean significant wave height along pass 138 of TP in the Yellow Sea. (c–d) are the same with (a–b), but for the East China Sea. In (c), bathymetry contours (units: m, blue), and the buoy location of the Japan Meteorology Agency (B22001, inverted red triangle) are also presented. In (d), data sources include TP, ERA-Interim reanalysis (ERA) and wave modeling (WW3). (a–b) are from He and Xu (2016), and (c–d) are from He *et al*. (2018a). Reproduced with permission of Springer Nature.

Extreme value like N-year return H_s is an important index in ocean engineering. In the YECS, satellite and modeling underestimate the yearly maximum H_s, and therefore, the N-year return H_s. For instance, at a buoy station, the 10-year return H_s from buoy, satellite and WW3 are 13.49, 8.56 and 7.95 m, respectively (He *et al*., 2018a). In essence, we uncover the patterns of extreme H_s (Fig. 1.2.6), where the extreme value near the Northwest Pacific is generally larger than that in the inner part of the ECS, and there is an obvious peak around west of Ryukyu Island. The peak is as high as 10 m, with an area covering 3.0 zonal degrees and 2.0 meridional degrees. The peak is closely related to the wind forcing; nonetheless, extreme values of wind forcing have more complex patterns than the H_s field (He *et al*., 2018a). As for Yellow Sea (YS), there are two weak peak extreme H_s in southeast of the YS (near 126.0°E, 32.0°N) and central Bohai Sea, which are also explainable by the extreme wind forcing (He and Xu, 2016).

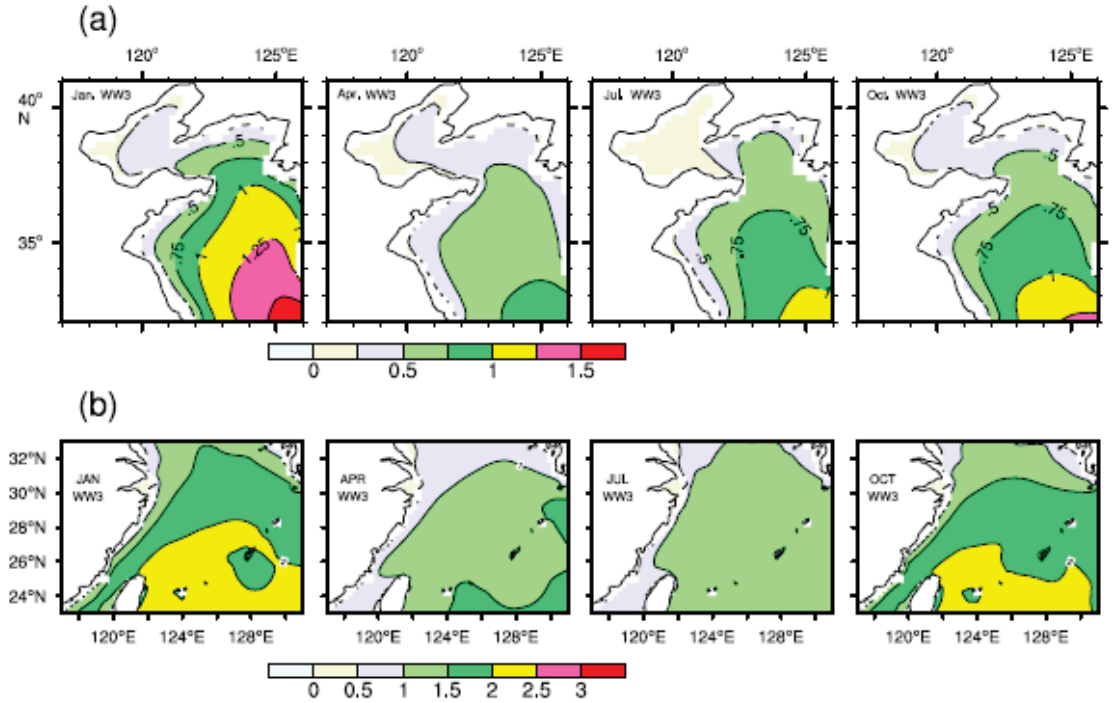

Fig. 1.2.5 Climatological monthly mean significant wave heights (units: m) from WW3 modeling in (a) Yellow Sea and (b) East China Sea. (a) is from He and Xu (2016), and (b) from He *et al*. (2018a). Reproduced with permission of Springer Nature.

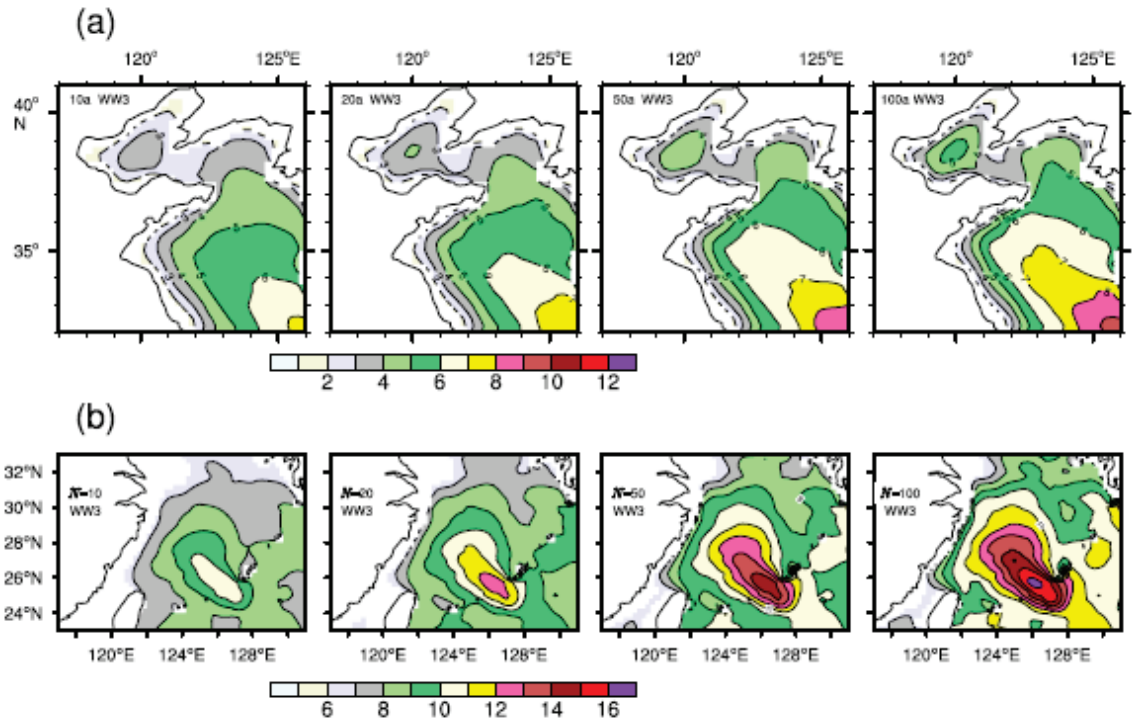

Fig. 1.2.6 N-year return significant wave heights (units: m) from WW3 modeling in (a) Yellow Sea and (b) East China Sea. (a) is from He and Xu (2016), and (b) from He *et al*. (2018a). Reproduced with permission of Springer Nature.

1.2.4 Internal tides

Distribution and energetics of the 1st-mode semidiurnal (M_2) internal tides (IT) around the shelf edge in the YECS were investigated using a three-dimensional numerical model (Niwa and Hibiya 2004; Liu *et al.*, 2019). In spite of only few *in-situ* or satellite remote sensing observations in a limited space and time, the observational results along with few modeling works suggest 1) multiple sources and local generations of ITs with complex topographic features, 2) multi- directional propagations of ITs with a wavelength of 15 to 40 km and an amplitude of *O*(10 m), and dominant mode-1 ITs with potential significance of mode-2 ITs. One of the modeling results demonstrates the effective generation of M_2 ITs over topographic features such as the subsurface ridges in the Luzon and Tokara straits, the ridges along the Ryuku Island chain, and shelf slope in the YECS (Fig. 1.2.7) where the M_2 barotropic tides are strong and bottom slopes are steep enough to form conditions favorable for IW generation. The M_2 ITs propagating away from these multiple source regions interfere to form a complicated pattern which agrees well with the satellite altimeter observations (Liu *et al.*, 2019). Niwa and Hibiya (2004) estimated roughly 10% of the energy conversion from the M_2 barotropic to baroclinic tides with a conversion rate of 35 GW although about half of the M_2 IT energy is subject to local dissipation in close proximity to the generation sites.

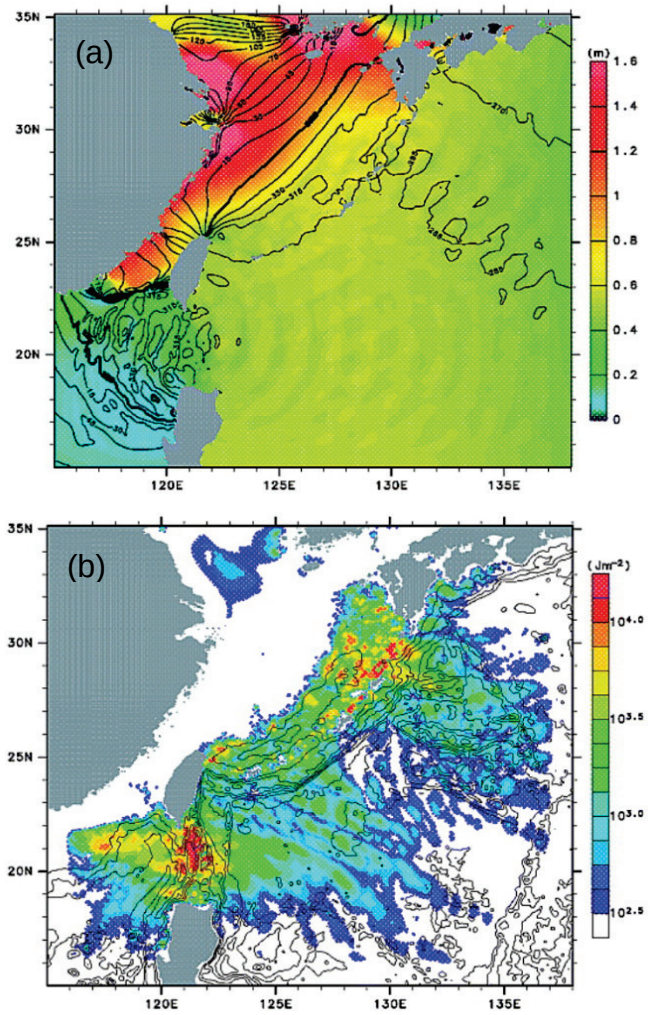

Fig. 1.2.7 (a) Amplitude (color, in cm) and phase (contour, in degrees) of the calculated surface elevation of the M_2 surface tide. (b) Model-predicted distribution of the depth-integrated kinetic energy of the M_2 internal tide (IT) averaged over the final 2 days of the calculation (Niwa and Hibiya, 2004). Reproduced with permission of Wiley & Sons.

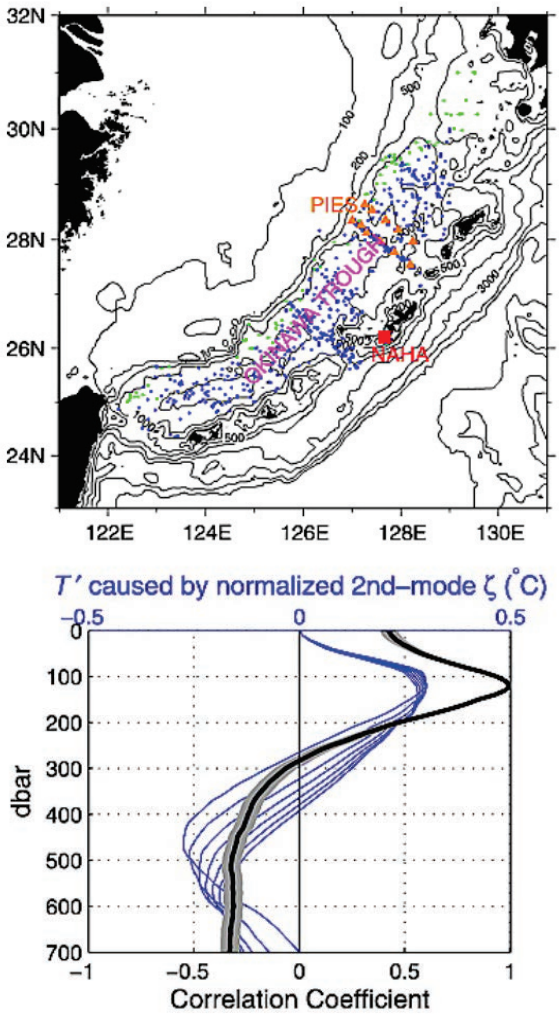

Fig. 1.2.8 (Top) Locations of instrument. NAHA coastal tide gauge (red square) and historical hydrocasts where acoustic travel time to 700 m is shorter than (blue dots) and longer than (green dots) 0.924 s. Bathymetry is in meters. (Bottom) Correlation coefficients between the instrument-derived water temperature at 120 m and those at other pressure levels with acoustic travel time to 700 m shorter than 0.924 s in the ECS (Park *et al*., 2006). Reproduced with permission of Wiley & Sons.

Structures of various (particularly 2nd-mode) ITs in the YECS have been confirmed from observations using an underwater sliding vehicle (Kuroda and Mitsudera, 1995) and an array of pressure-sensor-equipped inverted echo sounders (Park *et al*., 2006). Kuroda and Mitsudera (1995) presented and classified a variety of detailed structures of the lowest two modes of ITs with internal Froude numbers as a ratio between the speed of barotropic tidal current and the IW phase speed. In contrast to the dominance of 1st-mode ITs in the southern ECS, 2nd-mode ITs are most strongly generated at the shelf break in the central YECS and propagate onto the shelf in the north (Kuroda and Mitsudera, 1995). Park *et al*. (2006) also confirmed strong generation of 2nd-mode ITs in the Okinawa Trough region of the YECS from 2-year-long time series measurements during 2002–2004 and historical hydrocasts observations (Fig. 1.2.8), contrasting with no significant 2nd-mode ITs (1st-mode IT dominance) southeast of the Ryuku Islands. Vertical profiles of the correlation between the instrument-derived water temperature at 120 m and those at other pressure levels with acoustic travel time to 700 m shorter than 0.924 s in the Okinawa Trough region reflect the significance of 2nd-mode ITs (Fig. 1.2.8) contrasting with those in the southeast of the Ryuku Islands.

1.2.5 Nonlinear internal waves

The ITs at M_2 and other frequencies, and presumably near-inertial waves, in the YECS subsequently accompany shorter internal waves (IWs) at frequencies close to the buoyancy frequency as in other seas. They are also known as nonlinear IWs (NLIWs) or internal solitary waves due to their nonlinearity of different degrees, and have often been understood in the context of the Korteweg deVries (KdV) type models since Benjamin (1966), such as extended KdV or eKdV (*e.g.*, see Cho *et al.*, 2016 and references cited therein). NLIWs have been observed ubiquitously in stratified oceans of shelves and marginal seas though their characteristics and underlying dynamics still remain unclear in many regions, including the ECS, due to the lack of observations at required resolutions (in space and time) under a variety of background conditions. The NLIWs in the ECS are considered complex in perspectives of multiple (unknown) source regions for generation (Hsu *et al.*, 2000), multiple directions of propagation from multiple sources and consequent significance of their (wave-wave) interactions (Hsu *et al.*, 2000), relatively small amplitude of $O(10)$ m and slow propagation speed of $O(10^{-1}$ m s$^{-1})$, and multi-layered stratification implying a significant role of high-order-mode IWs (Liu *et al.*, 2009). These have been reported from only a few studies and fewer observations from *in-situ* field experiments and satellite imagery such as synthetic aperture radar (SAR).

The NLIWs were observed in the northwestern ECS (blue ellipse labeled (i) in Fig. 1.2.9 Top (a)) in 1996 August and 1997 July (Hsu *et al.*, 2000), and more recently southwestern ECS in 2007 August ((iv) in Fig. 1.2.9 Top (a), Li *et al.*, 2008) and northern ECS in August 2005, August 1998, and August 2008 ((ii), (iii), and (v) in Fig. 1.2.9 Top (a), Lee *et al.*, 2006; Teixeira *et al.*, 2006; Smith, 2010; Lozovatsky *et al.*, 2015). The amplitude, propagating speed, and characteristic width characterized from the observations range from 2 to 15 m, from 0.6 to 1.1 m s^{-1}, and from $O(10)$ m to $O(10^2$ m), respectively. The propagating speed and characteristic width of 1st-mode NLIWs are consistent with those predicted by the two-layered eKdV model for given amplitude and stratification where the latter varies in space (K1, K2, and K3 in Fig. 1.2.9), season (Fig. 1.2.9), and year (Cho *et al.*, 2016). Most recently, using satellite SAR images acquired in and around a shallow

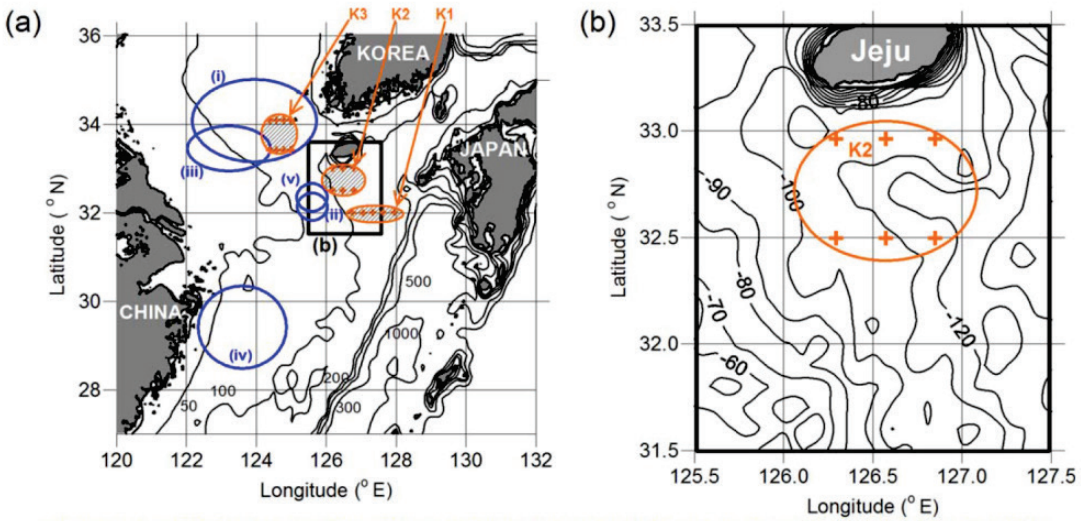

(i) Hsu et al. (2000), (ii) Lee et al. (2006), (iii) Teixeira et al, (2006), (iv) Li et al. (2008), (v) TAVEX (2008)/Smith (2010)

Fig. 1.2.9 (a) Five areas where internal wave (IW) observations were reported previously (blue circles, (i) to (v)) and three areas where historical hydrographic data were analyzed for characterizing 1st-mode nonlinear IWs (orange circles, K1 to K3). Depth contours are in meters. (b) Close-up of the K2 region around southern Jeju Island, Korea, corresponding to the black framed area in (a). The historical hydrographic data were collected from stations marked with orange crosses in the hatched areas.

sill named 'IEODO' in the ECS, along with *in-situ* observations and numerical models, various forms (spiral, wedge, and arc-like curvature patterns, Fig. 1.2.10) of NLIW fronts were presented, which are locally generated with wave energy radiating from the sill with a significant time lag dependent on background conditions (Nam *et al*., 2018).

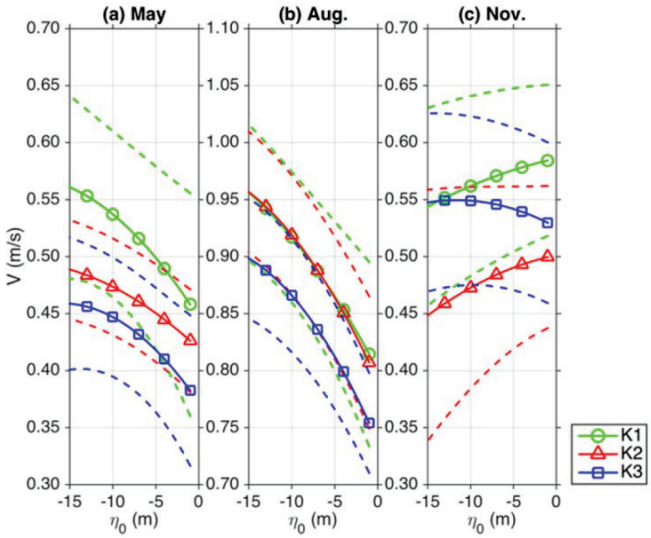

Fig. 1.2.9 Continued. Propagating speed for three areas (K1: green circles, K2: red triangles, and K3: blue boxes) as a function of the IW amplitude (η_0) based on the eKdV model: (a) May, (b) August, and (c) November. Symbols are sampled at 3 m intervals in amplitude starting from 1 m, and each pair of dashed curves represents a range of one standard deviation. All plots are from Cho *et al*. (2016). Reproduced with permission of Creative Commons.

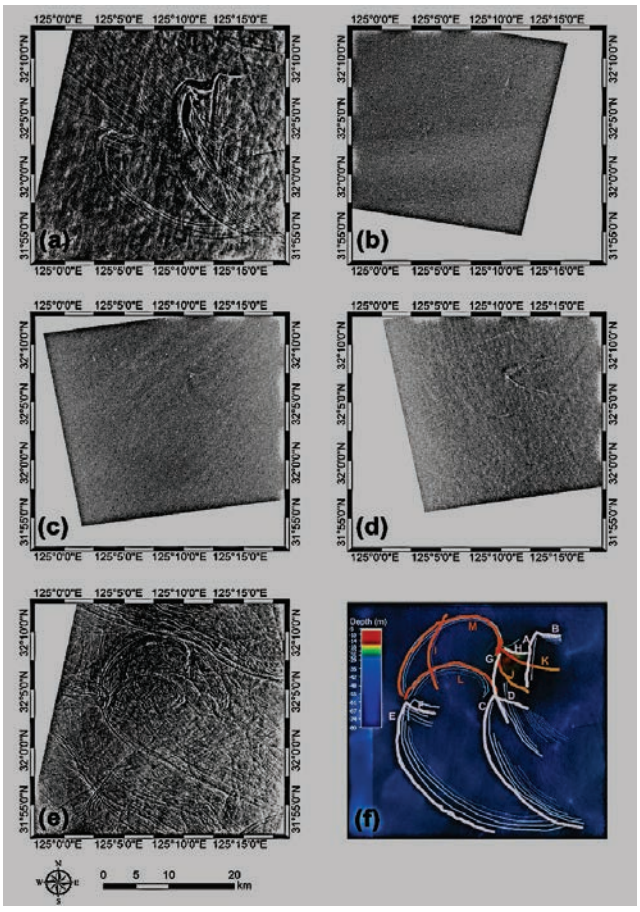

Fig. 1.2.10 Synthetic aperture radar (SAR) images in the vicinity of a small topographic sill known as IEODO in the northern ECS. The images taken on (a) 21:45:30 UTC September 10, 2014, (b) 09:43:54 UTC May 28, 2015, (c) 21:38:07 UTC June 3, 2015, (d) 21:31:17 UTC June 5, 2015, (e) 21:45:31 UTC June 12, 2015, and (f) bottom topography around the sill (color scale in the top-left), superimposed with a surface manifestation of IW fronts where the increased sea surface roughness is found in association with convergences of near-surface currents induced by IWs (from 'A' to 'H' in 2014; pink, from 'I' and 'M' in 2015; orange). All plots are from Nam *et al*. (2018). Reproduced with permission of Creative Commons.

The NLIWs play a significant role in transporting and redistributing heat, mass, energy, and materials, and they have been known to be important to the understanding of underwater acoustics (Williams *et al.*, 2001), submarine navigation and offshore engineering (Osborne *et al.*, 1978), marine biogeochemistry (Bogucki *et al.*, 1997; Lucas *et al.*, 2011), and the Earth's climate (Alford, 2003; Ferrari and Wunsch, 2009; Melet *et al.*, 2013). In spite of a few works on the NLIWs in the ECS, our understanding of generation, propagation, evolution, and dissipation of NLIWs remains in a primitive state. Increasing the number of *in-situ* and satellite observations at a better resolution in space and time will surely improve our understanding on these important processes in the ECS.

1.2.6 Future work

With the developing economy, human activities such as oceanic engineering and deep sea mining are growing fast, especially in high seas. Tides and waves exist everywhere in the ocean although the later presents mainly in the ocean surface layer. We need to study the role of tides and waves in broader aspects, such as the mixing role of tides and internal tides in the pelagic ocean and the mixing and resuspension role of tides in food-supply in the growing and breeding period of marine life. The need to study the destructive force of the internal waves on marine infrastructures and in oceanic engineering is also growing. Both nonlinear theory study (especially for internal waves) and *in-situ* observations are needed for future investigation of tides and internal tides.

For multi-scale surface wave study, we need to deploy more surface buoys, and obtain long-term time series. The surface model, where the sources terms need to be further improved into a near-perfect stage, is still under development. We should also pay attention to the data quality of boundary conditions, where the data quality of wind forcing is not as good as operational demands for extreme events like tropical cyclones. The model output of surface waves in the YECS calls for further validation, and the studies of surface waves in the YECS still leaves large room for future improvement.

1.2.7 References

Alford, M.H. 2003. Redistribution of energy available for ocean mixing by long-range propagation of internal waves. *Nature* **423**: 159–162, doi:10.1038/nature01628.

Baines, P.G. 1982. On internal tide generation models. *Deep Sea Res*. **29**: 307–338, doi:10.1016/0198-0149(82)90098-X.

Benjamin, T.B. 1966. Internal waves of finite amplitude and permanent form. *J. Fluid Mech*. **25**: 241–270, doi:10.1017/S0022112066001630.

Bogucki, D., Dickey, T. and Redekopp, L. 1997. Sediment resuspension and mixing by resonantly generated internal solitary waves. *J. Phys. Oceanogr*. **27**: 1181–1196, doi:10.1175/1520-0485(1997)027<1181:SRAMBR>2.0.CO;2.

Chen, G. 1992. Marine Atlas of Bohai Sea, Yellow Sea and East China Sea. Hydrology. China Ocean Press, Beijing.

Chen, G., Bi, S.W. and Ezraty, R. 2004. Global structure of extreme wind and wave climate derived from TOPEX altimeter data. *Int. J. Remote Sensing* **25**: 1005–1018, doi:10.1080/01431160310001598980.

Chen, Y.P., Xie, D.M., Zhang, C.K. and Qian, X.S. 2013. Estimation of long-term wave statistics in the East China Sea. *J. Coast. Res*. **65**: 177–182, doi:10.2112/SI65-031.1.

Chen, Z.B., He, Y.J. and Zhang, B. 2017. An automatic algorithm to retrieve wave height from X-band marine radar image sequences. *IEEE Trans. Geosci. Remote Sensing* **55**: 5084–5092.

Cho, C., Nam, S. and Song, H. 2016. Seasonal variation of speed and width from kinematic parameters of mode-1 nonlinear internal waves in the northeastern East China Sea. *J. Geophys. Res. Oceans* **121**: 5942–5958, doi:10.1002/2016JC012035.

Cui, H., He, H.L., Liu, X.H. and Li, Y. 2012. Effect of oceanic current on the typhoon-wave modeling in the East China Sea. *Chin. Phys. B* **21**: 109201, doi:10.1088/1674-1056/21/10/109201.

Dee, D.P., Uppala, S.M., Simmons, A.J., Berrisford, P., Poli, P., Kobayashi, S., Andrae, U., Balmaseda, M.A., Balsamo, G., Bauer, P., Bechtold, P., Beljaars, A.C.M., van de Berg, L., Bidlot, J., Bormann, N., Delsol, C., Dragani, R., Fuentes, M., Geer, A.J., Haimberger, L., Healy, S.B., Hersbach, H., Hólm, E.V., Isaksen, L., Kållberg, P., Köhler, M., Matricardi, M., McNally, A.P., Monge-Sanz, B.M., Morcrette, J.-J., Park, B.-K., Peubey, C., de Rosnay, P., Tavolato, C., Thépaut, J.-N. and Vitart, F. 2011. The ERA-Interim reanalysis: configuration and performance of the data assimilation system. *Quart. J. Roy. Meteorol. Soc*. **137**: 553–597, doi:10.1002/qj.828.

Ebuchi, N. and Kawamura, H. 1994. Validation of wind speeds and significant wave heights observed by the TOPEX altimeter around Japan. *J. Oceanogr*. **50**: 479–487, doi:10.1007/BF02234969.

Egbert, G.D. and Erofeeva, S.Y. 2002. Efficient inverse modeling of barotropic ocean tides. *J. Atmos. Ocean. Technol*. **19**: 183–204, doi:10.1175/1520-0426(2002)019<0183:EIMOBO>2.0.CO;2.

Egbert, G.D. and Ray, R.D. 2000. Significant dissipation of tidal energy in the deep ocean inferred from satellite altimeter data. *Nature* **405**: 775–778, doi:10.1038/35015531.

Fang, G. 1986. Tide and tidal current charts for the marginal seas adjacent to China. *Chinese J. Oceanol. Limnol*. **4**: 1–16, doi:10.1007/BF02850393.

Ferrari, R. and Wunsch, C. 2009. Ocean circulation kinetic energy: reservoirs, sources, and sinks. *Annu. Rev. Fluid Mech*. **41**: 253–282, doi:10.1146/annurev.fluid.40.111406.102139.

He, H.L. and Chen, D. 2011. Effects of surface wave breaking on the oceanic boundary layer. *Geophys. Res. Lett*. **38**: L07604, doi:10.1029/2011GL046665.

He, H.L. and Song, J.B. 2014. Determining the onset and strength of unforced wave breaking in a numerical wave tank. *Chin. Ocean Eng*. **28**: 501–509, doi:10.1007/s13344-014-0041-4.

He, H.L. and Xu, Y. 2016. Wind-wave hindcast in the Yellow Sea and the Bohai Sea from the year 1988 to 2002. *Acta Oceanol. Sin*. **35**: 46–53, doi:10.1007/s13131-015-0786-5.

He, H.L., Song, J.B., Lynett, P.J. and Li, S. 2009. Numerical study of energy loss due to wave breaking in the nearshore. *Chin. J. Oceanol. Limnol*. **27**: 621–629.

He, H.L., Song, J.B., Bai, Y.F., Xu, Y., Wang, J.J. and Bi, F. 2018a. Climate and extrema of ocean waves in the East China Sea. *Sci. China Series D: Earth Sci*. **61**: 980–994, doi:10.1007/s11430-017-9156-7.

He, H.L., Wu, Q.Y., Chen, D.K., Sun, J., Liang, C.J., Jin, W.F. and Xu, Y. 2018b. Effects of surface waves and sea spray on the air-sea fluxes during the passage of Typhoon Hagupit. *Acta Oceanol. Sin*. **37**: 1–7, doi:10.1007/s13131-018-1208-2.

Hsu, M.K., Liu, A.K. and Liu, C. 2000. A study of internal waves in the China Seas and Yellow Sea using SAR. *Cont. Shelf Res*. **20**: 389–410, doi:10.1016/S0278-4343(99)00078-3.

Hu, Z., Wang, D.P., Pan, D., He, X., Miyazawa, Y., Bai, Y., Wang, D. and Gong, F. 2016. Mapping surface tidal currents and Changjiang plume in the East China sea from geostationary ocean color imager. *J. Geophys. Res. Oceans* **121**: 1563–1572, doi:10.1002/2015JC011469.

Kuroda, Y. and Mitsudera, H. 1995. Observation of internal tides in the East China Sea with an underwater sliding vehicle. *J. Geophys. Res*. **100**: 10,801–10,816, doi:10.1029/95JC00473.

Kvale, E.P., Johnson, H.W., Sonett, C.P., Archer, A.W. and Zawistoski, A. 1999. Calculating lunar retreat rates using tidal rhythmites. *J. Sediment. Res*. **69**: 1154–1168, doi:10.2110/jsr.69.1154.

Lambeck, K. 1975. Effects of tidal dissipation in the oceans on the Moon's orbit and the Earth's rotation. *J. Geophys. Res*. **80**: 2917–2925, doi:10.1029/JB080i020p02917.

Lee, J.H., Lozovatsky, I., Jang, S.-T., Jang, C.J., Hong, C.S. and Fernando, H.J.S. 2006. Episodes of nonlinear internal waves in the northern East China Sea. *Geophys. Res. Lett*. **33**: L18601, doi: 10.1029/2006GL027136.

Li, S. and He, H.L. 2013. Simulating regular wave propagation over a submerged bar by boundary element method model and Boussinesq equation model. *Chin. Phys. B* **22**: 024701, doi:10.1088/1674-1056/22/2/024701.

Li, S., Li, M., Gerbi., G.P. and Song, J.B. 2013. Roles of breaking waves and Langmuir circulation in the surface boundary layer of a coastal ocean. *J. Geophys. Res. Oceans* **118**: 5173–5187, doi:10.1002/jgrc.20387.

Li, X., Zhao, Z., Han, Z. and Xu, L. 2008. Internal solitary waves in the East China Sea. *Acta Oceanol. Sin*. **27**: 51–59.

Liu, K., Sun, J., Guo, C., Yang, Y., Yu, W. and Wei, Z. 2019. Seasonal and spatial variations of the M_2 internal tide in the Yellow Sea. *J. Geophys. Res. Oceans* **124**: 1–24, doi:10.1029/2018JC014819.

Liu, Z., Wei, H., Lozovatsky, I.D. and Fernando, H.J. 2009. Late summer stratification, internal waves, and turbulence in the Yellow Sea. *J. Mar. Syst*. **77**: 459–472, doi:10.1016/j.jmarsys.2008.11.001.

Lozovatsky, I., Jinadasa, P., Lee, J.H. and Fernando, H.J. 2015. Internal waves in a summer pycnocline of the East China Sea. *Ocean Dyn*. **65**: 1051–1061, doi:10.1007/s10236-015-0858-2.

Lucas, A.J., Franks, P.J.S. and Dupont, C.L. 2011. Horizontal internal-tide fluxes support elevated phytoplankton productivity over the inner continental shelf. *Limnol. Oceanogr*. **1**: 56–74, doi: 10.1215/21573698-1258185.

Melet, A., Hallberg, R., Legg, S. and Polzin, K. 2013. Sensitivity of the ocean state to the vertical distribution of internal-tide-driven mixing. *J. Phys. Oceanogr*. **43**: 602–615, doi:10.1175/JPO-D-12-055.1.

Munk, W. and Wunsch, C. 1998. Abyssal recipes II: Energetics of tidal and wind mixing. *Deep Sea Res*. **45**: 1977–2010, doi:10.1016/S0967-0637(98)00070-3.

Nam, S., Kim, D.-J., Lee, S.-W., Kim, B.-K., Kang, K.-M. and Cho, Y.-K. 2018. Nonlinear internal wave spirals in the northern East China Sea. *Sci. Rep*. **8**: 3473, doi:10.1038/s41598-018-21461-3.

Niwa, Y. and Hibiya, T. 2004. Three-dimensional numerical simulation of M2 internal tides in the East China Sea. *J. Geophys. Res. Oceans* **109**: C04027, doi:10.1029/2003JC001923.

Osborne, A.R., Burch, T.L. and Scarlet, R.I. 1978. The influence of internal waves on deep-water drilling. *J. Petrol. Technol*. **30**: 1497–1504, doi:10.2118/6913-PA.

Park, J.-H., Andres, M., Martin, P.J., Wimbush, M. and Watts, D.R. 2006. Second-mode internal tides in the East China Sea deduced from historical hydrocasts and a model. *Geophys. Res. Lett*. **33**: L05602, doi:10.1029/2005GL024732.

Shao, W., Li, X., Hwang, P., Zhang, B. and Yang, X. 2017. Bridging the gap between cyclone wind and wave by C-band SAR measurements. J. *Geophys. Res. Oceans* **122**: 6714–6724, doi:10.1002/2017JC012908.

Smith, C.M. 2010. Effects of propagating internal waves on shallow-water acoustic propagation during the Transverse Acoustic Variability EXperiment of 2008. MSc thesis. Pennsylvania State University, 191 pp.

Song, J.B. 2009. The effects of random surface waves on the steady Ekman current solutions. *Deep Sea Res*. **56**: 659–671, doi:10.1016/j.dsr.2008.12.014.

Song, J.B., Fan, W., Li, S. and Zhou, M. 2015. Impact of surface waves on the steady near-surface wind profiles over the ocean. *Bound. Layer Meteorol*. **155**: 111–127, doi:10.1007/s10546-014-9983-6.

Teixeira, M., Warn-Varnas, A. and Apel, J. 2006. Analytical and observational studies of internal solitary waves in the Yellow Sea. *J. Coast. Res*. **22**: 1403–1416, doi:10.2112/04-0339.1.

Tolman, H.L., Balasubramaniyan, B., Burroughs, L.D., Chalikov, D.V., Chao, Y.Y., Chen, H.S. and Gerald, V.M. 2002. Development and implementation of wind generated ocean surface wave models at NCEP. *Wea. Forecast*. **17**: 311–333, doi:10.1175/1520-0434(2002)017<0311:DAIOWG>2.0.CO;2.

The Wamdi Group. 1988. The WAM model-a third generation ocean wave prediction model. *J. Phys. Oceanogr*. **18**: 1775–1810, doi:10.1175/1520-0485(1988)018<1775:TWMTGO>2.0.CO;2.

Wang, J., Dong, C.M. and He, Y.J. 2016. Wave climatological analysis in the East China Sea. *Cont. Shelf Res*. **120**: 26–40, doi:10.1016/j.csr.2016.03.010.

Williams, K.L., Henyey, F.S., Rouseff, D., Reynolds, S.A. and Ewart, T. 2001. Internal wave effects on high-frequency acoustic propagation to horizontal arrays - experiment and implications to imaging. *IEEE J. Oceanic Eng*. **26**: 102–112, doi:10.1109/48.917939.

Xu, Y., He, H.L., Song, J.B., Hou, Y.J. and Li, F.N. 2017. Observations and modelling of typhoon waves in the South China Sea. *J. Phys. Oceanogr*. **47**: 1307–1324, doi:10.1175/JPO-D-16-0174.1.

Yanagi, T., Morimoto, A. and Ichikawa, K. 1997. Co-tidal and co-range charts for the East China Sea and the Yellow Sea derived from satellite altimetric data. *J. Oceanogr*. **53**: 303–310.

Yang, W., Wei, H. and Zhao, L. 2017. Observations of tidal straining within two different ocean environments in the East China Sea: Stratification and near-bottom turbulence. *J. Geophys. Res. Oceans* **122**: 8876–8893, doi:10.1002/2017JC012924.

1.3 Water Masses

Fei Yu

Institute of Oceanology, Chinese Academy of Sciences, China

1.3.1 Introduction

The East China Sea (ECS) and Yellow Sea (YS) are located east of China on a broad continental shelf, which is one of the widest shelves in the world ocean, and is influenced by the East Asian monsoon system, with a strong northeast wind in winter and a weak southwest wind in summer. Because of the influence of the East Asian Monsoon, the climate of the ECS and YS shows typical seasonal characteristics. In winter, the climate of the YS is affected by the Siberian High pressure system such that a north and northwest wind prevails with an average wind speed between 6 and 10 m s^{-1}. Seasonal changes in solar radiation and other climatic/meteorological factors are responsible for the large seasonal variability of the ECS and YS hydrography. The major currents in the ECS and YS are the Kuroshio, which is the western boundary current of the North Pacific subtropical gyre, the Taiwan Strait Current (TSC) which transports the South China Sea (SCS) water through the Taiwan Strait (TS), the Tsushima Warm Current in the outer continental shelf with depths over 100 m, a branch of the Tsushima Warm Current–Yellow Sea Warm Current which transports high salinity water into the YS, the Taiwan Warm Current (TWC) in the middle continental shelf, with depths of 50–100 m, the Min-Zhe Coastal Current (MZCC) along the coasts of Fujian and Zhejiang Provinces (Min-Zhe coasts) and the Yellow Sea Coastal Current (YSCC) along Jiangsu Province in the inner continental shelf, shallower than 50 m (Fig. 1.3.1; Lie and Cho, 2002). The Changjiang River discharges a large volume of fresh water into the ECS. Obviously, these currents affect the oceanographic conditions as well as the distribution and properties of water masses in the ECS (Ichikawa and Chaen, 2000).

1.3.2 East China Sea

Current system background

The Kuroshio enters the ECS along east coast of Taiwan and the southernmost one of the Ryukyu Islands chain. Under the constraint of the ECS continental slope, the mainstream of the Kuroshio in the ECS runs stably along the 200-m isobath at a maximum velocity of 0.75 to 1.5 m s^{-1} (Nitanni, 1972). Passing through the Okinawa Trough, the Kuroshio hugs the shelf break of the ECS until it approaches the shoaling northern end of the trough, where it separates from the shelf and bends east-southeastward. After it turns eastward around 30°29′N, 129°E (Qiu and Imasato, 1990), the Kuroshio separates from the continental margin, and eventually flows into the Pacific Ocean through the Tokara Strait. The Kuroshio intrudes into the ECS from the subsurface water of Kuroshio northeast of Taiwan, upwells northwestward gradually from 300 to 60 m, then turns to

northeast in the region around 27.5°N, 122°E, and finally reaches 31°N off the mouth of the Changjiang River along approximately the 60-m isobath, forming bottom saline water off the coast of Zhejiang Province (Yang *et al.*, 2011). The Kuroshio has been known to have two branch currents entering the continental shelf of the ECS: the Taiwan Warm Current in the southwestern ECS and the Tsushima Warm Current in the southeastern ECS (*e.g.*, Guan and Mao, 1982). The two branches have a strong influence on water circulation and water mass distribution not only in the ECS, but also in the YS (*e.g.*, Kondo, 1985).

The TWC refers to the northward movement of warm water off the Min-Zhe coast. It was first observed in the late 1950s (Guan and Chen, 1964). Originating from the Kuroshio, the TWC runs through middle continental shelf and intrudes into the inner continental shelf outside the Changjiang mouth, influencing the coastal ecological, chemical and physical environments by transporting warm, saline and oligotrophic open ocean materials across the shelf into the ECS (*e.g.*, Miao and Yu, 1991; Zhang *et al.*, 2007). The TWC originates from two parts of waters (see Bai *et al.* (2004)): one is the Taiwan Strait Current (TSC) from Taiwan Strait (Su *et al.*, 1994) and the other is the Kuroshio Branch Current to the northeast of Taiwan (KBCNT) (Kondo, 1985; Ichikawa and Beardsley, 2002; Yang *et al.*, 2011; Lian *et al.*, 2016). The high salinity lower TWC water is considered derived from the KBCNT, and the high temperature and less saline surface TWC water originates both from the TSC and the KBCNT (Weng and Wang, 1984). As proposed by Su and Pan (1987), the TWC bifurcates into two branches near 28°N within the middle continental shelf: the inshore branch (TWCIB, this is the traditional TWC) which flows northward along approximately the 50-m isobath off the Min-Zhe coast and turns to the northeast off the mouth of the Changjiang River, and offshore branch (TWCOB) which first flows anticyclonically, then turns cyclonically and finally joins the western flank of the Kuroshio. However, there is no agreement on where the north end of the TWCIB is because of a lack of long-term current observations.

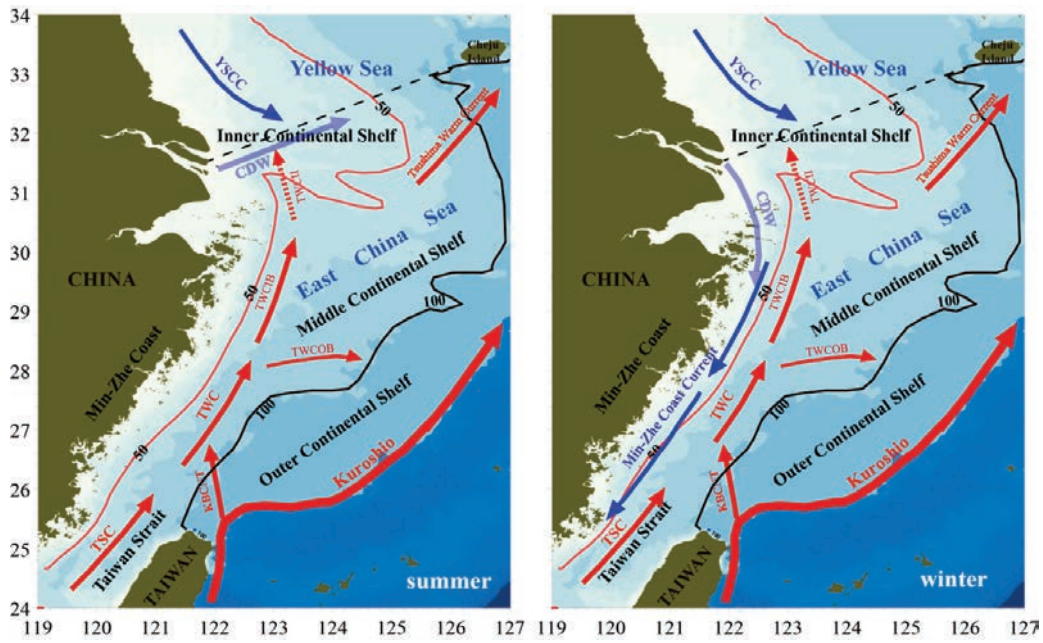

Fig. 1.3.1 Schematic circulation patterns in the ECS. Left panel indicates the circulation in summer and right panel indicates the circulation in winter.

The Tsushima Warm Current carries volume, heat, and salt from the ECS to the east and has a large impact on the surface circulation. The scientific questions for the Tsushima Warm Current in the ECS are its origin and volume. In general, there are two points of view on the origin of the Tsushima Warm Current. The first one is that the Tsushima Warm Current is considered as a northward branch of the Kuroshio when it separates southwest of Kyushu and that the Yellow Sea Warm Current (YSWC), separated from the Tsushima Warm Current southeast of Cheju Island, flows into the eastern Yellow Sea (Nitani, 1972). This point is supported by trajectories of satellite-tracked drifters (Lie and Cho, 1994). The second point of view is that the Tsushima Warm Current originates mainly from the Taiwan Strait (Beardsley *et al*., 1985). This was supported by current meter data over the continental shelf of the ECS (Fang *et al*., 1991). The volume transport of the Tsushima Warm Current is estimated from ferryboat acoustic Doppler current profiler (ADCP) data (Takikawa *et al*., 2005) and numerical models (Guo *et al*., 2006). The debates over the origin and volume of the Tsushima Warm Current are induced by lack of long-term direct current measurements.

The coastal currents in the ECS are complicated. Along the southern coast of the ECS, the northward flow through the Taiwan Strait is called the Taiwan Strait Warm Current (TSWC). The TSWC is reported flow northward along the Fujian–Zhejiang coast all year round, downwind in summer and upwind in winter (Su and Wang, 1987; Guan and Fang, 2006). As the extension of the South China Sea Warm Current (SCSWC), the TSWC brings high temperature and salinity SCS water into the ECS (Hu and Liu, 1992). Paralleling the TSWC on the coastal side, the MZCC exists in winter, induced by the winter monsoon, while there is no evidence of the existence of the MZCC in summer during the summer monsoon. Along the southern coast in the ECS, the YSCC moves southward in winter, but there is a conflict in the direction (Liu and Hu, 2009) of the YSCC in summer because of a lack of direct current measurements. The YSCC plays an important role in the evolution of the ECS water masses. Specifically, it causes the intensification of the MZCC and the YSWC water, and blocks the northeastward dispersion of the TWC water (Li *et al*., 2006).

Freshwater output from the Changjiang River forms a large-scale plume which plays a key role in physical processes in the adjacent ECS and YS. This water flux, known as Changjiang diluted water (CDW), is a prominent hydrographic feature in the ECS and YS. In summer, the CDW extends northeastward and forms a surface plume, while in winter it flows south in a narrow band along the eastern Chinese coast. The Changjiang River carries an enormous volume of fresh water, sediments, and nutrients to the ECS and YS, which significantly influences the water properties, circulation structure, sediment deposition, and ecosystems of the adjacent seas (Beardsley *et al*., 1985; Zhu and Shen, 1997). The influence of the Changjiang River on the water masses in the ECS is through the spreading of riverine plumes. The spreading of the plumes is strongly influenced by river discharge (Le, 1984), the East Asia monsoon (Zhu and Shen, 1997; Chang and Isobe, 2003), tidal mixing (Wu *et al*., 2011), coastal currents (Zhu *et al*., 1998), and continental shelf circulation. From salinity data, Mao *et al*. (1963) found that the CDW turns to the northeast in summer, but not to the south as would be expected, driven by the Coriolis force. The southerly summer monsoon is the dominant factor in the northeastward extension of the plume (Zhu and Shen, 1997; Chang and Isobe, 2003). In summer, the far-field diluted Changjiang water joins the northeastward shelf–current system and flows out of the ECS and YS through the Tsushima Strait where the year-round freshwater outflow is estimated to be at least 70% of the total Changjiang River discharge (Isobe *et al*., 2002; Chang and Isobe, 2003). In winter the CDW riverine plume flows south in a narrow band confined to the coast (*e.g*., Mao *et al*., 1963; Beardsley *et al*., 1985; Zhu and Shen, 1997).

Water masses

Previous studies on the ECS focus on typical seasons such as summer and winter. Because current observations were limited, most previous studies classified water masses according to their characteristic temperature and salinity, using different water mass analysis methods such as similar coefficients (Weng and Wang, 1984) and clustering method (Su and Weng, 1994; Qi *et al.*, 2014). However, different methods and datasets give different opinions. As described by Qi *et al.* (2014), there are eight water masses in summer and only five in winter in the ECS. Among these, Kuroshio Surface Water (KSW), Kuroshio Intermediate Water (KIW), ECS Surface Water (ECSSW), Continental Coastal Water (CCW), and Yellow Sea Surface Water (YSSW) exist throughout the year. Kuroshio Subsurface Water (KSSW), ECS Deep Water (ECSDW), and Yellow Sea Bottom Water (YSBW) are all seasonal water masses, occurring from May through October. The CCW, ECSSW and KSW all have significant seasonal variations. In addition, the CCW is affected by river runoff and ECSSW by the CCW and KSW (see Table 1.3.1).

Table 1.3.1 *T-S* characteristics of water masses in East China Sea.

Water mass		February	May	August	November
Continental Coastal Water (CCW)	*T*	7.0–15.5	13.4–23.5	22.0–28.0	15.5–21.5
	S	30.4–32.2	28.5–32.4	27.0–31.0	29.0–32.3
	D	0–30	0–20	0–20	0–30
East China Sea Surface Water (ECSSW)	*T*	11.5–20.5	14.5–24.5	23.0–28.5	17.0–25.0
	S	33.5–34.4	33.2–34.2	33.0–34.0	33.4–34.2
	D	0–200	0–50	0–75	0–200
East China Sea Deep Water (ECSDW)	*T*		13.5–21.5	15.5–24.5	
	S		33.5–34.4	33.4–34.4	
	D		50–200	75–200	
Kuroshio Surface Water (KSW)	*T*	14.2–24.4	19.0–27.8	23.7–30.2	15.0–26.0
	S	34.5–34.9	34.3–34.8	34.0–34.6	34.2–34.8
	D	0–450	0–60	0–75	0–400
Kuroshio Subsurface Water (KSSW)	*T*		13.0–23.3	13.0–25.0	
	S		34.6–35.0	34.5–35.0	
	D		50–400	60–400	
Kuroshio Intermediate Water (KIW)	*T*	7.4–13.5	6.5–13.6	7.0–13.8	6.6–13.9
	S	34.3–34.6	34.1–34.5	34.2–34.5	34.3–34.5
	D	>270	>240	>250	>280
Yellow Sea Surface Water (YSSW)	*T*	7.5–13.5	11.5–15.5	18.3–22.4	13.0–16.5
	S	32.5–33.6	32.0–33.2	31.5–32.4	32.0–33.4
	D	0–50	0–20	10–20	0–50
Yellow Sea Bottom Water (YSBW)	*T*		12.5–14.0	13.5–17.0	
	S		32.5–33.5	32.0–33.5	
	D		20–50	20–50	

Temperature, T (°C), Salinity, S, Depth, D (m)

Some other works have been carried out based on remote sensing data (*e.g.*, Yuan *et al.*, 2008) and models (*e.g.*, Yuan and Hsueh, 2010; Yang *et al.*, 2011; 2012). Yuan *et al.* (2008) studied the intrusion of the TWC into the Changjiang mouth and Subei using sea surface temperature (SST) and ocean color in winter. Yang *et al.* (2011, 2012) proposed an intrusion pathway of the Taiwan Warm

Current Inshore Branch (TWCIB) in summer. Using remote sensing data, we can only investigate phenomena in the sea surface, which is strongly influenced by solar heating and Changjiang runoff. It is difficult to study the phenomena in lower layers. Application of a local marginal sea model depends strongly on the artificial boundary conditions along the open boundary, where the vertical structures of currents and their temporal variations are difficult to set up (Guo *et al.*, 2003, 2006). The existing *T-S* diagram methods of analyzing water masses are useful in open ocean water mass analysis, but it is difficult to determine the core of original water masses in a shallow sea area by these methods because a large error may be introduced.

1.3.3 Yellow Sea

Current system background

The main water masses in the YS include the Yellow Sea Warm Current (YSWC) water mass, Yellow Sea Cold Water Mass (YSCWM) and the coastal water mass (Fig. 1.3.2). The water masses in the YS have distinct seasonal variation. The YSCWM appears mainly in summer and the YSWC mainly in winter.

Using hydrology observation data and drift bottle data, Uda (1934) drew the distribution of the current system of the Bohai Sea, YS and ECS. The YSWC is a unique current flowing against the wind direction in winter. The YSWC brings the open sea water into the YS and forms a high temperature and high salinity tongue from the southwest of Cheju Island toward the interior of the YS. It has great impact on the zooplankton ecosystem and the water exchange between the YS and ECS. Studies about the YSWC focus on its origin, formation mechanism, and path.

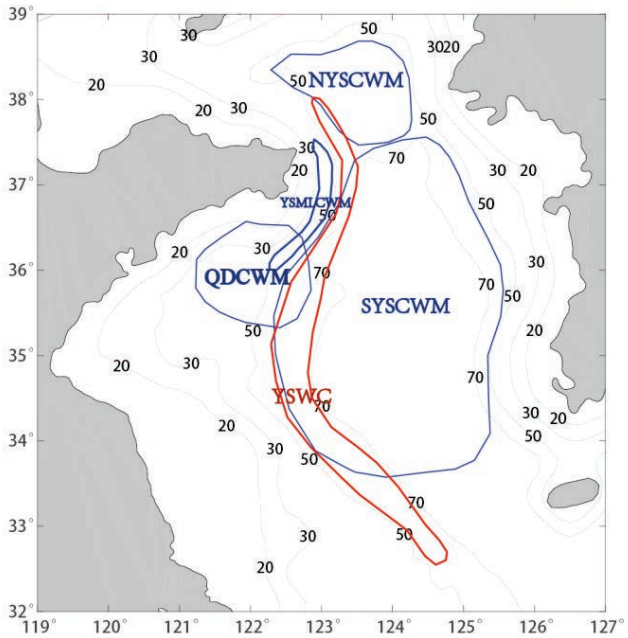

Fig. 1.3.2 Water mass distribution in the YS: Northern Yellow Sea Cold Water Mass (NYSCWM); Southern Yellow Sea Cold Water Mass (SYSCWM); Qingdao Cold Water Mass (QDCWM); Yellow Sea Middle Layer Cold Water (YSMLCW); Yellow Sea Warm Current (YSWC). Grey lines represent bathymetry in meters.

In the earlier times, the YSWC was thought to be a branch of the Tsushima Warm Current from the south of Cheju Island (Uda, 1934). This concept was supported by some scholars (Guan, 1962, 1994; Nitani, 1972; Chen *et al*., 1979; Park, 1986; Lie and Cho, 1994). However, based on current meter data obtained by Chinese researchers at day-night anchored stations, a new line of thought about the origin was considered. Fang *et al*. (1991) believed there was a current system, called the Taiwan-Tsushima-Tsugaru Warm Current System, placed on the ECS shelf and that the YSWC is a branch of this warm current system in the YS. Fang *et al*. (1997) proved this argument by numerical simulation. Another result of research suggested that the YSWC water is formed by lateral mixing of the Tsushima Warm Current water with the mixed water of the ECS southwest of Cheju Island (Lie *et al*., 2000) and that the mixed water of the YS and the Korean coastal water are also involved in the mixing process to some degree (Le and Mao, 1990; Le, 1992). In winter, the Tsushima Warm Current water with high temperature and high salinity meets the shelf water of the ECS with low temperature and low salinity and the mixing process forms a strong temperature and salinity front. The YSWC comes from this front area so it has the characteristic of mixed water. The YSWC matures in winter and disappears in summer (Beardsley *et al*., 1992; Lie, 1986; Park, 1986; Lie *et al*., 2000; Teague and Jacobs, 2000). However, the mature period of the TWC and Tsushima Warm Current is in summer. Further, no drifters, which were put in the northeastern area of the ECS, could get into the YS from the southwest of Cheju Island (Lie *et al*., 2000). These results show that the YSWC is mixed water other than a direct branch of the TWC or the Tsushima Warm Current. In other words, forcing of the TWC or the Tsushima Warm Current is not the formation mechanism of the YSWC.

Observation data and drifter trajectories show the YSWC has the characteristic of intermittent flow which may be related to the burst of the north wind in winter. Wind forcing in winter is widely thought to be the main dynamic mechanism of the YSWC. In climatology, the mean north wind in winter makes the coastal water of the YS flow toward the south. Because of mass conservation, there will be a northward compensation current in the middle YS (Fang *et al*., 1997; Yuan *et al*., 1982). The YSWC could be seen in a stable mode under a stable north wind. This viewpoint is consistent with the upwind circulation theory (Csanady, 1982). In meteorology, the forcing from a strong north wind makes the sea level at the south of the YS higher than that at the north of the YS. When the north wind recedes, a northward pressure gradient force causes the YSWC (Hsueh, 1988; Riedlinger and Jacobs, 2000; Teague and Jacobs, 2000). Strong winds produce the barotropic mode of the YSWC. Wan (2014) thought the YSWC is the superposition of the barotropic mode and the stable mode. The baroclinic effect on the YSWC is also considered (Lie, 1999; Lie *et al*., 2001, 2009, 2013). The coastal water and YSWC water form a strong front in winter, creating strong difference in temperature and salinity between the YSWC and coastal water. A strong north wind breaks the front and allows the high temperature and salinity water of the YSWC to flow into the YS. This mechanism results in the variation of the YSWC lagging behind that of the north wind (Zhao *et al*., 2011; Qu, 2014).

After formation, the YSWC is thought to flow to the north along the YS trough (Uda, 1932, 1933; Nitani, 1972; Chen *et al*., 1979; Guan, 1994). However, some scientists have held a different viewpoint: the YSWC axis is at the west side of the YS trough along the isobaths of 50 to 70 m (Mao *et al*., 1965; Kondo, 1985; Fang *et al*., 1997; Tang *et al*., 2001; Xu *et al*., 2005). The YSWC axis has seasonal and interannual variability and is located at the west side of the YS trough in most years (Tang *et al*., 1999, 2000, 2001). In some years, the YSWC axis shows a double-peak structure. One warm tongue is at the middle YS trough and the other is at the west side of the trough (Le and Mao, 1990; Ma *et al*., 2006). After the YSWC flows into the middle YS, a northwestward branch toward Shandong peninsula and a northwestward branch toward the north YS are generated (Su, 1986; Zhao *et al*., 2011).

The seasonal variation of the YSWC has a great impact on the characteristics of water masses. An earlier study (Park, 1986) pointed out that the YSWC is strong in winter and weak in summer. Analyzing CTD data from 1996 to 1999, Zou *et al*. (2000) found that the YSWC forms in winter, recedes in spring and disappears in the middle of spring. In early spring, the YSWC axis moves eastward compared with that in winter (Tang *et al*., 2001). Further, numerical simulation results show that the YSWC forms in December, matures in February, and recedes quickly in spring (Xu *et al*., 2005). Its axis moves to the west from December to February and reaches the 60- to 70-m isobath area. The YSWC remains stable at the bottom layer during the winter (Xu *et al*., 2005).

Water masses

In the central deep region of the YS, there is a water mass characterized by lower temperature (<10°C) and high salinity, called the Yellow Sea Cold Water Mass (YSCWM; Table 1.3.2). It occupies a third of the region above the deep and bottom layers of the YS in summer (Su and Weng, 1994) and exhibits a strong front in the YS. The YSCWM usually has three cold cores: one is the Northern Yellow Sea Cold Water Mass (NYSCWM, Fig. 1.3.2) and the other two form an eastern and western part of the Southern Yellow Sea Cold Water Mass (SYSCWM, Fig. 1.3.2) (Tang, 2005). The YSCWM is an important influence on the catches and fishing grounds of demersal fishes and has a great impact on the distribution of the biocenose and the acquisition of fishery resources (Cho, 1982; Du *et al*., 1996; Wang *et al*., 2003; Zhang *et al*., 2007).

Uda (1934) first found the existence of the YSCWM in 1934. He *et al*. (1959) first studied the formation mechanism of the YSCWM and concluded that it forms locally during the previous winter. This point of view is widely accepted. Further, Guan (1963) found that the temperature of the YSCWM has a relationship with the local air temperature during the previous winter and that the YSCWM shows cyclonic circulation pattern. Since then, quite a number of studies on the formation mechanism of the YSCWM have been made. The formation of a seasonal thermocline (Miu *et al*., 1991; Ren and Zhan, 2005), cooling at surface, strong mixing in winter (Hur *et al*., 1999), tidal mixing (Zhao, 1986; Lee and Beardsley, 1999; Ren and Zhan, 2005) and topography heat accumulation effect (Takahashi and Yanagi, 1995; Xu *et al*., 2003) are all important mechanisms during the formation of the YSCWM.

The YSCWM has clear seasonal variability based on *in-situ* observations and numerical simulations. With the seasonal change of the thermocline, the YSCWM forms in spring (approximately in May), matures in summer (approximately in August), recedes in autumn, and completely disappears in winter. Many research results have shown the seasonal characteristics of the YSCWM (Guan, 1963; Chu *et al*., 1997; Yu *et al*., 2006; Zhang *et al*., 2008; Bao *et al*., 2009; Yao *et al*., 2012). During the cooler season (from September to February), changes in the heat content of the YS are caused by variation in latent and sensible heat at the surface layer, which is related to the East Asian Winter Monsoon and the Arctic Oscillation (Wei *et al*., 2013).

The long-term variation of the YSCWM is still unclear. Following the accumulation of historical data, long-term variability of YSCWM has been analyzed. Weng *et al*. (1988) and Zhang and Yang (1996) explored the distribution range, volume, low temperature center and thermohaline characteristics of the YSCWM using the “similar coefficient” method and found that the YSCWM has obvious interannual variability. The SST of the YS has an increasing trend which is consistent with climate warming in northern China and the adjacent seas (Lin *et al*., 2005). Interannual variability in temperature has been discussed in some studies regarding the NYSCWM (Jiang *et al*., 2007; Li *et al*., 2015), with NYSCWM temperature showing an increasing trend. Temperature at the thermocline has the greatest temporal variance that is caused mainly by surface heating (Hu and Wang, 2004). Wei *et al*. (2010) reported that the summer *T-S* properties of the YSCWM correspond

to the YSWC in winter. Interannual variability of eastern part of the SYSCWM also deserves academic concern. Given the survey area, the study of the eastern part of the SYSCWM is mainly taken by Korean scientists. Park *et al*. (2011) conducted empirical orthogonal functional (EOF) and singular value decomposition (SVD) analyses on the Korea Oceanographic Data Center (KODC) dataset and described the temperature variability of the eastern part of the SYSCWM. He attributed the interannual temperature variation of the SYSCWM to winter forcing, including the Siberian High, Aleutian Low, Pacific Decadal Oscillation, East Asian Jet Stream, and Arctic Oscillation. Summer forcing could also intensify the temperature anomaly of the SYSCWM, for example, the SST of the Kuroshio and sea level pressure over the Asian continent. Yang *et al*. (2014) used the same data and simulation results to show that SST in the previous winter is associated with the southern limit of the SYSCWM in the following summer. Li (1991) pointed out that the YSCWM is in a warm phase in the year following a large meander of the Kuroshio, and in a cold phase when El Niño events occur. However, some studies have concluded that the temperature of the SYSCWM is not directly related to El Niño (Jia and Sun, 2002; Bai *et al*., 2004). Furthermore, winter processes play an important role in the interannual variability of the YSCWM. Wei *et al*. (2013) found that the heat content of the deep region of the YS is mainly influenced by lateral heat transport controlled by the YSWC, which also has a 4- to 7-year period of interannual variability (Wang *et al*., 2009).

Table 1.3.2 *T-S* characteristics of water masses in the Yellow Sea.

Water mass		
Northern Yellow Sea Cold Water Mass (NYSCWM)	*T* *S* *D*	6.0–10.0 32.5–34.0 50–70
Southern Yellow Sea Cold Water Mass (SYSCWM)	*T* *S* *D*	6–10 32.5–34.0 50–70
Qingdao Cold Water Mass (QDCWM)	*T* *S* *D*	6–10 31.7 40–60
Yellow Sea Middle Layer Cold Water (YSMLCW)	*T* *S* *D*	6–12 31.8–32.5 20–30
Yellow Sea Warm Current (YSWC)	*T* *S* *D*	8–14 32.5–34 50–70

Temperature, T (°C), Salinity, S, Depth, D (m)

Spring could be seen as a conversion period in which the YS changes from vertically homogeneous YSWC mode to vertical stratified YSCWM mode. More attention is usually given to how the YS changes in spring. In 1996, the Yellow Sea Middle Layer Cold Water (YSMLCW) and inversion layer was found during a China and Korea joint ocean investigation (Tang *et al*., 1999; Zou *et al*., 2000). Zou *et al*. (2000) explained the formation mechanism of YSMLCW: The YSWC weakens in spring. The mixed water of the western YS, which has a lower temperature, expands toward the east and south and spreads over the YSWC water. In the meantime, surface heating forms a thermocline. Observation data (Zou *et al*., 2001) and simulation results (Xu *et al*., 2001) show that the YSWC is one of main reasons for the formation of the YSMLCW. The Qingdao Cold Water Mass (QDCWM) is also a classic phenomenon of the YS in spring, forming offshore southeast of Qingdao. The

source of the QWCWM is coastal water that originates from the north YS (Zhang *et al*., 1996). The QDCWM has lowest temperature in spring. It forms in March, matures in April, and blends into the YSCWM gradually from May (Yu *et al*., 2006). Yu *et al*. (2006) found that the Inchon Offshore Cold Water Mass has the same seasonal characteristics as the QDCWM. The QDCWM has a great impact on the fishing grounds in the YS (Zheng and Zhang, 1983) by upwelling nutrients to the upper layer water. Long-term variation in water properties analysis shows that the QDCWM became stronger before the mid-1970s, and weakened after the mid-1970s. The interannual variability of the QDCWM strength is related to the ENSO events in which the QDCWM weakens during El Niño events (Zhang *et al*., 2004).

1.3.4 Future work

Influenced by the monsoon and currents system, the water masses of the ECS and YS are complex, showing strong seasonal variation and complex vertical structure. Influenced by global warming, the water masses of the ECS and YS also show a warming trend, with interannual or interdecadal variations. A deep understanding of the variation of water masses in the ECS and YS could give us better insight to ecological and environmental variations, and help us promote environmentally sustainable management ability.

For the Yellow Sea, new observations show that the southern YSCWM and YSWC exist concurrently in the southern Yellow Sea during spring and autumn and their co-existence time is more than half a year. The mechanism for this co-existence and the influence of the biogeochemical process in Yellow Sea needs to be studied further.

For the East China Sea, recent observations suggest that there exists some mesoscale water masses between the Kuroshio and Taiwan Warm Current waters. The seasonal-to-interannual variation characteristics of the mesoscale water masses should be analyzed and their influence on the ecology of the East China Sea should be studied in the future.

1.3.5 References

Bai, H., Hu, D.X., Chen, Y.L. and Wang, Q.Y. 2004. Statistic characteristics of thermal structure in the southern Yellow Sea in summer. *Chin. J. Oceanol. Limnol.* **22**: 237–243, doi:10.1007/BF02842554.

Bao, X.W., Li, N., Yao, Z.G. and Wu, D.X. 2009. Seasonal variation characteristics of temperature and salinity of the North Yellow Sea. *Period. Ocean Univ. China* **4**: 553–562 (in Chinese with English abstract).

Beardsley, R., Limeburner, R., Yu, H. and Cannon, G. 1985. Discharge of the Changjiang (Yangtze River) into the East China Sea. *Cont. Shelf Res*. **4**: 57–76, doi:10.1016/0278-4343(85)90022-6.

Beardsley, R.C., Limeburner, R., Kim, K. and Candela, J. 1992. Lagrangian flow observations in the East China, Yellow and Japan seas. *La mer* **30**: 297–314.

Chang, P.H. and Isobe, A. 2003. A numerical study on the Changjiang diluted water in the Yellow and East China Seas. *J. Geophys. Res. Oceans* **108**: 3299, doi:10.1029/2002JC001749.

Chen, Z.S., He, Y.C. and Lin, X.F. 1979. The situation of Yellow Sea circulation. *Ocean Res*. **3**: 1–42 (in Chinese).

Cho, K. 1982. On the influence of the Yellow Sea bottom cold water on the demersal fishing grounds. *Bull. Korean Fish. Technol. Soc*. **18**: 25–33.

Chu, P.C., Wells, S.K., Haeger, S.D., Szczechowski, C. and Carron, M. 1997. Temporal and spatial scales of the Yellow Sea thermal variability. *J. Geophys. Res. Oceans* **102**: 5655–5667, doi10.1029/96JC03428.

Csanady, G.T. 1982. Circulation in the coastal ocean. *Advances Geophys.* **23**: 101–183.

Du, B., Zhang, Y.J., Shan, Y.C. and Wang, H. 1996. The characteristics of Cold Water Mass variation at the bottom of the north Yellow Sea and its hydrological effects on the mortality of shellfish cultured in the waters of outor Chang-Shan Island. *Mar. Sci. Bull*. **15**: 17–28 (in Chinese with English abstract).

Fang, G., Zhao, B. and Zhu, Y. 1991. Water volume transport through the Taiwan Strait and the continental shelf of the East China Sea measured with current meters. *Elsevier Oceanogr. Ser.* **54**: 345–358, doi:10.1016/S0422-9894(08)70107-7.

Fang, Y., Zhang, Q.H. and Fang, G.H. 1997. A numerical study on the path and origin of the Yellow Sea Warm Current. *The Yellow Sea* **3**: 18–26.

Guan, B. and Chen, S. 1964. The current systems in the near-sea area of China Seas. *Initial Rep.* **5**: 1–85.

Guan, B. and Fang, G. 2006. Winter counter-wind currents off the southeastern China coast. *J. Oceanogr.* **62**: 1–24, doi:10.1007/s10872-006-0028-8.

Guan, B.X. 1962. Some problems concerning the study of the current structure of the near-shore area of China Sea. *Oceanol. Limnol. Sin*. **4**: 121–141 (in Chinese).

Guan, B.X. 1963. A preliminary study of the temperature variations and the characteristics of the circulation of the Cold Water Mass of the Yellow Sea. *Oceanol. Limnol. Sin.* **5**: 255–284 (in Chinese).

Guan, B.X. 1994. Patterns and structures of the currents in Bohai, Huanghai and East China Seas, pp. 17–26 *in:* Oceanology of China Seas, vol. 1 *edited by* D. Zhou, Y.-B. Liang and C.-K. Zeng (C.K. Tseng), Springer, Netherlands.

Guan, B.X. and Mao, H.L. 1982. A note on circulation of the East China Sea. *Chin. J. Oceanol. Limnol*. **1**: 5–16.

Guo, X., Hukuda, H., Miyazawa, Y. and Yamagata, T. 2003. A triply nested ocean model for simulating the Kuroshio-Roles of horizontal resolution on JEBAR. *J. Phys. Oceanogr*. **33**: 146–169, doi:10.1175/1520-0485(2003)033<0146:ATNOMF>2.0.CO;2.

Guo, X., Miyazawa, Y. and Yamagata, T. 2006. The Kuroshio onshore intrusion along the shelf break of the East China Sea: the origin of the Tsushima Warm Current. *J. Phys. Oceanogr*. **36**: 2205–2231, doi:10.1175/jpo2976.1.

He, C.B., Wang, Y.X., Lei, Z.Y. and Xu, S. 1959. A preliminary study of the formation of Yellow Sea cold mass and its properties. *Oceanol. Limnol. Sin*. **2**: 11–15 (in Chinese).

Hsueh, Y. 1988. Recent current observations in the eastern Yellow Sea. *J. Geophys. Res*. **93**: 6875–6884, doi:10.1029/JC093iC06p06875.

Hu, D.X. and Wang, Q.Y. 2004. Interannual variability of the southern Yellow Sea cold water mass. *Chin. J. Oceanol. Limnol*. **22**: 231–236, doi:10.1007/BF02842553.

Hu, J.Y. and Liu, M.S. 1992. The current structure during summer in southern Taiwan Strait. *Trop. Oceanol*. **11**: 42–47 (in Chinese with English abstract).

Hur, H., Jacobs, G. and Teague, W. 1999. Monthly variations of water masses in the Yellow and East China Seas. *J. Oceanogr*. **55**: 171–184, doi:10.1023/A:1007885828278.

Ichikawa, H. and Beardsley, R.C. 2002. The current system in the Yellow and East China Seas. *J. Oceanogr*. **58**: 77–92, doi:10.1023/A:1015876701363.

Ichikawa, H. and Chaen, M. 2000. Seasonal variation of heat and freshwater transports by the Kuroshio in the East China Sea. *J. Mar. Syst.* **24**: 119–129, doi:10.1016/S0924-7963(99)00082-2.

Isobe, A., Ando, M., Watanabe, T., Senjyu, T., Sugihara, S. and Manda, A. 2002. Freshwater and temperature transports through the Tsushima-Korea Straits. *J. Geophys. Res. Oceans* **107**: 3065, doi:10.1029/2000JC000702.

Jia, R. and Sun, L. 2002. Distribution features of the Yellow and Bohai Seas temperature in winter and summer. *Mar. Sci. Bull. (Tianjin)* **21**: 1–8 (Chinese edition).

Jiang, B.J., Bao, X.W., Wu, D.X. and Xu, J.P. 2007. Interannual variation of temperature and salinity of northern Huanghai Sea Cold Water Mass and its probable cause. *Acta Oceanol. Sin.* **29**: 1–10, doi:10.1002/cem.1038.

Kondo, M. 1985. Oceanographic investigations of fishing grounds in the East China Sea and the Yellow Sea, 1: Characteristics of the mean temperature and salinity distributions measured at 50m and near the bottom. *Bull. Seikai Region. Fish. Res. Lab*. **62**: 19–66.

Le, K.-T. 1984. A preliminary study of the path of the Changjiang Diluted Water. *Oceanol. Limnol. Sin*. **15**: 157–167 (in Chinese with English abstract).

Le, K.T. 1992. On the origin of Yellow Sea Warm Current Water in winter. *Acta Oceanol. Sin.* **14**: 9–19 (in Chinese).

Le, K.T. and Mao, H.L. 1990. Wintertime structure of temperature and salinity of the southern Huanghai (Yellow) Sea and its current system. *Oceanol. Limnol. Sin*. **21**: 505–514 (in Chinese with English abstract).

Lee, S.H. and Beardsley, R.C. 1999. Influence of stratification on residual tidal currents in the Yellow Sea. *J. Geophys. Res*. **104**: 15,679−15,701, doi:10.1029/1999JC900108.

Li, A., Yu, F., Diao, X.Y. and Si, G.C. 2015. Interannual variability of temperature of northerm Yellow Sea Cold Water Mass. *Acta Oceanol. Sin.* **37**: 30–42 (in Chinese with English abstract).

Li, G., Han, X., Yue, S., Wen, G., Rongmin, Y. and Kusky, T. 2006. Monthly variations of water masses in the East China Seas. *Cont. Shelf Res.* **26**: 1954–1970, doi:10.1016/j.csr.2006.06.008.

Li, K.P. 1991. The response of Yellow Sea Cold Water Mass to changes in ocean. *Acta Oceanol. Sin.* **13**: 779–785.

Lian, E., Yang, S., Wu, H., Yang, C., Li, C. and Liu, J.T. 2016. Kuroshio subsurface water feeds the wintertime Taiwan Warm Current on the inner East China Sea shelf. *J. Geophys. Res. Oceans* **121**: 4790–4803, doi:10.1002/2016JC011869.

Lie, H.J. 1986. Summertime hydrographic features in the southeastern Hwanghae. *Prog. Oceanogr*. **17**: 229–242, doi:10.1016/0079-6611(86)90046-7.

Lie, H.J. 1999. On the Huanghai (Yellow) Sea circulation: a review by current measurements. *Acta Oceanol. Sin*. **18**: 355–373.

Lie, H.J. and Cho, C.H. 1994. On the origin of the Tsushima Warm Current. *J. Geophys. Res. Oceans* **99**: 25,081–25,091, doi:10.1029/94JC02425.

Lie, H.J. and Cho, C.H. 2002. Recent advances in understanding the circulation and hydrography of the East China Sea. *Fish. Oceanogr.* **11**: 318–328, doi:10.1046/j.1365-2419.2002.00215.x.

Lie, H.J., Cho, C.H., Lee, J.H., Lee, S. and Tang, Y. 2000. Seasonal variation of the Cheju Warm Current in the northern East China Sea. *J. Oceanogr*. **56**: 197–211, doi:10.1023/A:1011139313988.

Lie, H.J., Cho, C.H., Lee, J.H., Lee, S., Tang, Y. and Zou, E. 2001. Does the Yellow Sea Warm Current really exist as a persistent mean flow? *J. Geophys. Res. Oceans* **106**: 22,199–22,210, doi:10.1029/2000JC000629.

Lie, H.J., Cho, C.H. and Lee, S. 2009. Tongue-shaped frontal structure and warm water intrusion in the southern Yellow Sea in winter. *J. Geophys. Res. Oceans* **114**: doi:10.1029/2007JC004683.

Lie, H.J., Cho, C.H. and Lee, S. 2013. Frontal circulation and westward transversal current at the Yellow Sea entrance in winter. *J. Geophys. Res. Oceans* **118**: 3851–3870, doi:10.1002/jgrc.20280.

Lin, C., Ning, X., Su, J., Lin, Y. and Xu, B. 2005. Environmental changes and the responses of the ecosystems of the Yellow Sea during 1976–2000. *J. Mar. Syst*. **55**: 223–234, doi:10.1016/j.jmarsys.2004.08.001.

Liu, Z. and Hu, D. 2009. Preliminary study on the Huanghai Sea coastal current and its relationship with local wind in summer. *Acta Oceanol. Sin.* **31**: 1–7 (in Chinese with English abstract).

Ma, J., Qiao, F., Xia, C. and Kim, C.S. 2006. Effects of the Yellow Sea Warm Current on the winter temperature distribution in a numerical mode. *J. Geophys. Res. Oceans* **111**: C11S04, doi:10.1029/2005JC003171.

Mao, H., Gan, Z. and Lan, S. 1963. Preliminary study on the Changjiang diluted water and its mixing natures. *Oceanol. Limnol. Sin*. **5**: 183–206 (in Chinese with English abstract).

Mao, H.L., Ren, Y.B. and Sun, G.D. 1965. The preliminary analysis of the hydrological characteristics and water types of the southern Yellow Sea and north East China Sea in summer. *Mar. Sci. Sin*. **1**: 78–125 (in Chinese).

Miao, Y. and Yu, H. 1991. Spatial and temporal variations of water type mixing characteristic in the East China Sea. *Trans. Sci. Survey Kuroshio Current* **3**: 193–203.

Miu, J.B., Liu, X.Q. and Hsueh, Y. 1991. Study on the formational mechanism of the northern Yellow (Huanghai) Sea Cold Water Mass (II) — Discussion on the solution of the model. *Sci. China Series B* **34**: 1271–1280.

Nitani, H. 1972. Beginning of the Kuroshio, pp. 353–369 *in:* Kuroshio—Its Physical Aspects *edited by* H. Stommel and K. Yoshida, University of Tokyo Press, Tokyo.

Park, S., Chu, P.C. and Lee, J.H. 2011. Interannual-to-interdecadal variability of the Yellow Sea Cold Water Mass in 1967–2008: characteristics and seasonal forcings. *J. Mar. Syst*. **87**: 177–193, doi: 10.1016/j.jmarsys.2011.03.012.

Park, Y.H. 1986. A simple theoretical model for the upwind flow in the southern Yellow Sea. *J. Oceanol. Soc. Korea* **21**: 203–210.

Qi, J., Yin, B., Zhang, Q., Yang, D. and Xu, Z. 2014. Analysis of seasonal variation of water masses in East China Sea. *Chin. J. Oceanol. Limnol.* **32**: 958–971, doi:10.1007/s00343-014-3269-1.

Qiu, B. and Imasato, N. 1990. A numerical study on the formation of the Kuroshio Counter Current and the Kuroshio Branch Current in the East China Sea. *Cont. Shelf Res.* **10**: 165–184, doi:10.1016/0278-4343(90)90028-k.

Qu, L.X. 2014. Study of the oceanic response to the winter strong wind events in the Yellow and Bohai Sea. M.Sc. thesis, University of China, Qingdao (in Chinese with English abstract).

Ren, H.J. and Zhan, J.M. 2005. A numerical study on the seasonal variability of the Yellow Sea cold water mass and the related dynamics. *J. Hydrodyn*. **20**(Suppl.): 887–896.

Riedlinger, S.K. and Jacobs, G.A. 2000. Study of the dynamics of wind-driven transports into the Yellow Sea during winter. *J. Geophys. Res. Oceans* **105**: 28,695–28,708, doi:10.1029/2000JC900127.

Su, J. and Pan, Y. 1987. On the shelf circulation north of Taiwan. *Acta Oceanol. Sin.* **6**(Suppl. I): 1–20.

Su, J. and Wang, W. 1987. On the sources of the Taiwan Warm Current from the South China Sea. *Chin. J. Oceanol. Limnol.* **5**: 299–308, doi:10.1007/BF02843812.

Su, J., Pan, Y. and Liang, X. 1994. Kuroshio intrusion and Taiwan Warm Current, pp. 59–70 *in:* Oceanology of China Seas, vol. 1 *edited by* D. Zhou, Y.-B. Liang and C.-K. Zeng (C.K.Tseng), Kluwer Academic, Dordrecht.

Su, Y.S. 1986. A survey of geographical environment, circulation systems and the central fishing grounds in the Huanghai Sea and East China Sea. *J. Ocean Univ. Qingdao* **16**: 12–27.

Su, Y.S. and Weng, X.C. 1994. Water masses in China seas, pp. 3–16 *in:* Oceanology of China Seas, vol. 1 *edited by* D. Zhou, Y.-B. Liang and C.-K. Zeng (C.K.Tseng), Kluwer Academic, Dordrecht.

Takahashi, S. and Yanagi, T. 1995. A numerical study on the formation of circulations in the Yellow Sea during summer. *La mer* **33**: 135–147.

Takikawa, T., Yoon, J.-H. and Cho, K.-D. 2005. The Tsushima Warm Current through Tsushima Straits estimated from ferryboat ADCP data. *J. Phys. Oceanogr.* **35**: 1154–1168, doi:10.1175/JPO2742.1.

Tang, Y.X. 2005. Yellow Sea Cold Water Mass, pp. 202–206 *in:* Hydrography of China Offshore *edited by* J. Su, Ocean Press, China (in Chinese).

Tang, Y.X., Zou, E.M. and Lie, H.J. 1999. Analysis of hydrographic features and circulation situation in the southern Huanghai Sea in early spring. *Acta Oceanol. Sin.* **21**: 1–11 (in Chinese).

Tang, Y.X., Zou, E.M. and Lie, H.J. 2000. Some features of circulation in the southern Huanghai Sea. *Acta Oceanol. Sin.* **22**: 1–16 (in Chinese).

Tang, Y.X., Zou, E.M. and Lie, H.J. 2001. On the origin and path of the Huanghai Warm Current during winter and early spring. *Acta Oceanol. Sin.* **23**: 1–12 (in Chinese).

Teague, W.J. and Jacobs, G.A. 2000. Current observations on the development of the Yellow Sea Warm Current. *J. Geophys. Res. Oceans* **105**: 3401–3411, doi:10.1029/1999JC900301.

Uda, M. 1932. The results of simultaneous oceanographical investigations in the Japan Sea and its adjacent waters in May and June. *J. Imp. Fish. Exp. Sta*. **5**: 57–190 (in Japanese with English summary).

Uda, M. 1933. Results of simultaneous oceanographic investigations in the Japan Sea and its adjacent waters in October and November. *J. Imp. Fish. Exp. Sta*. **7**: 91–151 (in Japanese with English summary).

Uda, M. 1934. Hydrographical reasearch on the normal monthly conditions in the Japan Sea, the Yellow Sea, and the Okhotsk Sea. *J. Imp. Fish. Exp. Sta*. 5: 191–236 (in Japanese with English summary).

Wan, K. 2014. The study on Yellow Sea Warm Current's mechanism and low-frequency sea level fluctuations in Bohai and Yellow Sea during winter storm. Ph.D. dissertation, Ocean University of China, Qingdao (in Chinese).

Wang, H.W., Yu, F., Lv, L.G., Diao, X.Y. and Guo, J.S. 2009. Characteristics of spatial and interannual variation in the Yellow Sea Warm Current area in winter. *Adv. Mar. Sci*. **27**: 140–148 (in Chinese with English abstract).

Wang, R., Zuo, T. and Wang, K. 2003. The Yellow Sea cold bottom water—an oversummering site for *Calanus sinicus* (Copepoda, Crustacea). *J. Plankt. Res*. **25**: 169–183, doi:10.1093/plankt/25.2.169.

Wei, H., Shi, J., Lu, Y. and Peng, Y. 2010. Interannual and long-term hydrographic changes in the Yellow Sea during 1977–1998. *Deep Sea Res. II* **57**: 1025–1034, doi:10.1016/j.dsr2.2010.02.004.

Wei, H., Yuan, C., Lu, Y., Zhang, Z. and Luo, X. 2013. Forcing mechanisms of heat content variations in the Yellow Sea. *J. Geophys. Res. Oceans* **118**: 4504–4513, doi:10.1002/jgrc.20326.

Weng, X. and Wang, C. 1984. A preliminary study on the TS characteristics and the origin of Taiwan Warm Current Water in summer. *Stud. Mar. Sinica* **21**: 113–133 (in Chinese with English abstract).

Weng, X.C., Zhang, Y.K., Wang, C.M. and Zhang, Q.L. 1988. The Variational characteristics of the Huanghai Sea (Yellow Sea) Cold Water Mass. *Oceanol. Limnol. Sin*. **19**: 368-379 (in Chinese).

Wu, H., Zhu, J., Shen, J. and Wang, H. 2011. Tidal modulation on the Changjiang River plume in summer. *J. Geophys. Res. Oceans* **116**: C08017, doi:10.1029/2011JC007209.

Xu, B.C., Wang, Z.S. and Zou, E.M. 2001. Self-simulation of vertical thermal structure for the Intermediate Cold Water in the west of Southern Huanghai Sea. *J. Oceanogr. Huanghai Bohai Seas* **19**: 1–7.

Xu, D.F., Yuan, Y.C. and Liu, Y. 2003. The baroclinic circulation structure of Yellow Sea cold water mass. *Sci. China Series D: Earth Sci*. **46**: 117–126.

Xu, Y., Yu, F. and Zhang, Z.X. 2005. Diagnostic computation of the Yellow Sea Warm Current in winter. *Adv. Mar. Sci*. **23**: 399–407 (in Chinese with English abstract).

Yang, H.W., Cho, Y.K., Seo, G.H., You, S.H. and Seo, J.W. 2014. Interannual variation of the southern limit in the Yellow Sea Bottom Cold Water and its causes. *J. Mar. Syst*. **139**: 119–127, doi: 10.1016/j.jmarsys.2014.05.007.

Yao, Z.G., Bao, X.W., Li, N., Li, X.B., Wan, K. and Song, J. 2012. Seasonal evolution of the northern Yellow Sea Cold Water Mass. *Period. Ocean Univ. China* **42**: 9–15 (in Chinese with English abstract).

Yang, D., Yin, B., Liu, Z. and Feng, X. 2011. Numerical study of the ocean circulation on the East China Sea shelf and a Kuroshio bottom branch northeast of Taiwan in summer. *J. Geophys. Res. Oceans* **116**: C05015, doi:10.1029/2010JC006777.

Yang, D., Yin, B., Liu, Z., Bai, T., Qi, J. and Chen, H. 2012. Numerical study on the pattern and origins of Kuroshio branches in the bottom water of southern East China Sea in summer. *J. Geophys. Res. Oceans* **117**: 1–16, doi:10.1029/2011JC007528.

Yu, F., Zhang, Z.X., Diao, X.Y., Gou, J.S. and Tang, Y.X. 2006. Analysis of evolution of the Huanghai Sea Cold Water Mass and its relationship with adjacent water masses. *Acta Oceanol. Sin*. **28**: 26–34, (in Chinese with English abstract), doi:10.3321/j.issn:0253-4193.2006.05.003.

Yuan, D. and Hsueh, Y. 2010. Dynamics of the cross-shelf circulation in the Yellow and East China Seas in winter. *Deep Sea Res. II:* **57**: 1745–1761, doi:10.1016/j.dsr2.2010.04.002.

Yuan, D., Zhu, J., Li, C. and Hu, D. 2008. Cross-shelf circulation in the Yellow and East China Seas indicated by MODIS satellite observations. *J. Mar. Syst.* **70**: 134–149, doi:10.1016/j.jmarsys.2007.04.002.

Yuan, Y.C., Su, J.L. and Zhao, J.S. 1982. A single layer model of thr continental shelf circulation in the East China Sea. *Acta Oceanol. Sin.* **4**: 1–11.

Zhang, J., Liu, S.M., Ren, J.L., Wu, Y. and Zhang, G.L. 2007. Nutrient gradients from the eutrophic Changjiang (Yangtze River) Estuary to the oligotrophic Kuroshio waters and re-evaluation of budgets for the East China Sea Shelf. *Prog. Oceanogr.* **74**: 449–478, doi:10.1016/j.pocean.2007.04.019.

Zhang, Q.L., Weng, X.C. and Yang, Y.L. 1996. Analysis of water masses in the south Yellow Sea in spring. *Oceanol. Limnol. Sin*. **27**: 421–428 (in Chinese).

Zhang, Q.L., Hou, Y.J., Cheng, M.H. *et al*. 2004. Variation features in Qingdao Cold Water Mass strength. *Stud. Mar. Sin*. **46**: 13–21 (in Chinese).

Zhang, S., Wang, Q., Lü, Y., Ciu, H. and Yuan, Y.L. 2008. Observation of the seasonal evolution of the Yellow Sea Cold Water Mass in 1996–1998. *Cont. Shelf Res.* **28**: 442–457, doi:10.1016/j.csr.2007.10.002.

Zhang, Y.K. and Yang, Y.L. 1996. Analyses of the variational characteristics of the north Huanghai Sea Cold Water Mass. *Mar. Forecasts* **13**: 15–21.

Zhao, B.R. 1986. The fronts of the Huanghai cold water mass (HCWM) induced by tidal mixing. *Chin. J. Oceanol. Limnol*. **4**: 159–170, doi:10.1007/BF02850432.

Zhao, S., Yu, F., Diao, X.Y. and Si, G.C. 2011. The path and mechanism of the Yellow Sea Warm Current. *Mar. Sci*. **35**: 73-80 (in Chinese).

Zheng, D. and Zhang, R.A. 1983. Analysis of spring water masses in the sea area off Yantai, Weihai and Shidao. *Mar. Sci. Bull*. **2**: 61–68.

Zhu, J. and Shen, H. 1997. Extension mechanisms of Changjiang Diluted Water. East China Normal University Press, Shanghai, pp. 18–176 (in Chinese with English abstract).

Zhu, J., Xiao, C. and Shen, H. 1998. Numerical model simulation of expansion of Changjiang diluted water in summer. *Acta Oceanol. Sin.* **20**: 13–22 (in Chinese with English abstract).

Zou, E.M., Guo, B.H. and Tang, Y.X. 2000. The hydrographic features and water masses analyses of the southern Huanghai Sea in the spring of 1996. *Acta Oceanol. Sin.* **22**: 17–26.

Zou, E.M., Guo, B.H. and Tang, Y.X. 2001. An analysis of summer hydrographic features and circulation in the southern Yellow Sea and the northern East China Sea. *Oceanol. Limnol. Sin*. **32**: 340–348.

1.4 Ocean Mixing

Takeshi Matsuno[1], Hao Wei[2], Jae Hak Lee[3] and Chuanjie Wei[4]

[1] Research Institute for Applied Mechanics, Kyushu University, Japan
[2] School of Marine Science and Technology, Tianjin University, China
[3] Korea Institute of Ocean Science and Technology, Korea
[4] Institute of Oceanography, Chinese Academy of Sciences, China

1.4.1 Introduction

Mixing processes in the ocean play an important role in dissipating energy and diffusing materials. Mixing can be divided into two types, horizontal and vertical, the features of which are quite different because of the ocean's large aspect ratio and stratified structure. While horizontal and vertical mixing are similar in many ways to isopycnal and diapycnal mixing, respectively, they are not identical because, for example, horizontal mixing should be diapycnal if there is a horizontal density gradient in a frontal region. Horizontal or isopycnal mixing may be important in basin-scale phenomena, such as the formation of North Pacific Intermediate Water. Very few reports have considered horizontal mixing processes or related topics in the East China Sea (ECS). Various aspects of vertical/diapycnal mixing in the ECS have, however, been reported, so mainly vertical mixing is considered in this section.

Vertical mixing plays a very important role in the stratification and transport of material in the ocean. It is particularly important to have a quantitative understanding of this process in the shelf region and coastal water because vertical mixing and stratification strongly control biogeochemical processes and the biological environment. The ECS is well-known for its high biological productivity, which is sustained by nutrients from land and sub-surface of the ocean, including the deep ocean. Therefore, the mixing processes that supply the necessary nutrients for primary production and control the transport of material need to be evaluated correctly. While the biological abundance and environmental conditions in the ECS have been studied extensively, there are very few quantitative surveys of the mixing processes. We therefore need to find out more about the physical and biological aspects of the mixing processes, and enhance our understanding of the marine environment in the ECS. In this context, a summary of the information that is currently available about vertical mixing in the ECS is essential.

Studies of turbulent mixing in the ECS can be divided into various phases. Some studies discuss turbulent mixing as a physical process that changes the stratification and ocean structure. Others consider turbulent mixing as a process that transports biogeochemical materials related to primary production, such as nutrients. Other research has focused on measuring the microstructure, and improving the accuracy of estimates of the turbulence intensity by parameterization.

From another perspective, the role that vertical mixing plays in physical and biological processes may be divided into three separate cases based on the relative position of the turbulent mixing, namely, the surface, intermediate, and bottom layers; this classification is particularly useful for the

shelf region. It is generally thought that mixing processes in the surface layer are related to the formation and evolution of the surface mixed layer and contribute to air–sea interactions. Vertical mixing in the intermediate layer seems to be related to the activities of internal waves, including internal tides, near-inertial internal gravity waves, and high frequency internal waves. Turbulence in the intermediate layer contributes to the evolution of stratification and the vertical flux of various materials. Turbulence in the bottom boundary layer (BBL) makes an important contribution to the flux of materials just above the sea floor. As well as these main layers, we should also carefully consider a sort of diffusive bottom layer (DBL), which, even though it is very thin, is very important for sediment–water exchange fluxes.

In this review, we summarize information about mixing processes in the different layers, including the physical processes and their influence on various phenomena, such as air–sea interactions, the supply of nutrients for primary production, and other marine environments.

1.4.2 Methods for estimating the turbulence intensity

Over recent decades, the most reliable estimates of the turbulence intensity have been based on measurements of microstructure from which the turbulent energy dissipation rate (ε) can be determined by integrating the shear spectrum within a specific wave number range, assuming isotropy (*e.g.*, Gregg, 1987). Although the assumption of isotropy may not be correct, particularly in strongly stratified situations, there is no standard method for estimating the intensity of anisotrophic turbulence in the ocean.

Various instruments, such as the Turbulence Ocean Microstructure Acquisition Profiler (TurboMAP) (Wolk *et al.*, 2002), Vertical Microstructure Profiler (VMP) (Lueck *et al.*, 2013), Microstructure profilers MSS (ISW Wassermesstechnik) and Micro-Structure-Turbulence (MST) profiler (Prandke and Stips, 1998), use shear probes to detect small-scale velocity shear and can be used to measure the microstructure. The velocity shear is measured at frequencies of between 512 and 1024 Hz when the instrument is freely descending at a speed of between 0.5 and 0.6 m s^{-1}. Turbulence in the ECS has been measured mostly with microstructure profilers (*e.g.*, Matsuno *et al.*, 2005, 2006; Lee *et al.*, 2006; Liu *et al.*, 2009).

Acoustic Doppler velocimeters (ADV) or acoustic Doppler current profilers (ADCP) (*e.g.*, Lozovatsky *et al.*, 2008) have been used to make high resolution measurements of the turbulence intensity, particularly in the BBL. These instruments give high frequency measurements of the current velocity at a fixed point, and the shear produced is calculated from the fluctuations.

Instead of measuring the turbulence directly, vertical mixing processes can be evaluated in other ways, for example, by assessing temporal changes in the vertical structure, or by using chemical tracers. In this review, we will mainly consider vertical mixing that is related to direct measurements of turbulence.

1.4.3 Characteristics of mixing processes

Surface layer

Because of its strong relationship with the heat flux through the sea surface, the turbulence in the surface mixed layer has been investigated thoroughly. Even so, some aspects remain unclear and, for example, it would be beneficial to quantitatively evaluate the interactions between the

turbulence and the waves. The turbulence intensity in the surface layer controls the formation of the surface mixed layer (SML), which then influences the sea surface temperature (SST). Therefore, the heat flux through the sea surface is controlled by the turbulence intensity. The turbulence intensity in the SML may be determined by the buoyancy flux and wind stress at the sea surface. Because of the contribution it makes to air–sea interactions, the turbulence intensity in the SML of oceans worldwide has been studied extensively.

That said, the turbulence in the SML of the ECS has not been studied so intensively, perhaps because of the large spatial and temporal variabilities. For example, Liu *et al*. (2009) analyzed hourly measurements of the microstructure and found that diurnal variations in the turbulence intensity in the surface layer of the Yellow Sea (YS) were associated with nighttime convection and daytime stratification. However, this does not occur throughout the YS, and other studies reported that the turbulence intensity varied over shorter time scales, probably because of variations in wind effects over shorter time scales.

While the assumptions of the dissipation method proposed by Osborn (1980) may not be applied when describing the equilibrium of turbulent kinetic energy (TKE) in the ECS, we generally do still use this assumption. Endoh *et al*. (2014) discussed the contribution of the transport term in the equilibrium equation for TKE, based on direct measurements of ε and indirect estimations of the buoyancy flux and shear production. They assumed the temporal variation in the TKE was zero and showed, with measurements collected with Lagrangian tracking surface drifters, that the TKE transport term made a significant contribution to the equilibrium of the TKE.

Because of their influence on turbulent mixing in the surface layer in the ECS, typhoons are discussed in relation to air–sea interactions and primary production. The passage of a typhoon can cause surface divergence because of the cyclonic wind field and strong stirring of the surface layer. The former is caused by Ekman transport, in which the thickness of the Ekman layer depends on the vertical eddy viscosity, and the latter generates turbulent energy production. Both are related to the turbulence intensity. Hung *et al*. (2013) and Tsai *et al*. (2013) discussed how a typhoon influenced the cold dome to the northeast of Taiwan along with the interaction between the Kuroshio and topography. They showed that the passage of the typhoon resulted in upwelling of cold and high nutrient water by Ekman divergence, and also mentioned the contribution of vertical mixing. Elsewhere, using Argo float and satellite data, Siswanto *et al*. (2008) showed that primary production was enhanced when a typhoon passed. While they did not directly discuss vertical mixing in their study, they suggested that upwelling of high nutrient water driven by the typhoon made a significant contribution to primary production in the ECS. Moon and Kwon (2012) suggested that, when typhoons passed over the Yellow Sea Bottom Cold Water regions in the northern parts of the ECS and the YS, the intensity of the typhoon decreased significantly because of cooling at the surface induced by the vertical mixing and upwelling.

As mentioned earlier, it is important to determine the depth of the SML and the SST. Numerous researchers have examined the mixing processes in the surface layer with numerical models but few of these studies have been presented concerning the ECS. Huang *et al*. (2008) suggested that the influence of waves needed to be considered when determining the depth of the SML and showed that, by including wave-induced mixing, the estimates of the SST were more accurate.

Sub-surface layer

Since there is no direct influence of wind or bottom stress, vertical mixing in the interior of the ocean should be controlled by internal processes, such as the breaking of internal waves and/or Kelvin–Helmholtz instability. Early studies related to turbulence in the ECS mainly considered the

relationship between enhanced turbulence and shear instability in the intermediate layer and in the BML, and there were limited direct measurements of turbulence (Matsuno *et al*., 1997). After 2000, there were more opportunities to obtain microstructure measurements. Matsuno *et al*. (2006) used microstructure observations from July 2003 and July 2004 to show the structure of the turbulence intensity in the outer shelf region of the ECS, and summarized the turbulence intensity in the upper, intermediate, and bottom layers. As shown in Fig. 1.4.1, the range of the observed turbulence in the intermediate layer was wider than the ranges in the upper and bottom layers, which means that vertical mixing was enhanced intermittently, and this intermittent strong turbulence may have been related to the development of internal waves. They also observed that the turbulence was enhanced along a characteristic ray of internal tides around the shelf break of the central ECS (Matsuno *et al*., 2005).

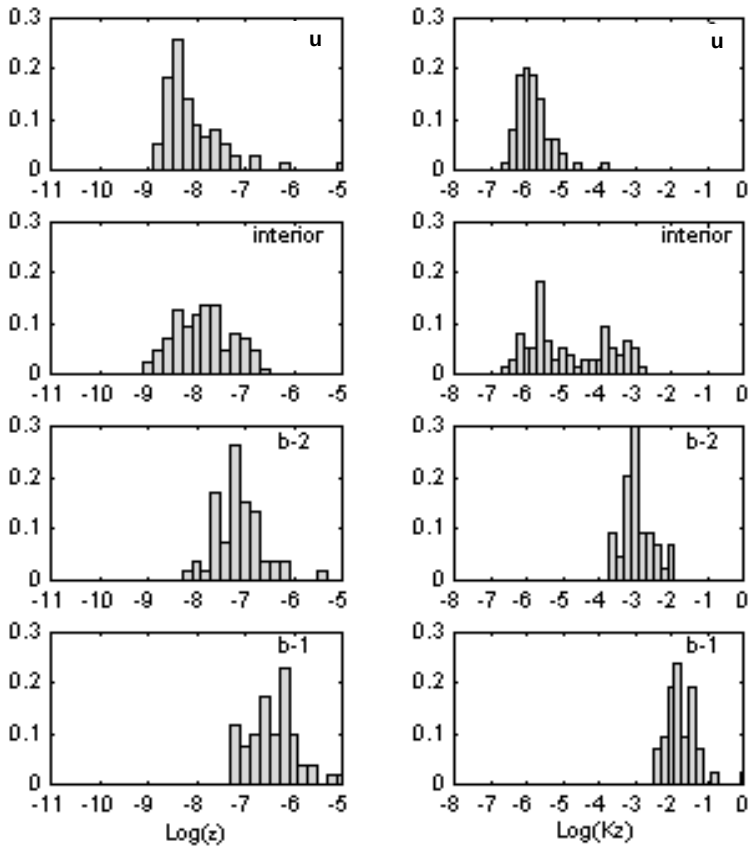

Fig. 1.4.1 Histograms showing the magnitude of turbulent dissipation rate, ε (left) and the vertical eddy diffusivity, K_z (right) in specified layers in the outer shelf region of the ECS in July 2004. The layers, u, b-2, and b-1 refer to the layer between 15 and 30 m below the surface, between 10 and 20 m above the bottom, and within 10 m of the bottom, respectively. From Matsuno *et al*. (2006). Reproduced with permission of Wiley & Sons.

Lee *et al*. (2006) observed short period nonlinear internal waves during a campaign on the shelf south of Jeju Island in August, 2005. While they were mainly interested in the evolution of internal solitary waves, they also found, by analyzing microstructure measurements, that the turbulence was intermittently intensified in the sub-surface. They found that the dissipation rate exceeded 10^{-7} W kg^{-1} around the pycnocline (Fig. 1.4.2), where K–H instability sometimes occurred, possibly associated with internal solitary waves. Liu *et al*. (2009) suggested that the internal waves influenced the turbulence intensity just below the pycnocline in the YS. While their observations showed that there was very small diffusivity within the pycnocline, the values of ε were relatively

large below the pycnocline, and may have been associated with internal waves propagated from a distance, as also reported by Lee *et al*. (2006). However, when the turbulence was enhanced around the pycnocline, there was no consistent aspect in the detailed structure of the turbulence intensity, that is, the turbulence may have been enhanced within the pycnocline in one case but may have been enhanced just above or below the pycnocline in other cases.

Other researchers have reported weak turbulence around the pycnocline. Wei *et al*. (2014) estimated the TKE dissipation rate and diffusivity in three seasons between 2006 and 2007 in the south YS and found that the vertical mixing tended to be more intensive in the near-surface and bottom layers than in the middle layer. They also showed that the pycnocline played an important role in preventing wind-induced mixing. They found that the mixing in summer was structured into two layers, one above and one below the pycnocline, and that the stratification inhibited the occurrence of shear instability and prevented vertical exchange across the pycnocline. The Yellow Sea Warm Current is a stable stratified current in which the mixing is quite weak. Enhanced mixing only occurs in the boundary of the warm current because of the shear instability. The depth of the upper mixed layer can be limited by the current in winter.

Lozovatsky *et al*. (2015), from their observations in August 2006 southwest of Jeju Island, also showed that the turbulence was intensified intermittently in the sub-surface layer in the shelf region of the ECS. They suggested that the ε was either negatively or positively correlated with the stratification, depending on the situation. When the stratification was relatively weak and was within the range $2 < N^2/N_0^2 < 6.3$, where N_0 was the standard buoyancy frequency in the deep ocean proposed by Garrett and Munk (1975) and $N_0 = 5 \times 10^{-3}$ s^{-1}, the relationship between ε and N^2 was clearly related with a power law $\varepsilon \sim (N^2)^{-3}$. This means that the turbulence was stronger when the stratification was weaker. However, when the stratification was stronger, internal waves tended to develop and break, resulting in intensified turbulence, so the relationship between ε and N^2 was positive, as proposed by Mackinnon and Gregg (2005). However, internal waves are not always generated under intensified stratification, and internal waves do not always break, which means that the relationship would only occasionally be positive, and it would be very difficult to give a universal description of the relationship between ε and N^2, at least in the shelf region.

Vertical mixing in the intermediate water changes the structure of the stratification and transports materials. From a biogeochemical perspective, vertical transport of materials is a very important process by which nutrients are supplied from dark lower layers to the upper euphotic zone. A subsurface chlorophyll maximum generally forms in the lower part of the euphotic zone. With the exception of the coastal region, nutrients are usually depleted in the surface layer of the ECS because the light is sufficiently intense, and a sub-surface chlorophyll maximum (SCM) forms with the nutrients supplied from the lower layer under dusky light conditions.

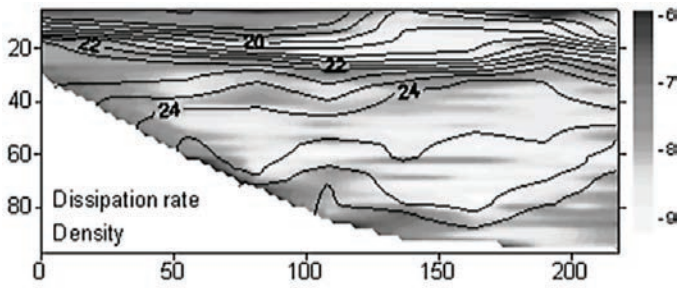

Fig. 1.4.2 Vertical distribution of ε (W kg^{-1}) shown on a log-scale along the northeast–southwest section south of Jeju Island. The gray-shaded plot of ε was overlain with contours of the specific potential density. The southwest end of the section is on the left. From Lee *et al*. (2006). Reproduced with permission of Wiley & Sons.

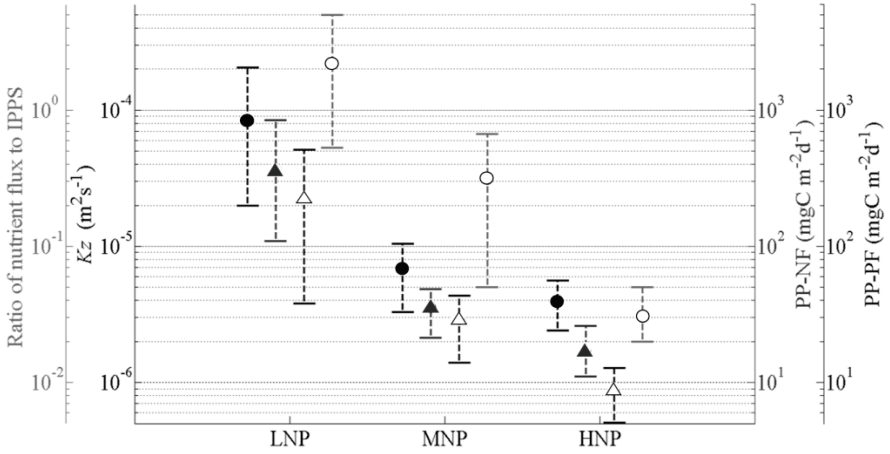

Fig. 1.4.3 Mean (marks) and 95% confidence interval (dotted line with two solid lines) of the vertical eddy diffusivity (K_z) (solid circle), primary production converted from the nitrate flux (solid triangle), primary production converted from the phosphate flux (open triangle), and the ratio of the nutrient flux to integrated primary production within the sub-surface chlorophyll maximum (open circle) for low, medium, and high Nitrogen/Phosphate ratios. From Lee *et al*. (2017). Reproduced with permission of Elsevier.

As mentioned above, nutrients may be supplied to the upper layer from the lower layer because of upwelling generated by divergence in the surface layer. However, SCM visible even in calm conditions suggests that there might be more frequent upward transport of nutrients. To evaluate the supply of nutrients to the SCM, we need to have a quantitative understanding of the vertical mixing around it. Using a relatively limited dataset of turbulence measurements from the eastern end of the ECS, Shiozaki *et al*. (2011) discussed how vertical fluxes of nutrients contributed to primary production. Recently, Lee *et al*. (2017) used cumulative data from the central part of the shelf region in the ECS to evaluate how vertical mixing helped to supply nutrients to the SCM. They showed that the nutrient supply to the SCM, because of vertical mixing, was notably large in some cases, but not in others, and that the difference was caused mainly by the magnitude of the vertical eddy diffusivity. As mentioned by Lozovatsky *et al.* (2015), large values for the eddy diffusivity around the pycnocline occurred intermittently, depending on the activities of internal waves. Lee *et al*. (2017) found that the large nutrient fluxes associated with intensified vertical mixing tended to correspond with low nitrogen/phosphorus (N/P) nutrient ratios around the SCM. When the N/P ratio was low, primary production in the SCM was thought to be supported by nutrients supplied from the lower layer via vertical mixing (Fig. 1.4.3). The N/P ratio may be a useful indicator of the nutrient sources, and low and high ratios may show whether the nutrients are from the lower layer or river discharge, respectively. The intensified turbulent mixing may transport nutrients from the lower layer into the SCM, and may be associated with the development and breaking of internal waves.

Bottom boundary layer

In shelf regions such as those in the ECS, the vertically well-mixed bottom boundary layer (BBL) commonly forms because of the force of strong tidal currents. Turbulence just above the sea floor also has a role in the formation of the BBL. Of all the mixing processes in the ECS, turbulence in the BBL has perhaps been studied most. In the shelf region of the ECS, noticeable periodicity caused by tidal motions may mean that the mixing processes show regular variations influenced by tidally variable bottom stress. Using time series of current velocity taken with a bottom-mounted ADV and ADCP on the inner shelf of the ECS, Lozovatsky *et al*. (2008) showed that there were clear variations in ε associated with tidal motion. They found that the TKE and ε were related in

both shallow and relatively deep areas in the YS; they also found that there was a different relationship under influence of convection in the deeper area (Fig. 1.4.4). They discussed the friction velocity that controls the mixing processes in the BBL and showed that, when the dissipation rate was scaled with the friction velocity, it was 50% larger for the rotating tidal currents than for reversing tidal currents at shallower sites near the coast.

By analyzing hourly repeated measurements made with a microstructure profiler, Liu *et al*. (2009) showed that there was temporal variation in the turbulence intensity in the BBL at shallow (38 m) and relatively deep (73 m) sites in the YS. The turbulence in the BBL was enhanced because of semi-diurnal tidal motions, and the well correlated relationship between the enhanced turbulence and the smaller values of the gradient Richardson number was shown using data obtained with a bottom-mounted ADCP at the shallow station. At the shallow station, the BBL was about 15 m thick and was mostly homogeneous; at the deep station, the BBL was thinner than at the shallow station, there was weak stratification, and turbulence seemed to be suppressed in the upper part of the BBL. Lozovatsky *et al*. (2015) discussed turbulence around the pycnocline and in the BBL in the shelf region south of Jeju Island. They suggested that ε decreased more quickly with the distance from the sea floor in a weakly stratified upper portion of the BBL compared with the homogeneous layer close to the sea floor.

We can gain an improved understanding of the turbulence processes by examining the weak stratification in the BBL. Yoshikawa *et al*. (2010) compared the shear production and ε from a time series of repeated measurements of microstructure with Lagrangian tracking of a drifting buoy in the shelf region of the ECS and showed that the production of buoyancy in the BBL was important. They mentioned that the eddy viscosity profile could provide useful insights into how Ekman dynamics changed in the BBL, and also showed that the turbulence intensity could affect the current velocity profiles in the bottom Ekman layer. They also found that the vertical profiles of the bottom Ekman spiral depended on the stratification, even when the BBL was weakly stratified.

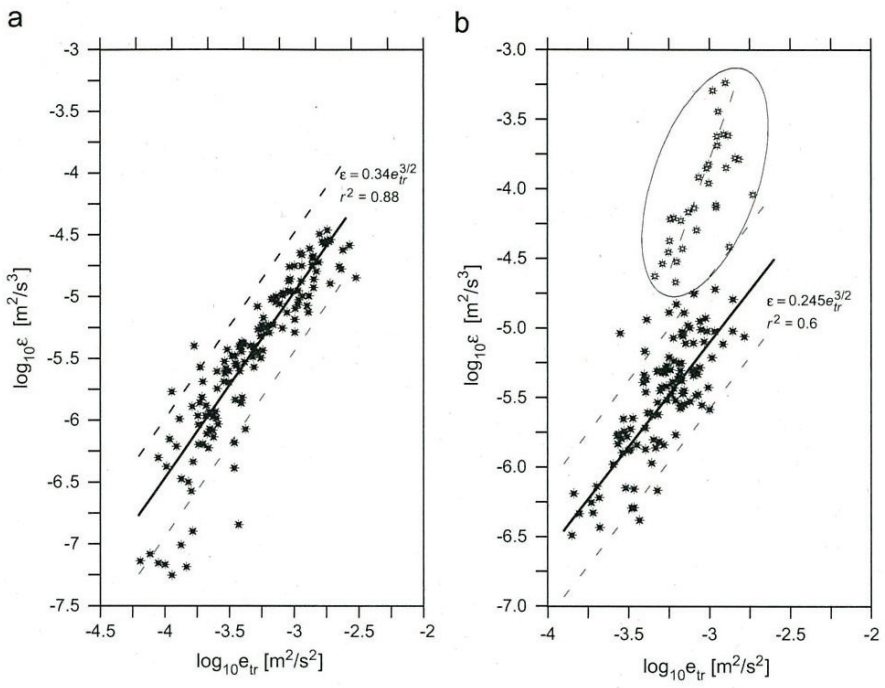

Fig. 1.4.4 Relationship between the turbulent kinetic energy (e_{tr}) and the ε in the bottom boundary layer at sites in (a) shallow and (b) relatively deep areas in the Yellow Sea, along with the relationship when the mixing was influenced by convection with advected warm water (open marks) in the deeper site. From Lozovatsky *et al*. (2008). Reproduced with permission of Elsevier.

The stratified structure of the BBL may be influenced by mixing processes associated with both the inclination of the bottom slope and the current direction. Endoh *et al*. (2016) found evidence for tidal straining, which is usually found in coastal waters or estuaries, even on the outer shelf of the ECS. They analyzed turbulence measurements and vertical profiles of the current velocity on the slightly inclined continental shelf and found that the stratification switched between unstable and stable with a semidiurnal period in the lower part of the BBL. This means that, where there was shear-induced convection (Lorke *et al*., 2005), the turbulence intensity just above the bottom depended on both the magnitude of the current and its direction. On the other hand, the turbulence intensity in the upper part of the BBL appeared to be related to the small diurnal variation in the stratification, which was caused by horizontal advection. The variation range of the bottom Ekman layer thickness was much larger for diurnal motion than for semidiurnal motion, which is why there was diurnal variation in the horizontal advection in the upper part of BBL. The energy dissipation rate was enhanced in the upper part of the BBL when the weakly stratified structure was advected with diurnal motion. The turbulence intensity around the BBL therefore strongly depends on stratification, even if the stratification is weak.

Turbulence in the BBL strongly affects the bottom stress, as observed by Lozovatsky *et al*. (2008, 2010). While the results of numerical models should be seriously influenced by the intensity of the bottom stress, most numerical models do not have enough vertical resolution to express the structure of the BBL in detail. From another perspective, the turbulence in the BBL is important to consider the resuspension of sediment, particularly in shallow areas. Yuan *et al*. (2008) deployed a bottom-mounted quadrapod equipped with an ADCP, ADV, and optical backscatter sensor (OBS) over two semidiurnal tidal cycles along the western coast of the YS. They combined these data with measurements from shipboard Conductivity-Temperature-Depth (CTD) profiling and a submersible laser-diffraction particle size analyzer (LISST-100), and constructed the temporal and spatial distributions of the tidal currents, TKE, suspended sediment concentration (SSC), and particle size distributions. The tidal-induced bottom shear stress was the main cause of stirring during the observations. The friction velocity was clearly related to both the SSC and particle size, as shown in Fig. 1.4.5.

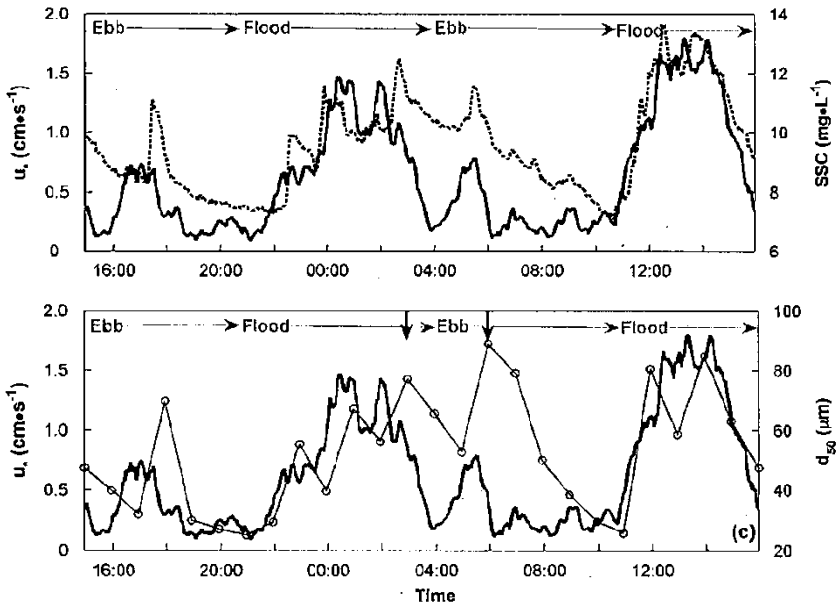

Fig. 1.4.5 Temporal variations in the friction velocity (solid lines), concentration of suspended sediment concentration; SSC (upper dotted line), and median size (d_{50}) (lower circles and line) of suspended sediments (SS) in the bottom boundary layer in a shallow area of the Yellow Sea. The SSC was estimated by calibrating the back-scattering intensity obtained from an Acoustic Doppler velocimeter set at 0.45 m above the sea floor. From Yuan *et al*. (2008). Reproduced with permission of Elsevier.

However, the weak tidal flow during the ebb phase was accompanied by two large- and median-sized SSC events. The interactions between seiche-induced oscillations and a weak ebb flow induced multiple flow reversals and provided a source of turbulence production which, in turn, stripped up the benthic fluff layers (only several millimeters). They also found that sediment was resuspended during the intermittent turbulent bursts and that the coherent structures were related to the sediment resuspension (Yuan *et al*., 2009). They found that most of the turbulent sediment flux was generated during 'ejection' (56%) and 'sweep' (42%) events, and that the contributions from outwards and inwards interactions were negligible. The wall turbulence containing coherent structures vertically transported momentum more efficiently than suspended sediments. By spectrally scaling the sediment concentration, they found that there were two types of suspended sediment clouds with different sizes during the peak flood. The large-sized particle clouds contained coarse sediments that were locally resuspended from the seabed, whereas the smaller particle clouds consisted of silts and clays, and acted as washload advected from Jiaozhou Bay and the YS by tidal flows. Finally, they found that wavelet transformations could provide a more intuitive way to study and visualize the relationship between the burst cycle and sediment suspension, and the results clearly showed that the intermittent Reynolds stress generation was accompanied by intense sediment resuspension.

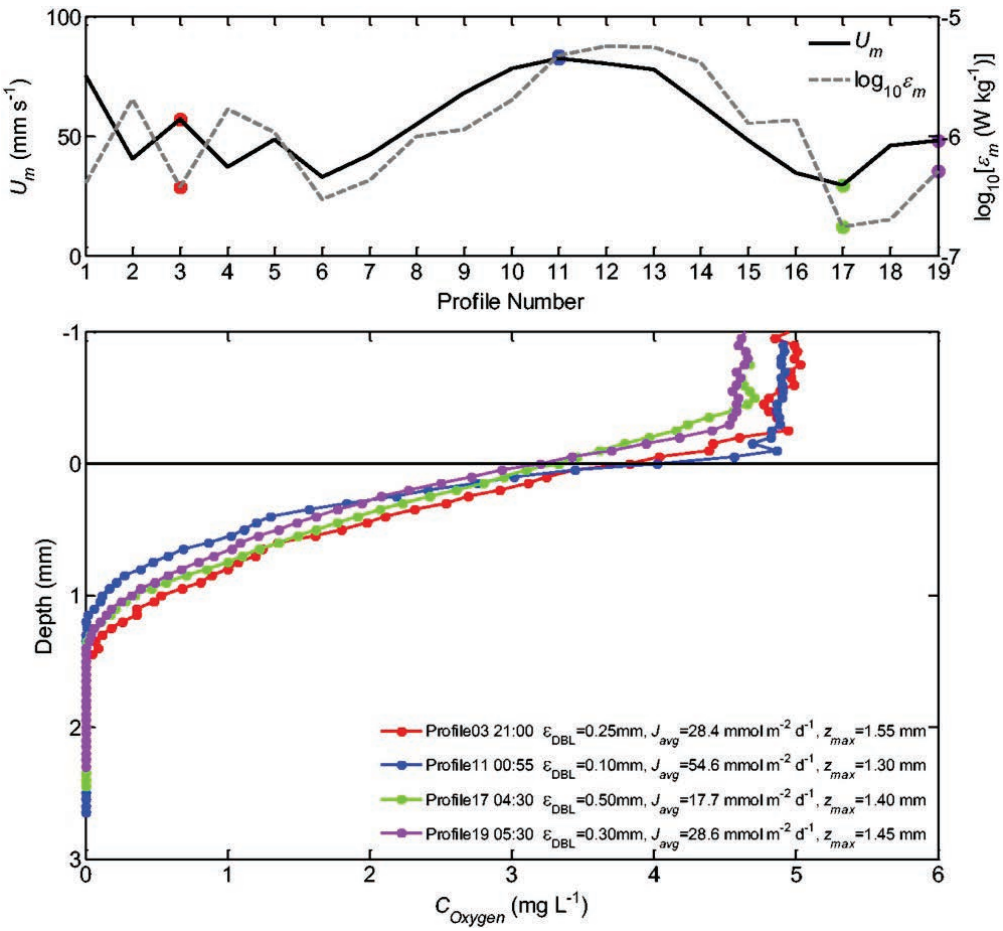

Fig. 1.4.6 (Top) Temporal variations in the current speed (U_m) and turbulent dissipation rate (ε_m) estimated with the friction velocity at 0.24 m above the seafloor obtained with Acoustic Doppler velocimeters set in a shallow area, 6.5 m deep, in the Bohai Bay. (Bottom) Vertical profiles of dissolved oxygen measured within very thin layers of water and sediments close to the seafloor (depth = 0 in the vertical axis), where the vertical resolution is 50 μm. From Wang *et al*. (2013). Reproduced with permission of Wiley & Sons.

Bian *et al*. (2013) surveyed the distribution of SSC over the extent of the YS and the ECS through four seasons and showed that the water in the surface layer in winter and spring was turbid and had a high SSC, reflecting the resuspension of sediments by intensified vertical mixing. The SSC was low in the surface layer during summer because resuspension of sediments was suppressed by stratification. The turbulence in the BBL therefore influenced the surface layer in the convective season, but not in the stratified season. Bian *et al*. (2013) also discussed the suspension of the sediment, and considered that wind-waves drove the sediment suspension in the coastal region, and that tidal motions were more important in the offshore region. In the BBL, SSC is mainly controlled by tidal motions and seasonal patterns are not so clear; further, upward movement of water with high SSC water is suppressed by stratification.

Wang *et al*. (2012, 2013, 2016) took *in situ* measurements of the DBL and BBL under different environmental and oxygen conditions at three sites in the coastal region of the ECS. As well as recording the usual suite of BBL variables, they measured oxygen concentration profiles with a Unisense Mini Profiler MP4 that was equipped with a Clark-type oxygen microsensor (OX25, Unisense A/S; Müller *et al*., 2002). Each oxygen profile had a vertical resolution of 50 μm, as shown in Fig. 1.4.6. Scaling methods for the DBL thickness (δ_{DBL}) rooted in the Batchelor length scale gave consistent dimensions for the three stations. They found that the method that represented the Batchelor length scale as a function of flow speed (U) was the most appropriate for scaling the δ_{DBL} when the law of the wall applied. The diffusive flux was controlled by the dynamic-forced δ_{DBL} and the difference in the oxygen concentration over the DBL (DC). Values of DC were scaled using the oxygen concentration of the BBL (CBBL) and the normalized benthic temperature. They developed a useful method for scaling the diffusive flux from measurements of the benthic temperature, salinity, U, CBBL, and estimates of the bottom roughness.

1.4.4 Concluding remarks

Researchers have made considerable progress in the area of vertical mixing in the YS and ECS since the 2000s. Studies have shown that vertical mixing is generally enhanced in the surface and bottom layers because of wind effects and tidal motions, but that the turbulence intensity is not always enhanced in the sub-surface layer. Various studies have suggested that the turbulence is enhanced intermittently around the pycnocline (Matsuno *et al*., 2006; Lozovatsky *et al*., 2015), perhaps because of the activities of internal waves. Shear instability associated with the breaking of internal waves might occur intermittently. Liu *et al*. (2009) found that there were large vertical variations in the eddy diffusivity K_z around the pycnocline, that is, the K_z was very small within, but was large just below, the pycnocline. It is very important to note that stratification is strongly related to the distribution of the turbulence intensity, and this occurs not only around the pycnocline, but also under weak stratification in the SML and BBL.

The relationship between the turbulence intensity and stratification is difficult to understand because stratification not only contributes to, but is also a result of, turbulent mixing. Given that the shear instability may cause enhanced turbulence, strong mixing might occur when the gradient Richardson number is small, which means the turbulence intensity should be negatively correlated with the stratification. However, as mentioned by Lozovatsky *et al*. (2015), even in the ECS, the turbulence intensity was positively correlated with the stratification in some cases, which suggests that it follows the parameterization of Mackinnon and Gregg (2005). The fact that the internal wave fields in the ECS were not fully developed, as expressed by the model of Garrett and Munk (1975), probably reflects various complicated boundary conditions. It would therefore be difficult to propose a universally applicable parameterization; instead, some specialized parameterizations that are specific to individual conditions would need to be developed so that the mixing processes in the ECS can be quantitatively evaluated.

1.4.5 Future work

We may have two issues for future research on turbulent mixing in the ECS. One is the relationship between the stratification and turbulence intensity, and the other is the contribution of surface waves. The former is strongly related to internal waves. The most mysterious and challenging issue relevant to mixing processes in the ECS would be the relationship between turbulence intensity and internal waves. As mentioned above, turbulence intensity in the subsurface has large variability, where a significant part of the large variability would be caused by the intermittent occurrence of internal waves. However, the behavior of internal waves has not been fully determined in this region, particularly their dissipation processes, which should be connected to mixing processes. Therefore, a full understanding of the internal wave activities, including internal tides and shorter time scale internal waves, would be one of the important issues for future work.

Another issue for future research is understanding the role of vertical mixing in the thermohaline fronts, especially in the northern ECS where the lateral intrusive structure in salinity or temperature appears frequently in the depth below the thermocline. Lateral intrusion in the front itself is indicative of the mixing process but no (repeated) observation has been conducted yet. A quantitative understanding of the frontal mixing is important to examine the material exchange across the front in the region.

Measurements of Reynolds stress could be important to evaluate the turbulence intensity because it determines the turbulence production. However, high frequency current velocity fluctuations contains not only turbulence but also (surface) waves, and turbulence intensity could depend partly on waves. It is an important issue for future work in identifying the contribution of waves after distinguishing wave motion from direct measurements of high frequency current velocity fluctuations.

Quantitative understanding of the contribution of internal and surface waves to the mixing processes must improve the parameterization for the vertical mixing, which should be formulated, depending on various situations, as mentioned above. The parameterization to shelf mixing under different conditions or different regions should be one of the most important future works, while linkages to theoretical and numerical studies are necessary.

Furthermore, as mentioned earlier, we did not discuss horizontal mixing in this review, mainly because horizontal mixing processes have rarely been observed *in situ* in the ECS and YS. However, we have frequently observed horizontal intrusion of low salinity and low temperature water into the sub-surface in the shelf region of the ECS, which probably affects the formation of the water masses and the biological environment in this region. Horizontal mixing processes should be quantitatively evaluated, and future studies should consider both horizontal and vertical mixing processes.

Acknowledgements

We thank Deborah Ballantine, PhD, from Edanz Group (www.edanzediting.com/ac) for editing a draft of this manuscript.

1.4.6 References

Bian, C., Jiang, W., Quan, Q., Wang, T., Greatbatch, R. and Li, W. 2013. Distributions of suspended sediment concentration in the Yellow Sea and the East China Sea based on field surveys during the four seasons of 2011. *J. Mar. Syst.* **121–122**: 24–35, doi:10.1016/j.jmarsys.2013.03.013.

Endoh, T., Matsuno, T., Yoshikawa, Y. and Tsutsumi, E. 2014. Estimates of the turbulent kinetic energy budget in the oceanic convective boundary layer. *J. Oceanogr.* **70**: 81–90, doi:10.1007/s10872-013-0215-3.

Endoh, T., Yoshikawa, Y., Matsuno, T., Wakata, Y., Lee, K.-J. and Umlauf, L. 2016. Observational evidence for tidal straining over a sloping continental shelf. *Cont. Shelf Res.* **117**: 12–19, doi:10.1016/j.csr.2016.01.018.

Garrett, C. and Munk, W. 1975. Space-time scales of internal waves: A progress report. *J. Geophys. Res.* **80**: 291–297, doi:10.1029/JC080i003p00291.

Gregg, M.C. 1987. Diapycnal mixing in the thermocline. A review. *J. Geophys. Res.* **92**: 5249–5286, doi: 10.1029/JC092iC05p05249.

Huang, C., Qiao, F. and Song, Z. 2008. The effect of the wave-induced mixing on the upper ocean temperature in a climate model. *Acta Oceanol. Sin.* **27**: 104–111.

Hung, C.C., Chung, C.C., Gong, G.C., Jan, S., Tsai, Y., Chen, K.-S., Chou, W.C., Lee, M.-A., Chang. Y., Chen, M.-H., Yang, W.-R., Tseng, C.-J. and Gawarkiewicz, G. 2013. Corrigendum to "Nutrient supply in the southern East China sea after typhoon Morakot". *J. Mar. Res.* **71**: 133–150, doi: 10.1357/002224013812587609.

Lee, J.H., Lozovatsky, I., Jang, S.-T., Jang, C.J. and Hong, C.S. 2006. Episodes of nonlinear internal waves in the northern East China Sea. *Geophys. Res. Lett.* **33**: L18601, doi:10.1029/2006GL027136.

Lee, K.-J., Matsuno, T., Endoh, T., Ishizaka, J., Zhu, Y., Takeda, S. and Sukigara, C. 2017. A role of vertical mixing on nutrient supply into the subsurface chlorophyll maximum in the shelf region of the East China Sea. *Cont. Shelf Res.* **143**: 139–150, doi:10.1016/j.csr.2016.11.001.

Liu, Z., Wei, H., Lozovatsky, I. and Fernando, H. 2009. Late summer stratification, internal waves, and turbulence in the Yellow Sea. *J. Mar. Syst.* **77**: 459–472, doi:10.1016/j.jmarsys.2008.11.001.

Lorke, A., Peters, F. and Wüest, A. 2005. Shear-induced convective mixing in bottom boundary layers on slopes. *Limnol. Oceanogr.* **50**: 1612–1619, doi:10.4319/lo.2005.50.5.1612.

Lozovatsky, I., Liu, Z., Wei, H. and Fernando, H.J.S. 2008. Tides and mixing in the northwestern East China Sea, Part II: Near-bottom turbulence. *Cont. Shelf Res.* **28**: 338–350, doi:10.1016/j.csr.2007.08.007.

Lozovatsky, I., Roget, E., Planella, J., Fernando, H.J.S. and Liu, Z. 2010. Intermittency of near-bottom turbulence in tidal flow on a shallow shelf. *J. Geophys. Res.* **115**: C05006, doi:10.1029/2009JC005325.

Lozovatsky, I., Jinadasa, S.U.P., Fernando, H.J.S., Lee, J.-H. and Hong, C.S. 2015. The wall-layer dynamics in a weakly stratified tidal bottom boundary layer. *J. Mar. Res.* **73**: 207–232, doi: 10.1357/002224015817391276.

Lueck, R., Wolk, F. and Black, K. 2013. Measuring tidal channel turbulence with a Vertical Microstructure Profiler (VMP). Rockland Scientific International, Partrac Ltd., Technical Note TN-026.

Mackinnon J. and Gregg, M.C. 2005. Near-inertial waves on the New England Shelf: The role of evolving stratification, turbulent dissipation, and bottom drag. *J. Phys. Oceanogr.* **35**: 2408–2424, doi:10.1175/JPO2822.1.

Matsuno, T., Hibiya, T., Kanari, S. and Kobayashi, C. 1997. Small scale internal waves and turbulent fluctuations near the continental shelf break in the East China Sea. *J. Oceanogr.* **53**: 259–269.

Matsuno, T., Shimizu, M., Morii, Y., Nishida, H. and Takaki, Y. 2005. Measurements of the turbulent energy dissipation rate around the shelf break in the East China Sea. *J. Oceanogr.* **61**: 1029–1037, doi:10.1007/s10872-006-0019-9.

Matsuno, T., Lee, J.-S., Shimizu, M., Kim, S.-H., Pang, I.-C. 2006. Measurements of the turbulent energy dissipation rate ε and an evaluation of the dispersion process of the Changjiang Diluted Water in the East China Sea. *J. Geophys. Res. Oceans* **111**: C11S09, doi:10.1029/2005JC003196.

Moon, I.-J. and Kwon, S.J. 2012. Impact of upper-ocean thermal structure on the intensity of Korean peninsular landfall typhoons. *Prog. Oceanogr.* **105**: 61–66, doi:10.1016/j.pocean.2012.04.008.

Müller, B., Maerki, M., Dinkel, C., Stierli, R. and Wehrli, B. 2002. In situ measurements in lake sediments using ion-selective electrodes with a profiling lander system, pp. 126–143 *in:* Environmental Electrochemistry *edited by* M. Taillefert and T.F. Rozan, American Chemical Society, doi:10.1021/bk-2002-0811.fw001.

Osborn, T.R. 1980. Estimates of the local rate of vertical diffusion from dissipation measurements. *J. Phys. Oceanogr*. **10**: 83–89, doi:10.1175/1520-0485(1980)010<0083:EOTLRO>2.0.CO;2.

Prandke, H. and Stips, A. 1998. Test measurements with an operational microstructure-turbulence profiler: Detection limits of dissipation rates. *Aquat. Sci.* **60**: 191–209, doi:10.1007/s000270050036.

Shiozaki, T., Furuya, K., Kurotori, H., Kodama, T., Takeda, S., Endoh, T., Yoshikawa, Y., Ishizaka, J. and Matsuno, T. 2011. Imbalance between vertical nitrate flux and nitrate assimilation on a continental shelf: Implications of nitrification. *J. Geophys. Res.* **116**: C10031, doi:10.1029/2010JC006934.

Siswanto, E., Ishizaka, J., Morimoto, A., Tanaka, K., Okamura, K., Kristijono, A. and Saino, T. 2008. Ocean physical and biogeochemical responses to the passage of Typhoon Meari in the East China Sea observed from Argo float and multiplatform satellites. *Geophys. Res. Lett.* **35**: L15604, doi:10.1029/2008GL035040.

Tsai, Y., Chern, C.-S., Jan, S. and Wang, J. 2013. Numerical study of cold dome variability induced by typhoon Morakot (2009) off Northeastern Taiwan. *J. Mar. Res.* **71**: 109–132, doi:10.1357/002224013807343434.

Wang, J., Zhao, L. and Wei, H. 2012. Variable diffusion boundary layer and diffusion flux at sediment-water interface in response to dynamic forcing over an intertidal mudflat. *Chin. Sci. Bull.* **57**: 1568–1577, doi:10.1007/s11434-012-4988-3.

Wang, J., Wei, H., Lu, Y. and Zhao, L. 2013. Diffusive boundary layer influenced by bottom boundary hydrodynamics in tidal flows. *J. Geophys. Res. Oceans* **118**: 5994–6005, doi:10.1002/2013JC008900.

Wang, J., Zhao, L., Fan, R. and Wei, H. 2016. Scaling relationships for diffusive boundary layer thickness and diffusive flux based on in situ measurements in coastal seas. *Prog. Oceanogr.* **144**: 1–14, doi:10.1016/j.pocean.2016.03.001.

Wei, C., Yu, F., Guo, J. and Diao, X. 2014. Seasonal variation of ocean turbulence in the western Yellow Sea. *Oceanol. Limnol. Sin.* **45**: 166–171 (in Chinese).

Wolk, F., Yamazaki, H., Seuront, L. and Lueck, R.G. 2002. A new free-fall profiler for measuring biophysical microstructure. *J. Atmos. Ocean. Technol.* **19**: 780–793, doi:10.1175/1520-0426(2002)019<0780:ANFFPF>2.0.CO;2.

Yoshikawa, Y., Endoh, T., Matsuno, T., Wagawa, T., Tsutsumi, E., Yoshimura, H. and Morii, Y. 2010. Turbulent bottom Ekman boundary layer measured over a continental shelf. *Geophys. Res. Lett.* **37**: L15605, doi:10.1029/2010GL044156.

Yuan, Y., Wei, H., Zhao, L. and Jiang, W. 2008. Observations of sediment resuspension and settling off the mouth of Jiaozhou Bay, Yellow Sea. *Cont. Shelf Res.* **28**: 2630–2643, doi:10.1016/j.csr.2008.08.005.

Yuan, Y., Wei, H., Zhao, L. and Cao, Y. 2009. Implications of intermittent turbulent bursts for sediment resuspension in a coastal bottom boundary layer: A field study in the western Yellow Sea, China. *Mar. Geol.* **263**: 87–96, doi:10.1016/j.margeo.2009.03.023.

1.5 Atmosphere–Ocean Interaction

Atsuhiko Isobe

Research Institute for Applied Mechanics, Kyushu University, Japan

1.5.1 Introduction

The “atmosphere–ocean interaction (air–sea interaction)” has been defined as a group of two-way coupling processes. Oceanic processes such as sea surface temperature (SST) field modify atmospheric processes such as sea surface winds and pressure fields, while the modified atmosphere again modifies the ocean in a feedback loop. However, unlike the ENSO event on a planetary scale, spatio-temporal scales are quite different between atmospheric and oceanic processes on the regional scale. Thereby, it seems unlikely to accomplish the two-way processes in a conventional manner over the Yellow and East China Sea shelves. Nonetheless, oceanic processes over shallow shelves are always vulnerable to atmospheric processes via momentum and/or heat fluxes through the sea surface, and thus, two-way coupling processes may occur if oceanic processes on the shelves modify the atmosphere. In this section, we start with the discussion on whether or not the Yellow and East China seas can modify extratropical cyclones on a sub-weekly timescale, one of the most energetic atmospheric processes over these shelves (subsection 1.5.2). Thereafter, two-way coupling processes longer than on a sub-weekly timescale are discussed in the subsection 1.5.3.

1.5.2 Two-way coupling process related to extratropical cyclones

The development of winter extratropical cyclones over warm oceans in a relatively short period (typically 2 to 3 hPa/6 h of surface pressure falls; Gulev *et al*., 2001) has been an important scientific topic in both meteorology and oceanography from a viewpoint of atmosphere–ocean interaction. In particular, many meteorologists have quantitatively estimated characteristics of the cyclone life cycle, including deepening rate. Warm ocean currents make conditions favorable for the formation of storm tracks in winter (Hoskins and Valdes, 1990). Thus, 50% of rapidly developing (faster than 6 hPa/6 h) cyclones are generated over the Gulf Stream or the Kuroshio in the Northern Hemisphere (Gulev *et al*., 2001). In fact, synoptic and sub-weekly-scale variability with a period of 2 to 6 days is prominent over these western boundary currents, in both standard deviation maps of 500 hPa geopotential height (Gulev *et al*., 2002) and sea surface heat flux (Zolina and Gulev, 2003). One may also refer to composite maps of intensive sea surface heat flux within an individual extratropical cyclone in Rudeva and Gulev (2011). The above statistics of extratropical cyclone deepening may have uncertainties because of various reanalysis datasets used in the studies. Nevertheless, recent intercomparison (Allen *et al*., 2010; Hodges *et al*., 2011) shows the similarity of cyclone occurrence in multiple reanalysis datasets, at least in the Northern Hemisphere.

Many publications indicate that winter extratropical cyclones deepen explosively over East Asia (*e.g.*, Chen *et al.*, 1991) as well as the Gulf Stream region. Rapid deepening of extratropical cyclones is reasonable because sub-weekly-scale baroclinic wave activity, with intra-seasonal, interannual, and decadal variations, is energetic over East Asia (Nakamura, 1992; Nakamura *et al.*, 2002), and because warm SST is sustained by intense horizontal heat transport by warm ocean currents such as the Kuroshio and Tsushima Current (Chen *et al.*, 1992). In fact, Yamamoto and Hirose (2007) used a numerical model approach with a high resolution SST field at the lower boundary to show that cyclogenesis is significantly enhanced north of Japan's islands. They asserted the primary importance of lower-level baroclinicity, enhanced by a sharp horizontal SST gradient for activation of winter extratropical cyclones. Furthermore, based on a long-term reanalysis dataset (JRA-25, Onogi *et al.*, 2007), Yoshiike and Kawamura (2009) found that the enhanced baroclinicity in the lower troposphere indeed intensifies winter extratropical cyclones north of Japan, especially during strong monsoon periods.

The oceanic influence of the Yellow and East China seas on the deepening of winter extratropical cyclones may be comparable with that in the area north of Japan, because both areas are at mid-latitudes between 30° and 50°N, with zonal width *O*(1000 km) sufficient for extratropical cyclone development. In addition to this geographical similarity, relatively high SST with sharp horizontal gradient is maintained in both areas, even in midwinter. Figure 1.5.1 shows a winter SST map averaged using 5-km resolution cloudless SST images (Isobe and Kako, 2012), in which infrared and microwave observations from multiple satellites are synthesized by the New Generation Sea Surface Temperature (NGSST) research group at Tohoku University (Guan and Kawamura, 2004).

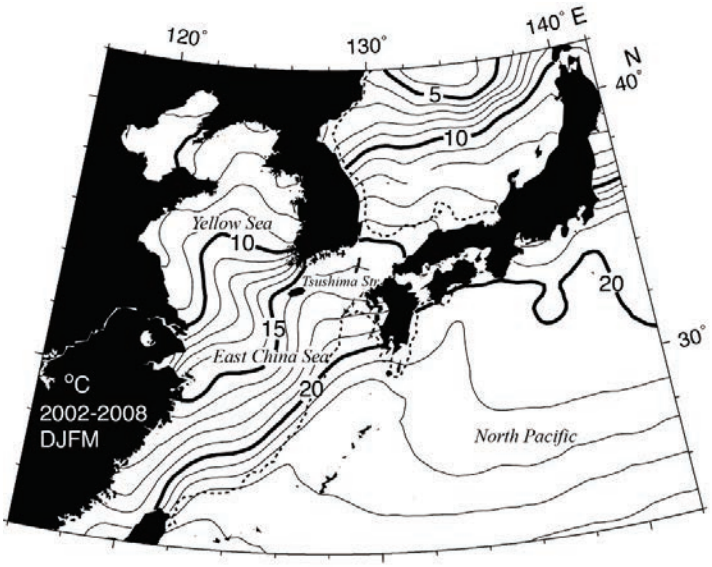

Fig. 1.5.1 Study area. Regional atmospheric model domain of this study is represented by the area surrounded by the bold line. The contour map denotes SST averaged over winters (December–March) from 2002 to 2008 in the area. Contour interval is 1°C. Dotted line is 200-m isobaths for indicating the shelf-break locations. Redrawn from Isobe and Kako (2012). ©American Meteorological Society. Used with permission.

Meteorological studies suggest, however, that the activity of winter extratropical cyclones over the Yellow and East China seas may be very different from that north and south of Japan, although this difference has received little attention. For instance, a well-known map of winter cyclone frequency within 5° boxes over the North Pacific (Figure 1 of Gyakum *et al.* (1989)) shows that surface cyclones are less common over the Yellow and East China seas in comparison with other

extratropical Pacific regions. Figure 1(b) in Yoshida and Asuma (2004) indicates that positions where extratropical cyclones develop faster than 1 bergeron are sparse in the Yellow and East China seas, suggesting that extratropical cyclones are prevented from developing in these areas. Based on 5° resolution surface pressure maps, however, Hanson and Long (1985) mentioned that winter cyclogenesis tends to be active above the Kuroshio in the East China Sea. Likewise, Xie *et al*. (2002) used a regional atmospheric numerical model to demonstrate that an extratropical synoptic-scale cyclone developed rapidly in February 2001 along the East China Sea shelf break, where lower-level baroclinicity is enhanced above the Kuroshio (see Figure 5 in Yoshiike and Kawamura (2009)).

Are the Yellow and East China seas favorable for extratropical cyclone development in winter? Both the objectively analyzed and reanalysis datasets are no doubt powerful tools for investigating extratropical mesoscale cyclones over the western North Pacific (*e.g.*, Yoshida and Asuma, 2004; Yoshiike and Kawamura, 2009). Nevertheless, horizontal resolution larger than 1° in both latitude and longitude (*e.g.*, 1.25° in the case of JRA-25) might still be too coarse for distinguishing oceanic influences of each East Asian marginal sea on cyclone activity. This is because their zonal scales are *O*(1000) km, and because horizontal scales of SST fronts and eddies are an order of magnitude smaller. In fact, Yamamoto and Hirose (2007) used the Pennsylvania State University/National Center for Atmospheric Research mesoscale model (MM5V3; Grell *et al*., 1994) with 10-km (~1/12°) grid cells to investigate the dependency of cyclogenesis on the sharpness of SST fronts in the model domain.

Isobe and Kako (2012) used Quick Scatterometer (QuikSCAT) data to investigate lower-troposphere vorticity fields with 0.25° resolution over the study area. Furthermore, using the NGSST dataset with SST condition at the finest resolution, they conducted numerical model experiments using MM5V3 at 12-km resolution to explore atmospheric and/or oceanic conditions favorable for extratropical cyclone development over the Yellow and East China seas. Standard deviations of the high-pass-filtered vorticity derived from the QuikSCAT data were computed at each grid cell over six winters (2002–2008) by removing low-frequency fluctuations with a 7-day box-car filter in each winter (Fig. 1.5.2).

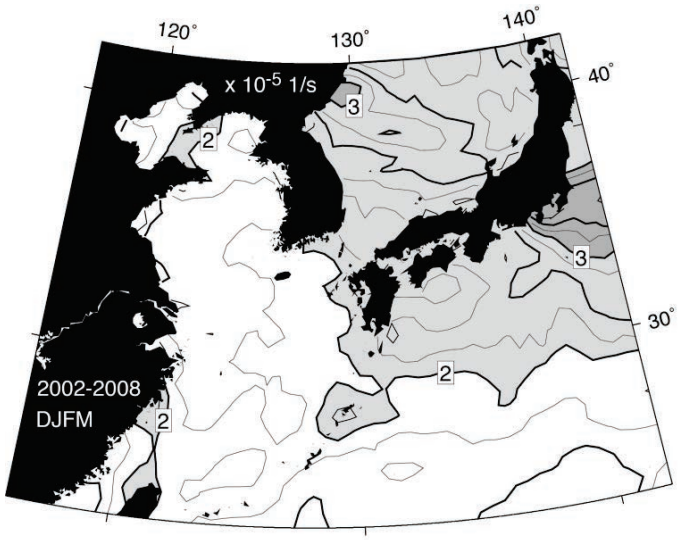

Fig. 1.5.2 Standard deviation map of sub-weekly-scale vorticity fluctuations computed from QuikSCAT-derived surface winds. Standard deviation was computed using vorticity high-pass filtered by a 7-day box filter over six winters from 2002 to 2008. Contour interval is 0.5 hPa. From Isobe and Kako (2012). ©American Meteorological Society. Used with permission.

This satellite-derived vorticity field demonstrates that, on average, extratropical cyclone activity is moderate over the warm Yellow and East China seas in winter. This is because enhanced lower-level baroclinicity (measured by the modeled gradient of equivalent potential temperature (EPT) at 925 hPa height) over these ocean areas is transferred as far as the shelf beak of the East China Sea by strong northwesterly surface winds (Fig. 1.5.3a). It seems that the disappearance of the areas with high baroclinicity over the Yellow and East China seas results from prevailing spatially homogeneous northwesterlies because of the absence of high mountains surrounding these areas. However, based on the numerical model results, it is found that the lower-level baroclinicity is enhanced over the Yellow and East China seas only when northwesterly surface winds weaken (Fig. 1.5.3b). Moderate winds are therefore required in the Yellow and East China seas for maintaining an oceanic influence on the atmospheric planetary boundary layer, and for enhancing cyclone activity in winter.

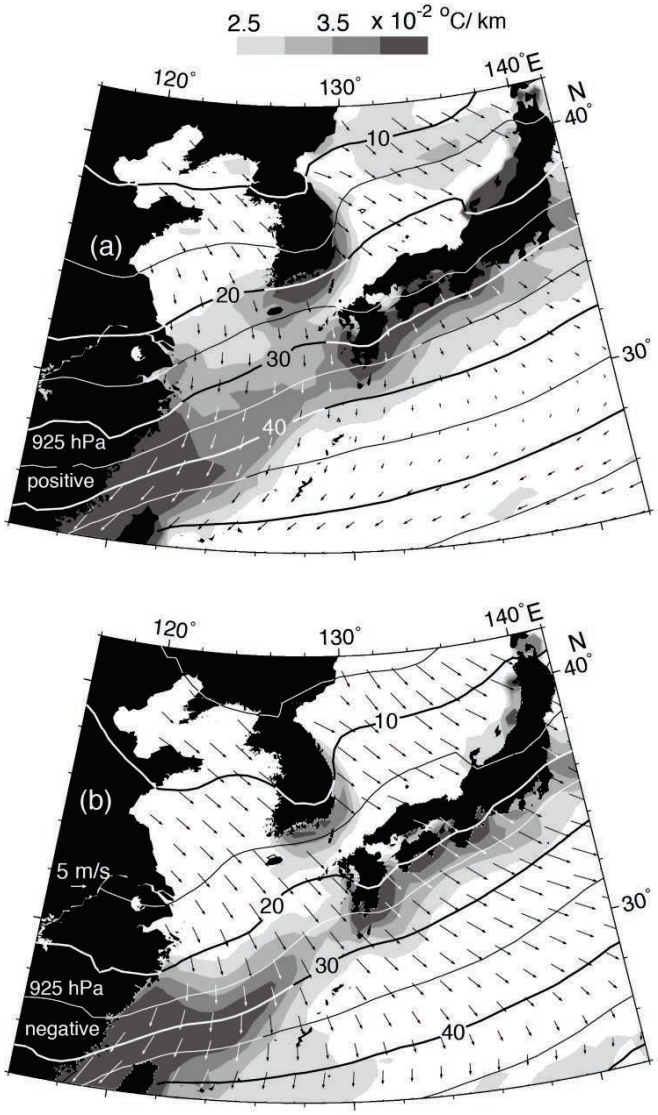

Fig. 1.5.3 Horizontal distribution of modeled equivalent potential temperature (EPT) at 925 hPa height (solid curves) along with its horizontal gradient depicted by shading. The two panels are shown in the (a) positive and (b) negative phases from the temporal mean of the EPT time series averaged over a box (30–36°N, 122–126°E) in the Yellow Sea. Contour interval of EPT is 5°C, and scale of shading is at the top of figures. Also shown are wind vectors at every tenth grid in each phase. All modeled data used here were low-pass-filtered by a 7-day box filter. From Isobe and Kako (2012). ©American Meteorological Society. Used with permission.

As well as winter cyclones, a two-way coupling process is accomplished in spring in the East China Sea. Kueh and Lin (2015) found that the springtime development of the Taiwan low depends on the preconditioning caused by the passage of a cold front and related cold-air outbreak. Using a regional atmosphere–ocean coupled model, they demonstrated that the strong wind during a cold-air outbreak results in SST lowered around the East China Sea shelf break owing to vertical mixing and retreat of the Kuroshio, and that the Taiwan low becomes stagnant over the upper ocean with the reduced heat content.

1.5.3 Two-way coupling processes longer than on a sub-weekly timescale

As mentioned above, lower-level baroclinicity (and hence, cyclone development) is activated owing to the SST gradient over the winter in the Yellow and East China seas, while the areas with high baroclinicity depend strongly on the northwesterly winter monsoon. In spring, the Taiwan low becomes stagnant because the SST is lowered by the cold-air outbreak. Although they are indeed an atmosphere–ocean interaction, their two-way processes are significant only during the passage of extratropical cyclones over the seas. We next examine atmosphere–ocean interaction maintained in the Yellow and East China seas, at least, over the intraseasonal timescale.

It is frequently found that surface winds are positively correlated with both SST and its gradient. This is partly because of vertical momentum mixing within the atmospheric boundary layer (Wallace *et al*., 1989), and partly because of the adjustment of the sea level pressure (SLP) above sharp oceanic fronts (Lindzen and Nigam, 1987), although a negative correlation was transiently observed at the onset of a cold-air outbreak over the warm Kuroshio in the East China Sea (Kasamo *et al*., 2014). Recent advances in satellite observations have revealed how ocean winds are modified above oceanic fronts on horizontal scales much smaller than typical atmospheric processes (*e.g*., Chelton *et al*., 2001; Nonaka and Xie 2003; Vecchi *et al*., 2004). For instance, Chelton *et al*. (2001) developed a quantitative procedure to examine the vertical mixing mechanism of winds modified by oceanic tropical instability waves, and showed that the perturbed wind stress curl (divergence) is linearly proportional to the crosswind (downwind) gradient of perturbed SST. Based on analyses of satellite microwave measurements over the North Pacific, Nonaka and Xie (2003) found a positive correlation between SST and wind speeds over the intense Kuroshio and Kuroshio Extension, whereas the correlation that is usually observed between these two properties is negative, especially above weak currents south of the Aleutian low. Furthermore, Vecchi *et al*. (2004) showed that low (high) wind velocities are observed over cold (warm) SST areas in the western Arabian Sea. As described above, a positive SST–wind correlation, which suggests an active influence of the mid-latitude ocean on the atmosphere, has been detected by satellite in various regions of the world.

In the Yellow and East China seas during winter, oceanic influences on atmospheric processes are likely to occur because, even in mid-winter, relatively warm water originating from the Kuroshio spreads over the sea surface, and because vertical momentum/heat transfer is enhanced by the cool, dry northerly monsoon winds prevailing over these warm seas at this time. In fact, Xie *et al*. (2002) showed a positive correlation between surface winds and SST over the winter in the Yellow and East China seas using wind speeds observed by the QuikSCAT/Seawinds and SST observed by the Tropical Rain Measuring Mission satellite’s microwave imager.

Meanwhile, in both conventional oceanography and meteorology, it has been considered that SST is passively influenced by the atmosphere via surface heat flux. In addition, the surface momentum flux, which drives ocean currents, also alters SST fields by the horizontal advection of heat. In fact, these processes of atmospheric forcing have a significant impact on the oceanic condition over the

Yellow Sea and East China Sea shelves because most of the area is shallower than 100 m. Xie *et al*. (2002) demonstrated that isotherms appear to lie parallel with isobaths over the Yellow Sea and East China Sea shelves in winter because shallow areas become much cooler owing to the smaller heat content compared with deeper areas. In addition, Hsueh (1988) and Isobe (2008) showed that strong northerly (southward) wind events over the Yellow Sea are followed by the occurrence of northward counter-wind ocean currents 1 to 2 days later. Thereafter, this northward ocean current alters the SST field in the Yellow Sea, as shown by Lie *et al*. (2001).

As mentioned above, the relatively warm Yellow and East China seas beneath the cool and dry air might play an active role in altering the wind field during winter, whereas the SST field must be altered passively due to the intense northerly winter monsoon winds prevailing over the seas. Different from the tropics, where a well-known interaction such as Bjerknes feedback exists on the ENSO timescale, the difficulty in accomplishing two-way processes in mid-latitude shelf seas stems from the considerably different spatio-temporal scales between oceanic and atmospheric processes. Note that the most energetic signal in the SST field in shallow shelf seas is the seasonal (regional) signal, whereas sub-weekly (synoptic) and monsoonal (planetary) signals are the more energetic in the wind field.

The most reliable method to find two-way oceanic and atmospheric processes longer than on a sub-weekly timescale is probably the regional atmosphere–ocean coupled model approach, corroborated by observed datasets. For instance, a regional coupled model developed by Fang *et al*. (2010) demonstrated that SST bias was revealed between the coupled and uncoupled (ocean general circulation) model owing to the mismatch of the surface heat flux. Also, in a recent study done by Iwasaki *et al*. (2014), both coupled and uncoupled models were built in order to compare their results with synthesized satellite-derived SSTs, and to evaluate how effective the coupled model was in reproducing the SST variability actually observed in the Yellow and East China seas in winter. Results of their study showed negative feedback between monsoon winds and SST in coastal waters during winter.

A regional atmosphere–ocean coupled model (Fig. 1.5.4) was developed by Iwasaki *et al*. (2014), based on the MM5V3 in conjunction with the Princeton Ocean Model (POM; Mellor, 2003), to investigate atmosphere–ocean interaction that might occur over the Yellow Sea and East China Sea shelves in winter. To examine how the coupled processes actually work in the ocean, SST fields computed in both coupled and uncoupled models were compared with those synthesized from multiple satellite observations. As mentioned above, the shallow areas, especially around the Chinese coasts, become much cooler owing to the smaller heat content compared with deeper areas. Their results, however, indicated that the coupled model significantly improves the negative SST bias revealed around the Chinese coast in the uncoupled model (Fig. 1.5.5).

Figure 1.5.6 shows a schematic of the negative feedback process accomplished in the shallow coastal waters of the Yellow and East China seas in winter. Northerly monsoonal winds prevail over the Yellow and East China seas in winter because, in general, the horizontal sea level pressure (SLP) gradient is sharp owing to the large landmass–ocean heat contrast (Fig. 1.5.6a). Enhanced cool and dry winds from the Asian landmass lower the SST, especially in shallow coastal waters, due to the intensive upward heat loss (Fig. 1.5.6b). Thereafter, the horizontal SLP gradient around the Chinese coast becomes moderate because the land–ocean heat contrast weakens due to the lowered SST in coastal areas (Fig. 7.5.6b). As a result, the wind speed is reduced in line with the moderated horizontal SLP gradient around the coast (Fig. 1.5.6b). Moreover, surface air temperature and specific humidity becomes high because cool and dry air is reduced due to the weakening of the northerly winds over the coastal waters. Hence, the upward heat flux in the coastal waters is reduced because of the weakening of the northerly winds and the decrease of cool and dry air and thus, this negative feedback process can suppress excessive cooling along the Chinese coast during winter.

The Yellow and East China seas meet two prerequisites favorable for the above mentioned negative feedback process to occur during winter. One is warm and shallow shelf seas neighboring a huge Asian landmass to maintain the sharp gradient in heat content (hence, SLP). The other is the offshore winds that carry cool and dry air over the warm ocean lowering the SST in coastal waters.

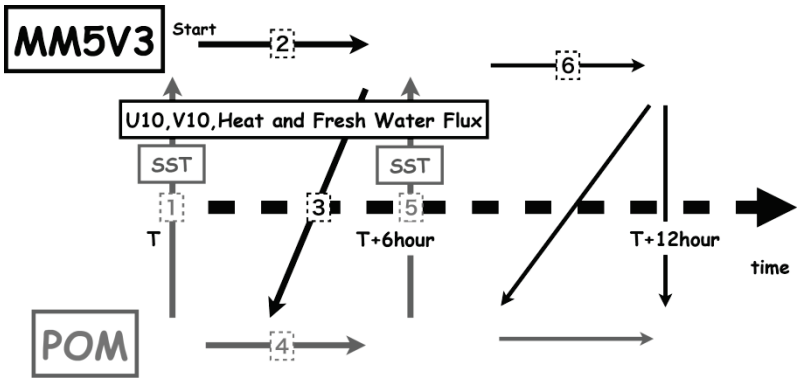

Fig. 1.5.4 Flow chart showing the coupling procedure between the atmospheric and oceanic models. The properties computed in these two models are exchanged in the order of numerals within the boxes. The Princeton Ocean Model (POM) gives SST to the Penn State Mesoscale Model (MM5V3), while the MM5V3 gives the momentum flux computed using wind speed at 10 m height (U10, V10), heat flux, and freshwater flux to POM. The exchange of the modeled properties are conducted every 6 hours. From Iwasaki *et al*. (2014). ©American Meteorological Society. Used with permission.

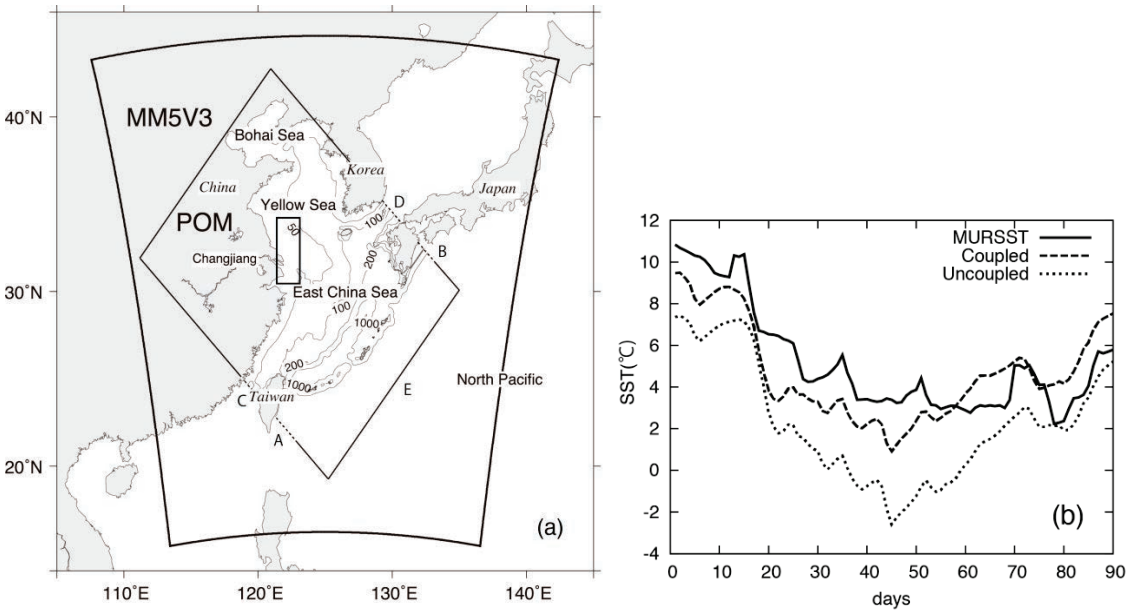

Fig. 1.5.5 (a) Model domain and bottom topography. Rectangles in panel (a) indicate the MM5V3 and POM domains. Letters A to C and B to D, placed beside the broken lines, indicate the locations of inflow, outflow, and sidewall boundaries. Isobaths are in meters. The small rectangle along the Chinese coast is used for panel (b), where temporal variations of daily SST averaged over the rectangle are depicted during winter of 2009 to 2010. Different line types in the upper right-hand corner are used for temperatures derived from MURSST (Multi-sensor Ultra-high Resolution SST), the coupled model, and uncoupled model. Abscissa indicates days elapsed from December 1. Redrawn from Iwasaki *et al*. (2014). ©American Meteorological Society. Used with permission.

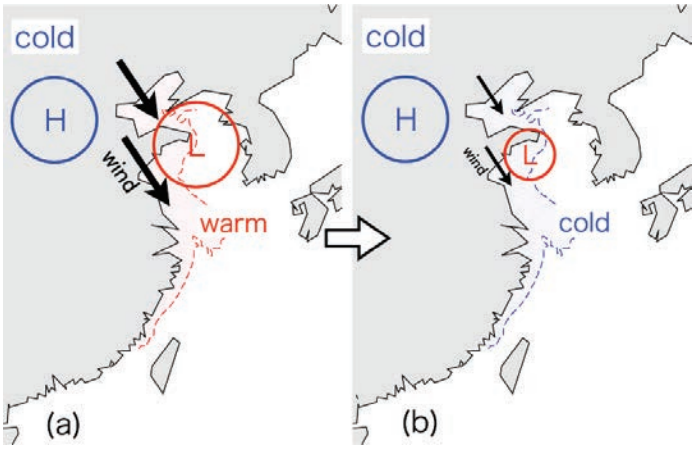

Fig. 1.5.6 Schematic view of the atmosphere–ocean coupled process over the coastal waters of the Yellow Sea and East China Sea in winter. The variation in sea level pressure before and after the negative feedback process is expressed by changing the size of the red circle with the letter "L". The variation in wind speeds in the coupled process is expressed by changing the thickness and length of the arrows. From Iwasaki *et al*. (2014). ©American Meteorological Society. Used with permission.

Besides winter processes mentioned above, one of the most remarkable intraseasonal atmospheric features in East Asia is the Baiu rainband in early summer. The oceanic (especially, Kuroshio) influence on the Baiu frontal zone has been pointed out by recent studies such as Sasaki *et al*. (2012), Kunoki *et al*. (2015), and Sato *et al*. (2016). The Kuroshio anchors the ascent motion of the Baiu frontal zone and large diabatic heating, and thus, the Kuroshio influence results in a deep atmospheric response extending to the upper troposphere (Sasaki *et al*., 2012). The two-way processes may occur if the modified Baiu frontal zone (hence, surface momentum and heat fluxes) again changes the ocean, although the accomplishment of such two-way processes should be further explored in terms of atmosphere–ocean interaction studies.

1.5.4 Future work

In this short review, our attention is focused only on physical processes. However, as suggested by Isobe *et al*. (2014), a coupling of physics and ocean biology is potentially capable of improving a regional atmospheric and oceanic model, which will be a challenging topic valuable to understanding the regional climate.

Acknowledgements

The critical and careful reading by Dr. Hanna Na is greatly appreciated.

1.5.5 References

Allen, J.T., Pezza, A.B. and Black, M.T. 2010. Explosive cyclogenesis: a global climatology comparing multiple reanalyses. *J. Climate* **23**: 6468–6484, doi:10.1175/2010JCLI3437.1.

Chelton, D.B., Esbensen, S.K., Schlax, M.G., Thum, N., Freilich, M.H., Wentz, F.J., Gentemann, C.L., McPhaden, M.J. and Schopf, P.S. 2001. Observations of coupling between surface wind stress and sea surface temperature in the eastern tropical Pacific. *J. Climate* **14:** 1479–1498, doi:10.1175/1520-0442(2001)014<1479:OOCBSW>2.0.CO;2.

Chen, S.-J., Kuo, Y.-H., Zhang, P.-Z. and Bai, Q.-F. 1991. Synoptic climatology of cyclogenesis over East Asia, 1958-1987. *Mon. Wea. Rev.* **119**: 1407–1418, doi:10.1175/1520-0493(1991)119<1407:SCOCOE>2.0.CO;2.

Chen, S.-J., Kuo, Y.-H., Zhang, P.-Z. and Bai, Q.-F. 1992. Climatology of explosive cyclones off the East Asian coast. *Mon. Wea. Rev.* **120**: 3029–3035, doi:10.1175/1520-0493(1992)120<3029:COECOT>2.0.CO;2.

Fang, Y., Zhang, Y., Tang, J. and Ren, X. 2010. A regional air-sea coupled model and its application over East Asia in the summer of 2000. *Adv. Atmos. Sci*. **27**: 583–593, doi:10.1007/S00376-009-8203-7.

Grell, G.A., Dudhia, J. and Stauffer, D.R. 1994. A description of the fifth-generation Penn State/NCAR mesoscale model (MM5). NCAR Technical Note, NCAR/TN-398+STR, 117 pp.

Guan, L. and Kawamura, H. 2004. Merging satellite infrared and microwave SSTs: methodology and evaluation of the new SST. *J. Oceanogr*. **60**: 905–912, doi:10.1007/s10872-004-5782-x.

Gulev, S.K., Zolina, O. and Grigoriev, S. 2001. Extratropical cyclone variability in the Northern Hemisphere winter from the NCEP/NCAR reanalysis data. *Climate Dyn.* **17**: 795–809, doi:10.1007/s003820000145.

Gulev, S.K., Jung, T. and Ruprecht, E. 2002. Climatology and interannual variability in the intensity of synoptic-scale processes in the North Atlantic from the NCEP-NCAR reanalysis data. *J. Climate* **15**: 809–828, doi:10.1175/1520-0442(2002)015<0809:CAIVIT>2.0.CO;2.

Gyakum, J.R., Anderson, J.R., Grumm, R.H. and Gruner, E.L. 1989. North Pacific cold-season surface cyclone activity: 1975-1983. *Mon. Wea. Rev.*, **117**: 1141–1155, doi:10.1175/1520-0493(1989)117<1141:NPCSSC>2.0.CO;2.

Hanson, H.P. and Long, B. 1985. Climatology of cyclogenesis over the East China Sea. *Mon. Wea. Rev.* **113**: 697–707.

Hodges, K.I., Lee, R.W. and Bengtsson, L. 2011. A comparison of extratropical cyclones in recent reanalyses ERA-Interim, NASA MERRA, NCEP CFSR, and JRA-25. *J. Climate* **24**: 4888–4906, doi:10.1175/2011JCLI4097.1.

Hoskins B.J. and Valdes, P.J. 1990. On the existence of storm-tracks. *J. Atmos. Sci.* **47**: 1854–1864, doi:10.1175/1520-0469(1990)047<1854:OTEOST>2.0.CO;2.

Hsueh, Y. 1988. Recent current observations in the eastern Yellow Sea. *J. Geophys. Res. Oceans* **93**: 6875–6884, doi:10.1029/JC093iC06p06875.

Isobe, A. 2008. Recent advances in ocean-circulation research on the Yellow and East China Sea shelves. *J. Oceanogr*. **64**: 569–584, doi:10.1007/s10872-008-0048-7.

Isobe, A. and Kako, S. 2012. A role of the Yellow and East China Seas in the development of extratropical cyclones in winter. *J. Climate* **25**: 8328–8340, doi:10.1175/JCLI-D-11-00391.1.

Isobe, A., Kako, S. and Iwasaki, S. 2014. Synoptic scale atmospheric motions modulated by spring phytoplankton bloom in the Sea of Japan. *J. Climate* **27**: 7587–7602, doi:10.1175/JCLI-D-14-00277.1.

Iwasaki, S. and Isobe, A. and Kako, S. 2014. Atmosphere-ocean coupled process along coastal areas of the Yellow and East China Seas in winter. *J. Climate* **27**: 155–167, doi:10.1175/JCLI-D-13-00117.

Kasamo, K., Isobe, A., Minobe, S., Manda, A., Nakamura, H., Ogata, K., Nishikawa, H., Tachibana, Y. and Kako, S. 2014. Transient and local weakening of surface winds observed above the Kuroshio front in the winter East China Sea. *J. Geophys. Res. Atmos.* **119**: 1277–1291, doi:10.1002/2013JD020610.

Kueh, M.-T. and Lin, P.-L. 2015. Upper ocean response and feedback to spring weather over the Kuroshio in the East China Sea: a coupled atmosphere-ocean model study. *J. Geophys. Res. Atmos*. **120**: 10,091–10,115, doi:10.1002/2015JD023386.

Kunoki, S., Manda, A., Kodama, Y., Iizuka, S., Sato, K., Fathrio, I., Mitsui, T., Seko, H., Moteki, Q, Minobe, S. and Tachibana, Y. 2015. Oceanic influence on the Baiu frontal zone in the East China Sea. *J. Geophys. Res. Atmos*. **120**: 449–463, doi:10.1002/2014JD022234.

Lie, H.-J., Cho, C.-H., Lee, J.-H. and Lee, S. 2001. Does the Yellow Sea Warm Current really exist as a persistent mean flow?. *J. Geophys. Res. Oceans* **106**: 22,199–22,210, doi:10.1029/2000JC000629.

Lindzen, R.S. and Nigam, S. 1987. On the role of sea surface temperature gradients in forcing low level winds and convergence in the tropics. *J. Atmos. Sci*. **44**: 2418–2436, doi:10.1175/1520-0469(1987)044<2418:OTROSS>2.0.CO;2.

Mellor, G.L. 2003. Users guide for a three-dimensional, primitive equation, numerical ocean model (June 2003 version). *Prog. Atmos. Ocean. Sci*., Princeton University, 53 pp.

Nakamura, H. 1992. Midwinter suppression of baroclinic wave activity in the Pacific. *J. Atmos. Sci.* **49**: 1629–1642, doi:10.1175/1520-0469(1992)049,1629:MSOBWA.2.0.CO;2.

Nakamura, H., Izumi, T. and Sampe, T. 2002. Interannual and decadal modulations recently observed in the Pacific storm track activity and East Asian winter monsoon. *J. Climate* **15**: 1855–1874, doi:10.1175/1520-0442(2002)015,1855:IADMRO.2.0.CO;2.

Nonaka, M. and Xie, S.-P. 2003. Covariations of sea surface temperature and wind over the Kuroshio and its extension: Evidence for ocean-atmospheric feedback. *J. Climate* **16**: 1404–1413.

Onogi, K., Tsutsui, J., Koide, H., Sakamoto, M., Kobayashi, S., Hatsushika, H., Matsumoto, T., Yamazaki, N., Kamahori, H., Takahashi, K., Kadokura, S., Wada, K., Kato, K., Oyama, R., Ose, T., Mannoji, N. and Taira, R. 2007. The JRA-25 reanalysis. *J. Meteorol. Soc. Jpn.* **85**: 369–432, doi:10.2151/jmsj.85.369.

Rudeva, I., and S. K. Gulev, 2011. Composite analysis of North Atlantic extratropical cyclones in NCEP-NCAR reanalysis data. *Mon. Wea. Rev*. **139**: 1419–1446, doi:10.1175/2010MWR3294.1.

Sasaki, Y., Minobe, S., Asai, T. and Inatsu, M. 2012. Influence of the Kuroshio in the East China Sea on the early summer (baiu) rain. *J. Climate* **25**: 6627–6645, doi:10.1175/JCLI-D-11-00727.1.

Sato, K., Manda, A., Moteki, Q., Komatsu, K.K., Ogata, K., Nishkawa, H., Oshika, M., Otomi, Y., Kunoki, S., Kanehara, H., Aoshima, T., Shimizu, K., Uchida, J., Shimoda, M., Yagi, M., Minobe, S. and Tachibana, Y. 2016. Influence of the Kuroshio on mesoscale convective systems in the baiu frontal zone over the East China Sea. *Mon. Wea. Rev*. **144**: 1017–1033, doi:10.1175/MWR-D-15-0139.1.

Vecchi, G.A., Xie, S.-P. and Fischer, A.S. 2004 Ocean-atmosphere covariability in the western Arabian Sea. *J. Climate* **17**: 1213–1224, doi:10.1175/1520-0442(2004)017<1213:OCITWA>2.0.CO;2.

Wallace, J.M., Mitchell, T.P. and Deser, C. 1989. The influence of sea surface temperature on surface wind in the eastern equatorial Pacific: Seasonal and interannual variability. *J. Climate* **2**: 1492–1499, doi:10.1175/1520-0442(1989)002<1492:TIOSST>2.0.CO;2.

Xie, S.-P., Hafner, J., Tanimoto, Y., Liu, W.T., Tokinaga, H. and Xu, H. 2002. Bathymetric effect on the winter sea surface temperature and climate of the Yellow and East China Seas. *Geophys. Res. Lett.* **29**: 2228, doi:10.1029/2002GL015884.

Yamamoto, M. and Hirose, N. 2007. Impact of SST reanalyzed using OGCM on weather simulation: A case of a developing cyclone in the Japan Sea area. *Geophys. Res. Lett*. **34**: L05808, doi:10.1029/2006GL028386.

Yoshida, A. and Asuma, Y. 2004. Structures and environment of explosively developing extratropical cyclones in the northwestern Pacific region. *Mon. Wea. Rev.* **132**: 1121–1142, doi:10.1175/1520-0493(2004)132<1121:SAEOED>2.0.CO;2.

Yoshiike, S. and Kawamura, R. 2009. Influence of wintertime large-scale circulation on the explosively developing cyclones over the western North Pacific and their downstream effects. *J. Geophys. Res. Atmos*. **114**: D13110, doi:10.1029/2009JD011820.

Zolina O. and Gulev, S.K. 2003. Synoptic variability of ocean-atmosphere turbulent fluxes associated with atmosphere cyclones. *J. Climate* **15**: 2717–2734.

1.6 Long-Term Variations of Physical Properties

Sang-Wook Yeh[1] and Jae-Hak Lee[2]

[1] Hanyang University, ERICA, Korea
[2] Korea Institute of Ocean Science and Technology, Korea

1.6.1 Introduction

There exist previous studies which reported that there is faster ocean warming around marginal seas than in other areas within ocean basins (Hansen *et al*., 2010; Burrows *et al*., 2011; Lima and Wethey, 2012). Such warming in marginal seas could be due to the increase of greenhouse gas forcing, natural variability, or the combined influence of both. In particular, it has been reported that the strongest warming in the globe has been observed in the East Asian marginal seas (Belkin, 2009; Yeh *et al*., 2010; Bao and Ren, 2014; Wu *et al*., 2017; Kim *et al*., 2018). Therefore, it is useful to understand the long-term variations of physical properties in the East Asian marginal seas. Among them is the Yellow Sea/East China Sea (hereafter, YECS), which is a shallow, semi-closed basin with depths < 100 m located in the northwestern Pacific Ocean (Fig. 1.6.1). The YECS is bounded

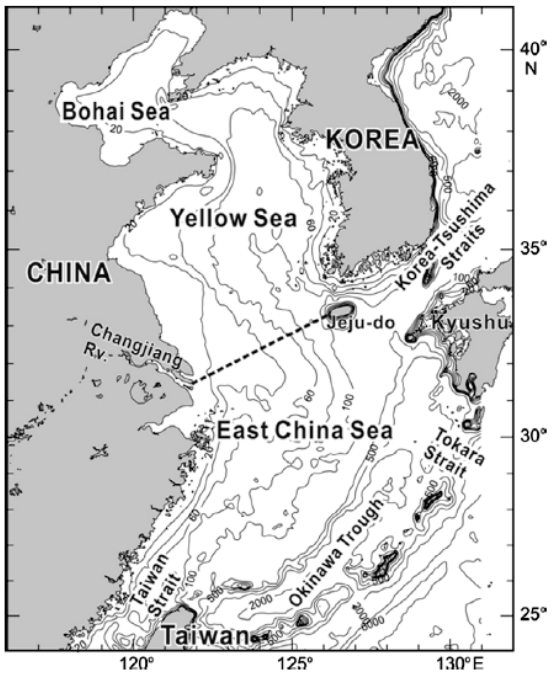

Fig. 1.6.1 The Yellow and East China seas (YECS). Continuous lines denote isobaths in meters. The dashed line connecting the Changjiang River mouth and Jeju-do indicates the geographical boundary between the Yellow Sea and East China Sea. From Lie and Cho (2016).

by the Korean Peninsula, the Ryukyu islands (East), China (West), Japan (North), and Taiwan Island (South) (Chu *et al*., 2005; Lie and Cho, 2016). The YECS is connected not only to the Pacific but also to two neighboring marginal seas through the Taiwan Strait to the southwest and the Korea–Tsushima Straits to the northeast. Therefore, the YECS plays a role as a shallow but large reservoir for water and materials originating from both land and ocean; it also serves as link supplier for the northwestern Pacific and the deep marginal seas. In addition, it is known that the social and economic conditions around the coast of East Asia marginal seas are largely influenced by the East Asian monsoon system, which is associated with the state of YECS sea surface temperature (SST) (Li *et al*., 2010). The SST condition in the YECS under global warming is able to regulate the growth of extratropical storms, which significantly modulates weather and climate conditions in East Asia (Inatsu *et al*., 2013). This review paper contains a brief summary of the physical properties of the YECS in terms of long-term variations of SST, sea level pressure and their associated atmospheric circulation.

1.6.2 Basic features of physical properties in the Yellow Sea and East China Sea

The physical properties of the YECS are relatively well known in terms of its hydrography, water mass features based on observations and high-resolution numerical modeling (Lie *et al*., 1998; Tseng *et al*., 2000; Lie *et al*., 2001; Ichikawa and Beardsley, 2002; Lie and Cho, 2002; Chu *et al*., 2005; Lie and Cho, 2016). The most important element of the YECS circulation system is the Kuroshio which flows northeastward along the continental slope of the ECS (Zheng and Klemas, 1982; Hickox *et al*., 2000; Park and Chu, 2008; Chen, 2009; Lee *et al*., 2014; Lie and Cho, 2016). The Kuroshio, which is a main driving forcing of the YECS, carries a large amount of heat, salt and oceanic materials from the tropical and subtropical ocean to the YECS. On the other hand, coastal currents in the YECS also carry a large amount of freshwater and materials from land to the offshore shelf. This results in the formation of various oceanic fronts between the Kuroshio region with a high salinity and coastal waters with a low salinity (Zheng and Klemas, 1982; Hickox *et al*., 2000; Park and Chu, 2008; Chen, 2009; Lee *et al.*, 2014).

On the other hand, the variability of SST in the YECS is usually associated with both local and non-local forcings. Local forcings include solar radiation, tide flow variations and atmosphere intraseasonal variability (Weng *et al*., 1993, Zeng *et al*., 2006). In general, the high frequency variability of SST in the YECS is mainly associated with local forcings (Weng *et al*., 1993). For example, the SST variability in the YECS on seasonal and sub-seasonal timescales is dominated by monsoons, oceanic advection, vertical mixing, bathymetry and so on (see, *e.g*., Tang *et al*., 1989; Bao *et al*., 2002; Furey and Bower, 2005; Liu *et al*., 2005). According to a recent study (Wu *et al*., 2016) in particular, over 90% of the temporal variability of SST in the YECS can be explained by the annual harmonic whose amplitude is one order larger than that of the semiannual harmonic. Similarly, Huang *et al.* (2012) argued that the SST in the YECS over the last 141 years (1870–2010) can be partitioned into an annual component (*i.e*., seasonal signal with zero mean) and an annual mean component (*i.e*., inter-annual, decadal and long-term trend). They further argued that the annual sinusoidal signal dominates the semi-annual signal by contributing greater than 94% to the annual range in general; the semi-annual signal contributes more than 10% to the annual range in the eastern Yellow Sea, particularly to the area south of the Korean Peninsula. The annual cycle of SST reaches its peak from mid-July in the south to early August in the north and central YECS.

In contrast, non-local forcing, including El Niño–Southern Oscillation (ENSO), Pacific Decadal Oscillation (PDO) and North Pacific Oscillation (NPO) is associated with the interannual SST variability in the YECS through ocean and atmospheric teleconnections (see, *e.g*., Park, 2000; Wu *et*

al., 2005). Using a fine resolution SST dataset, analysis indicates that a significant peak around 3.3 years exists in the YECS and such interannual variability of SST is linked with the ENSO teleconnection through which anomalous surface heat flux warms or cools the YECS during El Niño or La Niña events (Wu *et al*., 2016). Therefore, SST variations over the YECS exhibit multiple timescales and spatial patterns with different origins (Zhang *et al*., 2010).

1.6.3 Long-term variation of SST variability and sea level

The low-frequency variability of the YECS climate system has been extensively studied in terms of SST (*e.g*., Belkin *et al*., 2009; Huang *et al*., 2010; Yeh and Kim, 2010; Zhang *et al*., 2010; Kim *et al*., 2011; Park *et al*., 2011; Oey *et al*., 2013; Wang *et al*., 2013; Bao and Ren, 2014; Park *et al*., 2015, Wu *et al*., 2017, Kim *et al*., 2018). Previous studies have shown that SST over the coastal China seas demonstrates the strongest warming trend over the global ocean (Chen and Ho, 2002; Wu *et al*., 2012). Using a 38-year dataset collected from six costal stations, Lin *et al*. (2001) identified a warming trend in the Bohai Sea. The warming trends of the marginal seas of China for 1870–2011 are generally larger than the global and hemispheric averages, with the largest warming in the ECS (Bao and Ren, 2014). Yeh and Kim (2010) also examined the characteristics in the SST variability in the YECS during boreal winter for 1950–2008. They found that the mean SST in the YECS gradually increases until the late 2000s. A warming trend of a basin-scale SST is significant in most of the regions in the YECS. A broadly accepted conclusion from these studies indicates a robust and persistent SST increase in the YECS over recent decades, with the rates of 2 to 4 times faster than the global averaged trend of 0.13°C per decade (Trenberth *et al*., 2007).

In addition to the warming trend in the YECS, low-frequency SST variability is also dominant (Park and Ho, 2000). For example, Zhang *et al*. (2010) examined the mechanisms of SST low-frequency variations in the YECS using the HadISST (Rayner *et al*., 2006) for 1900–2006. They suggested that there are two distinct low-frequency modes in the YECS: a basin mode and a north–south dipole mode (Fig. 1.6.2). The former is characterized by a uniform warming over the entire coastal oceans, while the latter is characterized by a seesaw pattern over the shelf seas and the South China Sea. The basin mode is associated with global warming, but it is primarily attributed to oceanic advection. The dipole mode varies coherently with the PDO (Mantua *et al*., 1997). In contrast to the basin mode, the dipole mode is broadly associated with the surface heat flux, with oceanic advection acting to dampen SST in the shelf seas but sustaining SST in the South China Sea. Zhang *et al*. (2010) further argued that the basin mode and the dipole mode are dominant in boreal winter (December–January–February) and summer (June–July–August) despite some differences in the governing processes. Yeh and Kim (2010) argued that the NPO-like sea level pressure plays an important role to warm the YECS. The southern lobe of NPO-like sea level pressure over the North Pacific causes a weakening of northerly mean winds over the YECS during winter, which contributes to an increase in the SST in the YECS through the changes in the latent heat and sensible heat fluxes.

Figures 1.6.3a and b display the 11-year average of SST anomalies in the East Asian marginal seas, including the YECS in boreal winter and summer for 1980–2015, respectively. As suggested in previous studies, the decadal variations of SST anomalies in the YECS are evident in both boreal winter and summer. In particular, the SST in the YECS was characterized by a warming trend until the late 2000s. However, such a warming trend is not seen in the 21st century. The SST anomalies in the YECS for 2000–2015 are cooler than the climatology (1980–2015) in both winter and summer, respectively, indicating that the warming trend over the YECS has become weaker in the past decade.

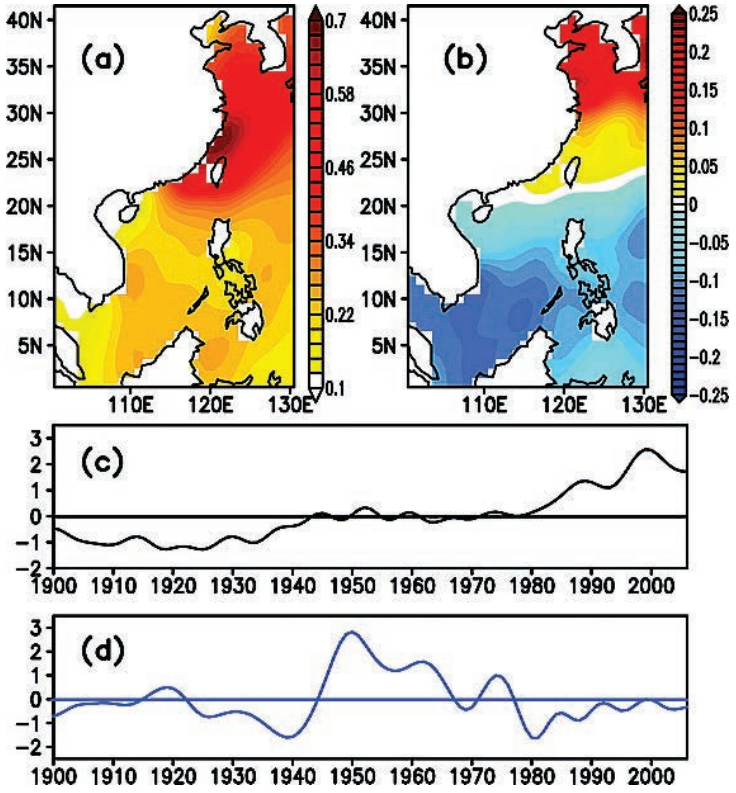

Fig. 1.6.2 Empirical orthogonal function (EOF) modes of low-pass-filtered (>7 years) sea surface temperature (SST) from the Hadley Centre Sea Ice and Sea Surface Temperature data over the coastal China seas: (a) first EOF, (b) second EOF, (c) first principle component (PC), and (d) second PC. Units in (a) and (b) are in °C. PCs have been normalized with a unit variance. From Zhang *et al*. (2010). Reproduced with permission of Wiley & Sons.

Recently, Bao and Ren (2014) showed that the warming in the marginal seas of China for 1998–2011 undergoes a slowdown in warming and such a slowdown is more evident than the global and northern hemispheric averages. Similarly, Wu *et al*. (2017) found that the most significant warming occurred in boreal winter during 1982–1998, based on four different SST datasets although the warming trends derived from these datasets differ in magnitude. Wu *et al*. (2017) argued that the rapid warming for 1982–1998 is a result of the asymmetry in the ENSO teleconnection, through which El Niño events induce significant warming over the eastern China Coastal Waters at its peak, whereas La Niña events fail to do the opposite that would completely reverse the trends. That is, more frequent occurrence of El Niño than La Niña events for 1982–1998 leads to the warming trend in the eastern China Coastal Waters. Since late 1998, however, a La Niña event occurs more frequently than the El Niño event. This also may contribute to the slowdown of the warming trend in the East Asian marginal seas.

Consistent with the result in Figure 1.6.3, Kim *et al*. (2018) also argued that a basin-scale cooling in the YECS followed after the warming of the sea surface reached a peak in the late 1990s (Fig. 1.6.4). They reasoned that this is closely associated with the variation in the Siberian High along with its intensification after the late 1990s. A contrasting relationship between the YECS SST and the Siberian High intensity is observed before and after the late 1990s, *i.e*., the two variables (YECS SST and Siberian High intensity) are barely correlated for 1982−1997, while their out-of-phase relationship becomes significant in the recent years (1998−2014) when the intensity of the Siberian High becomes stronger. This suggests that the Siberian High has played an increasing role in determining the state of the YECS since the late 1990s. On the other hand, there is a possibility that a low-frequency variability of YECS SST is associated with the changes in the relationship between the YECS SST variability and the PDO. While the YECS SST has a close correlation with the PDO index before the late 1990s, it weakens after the late-1990s, when the North Pacific regime shift occurred. In other words, the atmospheric–oceanic signals associated with the PDO were regionally confined to the eastern basin of the North Pacific after the late-1990s, and concurrently resulted in the decoupling of the YECS climate from the PDO.

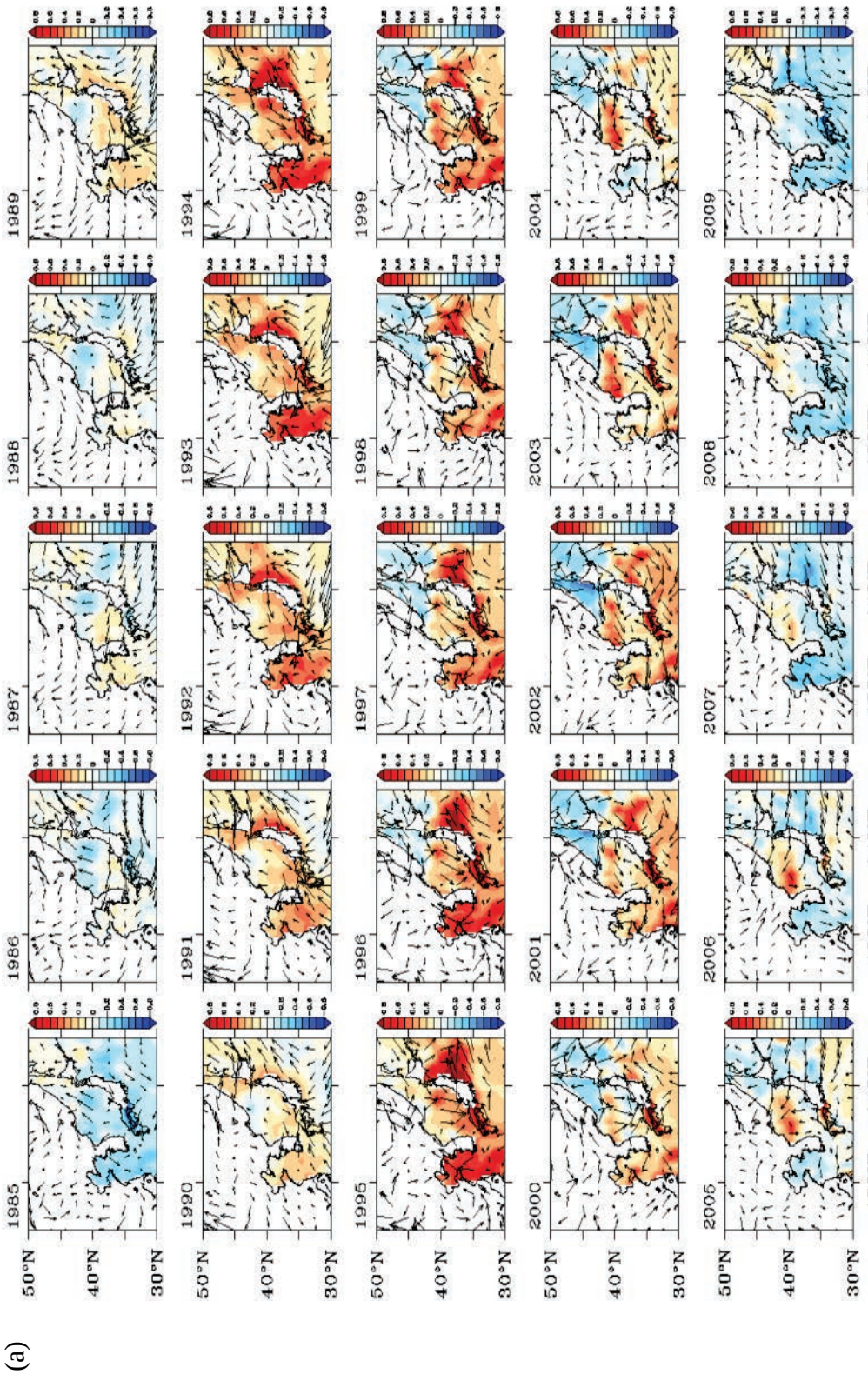

Fig. 1.6.3 The 11-year average of sea surface temperature (SST) anomalies in the East Asian marginal seas, including the Yellow Sea and East China Sea (YECS) in (a) boreal winter (December–January–February) and (b) summer (June–July–August) for 1980–2015. The year above in each figure indicates a center of year for the 11-year period. For example, 1985 denotes the SST anomalies averaged in 1980–1991.

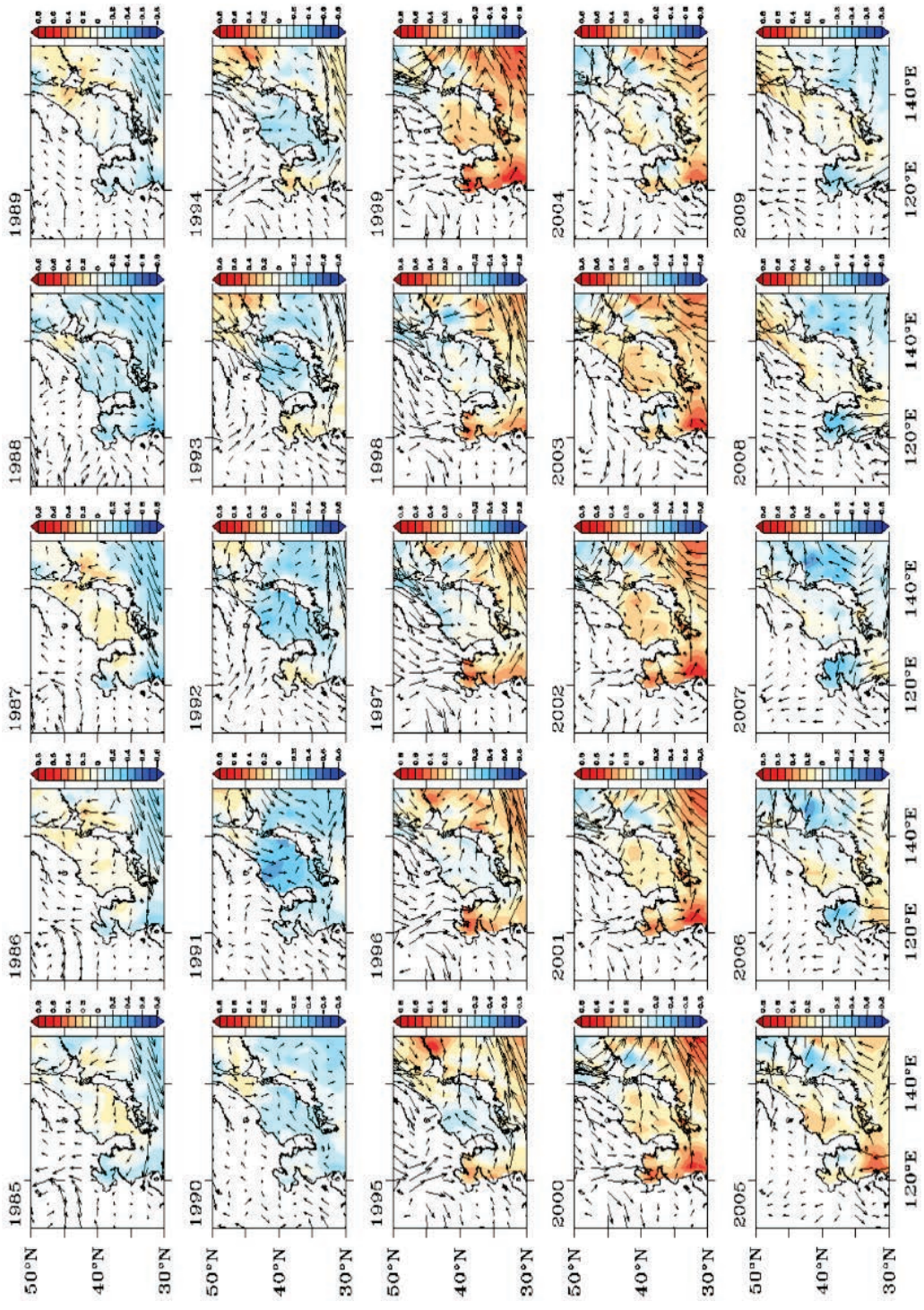

Fig. 1.6.3 Continued.

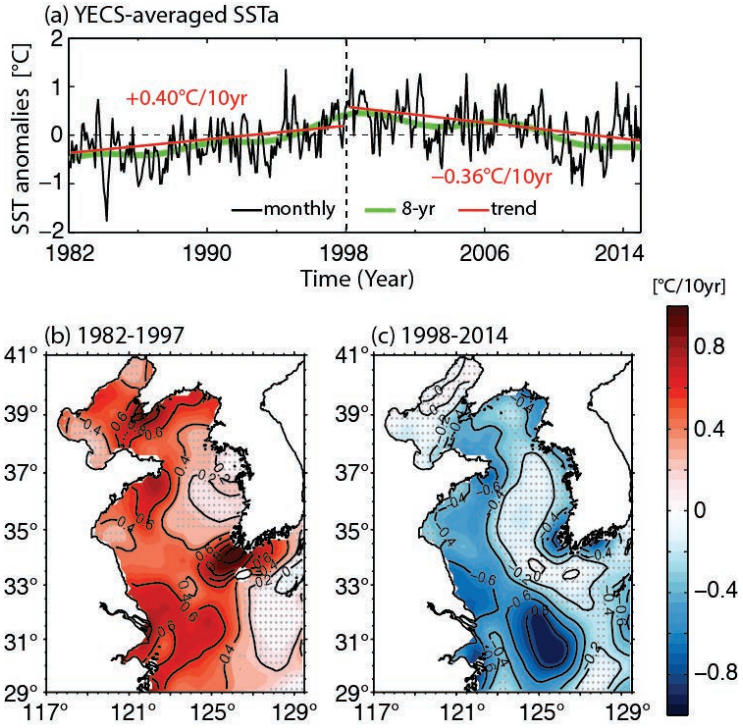

Fig. 1.6.4 (a) Time series of the monthly sea surface temperature (SST) anomaly averaged in the Yellow and East China seas (black); thick green and red lines indicate the 8-year low-pass filtered SST anomaly and the trends for the periods 1982−1997 and 1998−2014, respectively. The spatial distributions of the linear SST trends are illustrated for the periods (b) 1982−1997 and (c) 1998−2014. Gray dots show that the trends are insignificant trends at the 95% confidence level. From Kim *et al*. (2018). Reproduced with permission of Elsevier.

Sea level changes may affect regional tidal dynamics in shelf seas such as the YECS (Pickering *et al*., 2012; Ward *et al*., 2012). Therefore, coastal ecosystems and their communities in the YECS are closely associated with sea level variations (Chen *et al*., 2014). There are a number of studies investigating sea level variability in the YECS, including the coastline of China (Kang *et al*., 1995; Han *et al*, 2008; Pelling *et al*., 2013; Chen *et al*., 2014). It has been reported that the altimetric sea level rise rate is 0.64 cm yr^{-1} for 1992 to 2002, which is much larger than the rate of 0.24 cm yr^{-1} for 1980 to 2002 (Han *et al*., 2008). For the period of 1992 to 2002, in details, the altimetric annual harmonic has a magnitude of 10 to 30 cm in amplitude and is highest in summer in the ECS (Han *et al*., 2008). In particular, the interannual and longer-term sea level variability in the altimetric data are negatively correlated with the PDO, attributed in part to steric height change in the ECS (Han *et al*., 2008).

The tidal regime in the Bohai Sea has recently experienced rapid coastline changes due to natural developments of the Yellow River delta and to large-scale anthropogenic land reclamation (Pelling *et al*., 2013). It is reported that there have, indeed, been significant changes in the tidal regime in the Bohai Sea over the last 35 years (1976–2002), with M_2 amplitudes changing up to 20 cm in some parts. On the other hand, a significant increase in sea level extremes is found with trends in the range between 2.0 and 14.1 mm yr^{-1} adjacent to the Chinese coast for 1954–2012 (Feng and Tsimplis, 2014). Hourly sea level records at 20 tide gauges at and adjacent to the Chinese coasts show that tides and tropical cyclones determine the spatial distribution of sea level maxima. The interannual variability in the sea level extremes is also influenced by the changes in median sea level at the north and by the 18.6 year nodal cycle at the South China Sea.

1.6.4 Summary

Previous studies have shown that SST over the East Asian marginal seas is characterized by a strong warming trend. In addition, global warming has been thought to be a key mechanism leading to such a warming trend in the YECS. However, such a warming reached a peak in the late 1990s; subsequently, a basin-scale cooling has been observed in the recent past decade. Recent studies argue that a low frequency variability of YECS SST, which is associated with both atmospheric circulation and oceanic condition, is responsible for such a cooling trend in the YECS.

Because the variability of the YECS SST is closely connected to the Pacific Ocean SST on interannual-to-decadal timescales, including ENSO and PDO, in particular, it is important to examine the changes in the relationship of such phenomena with YECS SST variability. Recent studies have shown that the Pacific Ocean experienced an abrupt, systematic change, which can be characterized by: 1) the central Pacific El Niño having occurred more frequently than the conventional El Niño (Yeh *et al*., 2009); 2) the North Pacific Gyre Oscillation (NPGO), defined as the second sea surface height mode in the Eastern North Pacific (Di Lorenzo *et al*., 2008, 2010), becoming dominant compared to the PDO; 3) the low-frequency PDO index entering a negative regime from a positive one (Peterson and Schwing, 2003; Overland *et al*., 2008; Jo *et al*., 2015; Newman *et al*, 2016). It has been found that the SST in the YECS varied closely with the PDO before the late 1990s, indicating that the warming trend in the YECS SST was closely linked to the PDO. However, the recent SST in the YECS is largely influenced by the intensified Siberian High pressure system via enhanced heat losses in terms of latent and sensible heat fluxes. This indicates that the low frequency SST variability in the YECS might be determined largely by the relative role of the atmosphere and ocean system.

A number of studies have indicated that the sea level in the YECS, including the coastline of China, is rising, which is closely associated with regional tidal dynamics. In addition, the interannual variability of sea level variations is associated with a large scale of SST variations in the Pacific such as the PDO. In particular, a regional ocean general circulation model simulation showed that at the end of the 21st century, the sea level in the YECS will rise about 0.12 to 0.20 m, which is caused mainly by ocean mass redistribution due to the ocean dynamic change of the Pacific Ocean (Chen *et al*, 2014). These results indicate that it is essential to examine the relationship of the YECS and the surrounding Ocean to understand the SST and sea level variations in the YECS from the present to future.

1.6.5 Future work

Considering global warming due to the increase of greenhouse gas concentrations, it is necessary to examine more details on the impact of YECS SST by analyzing various observational datasets and multi-model datasets. In particular, it is essential to correctly project YECS SST to gain an understanding of anticipated changes in the marine ecosystem as well as climate variability within East Asia in a future climate. To do so, first of all, it is crucial to understand the details of physical processes associated with atmosphere–ocean coupled interactions in the YECS because of its shallow depth. On the other hand, it is also necessary to understand the inter-model diversity simulating YECS SST during the near future in climate models. Recently, Yi and Yeh (2019) examined the inter-model diversity when simulating East Asian marginal seas SST in the period 2020 to 2049 under four different Representative Concentration Pathway runs. They argued that the inter-model diversity of simulated tropical Pacific SST is associated with the diversity of East Asian marginal seas SST and is related to the wind speed associated with atmospheric teleconnections from the tropics to the western-to-central North Pacific (see Fig. 1.6.5). This indicates that it is

necessary to understand the details of physical connections of the YECS and its surrounding ocean basins, including the North Pacific and the tropical Pacific in both the observations and climate models.

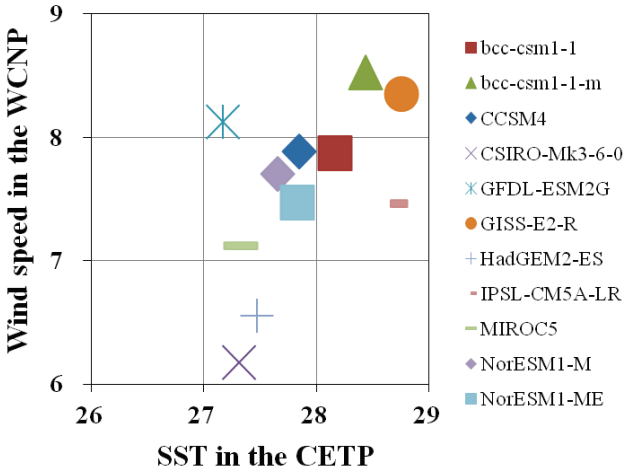

Fig. 1.6.5 Scatter plot of annual mean central-to-eastern tropical Pacific (170°W–120°W, 10°S–10°N) SST (°C) with western-to-central North Pacific (150°E–175°W, 35°N–50°N), wind speed (m s^{-1}) at 850 hPa for 11 climate models in the near future (2020–2049) in the RCP2.6 scenario. The simultaneous correlation coefficient between the two variables is 0.56, which is statistically significant at the 90% confidence level. From Yi and Yeh (2019). Reproduced with permission of Wiley & Sons.

1.6.6 References

Bao, B. and Ren, G. 2014. Climatological characteristics and long-term change of SST over the marginal seas of China. *Cont. Shelf Res*. **77**: 96–106, doi:10.1016/j.csr.2014.01.013.

Bao, X.W., Wan, X.Q., Gao, G.P. and Wu, D.X. 2002. Characteristics of the seasonal variability of the sea surface temperature field in the Bohai Sea, Yellow Sea and East China Sea from AVHRR data. *Acta Oceanol. Sin*. **24**: 125–133 (in Chinese).

Belkin, I.M. 2009. Rapid warming of large marine ecosystems. *Prog. Oceanogr*. **81**: 207–213, doi:10.1016/j.pocean.2009.04.011.

Burrows, M.T., Schoeman, D.S., Buckley, L.B., Moore, P., Poloczanska, E.S., Brander, K.M., Brown, C., Bruno, J.F., Duarte, C.M., Halpern, B.S., Holding, J., Kappel, C.V., Kiessling, W., O'Connor, M.I., Pandolfi, J.M., Parmesan, C., Schwing, F.B., Sydeman, W.J. and Richardson, A.J. 2011. The pace of shifting climate in marine and terrestrial ecosystems. *Science* **334**: 652–655, doi:10.1126/science.1210288.

Chen C.-T.A. 2009. Chemical and physical fronts in the Bohai, Yellow and East China seas. *J. Mar. Syst*. **78**: 394–410, doi:10.1016/j.jmarsys.2008.11.016.

Chen, Y.-L. and Ho, C.-R. 2002. A study on global and regional sea surface temperature trends. *J. Photogram. Remote Sens.* **7**: 41–58.

Chen, C.-L, Zuo, J.-C., Chen, M.-X., Gao, Z.-G. and Shuam, C.-K. 2014. Sea level change under IPCC-A2 scenario in Bohai, Yellow, and East China Seas. *Water Sci. Eng*. **7**: 446–456.

Chu, P., Yuchun, C. and Kuninaka, A. 2005. Seasonal variability of the Yellow Sea/East China Sea surface fluxes and thermohaline structure. *Adv. Atmos. Sci*. **22**:1–20, doi:10.1007/BF02930865.

Di Lorenzo, E., Schneider, N., Cobb, K.M., Franks, P.J.S., Chhak, K., Miller, A.J., McWilliams, J.C., Bograd, S.J., Arango, H., Curchitser, E., Powell, T.M. and Rivière, P. 2008. North Pacific Gyre Oscillation links ocean climate and ecosystem change. *Geophys. Res. Lett.* **35**: L08607, doi:10.1029/2007GL032838.

Di Lorenzo, E., Cobb, K.M., Furtado, J.C., Schneider, N., Anderson, B.T., Bracco, A., Alexander, M.A. and Vimont, D.J. 2010. Central Pacific El Niño and decadal climate change in the North Pacific Ocean. *Nat. Geosci*. **3**: 762−765, doi:10.1038/NGEO984.

Feng, X. and Tsimplis, M.N. 2014. Sea level extremes at the coast of China. *J. Geophys. Res. Oceans* **119**: 1593–1608, doi:10.1002/2013JC009607.

Furey, H.H. and Bower, A.S. 2005. Synoptic temperature structure of the East China and southeastern Japan/East Seas. *Deep Sea Res. II* **52**: 1421–1442, doi:10.1016/j.dsr2.2003.07.022.

Han, G. and Huang, W. 2008. Pacific Decadal Oscillation and sea level variability in the Bohai, Yellow and East China Sea. *J. Phys. Oceanogr*. **38**: 2772–2783, doi:10.1175/2008JPO3885.1.

Hansen, J., Ruedy, R., Sato, M. and Lo, K. 2010. Global surface temperature change. *Rev. Geophys*.**48**: doi:10.1029/2010RG000345.

Hickox, R., Belkin, I., Cornillon, P. and Shan, Z. 2000. Climatology and seasonal variability of ocean fronts in the East China, Yellow and Bohai Seas from satellite SST data. *Geophys. Res. Lett.* **27**: 2945–2948, doi:10.1029/1999GL011223.

Huang, D., Zhang, T. and Zhou, F. 2010. Sea-surface temperature fronts in the Yellow and East China Seas from TRMM microwave imager data. *Deep Sea Res. II* **57**: 1017–1024, doi:10.1016/j.dsr2.2010.02.003.

Huang, D., Ni, X., Tang, Q., Zhu, X. and Xu, D. 2012. Spatial and temporal variability of sea surface temperature in the Yellow Sea and East China Sea over the past 141 Years, pp. 213–234 *in:* Modern Climatolgy *edited by* S.Y. Wang and R. Gillies, www.intechopen.com, doi:10.5772/34236.

Inatsu, M., Mukougawa, H. and Xie, S.-P. 2013. Atmospheric response to zonal variations in midlatitude SST: Transient and stationary eddies and their feedback. *J. Climate* **16**: 3314–3329, doi:10.1175/1520-0442(2003)016<3314:ARTZVI>2.0.CO;2.

Jo, H.-S., Yeh, S.-W. and Lee, S.-K. 2015. Changes in the relationship in the SST variability between the tropical Pacific and the North Pacific across the 1998/1999 regime shift. *Geophys. Res. Lett*. **42**: 7171−7178, doi:10.1002/2015GL065049.

Kang, S.-K., Chung, J.-Y., Lee, S.-R. and Yum, K.-D. 1995. Seasonal variability of the M_2 tide in the seas adjacent to Korea. *Cont. Shelf. Res*. **15**: 1087–1113, doi:10.1016/0278-4343(94)00066-V.

Kim, S.-J., Woo, S.-H., Kim, B.-M. and Hur, S.-D. 2011. Trends in sea surface temperature (SST) change near the Korean Peninsula for the past 130 years. *Ocean Polar Res*. **33**: 281–290, doi:10.4217/OPR.2011.33.3.281.

Kim, Y.-S., Jang, C.-J. and Yeh, S-W. 2018. Recent surface cooling in the Yellow and East China Seas and the associated North Pacific climate regime shift. *Cont. Shelf. Res*. **156**: 43–54, doi:10.1016/j.csr.2018.01.009.

Lee, Y., Choi, J.K., Youn, S. and Roh, S. 2014. Influence of the physical forcing of different water masses on the spatial and temporal distributions of picophytoplankton in the northern East China Sea. *Cont. Shelf Res*. **88**: 216–227, doi:10.1016/j.csr.2014.08.001.

Li, H., Dai, A., Zhou, T. and Lu, J. 2010. Responses of East Asian summer monsoon to historical SST and atmospheric forcing during 1950–2000. *Climate Dyn*. **34**: 501–514, doi:10.1007/s00382-008-0482-7.

Lie, H.J. and Cho, C.H. 2002. Recent advances in understanding the circulation and hydrography of the East China Sea. *Fish. Oceanogr*. **11**: 318–328, doi:10.1046/j.1365-2419.2002.00215.x.

Lie, H.-J. and Cho, C.-H. 2016. Seasonal circulation patterns of the Yellow and East China Seas derived from satellite-tracked drifter trajectories and hydrographic observations. *Prog. Oceanogr*. **146**: 121–141, doi:10.1016/j.pocean.2016.06.004.

Lie, H.-J., Cho, C.-H. and Kaneko, A. 1998. On the branching of the Kuroshio and the formation of slope countercurrent in the East China Sea. Paper presented at Proceedings of Japan-China Joint Symposium on Cooperative Study of Subtropical Circulation System, 1–4 December 1997, Nagasaki, Japan.

Lie, H.J., Cho, C.H., Lee, J.H., Lee, S., Tang, Y. and Zou, E. 2001. Does the Yellow Sea Warm Current really exist as a persistent mean flow? *J. Geophys. Res. Oceans* **106**: 22,199–22,210, doi:10.1029/2000JC000629.

Lima, F.P. and Wethey, D.S. 2012. Three decades of high-resolution coastal sea surface temperatures reveal more than warming. *Nature Comm*. **3**: 704, doi:10.1038/ncomms1713.

Lin, C., Su, J., Xu, B. and Tang, Q. 2001. Long-term variations of temperature and salinity of the Bohai Sea and their influence on its ecosystem. *Prog. Oceanogr*. **49**: 7–19, doi:10.1016/S0079-6611(01)00013-1.

Liu, Q., Xie, S.P., Li, L. and Maximenko, N.A. 2005. Ocean thermal advective effect on the annual range of sea surface temperature. *Geophys. Res. Lett*. **32**: L24604, doi:10.1029/2005GL024493.

Mantua, N.J., Hare, S.R., Zhang, Y., Wallace, J.M. and Francis, R.C. 1997. A Pacific interdecadal climate oscillation with impacts on salmon production. *Bull. Meteorol. Amer. Soc*. **78**: 1069-1079, doi:10.1175/1520-0477(1997)078<1069:APICOW>2.0.CO;2.

Newman, M., Alexander, M.A., Ault, T.R., Cobb, K.M., Deser, C., Di Lorenzo, E., Mantua, N.J., Miller, A.J., Minobe, S., Nakamura, H., Schneider, N., Vimont, D.J., Phillips, A.S., Scott, J.D. and Smith, C.A. 2016. The Pacific decadal oscillation, revisited. *J. Clim*ate **29**: 4399−4427, doi:10.1175/JCLI-D-15-0508.1.

Oey, L.Y., Chang, M.C., Chang, Y.L., Lin, Y.C. and Xu, F.H. 2013. Decadal warming of coastal China Seas and coupling with winter monsoon and currents. *Geophys. Res. Lett*. **40**: 6288–6292, doi: 10.1002/2013GL058202.

Overland, J., Rodionov, S., Minobe, S. and Bond, N. 2008. North Pacific regime shifts: Definitions, issues and recent transitions. *Prog. Oceanogr*. **77**: 92−102, doi:10.1016/j.pocean.2008.03.016.

Park, K.-A., Lee, E.-Y., Chang, E. and Hong, S. 2015. Spatial and temporal variability of sea surface temperature and warming trends in the Yellow Sea. *J. Mar. Syst*. **143**: 24–38, doi:10.1016/j.jmarsys.2014.10.013.

Park, S. and Chu, P.C. 2008. Characteristics of thermal finestructure in the southern Yellow Sea and the East China Sea from airborne expendable bathythermograph measurements. *J. Oceanogr*. **64**: 859–875, doi:10.1007/s10872-008-0071-8.

Park, T., Jang, C.J., Jungclaus, J.H., Haak, H. and Park, W. 2011. Effects of the Changjiang river discharge on sea surface warming in the Yellow and East China Seas in summer. *Cont. Shelf Res*. **31**: 15–22, doi:10.1016/j.csr.2010.10.012.

Park, W. and Oh, I.-S. 2000. Interannual and interdecadal variations of sea surface temperature in the East Asian Marginal Seas. *Prog. Oceanogr.* **47**: 191–204, doi:10.1016/S0079-6611(00)00036-7.

Pelling, H.E., Green, J.A.M. and Ward, S.L. 2013. Modeling tides and sea level rise: To flood or not to flood, *Ocean Modell*. **63**: 21–29, doi:10.1016/j.ocemod.2012.12.004.

Peterson, W.T. and Schwing, F.B. 2003. A new climate regime in Northeast Pacific ecosystems. *Geophys. Res. Lett*. **30**: 1896, doi:10.1029/2003GL017528.

Pickering, M.D., Wells, N.C., Horsburgh, K.J. and Green, J.A.M. 2012. The impact of future sea-level rise on the European Shelf tides. *Cont. Shelf Res*. **35**: 1–15, doi:10.1016/j.csr.2001.11.011.

Rayner, N., Brohan, P., Parker, D., Folland, C., Kennedy, J., Vanicek, M., Ansell, T. and Tett, S. 2006. Improved analyses of changes and uncertainties in sea surface temperature measured in situ since the mid-nineteenth century: the HadSST2 dataset. *J. Climate* **19**: 446–469, doi:10.1175/JCLI3637.1.

Tang, M.Y., Liu, Y.Z., Li, H.H., Meng, Q.L., Qu, R.M., Gao, Z.H. and Sui, P. 1989. A preliminary analysis of the characteristics and formation causes of seasonal variability of averaged sea surface temperature field in the Bohai Sea, the Yellow Sea and the northern East China Sea. *Acta Oceanol. Sin*. **11**: 544–553 (in Chinese).

Trenberth, K.E., Jones, P., Ambenje, P., Bojariu, R., Easterling, D., Klein Tank, A., Parker, D., Rahimzadeh, F., Renwick, J. and Rusticucci, M. 2007. Observations: surface and atmospheric climate change. Climate change 2007. The physical science basis. Contribution of Working Group I to the Fourth Assessment Report of the Intergovernmental Panel on Climate Change *edited by* S. Solomon, D. Qin, M. Manning, Z. Chen, M. Marquis, K.B. Averyt, M. Tignor and H.L. Miller, Cambridge University Press, Cambridge.

Tseng, C., Lin, C., Chen, S. and Shyu, C. 2000. Temporal and spatial variations of sea surface temperature in the East China Sea. *Cont. Shelf Res*. **20**: 373–387, doi:10.1016/S0278-4343(99)00077-1.

Wang, F., Meng, Q., Tang, X. and Hu, D. 2013. The long-term variability of sea surface temperature in the seas east of China in the past 40 a. *Acta Oceanol. Sin*. **32**: 48–53, doi:10.1007/s13131-013-0288-2.

Ward, S.L., Green, J.A.M. and Pelling, H.E. 2012. Tides, sea-level rise and tidal power extraction on the European Shelf. *Ocean Dyn*. **62**: 1153–1167, doi:10.1007/s10236-012-0552-6.

Weng, X.C., Zhang, Q.L., Zhang, Y.K. and Yang, Y.L. 1993. Characteristics of the daily variations of water temperature in the Bohai Sea, Yellow Sea and East China Sea. *Mar. Sci*. **6**: 49–54 (in Chinese).

Wu, D.X., Li, Q., Lin, X.P. and Bao, X.W. 2005. The characteristics of the Bohai Sea SST anomaly interannual variability during 1990–1999. *Period. Ocean Univ. China* **35**: 173–176 (in Chinese).

Wu, L., Cai, W., Zhang, L., Nakamura, H., Timmermann, A., Joyce, T., McPhaden, M.J., Alexander, M., Qiu, B., Visbeck, M. and Chang, P. 2012. Enhanced warming over the global subtropical western boundary currents. *Nature Climate Change* **2**: 161–166, doi:10.1038/ NCLIMATE1353.

Wu, R., Lin, J. and Li, B. 2016. Spatial and temporal variability of sea surface temperature in eastern Marginal Seas of China. *Adv. Meteorol*. **2016**: doi:10.1155/2016/3820720.

Wu, R., Li, C. and Lin, J. 2017. Enhanced winter warming in the Eastern China coastal waters and its relationship with ENSO. *Atmos. Sci. Lett*. **18**: 11–18, doi:10.1002/asl.718.

Yeh, S.-W. and Kim, C.-H. 2010. Recent warming in the Yellow/East China Sea during winter and the associated atmospheric circulation. *Cont. Shelf Res*. **30**: 1428–1434, doi:10.1016/j.csr.2010.05.002.

Yeh, S.-W., Kug, J.-S., Dewitte, B., Kwon, M., Kirtman, B.P. and Jin, F.-F. 2009. El Niño in a changing climate. *Nature* **461**: 511–514, doi:10.1038/nature08316.

Yeh, S.-W., Park, Y.G., Min, H.S., Kim, C.H. and Lee, J.H. 2010. Analysis of characteristics in the sea surface temperature variability in the East/Japan Sea. *Prog. Oceanogr*. **85**: 213–223, doi:10.1016/j.pocean.2010.03.001.

Yi, D. and Yeh, S.-W. 2019. Understanding inter-model diversity of CMIP5 climate models in simulating East Asian Marginal Sea Surface Temperature in the near future (2020-2049). *J. Geophys. Res*. **124**: 5607–5617, doi:10.1029/2019JC015028.

Zeng, G.E., Lian, S.M., Cheng, X.H., Hua, Z.L. and Qi, Y.Q. 2006. EOF analysis of intra-seasonal variabilities of SST in the East China Sea and Yellow Sea. *Adv. Atmos. Sci*. **24**: 146–155 (in Chinese).

Zhang, L., Wu, L., Lin, X., and Wu, D. 2010. Modes and mechanisms of sea surface temperature low-frequency variations over the coastal China seas. *J. Geophys. Res. Oceans* **115**: doi:10.1029/2009JC006025.

Zheng, Q.A. and Klemas, V. 1982. Determination of winter temperature patterns, fronts, and surface currents in the Yellow Sea and East China Sea from satellite imagery. *Remote Sens. Environ*. **12**: 201–218.

Chemical Oceanography

Preface

The water in the Yellow Sea and the East China Sea originates mainly from the Kuroshio Current. The water resides for about 5 years in the Yellow Sea, which is one of the largest continental shelves in the world. This region receives disproportionally large amounts of anthropogenic materials from the continents via the atmosphere, rivers, and groundwater inputs. Owing to such oceanographic and environmental settings, vigorous biogeochemical alterations of natural and anthropogenic chemical constituents take place in this region. Thus, the observational results in this region may provide key information on the biogeochemical processes of human impacts in the ocean. This chapter aims at understanding the inputs of chemical constituents from rivers, the atmosphere, and groundwater, the biogeochemical reactions in seawater and sediments, and the fluxes in the Yellow Sea and the East China Sea to the Pacific Ocean.

The chapter includes six sections: (1) dissolved methane and nitrous oxide – distribution, controlling factors, and air–sea exchange; (2) nutrient biogeochemistry – spatial and temporal variations, distribution patterns, sources and sinks, and budgets; (3) hypoxia – hypoxia events, current features, organic matter decomposition, and impact of hypoxia; (4) biogeochemical tracers – trace elements and radioisotopes in seawater, sediments, and depositional fluxes; (5) persistent organic pollutants (POPs) and heavy metal pollution – OCPs, PCBs, SCCPs, Brominated POPs, Fluorinated POPs, and heavy metals; (6) atmospheric deposition – dusts, trace elements, and nutrients.

Although there has been remarkable progress in the accurate analyses of various chemical constituents in this region during the last few decades, the measurements are limited to specific areas in specific seasons. Therefore, more comprehensive studies covering the entire Yellow Sea and the East China Sea over different seasons are necessary to better understand biogeochemical characteristics and cycling. Since this region is included in the Exclusive Economic Zones of three countries, extensive collaboration is necessary for cooperative research cruises, sampling exchanges, and data exchanges. In order to compile the data from different laboratories and regions, inter-comparison of experiments and data validation steps are also necessary. All these cooperative activities can be performed more efficiently through international platforms such as PICES.

Jing Zhang, Su Mei Liu, Guebuem Kim

2.1 Dissolved Methane and Nitrous Oxide

Gui-Ling Zhang and Wang-Wang Ye

Key Laboratory of Marine Chemistry Theory and Technology, Ministry of Education, Ocean University of China, China

2.1.1 Introduction

Methane (CH_4), the simplest organic matter, is the most abundant hydrocarbon in the atmosphere. Despite its relatively low concentrations, short-lived CH_4 in the atmosphere is approximately 25 times more effective on a per molecule basis than carbon dioxide (CO_2) in trapping heat. Thus CH_4 has a significant influence on global climate change, the oxidative capacity of the atmosphere, and the chemistry of the stratospheric ozone. The global atmospheric CH_4 has increased significantly since the industrial revolution; the concentration was reported as 1803 ± 2 ppb in 2011, which is about 2.5-fold of that (722 ± 25 ppb) in 1750 (IPCC, 2013). The continuing rise of atmospheric CH_4 indicates an imbalance of sources and sinks. The ocean is one of the natural sources of atmospheric CH_4 (11–18 Tg CH_4 yr^{-1}, Bange *et al.*, 1994). However, CH_4 distributions and emissions in marine ecosystems have large spatial and temporal variations (Bange *et al.*, 1994; Zhang *et al.*, 2004, 2008a). The continental shelf and its margins are potentially the most significant sources of CH_4 to the oceans (Bange *et al.*, 1994; Rehder and Suess, 2001) and show great dynamics in CH_4 distributions and emissions due to complicated influencing factors.

Nitrous oxide (N_2O) is a potent greenhouse gas in the atmosphere, and has a global warming potential of about 300 times that of carbon dioxide and a long atmospheric lifetime of 118 to 131 years (IPCC, 2013). Despite its low atmospheric mixing ratio, N_2O contributes about 6% to the anthropogenic greenhouse effect (IPCC, 2013). It also has the ability to destruct stratospheric ozone (Ravishankara *et al.*, 2009). The N_2O atmospheric mixing ratio has increased up to 20% above pre-industrial levels, from 271 ppb in 1750 to 324 ppb in 2011 (IPCC, 2013), which indicates that sources are larger than sinks. The ocean is the second largest natural source of atmospheric N_2O, with major contributions from the open ocean (Nevison *et al.*, 1995), but disproportionally high contributions from coastal waters (Bange *et al.*, 1996). N_2O in oceanic environments, including estuaries, coastal seas, and the open ocean is produced by microbial processes (Freing *et al.*, 2012). It is mainly formed as a byproduct during nitrification ($NH_4^+ \rightarrow NH_2OH \rightarrow NO_2^- \rightarrow NO_3^-$) and as an intermediate during denitrification ($NO_3^- \rightarrow NO_2^- \rightarrow NO \rightarrow N_2O$) (Bange, 2006). In both processes, the yield of N_2O strongly depends on the concentration of dissolved oxygen. Marine N_2O production and emission show large spatial and temporal variability and may increase substantially as a result of eutrophication and expansion of marine hypoxic regions (Codispoti, 2010; Naqvi *et al.*, 2010). However, measurement of oceanic N_2O is still sparse, and the derived emission estimate has large uncertainties (Nevison *et al.*, 1995; Bange *et al.*, 1996; Seitzinger *et al.*, 2000; Bange, 2006). The quantification of the oceanic N_2O emissions and the identification of the marine pathways of nitrous oxide formation and consumption have received increasing attention during the last few decades.

2.1.2 CH_4 distribution in the East China Sea and Yellow Sea and the controlling factors

CH_4 concentrations in the East China Sea (ECS) and Yellow Sea (YS) have obvious spatial and seasonal variability due to the complex mixing of different water masses and other variables. Maximum CH_4 concentrations, sea–air and sediment–water fluxes all occur during summer. CH_4 concentrations decrease gradually from the coastal area to the open sea, and high levels of CH_4 generally appear near the Changjiang River Estuary and outside Hangzhou Bay (Zhang *et al*., 2004, 2008a,b; Sun *et al*., 2018). In early spring and winter, CH_4 in the shelf region has a uniform distribution from the surface to the bottom, while it increases gradually with depth in other seasons. Published CH_4 data for the ECS are summarized in Table 2.1.1. Horizontally, CH_4 in the surface water (usually 2–5 nM) shows a gradient from onshore to offshore, where the Changjiang River enters the ECS with abundant CH_4 and the Kuroshio intrudes onto the shelf with poor CH_4 concentrations (Zhang *et al*., 2004, 2008a,b; Sun *et al*., 2018). Vertically, three patterns can be generally summarized to differentiate the depth profile of CH_4 in the ECS, *i.e*., with and without the thermocline at the shelf region and deep water at the slope (Fig. 2.1.1). The first two patterns are usually present in the shallow shelf regions near the coast, where the wind and land-source inputs strongly influence the shelf. In summer and autumn, the water column is well stratified, resulting in CH_4 accumulation in the bottom water due to sedimentary release. In winter and early spring, however, the water column is well mixed and the absence of the thermocline at most regions of the ECS supports the diffusion of CH_4 from bottom to surface water and finally its release to the air. Hence CH_4 distribution is vertically uniform in the continental shelf zone in spring and winter. The third pattern is usually present in the deep waters, such as the edge of the shelf or the slope. It is similar to the vertical distribution of CH_4 in the pelagic zone because those areas are far from land and are mainly influenced by the Kuroshio. Specifically, CH_4 in the first 100 m depth is uniform but reaches a subsurface maximum in the next 100 m. Below the peak, CH_4 decreases with depth and stabilizes at the lowest level (~1.0–1.5 nM). Research has shown that high CH_4 is also found at the edge of the continental shelf, where organic matter flows from the coastal region to the oceanic zone and accumulates in the break areas. The YS is a semi-enclosed shelf sea and has shallow water. The horizontal distribution of CH_4 in the YS shows an onshore-to-offshore gradient with the CH_4 concentrations, decreasing with distance off the coast. The vertical profile of CH_4 in the YS is similar to the first two patterns of the ECS due to the shallow water depth (Zhang *et al*., 2004).

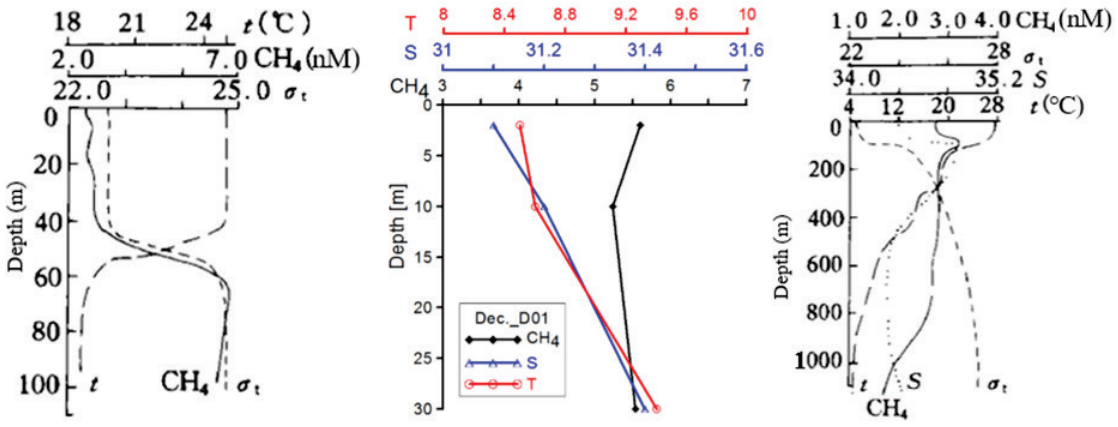

Fig. 2.1.1 Typical depth profiles of CH_4 in the ECS. Modified from Zang (1998) and Sun *et al*. (2018). Reproduced with permission of Elsevier.

Table 2.1.1 Summary of CH_4 measurements in surface waters of the ECS during 2011.

Region	Month	n	CH_4 con. (nM)	CH_4 sat. (%)	U_{10} ($m\ s^{-1}$)	$F_{W2014}(CH_4)$ ($\mu mol\ m^{-2}\cdot d^{-1}$)	$F_{N2000}(CH_4)$ ($\mu mol\ m^{-2}\ d^{-1}$)	$F'(CH_4)$ ($\mu mol\ m^{-2}\ d^{-1}$)
Coastal area (S≤32)	March	5	5.05~29.7 (11.6)	185~1063 (413)	0.2~12.6 (5.7)	0.05~53.7 (14.3)	0.33~50.7 (13.9)	0.85
	May	26	2.45~26.4 (9.09)	99~1107 (386)	1.2~14.8 (7.0)	–0.03~140 (23.7)	–0.03~131 (23.3)	4.46
	August	29	3.71~33.6 (8.84)	182~1644 (433)	1.9~8.9 (5.8)	1.75~119 (18.0)	2.11~121 (18.7)	3.85
	October	4	4.33~13.5 (7.00)	195~589 (344)	5.5~10.9 (8.4)	3.99~51.8 (26.7)	4.29~51.3 (26.3)	1.85
	December	2	5.60~12.1 (8.85)	193~439 (316)	4.7~7.5 (6.1)	2.69~25.5 (14.1)	3.00~25.8 (14.4)	0.57
Open sea (S>32)	March	31	2.39~4.36 (3.55)	96~165 (133)	0.3~13.5 (8.2)	–0.81~14.0 (3.62)	–0.77~13.2 (3.52)	3.36
	May	29	1.88~5.41 (3.14)	91~258 (148)	5.0~23.6 (11.5)	–2.63~86.9 (10.0)	–2.45~77.9 (9.35)	7.84
	August	8	4.03~10.7 (6.54)	206~557 (342)	5.1~8.4 (6.6)	5.65~25.3 (14.9)	5.92~26.4 (15.4)	12.0
	October	32	2.82~4.37 (3.80)	142~215 (190)	7.2~11.8 (9.1)	7.98~11.2 (9.11)	7.59~11.1 (9.01)	8.43
	December	34	3.12~6.67 (4.34)	135~280 (186)	3.7~14.1 (8.8)	1.36~26.9 (10.1)	1.61~25.6 (9.84)	9.57

Number in brackets is the mean value of each item.
CH_4con. and CH_4sat. denote CH_4 concentration and saturation rate, respectively.
U_{10} is the wind speed at 10 m above the sea surface.
$F_{W2014}(CH_4)$ and $F_{N2000}(CH_4)$ represent the sea–air flux density calculated by the W2014 and N2000 models, respectively.
$F'(CH_4)$ indicates the area-weighted mean sea–air CH_4 flux in each sub-area.

CH_4 distribution in the ECS is significantly influenced by complex mixing of various water masses, such as Changjiang diluted water, Taiwan Warm Current Water and Kuroshio (Zhang *et al.*, 2004; Sun *et al.*, 2018). The high CH_4 content (hundreds of nM) in the Changjiang River is an important source that impacts the CH_4 concentration along the coast, although most of CH_4 is removed via air–sea exchange and aerobic methane oxidation during the mixing in the estuary. The Kuroshio, however, with low CH_4 content, is an important sink of shelf CH_4. Export to the open sea via the Kuroshio accounts for 60% of total riverine input (Zhang *et al.*, 2004). Sediment release is another important source of dissolved CH_4 in the water column of the ECS and YS. CH_4 can be produced via bacterial degradation of organic matter in the sediments of the shelf and slope regions. The rivers carry high loads of nutrients, suspended particles and organic carbon into the ECS, which provide favorable conditions for methanogenesis. The annual average CH_4 release rate from sediments is about 1.11 $\mu mol\ m^{-2}\ d^{-1}$ on the continental shelf of the ECS (Sun *et al.*, 2018). The maximum CH_4 concentration and sediment–water CH_4 flux both occur in summer, which might be related to the occurrence of hypoxia in the bottom water.

Temperature can affect the gas solubility and microbial production rates of CH_4, which then leads to the seasonal variation of CH_4 in the ECS. Correlation between temperature and CH_4 has been found in the ECS, indicating that temperature is an important factor in regulating the distribution and emission of CH_4 (Sun *et al.*, 2018). Oxygen is another potential factor that regulates CH_4 distribution. CH_4 is traditionally thought to be produced in strictly anoxic environments, while it can be consumed in aerobic seawater by bacterial oxidation. High CH_4 concentrations (>13 nM) within hypoxic waters (DO < 2 mg L^{-1}) were observed at the bottom water and weak negative correlation

between CH_4 and oxygen was observed in the ECS during the seasonal hypoxia off the Yangtze River Estuary (Ye *et al*., 2016). Except for traditional production in the anoxic environment (*i.e*., sediment, suspended particles), CH_4 can also be formed in the oxygenated water via degradation of methyl compounds such as dimethylsulfoniopropionate (DMSP) and methylphosphonate (MPn), and these aerobic CH_4 production mechanisms have also been proved in the ECS and YS (Ye *et al*., 2020, 2021). In the coastal seawaters of the YS, CH_4 was observed to accumulate after MPn enrichment with high MPn-to-CH_4-conversion efficiency (~60%). Moreover, several *Vibrio* isolates isolated from the coastal waters were found to produce CH_4 while growing in culture using MPn as the sole phosphorus (P) source, thus indicating that *Vibrio* spp. are capable of cleaving MPn for P acquisition and might be the major contributors to MPn-dependent CH_4 production (Ye *et al*., 2020). Results from both laboratory and field incubations showed an increase in CH_4 after the addition of DMSP to the seawater from the ECS, indicating that the DMSP-dependent CH_4 production occurs in the coastal seawaters (Ye *et al*., 2021). For CH_4 oxidation, Tsurushima *et al*. (1996) estimated that the CH_4 turnover time in the ECS is longer than one year, which has a minor impact on CH_4 distribution, but might be shorter for coastal waters which contain a large amount of CH_4.

2.1.3 Distribution of N_2O in the East China Sea and Yellow Sea and the influencing factors

Previously published N_2O data are summarized in Table 2.1.2 which shows seasonal and spatial variations in the East China Sea and the Yellow Sea. N_2O concentrations showed an offshore decreasing trend in surface distribution, and a surface-to-bottom increasing gradient in the water column (Zhang *et al*., 2008a; Wang *et al*., 2016). The surface N_2O concentration was highest in summer, followed by fall, and the lowest N_2O usually was found in early spring.

Table 2.1.2 Summary of N_2O measurements in the surface waters of the Yellow Sea and East China Sea.

Study area	Date	Surface N_2O (nmol L^{-1})	N_2O saturation (%)	Flux (μmol m^{-2} d^{-1})	Reference
North Yellow Sea	2005.3	(11.94 ± 2.88)	(90 ± 22)	(–1.3 ± 4.0)[a] (–1.9 ± 6.2)[b]	Yang *et al*. (2009)
	2006.8	(11.68 ± 3.34)	(163 ± 45)	(6.5 ± 8.3)[a] (11.3 ± 13.4)[b]	
	2007.10	(11.90 ± 1.62)	(149 ± 20)	(7.9 ± 8.2)[a] (13.8 ± 14.3)[b]	
East China Sea	2003.9	5.75–24.1 (11.5 ± 4.5)	94–382 (191 ± 74)	(9.8 ± 16.0)[a] (17.1 ± 26.4)[b]	Zhang *et al*. (2008a)
	2011.5	6.31–11.88 (9.13 ± 1.45)	93–139 (119 ± 10)	(4.96 ± 6.12)[a] (10.25 ± 17.18)[b]	Ma *et al*. (2014)
	2013.8	6.33–11.07 (8.47 ± 0.85)	106–168 (140 ± 13)	0.6–42.0[b] (12.2 ± 10.8)[b] 0.8–31.9[d] (9.8 ± 8.2)[d]	Wang *et al*. (2016)

Numbers in brackets are average values.
[a] k_w was estimated by the LM86 equation; [b] k_w was estimated by the W92 equation; [d] k_w was estimated by the N00 equation.

The distribution of N_2O in the ECS was found to be influenced mainly by water temperature, mixing of water masses, and biological production. N_2O concentrations showed a negative correlation with temperature, but a positive one with suspended particulate matter concentration. There was no specific overall correlation observed between salinity and N_2O concentration, but a coupled increasing trend within the salinity range of 0–2 and a decreasing trend within the salinity range of 2–30 was found at the Changjiang River Estuary (Wang *et al*., 2016). Nitrification was considered to be the main process that controls the N_2O production. Prominent bottom water hypoxia occurred in the northern ECS in summer, where the nitrification and denitrification processes and the production of N_2O were expected to be enhanced, but only a slight increase of N_2O concentrations was found. The frequent vertical mixing of the water column prevented the accumulation of N_2O in the bottom waters to significantly high levels, and may lead to more emission of N_2O to the atmosphere (Wang *et al*., 2016).

2.1.4 Sea-to-air fluxes of CH_4 and N_2O in the East China Sea and Yellow Sea

The ECS and YS are net sources of atmospheric CH_4 and N_2O. CH_4 in the surface water of the ECS is usually at supersaturated levels (140–480%) (Zhang *et al*., 2004; Sun *et al*., 2018). The calculated sea-to-air fluxes of CH_4 ranged from 2.8–36.3 μmol m^{-2} d^{-1}, and CH_4 emissions from surface water in summer and autumn are higher than those in spring and winter. Sun *et al*. (2018) estimated the annual mean area-weighted sea–air flux density of CH_4 in the ECS to be about 10.7 μmol m^{-2} d^{-1} in 2011. Accordingly, an area-weighted, seasonally adjusted annual rate of CH_4 efflux from the ECS to the atmosphere was estimated to be 2.98 × 109 mol yr^{-1} (~0.05 Tg CH_4 yr^{-1}). Hence the ECS is an active site for CH_4 emissions to the atmosphere and contributes about 0.55% of total emissions from the global ocean. In the YS, the sea-to-air fluxes of CH_4 were 1.3 μmol m^{-2} d^{-1} in spring and 21.1 μmol m^{-2} d^{-1} in summer, respectively (Yang *et al*., 2010). The seasonal variability of the fluxes is mainly due to the variations in CH_4 surface concentration, temperature, and wind speed. Due to the large variations during different observations, CH_4 emissions from the YS and the ECS still have large uncertainties and are possibly underestimated.

Surface N_2O saturations in the ECS ranged from 90% to 660% (Zhang *et al*., 2008a; Wang *et al*., 2016). Wang *et al*. (2016) estimated the sea-to-air fluxes of N_2O as 30.6 ± 59.1 μmol m^{-2} d^{-1} from the Changjiang River Estuary, 9.8 ± 8.8 μmol m^{-2} d^{-1} from the coastal region and shelf, and 21.0 ± 12.7 μmol m^{-2} d^{-1} from the continental slope using the Wanninkhof (1992) equation. Annual N_2O emission from the ECS was estimated to be about 8.2 × 10^{-2} to 16.0 × 10^{-2} Tg N_2O yr^{-1}. Although the ECS only accounts for 0.2% of the world's oceanic area, it accounts for about 0.8% of global oceanic N_2O emission; hence the ECS is an active region for N_2O production and emission.

The saturation of dissolved N_2O in the North Yellow Sea showed obvious seasonal variations with higher values occurring in summer and autumn and lower values in spring, and the dissolved N_2O of the surface water changed from undersaturated to oversaturated with the water temperature, gradually increasing during three cruises in spring (Yang *et al*., 2009). Correlation analysis showed that temperature was the main factor influencing N_2O saturations. The estimated average N_2O fluxes ranged between 0.6 and 13.8 μmol m^{-2} d^{-1} for spring, summer, and autumn, which showed obvious seasonal variations, with the N_2O fluxes of summer and autumn higher than those of spring. Based on the average annual N_2O flux and the area of the North Yellow Sea, the annual N_2O emission from the studied area was estimated to be 5.3 × 10^{-3} to 9.2 × 10^{-3} Tg yr^{-1}. Hence, the North Yellow Sea is a net source of atmospheric N_2O.

2.1.5 Future perspective

Although previous research has given us a glimpse of CH_4 and N_2O cycling in the ECS and YS, we are still far from understanding the seasonal variations of CH_4 and N_2O distribution and emission, and quantification of CH_4 and N_2O sources and sinks in these areas. Most studies were based on discrete sampling and were conducted at large sampling intervals with coarse spatial resolution. In order to obtain high-quality data to evaluate the role of the ECS and YS in the global ocean, continuous measurements with higher temporal and spatial resolution are needed. Another prospect for future studies is the biological production processes of CH_4 and N_2O in seawater. The budget of CH_4 and N_2O in the ECS remains a puzzle because the contribution of microbial processes is still ambiguous. The explanation of "the oceanic methane paradox" is a hot topic, and aerobic CH_4 production in oxygenated water has been gradually revealed by recent studies. For the marginal seas of China, which pathway is the dominant one: the traditional one, the new one, or both? Is the CH_4 production mechanism the same as that in the open ocean, or does CH_4 in the ECS have a specific biogeochemical cycle due to the complicated conditions? The relative importance of the microbial processes (*i.e.*, nitrification, denitrification, and nitrifier denitrification) leading to the production and consumption of N_2O in the ECS and YS remains unclear. The isotopic composition of N_2O has been used to characterize local production and consumption mechanisms of dissolved N_2O in marine environments. Hopefully, new techniques (such as isotopes) may help us make progress on this in the future. Thus more studies on CH_4 and N_2O in the coastal and shelf waters of the ECS and YS are still needed to further enrich the global oceanic CH_4 and N_2O database, and to understand the biogeochemical cycles of CH_4 and N_2O in the shelf areas and their regional contribution to global oceanic CH_4 and N_2O emission.

2.1.6 References

Bange, H.W. 2006. Nitrous oxide and methane in European coastal waters. *Estuar Coast. Shelf Sci*. **70**: 361–374, doi:10.1016/j.ecss.2006.05.042.

Bange, H.W., Bartell, U.H., Rapsomanikis, S. and Andreae, M.O. 1994. Methane in the Baltic and North Seas and a reassessment of the marine emissions of methane. *Global Biogeochem. Cycles* **8**: 465–480, doi:10.1029/94GB02181.

Bange, H.W., Rapsomanikis, S. and Andreae, M.O. 1996. Nitrous oxide in coastal waters. *Global Biogeochem. Cycles* **10**: 197–207, doi:10.1029/95GB03834.

Codispoti, L.A. 2010. Interesting times for marine N_2O. *Science* **327**: 1339–1340, doi:10.1126/science.1184945.

Freing, A., Wallace, D.W.R. and Bange, H.W. 2012. Global oceanic production of nitrous oxide. *Philos. Trans. R. Soc. London Ser. B* **367**: 1245–1255, doi:10.1098/rstb.2011.0360.

IPCC (Intergovernmental Panel on Climate Change). 2013. Climate Change 2013: the physical science basis. Contribution of Working Group I to the Fifth Assessment Report of the Intergovernmental Panel on Climate Change *edited by* T.F. Stocker, D. Qin, G.K. Plattner, M. Tignor, S.K. Allen, J. Boschung, A. Nauels, Y. Xia, V. Bex and P.M. Midgley, Cambridge University Press, Cambridge.

Ma, X., Zhang, G.L., Cao, X.P., Song, G.D., Wang, L. and Liu, S.M. 2014. Distribution and air-sea fluxes of dissolved nitrous oxide in the East China Sea in spring. *Mar. Sci.* **38**: 21–28 (in Chinese).

Naqvi, S.W.A., Bange, H.W., Farias, L., Monteiro, P.M.S., Scranton, M.I. and Zhang, J. 2010. Coastal hypoxia/anoxia as a source of CH_4 and N_2O. *Biogeosciences* **7**: 2159–2190, doi:10.5194/bg-7-2159-2010, 2010.

Nevison, C.D., Weiss, R.F. and Erickson, D.J. 1995. Global oceanic emissions of nitrous oxide. *J. Geophys. Res. Oceans* **100**: 15,809–15,820, doi:10.1029/95JC00684.

Nevison, C.D., Lueker, T.J. and Weiss, R.F. 2004. Quantifying the nitrous oxide source from coastal upwelling. *Gobal Biogeochem. Cycles* **18**: doi:10.1029/2003GB002110.

Ravishankara, A.R., Daniel, J.S. and Portmann, R.W. 2009. Nitrous oxide (N_2O): The dominant ozone-depleting substance emitted in the 21st century. *Science* **326**: 123–125, doi:10.1126/science.1176985.

Rehder, G. and Suess, E. 2001. Methane and pCO_2 in the Kuroshio and the South China Sea during maximum summer surface temperatures. *Mar. Chem.* **75**: 89–108,doi:10.1016/S0304-4203(01)00026-3.

Seitzinger, S.P., Kroeze, C. and Styles, R.V. 2000. Global distribution of N_2O emissions from aquatic systems: natural emissions and anthropogenic effects. *Chemosphere Global Change Sci*. **2**: 267–279, doi:10.1016/S1465-9972(00)00015-5.

Sun, M.S., Zhang, G.L., Ma, X., Cao, X.P., Mao, X.Y., Li, J., Ye, W.W. and Liu, S.M. 2018. Dissolved methane in the East China Sea: Distribution, seasonal variation and emission. *Mar. Chem*. **202**: 12–26, doi:10.1016/j.marchem.2018.03.001.

Tsurushima, N., Watanabe, S. and Tsunogai, S. 1996. Methane in the East China Sea Water. *J. Oceanogr*. **52**: 221–233, doi:10.1007/BF02235671.

Wang, L., Zhang, G., Zhu, Z., Li, J., Liu, S., Ye, W. and Han, Y. 2016. Distribution and sea-to-air flux of nitrous oxide in the East China Sea during the summer of 2013. *Cont. Shelf Res*. **123**: 99–110, doi:10.1016/j.csr.2016.05.001.

Wanninkhof, R. 1992. Relationship between wind speed and gas exchange over the ocean. *J. Geophys. Res. Oceans* **97**: 7373–7382, doi:10.1029/92JC00188.

Yang, J., Zhang, G.-L., Zheng, L.-X. and Zhang, F. 2009. Seasonal variation of fluxes and distributions of dissolved nitrous oxide in the North Yellow Sea. *Environ. Sci*. **30**: 656–662 (in Chinese).

Yang, J., Zhang, G.-L., Zheng, L.-X., Zhang, F. and Zhao, J. 2010. Seasonal variation of fluxes and distributions of dissolved methane in the North Yellow Sea. *Cont. Shelf Res*. **30**: 187–192, doi: 10.1016/j.csr.2009.10.016.

Ye, W., Zhang, G., Zhu, Z., Huang, D., Han, Y., Wang, L. and Sun, M. 2016. Methane distribution and sea-to-air flux in the East China Sea during the summer of 2013: Impact of hypoxia. *Deep Sea Res. II* **124**(Suppl. C): 74–83, doi:10.1016/j.dsr2.2015.01.008.

Ye, W.-W., Wang, X.-L., Zhang, X.-H. and Zhang, G.-L. 2020. Methane production in oxic seawater of the western North Pacific and its marginal seas. *Limnol. Oceanogr.* **65**: 2352–2365, doi:10.1002/lno.11457.

Ye, W.-W., Du, G.-X., Zhang, H.-H. and Zhang, G.-L. 2021. Methane in the Yellow Sea and East China Sea: dynamics, distribution and production. *J. Oceanol. Limnol.* doi:10.1007/s00343-021-1010-4.

Zang, J. 1998. Dissolved methane in sea water of the East China Sea. *Acta Oceanol. Sin*. **20**: 52–59 (in Chinese).

Zhang, G.L., Zhang, J., Kang, Y.B. and Liu, S.M. 2004. Distributions and fluxes of methane in the East China Sea and the Yellow Sea in spring. *J. Geophys. Res. Oceans* **109**: doi:10.1029/2004JC002268.

Zhang, G., Zhang, J., Ren, J., Li, J. and Liu, S. 2008a. Distributions and sea-to-air fluxes of methane and nitrous oxide in the North East China Sea in summer. *Mar. Chem*. **110**: 42–55, doi:10.1016/j.marchem.2008.02.005.

Zhang, G., Zhang, J., Liu, S., Ren, J., Xu, J. and Zhang, F. 2008b. Methane in the Changjiang (Yangtze River) Estuary and its adjacent marine area: Riverine input, sediment release and atmospheric fluxes. *Biogeochemistry* **91**: 71–84, doi: 10.1007/s10533-008-9259-7.

2.2 Nutrients Biogeochemistry

Su Mei Liu[1,2] and Yu Umezawa[3]

[1] Frontiers Science Center for Deep Ocean Multispheres and Earth System, and Key Laboratory of Marine Chemistry Theory and Technology, Ministry of Education, Ocean University of China, China
[2] Qingdao National Laboratory for Marine Science and Technology, China
[3] Tokyo University of Agriculture and Technology, Japan

2.2.1 Introduction

Nutrient dynamics has been greatly altered by human disturbances and global change over the last century. Excessive nutrient discharges and changes in relative nutrient concentrations caused by land use transformation and anthropogenic emissions have been known to result in eutrophication, hence modifying aquatic food webs and causing severe hypoxic events in coastal environments. Water exchange between coastal and offshore waters can also be a very important factor affecting coastal ecosystems

Many rivers, such as the Yalujiang and Changjiang (Yangtze River) transport large amounts of water and suspended matter from the continent into the Yellow Sea and East China Sea (YECS, Fig. 2.2.1). Dust and soil particles from Northeast Asia are transported to these seas via the atmosphere and are deposited on the sea surface. The rainfall is 1000–2000 mm in the East China Sea (ECS) and 600–800 mm in the Yellow Sea (YS). Circulation, upwelling, riverine transport, and atmospheric deposition carry nutrients to the surface water of the YECS. The nutrient budgets for the YECS have

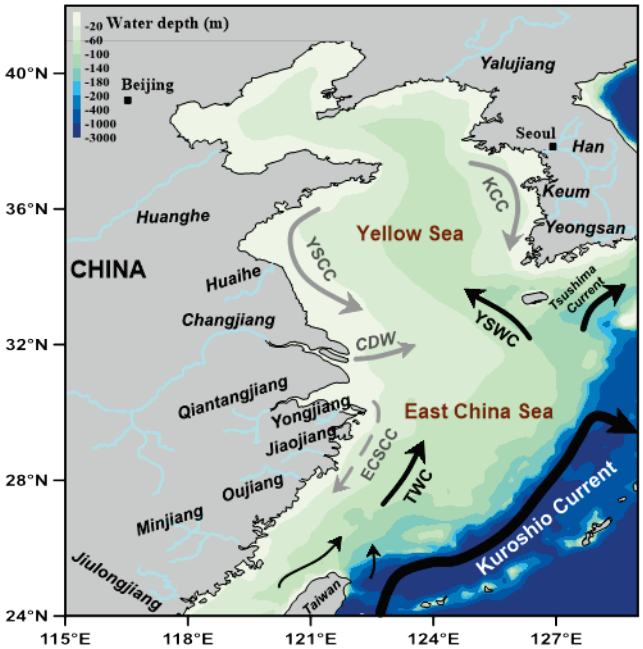

Fig. 2.2.1 Map of the Yellow Sea and East China Sea, showing the location of large rivers dealt with in this study. The circulation regimes and main water masses are also indicated, including the Yellow Sea Warm Current (YSWC), Yellow Sea Coastal Current (YSCC), Korea Coastal Current (KCC), Taiwan Warm Current (TWC), East China Sea Coastal Current (ECSCC), and Kuroshio.

been evaluated for the relative importance of external nutrient inputs *versus* physical transports and internal biogeochemical processes (Chen and Wang, 1999; Liu *et al*., 2003a; Zhang *et al*., 2007).

Historical observation of nutrients in this region started in the late 1950s, including several national and international cooperative programs in the 1980s. Most of these research activities focused on the distribution and variation of nutrients in the water column. The YECS is the area receiving the most extensive marine research, which forms a strong data basis for our knowledge of nutrient biogeochemistry in this region. However, there is almost no review that is internationally available.

2.2.2 Spatial and temporal variations of nutrients

Nutrients biogeochemistry is highly dynamic in the YECS, with different characteristics for various parts from the north to the south (Zhang and Su, 2006).

Nutrients in the Yellow Sea

High surface concentrations of nutrients are found in the coastal areas in summer, 5- to 10-fold higher than those in the Central YS, reflecting the effects of the Changjiang effluent plume, surface runoff in the west and east coasts and the circulation in the YS (Chung *et al*., 1999; Liu *et al*., 2003a; Zhang and Su, 2006). In winter, high concentrations of nutrients are found south of the YS, reflecting the influence of the YS warm current water originating from the Tushima warm current extending northwestward to enter the YS, but nutrients are deficient in the northwestern YS (Wang *et al*., 2003). In addition, nutrient concentrations in the central part of the YS are generally higher than those in coastal areas, owing to strong vertical mixing by northerly winds and reduction of land-source input (*e.g*., river) in winter (Zhang and Su, 2006). Moreover, the concentrations of nutrients in near-bottom waters are significantly higher in the Central YS (*i.e*., Yellow Sea Cold Water Mass: YSCWM) than those in the coastal region (Chung *et al*., 1999; Liu *et al*., 2003a). The high concentrations of nitrogen compounds and $Si(OH)_4$ in the Jiangsu coastal zone and southwest results most likely from the convergence of the Yellow Sea Coastal Current and the Changjiang effluent (Wu *et al*., 2011). Elevated suspended particulate matter in the Jiangsu coastal zone and southwest of the YS is responsible for the high concentration of nutrients, particularly particulate nitrogen (N) and particulate phosphorus (P), where the sediment mainly comes from the Changjiang Delta and the abandoned Huanghe Delta. The high concentration of PO_4^{3-} in the southern YS, especially the southeast part, indicates intrusion of waters from ECS and terrigenous inputs in the east and west sides (Liu *et al*., 2003a). In spring, high concentrations of nutrients cover the coastal areas affected by Changjiang Diluted Water (CDW) and the prevailing southerly winds. In contrast, the concentration of nutrients in the northern and eastern YS are very low. In autumn, high concentrations of nutrients are found in the southwestern and eastern coastal waters of the YS which are related to the low freshwater discharge and the prevailing northeasterly wind (Wang *et al*., 2003).

For total P (TP), dissolved organic phosphorus (DOP) is the dominant species, representing 50% of the TP, PO_4^{3-} and particulate P (PP) accounts for 30% and 20% of the TP, respectively. For nitrogen compounds, dissolved organic nitrogen (DON) is dominant in the upper 10 m water column, accounting for 70% of the total dissolved nitrogen (TDN), but only 30% of the TDN in near-bottom waters; particulate nitrogen (PN) represents 25% of the total nitrogen (TN). The high concentrations of DON and DOP should be considered in models of nutrients cycling, which could help to explain observations of nutrient limitation in ecosystems of the YS (Liu *et al*., 2003a).

The spring phytoplankton bloom is an important phenomenon in the YS. Jin *et al.* (2013) addressed the coupling between the nutrient condition and phytoplankton blooms in the YS. They indicate that abundant nutrients and the fitting nutrients ratios in the central YS provide favorable conditions for the onset of phytoplankton blooms. The upward nutrient fluxes from deep water to the euphotic zone by means of diffusion and turbulent entrainment are important nutrient sources to sustain the bloom, and they appear to represent 56 to 69% of the nutrients requested for phytoplankton growth (Jin *et al.*, 2013).

Nutrients in the East China Sea

The ECS receives a tremendous riverine supply of fresh water, suspended sediment and nutrients, notably from China. The salt marsh in the Changjiang Estuary plays an important ecological role in nutrient transport from the river to offshore areas, and increases P limitation (Liu *et al.*, 2016). Eutrophication has become an overwhelming phenomenon in the coastal environment off the Changjiang Estuary; high-level nutrients from land-sources are constrained to the inner and middle shelf region with P as a limiting element for phytoplankton growth (Zhang *et al.*, 2007; Gao *et al.*, 2015), red-tide events happen frequently and hypoxia exists in near-bottom waters (Zhu *et al.*, 2011, 2016, 2017; Liu *et al.*, 2015), while the open ECS shelf and slope waters remain oligotrophic (Zhang *et al.*, 2007). Across the ECS shelf, nutrients in surface waters gradually decrease from eutrophic coastal to oligotrophic open shelf waters, and the influence of land-source nutrients can be seen at the surface over a distance of up to 250–300 km from the coast (Wu *et al.*, 2003; Ren *et al.*, 2006). Taiwan Warm Current Water and Kuroshio Surface Water are devoid of nutrients. The Kuroshio Subsurface Water is rich in nutrients, and extensive exchange of water and nutrients between the ECS and Kuroshio occurs across the shelf break region through upwelling and frontal processes and spreads over a broad part of the shelf, reaching water depth of 50–100 m at mid-shelf (Chen *et al.*, 1995; Chen, 1996; Gong *et al.*, 1996; Liu *et al.*, 2000; Zhang *et al.*, 2007). The exchange across the shelf edge with the Kuroshio is of great importance for productive fisheries and the nutrient budget (Chen and Wang, 1999; Zhang and Su, 2006).

Nutrients in the Changjiang Estuary and the ECS show seasonal variations in terms of riverine input, biological activities, and current regime (Zhang *et al.*, 2007; Chen, 2008; Liu *et al.*, 2016). In summer, affected by riverine input, upwelling, and monsoons, high concentrations of nutrients cover the Changjiang Estuary and the river plume which extends towards Cheju Island, in the area southwest of Korea, and in an upwelling area northeast of Taiwan (Zhang *et al.*, 2007; Chen, 2008). In winter, cooling and strong vertical mixing result in the concentrations of nutrients generally exceeding those in summer, especially in the surface layer. Affected by the strong northeasterly monsoon, high concentrations of nutrients derive from the Changjiang flow southwestward along the coast of southeastern China (Zhang *et al.*, 2007; Chen, 2008). While the concentration of nutrients is deficient in the offshore area of the ECS, which is related to the influence of the Kuroshio and the Taiwan Warm Current intruding into the saline warm surface waters of the ECS, the Subei coastal current extends southeastward to enter the northern ECS, with low discharge and a prevailing northeasterly wind (Wang *et al.*, 2003; Chen, 2008). In spring and fall, spatial variations of nutrients are subject to transitions between summer and winter.

2.2.3 Main sources and sinks of nutrients

Riverine input

The Chinese rivers are characterized by high dissolved inorganic nitrogen (DIN) and low PO_4^{3-} concentrations with high DIN/PO_4^{3-} ratios. The dissolved silicate levels, in general, are higher in the

warm and high-flow South China rivers than those in the cold and low-flow North China rivers, due to differences in climate, rock type, and physical and chemical weathering (Zhang, 1996). Nutrient levels in the Chinese rivers are higher than those from the large and less-disturbed rivers in the world such as the Amazon and the Congo, but comparable to the values for the European and North American polluted and eutrophic rivers such as the Loire, Po, Rhine, and Seine (Zhang, 2002). The concentrations and fluxes of nutrients in the rivers that empty into the YECS are provided in Tables 2.2.1 and 2.2.2.

Table 2.2.1 Concentrations (μM) of nutrients in the major Chinese and Korean rivers discharging into the Yellow Sea and East China Sea. Data from Liu, S.M. *et al*. (2009) and references therein.

River	Season	NO_3^-	NO_2^-	NH_4^+	PO_4^{3-}	$Si(OH)_4$
Nutrient concentrations from rivers to the Yellow Sea						
Huaihe	Dec 2004–Feb 2005	76.3	1.71	16.5	4.02	38.1
Yalujiang	August 1992, 1994	268	0.37	2.38	0.30	127
Yalujiang	May 1996	76.3	0.17	5.78	0.09	146
Han	June 1992	57.1	2.0	75.8	3.5	36.9
Han	June 2000	97.6	12.7	217.5	–	–
Keum	1997–1998	160	1.5	26.5	1.4	85
Yeongsan	1998–2000	–	–	37.1	3.9	72.2
Nutrient concentrations from rivers to the East China Sea						
Changjiang*	January 1997–2001	62.7	0.61	16.0	0.49	112.0
Changjiang*	July 1997–2001	70.2	0.07	4.64	0.34	100.2
Qiantangjiang	August 2004	101	1.54	0.70	1.00	128
Yongjiang	May 2002	119	11.1	–	3.2	183
Jiaojiang	October 1994	123	–	0.59	2.21	162
Oujiang	August 2004	72.3	0.44	3.21	0.30	150
Minjiang	October 1986	65	–	4.13	1.45	208
Minjiang	June 1986	45	–	3.61	0.50	156
Jiulongjiang	Summer	36.2	–	10.7	0.61	261
Jiulongjiang	Winter	36.2	–	19.6	0.91	279.4

* Note: Part of the Changjiang freshwater discharge empties into the Yellow Sea (Liu *et al*., 2003a).

Nitrogen and phosphorus originate from both agricultural and domestic wastes, and nitrogen is preferentially leached from the drainage basin compared to reactive phosphorus. The longer residence time in the estuaries allows for greater utilization of nutrients by phytoplankton than in the rivers (Liu, S.M. *et al*., 2009).

Almost 30 rivers empty into the YS, including the Yalujiang, Huaihe, Han, Keum, and Yeongsan (Liu *et al*., 2003a). The Changjiang drains directly into the ECS, but the discharge of the Changjiang can be carried into the YS (Fig. 2.2.1), especially in summer when the Changjiang effluent may reach Cheju Island (Le, 1984). Twelve to 27% of the Changjiang discharge empties into the YS from June to October, with the highest discharge in August. About 10% of the Changjiang discharge empties into the YS in November and December while less than 5% of the Changjiang discharge empties into the YS from January to May. The annual water discharge to the YS is 14.1% (130×10^9 m^3) of the Changjiang discharge (Liu *et al*., 2003a). The riverine input fluxes of NO_3^-, NH_4^+, PO_4^{3-}, and $Si(OH)_4$ to the YS are 24 ± 12, 2.7 ± 1.4, 0.42 ± 0.21, and 23.2 ± 11.6 × 10^9 mol yr^{-1}, respectively. Compared to riverine nutrient inputs to the YS from China and

Korea, the NO_3^- inputs were mainly by Yalujiang (~50%) and Changjiang (~40%), the NH_4^+ and PO_4^{3-} inputs were mainly by Han River (~50%) and Changjiang (20–30%), and the $Si(OH)_4$ inputs were mainly by Changjiang (57%) and Yalujiang (~30%). This indicates that riverine inputs of NO_3^- and $Si(OH)_4$ are mainly from Chinese rivers (Changjiang and Yalujiang), while inputs of NH_4^+ and PO_4^{3-} are mainly by Korean rivers (*e.g.*, Han River), followed by a Chinese river (Changjiang).

Table 2.2.2 Nutrient fluxes ($\times 10^6$ mol d^{-1}) from rivers to the Yellow Sea and East China Sea. The data are from Liu, S.M. *et al*. (2009) and references therein.

River	Season	NO_3^-	NO_2^-	NH_4^+	PO_4^{3-}	$Si(OH)_4$
Nutrient fluxes transport from rivers to the Yellow Sea						
Huaihe	Dec 2004–Feb 2005	5.52	0.12	1.19	0.29	2.76
Yalujiang	August 1992, 1994	29.2	0.040	0.26	0.033	13.8
Yalujiang	May 1996	4.81	0.011	0.37	0.006	9.21
Han	June 1992, 2000	4.43	0.42	8.40	0.20	2.11
Keum	1997–1998	2.54	0.024	0.42	0.022	1.35
Yeongsan	1998–2000	–	–	0.21	0.022	0.42
Nutrient fluxes transport from rivers to the East China Sea						
Changjiang*	January 1997–2001	65.9	0.64	16.8	0.51	117.7
Changjiang*	July 1997–2001	277.4	0.28	18.3	1.34	395.9
Qiantangjiang	August 2004	9.46	0.14	0.066	0.094	12.0
Yongjiang	May 2002	1.12	0.11	–	0.030	1.73
Jiaojiang	October 1994	2.24	–	0.011	0.040	2.96
Oujiang	August 2004	2.89	–	0.13	0.012	6.00
Minjiang	Winter	4.48	0.11	0.28	0.10	14.3
Minjiang	Summer	12.5	0.23	1.00	0.14	43.2
Jiulongjiang	Summer	2.6	–	0.78	0.04	19.1
Jiulongjiang	Winter	0.5	–	0.30	0.01	4.2

* Note: Part of the Changjiang freshwater discharge empties into the Yellow Sea (Liu *et al*., 2003a).

This is due to the fact that Chinese rivers appear to be largely contaminated by agricultural practices and Korean rivers are largely contaminated by municipal sewage (Liu *et al*., 2003a). A number of rivers empty into the ECS, including the Changjiang, Jiaojiang, Oujiang, Minjiang, Jiulongjiang. In total, riverine input to the ECS is $63.2 \pm 19.8 \times 10^9$ mol yr^{-1} of NO_3^-, $6.01 \pm 2.21 \times 10^9$ mol yr^{-1} of NH_4^+, $0.41 \pm 0.10 \times 10^9$ mol yr^{-1} of PO_4^{3-}, and $103.5 \pm 29.2 \times 10^9$ mol yr^{-1} of $Si(OH)_4$ (Table 2.2.2).

Nutrients recycling in sediments

Although sediments of the coastal environment play an important role in nutrients recycling, there are limited studies in the YECS. Based on incubation experiments on a boat, the fluxes of NO_3^-, NH_4^+, PO_4^{3-}, and $Si(OH)_4$ at the sediment–water interface were 185 ± 14.3, -1.81 ± 0.24, 0.035 ± 0.012, and $138 \pm 35.4 \times 10^9$ mol yr^{-1}, respectively, in the YS in May 1998 (Liu *et al*., 2003a). The primary production of the YS sampled during three cruises in spring (April 1996, May 1995 and 1997) revealed values of 68–5303 mgC m^{-2} d^{-1} with an average of 2066 mgC m^{-2} d^{-1} (Yang *et al*., 1999). Based on Redfield ratios (C: N: P = 106:16:1), 0.86–66.7 mmol m^{-2} d^{-1} for nitrogen and

0.053–4.17 mmol m^{-2} d^{-1} for phosphorus can be estimated to support phytoplankton growth. Comparison with the benthic fluxes of nutrients reveals that sediment–water exchange could match 2 to 150% of the N requirement for phytoplankton, but could only match <1% of the P requirement for phytoplankton, which is indicative of either a rapid PO_4^{3-} recycling in the water column or important riverine and atmospheric inputs. These calculations indicate a smaller role for sediments in supplying nutrients for phytoplankton than for some other systems, for example, Chesapeake Bay and Mobile Bay (Cowan and Boynton, 1996; Cowan *et al*., 1996).

The fluxes of NH_4^+, NO_3^-, and $Si(OH)_4$ at the sediment–water interface were –2.6–3.4, –1.4–3.2, 0.13–13.2 mmol m^{-2} d^{-1}, respectively, in the Changjiang Estuary in June 1980, and August and November–December 1981 (Aller *et al*., 1985). This was the first study on benthic nutrient regeneration in Chinese seas. In spring 2001 and 2002, sediment-core incubations indicated that nutrient exchange fluxes in the ECS were –0.385–0.143 mmol m^{-2} d^{-1} for NO_3^-, –1.42–0.548 mmol $m^{-2}d^{-1}$ for NH_4^+, –0.078–0.006 mmol m^{-2} d^{-1} for PO_4^{3-}, and –0.673–2.63 mmol m^{-2} d^{-1} for $Si(OH)_4$, respectively, with a DIN:DIP ratio of 15–60 and DIN:Si ratio of 0.4–0.5 (Qi *et al*., 2003). Over the entire ECS shelf, nutrient exchange fluxes provided 3.6×10^9 mol yr^{-1} for NO_3^-, 32×10^9 mol yr^{-1} for NH_4^+, 0.8×10^9 mol yr^{-1} for PO_4^{3-}, and 79×10^9 mol yr^{-1} for $Si(OH)_4$ from sediment to water based on *in situ* incubations and pore-water profiles (Zhang *et al*., 2007).

Nitrogen transformation processes in sediments of the ECS are addressed based on the ^{15}N isotope pairing technique and by developing a mathematical model to correct the effects of DNRA (Dissimilatory Nitrate Reduction to Ammonium). N transformation processes are very complicated in the ECS sediments, including denitrification, anammox, and DNRA, as well as intracellular nitrate release (Song *et al*., 2013). The nitrate reduction rate was 16.2 ± 7.4 and 7.0 ± 3.7 nmol N cm^{-3} h^{-1} in June and October 2010, respectively, in which denitrification, anammox, and DNRA represented 46 ± 6% and 8.5 ± 0.1%, 20 ± 12% and 49% ± 20%, and 35% ± 10 and 43% ± 19%, respectively. The genuine N_2 production rate through denitrification was 0.26 ± 0.08 nmol N cm^{-3} h^{-1} in October 2010 (Song *et al*., 2013, 2016). Because nitrogen cycles in the sediment affect nutrient concentrations in pore-water, clarifying these processes are effective to evaluate nutrient fluxes from sediment into the water column of the ECS.

2.2.4 Nutrient budgets

Nutrient budget models for the YS (excepting the Bohai Sea) were developed based on LOICZ Biogeochemical Modelling Guidelines suggested by Gordon *et al*. (1996). For the model, the water and salt budgets were calculated first and then the mass balance of nutrients were built (Fig. 2.2.2). In calculation, we ignored the contribution from submarine groundwater and waste drainage, as the data were not available and had large uncertainties. The atmospheric inputs are becoming important relative to the riverine pathway with regard to the nutrient inputs. Moreover, advection dominates the nutrient budgetary issues; the active sink/source terms account for approximately 60 to 70% of annual input/export flux in the region (Liu *et al*., 2003a; Zhang and Su, 2006).

Nutrient dynamics are more complicated in the ECS than in the YS. The nutrient budget calculation for the ECS differs from previous LOICZ procedures (Gordon *et al*., 1996) because the limited data sets from the ECS do not allow specification of the ‘‘mixing terms’’ for water channels/straits and/or at the open boundary (Zhang *et al*., 2007). Nutrient budgets were first built for the ECS by Chen and Wang (1999). The revised budgets take into account monitoring and field observation data for river inputs, atmospheric dry and wet depositions, and sediment–water interface exchange fluxes, and separated nitrate and ammonium (Fig. 2.2.3). The results of the revised budgets suggest that the ECS shelf does not likely export substantial amounts of dissolved nutrients to the open

Northwest Pacific Ocean (Zhang *et al.*, 2007). Further study should focus on nutrient transformation processes, such as NO_3^- assimilation and nitrification, which play an important role in the nitrogen cycle on the ECS shelf (Liu *et al.*, 2020).

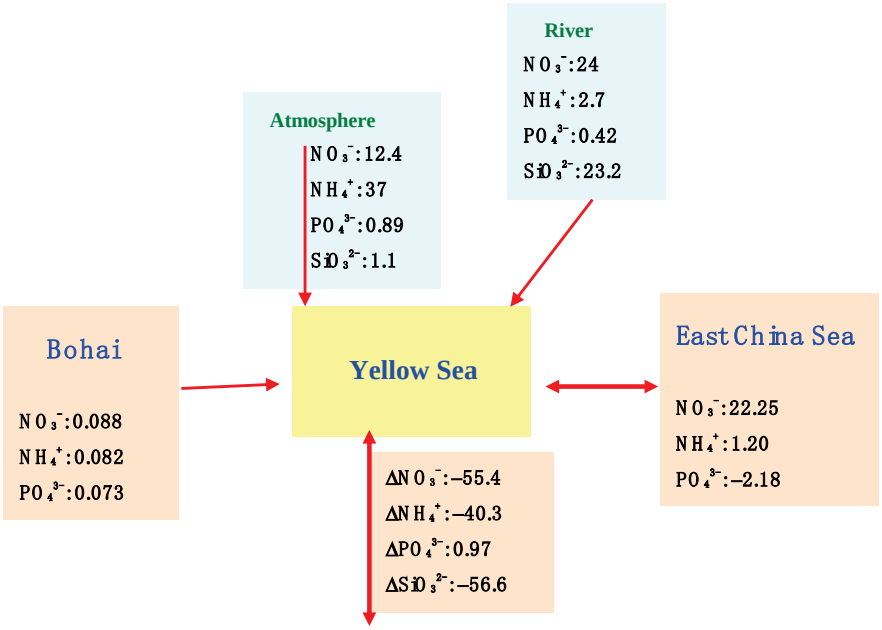

Fig. 2.2.2 Box model showing the nutrient budgets of the Yellow Sea, excluding the Bohai Sea. The negative and positive values in nutrient exchange and sink/source terms indicate nutrient loss from and input to the system, respectively ($\times 10^9$ mol yr^{-1}). Redrawn from Liu *et al.* (2003a). Reproduced with permission of Elsevier.

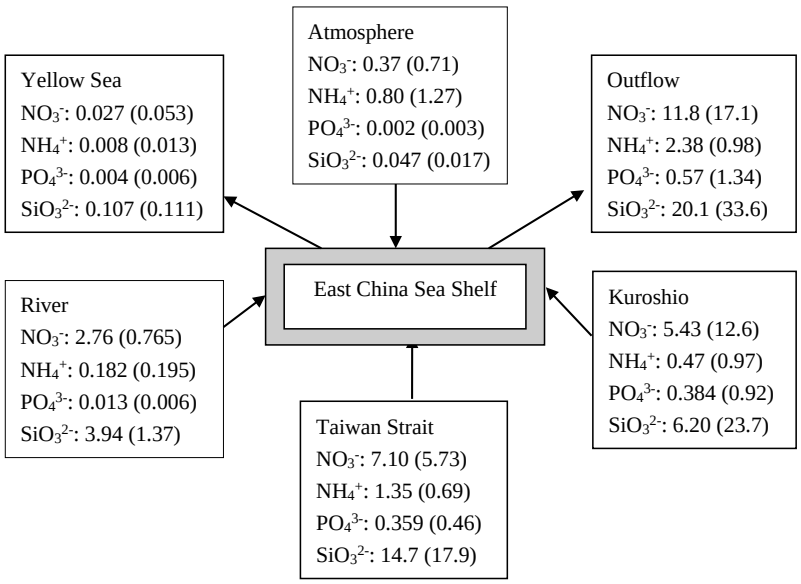

Fig. 2.2.3 Box model showing the nutrient budgets of the East China Sea Shelf, including the nutrient fluxes (kmol s^{-1}) in summer and winter (in brackets), respectively. Redrawn from Zhang *et al.* (2007).

2.2.5 Long-term changes of nutrients

Long-term environmental changes have been observed in the YS due to human activities and climate change: the concentrations of NO_3^- and dissolved inorganic nitrogen (DIN) in the southern YS have been continuously increasing since the 1980s, with a most rapid increase after the mid-1990s (Lin *et al*., 2005; Li *et al*., 2015; Wei *et al*., 2015). While the concentrations of $Si(OH)_4$ and PO_4^{3-} generally exhibited a decreasing trend before the mid-1990s, they then gradually increased (Wei *et al*., 2015). Nutrient composition also changed: the N:P ratio has been continuously increasing since the 1980s and reached a level of >16 (Redfield ratio) at the end of the last century; the Si:N ratio decreased rapidly from the mid-1980s to the mid-1990s and then maintained a low level of ~1; the Si:P ratio decreased from the 1970s to the mid-1990s and then increased gradually. In the southern YS there was an evolution from N limitation to P and Si limitation (Lin *et al*., 2005; Wei *et al*., 2015). The variations in the concentrations of nutrients were related to the variations of the riverine and atmospheric inputs.

Over the ECS shelf from the river to the shelf slope, nutrient concentrations and composition have changed differently. Based on monitoring observations in the lower reaches of Changjiang River, Li *et al*. (2007) indicated that concentrations and fluxes of DIN and PO_4^{3-} had increased greatly since the 1950s, while annual average concentration and flux of dissolved silicate had an opposite trend, showing a sharp decrease since the 1950s. They stated that fertilizer application peaking after the 1980s could be responsible for the high DIN and DIP levels, and construction of dams could be linked to the decrease of dissolved silica. Based on historical summertime data from 1959 to 2009, Jiang *et al*. (2014) reported similar results for the concentrations of NO_3^-, NO_2^-, NH_4^+, and PO_4^{3-} and ratios of N:P and N:Si in the freshwater and saline sections of the Changjiang Estuary which all increased because of persistent riverine loading, but $Si(OH)_4$ levels remained constant like previous studies (Liu *et al*., 2003b, Liu, S.M. *et al*., 2009). Further studies have indicated that the concentrations of PO_4^{3-} increased more rapidly than those of DIN and DIN:DIP molar ratio decreased by 60 to 70% over the period from 1995 to 2016 (Zhang *et al*., 2021). Moreover, $Si(OH)_4$ remained most likely stable, with a possible weak increase over the last 10 years due to erosion in the lower reach of the Changjiang (Wang *et al*., 2018; Ding *et al*., 2019; Zhang *et al*., 2021). As a result, microalgal biomass showed a dramatic increase with a decreasing diatom–dinoflagellate ratio and exacerbated harmful algal blooms, which is closely related to an increase in anthropogenic activities and climatic change (Jiang *et al*., 2014). Using historical *in situ* data sets from 1971 to 2001, an increase in DIN at summer surface water was also observed in the northern ECS, probably due to the combination of changes in Changjiang discharge and increase of nitrogen fertilizer use in China (Siswanto *et al*., 2008a). Although scientists are paying much attention to the response of the ECS ecosystem to changes in the nutrient supply arising from the Three Gorges Dam project, it is still not clear if there are any changes because of the lack of time-series data and the complex interactions in the Changjiang Estuary (Gong *et al*., 2006; Jiang *et al*., 2014).

Environmental change in the ECS slope and Kuroshio region is also not clear due to a limited data set. Based on *in situ* data from 1987 to 2009 in the ECS outer shelf/slope region, nitrate concentrations and nitrate flux in the Kuroshio were examined; Guo *et al*. (2012) indicated that although the nitrate concentration in the middle and bottom layers across the Kuroshio was found to increase significantly over the 23-year period especially after 2004, nutrient transport did not increase significantly due to decreased current velocity.

2.2.6 Isotopic applications in nutrient biogeochemistry studies

Complicated spatial and temporal variations and limited shipboard sampling lead to uncertainty in the extrapolation of direct measurements of nutrient transports at regional and global scales. Isotopes, however, can solve these constraints to some extent.

Phosphorus

Using natural activities of produced radioisotopes ^{32}P and ^{33}P in total dissolved phosphorus (TDP), Zhang *et al*. (2004) provided the first direct estimates of residence times of dissolved and biological P pools within the upper water column of the ECS. They indicated that the dissolved P turnover rates varied with residence times of 3 to 4 days for TDP in coastal waters, which suggested that low P concentrations could support relatively high levels of primary production. The short residence times of TDP suggest that studies of dissolved nutrient concentrations alone are insufficient for determining either nutrient limitation or maximal primary production.

Silicon

Zhang *et al*. (2015) measured the dissolved silicate concentration and silicon isotopic composition ($\delta^{30}Si$) in the surface water of the Changjiang estuary in summer and winter to study the behavior of dissolved silicate fluvial inputs into the ECS. The dissolved silicate concentration decreased away from the estuary and had a negative linear relationship with salinity affected by mixing between river water and seawater, similar to previous studies (Zhang *et al*., 2007). Measured $\delta^{30}Si$ in the Changjiang estuary ranged from +1.48‰ to +2.35‰ in summer, and from +1.54‰ to +1.95‰ in winter. As a result of low light levels and abundant dissolved silicate riverine inputs, dissolved silicate and the isotope remain relatively unaffected by biological utilization and fractionation in the near-shore region. Beyond a salinity level of 20, an obvious increase in $\delta^{30}Si$ was observed, indicating a significant increase in biological utilization and fractionation of dissolved silicate in high salinity waters in summer. Lower water temperatures and light levels that prevail over the winter lead to the reduced fractionation of dissolved silicate compared with that in summer.

Nitrogen

In comparison to phosphorus and silicon, there are many more works that apply nitrogen isotopes to address nitrogen biogeochemistry in the YECS. The dual isotopes ($\delta^{15}N$ and $\delta^{18}O$) of nitrate and nitrite and other nitrogen isotopes (*e.g*., $\delta^{15}N$ in NH_4^+, DON and PON) are powerful approaches to separate nitrogen flux processes in the ocean that are difficult to obtain through more traditional measurements of solute concentration or direct rate determination (Liu and Kaplan, 1989; Sigman *et al*., 2005). The earliest work in this region was done by Kon-Kee Liu, who reported the NO_3^-–$\delta^{15}N$ value of +4.7 ± 0.6‰ in Kuroshio upwelling water northeast of Taiwan measured 20 years ago (Liu *et al*., 1996), which was comparable to the $\delta^{15}N$ values for NO_3^- in the Kuroshio Subsurface Water observed recently (Umezawa *et al*., 2014; Liu *et al*., 2020). Based on isotope balance in the water column, Liu *et al*. (1996) also estimated the nitrogen fixation flux to be 0.5 mg m^{-2} day^{-1} N in the Okinawa Trough.

The seasonal variations of $\delta^{15}N$–NO_3^- values were measured in the Changjiang Estuary in 2006 and 2010 and the effects of nitrogen transform processes (nitrate assimilation, nitrification, and denitrification) and human activities (fertilizer, sewage, and manure) were discussed (Liu, X. *et al*., 2009; Yu *et al*., 2015; Liu *et al*., 2020). Chen *et al*. (2013) measured $\delta^{15}N$ and $\delta^{18}O$ values of NO_3^-

in the Changjiang Estuary in spring and studied the influence of nitrification, nitrate assimilation, and water stratification. Wang *et al*. (2016) measured nitrate dual isotopes in the southern ECS and the east of Taiwan in spring 2014, and indicated nitrate assimilation happened in the euphotic layer, causing 5‰ isotope fractionation, and nitrification occurred in the bottom water when Kuroshio Subsurface Water intruded into the ECS and oxygen consumption concomitantly. On the shelf of southern Cheju Island, the $\delta^{15}N$ and $\delta^{18}O$ of NO_3^- were useful for clarifying the sources of NO_3^- (*i.e.*, CDW, YSCWM and Kuroshio Subsurface Water-derived NO_3^-), which were actually assimilated by phytoplankton. Although isotopic fractionation during NO_3^- uptake by phytoplankton seemed to drastically increase $\delta^{15}N$ and $\delta^{18}O$ in summer, the relatively light nitrate with $\delta^{15}N$ lower than expected from this fractionation effect might be explained by contribution of atmospheric nitrogen and/or nitrification to NO_3^- dynamics in the surface and subsurface layers (Umezawa *et al*., 2014). Off the Changjiang Estuary to the ECS continental slope in summer, phytoplankton assimilation leads to high $\delta^{15}N$ and $\delta^{18}O$ values for NO_3^- in the upper water layers; organic matter remineralization, nitrification, and coupled sedimentary nitrification and denitrification results in low NO_3^- isotope values in the lower water layers; assimilation, nitrification, and N_2 fixation results in high $\delta^{15}N$ and $\delta^{18}O$ values and low $\Delta(15, 18)$ values in the upper water layers of the ECS continental slope. Moreover, NO_2^- in the ECS is dominated by NH_4^+ oxidation, and NO_2^- oxidation plays an important role in depleting NO_2^- in $\delta^{15}N$ values (Liu *et al.*, 2020).

Compared to the ECS, studies on nitrate isotopes in the YS are limited. Liu *et al*. (2017) reported that the $\delta^{15}N$ and $\delta^{18}O$ values for NO_3^- in the YS in spring varied among the different water masses. The high level of $\delta^{18}O$ relative to $\delta^{15}N$ in NO_3^- in the YS was related to the decomposition of organic matter and subsequent nitrification, as well as atmospheric deposition. Moreover, nutrient regeneration from sediments was an important source of water column NO_3^-.

2.2.7 Regeneration of nutrients

The relatively lower *f*-ratio (ratio of nitrate-based new production to total primary production) in the shelf water and Kuroshio region compared with that in the upwelling area and Changjiang-influenced coastal waters (Chen *et al*., 2001; Chen and Chen, 2003) suggested that nutrients re-mineralized from organic matter are also non-negligible nutrient sources to support primary production in the shelf mixed water. Although NH_4^+ is primarily remineralized DIN and is preferentially incorporated into phytoplankton, NH_4^+ is easily converted to nitrate through nitrification at oxic conditions. Therefore, the extent of nitrification in the euphotic layer may imply the importance of regenerated nutrients.

Nitrification rate and nitrate assimilation rate have been examined using ^{15}N incubation technique in the Changjiang Estuary and the ECS. Hsiao *et al*. (2014) determined the nitrification rate in the Changjiang plume in August 2011. They reported the nitrification rate of bulk water (NR_b) was positively correlated with NH_4^+ concentration that ranged from undetectable up to 4.6 μmol L^{-1} d^{-1}, peaking at a salinity of ~29. In the river mouth and the inner plume, NR_b was much higher than that at particle-free water (particle >3 μm eliminated), indicating that the nitrifying microorganism is mainly particle associated. Shiozaki *et al*. (2011) determined the nitrate assimilation rate and diapycnal nitrate flux in the northeast of the ECS and simultaneously examined the potential distribution of nitrification activity. Active nitrate assimilation larger than diapycnal nitrate flux was observed when the surface nitrate was depleted (<0.1 μM), with mean rates of 1400 and 96 μmol N m^{-2} d^{-1} in the ECS and the Kuroshio Current, respectively. Archaeal *amoA* was observed at shallow light depths at or above 10% light depth, suggesting that nitrification occurred within the euphotic zone in the ECS. Shiozaki *et al*. (2011) concluded that nitrification within the euphotic zone would be attributed to at least, in part, the observed discrepancy between nitrate assimilation and vertical

flux. In the ECS in the period from 1993 to 1996, Kanda *et al*. (2003) reported that the nitrate uptake rate integrated over the euphotic zone was higher on the ECS shelf (56 mg N m^{-2} d^{-1}) than in the shelf-break and slope region (21 mg N m^{-2} d^{-1}). Both seasonal and spatial variations were larger on the shelf. Uptake rates were low in summer due to low nitrate concentration when the water columns were stratified and were also low in well-mixed water columns in winter and spring when the water temperature was low. High rates of uptake were observed in the spring bloom and in autumn. These findings suggest that nutrient fluxes based on the budget model alone do not necessarily indicate the contribution of each nutrient source to primary production because NO_3^- uptake rate by phytoplankton is affected by many environmental and physiological factors.

2.2.8 Other nutrient sources

In addition to remineralized nutrients, there are several nutrient sources to support primary production in the nutrient-depleted surface water of the ECS, especially during summer.

Shiozaki *et al*. (2010) reported that there was a patch of higher abundance of N_2-fixing filamentous diazotrophs, *Trichodesmium* spp., in the surface water of the ECS and Kuroshio region, and the median N_2 fixation activity at the observed stations was about 3.0 nmol N L^{-1} d^{-1}, with an order of higher values at several locations (*i.e*., 14 or 28 nmol N L^{-1} d^{-1}). Unicellular diazotrophic cyanobacteria such as UCYN-A are also major agents to carry out N_2 fixation, and their activity in the Kuroshio-influenced ECS area is equal to or greater than that of *Trichodesmium* and diatom–diazotroph associations containing the cyanobiont (Wu *et al*., 2018). Because *Trichodesmium* is capable of hydrolyzing DOP compounds as phosphorus sources (Mulholland *et al*., 2002) as well as many of the phytoplankton species, the bloom of these N_2-fixing cyanobacteria can become additional nutrient (DIN and DIP) sources for other microorganisms through biological decomposition.

In the ECS, the DOP concentration generally exceeded the DIP concentration in the surface layer (<100 m) of the outer shelf, while DIP is the major form of dissolved P, accounting for more than 70% of the TDP pool in inner and middle shelf waters (Fang, 2004). Because excess nitrogen supplies to surface water of the ECS have occurred due to increasing atmospheric deposition (Kim *et al*., 2011) and terrestrial input (Liu *et al*., 2016), the availability of DOP is an essential factor to consider nutrient supplies supporting primary production at offshore waters. Because one of the DOP components, phosphomonoesters, is hydrolyzed into phosphate by an extracellular enzyme, alkaline phosphatase (AP), its activity (APA) has been used to check whether microphytoplankton experience phosphorus stress (Dyhrman and Ruttenberg, 2006). APA is very low at the upwelling zone where DIP is supplied from deeper layers, while APA is enhanced at DIP-depleted surface Kuroshio waters (Liu *et al*., 2010), suggesting the potential use of DOP as a nutrient supply.

Typhoon-induced mixing is an important physical factor to lift up nutrients from the subsurface layer to surface waters. Typhoon passages crossing the shelf-slope push the Kuroshio current axis shelfward and lead to the upwelling and vertical mixing of subsurface Kuroshio water with plenty of nutrients, in addition to enhancing input of nutrient-replete terrestrial waters. Hung *et al*. (2013) reported that nitrate and phosphate supplies to the water column in the southern ECS after the typhoon's passage were 5.6×10^{11} g-N d^{-1} and 7.8×10^{10} g-P d^{-1}, respectively, which were significantly higher than those before the typhoon occurred (nitrate supply = 1×10^9 g-N d^{-1}, phosphate supply = 1.6×10^8 g-P d^{-1}), which account for approximately 86% and 87% of summer nitrate and phosphate supplies, respectively, to the southern ECS. Enhanced phytoplankton chlorophyll-a and primary productivity (Siswanto *et al*., 2008b, 2009; Hung *et al*., 2013) and sinking particulate organic carbon (POC) fluxes (Hung *et al*., 2010) were observed after the typhoon passages.

2.2.9 Future perspective

Extensive marine research on nutrient biogeochemistry has been carried out in the YECS, including spatial and temporal variations of nutrients, and the main sources of nutrients (such as riverine inputs and atmospheric deposition). However, more studies should focus on the following aspects: (1) sources derived from nutrients regeneration in the water column and sediments; (2) nutrients exchange between the YECS with offshore seawaters, such as the effects of the Yellow Sea Warm Water input into the YS and water exchange between the ECS and open sea; (3) quantifying transformation rates between nutrient species, such as nitrification rate and nitrate assimilation; (4) the effects of dissolved organic nutrients; (5) POM dynamics including export of PON/P as sinking matter from the shelf to deeper ocean, Okinawa Trough, by the Continental Shelf Pump (Tsunogai, 2002); (6) response of the YECS ecosystem to the change of nutrient dynamics.

Acknowledgments

The authors are very grateful to the Advisory Panel for a Circulation Study of East Asian Marginal Seas (AP-CREAMS) of North Pacific Marine Science Organization (PICES) for organization and discussion a Scientific Report; Zhaomeng Xu for his contribution to preparing Figure 1; and Dr. Dongseon Kim for constructive comments and suggestions. This study was funded by the Natural Sciences Foundation of China (NSFC: 41776087, 42176040), the Taishan Scholars Programme of Shandong Province, Aoshan Talents Program supported by Qingdao National Laboratory for Marine Science and Technology (No. 2015ASTP-OS08).

2.2.10 References

Aller, R.C., Mackin, J.E., Ullman, W.J., Wang, C., Tsai, S., Jin, J., Sui, Y. and Hong, J. 1985. Early chemical diagenesis, sediment-water solute exchange, and storage of reactive organic matter near the mouth of the Changjiang, East China Sea. *Cont. Shelf Res.* **4**: 227–251, doi:10.1016/0278-4343(85)90031-7.

Chen, C.-T. A. 1996. The Kuroshio Intermediate Water is the major source of nutrients on the East China Sea continental shelf. *Oceanol. Acta* **19**: 523–527.

Chen, C.-T. A. 2008. Distribution of nutrients in the East China Sea and the South China Sea connection. *J. Oceanogr*. **64**: 737–751, doi:10.1007/s10872-008-0062-9.

Chen, C.-T.A. and Wang, S.-L. 1999. Carbon, alkalinity and nutrient budgets on the East China Sea continental shelf. *J. Geophys. Res. Oceans* **104**: 20,675–20,686, doi:10.1029/1999JC900055.

Chen, C.-T. A., Ruo, R., Pai, S.C., Liu, C.T. and Wong, G.T.F. 1995. Exchange of water masses between the East China Sea and the Kuroshio off northeastern Taiwan. *Cont. Shelf Res.* **15**: 19–39, doi: 10.1016/0278-4343(93)E0001-O.

Chen, F., Chen, J., Jia, G., Jin, H., Xu, J., Yang, Z., Zhuang, Y., Liu, X. and Zhang, H. 2013. Nitrate $\delta^{15}N$ and δ^{18} evidence for active biological transformation in the Changjiang Estuary and the adjacent East China Sea. *Acta Oceanol. Sin*. **32**: 11–17.

Chen, Y.L.L., Chen, H.Y., Lee, W.H., Hung, C.C., Wong, G.T.F. and Kanda, J. 2001. New production in the East China Sea, comparison between well-mixed winter and stratified summer conditions. *Cont. Shelf Res*. **21**: 751–764, doi:10.1016/S0278-4343(00)00108-4.

Chen, Y.L.L. and Chen, H.Y. 2003. Nitrate-based new production and its relationship to primary production and chemical hydrography in spring and fall in the East China Sea. *Deep Sea Res. II* **50**: 1249–1264, doi:10.1016/S0967-0645(03)00021-3.

Chung, C.S., Hong, G.H., Kim, S.H., Park, J.K., Kim, Y.I., Moon, D.S., Bang, I.K., Wang, B.D., Wang G.Y. and Yang, D.B. 1999. The distributional characteristics and budget of dissolved inorganic nutrients in the Yellow Sea, pp. 11-20 *in:* Biogeochemical Processes in the Bohai and Yellow Sea *edited by* G.H. Hong, J. Zhang and C.S. Chung, The Dongjin Publication Association, Seoul.

Cowan, J.L.W. and Boynton, W.R. 1996. Sediment-water oxygen and nutrient exchanges along the longitudinal axis of Chesapeake Bay: seasonal patterns, controlling factors and ecological significance. *Estuaries* **19**: 562–580, doi:10.2307/1352518.

Cowan, J.L.W., Pennock, J.R. and Boynton, W.R. 1996. Seasonal and interannual patterns of sediment-water nutrient and oxygen fluxes in Mobile Bay, Alabama (USA): regulating factors and ecological significance. *Mar. Ecol. Prog. Ser*. **141**: 229–245, doi:10.3354/meps141229.

Ding, S., Chen, P., Liu, S.M., Zhang, G., Zhang, J. and Dan, S.F. 2019. Nutrient dynamics in the Changjiang and retention effect in the Three Gorges Reservoir. *J. Hydrol.* **574**: 96–109, doi: 10.1016/j.jhydrol.2019.04.034.

Dyhrman, S.T. and Ruttenberg, K.C. 2006. Presence and regulation of alkaline phosphatase activity in eukaryotic phytoplankton from the coastal ocean: Implications for dissolved organic phosphorus remineralization. *Limnol. Oceanogr*. **51**: 1381–1390, doi:10.4319/lo.2006.51.3.1381.

Fang, T.-H. 2004. Phosphorus speciation and budget of the East China Sea. *Cont. Shelf Res*. **24**: 1285–1299, doi:10.1016/j.csr.2004.04.003.

Gao, L., Li, D., Ishizaka, J., Zhang, Y., Zong, H. and Guo, L. 2015. Nutrient dynamics across the river-sea interface in the Changjiang (Yangtze River) estuary—East China Sea region. *Limnol. Oceanogr*. **60**: 2207–2221, doi:10.1002/lno.10196.

Gong G.C., Chen, Y.L. and Liu, K.K. 1996. Chemical hydrography and chlorophyll a distribution in the East China Sea in summer: Implications in nutrient dynamics. *Cont. Shelf Res*. **16**: 1561–1590.

Gong, G.-C., Chang, J., Chiang, K.-P., Hsiung, T.-M., Hung, C.-C., Duan, S.-W. and Codispoti, L.A. 2006. Reduction of primary production and changing of nutrient ratio in the East China Sea: Effect of the Three Gorges Dam? *Geophys. Res. Lett*. **33**: L07610, doi:10.1029/2006GL025800.

Gordon, D.C., Boudreau, P.R., Mann, K.H., Ong, J.-E., Silvert, W.L., Smith, S.V., Wattayakorn, G., Wulff, F. and Yanagi, T. 1996. LOICZ Biogeocchemical Modelling Guidelines. LOICZ Reports and Studies 5, LOICZ, Texel, The Netherlands, 96 pp.

Guo, X., Zhu, X.-H., Wu, Q.-S. and Huang, D. 2012. The Kuroshio nutrient stream and its temporal variation in the East China Sea. *J. Geophys. Res. Atmos.* **117**: C01026, doi:10.1029/2011JC007292.

Hsiao, S. S.-Y., Hsu, T.-C., Liu, J.-W., Xie, X., Zhang, Y., Lin, J., Wang, H., Yang, J.-Y. T., Hsu, S.-C., Dai, M. and Kao, S.-J. 2014. Nitrification and its oxygen consumption along the turbid Chang Jiang River plume. *Biogeosciences* **11**: 2083–2098, doi:10.5194/bg-11-2083-2014.

Hung, C.-C., Gong, G.-C., Chou, W.-C., Chung, C.-C., Lee, M.-A., Chang, Y., Chen, H.-Y., Huang, S.-J., Yang, Y., Yang, W.-R., Chung, W.-C., Li, S.-L. and Laws, E. 2010. The effect of typhoon on particulate organic carbon flux in the southern East China Sea. *Biogeosciences* **7**: 3007–3018, doi: 10.5194/bg-7-3007-2010.

Hung, C.-C., Chung, C.-C., Gong, G.-C., Jan, S., Tsai, Y., Chen, K.-S., Chou, W.C., Lee, M.-A., Chang, Y., Chen, M.-H., Yang, W.-R., Tseng, C.-J. and Gawarkiewicz, G. 2013. Nutrient supply in the Southern East China Sea after Typhoon Morakot. *J. Mar. Res*. **71**: 133–149, doi:10.1357/002224013807343425.

Jiang, Z., Liu, J., Chen, J., Chen, Q., Yan, X., Xuan, J. and Zeng, J. 2014. Responses of summer phytoplankton community to drastic environmental changes in the Changjiang (Yangtze River) estuary during the past 50 years. *Water Res*. **54**: 1-11, doi:10.1016/j.watres.2014.01.032.

Jin, J., Liu, S.M., Ren, J.L., Liu, C.G., Zhang, J., Zhang, G.L. and Huang, D.J. 2013. Nutrient dynamics and coupling with phytoplankton species composition during the spring blooms in the Yellow Sea. *Deep Sea Res. II* **97**: 16–32, doi:10.1016/j.dsr2.2013.05.002.

Kanda, J., Itoh, T., Ishikawa, D. and Watanabe, Y. 2003. Environmental control of nitrate uptake in the East China Sea. *Deep Sea Res. II* **50**: 403–422, doi:10.1016/S0967-0645(02)00464-2.

Kim, T.-W., Lee, K., Najjar, R.G., Jeong, H.-D. and Jeong, H.J. 2011. Increasing N abundance in the northwestern Pacific Ocean due to atmospheric nitrogen. *Science* 334: 505–509, doi:10.1126/science.1206583.

Le, K. 1984. A preliminary study of the path of the Changjiang Diluted Water. *Chin. J. Oceanol. Limnol.* **2**: 157–167 (in Chinese).

Li, M., Xu, K., Watanabe, M. and Chen, Z. 2007. Long-term variations in dissolved silicate, nitrogen, and phosphorus flux from the Yangtze River into the East China Sea and impacts on estuarine ecosystem. *Estuar. Coast. Shelf Sci*. **71**: 3–12, doi:10.1016/j.ecss.2006.08.013.

Li, H.-M., Zhang, C.-S., Han, X.-R. and Shi, X.-Y. 2015. Changes in concentrations of oxygen, dissolved nitrogen, phosphate, and silicate in the southern Yellow Sea, 1980-2012: Sources and seaward gradients. *Estuar. Coast. Shelf Sci*. **163**: 44–55, doi:10.1016/j.ecss.2014.12.013.

Lin, C.L., Ning, X.R., Su, J.L., Lin, Y. and Xu, B. 2005. Environmental changes and responses of ecosystem of the Yellow Sea during 1976–2000. *J. Mar. Syst*. **55**: 223–234, doi:10.1016/j.jmarsys.2004.08.001.

Liu, H., Gong, G. and Chang, J. 2010. Lateral water exchange between shelf-margin upwelling and Kuroshio waters influences phosphorus stress in microphytoplankton. *Mar. Ecol. Prog. Ser*. **409**: 121–130, doi:10.3354/meps08603.

Liu, K.K. and Kaplan, I.R. 1989. The eastern tropical Pacific as a source of ^{15}N-enriched nitrate in seawater off southern California. *Limnol. Oceanogr*. **34**: 820–830, doi:10.4319/lo.1989.34.5.0820.

Liu, K.K., Su, M.-J., Hsueh, C.-R. and Gong, G.-C. 1996. The nitrogen isotopic composition of nitrate in the Kuroshio water northeast of Taiwan: evidence for nitrogen fixation as a source of isotopically light nitrate. *Mar. Chem*. **54**: 273–292, doi:10.1016/0304-4203(96)00034-5.

Liu, K.-K., Tang, T.Y., Gong, G.-C., Chen, L.-Y. and Shiah, F.-K. 2000. Cross-shelf and along-shelf nutrient fluxes derived from flow fields and chemical hydrography observed in the southern East China Sea off northern Taiwan. *Cont. Shelf Res*. **20**: 493–523, doi:10.1016/S0278-4343(99)00083-7.

Liu, K.-K., Yan, W., Lee, H.-J., Chao, S.-Y., Gong, G.-C. and Yeh, T.-Y. 2015. Impacts of increasing dissolved inorganic nitrogen discharged from Changjiang on primary production and seafloor oxygen demand in the East China Sea from 1970 to 2002. *J. Mar. Syst*. **141**: 200–217, doi:10.1016/j.jmarsys.2014.07.022.

Liu, S.M., Zhang, J., Chen, S.Z., Chen, H.T., Hong, G.H., Wei, H. and Wu, Q.M. 2003a. Inventory of nutrient compounds in the Yellow Sea. *Cont. Shelf Res*. **23**: 1161–1174, doi:10.1016/S0278-4343(03)00089-X.

Liu, S.M., Zhang, J., Chen, H.T., Wu, Y., Xiong, H. and Zhang, Z.F. 2003b. Nutrients in the Changjiang and its tributaries. *Biogeochemistry* **62**: 1–18, doi:10.1023/A:1021162214304.

Liu, S.M., Hong, G.-H., Zhang, J., Ye, X.W. and Jiang, X.L. 2009. Nutrient budgets for large Chinese estuaries. *Biogeosciences* **6**: 2245–2263, doi:10.5194/bg-6-2245-2009.

Liu, S.M., Qi, X.H., Li, X., Ye, H.R., Wu, Y., Ren, J.L., Zhang, J. and Xu, W.Y. 2016. Nutrient dynamics from the Changjiang (Yangtze River) estuary to the East China Sea. *J. Mar. Syst*. **154**: 15–27, doi: 10.1016/j.jmarsys.2015.05.010.

Liu, S.M., Altabet, M.A., Zhao, L., Larkum, J., Song, G.D., Zhang, G.L., Jin, H. and Han, L.J. 2017. Tracing nitrogen biogeochemistry during the beginning of a spring phytoplankton bloom in the Yellow Sea using coupled nitrate nitrogen and oxygen isotope ratios. *J. Geophys. Res. Biogeosci.* **122**: 2490–2508, doi:10.1002/2016JG003752.

Liu, S.M., Ning, X., Dong, S., Song, G., Wang, L., Altabet, M.A., Zhu, Z., Wu, Y., Ren, J.L., Liu, C.G., Zhang, J. and Huang, D. 2020. Source vs recycling influences on the isotopic composition of nitrate and nitrite in the East China Sea. *J. Geophys. Res. Oceans* **125**: e2020JC016061. doi:10.1029/2020JC016061.

Liu, X., Yu, Z., Song, X. and Cao, X. 2009. The nitrogen isotopic composition of dissolved nitrate in the Yangtze River (Changjiang) estuary, China. *Estuar. Coast. Shelf Sci*. **85**: 641–650, doi:10.1016/j.ecss.2009.09.017.

Mulholland, M.R., Floge, S., Carpenter, E.J. and Capone, D.G. 2002. Phosphorus dynamics in cultures and natural populations of *Trichodesmium* spp. *Mar. Ecol. Prog. Ser*. **239**: 45–55, doi:10.3354/meps239045.

Qi, X.H., Liu, S.M., Zhang, J. and Chen, H.T. 2003. Nutrient regeneration rate of sediments in HABs (Harmful Algal Blooms) area of the East China Sea. *Chin. J. Appl. Ecol*. **14**: 1112–1116 (in Chinese).

Ren, J.L., Zhang, J., Li, J.B., Yu, X.Y., Liu, S.M. and Zhang, E.R. 2006. Dissolved aluminum in the Yellow Sea and East China Sea – Al as a tracer of Changjiang (Yangtze River) discharge and Kuroshio incursion. *Estuar. Coast. Shelf Sci*. **68**: 165–174, doi:10.1016/j.ecss.2006.02.004.

Shiozaki, T., Furuya, K., Kodama, T., Kitajima, S., Takeda, S., Takemura, T. and Kanda, J. 2010. New estimation of N fixation in the western and central Pacific Ocean and its marginal seas. *Global Biogeochem. Cycles* **24**: GB1015, doi:10.1029/2009GB003620.

Shiozaki, T., Furuya, K., Kurotori, H., Kodama, T., Takeda, S., Endoh, T., Yoshikawa, Y., Ishizaka, J. and Matsuno, T. 2011. Imbalance between vertical nitrate flux and nitrate assimilation on a continental shelf: Implications of nitrification. *J. Geophys. Res*. *Oceans* **116**: C10031, doi:10.1029/2010JC006934.

Sigman, D.M., Granger, J., DiFiore, P.J., Lehmann, M.F., Ho, R., Cane, G. and van Geen, A. 2005. Coupled nitrogen and oxygen isotope measurements of nitrate along the eastern North Pacific margin. *Global Biogeochem. Cycles* **19**: GB4022, doi:10.1029/2005GB002458.

Siswanto, E., Nakata, H., Matsuoka, Y., Tanaka, K., Kiyomoto, Y., Okamura, K., Zhu, J., and Ishizaka, J. 2008a. The long-term freshening and nutrient increases in summer surface water in the northern East China Sea in relation to Changjiang discharge variation. *J. Geophys. Res*. *Atmos*. **113**: C10030, doi: 10.1029/2008JC004812.

Siswanto, E., Ishizaka, J., Morimoto, A., Tanaka, K., Okamura K., Kristijono, A. and Saino, T. 2008b. Ocean physical and biogeochemical responses to the passage of Typhoon Meari in the East China Sea observed from Argo float and multiplatform satellites. *Geophys. Res. Lett*. **35**: L15604, doi: 10.1029/2008GL035040.

Siswanto, E., Morimoto, A. and Kojima S. 2009. Enhancement of phytoplankton primary productivity in the southern East China Sea following episodic typhoon passage. *Geophys. Res. Lett*. **36**: L11603, doi:10.1029/2009GL037883.

Song, G.D., Liu, S.M., Marchant, H., Kuypers, M.M.M. and Lavik, G. 2013. Anammox, denitrification and dissimilatory nitrate reduction to ammonium in the East China Sea sediment. *Biogeosciences* **10**: 6851–6864, doi:10.5194/bg-10-6851-2013.

Song, G.D., Liu, S.M., Kuypers, M.M.M. and Lavik, G. 2016. Application of the isotope pairing technique in sediments where anammox, denitrification, and dissimilatory nitrate reduction to ammonium coexist. *Limnol. Oceanogr.: Methods* **14**: 801–815, doi:10.1002/lom3.10127.

Tsunogai, S. 2002. The western North Pacific playing a key role in global biogeochemical fluxes. *J. Oceanogr*. **58**: 245–257, doi:10.1023/A:1015805607724.

Umezawa, Y., Yamaguchi, A., Ishizaka, J., Hasegawa, T., Yoshimizu, C., Tayasu, I., Yoshimura, H., Morii, Y., Aoshima, T. and Yamawaki, N. 2014. Seasonal shifts in the contributions of the Changjiang River and the Kuroshio Current to nitrate dynamics in the continental shelf of the northern East China Sea based on a nitrate dual isotopic composition approach. *Biogeosciences* **11**: 1297–1317, doi:10.5194/bg-11-1297-2014.

Wang, B-D., Wang, X-L. and Zhan, R. 2003. Nutrient conditions in the Yellow Sea and the East China Sea. *Estuar. Coast. Shelf Sci*. **58**: 127–136, doi:10.1016/S0272-7714(03)00067-2.

Wang, W., Yu, Z., Song, X., Wu, Z., Yuan, Y., Zhou, P. and Cao, X. 2016. The effect of Kuroshio Current on nitrate dynamics in the southern East China Sea revealed by nitrate isotopic composition. *J. Geophys. Res. Oceans* **121**: 7073–7087, doi:10.1002/2016JC011882.

Wang, X., Yang, S., Ran, X., Liu, X.-M. Bataille, C.P. and Su, N. 2018. Response of the Changjiang (Yangtze River) water chemistry to the impoundment of Three Gorges Dam during 2010–2011. *Chem. Geol.* **487**: 1–11, doi:10.1016/j.chemgeo.2018.04.006.

Wei, Q., Yao, Q., Wang, B., Wang, H. and Yu, Z. 2015. Long-term variation of nutrients in the southern Yellow Sea. *Cont. Shelf Res.* **111**: 184–196, doi:10.1016/j.csr.2015.08.003.

Wu, C., Fu, F-X., Sun J., Thangaraj S. and Pujari L. 2018. Nitrogen fixation by *Trichodesmium* and unicellular diazotrophs in the northern South China Sea and the Kuroshio in summer. *Sci. Rep*. **8**: 2415, doi:10.1038/s41598-018-20743-0.

Wu, H., Zhu, J., Shen, J. and Wang, H. 2011. Tidal modulation on the Changjiang River plume in summer. *J. Geophys. Res. Oceans* **116**: C08017, doi:10.1029/2011JC007209.

Wu, Y., Zhang, J., Li, D.J., Wei, H. and Lu, R.X. 2003. Isotope variability of particulate organic matter at the PN section in the East China Sea. *Biogeochemistry* **65**: 31–49, doi:10.1023/A:1026044324643.

Yang, S.R., Park, M.G., Hong, G.H., Chung, C.S. and Yang, D.B. 1999. New andregenerated production in the Yellow Sea, pp. 69–99 *in:* Biogeochemical Processes in the Bohai andYellow Sea *edited by* G.H. Hong, J. Zhang and C.S. Chung, Dongjin Publication Association, Seoul.

Yu, H., Yu, Z., Song, X., Cao, X., Yuan, Y. and Lu, G. 2015. Seasonal variations in the nitrogen isotopic composition of dissolved nitrate in the Changjiang River estuary, China. *Estuar. Coast. Shelf Sci*. **155**: 148–155, doi:10.1016/j.ecss.2015.01.017.

Zhang, A.Y., Zhang, J., Hu, J., Zhang, R.F. and Zhang, G.S. 2015. Silicon isotopic chemistry in the Changjiang Estuary and coastal regions: Impacts of physical and biogeochemical processes on the transport of riverine dissolved silica. *J. Geophys. Res. Oceans* **120**: 6943–6957, doi:10.1002/2015JC011050.

Zhang, J. 1996. Nutrient elements in large Chinese estuaries. *Cont. Shelf Res*. **16**: 1023–1045, doi:10.1016/0278-4343(95)00055-0.

Zhang, J. 2002. Biogeochemistry of Chinese estuarine and coastal waters: nutrients, trace metals and biomarkers. *Reg. Environ. Change* **3**: 65–76, doi:10.1007/s10113-001-0039-3.

Zhang, J. and Su, J.L. 2006. Nutrient dynamics of the China Seas: the Bohai Sea, Yellow Sea, East China Sea and South China Sea, pp. 637–671 *in:* The Sea, vol. 14 *edited by* A.R. Robinson and K.H. Brink, Harvard University Press, Cambridge.

Zhang, J., Liu, S.M., Ren, J.L., Wu, Y. and Zhang, G.L. 2007. Nutrient gradients from the eutrophic Changjiang (Yangtze River) Estuary to the oligotrophic Kuroshio waters and re-evaluation of budgets for the East China Sea Shelf. *Progr. Oceanogr.* **74**: 449–478, doi:10.1016/j.pocean.2007.04.019.

Zhang, J., Du, Y.N., Zhang, G.S., Chang, Y., Zhou, Y.C., Zhang, Z.F., Wu, Y., Chen, J.W., Zhang, A.Y., Zhu, Z.Y. and Liu, S.M. 2021. Increases in the seaward river flux of nutrients driven by human migration and land-use changes in the tide-influenced delta. *Sci. Total Environ.* **761**: 144501, doi:10.1016/j.scitotenv.2020.144501.

Zhang, Y., Zhu, L., Zeng, X. and Lin, Y. 2004. The biogeochemical cycling of phosphorus in the upper ocean of the East China Sea. *Estuar. Coast. Shelf Sci*. **60**: 369–379, doi:10.1016/j.ecss.2004.02.001.

Zhu, Z.-Y., Zhang, J., Wu, Y., Zhang, Y.-Y., Lin, J. and Liu, S.-M. 2011. Hypoxia off the Changjiang (Yangtze River) Estuary: Oxygen depletion and organic matter decomposition. *Mar. Chem*. **125**: 108–116.

Zhu, Z.-Y., Hu, J., Song, G.-D., Wu, Y., Zhang, J. and Liu, S.M. 2016. Phytoplankton-driven dark plankton respiration in the hypoxic zone off the Changjiang Estuary, revealed by in vitro incubations. *J. Mar. Syst*. **154**: 50–56, doi:10.1016/j.jmarsys.2015.04.009.

Zhu, Z.-Y., Wu, H., Liu, S.-M., Wu, Y., Huang, D.-J., Zhang, J. and Zhang, G.-S. 2017. Hypoxia off the Changjiang (Yangtze River) estuary and in the adjacent East China Sea: Quantitative approaches to estimating the tidal impact and nutrient regeneration. *Mar. Pollut. Bull*. **125**: 103–114, doi:10.1016/j.marpolbul.2017.07.029.

2.3 Hypoxia

Zhuoyi Zhu

School of Oceanography, Shanghai Jiao Tong University, China

2.3.1 The occurrence of hypoxia

Hypoxia means dissolved oxygen (DO) content in the water column is lower than a certain value. The most commonly accepted threshold value is 2 mg/L (or 62.5 μM). Namely, when DO content in the water column is lower than 2 mg/L, the water is termed hypoxic.

Due to biological respiration and chemical redox reaction, DO in the water column is being consumed all the time. On the other hand, the processes of primary production (and hence regeneration of DO), exchange with air via the water–atmosphere interface, and DO-rich water supply (*e.g.*, lateral advection) tend to increase DO content. When balanced with air, DO in the surface water is around 7.5 mg/L (or 233 μM) at 20°C and salinity of 33. Hypoxia takes place when the DO consumption rate in the water column exceeds the DO generation rate, and this imbalance is long enough in time to drop the DO concentration to a value lower than the threshold (*i.e.*, 2 mg/L).

The basic mechanism for the occurrence of hypoxia is very clear, namely stratification and excess organic matter decay in the near-bottom waters are the key factors that induce hypoxia (Diaz, 2001). Therefore, at regions where hypoxia take place, the water column profiles are usually similar: lower salinity and/or higher temperature is found in the surface waters with higher salinity and/or lower temperature in the near-bottom waters; in the meantime, dissolved nutrients are very low in the surface waters, and a clear increase can be found in the near-bottom waters (see Fig. 2.3.2).

Stratification is common in estuarine and coastal zones, but under the eutrophication trend worldwide, an excess of organic matter that is input into the near-bottom waters is basically due to anthropogenic activities, and it usually becomes the main reason for the coastal hypoxia when compared with past times (Diaz, 2001). The source of this decaying organic matter is interesting as well as important, especially in the assessment of hypoxia and further environmental policy amendments. There are two possible sources of organic matter. One is the organic matter that is produced in the overlying water column due to intensive primary production (which is promoted by excess nutrients input due to anthropogenic activities), and the other is from terrestrial sources (*e.g.*, from soil or sewage). In that case, a case by case study may be needed to distinguish which organic matter is the main source of decaying organic matter that causes the bottom hypoxia.

Organic matter decay is usually suggested as the main process that induces oxygen depletion; in some cases, however, nitrification is also found to be very important. In the Pearl River estuary, for example, hypoxic water is reported in the surface waters, and in this case, nitrification is suggested to be one of the key reasons (He *et al.*, 2014).

2.3.2 Yellow Sea and East China Sea background

The Yellow Sea (YS) and the East China Sea (ECS) are strongly impacted by strong monsoons. Summer is the wet season when southerly winds prevail, and stratification becomes very common in estuarine and coastal zones. However, there are usually several cyclones (typhoons) passing by in this region (on average, six) in summer, which cause strong vertical water column mixing and can temporarily interrupt the water column stratification. Further, carried by riverine water, more terrestrial materials (*e.g.*, nutrients) are input into the coastal zone, which usually causes elevated primary production. Hence an abundance of organic matter is produced and settles down beneath the pycnocline, where decomposition, which then consumes DO in the near-bottom waters, takes place. In winter, strong northerly winds prevail which usually mix the water column quite well, and river discharge is also usually much smaller when compared to that in summer.

The YS and ECS are bordered by coastlines having among the highest population densities in the world. Industrialization and urbanization are very predominant and fast-growing in this region. Also, there are several big rivers that empty into the YS and ECS, with the Changjiang River (also known as the Yangtze River) being one of the biggest rivers in the world. All of these aspects make the YS and ECS prone to very strong anthropogenic activities. Nutrients from many of China's rivers that empty into the Yellow Sea and/or the East China Sea have increased a lot in the past few decades. For example, the Changjiang River dissolved inorganic nitrogen concentration increased from 0.1 mg/L in the 1960s to 1.5 mg/L in the 1990s (Yan and Zhang, 2003). Smaller Chinese rivers also show an increase in nutrient concentrations under strong anthropogenic activities (Zhang, 1996). For the estuaries and adjacent coastal zones, like the vast area close to the Changjiang River mouth, it is clear that eutrophication has become an overwhelming phenomenon. Harmful algal blooms have increased a lot in the YS and ECS from the 1980s to the 21st century (Wang, 2006). In addition to the era with available historical and/or instrumental data, in an even longer time scale, like from the 1850s to now, there is still likely to be a mild eutrophication trend (Zhu *et al.*, 2014).

2.3.3 Overview of hypoxia in the Yellow Sea and East China Sea

Hypoxia takes place widely in the shallow coastal zones, namely from the coasts of Korea, Japan, and China. For example, hypoxia has been reported in Chinhae Bay, the Youngsan River estuarine bay, Chonsu Bay, and Kamak Bay (Lim *et al.*, 2006 and ref. therein), Jinzhou Bay, Liaohe Estuary, Laizhou Bay, (Zhu, 2007 and ref. therein) and the Changjiang Estuary (Zhu *et al.*, 2011).

Due to the monsoon season, hypoxia in the YS and the ECS usually occurs in summer (usually in August), whereas in winter, oxygen depletion in the near-bottom waters is usually alleviated (Lim *et al.*, 2006; Tishchenko *et al.*, 2013; Zhu *et al.*, 2017). All of the hypoxic areas are located in the estuarine and coastal region of the YS and ECS (Fig. 2.3.1). These regions are zones where the water column is strongly stratified in summer, organic matter is abundant, and there is strong eutrophication.

Of all the reported hypoxic zones in the area, most of the hypoxic zones in the YS and ECS are on the order of a few hundred square kilometers (or even less). The biggest hypoxic zone is located in the region off the Changjiang Estuary adjacent to the ECS. In 2006 it was found to cover an area as large as 15,400 km^2 (Zhu *et al.*, 2011).

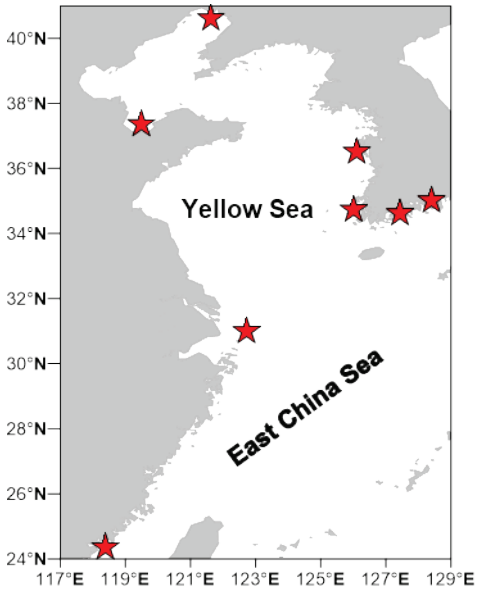

Fig. 2.3.1 Schematic of the hypoxia areas of concern (stars) in the pan-area of the Yellow Sea and East China Sea.

In addition to hypoxia in the estuarine and coastal zones, and lagoons, oxygen depletion also takes place in the deep Kuroshio waters where water depth can be over thousands of meters. However, no hypoxia has been found in these regions, and the DO minimum in the deep Okinawa Trough in the southern ECS can be as low as 2.37 mg/L (at 1450 m depth, our unpublished data), and higher than 2 mg/L.

2.3.4 The biggest hypoxia event in the Yellow Sea and East China Sea

The hypoxia event and its current features

Hypoxia off the Changjiang Estuary and adjacent ECS is likely the biggest hypoxia area in the YS and ECS. It was first revealed in 1959, located at around 31.5°N, 123°E with a DO minimum of 0.49 mg/L, according to the Office of Integrated Oceanographic Survey of China (1961). In that event, the hypoxic zonal area was calculated as 1900 km^2 (Zhu *et al.*, 2011). In a dissolved oxygen maximum study (Gu, 1980), a DO minimum (< 2 mg/L) zone was found off the Changjiang Estuary, though the area is hard to quantify. After the 1980s, DO depletion and further hypoxia were more frequently reported (Limeburner *et al.*, 1983; Chen *et al.*, 1988). In 1988, a further hypoxia event was discovered by Tian and his colleagues, which was located at around 30.83°N, 123°E (Tian *et al.*, 1993). In the 1990s, Li and his colleagues revealed a large hypoxia event, with an area up to 13,700 km^2 (Li *et al.*, 2002). In the 21st century, additional hypoxia events were found and studied (*e.g.*, Chen *et al.*, 2007; Wei *et al.*, 2007; Rabouille *et al.*, 2008; Wang *et al.*, 2012; Wei *et al.*, 2017). Oxygen depletion in the water column is also recorded in the sediment core via redox sensitive elements (*e.g.*, Mo, V, Fe Mn and U). Based on cores of tens of years time scale, upcore increasing trends of Mo, V, and U in an E3 core match well with a general lowering trend of bottom water DO minima since the mid-1980s (Wu *et al.*, 2020). Further, a less DO-depleted period 1991–1997 is also suggested in the identical research (Wu *et al.*, 2020). Based on benthic foraminifera and elemental geochemistry, hypoxia in an even longer time scale (3000 years) is further reconstructed

from a core named YD0902 (Ren *et al*., 2019). Based on their reconstructed hypoxia history over the past 3000 years, it is interesting to find that hypoxia likely occurred during a warm climate but lessened in a cold climate (Ren *et al*., 2019).

Though hypoxic areas can be traced back as early as in the 1950s, large ones (*i.e*., >10,000 km^2) were all found after 1999. Hence it is generally accepted that oxygen depletion is becoming more severe in recent decades (Chen *et al*., 2007; Zhu *et al*., 2011; Wang *et al*., 2012). Different from other large coastal hypoxia zones like the Gulf of Mexico, the northern part of the Black Sea, and the central Baltic Sea, where perennial hypoxia events are found, hypoxia off the Changjiang Estuary and adjacent ECS is recurrent and unstable in both time and space. Temporally, hypoxia events were found in summer (usually in August), and quickly disappeared in autumn (Zhu *et al*., 2011). Continuous measurement data from a bottom-mounted system further revealed that hypoxia can develop within 17–18 days and last for half a month, and is finally interrupted by strong wind mixing (Ni *et al*., 2016). In winter, no hypoxia was found in the ECS (Zhu *et al*., 2017). In space, the hypoxia zone can be sporadically distributed (Wei *et al*., 2007; Zhu *et al*., 2011). In August 2013, three hypoxic zones were found during a survey off the Changjiang Estuary and adjacent ECS, with a total area of 11,150 km^2 (Zhu *et al*., 2017). Despite the sporadic distribution pattern, the hypoxia zones were all found between 30°N and 32°N before the 2000s. In August 2006, hypoxia was found at 33°N (Zhu *et al*., 2011) and further confirmed in August 2013 (Zhu *et al*., 2017; Fig. 2.3.2a). Whether or not the hypoxia zone is moving northwards requires more field observation to confirm.

The area of the hypoxic zone was first reported as 1900 km^2 (Office of Integrated Oceanographic Survey of China, 1961). In the 1980s, it was hard to derive its area, which was conservatively estimated as smaller than the area found in the 1950s (Fig. 2.3.2b). As shown in Figure 2.3.2b, after the 1990s the hypoxia area became much larger. In 1999, it was found to be 13,700 km^2 (Li *et al*., 2002), 15,400 km^2 in 2006 (Zhu *et al*., 2011), and 11,150 km^2 in 2013 (Zhu *et al*., 2017). These three hypoxia events are, so far, the largest events that were ever found. In the three big hypoxia events (*i.e*., hypoxia in 1999, 2006, and 2013, the same hereafter), oxygen depletion was estimated as 4.7, 7.2, and 5.1 million tons, respectively (Zhu *et al*., 2017). The methods used in the published literature basically include the traditional Winkler titration method and DO probe (via DO meter or DO probe on a CTD). Different methods give different precisions/detection limits, and hence over the past a few decades, it remains difficult for us to determine the DO minimum trend before the precision and detection limit of every DO data set was clear. However, in the three big hypoxia events, DO minimum was found to show a descending trend, from 30.1 μM (1999), to 29.3 μM (2006) and finally 22.7 μM (2013), with a comparable DO measurement precision as discussed (Zhu *et al*., 2017).

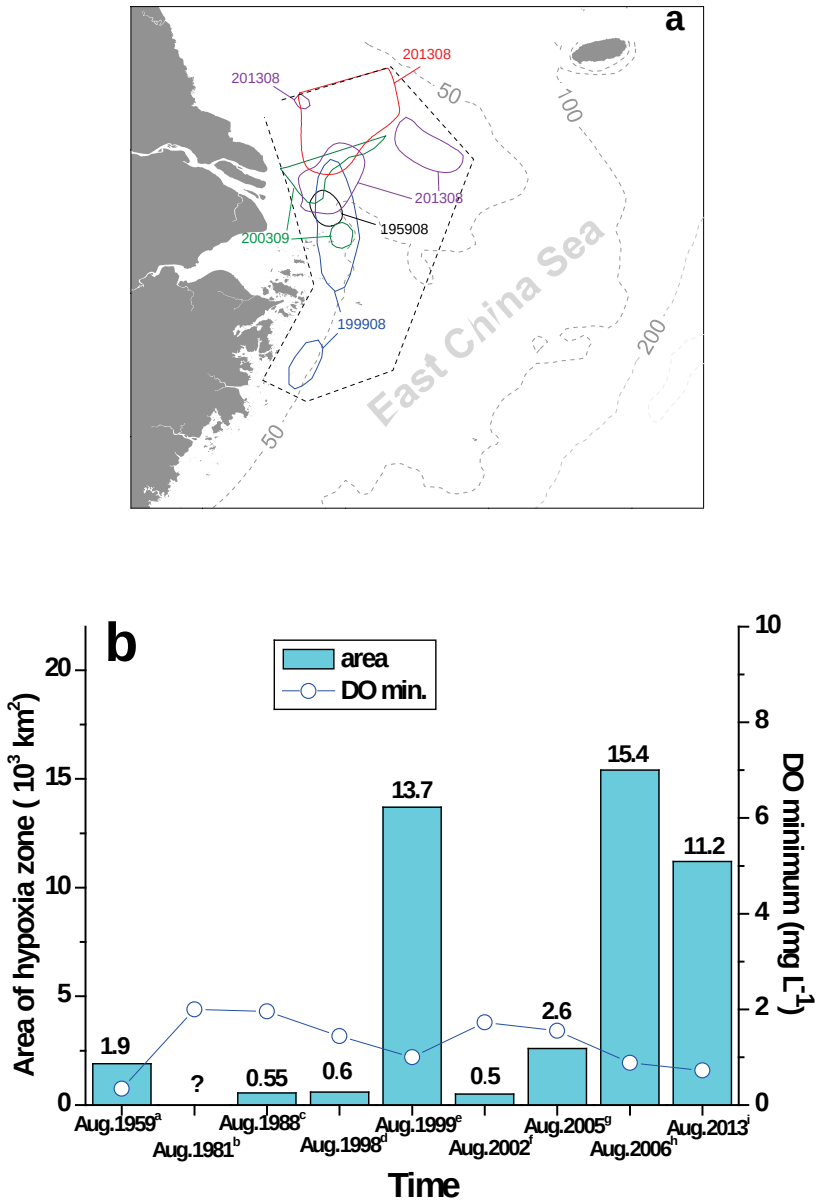

Fig. 2.3.2 Pooled key hypoxia zone of its a) locations and b) areas in the region off the Changjiang Estuary and adjacent ECS. Plots after Zhu *et al*. (2011); a: Office of Integrated Oceanographic Survey of China (1961), b: Limeburner *et al*. (1983), c: Tian *et al*. (1993), d: Wang and Wang (2007), e: Li *et al*. (2002), f: Wang (2009) and ref. therein, g: our unpublished data, h: Zhu *et al*. (2011), i: Zhu *et al*. (2017).

The occurrence of the hypoxia: Basic physical and biochemical factors

Two conditions are required before oxygen depletion can be observed and further hypoxia develops, namely physical background (stratification of the water column) and further, a biochemical process that consumes DO (organic matter decay in the bottom layers) (Diaz, 2001). Physically, strong terrestrial freshwater input in summer (basically from the Changjiang River) enhances strong stratification of the water column. In the upper layer, the brackish Changjiang Diluted Water is the main water mass, whereas in the bottom layer, the marine water prevails. A low DO (< 3 mg/L) distribution pattern was found to be similar to the area of the pycnocline (> 2.0 kg/m^4) (Zhu, J.R. *et al*., 2016), suggesting the stratification as the basic background in hypoxia occurrence. A *Q* quantitative relation was further presented (r = 0.66, p < 0.001, n = 86) between bottom water AOU

(apparent oxygen utilization) and delta σ (bottom water density minus surface water density) (Zhu *et al*., 2011). When delta σ is bigger than 5 kg/m^3, bottom AOU does not show a positive relation with delta σ, and instead of the correlation changes from positive to constant (Zhu *et al*., 2011). In addition to the stratification, the tide is another important physical background control on the bottom DO distribution, which is fundamental in estuarine and coastal regions. Tide is usually considered as a factor that alleviates the bottom DO, as it commonly generates currents that enhance vertical exchange in the water column (Luo *et al*., 2009; Tyler *et al*., 2009). Indeed, hypoxia is mostly found in August, when the estuarine region shows the smallest residual tidal currents (Zhu, J.R. *et al*., 2016). Also, numerical model application suggests that the hypoxia area may be reduced by the tide, especially destroying the bottom hypoxia in the region where stratification would be weakened due to tide (Chen *et al*., 2015). In addition to the numerical models, field data from diel observations (24 hours continuous observation at 3-h intervals), however, indicates that at least at some sites, the tide may cause the bottom waters to move back and forth, while the stratification of the water column is not interfered with. As a result, horizontally hypoxic water undergoes back and forth movement, whereas, at a given point (station), bottom DO concentration would show a tidal pattern over diel observations (Zhu *et al*., 2017). A sinusoidal model has been further applied to the diel observation bottom DO data, which yields 12 hours (r^2 = 0.6) for the bottom DO data (Zhu *et al*., 2017). This is consistent with the tidal period in this region (~13 hours). Given that tide causes the hypoxic waters to move back and forth in the bottom layer (at least at over a tidal time cycle time scale), a more accurate assessment of the hypoxia and its further environmental impact becomes more complicated. Almost certainly the region that undergoes hypoxia will be different from what we suggest now, as these results are all based on grid station data, in which no tide is considered when carrying out the field investigation. The numerical model further implies that the tidal excursion (*i.e*., the distance over which a water particle travels up and down the estuary with the flood and ebb tides) is larger in the northern Changjiang Estuary (~15 km) when compared to that in the southern Estuary (< 5 km). Given that hypoxia is happening more often in the northern Estuary (Fig. 2.3.2a), it is hence expected to influence a larger area under the tidal impact, when compared to hypoxic zones that have happened in the southern Estuary (Zhu *et al*., 2017). The wind is found to play an important role in determination of the water column physical structure. Strong winds not only cause vertical mixing, which alleviates bottom oxygen depletion (Ni *et al*., 2016), but also proper winds favor the near-bottom waters to dwell and develop hypoxia (Zhang *et al*., 2019).

With respect to the second factor, namely the biogeochemical process that consumes DO in the waters due to strong anthropogenic activity, the Changjiang River nutrient flux has been found to be increasing in the past decades (Zhang *et al*., 1999) and eutrophication is hence suggested to play a more prominent role in the estuarine region and adjacent ECS (Wang, 2006). In addition to the trend in eutrophication in recent decades, sediment core studies further imply that the marginal sea has been under mild eutrophication over the past 100 years (Zhu *et al*., 2014). Elevated terrestrial materials input from the Changjiang River (and a minor contribution from those small rivers along Zhejiang province) into the estuarine zone and adjacent ECS promote the *in situ* production. Indeed, blooms become common from May to August in the region off the Changjiang Estuary and adjacent ECS (Zhu *et al*., 1997). The vigorous primary production in the upper layer generates excess organic matter, part of which sinks to the bottom layer, and finally decays there. In the vicinity of the Changjiang River mouth, terrestrial organic matter may be an important source of decaying organic matter in the bottom waters that consumes bottom DO. However, we think the majority of the decaying organic matter in this region (*i.e*., where hypoxia is frequently found) should be of marine origin. Taking the whole area where hypoxia was most frequently reported into consideration (*i.e*., the black dashed line area in Figure 2.3.2a), it is estimated to be 180,100 km^2, and this area is also most likely to be receiving the Changjiang export material in a 100% manner. On one hand, the Changjiang annual particulate organic carbon (POC) flux is 1.8–4.2 × 10^6 tons

(Zhang *et al*., 1999), or more recently 1.3 × 10^6 tons (Gao *et al*., 2012). On the other hand, the *in situ* primary production within this area is likely to be 115 g C m^{-2} yr^{-1} (Gong *et al*., 2003) or an annual value of 21 × 10^6 tons (multiplied by the area 180,100 km^2). Given the *f*-ratio of 0.4 (Chen, 2003), the new production would yield an annual POC amount of 8.4 × 10^6 tons. As we emphasize the organic matter produced above the thermocline (not concerning export out of the shelf), hence there is not an overestimate of the *f*-ratio here (Chen, 2003). A more precise calculation in summer (*i.e*., August) gives a monthly POC flux of 0.2 × 10^6 tons for the Changjiang River (Gao *et al*., 2012), and a monthly new production rate of 5 × 10^6 tons (Gong *et al*., 2003) or 11 × 10^6 tons (Chen *et al*., 2001). So the ratio between the two sources (*i.e*., terrestrial and marine) within the area is annually as 1.3:8.4 (or 15%), or monthly (*i.e*., August) as 0.2:11–0.2:5 (*i.e*., 1.8–4%). As the estuarine filter effect and the decomposition process before the terrestrial organic matter finally reaches the bottom layer is not yet considered, hence the actual percentage is likely to be even smaller. In other words, terrestrial organic matter would play an even smaller role. The main uncertainty in the above estimate approach lies in the primary production and further new production value, which may show a large spatial distribution gradient and hence making the estimate of *in situ* produced organic carbon involves great error. Furthermore, from the aspect of chemical lability, *in situ* produced organic matter is more labile and easy to decompose, whereas the terrestrial organic matter that finally escapes from the estuarine filtration effect is expected to be more refractory. Recently, Wang and her colleagues used a mixing model to discuss the decaying organic matter in the bottom waters and identified a surface diatom bloom as the major source of the organic carbon (Wang *et al*., 2017). Further, carbon isotope study provided direct evidence that the decaying organic matter in the bottom layer is of marine origin (Wang *et al*., 2016).

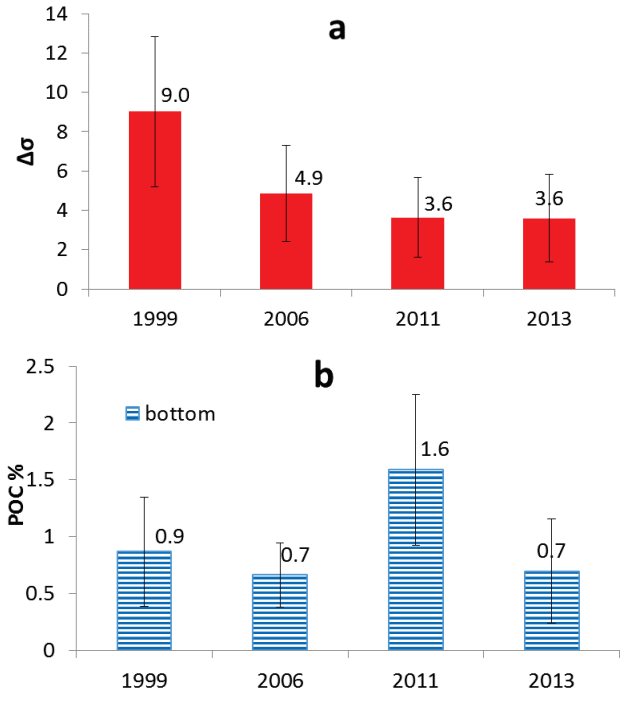

Fig. 2.3.3 Comparison of the factors that form hypoxia in the three big hypoxia events in 1999, 2006 and 2013: a) stratification as indicated by water density difference $\Delta\sigma$ (in kg/m^3) and b) organic matter decay as indicated by POC (particulate organic carbon) content (in %) in the total suspended matter in the bottom layers. (Data in August 2011 are also shown as a comparison, when no hypoxia was found; data in 1999 are derived from Li *et al*. (2002), data in 2006 are derived from Zhu *et al*. (2011) and data in 2011/2013 are derived from Zhu *et al*. (2017).

In the three big hypoxia events in 1999, 2006 and 2013, the physical (*e.g.*, stratification) and biochemical DO-consumption process (*e.g.*, organic matter decay) differed from each other (Fig. 2.3.3). In 1999, stratification was most severe (Fig. 2.3.3a), whereas the organic matter decay seems to be most thorough in 2006 and 2013 (Fig. 2.3.3b). Though stratification in 2011 was also very strong (Fig. 2.3.3a), POC content in the total suspended matter (TSM) of the bottom layer remained very high (Fig. 2.3.3b), which implies that the organic matter decaying process may not occur thoroughly when compared to the other three years (*i.e.*, 1.6% in 2011 *vs.* 0.9 in 1999, 0.7 in 2006, and 0.7 in 2013; Fig. 2.3.3b). As a result, no hypoxia was found in 2011, though a large area of low DO zone was detected *(i.e.*, 2 mg/L < bottom DO < 3 mg/L) (Zhu *et al.*, 2017).

The occurrence of the hypoxia: Its instabilities

The entire ECS lies over a broad continental shelf (over 500 km), which extends from the Chinese coast to the Okinawa Trough, and the water column of the vast ECS is hence usually very shallow. In the region off the Changjiang Estuary, it can be as shallow as 50 m when it is already over 100 km away from the mainland. The hypoxia usually occurs in the region with water depth < 50 m (Fig. 2.3.2a). In addition to occasional northerly wind events, there are usually three to six typhoons in the summer season in the ECS (Wei *et al.*, 2007). Given the shallow water depth of the hypoxia zone, the stratification of the water column can be easily interrupted during these weather events and hence can terminate the hypoxia. Therefore, different from other regions where hypoxia is perennial (like the Gulf of Mexico, the northern part of the Black Sea, the central part of the Baltic Sea), hypoxia off the Changjiang Estuary and adjacent ECS is recurrent and unstable. Ni and his colleagues (2016) found that hypoxia developed within 17–18 days, lasted for around two weeks, and was then quickly destroyed due to a strong wind event. The interesting part is that after the strong vertical mixing, the water column stabilized again, and it took another 17–18 days to develop another hypoxia event (Ni *et al.*, 2016). The repeated occurrence of hypoxia within the summer season (or even within the same month) alleviates the bottom oxygen-deficient environment, as DO would be occasionally supplied due to vertical mixing. The corresponding nutrient regeneration, however, would also be repeated (and hence enhanced), as each hypoxia event means organic matter decay and corresponding nutrient regeneration.

When discussing the recurrent nature of the hypoxia off the Changjiang Estuary and in the adjacent ECS, which is quite different from other similar regions like the Gulf of Mexico, one would naturally consider the annual variability of the Changjiang River impact (*e.g.*, annual discharge and nutrient export variability), as well as annual weather differences (*e.g.*, occurrence of typhoons differs from year to year). However, we argue that the marine background may also be essential. The water residence time of the ECS is on the order of one year (Li, 1994). Hence, oxygen depletion impact in the previous summer can hardly be delivered to the next summer as the waters are almost totally renewed in the following year. Against this background, we need to keep an eye on the nature of the source water as it impacts the summer hypoxia annually (Qian *et al.*, 2017).

Respiration rate estimates and comparison with sedimentary contribution

Organic matter decay is the key process that drops DO concentration, and hence its rate, and further, the plankton community respiration rate is essential in hypoxia studies. In the Changjiang Estuary and adjacent ECS, direct studies about the bottom plankton community respiration rate are limited (Wang *et al.*, 2017). Within the euphotic layer, the plankton community respiration rate was measured previously and is summarized in another section of this report (see subsection 3.1.9). Briefly, the plankton community respiration rate in the region off the Changjiang Estuary and adjacent ECS (*i.e.*, stations 18, 19, 20, 29) ranged from 0.04 to 0.10 mg O_2/L/day in autumn

(October/November; Chen *et al*., 2003), and ranged from 0.03 to 0.26 mg O_2/L/day in summer (August; Chen *et al*., 2006). The rate in summer is higher when compared to that in autumn, and is much higher when compared to that in the northern YS (~0.03 mg O_2/L/day; Zhai *et al*., 2014). By measuring dissolved inorganic carbon and further calculations, Wang and her colleagues suggested that the bottom water should be characterized by a community respiration rate of 2.4 g O_2/m^2/day (Wang *et al*., 2017). Assuming the bottom water depth as 20 m, a respiration rate of 2.4 g O_2/m^2/day (Wang *et al*., 2017) then equals 0.12 mg O_2/L/day, and this value is comparable to the mean value (*i.e*., (0.03 + 0.26)/2 = 0.145 mg O_2/L/day) reported by Chen *et al*. (2006), though which focused in the upper water column. It should be noted that when the DO decreasing rate is constant with time (linear decreasing of organic matter at a given oxygen level), it means the kinetics has a formal zero-order with regard to organic matter, whereas when the rate of oxygen decreasing is not constant with time and depends on oxygen concentration, kinetics has at least first-order regarding oxygen. Using time-serial observations of oxygen depletion near the bottom in Amursky Bay, kinetics first-order was successfully used for the modeling process (Tishchenko *et al*., 2016). Therefore, the aforementioned oxygen consumption rates from different scientific groups should be viewed and compared with care.

With respect to the organic matter decay rate, an *in situ* incubation experiment based on bottom waters indicated that decay of POC over the entire incubation period (8 days) roughly followed a linear decrease, and the rate averaged 0.3 mmol C/m^3/day in the low DO condition (DO < 50%) whereas the mean rate was 1.5 mmol C/m^3/day in the high DO (DO > 95%) condition (Zhu *et al*., 2013). For dissolved organic carbon, its decay follows the exponential pattern, and the decaying constant *k* ranged from 0.12– 0.29/hour (Gao *et al*., 2015).

Based on $^{224}Ra/^{228}Th$ disequilibrium in the sediment, Cai and his colleagues suggested that the sediment process contributes 6 to 61% bottom AOU (Cai *et al*., 2014). Direct *in situ* DO consumption incubation experiments suggested that the sedimentary respiration rate ranged from 7.6 to 10.2 mmol O_2/m^2/day (Song *et al*., 2016); a corresponding bottom water respiration rate can be derived from the aforementioned POC decay rate, and phytoplankton further drives the community respiration rate (Zhu, Z.Y. *et al*., 2016), which ranges from 27 to 300 mmol O_2/m^2/day. Together, sedimentary respiration and the bottom water respiration rate give sediment and bottom water contribution of bottom AOU as 14.5% and 85.5%, respectively.

More recently, a $\delta^{18}O$ technique was applied in the hypoxia study off the Changjiang Estuary and in the ECS (Zhou *et al*., 2021), which can simultaneously quantify the contribution of oxygen depletion from both water respiration and sedimentary respiration. The rationale behind this is that the oxygen isotope fractionation during water column respiration and sedimentary respiration differs greatly. The interesting point is that at a given site, the water column respiration and sedimentary respiration contribution to oxygen depletion is not stationary and instead, changes along with surface water production, or along with how much organic matter is sinking into the near-bottom waters. From the viewpoint of observations, the lower the bottom water DO, the greater the contribution from water column respiration. Generally, hypoxia off the Changjiang Estuary and in the adjacent ECS is caused by water column respiration (contributing over 70% of oxygen depletion) and the rest is contributed by sedimentary respiration (Zhou *et al*., 2021).

2.3.5 Impact of hypoxia

The most prominent and well-known impact of hypoxia is its negative influence on the ecosystem and fishery resources. In the Changjiang Estuary and adjacent ECS, the heterotrophic bacteria to autotrophic species ratio increased, fish biomass was reduced, and there was a change in

biodiversity and dominance of economic species (Zhang, J. *et al*., 2010). Overfishing may be the main reason, but environmental quality retreat, including hypoxia, worsens the problem. Quantitative assessment of the impact of hypoxia on fishery resources requires further study.

Also, hypoxia changes the microenvironment; hence the bacteria community structure under hypoxic conditions may be different from that in normal DO level conditions (Liu *et al*., 2012; Ye *et al*., 2016). Microbial activities accordingly enhance processes like anaerobic ammonium oxidation, denitrification, and/or dissimilatory nitrate reduction to ammonium, which generates notable greenhouse gas effects like N_2O and CH_4 (Zhang G.L. *et al*., 2008, 2010;). N_2O and CH_4 gas emission rates were reported as 22 and 38 μmol/m^2/day in the Changjiang Estuary and adjacent ECS, respectively, where a large area of hypoxia was found (Zhang *et al*., 2008). When compared to other large hypoxia zones, the greenhouse emission rate from the region off the Changjiang Estuary and adjacent ECS is among the highest (Zhang, J. *et al*., 2010). Also, bottom hypoxia and consequential hydrogen sulfide (H_2S) release from sediment in eutrophic estuaries is another major global environmental issue (Rathnayake *et al*., 2017).

Further, hypoxia plays an important role in the cycling of materials, and nutrients generated from bottom hypoxia and oxygen depletion is as efficient as the Changjiang River flux (Zhu *et al*., 2017). A conservative estimate to nutrient amounts that were regenerated in the three big hypoxia events off the Changjiang Estuary and adjacent ECS suggested that the N (nitrate) and P (phosphate) regeneration amount can be as high as 30,000 and 4100 tons, respectively (Zhu *et al*., 2017). Given that hypoxia can develop within 17–18 days (Ni *et al*., 2016), or even within 6 days (Wang *et al*., 2017), the nutrient regeneration rate is similar to that of the Changjiang River nutrient discharge (as 17–18 days) or even higher if 6 days of development into hypoxia would be considered (Zhu *et al*., 2017).

2.3.6 Uncertainties, unknowns, and perspectives

The YS and ECS is a region under extremely strong anthropogenic activity, including eutrophication and big hydrology projects (like the Three Gorges Dam project in the Changjiang River). While eutrophication promotes vigorous phytoplankton growth, the Three Gorges Dam interferes with the large river suspended load discharge pattern, and modifies the stoichiometry of riverine nutrients that are being finally emptied into the ECS. It has been found that suspended load in the Changjiang River water has been decreasing since the Three Gorges Dam project (Yang *et al*., 2007). Less total suspended matter in the estuarine surface water means the alleviation of light limitation for phytoplankton growth. Also, silicate, nitrate, and phosphate concentrations have been found to change in the past few decades. The ratio between these nutrients hence also changes, which may cause a phytoplankton structure shift in the estuary. A shift from diatom to dinoflagellates blooms in the Changjiang Estuary and adjacent ECS has been reported (Tang *et al*., 2006), and further evidence has also been found in sediment cores (Zhu *et al*., 2014). Anthropogenic activities, contributing to ecosystem changes, induce additional challenges to the YS and ECS environment, and hence further the development of bottom hypoxia.

Overall, hypoxia in the YS and ECS is a subject of strong scientific interest and attention, but we are still unaware of many key details when compared to other large coastal hypoxia regions like the central Baltic Sea and the Gulf of Mexico. For example, hypoxia and its feedback to the ecosystem via nutrient modification remain largely unknown, while in the Baltic Sea, it is clear that hypoxia alleviates P limitation, promotes further phytoplankton blooms and hence enhances further hypoxia occurrence (Zilius *et al*., 2014). Also, whether the hypoxia is highly related to terrestrial output seems more complex when compared to the case in the Gulf of Mexico, where a simple relation was

found between terrestrial N flux and the following bottom hypoxia (Turner *et al*., 2012). Another important puzzle is the role of sub-ground marine water discharge in bottom hypoxia; yet we know very little in this aspect.

In addition to these unknowns, the numerical study of hypoxia remains very limited (Chen *et al*., 2015). This is fundamental when making quantitative predictions to the public and government. To pave the road for a pertinent numerical study, the key parameters should be quantitatively confirmed by field observations or *in situ* incubation experiments, although this corresponding work is still limited (Zhu, Z.Y. *et al*., 2016).

2.3.7 References

Cai, P.H., Shi, X.M., Moore, W.S., Peng, S.Y., Wang, G.Z. and Dai, M.H. 2014. ^{224}Ra:^{228}Th disequilibrium in coastal sediments: Implications for solute transfer across the sediment–water interface. *Geochim. Cosmochim. Acta* **125**: 68–84.

Chen, C.C., Shiah, F.K., Gong, G.C. and Chiang, K.P. 2003. Planktonic community respiration in the East China Sea: importance of microbial consumption of organic carbon. *Deep Sea Res. II* **50**: 1311–1325, doi:10.1016/S0967-0645(03)00025-0.

Chen, C.-C., Chiang, K.-P., Gong, G.-C., Shiah, F.-K., Tseng, C.-M. and Liu, K.-K. 2006. Importance of planktonic community respiration on the carbon balance of the East China Sea in summer. *Global Biogeochem. Cycles* **20**: GB4001, doi:10.1029/2005GB002647.

Chen, C.-C., Gong, G.-C. and Shiah, F.-K. 2007. Hypoxia in the East China Sea: One of the largest coastal low-oxygen areas in the world. *Mar. Environ. Res*. **64**: 399–408, doi:10.1016/j.marenvres.2007.01.007.

Chen, C.T.A. 2003. New vs. export production on the continental shelf. *Deep-Sea Res. II* **50**: 1327–1333, doi:10.1016/S0967-0645(03)00026-2.

Chen, J.Y., Chen, X.L. and Yang, S.L. 1988. Report of the survey to the Shanghai coastal zone and tidal flat resources. Shanghai Scientific and Technical Publishers, Shanghai.

Chen, X.F., Shen, Z.Y., Li, Y.Y. and Yang, Y. 2015. Tidal modulation of the hypoxia adjacent to the Yangtze Estuary in summer. *Mar. Pollut. Bull*. **100**: 453–463, doi:10.1016/j.marpolbul.2015.08.005.

Chen, Y.L.L., Chen, H.-Y., Lee, W.-H., Hung, C.-C., Wong, G.T.F. and Kanda, J. 2001. New production in the East China Sea, comparison between well-mixed winter and stratified summer conditions. *Cont. Shelf Res.* **21**: 751–764, doi:10.1016/S0278-4343(00)00108-4.

Dai, M., Guo, X., Zhai, W., Yuan, L., Wang, B., Wang, L., Cai, P., Tang, T. and Cai, W.-J. 2006. Oxygen depletion in the upper reach of the Pearl River estuary during a winter drought. *Mar. Chem*. **102**: 159–169, doi:10.1016/j.marchem.2005.09.020.

Diaz, R.J. 2001. Overview of hypoxia around the world. *J. Environ. Qual*. **30**: 275–281, doi: 10.2134/jeq2001.302275x.

Fujiwara, T., Takahashi, T., Kasai, A., Sugiyama, Y. and Kuno, M. 2002. The role of circulation in the development of hypoxia in Ise Bay, Japan. *Estuar. Coast. Shelf Sci*. **54**: 19–31, doi:10.1006/ecss.2001.0824.

Gao, L., Li, D.J. and Zhang, Y.W. 2012. Nutrients and particulate organic matter discharged by the Changjiang (Yangtze River): Seasonal variations and temporal trends. *J. Geophys. Res. Biogeosci.* **117**: G04001, doi:10.1029/2012JG001952.

Gao, X.F., Wu, Y. and Zhu, Z.Y. 2015. Degradation of dissolved organic matter from dead phytoplankton off the Changjiang River Estuary and the resulting dissolved oxygen consumption. *Oceanol. Limnol. Sin*. **46**: 1010–1017 (in Chinese).

Gong, G.C., Wen, Y.H., Wang, B.W. and Liu, G.J. 2003. Seasonal variation of chlorophyll *a* concentration, primary production and environmental conditions in the subtropical East China Sea. *Deep Sea Res. II* **50**: 1219–1236, doi:10.1016/S0967-0645(03)00019-5.

Gu, H.K. 1980. The maximum value of dissolved oxygen in its vertical distribution in Yellow Sea. *Acta Oceanol. Sin*. **2**: 70–80. (in Chinese with English abstract).

He, B.Y., Dai, M.H., Zhai, W.D., Guo, X.H. and Wang, L.F. 2014. Hypoxia in the upper reaches of the Pearl River Estuary and its maintenance mechanisms: A synthesis based on multiple year observations during 2000–2008. *Mar. Chem*. **167**: 13–24, doi:10.1016/j.marchem.2014.07.003.

Kasai, A., Yamada, T. and Takeda, H. 2007. Flow structure and hypoxia in Hiuchi-nada, Seto Inland Sea, Japan. *Estuar. Coast. Shelf Sci*. **71**: 210–217, doi:10.1016/j.ecss.2006.08.001.

Kodama, K. and Horiguchi, T. 2011. Effects of hypoxia on benthic organisms in Tokyo Bay, Japan: a review. *Mar. Pollut. Bull*. **63**: 215–220, doi:10.1016/j.marpolbul.2011.04.022.

Li, D.J., Zhang, J., Huang, D.J., Wu, Y. and Liang, J. 2002. Oxygen depletion off the Changjiang (Yangtze River) Estuary. *Sci. China Series D: Earth Sci.* **45**: 1137–1146.

Li, Y.-H., 1994. Material exchange between the East China Sea and the Kuroshio current. *Terrest. Atmos. Ocean. Sci.* **5**: 625–631, doi:10.3319/TAO.1994.5.4.625(O).

Lim, H.-S., Diaz, R.J., Hong, J.-S. and Schaffner, L.C. 2006. Hypoxia and benthic community recovery in Korean coastal waters. *Mar. Pollut. Bull*. **52**: 1517–1526, doi:10.1016/j.marpolbul.2006.05.013.

Limeburner, R., Beardsley, R.C. and Zhao, J. 1983. Water masses and circulation in the East China Sea. Proceedings of the International Symposium on Sedimentation on the Continental Shelf, with Special Reference to the East China Sea. China Ocean Press, Hangzhou, pp. 285–294.

Liu, M., Xiao, T., Wu, Y., Zhou, F., Huang, H.Q., Bao, S.X. and Zhang, W.C. 2012. Temporal distribution of bacterial community structure in the Changjiang Estuary hypoxia area and the adjacent East China Sea. *Environ. Res. Lett*. **7**: 025001, doi:10.1088/1748-9326/7/2/025001.

Luo, L., Li, S. and Wang, D. 2009. Hypoxia in the Pearl River Estuary, the South China Sea, in July 1999. *Aquat. Ecosyst. Health Mgmt*. **12**: 418–428, doi:10.1080/14634980903352407.

Ni, X.B., Huang, D.J., Zeng, D.Y., Zhang, T., Li, H.L. and Chen, J.F. 2016. The impact of wind mixing on the variation of bottom dissolved oxygen off the Changjiang Estuary during summer. *J. Mar. Syst*. **154**: 122–130, doi:10.1016/j.jmarsys.2014.11.010.

Office of Integrated Oceanographic Survey of China. 1961. Dataset of the national integrated oceanographyic survey. vol 1. Survey data of hydrometeorological and chemical elements in the bohai, Huanghai and East China Seas, Beijing, 811 pp.

Qian, W., Dai, M.H., Xu, M., Kao, S.J., Du, C.J., Liu, J.W., Wang, H.J., Guo, L.G. and Wang, L.F. 2017. Non-local drivers of the summer hypoxia in the East China Sea off the Changjiang Estuary. *Estuar. Coast. Shelf Sci*. **198**: 393–399, doi:10.1016/j.ecss.2016.08.032.

Rabouille, C., Conley, D.J., Dai, M.H., Cai, W.J., Chen, C.T.A., Lansard, B., Green, R., Yin, K., Harrison, P.J., Dagg, M. and McKee, B. 2008. Comparison of hypoxia among four river-dominated ocean margins: The Changjiang (Yangtze), Mississippi, Pearl, and Rhone rivers. *Cont. Shelf Res*. **28**: 1527–1537, doi:10.1016/j.csr.2008.01.020.

Rathnayake, R.M.L.D., Sugahara, S., Maki, H., Kanaya, G., Seike, Y. and Satoh, H. 2017. High spatial resolution analysis of the distribution of sulfate reduction and sulfide oxidation in hypoxic sediment in a eutrophic estuary. *Water Sci. Technol*. **75**: 418–426, doi:10.2166/wst.2016.516.

Ren, F., Fan, D., Wu, Y. and Zhao, Q. 2019. The evolution of hypoxia off the Changjiang Estuary in the last 3000 years: Evidence from benthic foraminifera and elemental geochemistry. *Mar. Geol*. **417**: 106039, doi:10.1016/j.margeo.2019.106039.

Song, G.D., Liu, S.M., Zhu, Z.Y., Zhai, W.D., Zhu, C.J. and Zhang, J. 2016. Sediment oxygen consumption and benthic organic carbon mineralization on the continental shelves of the East China Sea and the Yellow Sea. *Deep Sea Res. II* **124**: 53–63, doi:10.1016/j.dsr2.2015.04.012.

Tang, D.L., Di, B.P., Wei, G.F., Ni, I.H., Oh, I. and Wang, S.F. 2006. Spatial, seasonal and species variations of harmful algal blooms in the South Yellow Sea and East China Sea. *Hydrobiol*. **568**: 245–253, doi:10.1007/s10750-006-0108-1.

Tian, R.C., Hu, F.X. and Martin, J.M. 1993. Summer nutrient fronts in the Changjiang (Yantze River) Estuary. *Estuar. Coast. Shelf Sci*. **37**: 27–41, doi:10.1006/ecss.1993.1039.

Tishchenko, P.Y., Lobanov, V.B., Zvalinsky, V.I., Sergeev, A.F., Koltunov, A., Mikhailik, T.A., Tishchenko, P.P., Shvetsova, M.G., Sagalaev, S. and Volkova, T. 2013. Seasonal hypoxia of Amursky Bay in the Japan Sea: Formation and destruction. *Terrest. Atmos. Ocean. Sci.* **24**: 1033–1050, doi: 10.3319/tao.2013.07.12.01(oc).

Tishchenko, P., Tishchenko, P., Lobanov, V., Sergeev, A., Semkin, P. and Zvalinsky, V. 2016. Summertime in situ monitoring of oxygen depletion in Amursky Bay (Japan/East Sea). *Cont. Shelf Res*. **118**: 77–87, doi:10.1016/j.csr.2016.02.014.

Turner, R.E., Rabalais, N.N. and Justić, D. 2012. Predicting summer hypoxia in the northern Gulf of Mexico: Redux. *Mar. Pollut. Bull*. **64**: 319–324, doi:10.1016/j.marpolbul.2011.11.008.

Tyler, R.M., Brady, D.C. and Targett, T.E. 2009. Temporal and spatial dynamics of diel-cycling hypoxia in estuarine tributaries. *Estuar. Coasts* **32**: 123–145, doi:10.1007/s12237-008-9108-x.

Wang, B., Chen, J.F., Jin, H.Y., Li, H.L., Huang, D.J. and Cai, W.J. 2017. Diatom bloom-derived bottom water hypoxia off the Changjiang estuary, with and without typhoon influence. *Limnol. Oceanogr*. **62**: 1552–1569, doi:10.1002/lno.10517.

Wang, B.D. 2006. Cultural eutrophication in the Changjiang (Yangtze River) plume: History and perspective. *Estuar. Coast. Shelf Sci*. **69**: 471–477, doi:10.1016/j.ecss.2006.05.010.

Wang, B.D. 2009. Hydromorphological mechanisms leading to hypoxia off the Changjiang estuary. *Mar. Environ. Res*. **67**: 53–58, doi:10.1016/j.marenvres.2008.11.001.

Wang, B.D. and Wang, X.L. 2007. Chemical hydrography of coastal upwelling in the East China Sea. *Chin. J. Oceanol. Limnol*. **25**: 16–26, doi:10.1007/s00343-007-0016-x.

Wang, B.D., Wei, Q.S., Chen, J.F. and Xie, L.P. 2012. Annual cycle of hypoxia off the Changjiang (Yangtze River) Estuary. *Mar. Environ. Res*. **77**: 1–5, doi:10.1016/j.marenvres.2011.12.007.

Wang, H.J., Dai, M.H., Liu, J.W., Kao, S.-J., Zhang, C., Cai, W.-J., Wang, G.Z., Qian, W., Zhao, M.X. and Sun, Z.Y. 2016. Eutrophication-driven hypoxia in the East China Sea off the Changjiang Estuary. *Environ. Sci. Technol*. **50**: 2255–2263, doi:10.1021/acs.est.5b06211.

Wei, H., He, Y., Li, Q., Liu, Z. and Wang, H. 2007. Summer hypoxia adjacent to the Changjiang Estuary. *J. Mar. Syst.* **67**: 292–303, doi.org/10.1016/j.jmarsys.2006.04.014.

Wei, Q.S., Wang, B.D., Yu, Z.G., Chen, J.F. and Xue, L. 2017. Mechanisms leading to the frequent occurrences of hypoxia and a preliminary analysis of the associated acidification off the Changjiang Estuary in summer. *Sci. China Earth Sci*. **60**: 360–381 (in Chinese), doi:10.1007/s11430-015-5542-8.

Wu, Y., Fan, D., Wang, D. and Yin, P. 2020. Increasing hypoxia in the Changjiang Estuary during the last three decades deciphered from sedimentary redox-sensitive elements. *Mar. Geol*. **419**: doi:10.1016/j.margeo.2019.106044.

Yamamuro, M. 2012. Herbicide-induced macrophyte-to-phytoplankton shifts in Japanese lagoons during the last 50 years: consequences for ecosystem services and fisheries. *Hydrobiol.* **699**: 5–19, doi:10.1007/s10750-012-1150-9.

Yan, W.J. and Zhang, S. 2003. How do nitrogen inputs to the Changjiang basin impact the Changjiang River nitrate: A temporal analysis for 1968-1997. *Global Biogeochem. Cycles* **17**: 1091, doi: 10.1029/2002GB002029.

Yang, S.L., Zhang, J. and Xu, X.J. 2007. Influence of the Three Gorges Dam on downstream delivery of sediment and its environmental implications, Yangtze River. *Geophys. Res. Lett.* **34**: L10401, doi:10.1029/2007GL029472.

Ye, Q., Wu, Y., Zhu, Z.Y., Wang, X.N., Li, Z.Q. and Zhang, J. 2016. Bacterial diversity in the surface sediments of the hypoxic zone near the Changjiang Estuary and in the East China Sea. *Microbiol. Open* **5**: 323–339, doi:10.1002/mbo3.330.

Yin, K.D., Lin, Z.F. and Ke, Z.Y. 2004. Temporal and spatial distribution of dissolved oxygen in the Pearl River Estuary and adjacent coastal waters. *Cont. Shelf Res*. **24**: 1935–1948, doi:10.1016/j.csr.2004.06.017.

Zhai, W.D., Zheng, N., Huo, C., Xu, Y., Zhao, H.D., Li, Y.W., Zang, K.P., Wang, J.Y. and Xu, X.M. 2014. Subsurface pH and carbonate saturation state of aragonite on the Chinese side of the North Yellow Sea: seasonal variations and controls. *Biogeosciences* **11**: 1103–1123, doi:10.5194/bg-11-1103-2014.

Zhang, G.L., Zhang, J., Ren, J.L., Li, J.B. and Liu, S.M. 2008. Distributions and sea-to air fluxes of methane and nitrous oxide in the North East China Sea in summer. *Mar. Chem*. **110**: 42–55.

Zhang, G.L., Zhang, J., Liu, S.M., Ren, J.L. and Zhao, Y.C. 2010. Nitrous oxide in the Changjiang (Yangtze River) Estuary and its adjacent marine area: Riverine input, sediment release and atmospheric fluxes. *Biogeosciences* **7**: 3505–3516, doi:10.5194/bg-7-3505-2010.

Zhang, J. 1996. Nutrient elements in large Chinese estuaries. *Cont. Shelf Res*. **16**: 1023–1045, doi: 10.1016/0278-4343(95)00055-0.

Zhang, J., Zhang, Z.F., Liu, S.M., Wu, Y., Xiong, H. and Chen, H.T. 1999. Human impacts on the large world rivers: Would the Changjiang (Yangtze River) be an illustration? *Global Biogeochem. Cycles* **13**: 1099–1105, doi:10.1029/1999GB900044.

Zhang, J., Gilbert, D., Gooday, A.J., Levin, L., Naqvi, S.W.A., Middelburg, J.J., Scranton, M., Ekau, W., Peña, A., Dewitte, B., Oguz, T., Monteiro, P.M.S., Urban, E., Rabalais, N.N., Ittekkot, V., Kemp, W.M., Ulloa, O., Elmgren, R., Escobar-Briones, E. and Van der Plas, A.K. 2010. Natural and human-induced hypoxia and consequences for coastal areas: synthesis and future development. *Biogeosciences* **7**: 1443–1467, doi:10.5194/bg-7-1443-2010.

Zhang, W.-X., Wu, H., Hetland, R.D. and Zhu, Z.-Y. 2019. On mechanisms controlling the seasonal hypoxia hot spots off the Changjiang River Estuary. *J. Geophys. Res. Oceans* **124**: 8683–8700, doi: 10.1029/2019jc015322.

Zhou, J., Zhu, Z.-Y., Hu, H.-T., Zhang, G.-L. and Wang, Q.-Q. 2021. Clarifying water column respiration and sedimentary oxygen respiration under oxygen depletion off the Changjiang Estuary and adjacent East China Sea. *Front. Mar. Sci*. **7**: doi:10.3389/fmars.2020.623581.

Zhu, J.R., Zhu, Z.Y., Lin, J., Wu, H. and Zhang, J. 2016. Distribution of hypoxia and pycnocline off the Changjiang Estuary, China. *J. Mar. Syst*. **154**: 28–40, doi:10.1016/j.jmarsys.2015.05.002.

Zhu, M.Y., Li, R.X., Mu, X.Y. and Ji, R.B. 1997. Harmful algal blooms in China seas. *Ocean Res*. **19**: 173–184.

Zhu, Z.Y. 2007. Hypoxia in the Changjiang estuary and its adjacent area-started with phytoplankton pigments. State Key Laboratory of Estuarine and Coastal Research. East China Normal University Press, Shanghai, 226 pp.

Zhu, Z.Y., Zhang, J., Wu, Y., Zhang, Y.Y., Lin, J. and Liu, S.M. 2011. Hypoxia off the Changjiang (Yangtze River) Estuary: Oxygen depletion and organic matter decomposition. *Mar. Chem*. **125**: 108–116, doi:10.1016/j.marchem.2011.03.005.

Zhu, Z.Y., Zhang, J., Wu, Y., Zhang, Y.Y., Lin, J. and Ji, Q. 2013. A study of particulate organic carbon and phytoplankton pigments early degradation rate under different dissolved oxygen level off the Changjiang (Yangtze) River Estuary. *Oceanol.Limnol. Sin*. **44**: 1–8 (in Chinese with English abstract).

Zhu, Z.Y., Wu, Y., Zhang, J., Du, J.Z. and Zhang, G.S. 2014. Reconstruction of anthropogenic eutrophication in the region off the Changjiang Estuary and central Yellow Sea: From decades to centuries. *Cont. Shelf Res*. **72**: 152–162, doi:10.1016/j.csr.2013.10.018.

Zhu, Z.Y., Hu, J., Song, G.D., Wu, Y., Zhang, J. and Liu, S.M. 2016. Phytoplankton-driven dark plankton respiration in the hypoxic zone off the Changjiang Estuary, revealed by in vitro incubations. *J. Mar. Syst*. **154**: 50–56, doi:10.1016/j.jmarsys.2015.04.009.

Zhu, Z.Y., Wu, H., Liu, S.M., Wu, Y., Huang, D.J., Zhang, J. and Zhang, G.S. 2017. Hypoxia off the Changjiang (Yangtze River) Estuary and in the adjacent East China Sea: quantitative approaches to estimating the tidal impact and nutrient regeneration. *Mar. Pollut. Bull*. **125**: 103–114, doi: 10.1016/j.marpolbul.2017.07.029.

Zilius, M., Bartoli, M., Bresciani, M., Katarzyte, M., Ruginis, T., Petkuviene, J., Lubiene, I., Giardino, C., Bukaveckas, P.A., de Wit, R. and Razinkovas-Baziukas, A. 2014. Feedback mechanisms between cyanobacterial blooms, transient hypoxia, and benthic phosphorus regeneration in shallow coastal environments. *Estuar. Coasts* **37**: 680–694, doi:10.1007/s12237-013-9717-x.

2.4 Biogeochemical Tracers

Jing Zhang[1] and Guebuem Kim[2]

[1] University of Toyama, Japan
[2] Seoul National University, Korea

2.4.1 Introduction

Trace elements and their isotopes (TEls) are key parameters of the GEOTRACES program (https://www.geotraces.org/). Many trace elements (*e.g.*, Fe, Co, Cu) are micronutrients that play critical roles in the ocean ecosystem, and therefore control the structure and productivity of marine ecosystems as well as carbon cycling. Other trace elements and isotopes can be used to assess ocean processes. For example, Al, Mn, rare earth elements (REEs; Zhang *et al.*, 2019), $^{143}Nd/^{144}Nd$, and Ra isotopes have been used to identify and quantify mixing of various water masses, including riverine input and submarine groundwater discharge. Given the crucial importance of TEls and isotopes that serve as biogeochemical tracers, knowledge on their processes and fluxes which control their distribution and internal cycling is required.

2.4.2 Water column

Distribution of TEls in the Changjiang Estuary and East China Sea

Aluminium

The distribution of dissolved Aluminum (Al) in the Changjiang Estuary and East China Sea (ECS) was reported as early as 1984 by Mackin and Aller (1984). Dissolved Al in the Changjiang Estuary varies widely (18–200 nmol L^{-1}) at very low salinity, but seems to be constant when the salinity is between 1 and 30 (Ren *et al.*, 2006). The concentration of dissolved Al generally decreases gradually from the Changjiang Estuary to the central shelf, and then decreases sharply at the shelf break. Dissolved Al ranges from 2 to 113 nmol L^{-1} on the ECS shelf (Minakawa and Watanabe, 1998; Ren *et al.*, 2006, 2015). The average residence time of dissolved Al is 339 ± 118 days (Ren *et al.*, 2006). Ren *et al.* (2015) calculated the cross-shelf transport of Al flux at the subsurface layer and found that the coastal enriched Al water was mainly exported to the marginal sea north of Japan and the northwestern Pacific Ocean. The presence of an Al plume indicates cross-shelf transport over the ECS shelf which is evident at the isopycnal layers at Sq = 23.5 ± 0.5 kg m^{-3}. The possible transport passage originates from the near-bottom layer of the Min-Zhe coast, extends northeastward and then shifts southeastward through the ECS shelf to the Kuroshio water at 30° N (Wang *et al.*, 2018).

Manganese

The dissolved Manganese (Mn) concentrations in the ECS range from 2 to 141 nmol L^{-1}, with an average of 8 nmol L^{-1}. Seasonal variations of dissolved Mn in the ECS are significant, with the highest concentrations occurring in summer and the maximum concentrations (141 nmol L^{-1}) occurring in near-bottom waters of the suboxic zone. Extensive consumption of oxygen results in the regeneration of dissolved Mn in near-bottom waters of the suboxic zone (Wang *et al.*, 2016). Dissolved Mn in the Changjiang Estuary behaves nonconservatively and is removed significantly by net sorption onto suspended particles. The concentration of dissolved Mn decreases across the ECS with distance from the coast. Mn-rich ECS shelf waters are exported to the Kuroshio waters and may have the potential to influence the northwestern Pacific Ocean as well as the marginal sea north of Japan. The estimated average residence time for dissolved Mn is 76 to 350 days in the ECS (Wang *et al.*, 2016).

Iron

The average concentrations of total dissolved iron (D-Fe) in the surface water of the Changjiang Estuary in spring and autumn are 40 ± 27 nmol L^{-1} and 21 ± 11 nmol L^{-1}, respectively. The average bottom D-Fe concentrations in the estuary in spring and autumn are 76 ± 59 nmol L^{-1} and 79 ± 39 nmol L^{-1}, respectively. The average D-Fe concentration in both surface and bottom waters in spring is higher than that in autumn. The average surface concentrations of Fe organic ligands (L_t) in the estuary in spring are higher than those in autumn (40 ± 27 vs 23 ± 8 nmol L^{-1}). Both D-Fe and L_t are elevated in the Changjiang Estuary and Hangzhou Bay but are depleted with distance away in the offshore of the ECS (Su *et al.*, 2015). The dissolved Fe is significantly correlated with L_t, and the limitation of total dissolved phosphate (TDP) decreases the uptake of Fe (Su *et al.*, 2017).

Other trace elements

In the coastal waters of the ECS, the average concentrations of dissolved Zinc (Zn), Copper (Cu), Cobalt (Co), and Vanadium (V) are 14 ± 9.0, 23 ± 5, 0.9 ± 0.2, and 20 ± 6 nmol L^{-1}, respectively (Su *et al.*, 2017). TDP is associated with dissolved Fe, Cu, Zn, and Co, but not with V. Su *et al.* (2017) highlighted that the limitation of TDP decreased the uptake of Fe.

Distributions of trace elements in the Yellow Sea and Bohai Sea

The studies on dissolved Al in the Yellow Sea (YS) are very limited; the concentration of dissolved Al ranges from 8 to 71 nmol L^{-1} (Ren *et al.*, 2006), but was observed to be as high as 197 nmol L^{-1} due to the influence of dust storms (Ren *et al.*, 2011). Dissolved Al in the southern YS is high in the coastal area and decreases towards the central area, and is regulated by the mixing of different water masses, including the Yellow Sea Coastal Current, Korea Coastal Current and Yellow Sea Warm Current (Ren *et al.*, 2011). The residence time of dissolved Al in the YS is 148 ± 32 days.

In general, the average metal (Cu, Co, Cd, and Ni) concentrations found in the southern YS are lower than those in the Bohai Sea (BS; Li *et al.*, 2015, 2017). The average concentrations of Cu, Co, Cd, and Ni are 8, 0.1, 0.4, and 7 nmol kg^{-1}, respectively in the southern YS, while they are 19, 0.3, 0.8, and 13 nmol kg^{-1}, respectively in the Central BS (Li *et al.*, 2017). These trace elements are affected by river discharge and biological uptake.

Overall, current studies are mainly focused on the distributions of trace elements in the water column; studies on the processes (desorption/adsorption, generation) and fluxes of biogeochemical tracers are still very limited. Lee *et al.* (2014) quantified the fraction of Changjiang Diluted Water

(CDW) using ^{223}Ra and ^{228}Ra. They found that CDW contributes >20% to the northern ECS. This result is comparable with the estimate from Che and Zhang (2018). Furthermore, the contribution of Kuroshio Subsurface Water to the Changjiang Estuary is >80% using ^{143}Nd/^{144}Nd (Che and Zhang, 2018); Kuroshio water was found to be the major source, at 98–99%, in the bottom water (100 m depth) of the ECS central shelf using REEs in combination with salinity and potential temperature (Zhang *et al*., 2018). The water contributions from the ECS to the northwestern Pacific and to the marginal sea north of Japan are ~6% and 10%, respectively. Ren *et al*. (2015) evaluated Al export from the ESC along the 100 m isobath to be 1.67×10^{10} g yr^{-1}. Those studies suggested that the ECS might be an important material source to the northwestern Pacific Ocean.

Distribution of radionuclides in the East China Sea and Yellow Sea

Ra isotopes

Radium (Ra) isotopes are very useful for tracing complicated water mixing and transport since they are soluble in seawater and have different half-lives: ^{228}Ra (half-life: 5.75 years), ^{226}Ra (half-life: 1,602 years), ^{223}Ra (half-life: 11.4 days), and ^{224}Ra (half-life: 3.66 days). In the ECS, the activities of ^{226}Ra and ^{228}Ra have ranged from 5 to 26 dpm 100L^{-1} with a mean value 14 dpm 100L^{-1} and from 1 to 73 dpm 100L^{-1} with a mean value 34 dpm 100L^{-1}, respectively (Nozaki *et al*., 1991; Inoue *et al*., 2012; Su *et al*., 2013; Men and Liu, 2015). The highest concentrations of long-lived ^{226}Ra were observed in the river plume area (Fig. 2.4.1), associated with the efficient desorption of Ra from fresh riverine sediments. In contrast, the highest concentration of ^{228}Ra were observed in the central YS water. This trend is due to much larger inputs of ^{228}Ra from bottom sediments, ingrown from ^{232}Th in sediments, although there are significant inputs of ^{228}Ra from riverine sediments (Fig. 2.4.1).

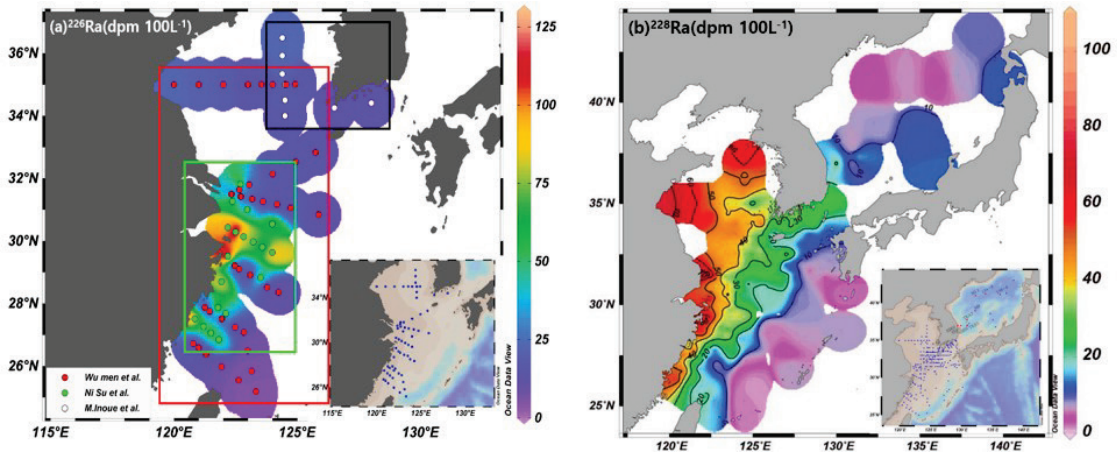

Fig. 2.4.1 Locations of sampling sites and the distributions of (a) ^{226}Ra and (b) ^{228}Ra activities in the surface water of the East China Sea obtained in previous studies (Okubo, 1980; Nozaki *et al*., 1991; Yeh and Chung, 1997; Kim *et al*., 2005; Zhang *et al*., 2007; Inoue *et al*., 2010, 2012; Su *et al*., 2013; Lee *et al*., 2014; Kim *et al*., 2015; Men and Liu, 2015).

The activities of ^{226}Ra and ^{228}Ra have been successfully utilized to evaluate the mixing of multiple water masses (Zhang *et al*., 2007; Lee *et al*., 2014) and water circulation patterns on the surface (Nozaki *et al*., 1991). For example, Lee *et al*. (2014) concluded that CDW contributes >20% to the northern ECS. In addition, the decay of ^{228}Ra relative to ^{226}Ra in the YS has been used to estimate the water residence time (Nozaki *et al*., 1991; Kim *et al*., 2005). These Ra isotopes were also used

to estimate Submarine Groundwater Discharge in this region (Kim *et al*., 2005; Kim *et al*., 2015). Su *et al*. (2013) used ^{226}Ra and ^{228}Ra to estimate the diffusivity and advection velocities in this region.

In the ECS, the distributions of short-lived ^{224}Ra and ^{223}Ra were also utilized successfully for tracing water-mass transport rates from the river plume to the upstream and vertical water mixing in the shelf region after a typhoon (Lee *et al*., 2014). As such, Gu *et al*. (2012) used these isotopes to estimate the water residence time and the contribution of Submarine Groundwater Discharge in the Changjiang effluent plume.

^{210}Po and ^{210}Pb

Of the naturally occurring radionuclides, the Polonium isotope ^{210}Po (half-life: 138 days) is produced by ^{210}Pb (half-life: 22.3 years) decay, and ^{210}Pb is produced by ^{226}Ra decay, via ^{222}Rn. Both Pb and Po are particle reactive. Especially, Po is known to be more preferentially taken up by biota (Kim, 2001). Due to their slightly different chemical properties, the ratios of ^{210}Po/^{210}Pb in the ocean can vary in the water column.

In the ECS and YS, total ^{210}Pb activities range from 2 to 45 dpm 100 L^{-1} (with a mean value of 15 ± 9 dpm100 L^{-1}) and total ^{210}Po activities range from 1 to 30 dpm100 L^{-1} (with a mean value of 8 ± 7 dpm 100L^{-1}) in the surface ocean. In general, both nuclides show considerably large seasonal and regional variations in the surface water layer, depending on atmospheric depositions, marine productivity, and sediment amounts. The activities of ^{210}Pb and ^{210}Po in the shelf water are considerably lower than those in the Kuroshio Current (Fig. 2.4.2), perhaps due to their particle reactive characteristics.

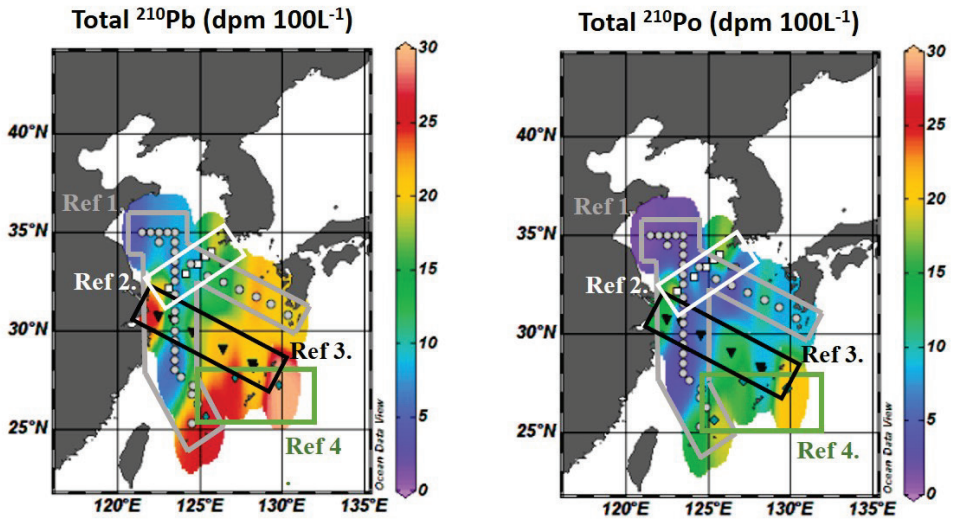

Fig. 2.4.2 Maps showing the locations of the data acquired and the distributions of ^{210}Pb and ^{210}Po in previous studies. Data from Nozaki *et al*. (1990, 1991), Hong *et al*. (1999) and Su *et al*. (2017).

The activities of both nuclides are higher in the vicinity of the Changjiang Estuary and the southwest region of Korea, perhaps due to higher suspended sediment loadings. Similarly, excess dissolved ^{210}Po activities have been observed in the western and eastern shallow shelf areas in the mouth of the YS, due to high suspended particle content (Hong *et al*., 1999). Based on a mass balance model, the residence time of ^{210}Pb was calculated to be approximately two months on the

shelf, and seven months in the Kuroshio Current (Nozaki *et al*., 1991). Nozaki *et al*. (1990) found a large ^{210}Po deficiency relative to ^{210}Pb in the upper 1000 m water column of the ECS and the Philippine Sea.

^{137}Cs and ^{90}Sr

Among artificial radionuclides, the Cesium isotope ^{137}Cs (half-life: 30.17 years) and Strontium isotope ^{90}Sr (half-life: 28.7 years) have received particular attention due to their long half-lives in the ocean. The main source of both nuclides is atmospheric fallout from global weapon testing during the 1960s in the western Pacific. Thus, in general, the distribution of water-soluble ^{137}Cs depends on ocean currents, radioactive decay, water mixing, and inputs through the remobilization of terrestrial sources, while the distribution of ^{90}Sr is influenced significantly by local biogeochemistry and physical mixing of different water masses.

The activity of ^{137}Cs in surface seawater in the ECS ranges from 0.4 to 1.8 Bq m^{-3} with a mean value of 1.0 ± 0.1 Bq m^{-3} in 2011 (Wu, 2018; Zhao *et al*., 2018; Fig. 2.4.3). It is similar to the range from the South China Sea (1.1–1.4 Bq m^{-3} with a mean value of 1.3 ± 0.1 Bq m^{-3}, Wu *et al*., 2013). In the YS and the southern sea off Korea, ^{137}Cs activity ranges from 1.5 to 2.3 Bq m^{-3} and from 1.0 to 2.0 Bq m^{-3}, respectively (KINS, 2012) (Fig. 2.4.3). The ranges of ^{137}Cs activity show similar values for the period 2007–2011 (1.0–3.0 Bq m^{-3}, KINS, 2012). The higher activities of ^{137}Cs in the center of the YS seem to be associated with the accumulation of terrestrial ^{137}Cs over a water residence time of about five years.

The ^{90}Sr activity in surface seawater of the ECS ranged from 2.0 to 3.0 Bq m^{-3} in 1994 (Fig. 2.4.3, Hong *et al*., 2006). In the YS, the activity of ^{90}Sr ranged from 1.0 to 4.0 Bq m^{-3} for the period 1994–2000 and 2012 (Fig. 2.4.3, Hong *et al*., 2006; KINS, 2012). Hong *et al*. (2006) suggested that river waters are the main source of ^{90}Sr in the YS based on a correlation between ^{90}Sr activity and salinity. As such, ^{90}Sr activities were higher towards the river mouth and the YS.

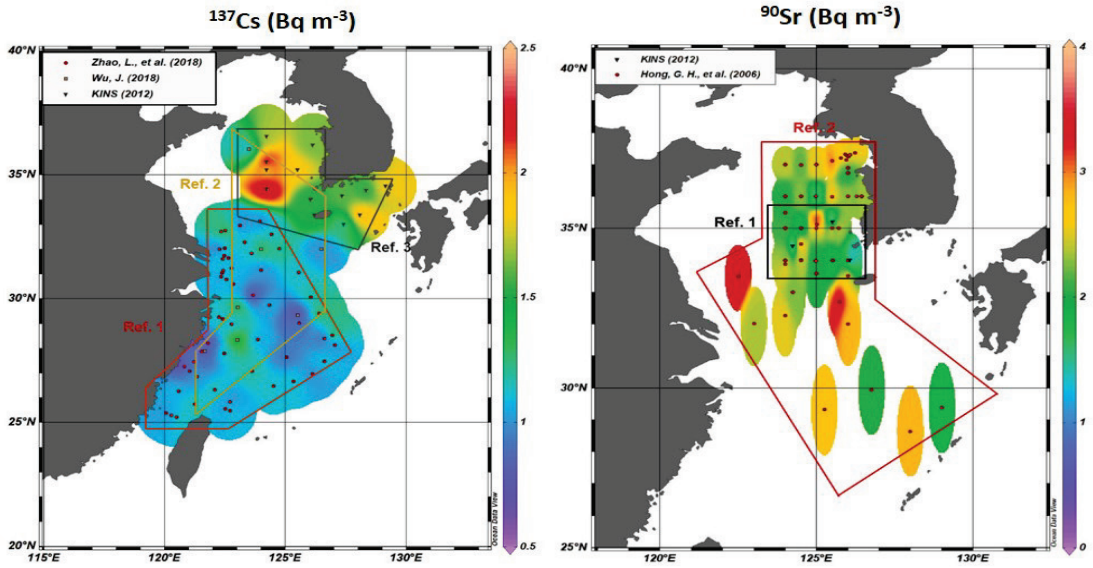

Fig. 2.4.3 The spatial distribution of ^{137}Cs activities in surface water of the East China Sea, the Yellow Sea, and the southern sea off Korea. Data from KINS (2012), Wu (2018) and Zhao *et al*. (2018). The spatial distribution of ^{90}Sr activities in surface water of the East China Sea and the Yellow Sea. Data from Hong *et al*. (2006) and KINS (2012).

2.4.3 Sediment

As one of major GEOTRACES ocean interfaces, the biogeochemical reaction between sediments and the overlying water column influences the net sources and sinks for dissolved TEIs in seawater as well as the internal cycling of TEIs in the ocean (GEOTRACES Science Plan, 2006). However, as the largest marginal shelf adjacent to the northwestern Pacific Ocean, little is known about net supplies of TEIs from sediments or about the key processes and key areas of the supplies in the ECS, YS, and BS.

Meanwhile, the signal from land changes and anthropogenic activities with the injection of Changjiang and Yellow River water, and the signal from ocean processes have been recorded synthetically in the sediments. However, there are few systematic studies that focus on these signals.

Some trace metals play a key role in controlling biogeochemical processes in the ocean, such as Fe, Cu, Zn, Co, Cd, and Mn. Meanwhile, some trace metals are harmful to the natural and human environment due to their toxicity and/or radioactivity, such as Lead (Pb), Mercury (Hg), Cadmium (Cd), Arsenic (As), Zinc (Zn). Studies (Huang *et al.*, 2014; Hu *et al.*, 2015) in recent years have advanced our understanding of the distribution of these micronutrients and pollutant trace metals in the continental shelves of the ECS, YS, and BS.

East China Sea

Higher heavy metal (Cu, Pb, Zn, Cd, As, Hg) concentrations are found at the entrance to the Changjiang, decreasing toward the northeast. The vertical distribution of contamination levels and its ecological risk can be divided into four periods based on the down core variation in heavy metals: pre-1940s, 1940s–1970s, 1970s–1990s, and late 1990s to the present (Hu *et al.*, 2015). Higher concentrations of metals (Cu, Mn, Ni, Zn, Pb, Fe) are generally found in the inner ECS shelf and decreasing seaward. The sequences of the enrichment factor (EF) of the studied metals are Cu > Mn > Ni > Zn > Pb > Fe. The metal contamination in the middle and outer shelves of the ECS is still minor (Fang *et al.*, 2009). Total concentrations for As, Hg, Selenium (Se), Antimony (Sb), Tellerium (Te), Tin (Sn), Bismuth (Bi), and Germanium (Ge) ae 4.6–30, 0.01–0.40, 0.04–0.38, 0.36–1.48, 0.02–0.10, 0.48–6.58, 0.13–0.64 and 0.83–2.43 mg/g, respectively, in the Changjiang Estuary and Hangzhou Bay. As, Hg and Sn are at low risk, whereas Bi, Se, Sb, Te and Ge are at medium risk (Duan *et al.*, 2014).

The results of sequential extraction, the geoaccumulation index (Igeo) and principal component analysis indicate that Se and Sn come mainly from natural inputs (crustal and biological inputs) while As, Sb, Hg, Bi and Te come from both crustal and anthropogenic inputs via the atmosphere and rivers, whereas Ge possibly come from natural (crustal and biological inputs) and anthropogenic inputs (Duan *et al.*, 2014). Distributions of enrichment factors (EFs) and labile fractions reveal that the input of anthropogenic Cd and Cu is mainly through the Changjiang River, Pb is delivered both through the Changjiang River and the atmosphere, while Zn pollution is carried from land through the Changjiang River and Hangzhou Bay (Yu *et al.*, 2013).

The annual sedimentation fluxes of trace metals in the ECS are: Fe, 4–107 t yr^{-1}; Mn, 9–105 t yr^{-1}; Zn, 1–105 t yr^{-1}; Ni, 4–104 t y^{-1}; Pb, 4–104 t yr^{-1} and Cu, 3–104 t yr^{-1}, respectively, and approximately 55–70% and 10–17% of the sedimentation fluxes of trace metals are deposited to the inner shelf and the Changjiang Estuarine zone, respectively (Fang *et al.*, 2009). The budget calculation shows that the Changjiang contributes 82–90% of potentially harmful elements (PHEs, V, Cr, Co, Ni, Cu, Zn, Mo, Cd and Pb) influxes, while 38–77% of PHEs are buried in sediment, mainly along the inner shelf (Yu *et al.*, 2013).

Yellow Sea

Higher concentrations of heavy metals (Cu, Mn, Cd, Hg, Pb, Zn, Fe, Al) are generally found in the central part of the southern YS, and according to the calculated EF of the studied metals, Cd in the sediments poses a high risk to local environments, while Mn, Hg, Pb, and Zn are at moderate risk levels (Yuan *et al*., 2012).

The values of the EF values suggest that Pb, Cd and Cu in the northwestern YS region originate from both anthropogenic and natural inputs, while Pb, Cd, and Cu in the eastern and northern YS as well as Zn, Cr, Ni, and Co in the YS mainly come from natural sources, including terrestrial weathering delivered to the YS through rivers and atmospheric deposition (Huang *et al*., 2014).

The annual sedimentation fluxes of heavy metals in the west part of YS are Fe, 1–106 t yr^{-1}; Mn, 2–104 t yr^{-1}; Cu, 9–102 t yr^{-1}; Zn, 3–103 t yr^{-1}; Pb, 1–103 t yr^{-1}; Cd, 4.9 t yr^{-1}; Cr, 1–104 t yr^{-1}; Ni, 1–103 t yr^{-1} and Co, 5–102 t yr^{-1} (Huang *et al*., 2014).

Bohai Sea

High concentrations of Cu, Co, Ni, Zn, and Cr are found in the sediments off the coast of the Bohai Bay and in the central Bohai Sea mud, while high concentrations of Cd and Pb are found in the sediments in the whole Bohai Sea. The sediments in the Bohai Sea are unpolluted with respect to the heavy metals of Co, Ni, and Cr and unpolluted to moderately polluted with respect to Cu, Zn, Cd, and Pb (Liu *et al*., 2016).

2.4.4 Atmosphere

The influence of trace elements on the surface ocean

It has been recently recognized that atmospheric inputs of particles (dry deposition) and rainwater (wet deposition) result in significant fluxes of REEs and other trace elements (TE) to the oceans. These inputs are frequent and even more significant than riverine inputs (*e.g*., Duce *et al*., 1991; Sholknovitz *et al*., 1993; Greaves *et al*., 1994; Spokes *et al*., 2001).Transition metals such as Fe, Mn, Cu, and Zn are all essential nutrients for marine phytoplankton. Iron, with low solubility in seawater, has become an important factor limiting primary productivity in most areas of the sea, especially in the high nutrient and low chlorophyll regions (Martin *et al*., 1994; Boyd *et al*., 2000; Tsuda *et al*., 2011). The lack of Mn and Zn sometimes will be the factor that limits the growth of phytoplankton, while some other TE such as Cu and As will have a toxic effect on phytoplankton (Bruland *et al*., 1989; de Baar *et al*., 1990; Paytan *et al*., 2009; Szivák, 2009).

Sources of trace elements in the atmosphere

There is a lot of evidence showing that the concentration of heavy metals in the environment has significantly increased since the industrial revolution, and the concentration continues to grow (Huisman *et al*., 1997; Couture *et al*., 2008). The origins of TE in atmospheric wet deposition are extremely complex owing to the mixing impacts from multiple anthropogenic activities and natural sources (Vuai and Tokuyama, 2011; Montoya Mayor *et al*., 2013). Except for Al and Fe, which are absolute crust-derived elements, the elements Mn, Co, Zn, Se, Pb, Cd, and Cr are all derived from human activities, based on a one-year study on dissolved TE in the atmospheric wet deposition at Jiaozhou Bay (Xing *et al*., 2017). Studies on the trend of metal elements in atmospheric aerosols in Beijing showed that Cu, Zn, Cd, and Pb were all affected by coal-burning emissions (Okuda *et al*.,

2008). In addition, transportation means and materials, such as exhaust emissions, tire wear, road paint and brake pads, are important sources of Cu, Zn and Cr (Manalis *et al*., 2005). The concentrations of Cd, Cr, Co, Ni, As, and Zn are also affected by the burning of garbage, which suggests that waste incineration is another important source of heavy metals in urban aerosols (Hu *et al*., 2003).

Depositional fluxes of trace elements

The atmospheric deposition of TE has a profound influence on marine biogeochemical processes; thus they have attracted increasing attention from the academic community (Song, 2010), with studies being carried out on dissolved TE and dry deposition velocities of marine aerosol (Voutsa and Samara, 2002; Cizmecioglu and Muezzinoglu, 2008; Buck *et al*., 2010, 2013). The research in this area is mainly focused on total concentrations and less focused on TE dissolved in aerosols (Ben *et al*., 2015), which has seriously restricted the understanding of the effects of bioavailability and geochemical migration on atmospheric deposition. The dry deposition flux of dissolved TE in the ECS aerosol is lower than that at Tokyo and higher than that in the Pacific (Sakata and Marumoto, 2004; Hsu *et al*., 2010; Buck *et al*., 2013). Xing *et al*. (2017) observed that the input of Zn, Cd, and Cr by the atmospheric wet deposition accounted for 24%, 0.07%, and 1.4%, respectively, compared with the riverine input in Jiaozhou Bay. The deposition fluxes of atmospheric dissolved TEls in the ECS and YS are listed in Table 2.4.1.

Table 2.4.1 Deposition fluxes of atmospheric dissolved trace elements in the ECS and YS ($\times 10^7$ g yr^{-1}).

	Al	Fe	Mn	Co	Zn	Se	Pb	Cd	Cr	Reference
Wet deposition	3400	1600	270	10	2800	83	250	15.0	77	Xing *et al*., 2017
Dry deposition	1700	1600	280	2.9	800	11	100	7.9	9.7	Hsu *et al*., 2010

Depositional fluxes of rare earth elements

Heaton *et al*. (1990) and Sholknovitz *et al*. (1993) investigated the concentration of REEs in rainwater samples. However, the concentrations of REEs in the rainwater were below the instrumental detection limit by neutron activation analysis (INAA) method. Freydier *et al*. (1998) determined the total REE concentration in precipitation samples from Lamto (Niger) and Kollo (Ivory Coast), but they did not separate the dissolved phase from the particulate phase. Ryu *et al*. (2007) carried out a systematic research on REE concentrations in rain, river waters, and total suspended particles (TSP) in air in Korea. One possible reason for the high REE concentrations in the Han River might be the seasonal contribution of atmospheric input. For REE concentrations during the Asian dust period, TSP were much higher than the average concentrations, suggesting that atmospheric input from China (the Yellow sand) could affect the REE concentrations on the Korean Peninsula. The dissolved REE concentrations in rainwater collected from Guiyang in the acid rain impacted zone of southwest China were negatively correlated with pH. Speciation calculations predicted that the free REE metal ions, sulfate, oxalate and fluoride complexes are important forms of dissolved REEs (Zhu *et al*., 2016). The ECS and the YS, as a linking passage between the Asian continent and the northwestern Pacific Ocean, plays an important role in atmospheric transportation. However, few studies have focused on the deposition flux of REEs in this area since the work of Zhang and Liu (2004). They first determined REEs together with major ion composition in rainwater samples collected from the marginal sea north of Japan and the ECS. The results showed large differences in major ion compositions and REE patterns of the samples which reflected mixing of oceanic, crustal, and anthropogenic sources. The wet deposition fluxes of

atmospheric dissolved REEs in the ECS and YS calculated by the data of Zhang and Liu (2004) are listed Table 2.4.2.

Table 2.4.2 Wet deposition fluxes of atmospheric dissolved rare earth elements in the ECS and the YS ($\times 10^3$ mol yr^{-1}).

Y	La	Ce	Pr	Nd	Sm	Eu	Gd	Tb	Dy	Ho	Er	Tm	Yb	Lu
37	44	140	10	33	3.9	0.83	3.2	0.47	2.7	0.65	2.1	0.33	2.49	0.36

Y = Yttrium, La = Lanthanum, Ce = Cerium, Pr = Praseodymium, Nd = Neodymium, Sm = Samarium, Eu = Europium, Gd = Gadolinium, Tb = Terbium, Dy = Dysprosium, Ho = Holmium, Er = Erbium, Tm = Thulium, Yb = Ytterbium, Lu = Lutetium

The sources of rare earth elements in the atmosphere

Four main types of shale-normalized patterns are identified from the data obtained for the dissolved REEs in rainwater: (middle) MREE-enrichment, flat REE, (heavy) HREE-enrichment, and (light) LREE enrichment (Sholkovitz *et al*., 1993; Aubert *et al*., 2002; Zhang and Liu, 2004; Ryu *et al*., 2007; Iwashita *et al*., 2011; Soyol-Erdene *et al*., 2011). The REEs have also been found to be a potential indicator of environmental pollution, since anthropogenic inputs show characteristic signatures of REE composition (Olmez and Gordon, 1985; Olmez *et al*., 1991; Chiarenzelli *et al*., 2001; Zhang *et al*., 2001). In addition, large anomalies of La, Eu, and Gd were also noted in rainwater. The La anomaly might be derived from automobile emissions and REE-fertilizers (Zhu *et al*., 2016). The Eu anomaly in rainwater is geologically inherited through chemical weathering of rocks and minerals (Sholkovitz *et al*., 1993). The Gd-DTPA used as a Magnetic Resonance Imaging (MRI) contrasting agent may be the main anthropogenic source for Gd in rainwater (Kulaksız and Bau, 2013).

2.4.5 Future perspectives

Taken together, biogeochemical tracers can provide direct evidence for understanding the oceanic processes of physics and biology as well as their controlling factors. Field observation data will help the setup, improvement, and validation of simulations; meanwhile, models will provide a framework to design and evaluate the observations. The synergy of numerical simulations and observation data will facilitate the establishment of methods of interdisciplinary cooperation. Finally, the international GEOTRACES program, working on the studies of marginal seas, will improve the framework for regional cooperation by the co-observation of cross-over stations. Future work needs to be addressed as follows: (1) key mechanisms and biogeochemical processes on long-term scales are still not clear in the ECS and its adjacent marginal seas and (2) speciation of biogeochemical elements and their implications for climate change and the ocean ecosystem are largely unknown.

Acknowledgements

We are grateful to Qian Liu, Huijun He, Qian He, Wenkai Guan, Hojong Seo, Jun Hyung Seo, Yongjin Han and Ji Hyun Kim in organizing the data tables, figures, and references.

2.4.6 References

Aubert, D., Stille, P., Probst, A., Gauthier-Lafaye, F., Pourcelot, L. and Nero, M.D. 2002. Characterization and migration of atmospheric REE in soils and surface waters. *Geochim. Cosmochim. Acta* **66**: 3339–3350.

Ben, X.Y., Shi, J.H., Qiu, S., Yan, X.H. and Gao H.W. 2015. Solubility of iron in atmospheric aerosols and related influence factors in Qingdao, China. *Acta Scientiae Circumst.* **35**: 65–71.

Boyd, P.W., Watson, A.J., Law, C.S., Abraham, E.R., Trull, T., Murdoch, R., Bakker, D.C., Bowie, A.R., Buesseler, K.O., Chang, H., Charette, M., Croot, P., Downing, K., Frew, R., Gall, M., Hadfield, M., Hall, J., Harvey, M., Jameson, G., LaRoche, J., Liddicoat, M., Ling, R., Maldonado, M.T., McKay, R.M., Nodder, S., Pickmere, S., Pridmore, R., Rintoul, S., Safi, K., Sutton, P., Strzepek, R., Tanneberger, K., Turner, S., Waite, A. and Zeldis, J. 2000. A mesoscale phytoplankton bloom in the polar Southern Ocean stimulated by iron fertilization. *Nature* **407**: 695–702, doi:10.1038/35037500.

Bruland, K.W. 1989. Complexation of zinc by natural organic ligands in the central North Pacific. *Limnol. Oceanogr.* **34**: 269–285, doi:10.4319/lo.1989.34.2.0269.

Buck, C.S., Landing, W.M. and Resing, J.A. 2010. Particle size and aerosol iron solubility: A high-resolution analysis of Atlantic aerosols. *Mar. Chem*. **120**: 14–24, doi:10.1016/j.marchem.2008.11.002.

Buck, C.S., Landing, W.M. and Resing, J. 2013. Pacific Ocean aerosols: deposition and solubility of iron, aluminum, and other trace elements. *Mar. Chem.* **157**: 117–130, doi:10.1016/j.marchem.2013.09.005.

Che, H. and Zhang, J. 2018. Water mass analysis and end−member mixing contribution using coupled radiogenic Nd isotopes and Nd concentrations: interaction between marginal seas and the northwestern Pacific. *Geophys. Res. Lett.* **45**: 2388–2395, doi:10.1002/2017GL076978.

Cizmecioglu, S.C. and Muezzinoglu, A. 2008. Solubility of deposited airborne heavy metals. *Atmos. Res.* **89**: 396–404, doi:10.1016/j.atmosres.2008.03.012.

Chiarenzelli, J., Aspler, L., Dunn, C., Cousens, B., Ozarko, D. and Powis, K. 2001. Multi-element and rare earth element composition of lichens, mosses, and vascular plants from the Central Barrenlands, Nunavut, Canada. *Appl. Geochem*. **16**: 245–270, doi:10.1016/S0883-2927(00)00027-5.

Couture, R.M., Gobeil, C. and Tessier, A. 2008. Chronology of atmospheric deposition of arsenic inferred from reconstructed sedimentary records. *Environ. Sci. Technol.* **42**: 6508–6513, doi:10.1021/es800818j.

de Baar, H.J.W., Buma, A.G.J., Nolting, R.F., Cadée, G.C., Jacques, G. and Tréguer, P.J. 1990. On iron limitation of the Southern Ocean: experimental observations in the Weddell and Scotia Seas. *Mar. Ecol. Prog. Ser.* **65**: 105–122, doi:10.3354/meps065105.

Duan, L.Q., Song, J.M., Yuan, H.M., Li, X.G., Li, N. and Ma, J.K. 2014. Distribution, chemical speciation and source of trace elements in surface sediments of the Changjiang Estuary. *Environ. Earth Sci.* **72**: 3193–3204, doi:10.1007/s12665-014-3225-6.

Duce, R.A., Liss, P.S., Merrill, J.T., Atlas, E.L., Buat-Menard, P., Hicks, B.B., Miller, J.M., Prospero, J.M., Arimoto, R., Church, T.M., Ellis, W., Galloway, J.N., Hansen, L., Jickells, T.D., Knap, A.H., Reinhardt, K.H., Schneider, B., Soudine, A., Tokos, J.J., Tsunogai, S., Wollast, R. and Zhou, M. 1991. The atmospheric input of trace species to the world ocean. *Global Biogeochem. Cycles* **5**: 193–259, doi:10.1029/91GB01778.

Fang, T.H., Li, J.Y., Feng, H.M. and Chen, H.Y. 2009. Distribution and contamination of trace metals in surface sediments of the East China Sea. *Mar. Environ. Res.* **68**: 178–187, doi:10.1016/j.marenvres.2009.06.005.

Freydier, R., Dupre, B. and Lacaux, J.P. 1998. Precipitation chemistry in intertropical Africa. *Atmos. Environ.* **32**: 749–765.

GEOTRACES Science Plan. 2006. An International Study of Marine Biogeochemical Cycles of Trace Elements and Isotopes. 87 pp., https://geotracesold.sedoo.fr/libraries/documents/Science_plan.pdf.

Greaves, M.J., Statham, P.J. and Elderfield. H. 1994. Rare earth element mobilization from marine atmospheric dust into seawater. *Mar. Chem.* **46**: 255–260, doi:10.1016/0304-4203(94)90081-7.

Gu, H., Moore, W.S., Zhang, L., Du, J. and Zhang, J. 2012. Using radium isotopes to estimate the residence time and the contribution of submarine groundwater discharge (SGD) in the Changjiang effluent plume, East China Sea. *Cont. Shelf Res.* **35**: 95–107, doi:10.1016/j.csr.2012.01.002.

Heaton, R.W., Rahn, K.A. and Lowenthal, D.H. 1990. Determination of trace elements, including regional tracers, in Rhode Island precipitation. *Atmos. Environ.* **24**: 147–153, doi:10.1016/0960-1686(90)90450-2.

Hong, G.H., Park, S.K., Baskaran, M., Kim, S.H., Chung, C.S. and Lee, S.H. 1999. Lead-210 and polonium-210 in the winter well-mixed turbid waters in the mouth of the Yellow Sea. *Cont. Shelf Res.* **19**: 1049–1064, doi:10.1016/S0278-4343(99)00011-4.

Hong, G.H., Chung, C.S., Lee, S.H., Kim, S.H., Baskaran, M. and Lee, H.M. 2006. Artificial radionuclides in the Yellow Sea: inputs and redistribution. *Radioact. Environ.* **8**: 96–133, doi:10.1016/S1569-4860(05)08007-1.

Hsu, S.C., Wong, G.T.F., Gong, G.C., Shiah, F.K., Huang, Y.T., Kao, S.J., Tsai, F., Lung, S.C.C., Lin, F.J., Lin, I.I., Hung, C.C. and Tseng, C.M. 2010. Sources, solubility, and dry deposition of aerosol trace elements over the East China Sea. *Mar. Chem.* **120**: 116–127, doi:10.1016/j.marchem.2008.10.003.

Hu, C.W., Chao, M.R., Wu, K.Y., Chang-Chien, G.P., Lee, W.J. and Chang, L.W. and Lee, W.S. 2003. Characterization of multiple airborne particulate metals in the surroundings of a municipal waste incinerator in Taiwan. *Atmospheric Environ.* **37**: 2845–2852, doi:10.1016/S1352-2310(03)00208-5.

Hu, G., Bi, S., Xu, G., Zhang, Y., Mei, X. and Li, A. 2015. Distribution and assessment of heavy metals off the Changjiang River mouth and adjacent area during the past century and the relationship of the heavy metals with anthropogenic activity. *Mar. Pollut. Bull.* **96**: 434–440, doi:10.1016/j.marpolbul.2015.05.009.

Huang, P., Li, T.G., Li, A.C., Yu, X.K. and Hu, N.J. 2014. Distribution, enrichment and sources of heavy metals in surface sediments of the north Yellow Sea. *Cont. Shelf Res.* **73**: 1–13, doi:10.1016/j.csr.2013.11.014.

Huisman, D.J., Vermeulen, F.J.H., Baker, J., Veldkamp, A., Kroonenberg, S.B. and Klaver, G.T. 1997. A geological interpretation of heavy metal concentrations in soils and sediments in the southern Netherlands. *J. Geochem. Explor.* **59**: 163–174, doi:10.1016/S0375-6742(97)00018-6.

Inoue, M., Nakano, Y., Kiyomoto, Y., Kofuji, H., Hamajima, Y. and Yamamoto, M. 2010. Seasonal variation of ^{228}Ra/ ^{226}Ra ratio in surface water from the East China Sea and the Tsushima Strait. *J. Oceanogr.* **66**: 425–428, doi:10.1007/s10872-010-0036-6.

Inoue, M., Yoshida, K., Minakawa, M., Kiyomoto, Y., Kofuji, H., Nagao, S., Hamajima, Y. and Yamamoto, M. 2012. Spatial variations of ^{226}Ra, ^{228}Ra, and ^{228}Th activities in seawater from the eastern East China Sea. *Geochem. J.* **46**: 429–441, doi:10.2343/geochemj.2.0221.

Iwashita, M., Saito, A., Arai, M., Furusho, Y. and Shimamura, T. 2011. Determination of rare earth elements in rainwater collected in suburban Tokyo. *Geochem. J.* **45**: 187–197, doi:10.2343/geochemj.1.0121.

Kim, G. 2001. Large deficiency of polonium in the oligotrophic ocean's interior. *Earth Planet. Sci. Lett.* **192**: 15–21, doi:10.1016/S0012-821X(01)00431-9.

Kim, G., Ryu, J.W., Yang, H.S. and Yun. S.T. 2005. Submarine groundwater discharge (SGD) into the Yellow Sea revealed by ^{228}Ra and ^{226}Ra isotopes: implications for global silicate fluxes. *Earth Planet. Sci. Lett.* **237**: 156–166, doi:10.1016/j.epsl.2005.06.011.

Kim, I. and Kim, G. 2015. Role of colloids in the discharge of trace elements and rare earth elements from coastal groundwater to the ocean. *Mar. Chem.* **176**: 126–132, doi:10.1016/j.marchem.2015.08.009.

Kim, J., Cho, H.M. and Kim, G. 2015. ^{228}Ra flux in the northwestern Pacific marginal seas: Implications for disproportionally large submarine groundwater discharge. *Ocean Sci. J.* **50**: 195–202, doi:10.1007/s12601-015-0015-3.

KINS (Korea Institute of Nuclear Safety). 2012. Marine Environmental Radioactivity Survey, KINS/ER-092, 8 (in Korean).

Kulaksız, S. and Bau, M. 2013. Anthropogenic dissolved and colloid/nanoparticle-bound samarium, lanthanum and gadolinium in the Rhine River and the impending destruction of the natural rare earth element distribution in rivers. *Earth Planet. Sci. Lett.* **362**: 43–50, doi:10.1016/j.epsl.2012.11.033.

Lee, H., Kim, G., Kim, J., Park, G. and Song, K. 2014. Tracing the flow rate and mixing ratio of the Changjiang Diluted Water in the northwestern Pacific marginal seas using radium isotopes. *Geophys. Res. Lett.* **41**: 4637–4645, doi:10.1002/2014GL060230.

Li, L., Liu, J., Wang, X. and Shi, X. 2015. Dissolved trace metal distributions and Cu speciation in the southern Bohai Sea, China. *Mar. Chem.* **172**: 34–45, doi:10.1016/j.marchem.2015.03.002.

Li, L., Wang, X.J., Liu, J.H. and Shi, X.F. 2017. Dissolved trace metal (Cu, Cd, Co, Ni, And Ag) distribution and Cu speciation in the southern Yellow Sea and Bohai Sea, China. *J. Geophys. Res. Oceans* **122**: 1190–1205, doi:10.1002/2016JC012500.

Liu, M., Fan, D., Liao, Y., Chen, B. and Yang, Z. 2016. Heavy metals in surficial sediments of the central Bohai Sea: their distribution, speciation and sources. *Acta Oceanol. Sin.* **35**: 98–110, doi:10.1007/s13131-016-0926-6.

Mackin, J.E. and Aller, R.C. 1984. Diagenesis of dissolved aluminum in organic-rich estuarine sediments. *Geochim. Cosmochim. Acta*. **48**: 299–313, doi:10.1016/0016-7037(84)90252-7.

Manalis, N., Grivas, G., Protonotarios, V., Moutsatsou, A., Samara, C. and Chaloulakou, A. 2005. Toxic metal content of particulate matter (PM_{10}), within the greater area of Athens. *Chemosphere* **60**: 557–566, doi:10.1016/j.chemosphere.2005.01.003.

Martin, J.H., Coale, K.H., Johnson, K.S., Fitzwater, S.E., Gordon, R.M., Tanner, S.J., Hunter, C.N., Elrod, V.A., Nowicki, J.L., Coley, T.L., Barber, R.T., Lindley, S., Watson, A.J., Van Scoy, K., Law, C.S. Liddicoat, M.I., Ling, R., Stanton, T., Stockel, J., Collins, C., Anderson, A., Bidigare, R., Ondrusek, M., Latasa, M., Millero, F.J., Lee, K., Yao, W., Zhang, J.Z., Friederich, G., Sakamoto, C., Chavez, F., Buck, K., Kolber, Z., Greene, R., Falkowski, P., Chisholm, S.W., Hoge, F., Swift, R., Yungel, J., Turner, S., Nightingale, P., Hatton, A., Liss, P. and Tindale, N.W. 1994. Testing the iron hypothesis in ecosystems of the equatorial Pacific Ocean. *Nature* **371**: 123–129, doi:10.1038/371123a0.

Men, W. and Liu, G. 2015. Distribution of ^{226}Ra and the residence time of the shelf water in the Yellow Sea and the East China Sea. *J. Radioanal. Nucl. Chem.* **303**: 2333–2344, doi:10.1007/s10967-014-3749-y.

Minakawa, M. and Watanabe, Y. 1998. Aluminum in the East China Sea and Okinawa Trough, marginal sea areas of the western North Pacific. *J. Oceanogr.* **54**: 629–640, doi:10.1007/BF02823283.

Montoya-Mayor, R., Fernández-Espinosa, A.J., Seijo-Delgado, I. and Ternero-Rodríguez, M. 2013. Determination of soluble ultra-trace metals and metalloids in rainwater and atmospheric deposition fluxes: a 2-year survey and assessment. *Chemosphere* **92**: 882–891, doi:10.1016/j.chemosphere.2013.02.044.

Nozaki, Y., Ikuta, N. and Yashima, M. 1990. Unusually large ^{210}Po deficiencies relative to ^{210}Pb in the Kuroshio Current of the East China and Philippine seas. *J. Geophys. Res. Oceans* **95**: 5321–5329, doi:10.1029/JC095iC04p05321.

Nozaki, Y., Tsubota, H., Kasemsupaya, V., Yashima, M. and Naoko, I. 1991. Residence times of surface water and particle-reactive ^{210}Pb and ^{210}Po in the East China and Yellow Seas. *Geochim. Cosmochim. Acta* **55**: 1265–1272, doi:10.1016/0016-7037(91)90305-O.

Okubo, T. 1980. Radium-228 in the Japan Sea. *J. Oceanogr. Soc. Japan* **36**: 263–268.

Olmez, I. and Gordon, G.E. 1985. Rare earths: atmospheric signatures for oil-fired power plants and refineries. *Science* **229**: 966–968, doi:10.1126/science.229.4717.966.

Olmez, I., Sholkovitz, E.R., Hermann, D. and Eganhouse, R. 1991. Rare earth elements in sediments off Southern California: a new anthropogenic indicator. *Environ. Sci. Technol.* **25**: 310–316, doi:10.1021/es00014a015.

Paytan, A., Mackey, K.R., Chen, Y., Lima, L.D., Doney, S.C., Mahowald, N., Labiosa, R. and Post, A.F. 2009. Toxicity of atmospheric aerosols on marine phytoplankton. *Proc. Natl. Acad. Sci. USA* **106**: 4601–4605, doi:10.1073/pnas.0811486106.

Ren, J.L., Zhang, J., Li, J.B., Yu, X.Y., Liu, S.M. and Zhang, E.R. 2006. Dissolved aluminum in the Yellow Sea and East China Sea – Al as a tracer of Changjiang (Yangtze River) discharge and Kuroshio incursion. *Estuar. Coast. Shelf Sci.* **68**: 165–174, doi:10.1016/j.ecss.2006.02.004.

Ren, J.L., Zhang, G.L., Zhang, J., Shi, J.H., Liu, S.M., Li, F.M., Jin, J. and Liu, C.G. 2011. Distribution of dissolved aluminum in the southern Yellow Sea: influences of a dust storm and the spring bloom. *Mar. Chem.* **125**: 69–81, doi:10.1016/j.marchem.2011.02.004.

Ren, J.L., Xuan, J.L., Wang, Z.W., Huang, D. and Zhang, J. 2015. Cross-shelf transport of terrestrial Al enhanced by the transition of northeasterly to southwesterly monsoon wind over the East China Sea. *J. Geophys. Res. Oceans* **120**: 5054–5073, doi:10.1002/2014JC010655.

Ryu, J.S., Lee, K.S., Lee, S.G., Lee, D. and Chang, H.W. 2007. Seasonal and spatial variations of rare earth elements in rainwaters, river waters and total suspended particles in air in South Korea. *J. Alloys Compounds* **437**: 344–350, doi:10.1016/j.jallcom.2006.08.002.

Sakata, M. and Marumoto, K. 2004. Dry deposition fluxes and deposition velocities of trace metals in the Tokyo metropolitan area measured with a water surface sampler. *Environ. Sci. Technol.* **38**: 2190–2197, doi:10.1021/es030467k.

Sholkovitz, E.R., Church, T.M. and Arimoto, R. 1993. Rare earth element composition of precipitation, precipitation particles, and aerosols. *J. Geophys. Res. Atmos.* **98**: 20,587–20,599, doi:10.1029/93JD01926.

Soyol-Erdene, T.O., Han, Y., Lee, B. and Huh, Y. 2011. Sources and fluxes of Pt, Ir and REE in the Seoul metropolitan area through wet scavenging processes. *Atmos. Environ.* **45**: 1970–1978, doi:10.1016/j.atmosenv.2011.01.023.

Spokes, L., Jickells, T. and Jarvis, K. 2001. Atmospheric inputs of trace metals to the northeast atlantic ocean: the importance of southeasterly flow. *Mar. Chem.* **76**: 319–330, doi:10.1016/S0304-4203(01)00071-8.

Su, H., Yang, R., Zhang, A. and Li, Y. 2015. Dissolved iron distribution and organic complexation in the coastal waters of the East China Sea. *Mar. Chem.* **173**: 208–221, doi:10.1016/j.marchem.2015.03.007.

Su, H., Yang, R., Zhang, A., Li, Y., Qu, S. and Wang, X. 2017. Characteristics of trace metals and phosphorus in seawaters offshore the Yangtze River. *Mar. Pollut. Bull.* **124**: 1020–1032, doi: 10.1016/j.marpolbul.2017.01.022.

Su, N., Du, J., Li, Y. and Zhang, J. 2013. Evaluation of surface water mixing and associated nutrient fluxes in the East China Sea using ^{226}Ra and ^{228}Ra. *Mar. Chem.* **156**: 108–119, doi:10.1016/j.marchem.2013.04.009.

Szivák, I., Behra, R. and Sigg, L. 2009. Metal-induced reactive oxygen species production in *Chlamydomonas reinhardtii* (Chlorophyceae). *J. Phycol.* **45**: 427–435, doi:10.1111/j.1529-8817.2009.00663.x.

Tsuda, A., Takeda, S., Saito, H., Nishioka, J., Nojiri, Y., Kudo, I., Kiyosawa, H., Shiomoto, A, Imai, K., Ono, T., Shimamoto, A., Tsumune, D., Yoshimura, T., Aono, T., Hinuma, A., Kinugasa, M., Suzuki, K., Sohrin, Y., Noiri, Y., Tani, H., Deguchi, Y., Tsurushima, N., Ogawa, H., Fukami, K., Kuma, K. and Saino, T. 2003. A mesoscale iron enrichment in the western subarctic Pacific induces a large centric diatom bloom. *Science* **300**: 958–961, doi:10.1126/science.1082000.

Voutsa, D. and Samara, C. 2002. Labile and bioaccessible fractions of heavy metals in the airborne particulate matter from urban and industrial areas. *Atmos. Environ.* **36**: 3583–3590, doi:10.1016/S1352-2310(02)00282-0.

Vuai, S.A.H. and Tokuyama, A. 2011. Trend of trace metals in precipitation around Okinawa Island, Japan. *Atmos. Res.* **99**: 80–84, doi:10.1016/j.atmosres.2010.09.010.

Wang, Z., Ren, J., Jiang, S., Liu, S., Xuan, J. and Zhang, J. 2016. Geochemical behavior of dissolved manganese in the East China Sea: seasonal variation, estuarine removal, and regeneration under suboxic conditions. *Geochem. Geophys. Geosyst.* **17**: 282–299, doi:10.1002/2015GC006128.

Wang, Z., Ren, J., Xuan, J., Li, F., Yang, T. and Guo, Y. 2018. Processes controlling the distribution and cycling of dissolved manganese in the northern South China Sea. *Mar. Chem.* **204**: 152–162, doi:10.1016/j.marchem.2018.07.003.

Wu, J. 2018. Impacts of Fukushima Daiichi Nuclear Power Plant accident on the Western North Pacific and the China Seas: Evaluation based on field observation of ^{137}Cs: *Mar. Pollut. Bull.* **127**: 45–53, doi:10.1016/j.marpolbul.2017.11.056.

Wu, J.W., Zhou, K.B. and Dai, M.H. 2013. Impacts of the Fukushima nuclear accident on the china seas: evaluation based on anthropogenic radionuclide ^{137}Cs. *Sci. Bull.* **58**: 552–558, doi:10.1007/s11434-012-5426-2.

Xing, J., Song, J., Yuan, H., Wang, Q., Li, X., Li, N., Duan, L. and Qu, B. 2017. Atmospheric wet deposition of dissolved trace elements to Jiaozhou Bay, north China: fluxes, sources and potential effects on aquatic environments. *Chemosphere* **174**: 428–436, doi:10.1016/j.chemosphere.2017.02.004.

Yeh, J.C. and Chung, Y.C. 1997. ^{228}Ra and ^{226}Ra Distributions off north and southwest Taiwan. *Terrest. Atmos. Ocean. Sci.* **8**: 141–154, doi:10.3319/TAO.1997.8.1.141(O).

Yu, Y., Song, J., Li, X., Yuan, H. and Li, N. 2013. Fractionation, sources and budgets of potential harmful elements in surface sediments of the East China Sea. *Mar. Poll. Bull.* **68**: 157–167, doi:10.1016/j.marpolbul.2012.11.043.

Yuan, H., Song, J., Li, X., Li, N. and Duan, L. 2012. Distribution and contamination of heavy metals in surface sediments of the South Yellow Sea. *Mar. Pollut. Bull.* **64**: 2151–2159, doi:10.1016/j.marpolbul.2012.07.040.

Zhang, J. and Liu C.Q. 2004. Major and rare earth elements in rainwater from Japan and East China Sea: Natural and anthropogenic sources. *Chem. Geol.* **209**: 315–326, doi:10.1016/j.chemgeo.2004.06.014.

Zhang, L., Liu, Z., Zhang, J., Hong, G.H., Park, Y. and Zhang, H.F. 2007. Reevaluation of mixing among multiple water masses in the shelf: An example from the East China Sea. *Cont. Shelf Res.* **27**: 1969–1979, doi:10.1016/j.csr.2007.04.002.

Zhao, L., Liu, D., Wang, J., Du, J., Hou, X. and Jiang, Y. 2018. Spatial and vertical distribution of radiocesium in seawater of the East China Sea. *Mar. Pollut. Bull.* **28**: 361–368, doi:10.1016/j.marpolbul.2018.01.047.

Zhu, Z., Liu, C.Q., Wang, Z.L., Liu, X. and Li, J. 2016. Rare earth elements concentrations and speciation in rainwater from Guiyang, an acid rain impacted zone of southwest China. *Chem. Geol.* **442**: 23–34, doi:10.1016/j.chemgeo.2016.08.038.

Zhang, F.S., Yamasaki, S. and Kimura, K. 2001. Rare earth element content in various waste ashes and the potential risk to Japanese soils. *Environ. Int.* **27**: 393–398, doi:10.1016/S0160-4120(01)00097-6.

Zhang, J., Liu, Q., Bai, L-L. and Matsuno, T. 2018. Water mass analysis and contribution estimation using heavy rare earth elements: Significance of Kuroshio intermediate water to Central East China Sea shelf water. *Mar. Chem.* **204**: 174–180, doi:10.1016/J.MARCHEM.2018.07.011.

Zhang, J., Liu, Q., He, Q. and Nozaki, Y. 2019. Rare earth elements and their isotopes in the ocean, pp. 181–197 *in:* The Encyclopedia of Ocean Sciences, 3rd edition, vol. 1, *edited by* J.K. Cochran, J.H. Bokuniewicz and L.P. Yager, Elsevier, Oxford.

2.5 Persistent Organic Pollutants and Heavy Metal Pollution

Xianguo Li[1,2] and Yanbin Li[1,2]

[1] College of Chemistry and Chemical Engineering, Ocean University of China, China
[2] Key Laboratory of Marine Chemistry Theory and Technology, Ministry of Education, Ocean University of China, China

2.5.1 Introduction

Over the past few decades rapid population growth and intensive anthropogenic activities, as well as unprecedented industrialization and urbanization, have led to large amounts of heavy metals and persistent organic pollutants (POPs) being emitted into the environment. Due to their environmental persistence, bioaccumulation and biomagnification via the food chain, toxicity to humans and wildlife, and long-range transport, they have aroused increasing public concerns in recent years. The Stockholm Convention, aimed to protect humans and the environment from exposure to hazardous and toxic POPs, initially listed twelve "legacy" POPs in 2001, including eight types of organochlorine pesticides (OCPs), two kinds of industrial chemicals (polychlorinated biphenyls (PCBs) and hexachlorobenzene), and two types of byproducts (polychlorinated dibenzo-p-dioxins and polychlorinated dibenzofurans) (UNEP, 2001). Meanwhile, polycyclic aromatic hydrocarbons (PAHs) were also classified as POPs under the Aarhus Protocol (UNECE, 1998). In 2009, nine new chemicals of emerging environmental concern ("emerging" POPs), with potential POPs-like behavior, were added to Stockholm Convention (UNEP, 2009), among which polybrominated diphenyl ethers (PBDEs) and perfluoroalkyl substances (PFASs) were of the most concern. Additionally, hexabromocyclododecane and short-chain chlorinated paraffins (SCCPs) were listed in Annex A of the Stockholm Convention on POPs in 2013 (UNEP, 2013a). In 2013, the Minimata Convention, aimed to protect human health and the environment from the adverse effects of mercury, was lanched by the UNEP (UNEP, 2013b). Mercury is among the heavy metals drawing the most public concern world-wide.

POPs are hydrophobic with octanol-water partition coefficients (log K_{ow}) ranging from 3.0 to 7.0 (Jones and De Voogt, 1999; Meng *et al.*, 2017). Thus, POPs are prone to being trapped in marine sediments after entering marine systems. Marine sediments are then generally regarded as one of the major sinks of POPs. Moreover, the solubility of POPs decreases significantly in seawater, due to greater ionic strength, compared to that in freshwater (Turner and Millward, 2002). When POPs are transported from rivers to seas, the adsorption of POPs onto suspended particles and accumulation in sediments increases in the estuaries and coastal areas. Meanwhile, POPs in sediments can be re-released to aquatic environments, leading to secondary pollution of water systems (Zhen *et al.*, 2016). Aquatic (especially benthic) organisms can ingest these POPs from the water phase and sediments, and thus introduce them to the food chain, posing great risks to the marine ecosystem and even to humans (Li *et al.*, 2007; Jiao *et al.*, 2016). Consequently, sediments play an important role in evaluating the overall environmental quality of aquatic systems.

The rapid growth of the economy, coupled with intensively increasing anthropogenic activities, has accelerated the environmental deterioration in the Yellow Sea (YS) and the East China Sea (ECS). Additionally, about 10% of the worldwide riverine sediments, predominantly from the Yellow River and Yangtze (Changjiang) River, are delivered into the YS and ECS (Milliman and Meade, 1983). As a result, rivers play an important role in controlling the physical and biogeochemical features of the sediments as well as the associated POPs and heavy metals in the adjacent estuaries and coastal margins of the YS and ECS (Gao *et al*., 2008; Wang, 2008; Liu *et al*., 2009b; Hu *et al*., 2011; Ci *et al*., 2014; NBO, 2016). Besides, the YS and ECS are in the pathway of Asian dust in spring and winter, thus receiving large amounts of atmospheric particles and associated POPs and heavy metals (Liu *et al*., 2005; Guo *et al*., 2006; Lammel *et al*., 2006; Hu *et al*., 2011). The YS and ECS have become one of the most heavily polluted sea areas and thus act as a sink and possible long-term sources of POPs and heavy metals, causing increasing concerns among researchers and the general public. This review summarizes the distributions, potential sources and fates of a few legacy and emerging POPs (OCPs, PCBs, SCCPs, PBDEs and PFASs) commonly detected in sediments from the YS and ECS, as well as the distribution of heavy metals in sediment, water and biota, and the cycling of heavy metals in both marine systems. Discrepancies in environmental conditions between the YS and ECS are also documented in the present review.

2.5.2 Legacy and emerging persistent organic pollutants in sediments of the Yellow Sea and East China Sea

Chlorinated POPs

Organochlorine pesticides

Organochlorine pesticides (OCPs), one of the typical legacy POPs, continue to attract considerable scientific and regulatory interest because of their historically high production volumes, persistence, bioaccumulation and potential adverse impacts on non-target organisms (Yang *et al*., 2005a). OCPs can be transported from pollution sources (mainly pesticide plants and related non-point sources) to marine systems through pathways such as atmospheric transport and deposition, direct and indirect local discharge, riverine inputs and surface runoff of contaminated soils (Zhou *et al*., 2014). Due to their hydrophobicity, OCPs tend to strongly partition into particulate matter and settle down through the water column to coastal sediments, and then are transported towards offshore areas (Chen *et al*., 2002). On the other hand, resuspension in estuarine and coastal areas may act as a source of OCPs to the overlying water column and offshore sediments (Eggleton and Thomas, 2004).

Among OCPs, dichloro-diphenyl-trichloroethane (DDT) and hexachlorocyclohexane (HCH) were widely used in China from the 1950s until their officially banning in 1983 (Gong *et al*., 2007). To monitor the pollution status, the occurrences of DDTs and HCHs were extensively investigated in estuarine, coastal and oceanic sediments from the YS and ECS (Fig. 2.5.1). As shown in Figure 2.5.1, concentrations of DDTs and HCHs vary greatly among these areas. In the YS, the highest level of DDTs was detected in Jiaozhou Bay, with a mean value of 10.3 ng g^{-1} dry weight (d.w.) (Liu *et al*., 2013). The concentrations of HCHs in sediments were distinctly lower than those of DDTs, with the highest level of 8.08 ng g^{-1} d.w. in the Qingdao coastal area (Wang, J. *et al*., 2010), for which the higher potential of degradation for HCHs and the widespread usage of technical DDTs over HCHs in China (Jones and De Voogt, 1999; Peng *et al*., 2015) might be responsible. To evaluate the ecotoxicological effects of DDTs and HCHs, the concentration data in this review were compared with quality guideline values. HCHs from most of the studied areas were higher than probable effect level (PEL: 0.99 ng g^{-1} d.w.; Feng *et al*., 2011), indicating potentially adverse

effects to the benthic environment and wildlife. However, DDTs were overall lower than PEL (46.1 ng g^{-1} d.w.; Feng *et al*., 2011), suggesting that the ecotoxicological risks of DDTs in the YS might be negligible. Over the entire studied areas in the YS, OCP concentrations in sediments from rivers, estuaries and bays were overall higher than those from the open seas (Fig. 2.5.1). Moreover, Hu *et al*. (2011) found that OCP levels showed a significantly decreasing trend with increasing distance from shoreline in the northern YS, indicating land-based sources and intensive land–sea migration.

In the ECS and adjacent estuaries, the average OCP concentrations ranged from 1.2 to 15.3 ng g^{-1} d.w., with the highest level in the Yangtze River Estuary for DDTs and Minjiang Estuary for HCHs (Fig. 2.5.1). Compared with the YS, the OCP concentrations were overall higher in the ECS. This discrepancy could be attributed to the variations in environmental conditions between the YS and ECS, as well as the high urbanization and industrialization in the Yangtze River Delta and adjacent coastal regions (An *et al*., 2009; Hu *et al*., 2011). In addition, the Yangtze River Delta is an important production base for cereals, and has a record of the highest pesticide application in China (Li *et al*., 2001; Zhang, H. *et al*., 2009). Over the inner shelf area of the ECS, OCP levels showed a decreasing trend from the Yangtze River Estuary toward the south, indicating the important role the Yangtze River plays on OCP pollution in the ECS (Yang *et al*., 2005b; Li *et al*., 2014; Zhou *et al*., 2014). Similar to the YS, the levels of DDTs were overall higher than those of HCHs, indicating the extensive usage of technical DDTs in China. Compared with the quality guidelines, the HCHs in the Yangtze River Estuary and Minjiang Estuary were distinctly higher than PEL, while DDTs were lower than PEL in all the studied areas. Considering the high inputs of the Yangtze River to the ECS, more attention should also be paid to DDTs and HCHs in this aquatic environment.

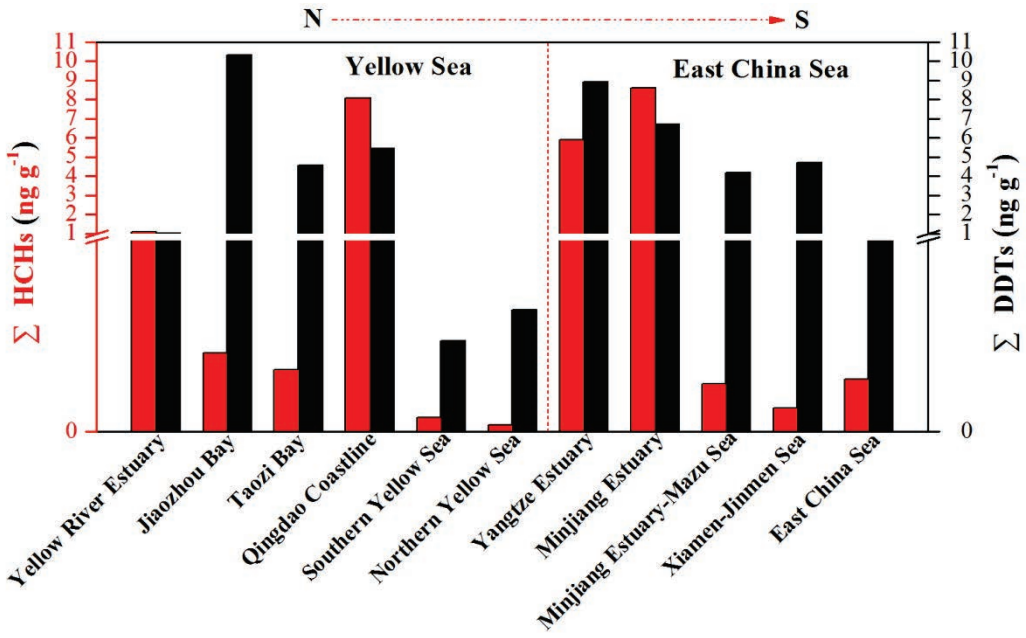

Fig. 2.5.1 Average concentrations (ng g^{-1} d.w.) of HCHs and DDTs in surface sediments from nearshore and offshore regions of the Yellow Sea and East China Sea. Data were collected from Chen *et al*. (1996), Zhang and Lin (2004), Yang *et al*. (2005b), Chen *et al*. (2010), Wang, G.L. *et al*. (2010), Wang, J. *et al*. (2010b), Hu *et al*. (2011), Liu *et al*. (2013), Li *et al*. (2014) and Zhou *et al*. (2014).

Polychlorinated biphenyls

Up to about 50 years ago polychlorinated biphenyls (PCBs) were widely used in transformers, capacitors, paints and printing ink, as well as in some other industrial applications (Erickson and Kaley, 2011). Concerns about their toxicity and bioaccumulation led to their banning throughout the world in the late 1970s (Erickson and Kaley, 2011; Duan *et al*., 2013a). In China, approximately 10,000 tons of PCBs were produced from 1965 to 1974, with 9000 tons for trichlorobiphenyls and 1000 tons for pentachlorobiphenyls (Mai *et al*., 2005b). A series of studies were conducted across the whole area covered in this review (Fig. 2.5.2). In general, PCB concentrations in sediments were distinctly higher than OCPs in the YS and ECS (Figs. 2.5.1 and 2.5.2). PCB concentrations in the studied areas varied greatly. In the YS, the highest concentration of PCBs was detected in Jiaozhou Bay (an average of 10.3 ng g^{-1} d.w.; Guo *et al*., 2011), which was 3- to 10-fold higher than that in other areas. In the ECS, Yueqing Bay had the highest PCB level, with a mean value of 14.1 ng g^{-1} d.w. (Yang, H. *et al*., 2011). Over the entire studied areas, PCBs in sediments generally followed the order of bays > rivers > coastal areas > open seas (Fig. 2.5.2) in both the YS and ECS, indicating land-based sources and intensive transport from source to sink. In addition, a decreasing trend of PCBs could be observed from 2004 to 2011 in the YS (Zhang *et al*., 2007; Duan *et al*., 2013b) and from 2007 to 2011 (Yang *et al*., 2012; Duan *et al*., 2013a) in the ECS. This was also confirmed by data from sediment cores in the area (Zhang, P. *et al*., 2009; Duan *et al*., 2013a), attributed to the ban on production and usage of PCBs as well as to the regulatory strategies implemented in China. However, Zhang, P. *et al*. (2009) and Duan *et al*. (2013a) reported relatively high proportions of heavier homologs (6–8Cl PCBs) in recent years. According to previous reports, PCBs produced unintentionally by industrial processes (Aries *et al*., 2006; Liu, G. *et al*., 2009), waste incineration (Shibamoto *et al*., 2007) and vehicle exhaust (Broz *et al*., 2000) were dominated by heavier congeners (predominated by 7–8Cl PCBs). Consequently, the elevated proportions of heavier homologs in recent years might be attributed to the intensive influence of local anthropogenic activities mentioned above.

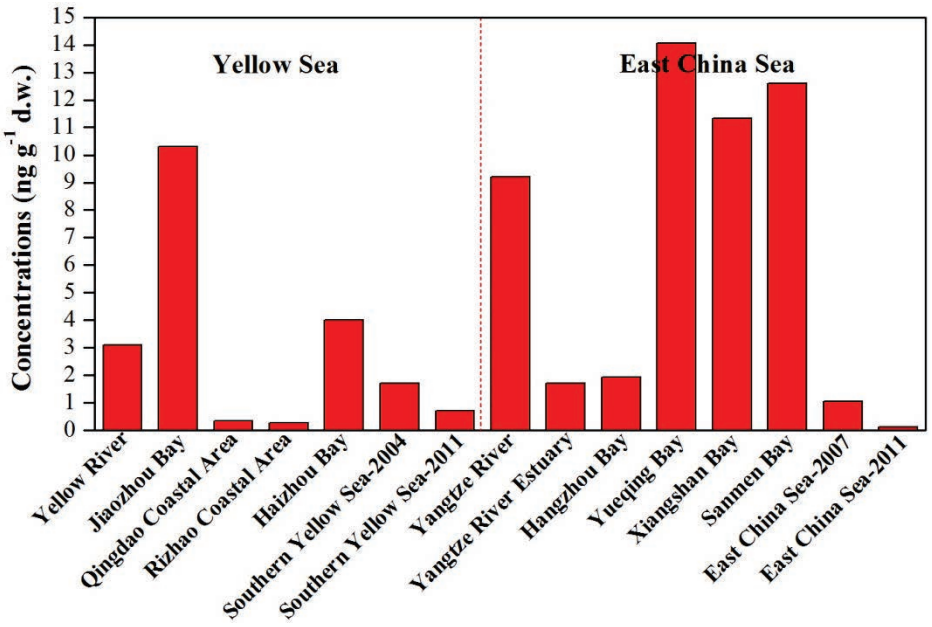

Fig. 2.5.2 Average concentrations (ng g^{-1} d.w.) of PCBs in surface sediments from nearshore and offshore regions of the Yellow Sea and East China Sea. Data were collected from He *et al*. (2006), Zhang *et al*. (2007), An *et al*. (2009), Yang *et al*. (2009), Pan *et al*. (2010), Yang, H. *et al*. (2011), Duan *et al*. (2013a,b), Liu *et al*. (2013), Yang *et al*. (2012) and Zhang *et al*. (2014).

To have an insight into the sources of PCBs in the YS, Duan *et al*. (2013b) applied partial least-squares regression (PLSR) to analyze PCBs in marine sediments from the central mud area in the southern YS. The results showed that PCBs produced unintentionally by industrial and other processes appeared to be the major sources in sediments, accounting for 60.5%. Industrially synthesized PCBs with 3Cl and 5Cl accounted for 15.5% and 24.0%, respectively. Among these PCBs, atmospheric deposition was the main pathway (84.5%), followed by continental runoff (15.5%). In the ECS, Duan *et al*. (2013a) observed that lower chlorinated congeners were mainly introduced by the Yangtze River, to be finally buried in sediments of the estuarine regions and vicinity. However, higher chlorinated congeners were mainly imported via direct emission from local sources, to be finally buried in sediments far away from the estuary. Of the PCBs in surface sediments, 40.1% came from the Yangtze River, 37.9% from local sources and the rest of 22.0% from atmospheric deposition. Additionally, Fan *et al*. (2014) used the lipid biomarker ($\sum C_{27} + C_{29} + C_{31}$ *n*-alkanes) of terrestrial organic matter to identify the regional sources of PCBs in marine sediments from the ECS. The results indicated that the sedimentary PCBs in the mud area southwest of Cheju Island, northern inner shelf and southern inner shelf of 29°N were mainly from atmospheric deposition, riverine input of the Yangtze River, and local coastal sources via atmospheric deposition, respectively.

Short-chain chlorinated paraffins

As a kind of emerging POPs, chlorinated paraffins (CPs) are highly complex technical mixtures of alkanes containing thousands of different isomers, enantiomers and diastereomers (Bayen *et al*., 2006). They have a general formula of $C_xH_{(2x+2)-y}Cl_y$ with a degree of chlorination between 30% and 70%. According to the carbon chain length, CPs can be subdivided into short-chain (SCCPs, C_{10}–C_{13}), medium-chain (MCCPs, C_{14}–C_{17}) and long-chain CPs (LCCP, $C_{>17}$; Tomy *et al*., 1998). Because of their high chemical and thermal stabilities, CPs are widely used as flame retardants, plasticizers and additives in paints, sealants and metal working fluids (Stejnarová *et al*., 2005). Compared to the other two groups, SCCPs have caused growing environmental concerns worldwide, due to their persistence, greater potential of long-range atmospheric transport, bioaccumulation in food webs and higher toxicity to aquatic organisms (Reth *et al*., 2005). To date, the quantification of SCCPs in environmental samples is challenging, particularly because of the lack of suitable standards, their low response in various detection systems and their high complex nature, leading to great difficulties in chromatographic separation among CP congeners and between SCCPs and other organohalogen compounds (Mourik *et al*., 2015). In China, information on SCCPs in the environment is still scare, and the investigations were mainly implemented in the Bohai Sea (BS) and vicinity. Thus, the pollution status of SCCP in the BS was also considered in this review. To understand the transport mechanisms and fates of SCCPs from terrestrial sources to marine environments, data of SCCPs in nearshore and offshore sediments from the BS, YS and ECS were summarized in the present review (Fig. 2.5.3). The SCCP levels in Dalian Bay (with a mean value of 4040 ng g^{-1} d.w.) were significantly higher than in Jinzhou Bay (with a mean value of 667 ng g^{-1} d.w.; Yu, 2012), reflecting the influence of heavier industrial activities along Dalian Bay. Considerable amounts of SCCPs were detected in sediments from nearshore regions of the BS (97.6–1760 ng g^{-1} d.w.; Ma *et al*., 2014a), Liaohe Estuary (64.9–1680 ng g^{-1} d.w.; Chen *et al*., 2014), Liaodong Bay (65.0–541 ng g^{-1} d.w.; Ma *et al*., 2014b), Laizhou Bay (1.0–1200 ng g^{-1} d.w. ; Pan, 2010), the mouth of Daliao River (64.9–407 ng g^{-1} d.w.; Gao *et al*., 2010), and coastal estuaries of China (242–1450 ng g^{-1} d.w.; Yu, 2012). Tang and Yao (2005) reported that SCCP sources around the BS and vicinity might come primarily from the usage of technical CP-42, CP-52 and CP-72 because their production volumes around the BS were estimated at 18, 39 and 5.5 kt, respectively (Tang and Yao, 2005).

Compared with nearshore sediments, approximately 1 to 2 orders of magnitude lower levels were found in offshore sediments (Fig. 2.5.3), suggesting that only a minor fraction of SCCPs was transported to offshore areas. According to a large-scale research project on the occurrence of SCCPs in the BS and YS, SCCPs decreased in concentration (14.5–85.2 ng g^{-1} d.w.), but the relative abundances of C_{10} with Cl_5 congeners increased with increasing distance from coast to the open sea (Zeng *et al*., 2013). The spatial distribution and correlation analysis implied that SCCPs originated mainly from riverine inputs via ocean currents and partly from atmospheric deposition by East Asian monsoons. Similarly, SCCP levels in the ECS sediments (5.8–64.8 ng g^{-1} d.w.) also showed a decreasing gradient, and the proportion of lighter SCCP congeners increased from inner shelf to the open sea (Zeng *et al*., 2012; Zhao *et al*., 2013a). As shown in Figure 2.5.3, the variation in congener profiles, between sites proximal and distal to the coastline, indicated a combinatorial influence of emission sources and the fractionation during long-range atmospheric and/or oceanic transports, which was consistent with observations in air (Wang, 2012), water (Ma *et al*., 2014b) and soil (Wang *et al*., 2013). Especially, a sharp increase in abundance of C_{10} in offshore sediments (Fig. 2.5.3) further verified the fact that lighter SCCP congeners were subjected to greater long-range transport due to their high volatility and solubility compared with heavier congeners. In addition to the spatial distribution of SCCPs, investigations have also been carried out in sediment cores from the YS and ECS to explore the temporal trends and potential degradation of SCCPs (Zeng *et al*., 2012; Zeng *et al*., 2013). In both YS and ECS, extremely high concentrations of SCCPs were detected in the upper layers, which was consistent with the rapidly increasing production and consumption of technical SCCPs in recent years in China. Thereafter, SCCP levels overall decreased exponentially with increasing depth. Additionally, the trend of increasing proportions of short-chain and lower chlorinated congeners with increasing depth suggests the occurrence of microbially mediated transformation of SCCPs and/or more down-core migration of lighter congeners (Chen *et al*., 2011; Zeng *et al*., 2014).

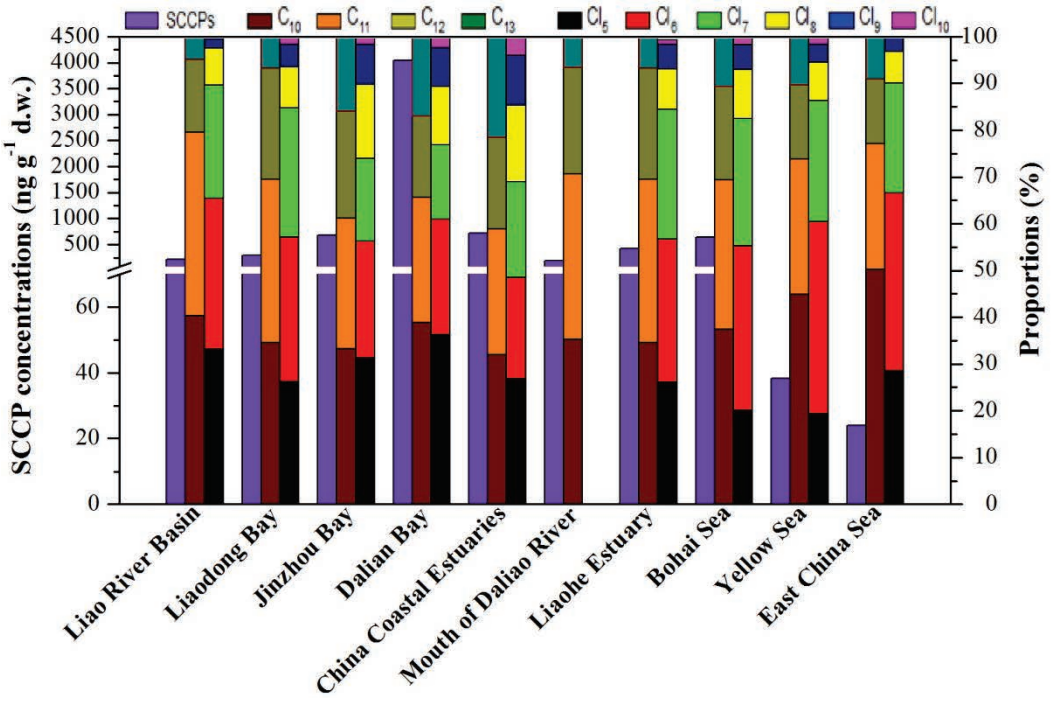

Fig. 2.5.3 Average concentrations (ng g^{-1} d.w.) and composition profiles (%) of short-chain chlorinated paraffins (SCCPs) in surface sediments from nearshore and offshore regions of the Bohai Sea, Yellow Sea and East China Sea. Data were collected from Gao *et al*. (2010, 2012), Yu (2012), Zeng *et al*. (2013), Zhao *et al*. (2013a), Chen *et al*. (2014) and Ma *et al*. (2014a,b).

Brominated POPs

As typical emerging brominated POPs, polybrominated diphenyl ethers (PBDEs) have been extensively used as flame retardants in commercial and industrial products, such as plastics, textiles, furnishing foams, electronic equipment and building materials (Jiang *et al*., 2010). Primarily, there have been three PBDE commercial formulae in use, *i.e*., Penta- (over 70% of BDE-47 and BDE-99), Octa- (over 40% of BDE-183), and Deca- (over 98% of BDE-209) BDEs (Alaee *et al*., 2003). In China, the domestic production of PBDEs was up to 10,000 tons in 2000, with Deca-BDE as the dominant products (Mai *et al*., 2005a). With the rapid development of electrical and electronic industries in recent decades, China has become one of the largest consumers of PBDE flame retardants, with an estimated annual growth rate of 7% in 2005 (Wang *et al*., 2016b). PBDEs are easily released into the general environment during the production, application and disposal processes because they are added into products without chemical bonding (Rahman *et al*., 2001).

To date, several studies have been conducted on PBDEs in sediments from areas along the YS and ECS (Fig. 2.5.4). As shown in Figure 2.5.4, relatively high concentrations were observed in Dagu River (0.65 ng g^{-1} d.w. for ∑PBDEs (the sum of PBDEs without BDE-209) and 3.27 ng g^{-1} d.w. for BDE-209; Zhen *et al*., 2016), Yellow River Estuary (0.69 ng g^{-1} d.w. for ∑PBDEs and 2.79 ng g^{-1} d.w. for BDE-209; Yuan *et al*., 2016) and Sanggou Bay (0.52 ng g^{-1} d.w. for ∑PBDEs and 3.66 ng g^{-1} d.w. for BDE-209; Wang *et al*., 2017) in the YS, where the levels of PBDEs were 1 to 2 orders of magnitude higher than those in other regions. Elevated levels in Dagu River and Yellow River Estuary indicated the intensive influence of anthropogenic activities along the drainage basins. However, the concentrations of ∑PBDEs and BDE-209 in Sanggou Bay were surprisingly higher than in other bays, such as Taozi Bay, Sishili Bay and Jiaozhou Bay in the vicinity of the YS (Fig. 2.5.4). Wang *et al*. (2017) reported that Gu River is the main entrance to Sanggou Bay, to which large quantities of household and industrial wastewater are transported, accounting for about 99% of the pollutants in the bay. In addition, traffic and shipping activities in a large multifunction harbor, located in the northwest of Sanggou Bay, may serve as another source of PBDEs. Undoubtedly, low levels of PBDEs were detected in offshore marine sediments from the southern YS (0.24 ng g^{-1} d.w. for ∑PBDEs and 0.65 ng g^{-1} d.w. for BDE-209; Wang *et al*., 2016a), indicating the land–sea migration of PBDEs. Principal component analysis (PCA) revealed that PBDEs in the SYS were mainly from continental runoff (69.0%) and atmospheric deposition (31.0%) (Wang *et al*., 2016a).

In the ECS and adjacent areas, relatively higher levels were detected in the mouth of Qiantang River (0.55 ng g^{-1} d.w. for ∑PBDEs and 4.57 ng g^{-1} d.w. for BDE-209), followed by Yangtze River Estuary (0.37 ng g^{-1} d.w. for ∑PBDEs and 3.17 ng g^{-1} d.w. for BDE-209) and Hangzhou Bay (0.16 ng g^{-1} d.w. for ∑PBDEs and 2.29 ng g^{-1} d.w. for BDE-209) (Chen *et al*., 2006). This is an indication that Qiantang River might be one of the sources of PBDEs in Hangzhou Bay. PBDE concentrations dramatically decreased in offshore marine sediments of the ECS, with mean values of 0.12 and 0.54 ng g^{-1} d.w. for ∑PBDEs and BDE-209, respectively (Wang *et al*., 2016b). Input of the Yangtze River significantly influenced the distribution of higher brominated congeners in the ECS inner shelf north of 28°N (Wang *et al*., 2016b). PLSR revealed that PBDEs in the coastal ECS were mainly from direct discharge of local anthropogenic activities (80.7%), followed by surface runoff of contaminated soils (15.1%), microbial degradation after sedimentation (2.6%) and photodegradation during atmospheric transportation (1.6%). Moreover, the potential cancer risk, via fish consumption, of human exposure to BDE-209 at 95% confidence level was 3.09×10^{-7}, 1.67×10^{-7} and 8.86×10^{-7} for children, teens and adults, respectively, significantly lower than the threshold level (10^{-6}). Hazard index (HI) calculated for non-cancer risk was also far less than 1 for the three groups, suggesting negligible non-cancer risk. The ecological risk of PBDEs in marine sediments of the ECS was also evaluated.

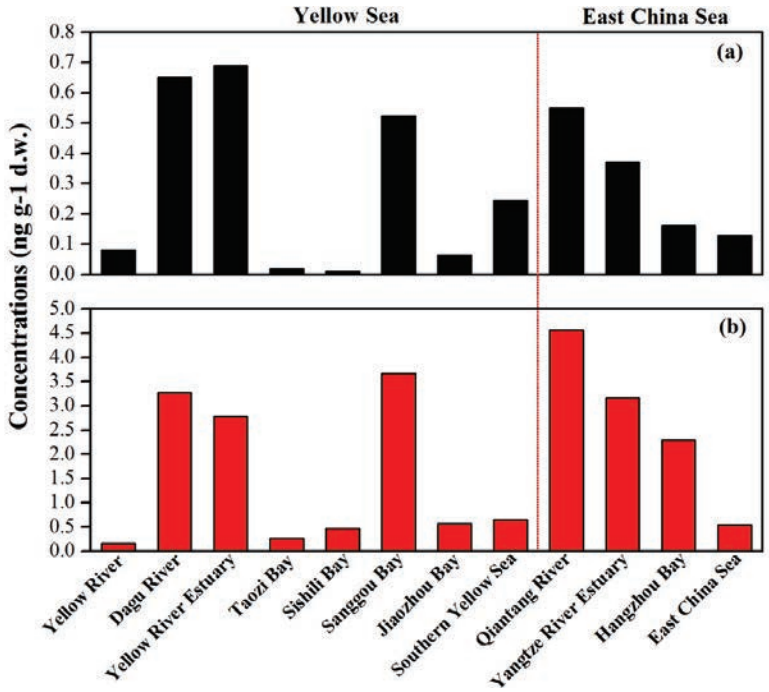

Fig. 2.5.4 Average concentrations (ng g^{-1} d.w.) of (a) ∑PBDEs and (b) BDE-209 in surface sediments from nearshore and offshore regions of the Yellow Sea and East China Sea. Data were collected from Chen *et al*. (2006), Chen *et al*. (2012), Wang *et al*. (2016a,b), Yuan *et al*. (2016), Zhen *et al*. (2016) and Wang *et al*. (2017).

Li *et al*. (2016) conducted a large-scale investigation on temporal trends of sedimentary PBDEs in Chinese marginal seas, including the YS and ECS. The results showed that there was a persistent increase from the 1970s and almost no clear sign of decline of PBDEs until recently in China. More importantly, there was a faster increase of PBDEs from the 1990s in China, while in developed countries, a gradual leveling off or even declining trend was usually observed in this period (Zegers *et al*., 2003; Zhu and Hites, 2005). Wang *et al*. (2016b) reported a similar increasing trend for PBDEs from the 1990s by analyzing sediment cores collected from the ECS. The persistently increasing trend of PBDEs in China since the 1990s could be largely attributed to the booming of the manufacturing industry and unexpected transfer of PBDEs pollution from developed countries to China (Schwarzer *et al*., 2005; Chen *et al*., 2009). Besides, relatively high concentrations and fluxes of PBDEs in a core from coastal ECS located near a well-known electrical/electronic waste (e-waste) recycling area suggested a significant contribution of PBDE emissions from e-waste recycling in China (Han *et al*., 2009; Luo *et al*., 2009; Wang, Y. *et al*., 2011). Although enormous efforts in monitoring of PBDE contamination have been paid over the last decade, China is still lagging behind in terms of nationwide regulation of PBDE usage and disposal of PBDE-containing products.

Fluorinated POPs

Per- and polyfluoroalkyl substances (PFASs), a typical emerging fluorinated POP, have been widely used in the past six decades as additives in surface coating of carpets, leather, papers and textiles, as well as in firefighting foams, pesticides and paints (Gao, Y. *et al*., 2014). Among these PFASs, perfluorooctane sulfonate (PFOS) and perfluorooctanoic acid (PFOA) are the most frequently detected compounds in the environment (Kannan, 2011). In China, large-scale production of PFASs started in 2003, and the total output of PFOS is about 230 t yr^{-1} in the past several years (Xie *et al*.,

2013). However, data on PFASs in marine environments are very limited in China, and investigations have been conducted mainly in the BS and adjacent areas. Thus, PFASs data in the BS were also included in the present review. As shown in Figure 2.5.5, concentrations of PFOS and PFOA in sediments from the northern BS coastal areas were non-detectable to 1.97 ng g^{-1} d.w. and n.d.– 0.54 ng g^{-1} d.w., respectively (Wang, T. *et al.*, 2011), while those in the southern BS coastal areas were 0.03–0.44 and 0.005–29.02 ng g^{-1} d.w. (Zhu *et al.*, 2014), respectively. The highest concentration was observed in Xiaoqing River, where PFOA was dominant and its concentrations were between 3.86 and 456.20 ng g^{-1} d.w., likely because of the presence of local fluorine chemical industries (Sun *et al.*, 2016). Pollution of PFASs in water and sediment of Liaodong Bay was also investigated, and the results showed that the pollution status in the Daling River were relatively severe (PFOA: 0.18–18 ng g^{-1} d.w.) (Chen *et al.*, 2015). In addition, studies in Liaohe, Haihe and Yellow River were also carried out (Fig. 2.5.5). Since there was no obvious production of PFASs and related products, PFOS and PFOA in sediments were less than 10 ng g^{-1} d.w. in these rivers.

Occurrences and fates of PFASs in marine sediments from the BS, YS and ECS were also reported (Fig. 2.5.5). In the BS, concentrations of PFOS and PFOA were n.d.–0.15 ng g^{-1} d.w. and 0.06–2.70 ng g^{-1} d.w., respectively, among which relatively high concentrations were found near Liaodong Bay (Gao, Y. *et al.*, 2014). In the YS, concentrations of PFOS and PFOA were n.d.–0.40 ng g^{-1} d.w. and n.d.–1.52 ng g^{-1} d.w., respectively (Gao, Y. *et al.*, 2014), which was due to fluorine chemical plants in the Daling and Xiaoqing river basins (Bao *et al.*, 2010). However, among the three seas, the lowest levels of PFOS (n.d.–0.89 ng g^{-1} d.w.) and PFOA (n.d.–0.87 ng g^{-1} d.w.) were detected in the ECS, which was attributed to no fluorine industrial plants in adjacent areas of the ECS (Gao, Y. *et al.*, 2014). Over the entire studied areas in this review, it was noted that concentrations of PFOA were generally higher than those of PFOS, indicating the wide usage and production of PFOA in China. Moreover, both of PFOS and PFOA concentrations did not exceed water quality guidelines, avian wildlife values (AWV) or criteria continuous concentration (CCC) (Giesy *et al.*, 2010) in sediments around the BS, YS and ECS, suggesting that they have no adverse effects to aquatic organisms and humans at present.

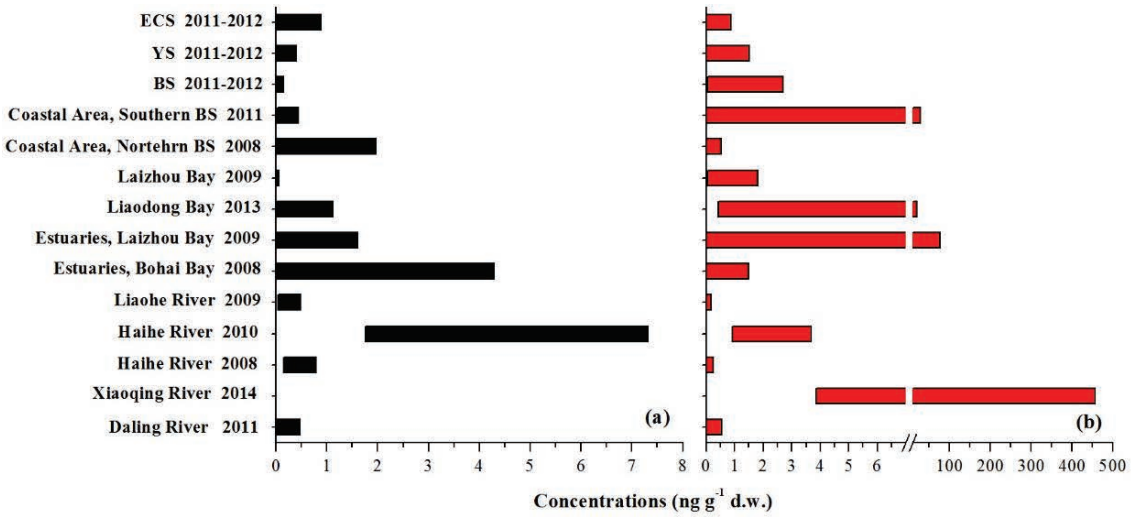

Fig. 2.5.5 Ranges of (a) perfluorooctane sulfonate (PFOS) and (b) perfluorooctanoic acid (PFOA) concentrations (ng g^{-1} d.w.) in surface sediments from nearshore and offshore regions of the Bohai Sea, Yellow Sea and East China Sea. Data were collected from Li *et al.* (2011), Pan *et al.* (2011), Wang, T. *et al.* (2011), Yang, L *et al.* (2011), Wang *et al.* (2012), Zhao *et al.* (2013b), Gao, Y. *et al.* (2014), Chen *et al.* (2015), Meng *et al.* (2015) and Sun *et al.* (2016).

2.5.3 Heavy metals in the Yellow Sea and East China Sea

Sources of heavy metals in the Yellow Sea and East China Sea

Heavy metals in marine systems originate from both naturally occurring and anthropogenic processes. Compared with natural sources, the increase in anthropogenic discharge is deemed to be the major cause of intensified heavy metal pollution in coastal environments (Kennish, 1997) in the past several decades. Heavy metals released from these anthropogenic and natural sources then enter the ocean via a variety of pathways, *e.g.*, river input, atmospheric deposition, waste water discharge, coastal erosion, *etc*.

Geological activities, such as structure activity, volcanic eruption, rock weathering, coastal erosion and geothermal emissions are the major natural sources of heavy metals. These processes have a great effect on the natural abundance (background values) and distribution of heavy metals in ocean. Limited studies have been conducted to determine the background values of heavy metals in the YS and ECS (Chen *et al*., 2017; Xiao *et al*., 2017). The background values of As, Cd, Cr, Cu, Ni, Pb, Zn, Hg and Mg in the YS were determined to be 6.26, 0.032, 57.77, 15.34, 31.48, 13.43, 69.12, 0.019 and 13327 mg/kg, respectively (Xiao *et al*., 2017), while the background values of Cr, Cu, Ni, Pb, Zn were reported to be 59.9, 29.7, 53.9, 26.0 and 84.9 mg/kg in the Yangtze River Estuary and adjacent areas (Chen *et al*., 2017).

The atmosphere is an important pool of toxic metals and it receives metals from both natural sources, *e.g.*, volcanic emissions, geysers, thermal springs, forest fires, and anthropogenic sources, *e.g.*, coal combustion, fossil fuels combustion, and volatilization of metals such as Hg and Se from ore deposits. Heavy metals in atmospheric gases, aerosols and particulates can be subsequently deposited into marine ecosystems by wet and dry deposition. It has been estimated that approximately 7000 and 6000 tons of heavy metals are deposited into the YS and ECS annually (Liu *et al*., 2005; Lammel *et al*., 2006).

Terrestrial runoff is among the most import routes for heavy metals entering the coastal marine environment. Agricultural fertilizers, mining tailings, and industrial and municipal discharges are the main sources of metals released into rivers, and they are eventually carried into the coastal environments. The Yangtze River (the third largest river in the world), Yalu River, Qiantang River and dozens of other rivers flow directly into the YS and ECS. The Yangtze River, Qiantang River and Yalu River are estimated to discharge approximately 14,000 tons of metals into coastal area, accounting for > 60% of riverine input of heavy metals from Chinese terrestrial areas into the ocean (Gao *et al*., 2008; Wang, 2008; Ci *et al*., 2014; NBO, 2016). The riverine discharge of some heavy metals into the YS and ECS has been reported to have increased dramatically since the 1980s (Wang, 2008; Liu *et al*., 2016). Industrial wastewater and domestic sewage water that are directly discharged into coastal seas are another important source of heavy metals in the YS and ECS. However, there is still a lack of sufficient data for the discharge of heavy metals into the YS and ECS from this source.

Heavy metals in the waters of the Yellow Sea and East China Sea

A number of previous studies were conducted to investigate the heavy metal levels in the seawater of the YS and ECS (Tian *et al*., 2009; Shen, 2013), most of which were in coastal bays and river estuaries, such as Jiaozhou Bay (Ling, 2010), Hangzhou Bay (Li *et al*., 2013), Yangtze River Estuary (Sun *et al*., 2009), and Yalu River Estuary (Li *et al*., 2017). As shown in the Table 2.5.1, concentrations of Cd, Cu, Hg, Pb and Zn were determined to be 0.14, 0.8, 0.0016, 0.35 and 3.8 μg L^{-1} in the north YS (Tian *et al*., 2009; Ci *et al*., 2011). Concentration of As in the south YS was

reported to be 2.33 μg L^{-1} (He *et al*., 2009). In comparison to the YS, concentrations of heavy metals in the ECS were relatively lower (Cd, 0.02 μg L^{-1}; Hg, 0.0015 μg L^{-1}; Pb, 0.13 μg L^{-1}; Zn, 1.2 μg L^{-1}) except Cu (1.4 μg L^{-1}) (Wang, 2008). Concentrations of heavy metals in the offshore areas of YS and ECS water were lower than the Criterion Continuous Concentration (chronic effects) in saltwater (US EPA, 2004), suggesting that both ecosystems may be only slightly polluted by heavy metals. In contrast, heavy metal concentrations in the coastal bays and river estuaries of both seas were relatively higher (Table 2.5.1). For example, concentrations of Zn (48.93 μg L^{-1}) and Pb (22.72 μg L^{-1}) in Jiaozhou Bay seawater were approximately 10 and 20 times higher than that in the Yellow Sea (Ling, 2010). Mercury in the water collected in the Yangtze River Estuary was much higher than that in the ECS (Sun *et al*., 2009). A decreasing trend was observed for Cu, Pb, Zn and Cr from inshore to offshore in the north YS surface water (Tian *et al*., 2009), suggesting the effect of anthropogenic discharge. In addition, heavy metals were found to decrease dramatically once discharged into the ocean (Gao, X.L. *et al*., 2014), possibly due to their rapid settlement at estuaries (Pan and Wang, 2012). This could explain the inconsistency between the relatively low level of most heavy metals in the offshore water and the large amount of heavy metals discharged into both seas from various sources. By using a single factor contaminant index method, Pb was assessed to be the heavy metal posing great risks in the YS (Tian *et al*., 2009), while Cu and Pb were the ones with potential risks in the ECS using Seawater Environmental Quality Index (SEQI) method (Shen, 2013). Heavy metals in the water are directly associated with the toxicity and risk of them to pelagic organisms. Instead of a single factor index method, ecosystem-based methods, *e.g*., species sensitivity distributions (SSDs, non-mechanistic) (Newman *et al*., 2000) and food web models (mechanistic) (Hernout *et al*., 2015), have been widely used to evaluate the risk of contaminants to pelagic organisms in recent years. More work should be conducted in the YS and BS to determine the pollution impact of heavy metals in YS and BS water, especially the offshore areas, and evaluate the risks of heavy metals to pelagic organisms at the ecosystem level.

Heavy metals in the sediments of Yellow Sea and East China Sea

Sediment is an important sink of heavy metals, and heavy metals in sediments come from aqueous phase deposition via physical, chemical or biological ways. Heavy metals in sediments are good indicators for both historical and present environmental pollution. More studies were conducted on investigating the pollution of toxic metals in the sediment of YS and ECS (Table 2.5.2) in comparison to that in the water column. Arsenic, Cd, Cr, Cu, Hg, Ni, Pb and Zn were measured to be in the range of 1.46–32.31, 0.07–0.455, 14.28–73.00, 3.08–34.87, 0.015–0.362, 4.48–45.59, 6.36–30.61 and 16.43–117.57 mg kg^{-1}, respectively, in YS sediments collected in 2013–2014 (Xiao *et al*., 2017). Mean concentrations of Cd, Cr, Cu, Hg, Ni, Pb and Zn in ECS sediments were measured to be 0.2, 71.4, 15, 0.09, 26, 27 and 60 mg kg^{-1} respectively (Fang *et al*., 2009; Duan *et al*., 2015). Compared with the offshore areas, concentrations of heavy metals were generally higher in bays and estuaries, indicating the effects of anthropogenic discharges of heavy metals. For instance, concentrations of Cu in the Yalu River Estuary were several times higher than those in the YS and ECS (Gao *et al*., 2008).

Heavy metal concentrations in the sediment can be used to assess the ecological risk of heavy metals, and several methods have been commonly used, *e.g*., the potential ecological risk index (PERI) (Hakanson, 1980) and sediment quality guidelines (SQGs) (Long *et al*., 1995; Macdonald *et al*., 1996). Sediment-based risk assessment methods have been proven to be a useful tool for identifying toxic metals with potential risks in aquatic environments. By analyzing the potential risks of eight heavy metals in the YS using the PERI and SQGs, Hg, As and Cd were identified to be listed as the priority contaminant metals in BS and YS sediments (Xiao *et al*., 2017). Guo (2011) reported that the potential risks of heavy metals showed an order of Cd > Hg > Cu >Pb> Cr > Zn at the Yangtze River Estuary and adjacent seas. Xu *et al*. (2015) reported that Pb in the ECS was the most polluted metal and had higher potential ecological risk.

Table 2.5.1 Summary of heavy metal concentrations (μg L^{-1}) in the waters of the Yellow Sea and East China Sea.

System	As	Cd	Cr	Cu	Hg	Ni	Pb	Zn	Reference
North Yellow Sea	nd	0.14	nd	0.8	0.0017	nd	0.35	3.8	Tian *et al.*, 2009; Ci *et al.*, 2011
South Yellow Sea	2.33	0.078	nd	1.41	0.0036	nd	0.37	6.21	He *et al.*, 2009
Yellow River Estuary	0.43–1.40	0.10–3.22	nd	0.10–4.46	0.004–0.028	nd	0.22–1.33	12.00–81.84	Tang *et al.*, 2010
Lianyungang	nd	0.131	nd	1.93	nd	nd	0.21	12.9	Ge *et al.*, 2010
Jiaozhou Bay	nd	1.13	nd	3.48	0.028	nd	22.72	48.93	Ling, 2010
Yalu River Estuary	1.60–2.05	0.83–1.33	0.113-0.14	1.80–4.70	0.006–0.049	nd	0.40–1.80	9.20–19.60	Li *et al.*, 2017
Yangtze River Estuary	3.6	0.387	nd	1.99	0.172	nd	0.9	6.1	Sun *et al.*, 2009
Luoyuan Bay	9.31	2.50	nd	5.58	0.04	nd	0.16	4.99	Qu *et al.*, 2009
Hangzhou Bay	1.9	0.13	0.52	1.76	0.042	nd	nd	nd	Li *et al.*, 2013
East China Sea	nd	0.02	nd	1.40	0.0015	nd	0.13	1.2	Wang, 2008; Wang, C.J. *et al*, 2016

nd = no data

Table 2.5.2 Summary of heavy metals concentrations (mg kg^{-1}) in the sediments of the Yellow Sea and East China Sea.

System	As	Cd	Cr	Cu	Hg	Ni	Pb	Zn	Reference
Yellow Sea	1.46–32.31	0.07–0.455	14.28–73.00	3.08–34.87	0.015–0.362	4.48–45.59	6.36–30.61	16.43–117.57	Xiao *et al.*, 2017
Yellow Sea	nd	0–8.12	nd	4.95–26.1	0.007–0.398	8.31–32.4	4.31–21.9	18.8–96.2	Jiang *et al.*, 2014; Meng *et al.*, 2014
South Yellow Sea	nd	0.06–1.54	nd	6.00–32.9	0.006–0.069	nd	6.20–39.3	24.6–244	Yuan *et al.*, 2012
Yellow River Estuary	6.5–12.6	0.11–0.2	nd	21–38	0.03–0.05	16.8–23.5	11.6–15.0	21–38	Wu *et al.*, 2007
Haihe Estuary	nd	0.4–2.1	63.2–155	21–246	nd	nd	21.7–78.9	nd	Liu *et al.*, 2006
Jiaozhou Bay	2.04–20.1	0–1	0.714–130	4.45–211	0.005–4.1	nd	12.3–109	10–384	He *et al.*, 2013
Qingdao coastal	8.4	0.1	55.61	22	0.05	nd	27.6	58	Ye *et al.*, 2007
Yalu River Estuary	7.1	0.24	52.3	93.15	0.07	21.2	29.6	108.4	Gao *et al.*, 2008
Lianyungang coastal	8.4	0.1	nd	36	0.05	nd	14.8	nd	He *et al.*, 2008
Yangtze River Estuary	nd	0.261	78.9	30.7	0.12	31.8	27.3	94.3	Zhang, W.G. *et al.*, 2009
Luoyuan Bay	9.28	0.075	nd	21.2	0.041	nd	29.5	90.86	Qu *et al.*, 2009; Chen, 2011
Hangzhou Bay	8.27	0.112	nd	23.2	0.080	nd	26.3	78.4	Cai, 2015
East China Sea	nd	0.2	71.4	15	0.09	26	27	60	Fang *et al.*, 2009; Duan *et al.*, 2015

nd = no data

In addition to the total amounts, the speciation of heavy metals plays an important role in the cycling and risk of heavy metals in marine sediments. Heavy metals are present in several major forms in the sediment, including acid soluble, reducible, oxidizable and residual (Gao and Li, 2012), which have different bioavailabilities and toxicities. By using a BCR (Community Bureau of Reference) method, Chen *et al.* (2012) investigated the fraction of eight heavy metals in Rongcheng Bay (in Yellow Sea) sediments. The residual form (78.16% and 65.89%) was found to be the major species of Zn and Cr in the sediment, while more Cu and Pb were present in more active form (bound to Fe and Mn oxides). Most Cu, Zn, Cd, Pb and Hg were found to be present in the residual fraction in the ECS (Yu *et al.*, 2013; Duan *et al.*, 2015), while organic matter fraction was found to be the main component of their labile fractions (Duan *et al.*, 2015). As the toxicity of heavy metals depends on not only the total amounts but also the speciation, the speciation of heavy metals should be taken into account when evaluating the risks of heavy metals in the YS and ECS.

Heavy metals in the organisms of Yellow Sea and East China Sea

Marine organisms can absorb heavy metals from seawater, suspended particles and sediments, and eventually are bioaccumulated via the food chain to high concentrations in high trophic level organisms. Heavy metals in organisms draw the most public concerns due to their threat to human health. Most investigations on heavy metal concentrations and their potential risks in marine organisms have been conducted in coastal cities, bays and estuaries of the YS and ECS (Sun and Yang, 1992; Yan, 1993; Fang *et al.*, 2004; Asante *et al.*, 2008; Liu *et al.*, 2008; Qu *et al.*, 2009; Luo *et al.*, 2012, 2013; Yi and Zhang, 2012; Zhang *et al.*, 2012; Li *et al.*, 2013; Xia *et al.*, 2013; Jiang *et al.*, 2015; Liu *et al.*, 2017) (Table 2.5.3). In general, organisms in the YS and ECS are not heavily polluted by heavy metals. Their concentrations are comparable to or even lower than those reported in the other marine systems (Asante *et al.*, 2008). Among the eight common heavy metals, Pb in shrimp and crab (Zhang *et al.*, 2012) and Cd in fish (Xia *et al.*, 2013) have been detected to be over the Codex Alimentarius Commission (CAC) and European Commission Regulation in the YS. Arsenic in sea cucumber was assessed to be over maximum residue limits (MRLs) in the YS (Jiang *et al.*, 2015). Mercy and Zn over the Criterion Continuous Concentration and Limit of the Food and Agriculture Organization of the United Nations (Luo *et al.*, 2012) were detected in crabs along the coast of the northern YS. High Zn and Cu concentrations (exceeding the maximum limits in China) were detected in oysters collected from the coast of Zhejiang province (Li *et al.*, 2013; Lu *et al.*, 2017). Trophic level is among the most important factors controlling the levels of heavy metals in the organisms. Mercury in fishes was observed to increase significantly with increasing trophic level (Xia *et al.*, 2013). The consumption of marine organisms is one of the primary pathways of exposure to Hg for humans. By using the Target Hazard Quotient (THQ) method, shellfish consumption was estimated to result in the low risk of Hg exposure to residents near Jiaozhou Bay (Zhang and Zhang, 2015).

Table 2.5.3 Summary of heavy metals in the organisms (mg kg^{-1}) of the Yellow Sea and East China Sea.

System	Organism	As	Cd	Cr	Cu	Hg	MeHg	Ni	Pb	Zn	Reference
Yellow Sea	bivalve	0.52	0.54	nd	nd	0.012	nd	nd	0.23	nd	Liu *et al.*, 2008
	fish	nd	0.07	0.50	0.51	0.13	nd	nd	0.60	nd	Yan, 1993
	molluscs	nd	0.22–3.50	nd	0.48–2.30	nd	nd	nd	0.05–0.81	7.20–89.8	He, 1996
Northern Yellow Sea coastal	crab	nd	0.29	nd	nd	0.68	0.55	nd	nd	44	Luo *et al.*, 2012
	sea cucumber	0.372	0.161	0.108	0.179	0.034	nd	nd	0.065	2.634	Luo *et al.*, 2013
Dalian coastal	fish					0.023	0.021				Xia *et al.*, 2013
	sea cucumber	0.368	0.079	0.118	0.204	0.037	nd	nd	0.085	2.987	Jiang *et al.*, 2015
	mussel	13.50	2.30	2.18	1.83	0.028	nd	1.50	0.51	76.89	Fung *et al.*, 2004
Yantai coastal	shrimp	14.11–23.65	nd	1.55–5.24	73.13–163.84	nd	nd	5.77–23.13	1.82–4.95	74.6–97.09	Zhang *et al.*, 2012
Jiaozhou Bay	fish	nd	nd	0.10–2.35	0.13–1.02	nd	nd	nd	0.095–1.81	1.42–10.59	Sun and Yang, 1992
	molluscs	nd	nd	0.20–1.67	1.12–14.46	nd	nd	nd	0.18–2.13	10.60–23.79	Sun and Yang, 1992
	shellfish	nd	nd	1.22	1.45–7.57	0.001–1.096	nd	nd	0.36–0.80	11.58–12.86	Zhang and Zhang, 2015
	clam	8.32–14.33	0.39–0.68	0.96–4.04	7.70–9.14	0.53–1.42	nd	nd	0.53–1.42	62.20–87.11	Ma *et al.*, 2009
Qingdao coastal	fish					0.023	0.014				Xia *et al.*, 2013
	mussel	12.93	1.27	8.33	22.08	0.27	nd	3.31	0.90	107.6	Fung *et al.*, 2004
Yalu River Estuary	sea cucumber	0.40	0.18	0.24	0.26	0.062	nd	nd	0.15	3.32	Jiang *et al.*, 2015
Lianyungang coastal	fish	nd	0.01–0.36	0.02–0.99	0.37–0.71	0.05–0.32	nd	nd	0–0.43	nd	Yan, 1993
Shanghai coastal	fish	nd	0–0.09	0–0.04	2.31–6.72	0.03–0.11	nd	nd	0.31–0.61	nd	Yan, 1993
						0.024	0.014				Xia *et al.*, 2013
	mussel	24.55	2.81	6.07	3.32	0.058	nd	2.91	0.71	141.3	Fung *et al.*, 2004
Zhejiang coastal	fish	<DL–7.6	0.001–0.131	nd	0.10–1.95	0.002–0.032	nd	nd	0.008–0.142	3.6–42.4	Fang *et al.*, 2004
	shellfish	0.7–2.4	0.067–13	nd	0.87–135	0.009–0.044	nd	nd	0.029–0.348	5.42–244	Fang *et al.*, 2004
	shrimp	1.1–9.2	0.046–1.12	nd	1.43–23.4	0.004–0.028	nd	nd	0.006–0.244	5.49–15.4	Fang *et al.*, 2004

Table 2.5.3 Continued.

System	Organism	As	Cd	Cr	Cu	Hg	MeHg	Ni	Pb	Zn	Reference
Zhoushan coastal	fish					0.019	0.012				Xia *et al*., 2013
	mussel	17.7	4.96	5.94	22.58	0.037		2.44	0.67	128.1	Fung *et al*., 2004
Yangtze River Estuary	fish	nd	0.091	0.93	0.17	0.012	nd	nd	0.52	4.75	Yi and Zhang, 2012
Luoyuan Bay	fish	0.45	0.01	nd	0.2	0.032	nd	nd	0.19	12.44	Qu *et al*., 2009
	shrimp	0.5	nd	nd	3.1	0.023	nd	nd	0.04	9.07	Qu *et al*., 2009
	shellfish	0.7	1.28	nd	39.53	0.081	nd	nd	0.06	15.88	Li *et al*., 2013
Hangzhou Bay	oyster	1.2	1.70	0.35	123.05	0.032	nd	nd	1.59	nd	Li *et al*., 2013
Nantong coastal	fish	0.46–14.31	0–3.84	0.17–3.42	0.06–30.7	0.02–0.18	nd	0.07–0.75	0.01–0.41	0–68.65	Liu *et al*., 2017
East China Sea	fish	1.3–200	0.04–168	0.028–2.4	1.29–1040	<0.05–2.1	0.003–0.057	0.004–0.041	0.034–36.5	29.8–334	Asante *et al*., 2008

nd = no data, DL = detection limit

Cycling of heavy metals in the Yellow Sea and East China Sea

After entering the marine system, heavy metals undergo a variety of biogeochemical processes before they are sequestered in the deep sediments or accumulated in organisms. These processes include adsorption/desorption, transformations of heavy metals, diffusion from sediment to the water column, sedimentation/re-suspension, and exchange with nearby oceans. Limited studies (Lin *et al*., 2000; Ren *et al*., 2010; Ci *et al*., 2016) have been conducted on investigating the cycling of heavy metals in a limited part of the YS and ECS, most of which are only focused on the sedimentation of heavy metals in both ecosystems. Sedimentation has been deemed to be a dominant sink of heavy metals in the coastal sea and most reactive heavy metals discharged through rivers from the continent to the ECS continental shelf were estimated to deposit on the bottom sediments prior to transporting to the open ocean (Zhang, 1995; Pan and Wang, 2012; Liu *et al*., 2016). Fang *et al*. (2009) calculated that the annual sedimentation fluxes of trace metals in the ECS were 1.08×10^5, 4.48×10^4, 4.32×10^4 and 3.10×10^4 t per year for Zn, Ni, Pb and Cu, respectively. Approximately 55–70% and 10–17% of the sedimentation fluxes of trace metals were deposited in the inner shelf and the Yangtze River Estuary zone (Pan and Wang, 2012). Since the fate, bioavailability and toxicity of heavy metals depend highly on the transport and transformations of heavy metals in the marine system, there is an urgent need to elucidate the major processes controlling their concentrations and speciation in the YS and ECS.

2.5.4 Conclusions and recommendations

The YS and ECS receive a large quantity of pollutants from anthropogenic sources, including legacy and emerging POPs and heavy metals from riverine input, sewage discharge and atmospheric deposition. The total input fluxes of pollutants into both seas have increased dramatically since the 1980s, resulting in POP and heavy metal contamination in the water, sediment and organisms. In the present review, spatial distributions and potential risks of several POPs and heavy metals in the YS and ECS were summarized. Results of data review suggest that sources of different POPs were independent, and some hotspot areas with greater production of certain chemicals were identified. Mercury, Cd and Pb were identified to be the major heavy metals posing risks to human and ecosystem health in the YS and ECS.

However, it should be noted that studies on emerging POPs such as SCCPs, PBDEs and PFASs in the marine system are still very limited. In addition, environmental quality guidelines of POPs for protection of the coastal ecosystem have not been established in China. Given their ubiquity, persistence, long-range atmospheric transport, bioaccumulation and biomagnification through food webs, as well as their potential adverse risks to the environment and human health, actions are required to bridge the knowledge gaps in the environmental occurrence, and to evaluate the risks to organisms and humans.

We propose the following research directions: (1) Particularly in light of the continued and large-scale production and usage of emerging POPs, future monitoring studies should be designed according to the knowledge gaps in terms of geographical distributions and environmental matrices; (2) Despite of some efforts to study the environmental behaviors of POPs, more information is urgently needed to explore the migration and transformation processes and mechanisms of POPs after they enter the seas. For example, how does the hydrodynamic sorting of sediments affect the distribution and environmental fates of POPs in the seas? How do the complex biochemical processes affect the migration and transformation of POPs in the seas? How do their physicochemical properties (such as chemical structure, solubility, and partitioning coefficients) affect these processes and their environmental fates? (3) In aquatic environments, sedimentary total

organic carbon is commonly considered to be a key factor controlling the distribution and accumulation of hydrophobic organic pollutants due to their high affinity. However, very limited information is available about the different effects of terrestrial (TOM) and marine organic matters (MOM) on the environmental behavior of organic pollutants in the seas. The molecular mechanism for interaction between POPs and organic matter still remains unclear; (4) Further work is needed to study the biomagnification of POPs in the food web and related influencing factors (such as the intake rate, degradation, and transformation), as well as the mechanisms of toxicity of POPs, and thus to evaluate the exposure pathways and ecological and health risks of POPs to organisms and humans; (5) Additional biomonitoring data are needed to understand the routes of POPs uptake in the human body and the levels present in tissues, and more efforts are necessary to conduct a comprehensive risk assessment and evaluate the relative importance of the various exposure routes (such as dietary intake, inhalation, dust ingestion, and dermal contact) for different populations.

Besides these previous studies on heavy metals in the YS and ECS, more effort should be made on several aspects in this field. First, most studies on the sources of heavy metals were done on the discharge from the major rivers. A comprehensive study that covers all the rivers and other sources (atmospheric deposition, sewage discharge, coastal erosion, and submarine ground water discharge) should be conducted to elucidate these sources. Second, the risks of heavy metals were assessed by comparing their criteria in water, sediments and organisms. An integrated method with the consideration of heavy metals in all these matrices should be developed to evaluate the risks of these heavy metals in the YS and ECS. In addition, since the toxicity and risks of heavy metals depend highly on their species, these risk assessment methods should take the speciation of heavy metals into account. Third, more efforts should be made on identifying the controlling biogeochemical processes and the mechanisms underlining these important processes to better understand the cycling and fate of heavy metals in the YS and ECS.

2.5.5 References

Alaee, M., Arias, P., Sjödin, A. and Bergman, Å. 2003. An overview of commercially used brominated flame retardants, their applications, their use patterns in different countries/regions and possible modes of release. *Environ. Int.* **29**: 683–689, doi:10.1016/S0160-4120(03)00121-1.

An, Q., Wu, Y., Wang, J. and Li, Z. 2009. Heavy metals and polychlorinated biphenyls in sediments of the Yangtze river estuary, China. *Environ. Earth Sci*. **59**: 363–370, doi:10.1007/s12665-009-0034-4.

Aries, E., Anderson, D.R., Fisher, R., Fray, T.A. and Hemfrey, D. 2006. PCDD/F and "Dioxin-like" PCB emissions from iron ore sintering plants in the UK. *Chemosphere* **65**: 1470–1480, doi:10.1016/j.chemosphere.2006.04.020.

Asante, K., Agusa, T., Mochizuki, H., Ramu, K., Inoue, S., Kubodera, T., Takahashi, S., Subramanian, A. and Tanabe, S. 2008. Trace elements and stable isotopes (delta^{13}C and delta^{15}N) in shallow and deep-water organisms from the East China Sea. *Environ. Pollut*. **156**: 862–873, doi:10.1016/j.envpol.2008.05.020.

Bao, J., Liu, W., Liu, L., Jin, Y., Dai, J., Ran, X., Zhang, Z. and Tsuda, S. 2010. Perfluorinated compounds in the environment and the blood of residents living near fluorochemical plants in Fuxin, China. *Environ. Sci. Technol*. **45**: 8075–8080, doi:10.1021/es102610x.

Bayen, S., Obbard, J.P. and Thomas, G.O. 2006. Chlorinated paraffins: a review of analysis and environmental occurrence. *Environ. Int*. **32**: 915–929, doi:10.1016/j.envint.2006.05.009.

Broz, J., Grabic, R., Kilián, J., Lojkásek, M., Marklund, S., Ocelka, T., Pekárek, V., Pribyl, J., Tydlitát, V. and Výska, J. 2000. The effect of oils on PAH, PCDD, PCDF, and PCB emissions from a spark engine fueled with leaded gasoline. *Chemosphere* **41**: 1905–1911, doi:10.1016/s0045-6535(00)00053-9.

Cai, X.P. 2015. Distribution and assessment of heavy metals in the surface sediments of Hangzhou Bay and its adjacent sea waters. Master's thesis (in Chinese), Zhejiang University, Hangzhou, China.

Chen, B., Liu. J., Qiu, J.D., Zhang, X.L., Wand, S. and Liu, J.Q. 2017. Spatio-temporal distribution and environmental risk of sedimentary heavy metals in the Yangtze River Estuary and its adjacent areas. *Mar. Pollut. Bull*. **116**: 469–478, doi:10.1016/j.marpolbul.2016.11.055.

Chen, C., Ma, X., Guo, W., Zhao, Y., Lü, J., Wang, Z. and Yao, Z. 2014. Congener specific distribution and bioaccumulation of short-chain chlorinated paraffins in Liao estuary. *Chinese Sci. Bull*. **59**: 578–585.

Chen, D., Bi, X., Zhao, J., Chen, L., Tan, J., Mai, B., Sheng, G., Fu, J. and Wong, M. 2009. Pollution characterization and diurnal variation of PBDEs in the atmosphere of an E-waste dismantling region. *Environ. Pollut*. **157**: 1051–1057, doi:10.1016/j.envpol.2008.06.005.

Chen, H., Zhang, C., Han, J., Sun, R., Kong, X., Wang, X. and He, X. 2015. Levels and spatial distribution of perfluoroalkyl substances in China Liaodong Bay basin with concentrated fluorine industry parks. *Mar. Pollut. Bull*. **101**: 965–971, doi:10.1016/j.marpolbul.2015.10.024.

Chen, H.R. 2011. Distribution and potential ecological risk assessment of heavy metals in surface sediments of Luoyuan Bay. *J. Fujian Fish*. **33**: 45–49 (in Chinese).

Chen, J., Zhao, H., Qiao, X., Xie, Q. and Zhang, Y. 2012. Polybrominated diphenyl ethers in soils of the modern Yellow River Delta, China: occurrence, distribution and inventory. *Chemosphere* **88**: 791–797, doi:10.1016/j.chemosphere.2012.03.084.

Chen, J.-F., Xia, X.-M., Ye, X.-R. and Jin, H.-Y. 2002. Marine organic pollution history in the Changjiang Estuary and Zhejiang coastal area—HCHs and DDTs stratigraphical records. *Mar. Pollut. Bull*. **45**: 391–396, doi:10.1016/S0025-326X(02)00093-0.

Chen, M.-Y., Luo, X.-J., Zhang, X.-L., He, M.-J., Chen, S.-J. and Mai, B.-X. 2011. Chlorinated paraffins in sediments from the Pearl River Delta, South China: Spatial and temporal distributions and implication for processes. *Environ. Sci. Technol*. **45**: 9936–9943, doi:10.1021/es202891a.

Chen, S.-J., Gao, X.-J., Mai, B.-X., Chen, Z.-M., Luo, X.-J., Sheng, G.-Y., Fu, J.-M. and Zeng, E.Y. 2006. Polybrominated diphenyl ethers in surface sediments of the Yangtze River Delta: levels, distribution and potential hydrodynamic influence. *Environ. Pollut*. **144**: 951–957, doi:10.1016/j.envpol.2006.01.044.

Chen, W., Zhang, L., Xu, L., Wang, X. and Hong, H. 1996. Concentrations and distributions of HCHs, DDTs and PCBs in surface sediments of sea area between Xiamen and Jinmen. *J. Xiamen Univ*. **35**: 936–940 (in Chinese).

Chen, W., Hong, H., Zhang, L., Xu, L., Wang, X. and Hong, L. 2010. Levels of residues of POPs in surface sediments in Minjiang Estuary-Mazu seas and their distribution characteristics. *Environ. Rep*. **19**: 53–58.

Ci, Z., Zhang, X., Yin, Y., Chen, J. and Wang, S. 2016. Mercury redox chemistry in waters of the Eastern Asian Seas: From polluted coast to clean open ocean. *Environ. Sci. Technol*. **50**, 2371–2380, doi: 10.1021/acs.est.5b05372.

Ci, Z.J., Zhang, X.S., Wang, Z.W., Niu, Z.C., Diao, X.Y. and Wang, S.W. 2011. Distribution and air-sea exchange of mercury (Hg) in the Yellow Sea. *Atmos. Chem. Phys*. **11**: 2881–2892, doi:10.5194/acp-11-2881-2011.

Ci, Z.J., Zhang, X.S. and Wang, Z.W. 2014. Mass balance of mercury for the Yellow Sea downwind and downstream of East Asian: the preliminary results, uncertainties and future research priorities. *Biogeochemistry* **118**: 243–255, doi:10.1007/s10533-013-9925-2.

Duan, L.Q., Song, J.M., Yu, Y., Yuan, H.M., Li, X.G. and Li, N. 2015. Spatial variation, fractionation and sedimentary records of mercury in the East China Sea. *Mar. Pollut. Bull*. **101**: 434–441, doi: 10.1016/j.marpolbul.2015.09.050.

Duan, X., Li, Y., Li, X., Li, M. and Zhang, D. 2013a. Distributions and sources of polychlorinated biphenyls in the coastal East China Sea sediments. *Sci. Total Environ*. **463–464**: 894–903, doi: 10.1016/j.scitotenv.2013.06.102.

Duan, X., Li, Y., Li, X., Zhang, D. and Li, M. 2013b. Polychlorinated biphenyls in sediments of the Yellow Sea: Distribution, source identification and flux estimation. *Mar. Pollut. Bull*. **76**: 283–290, doi:10.1016/j.marpolbul.2013.08.024.

Eggleton, J. and Thomas, K.V. 2004. A review of factors affecting the release and bioavailability of contaminants during sediment disturbance events. *Environ. Int*. **30**: 973–980, doi:10.1016/j.envint.2004.03.001.

Erickson, M.D. and Kaley, R.G. 2011. Applications of polychlorinated biphenyls. *Environ. Sci. Pollut. Res*. **18**: 135–151, doi:10.1007/s11356-010-0392-1.

Fan, Y., Lan, J., Li, H., Cao, Y., Zhao, Z., Wang, J., Zhao, M. and Jiang, G. 2014. Use of lipid biomarkers for identification of regional sources and dechlorination characteristics of polychlorinated biphenyls in the East China Sea. *Sci. Total Environ*. **490**: 766–775, doi:10.1016/j.scitotenv.2014.05.054.

Fang, J., Wang, K.X., Tang, J.L., Wang, Y.M., Ren, S.J., Wu, H.Y. and Wang, J. 2004. Copper, lead, zinc, cadmium, mercury, and arsenic in marine products of commerce from Zhejiang coastal area, China, May 1998. *Bull. Environ. Contam. Toxicol*. **73**: 583–590, doi:10.1007/s00128-004-0468-z.

Fang, T.H., Li, J.Y., Feng, H.M. and Chen, H.Y. 2009. Distribution and contamination of trace metals in surface sediments of the East China Sea. *Mar. Environ. Res*. **68**: 178–187, doi:10.1016/j.marenvres.2009.06.005.

Feng, J., Zhai, M., Liu, Q., Sun, J. and Guo, J. 2011. Residues of organochlorine pesticides (OCPs) in upper reach of the Huaihe River, East China. *Ecotoxicol. Environ. Safe*. **74**: 2252–2259, doi: 10.1016/j.ecoenv.2011.08.001.

Fung, C.N., Lam, J.C.W., Zheng, G.J., Connell, D.W., Monirith, I., Tanabe, S., Richardson, B.J. and Lam, P.K.S. 2004. Mussel-based monitoring of trace metal and organic contaminants along the east coast of China using *Perna viridis* and *Mytilus edulis*. *Environ. Pollut.* **127**: 203–216, doi:10.1016/j.envpol.2003.08.007.

Gao, J.H., Li, J., Wang, Z.Y., Wang, Y.P., Bai, F.L. and Cheng, Y. 2008. Heavy metal distribution and their influence factors in sediments of Yalu River Estuary and its adjacent sea area. *Geochimica* **37**: 430–438 (in Chinese).

Gao, X. and Li, P. 2012. Concentration and fractionation of trace metals in surface sediments of intertidal Bohai Bay, China. *Mar. Pollut. Bull*. **64**: 1529–1536, doi:10.1016/j.marpolbul.2012.04.026.

Gao, X.L., Zhou, F.X. and Chen, C.T.A. 2014. Pollution status of the Bohai Sea: An overview of the environmental quality assessment related trace metals. *Environ. Pollut*. **62**: 12–30, doi:10.1016/j.envint.2013.09.019.

Gao, Y., Wang, C., Zhang, H., Zou, L., Tian, Y. and Chen, J. 2010. Analysis of short-chain chlorinated paraffins in sediment samples from the mouth of the Daliao river by HRGC/ECNI-LRMS. *Environ. Sci*. **31**: 1904–1908 (in Chinese).

Gao, Y., Zhang, H., Su, F., Tian, Y. and Chen, J. 2012. Environmental occurrence and distribution of short chain chlorinated paraffins in sediments and soils from the Liaohe River Basin, PR China. *Environ. Sci. Technol*. **46**: 3771–3778, doi:10.1021/es2041256.

Gao, Y., Fu, J., Zeng, L., Li, A., Li, H., Zhu, N., Liu, R., Liu, A., Wang, Y. and Jiang, G. 2014. Occurrence and fate of perfluoroalkyl substances in marine sediments from the Chinese Bohai Sea, Yellow Sea, and East China Sea. *Environ. Pollut*. **194**: 60–68, doi:10.1016/j.envpol.2014.07.018.

Ge, X.J., Wu, S.J. and Wu, J.X. 2010. Study on the distribution law of heavy metal near Lianyungang Harbour. *J. Huaihai. Inst. Technol*. (Nat. Sci. Ed.). **19**: 89–92 (in Chinese).

Giesy, J.P., Naile, J.E., Khim, J.S., Jones, P.D. and Newsted, J.L. 2010. Aquatic toxicology of perfluorinated chemicals. *Rev. Environ. Contam. Toxicol.* **202**: 1–52, doi:10.1007/978-1-4419-1157-5_1.

Gong, X., Qi, S., Wang, Y., Julia, E. and Lv, C. 2007. Historical contamination and sources of organochlorine pesticides in sediment cores from Quanzhou Bay, Southeast China. *Mar. Pollut. Bull*. **54**: 1434–1440, doi:10.1016/j.marpolbul.2007.05.006.

Guo, F.X. 2011. Distribution of heavy metals and biogenic elements in the sediments and their ecological risk assessment in the East China Sea. PhD thesis (in Chinese), Jinan University, Guangzhou, China.

Guo, J., Yin, Y., Zheng, L., Yu, W., Zhao, H. and Yang, D. 2011. The distribution and risk assessment of polychlorinated biphenyl in surface sediments in estuaries of Jiaozhou bay, China. *J. Agro-Environ. Sci*. **30**: 965–972.

Guo, Z., Lin, T., Zhang, G., Yang, Z. and Fang, M. 2006. High-resolution depositional records of polycyclic aromatic hydrocarbons in the central continental shelf mud of the East China Sea. *Environ. Sci. Technol*. **40**: 5304–5311, doi:10.1021/es060878b.

Hakanson, L. 1980. An ecological risk index for aquatic pollution control. A sedimentological approach. *Water Res*. **14**: 975–1001, doi:10.1016/0043-1354(80)90143-8.

Han, W., Feng, J., Gu, Z., Chen, D., Wu, M. and Fu, J. 2009. Polybrominated diphenyl ethers in the atmosphere of Taizhou, a major e-waste dismantling area in China. *Bull. Environ. Contam. Toxicol*. **83**: 783–788, doi:10.1007/s00128-009-9855-9.

He, G.K. 1996. Levels of heavy metals in molluscs from the coastal region of the Bohai Sea and Huanghai Sea. *Chin. Environ. Sci*. **16**: 96–100 (in Chinese).

He, M.C., Sun, Y., Li, X.R. and Yang, Z.F. 2006. Distribution patterns of nitrobenzenes and polychlorinated biphenyls in water, suspended particulate matter and sediment from mid- and down-stream of the Yellow River (China). *Chemosphere* **65**: 365–374, doi:10.1016/j.chemosphere.2006.02.033.

He, S.J., Li, G.X. and Shi, J. 2013. Distribution of heavy metals in surficial sediment of Jiaozhou Bay and its influencing factors. *Mar. Geol. Front*. **4**: 41–48.

He, X.R., Chen, B.L. and Yin, W.Q. 2008. Study on the vertical distribution of heavy metals in sediments of Lianyungang near-shore area. *J. Huaihai. Inst. Technol*. (Nat. Sci. Ed.). **17**: 45–48 (in Chinese).

He, Z.P., Song, J.M. and Zhang, N.X. 2009. Variation characteristics and controlling factors of heavy metals in the South Yellow Sea surface seawaters. *Environ. Sci*. **29**: 1153–1162 (in Chinese).

Hernout, B.V., Bowman, S.R., Weaver, R.J., Jayasinghe, C.J. and Boxall, A.B.A. 2015. Implications of in vitro bioaccessibility differences for the assessment of risks of metals to bats. *Environ. Toxicol. Chem*. **34**: 898–906, doi:10.1002/etc.2871.

Hu, L.M., Lin, T., Shi, X.F., Yang, Z.S., Wang, H.J., Zhang, G. and Guo, Z.G. 2011. The role of shelf mud depositional process and large river inputs on the fate of organochlorine pesticides in sediments of the Yellow and East China seas. *Geophys. Res. Lett*. **38**: 246–258, doi:10.1029/2010GL045723.

Jiang, H., Tang, S., Qin, D., Chen, Z., Wang, J., Bai, S. and Mou, Z. 2015. Heavy metals in sea cucumber juveniles from coastal areas of Bohai and Yellow seas, north China. *Bull. Environ. Contam. Toxicol*. **94**: 577–582, doi:10.1007/s00128-014-1432-1.

Jiang, X., Teng, A., Xu, W. and Liu, X. 2014. Distribution and pollution assessment of heavy metals in surface sediments in the Yellow Sea. *Mar. Pollut. Bull*. **83**: 366–375, doi:10.1016/j.marpolbul.2014.03.020.

Jiang, Y., Wang, X., Zhu, K., Wu, M., Sheng, G. and Fu, J. 2010. Occurrence, compositional profiles and possible sources of polybrominated diphenyl ethers in urban soils of Shanghai, China. *Chemosphere* **80**: 131–136, doi:10.1016/j.chemosphere.2010.04.007.

Jiao, R., Wang, X., Wang, C., Ping, G., Wang, X. and Yao, T. 2016. Biomagnification of persistent organic pollutants along a high-altitude aquatic food chain in the Tibetan Plateau: Processes and mechanisms. *Environ. Pollut*. **220**: 636–643, doi:10.1016/j.envpol.2016.10.019.

Jones, K.C. and De Voogt, P. 1999. Persistent organic pollutants (POPs): state of the science. *Environ. Pollut.* **100**: 209–221, doi:10.1016/s0269-7491(99)00098-6.

Kannan, K. 2011. Perfluoroalkyl and polyfluoroalkyl substances: current and future perspectives. *Environ. Chem*. **8**: 333–338, doi:10.1071/EN11053.

Kennish, M.J. 1997. Heavy metals: Practical Handbook of Estuarine and Marine Pollution, CRC Press, New York, USA, pp. 253–298.

Lammel, G., Ghim, Y.S., Broekaert, J.A.C. and Gao, H.W. 2006. Heavy metals in air of an eastern China coastal urban area and the Yellow Sea. *Fresen. Environ. Bull*. **15**: 1539–1548.

Li, F., Sun, H., Hao, Z., He, N., Zhao, L., Zhang, T. and Sun, T. 2011. Perfluorinated compounds in Haihe River and Dagu drainage canal in Tianjin, China. *Chemosphere* **84**: 265–271, doi:10.1016/j.chemosphere.2011.03.060.

Li, H., Lin, L., Ye, S., Li, H. and Fan, J. 2017. Assessment of nutrient and heavy metal contamination in the seawater and sediment of Yalujiang Estuary. *Mar. Pollut. Bull*. **117**: 499–506, doi:10.1016/j.marpolbul.2017.01.069.

Li, J.Y., Cui, Y., Xiao, L., Wu, H.X. and Xue, J.Z. 2013. Analysis and evaluation on the heavy metal pollution of seawater and marine organisms from Zhoushan sea area and north bank in the Hangzhou Bay. *Mar. Sci. Bull*. **32**: 440–445.

Li, X., Zhang, Q., Gan, Y., Zhou, J., Dai, J., Cao, H. and Xu, M. 2007. Bioaccumulation and biomagnification of persistent organic pollutants POPs in food chain. *Chin. J. Appl. Environ. Biol*. **13**: 901–905.

Li, Y., Niu, J., Shen, Z., Zhang, C., Wang, Z. and He, T. 2014. Spatial and seasonal distribution of organochlorine pesticides in the sediments of the Yangtze Estuary. *Chemosphere* **114**: 233–240, doi: 10.1016/j.chemosphere.2014.04.112.

Li, Y., Lin, T., Hu, L., Feng, J. and Guo, Z. 2016. Time trends of polybrominated diphenyl ethers in East China Seas: Response to the booming of PBDE pollution industry in China. *Environ. Int*. **92**: 507–514, doi:10.1016/j.envint.2016.04.033.

Li, Y.F., Cai, D.J., Shan, Z.J. and Zhu, Z.L. 2001. Gridded usage inventories of technical hexachlorocyclohexane and lindane for China with 1/6° latitude by 1/4° longitude resolution. *Arch. Environ. Contam. Toxicol.* **41**: 261–266, doi:10.1007/s002440010247.

Lin, F.J., Hsu, S.C. and Jeng, W.L. 2000. Lead in the southern East China Sea. *Mar. Environ. Res.* **49**: 329–342, doi:10.1016/S0141-1136(99)00076-8.

Ling, M. 2010. Study on the mercury species and release of mercury from sea water to the atmosphere in Jiaozhou Bay in winter. Master's thesis (in Chinese), Ocean University of China, Qingdao.

Liu, C.L., Zhang, G.S., Ren, H.B. and Zhang, J. 2005. Distribution of heavy metals and nutrients in rainwater in coastal regions between the southern Yellow Sea and East China Sea. *Chin. J. Oceanol. Limnol*. **23**: 230–237.

Liu, G., Zheng, M., Ba, T., Liu, W. and Guo, L. 2009. A preliminary investigation on emission of polychlorinated dibenzo-p-dioxins/dibenzofurans and dioxin-like polychlorinated biphenyls from coke plants in China. *Chemosphere* **75**: 692–695, doi:10.1016/j.chemosphere.2009.01.006.

Liu, J., Chen, B.Y., Jefferson, T.A., Wang, H. and Yang, G. 2017. Trace element concentrations, risks and their correlation with metallothionein genes polymorphism: A case study of narrow-ridged finless porpoises (*Neophocaena asiaeorientalis*) in the East China Sea. *Sci. Total Environ.* **575**: 628–638, doi:10.1016/j.scitotenv.2016.09.062.

Liu, J.P., Xue, Z., Ross, K., Yang, Z.S. and Gao, S. 2009. Fate of sediments delivered to the sea by Asian large rivers: Long-distance transport and formation of remote alongshore clinothems. *Sediment. Rec*. **7**: 4–9, doi:10.2110/SEDRED.2009.4.4.

Liu, L., Xiong, D.Q., Gao, X.H., Song, C.Y. and Li, F.S. 2006. Characteristics of heavy metals contamination and distribution in surficial sediment of Haihe River and the adjacent sea area. *Mar. Environ. Sci*. **25**: 40–44 (in Chinese).

Liu, M.D., Chen, L., Wang, X.J., Zhang, W., Tong, Y.D., Ou, L.B., Xie, H., Shen. H.Z., Ye, X.J., Deng, C.Y. and Wang, H. 2016. Mercury export from mainland China to adjacent seas and its influence on the marine mercury balance. *Environ. Sci. Techol*. **50**: 6224–6232, doi:10.1021/acs.est.5b04999.

Liu, W.X., Hu, J., Chen, J.L., Fan, Y.S., Xing, B. and Tao, S. 2008. Distribution of persistent toxic substances in benthic bivalves from the inshore areas of the Yellow Sea. *Environ. Toxicol. Chem*. **27**: 57–66, doi:10.1897/07-115.1.

Liu, Y., Zhong, G., Tang, J., Pan, X., Tian, C. and Chen, Y. 2013. Concentrations and distribution of organochlorine pesticides in the surface sediments of Jiaozhou Bay, Taozi Bay and Sishili Bay. *Environ. Sci*. **34**: 129–136 (in Chinese).

Long, E.R., MacDonald, D.D., Smith, S.L. and Calder, F.D. 1995. Incidence of adverse biological effects within ranges of chemical concentrations in marine and estuarine sediments. *Environ. Mgmt*. **19**: 81–97, doi:10.1007/BF02472006.

Lu, G.Y., Ke, C.H., Zhu, A.J. and Wang, W.X. 2017. Oyster-based national mapping of trace metals pollution in the Chinese coastal waters. *Environ. Pollut.* **224**: 658–669, doi:10.1016/j.envpol.2017.02.049.

Luo, W., Wang, T.Y., Jiao, W.T., Hu, W.Y., Naile, J.E., Khim, J.S., Giesy, J.P. and Lu, Y.L. 2012. Mercury in coastal watersheds along the Chinese Northern Bohai and Yellow Seas. *J. Hazard. Mater*. **215**: 199–207, doi:10.1016/j.jhazmat.2012.02.052.

Luo, W., Lu, Y.L., Wang, T.Y., Kong, P.R., Jiao, W.T. and Hu, W.Y. 2013. Environemntal concentrations and bioaccumulations of cadmium and zinc in coastal watersheds along the Chinese Nortern Bohai and Yellow Seas. *Environ. Toxicol. Chem*. **32**: 831–840, doi:10.1002/etc.2136.

Luo, Y., Luo, X.-J., Lin, Z., Chen, S.-J., Liu, J., Mai, B.-X. and Yang, Z.-Y. 2009. Polybrominated diphenyl ethers in road and farmland soils from an e-waste recycling region in Southern China: concentrations, source profiles, and potential dispersion and deposition. *Sci. Total Environ*. **407**: 1105–1113, doi:10.1016/j.scitotenv.2008.10.044.

Ma, H.Q., Song, Q. and Wang, X.C. 2009. Accumulation of petroleum hydrocarbons and heavy metals in clams (*Ruditapes philippinarum*) in Jiaozhou Bay, China. *Chin. J. Oceanol. Limnol*. **27**: 887–897, doi:10.1007/s00343-009-9223-y.

Ma, X., Chen, C., Zhang, H., Gao, Y., Wang, Z., Yao, Z., Chen, J. and Chen, J. 2014a. Congener-specific distribution and bioaccumulation of short-chain chlorinated paraffins in sediments and bivalves of the Bohai Sea, China. *Mar. Pollut. Bull*. **79**: 299–304, doi:10.1016/j.marpolbul.2013.11.020.

Ma, X., Zhang, H., Wang, Z., Yao, Z., Chen, J. and Chen, J. 2014b. Bioaccumulation and trophic transfer of short chain chlorinated paraffins in a marine food web from Liaodong Bay, North China. *Environ. Sci. Technol*. **48**: 5964–5971, doi:10.1021/es500940p.

Macdonald, D.D., Carr, R.S., Calder, F.D., Long, E.R. and Ingersoll, C.G. 1996. Development and evaluation of sediment quality guidelines for Florida coastal waters. *Ecotoxicology* **5**: 253–278, doi: 10.1007/BF00118995.

Mai, B., Chen, S., Chen, S., Luo, X., Chen, L., Chen, L., Yang, Q., Sheng, G., Peng, P., Fu, J. and Zeng, E.Y. 2005a. Distribution of polybrominated diphenyl ethers in sediments of the Pearl River Delta and adjacent South China Sea. *Environ. Sci. Technol*. **39**: 3521–3527, doi:10.1021/es048083x.

Mai, B., Zeng, E.Y., Luo, X., Yang, Q., Zhang, G., Li, X., Sheng, G. and Fu, J. 2005b. Abundances, depositional fluxes, and homologue patterns of polychlorinated biphenyls in dated sediment cores from the Pearl River Delta, China. *Environ. Sci. Technol*. **39**: 49–56, doi:10.1021/es049015d.

Meng, J., Wang, T., Wang, P., Zhu, Z., Li, Q. and Lu, Y. 2015. Perfluoroalkyl substances in daling river adjacent to fluorine industrial parks: Implication from industrial emission. *Bull. Environ. Contam. Toxicol*. **94**: 34–40, doi:10.1007/s00128-014-1419-y.

Meng, J., Hong, S., Wang, T., Li, Q., Yoon, S.J., Lu, Y., Giesy, J.P. and Khim, J.S. 2017. Traditional and new POPs in environments along the Bohai and Yellow Seas: An overview of China and South Korea. *Chemosphere* **169**: 503–515, doi:10.1016/j.chemosphere.2016.11.108.

Meng, M., Shi, J.B., Yun, Z.J., Zhao, Z.S., Li, H.J., Gu, Y.X., Shao, J.J., Chen, B.W., Li, X.D. and Jiang, G.B. 2014. Distribution of mercury in coastal marine sediments of China: Sources and transport. *Mar. Pollut. Bull*. **88**: 347–353, doi:10.1016/j.marpolbul.2014.08.028.

Milliman, J.D. and Meade, R.H. 1983. World-wide delivery of river sediment to the oceans. *J. Geol*. **91**: 1–21.

Mourik, L.M.V., Leonards, P.E.G., Gaus, C. and Boer, J.D. 2015. Recent developments in capabilities for analysing chlorinated paraffins in environmental matrices: A review. *Chemosphere* **136**: 259–272, doi:10.1016/j.chemosphere.2015.05.045.

NBO (National Bureau of Oceanography of China). 2016. Bulletin of Marine Environmental Quality.

Newman, M.C., Ownby, D.R., Mézin, L.C.A., Powell, D.C., Christensen, T.R.L., Lerberg, S.B. and Anderson, B.A. 2000. Applying species-sensitivity distributions in ecological risk assessment: assumptions of distribution type and sufficient numbers of species. *Environ. Toxicol. Chem*. **19**: 508–515, doi:10.1897/1551-5028(2000)019<0508:ASSDIE>2.3.CO;2.

Pan, J., Yang, Y., Geng, C., Yeung, L., Cao, X. and Dai, T. 2010. Polychlorinated biphenyls, polychlorinated dibenzo-p-dioxins and dibenzofurans in marine and lacustrine sediments from the Shandong Peninsula, China. *J. Hazard. Mater*. **176**: 274–279, doi:10.1016/j.jhazmat.2009.11.024.

Pan, K. and Wang, W.X. 2012. Trace metal contamination in estuarine and coastal environments in China. *Sci. Total Environ*. **421**: 3–16, doi:10.1016/j.scitotenv.2011.03.013.

Pan, X.H. 2010. Polychlorinated naphthalenes, polybrominated diphenyl ethers and polychlorinated paraffins in surface sediments from the Laizhou Bay area. PhD thesis (in Chinese), University of Chinese Academy of Sciences, Yantai, Shandong, China.

Pan, Y., Shi, Y., Wang, J., Jin, X. and Cai, Y. 2011. Pilot investigation of perfluorinated compounds in river water, sediment, soil and fish in Tianjin, China. *Bull. Environ. Contam. Toxicol*. **87**: 152–157, doi:10.1007/s00128-011-0313-0.

Peng, L., Dai, X. and Yu, A. 2015. Assessment of the spatial and temporal distribution of legacy persistent organic pollutants and recommendations for sample collection from the surficial sediments of estuaries and seas in China. *Chemosphere* **119**: S138–S144, doi:10.1016/j.chemosphere.2014.04.004.

Qu, H.X., Dong, S.G., Tang, Z.H. and Wu, Y.P. 2009. Distribution and ecological evaluation of heavy metals in multi-medium of Luoyuan Bay. *Mar. Environ. Sci*. **28**: 298–308 (in Chinese).

Rahman, F., Langford, K.H., Scrimshaw, M.D. and Lester, J.N. 2001. Polybrominated diphenyl ether (PBDE) flame retardants. *Sci. Total Environ*. **275**: 1–17, doi:10.1016/s0048-9697(01)00852-x.

Ren, J.L., Zhang, J., Li, D.D., Cheng, Y. and Liu, S.M. 2010. Behavior of dissolved inorganic arsenic in the Yellow Sea and East China Sea. *Deep Sea Res. II* **57**: 1035–1046, doi:10.1016/j.dsr2.2010.02.005.

Reth, M., Zencak, Z. and Oehme, M. 2005. First study of congener group patterns and concentrations of short- and medium-chain chlorinated paraffins in fish from the North and Baltic Sea. *Chemosphere* **58**: 847–854, doi:10.1016/j.chemosphere.2004.09.036.

Schwarzer, S., De Bono, A., Giuliani, G., Kluser, S. and Peduzzi, P. 2005. E-waste, the hidden side of IT equipment's manufacturing and use. *Environ. Alert Bull*. **5**, United Nations Environment Programme.

Shen, Y.Q. 2013. Optimal design of monitoring network and comprehensive assessment of the seawater quality in China Seas. PhD thesis (in Chinese), Shanghai Jiao Tong University, Shanghai.

Shibamoto, T., Yasuhara, A. and Katami, T. 2007. Dioxin formation from waste incineration. *Rev. Environ. Contam. Toxicol*. **190**: 1–41, doi:10.1007/978-0-387-36903-7_1.

Stejnarová, P., Coelhan, M., Kostrhounová, R., Parlar, H. and Holoubek, I. 2005. Analysis of short chain chlorinated paraffins in sediment samples from the Czech Republic by short-column GC/ECNI-MS. *Chemosphere* **58**: 253–262, doi:10.1016/j.chemosphere.2004.08.083.

Sun, W.P., Pan, J.M., Lu, H.Y. and Xue, B. 2009. Distribution of dissolved trace metals in summer and winter of 2006 in Changjiang River Estuary and Hangzhou Bay. *J. Mar. Sci*. **31**: 79–84 (in Chinese).

Sun, Y. and Yang, Q.F. 1992. Heavy metal contents in economically important organisms of Jiaozhou Bay. *Mar. Sci*. **4**: 61–65 (in Chinese).

Sun, Y., Wang, T., Peng, X., Wang, P. and Lu, Y. 2016. Bacterial community compositions in sediment polluted by perfluoroalkyl acids (PFAAs) using Illumina high-throughput sequencing. *Environ. Sci. Pollut. Res. Int*. **23**: 10,556–10,565, doi:10.1007/s11356-016-6055-0.

Tang, A., Liu, R., Ling, M., Xu, L. and Wang, J. 2010. Distribution characteristics and controlling factors of soluble heavy metals in the Yellow River Estuary and adjacent sea. *Procedia Environ. Sci*. **2**: 1193–1198, doi:10.1016/j.proenv.2010.10.129.

Tang, E. and Yao, L. 2005. Industry status of chlorinated paraffin and its development trends. *China Chlor-Alkali* **2**: 1–3.

Tian, L., Chen, H.T., Du, J.T. and Wang, X.H. 2009. Factors influencing distribution of soluble heavy metals in North Yellow Sea surface seawaters. *Period. Ocean Univ. China* **39**: 617–621 (in Chinese).

Tomy, G.T., Fisk, A.T., Westmore, J.B. and Muir, D.C. 1998. Environmental chemistry and toxicology of polychlorinated n-alkanes. *Rev. Environ. Contam. Toxicol*. **158**: 53–128, doi:10.1007/978-1-4612-1708-4_2.

Turner, A. and Millward, G.E. 2002. Suspended particles: Their role in estuarine biogeochemical cycles. *Estuar. Coast. Shelf Sci*. **55**: 857–883, doi:10.1006/ecss.2002.1033.

UNECE (UN Economic Commission for Europe). 1998. The 1998 Aarhus Protocol on Persistent Organic Pollutants (POPs). Protocol to the 1979 Convention on Long-Range Transboundary Air Pollution on Persistent Organic Pollutants. United Nations Economic Commission for Europe. https://unece.org/environment-policyair/protocol-persistent-organic-pollutants-pops.

UNEP (UN Environment Programme). 2001. Final Act of the Plenipotentiaries on the Stockholm Convention on Persistent Organic Pollutants. United Nations Environment Program Chemicals, Geneva, Switzerland, 445 pp.

UNEP. 2009. The New POPs under the Stockholm Convention. http://chm.pops.int/TheConvention/ThePOPs/TheNewPOPs/tabid/2511/Default.aspx.

UNEP. 2013a. Listing of Hexabromocyclododecane. http://www.pops.int/TheConvention/ThePOPs/TheNewPOPs/tabid/2511/Default.aspx.

UNEP. 2013b. Minamata Convention on Mercury. http://www.mercuryconvention.org/Portals/11/documents/Booklets/Minamata%20Convention%20on%20Mercury_booklet_English.pdf.

US EPA (US Environmental Protection Agency). 2004. National Recommended Water Quality Criteria. https://www.epa.gov/sites/production/files/2015-06/documents/nrwqc-2004.pdf.

Wang, C.J., Ci, Z.J., Wang, Z.W. and Zhang, X.S. 2016. Air-sea exchange of gaseous mercury in the East China Sea. *Environ. Pollut*. **212**: 535–543, doi:10.1016/j.envpol.2016.03.016.

Wang, C.Y. 2008. The studies of environmentally ecological effects assessment and environmental capacity estimation of the heavy metal Cu, Pb, Zn and Cd in the East China Sea. PhD thesis (in Chinese), Ocean University of China, Qingdao.

Wang, G., Peng, J., Xu, X., Zhang, D. and Li, X. 2016a. Polybrominated diphenyl ethers in sediments from the Southern Yellow Sea: Concentration, composition profile, source identification and mass inventory. *Chemosphere* **144**: 2097–2105, doi:10.1016/j.chemosphere.2015.10.088.

Wang, G., Peng, J., Zhang, D. and Li, X. 2016b. Characterizing distributions, composition profiles, sources and potential health risk of polybrominated diphenyl ethers (PBDEs) in the coastal sediments from East China Sea. *Environ. Pollut*. **213**: 468–481, doi:10.1016/j.envpol.2016.02.054.

Wang, G.L., Ma, L.M., Sun, J.H. and Gan, Z. 2010. Occurrence and distribution of organochlorine pesticides (DDT and HCH) in sediments from the middle and lower reaches of the Yellow River, China. *Environ. Monit. Assess*. **168**: 511–521, doi:10.1007/s10661-009-1131-2.

Wang, J., Tan, L., Zhang, W. and Lian, Z. 2010. Concentrations and distribution characteristic of PAHs, PCBs and OCPs in the surface sediments of Qingtao coastal area. *Environ. Sci*. **31**: 2713–2722 (in Chinese).

Wang, L., Ge, W., Chai, C., Xia, B. and Jiang, T. 2017. Polybrominated diphenyl ethers in marine sediments of Sanggou Bay in east China. *Mar. Pollut. Bull*. **115**: 459–464, doi:10.1016/jmarpolbul.2016.10.065.

Wang, T., Lu, Y., Chen, C., Naile, J.E., Khim, J.S., Park, J., Luo, W., Jiao, W., Hu, W. and Giesy, J.P. 2011. Perfluorinated compounds in estuarine and coastal areas of north Bohai Sea, China. *Mar. Pollut. Bull*. **62**: 1905–1914, doi:10.1016/j.marpolbul.2011.05.029.

Wang, T., Lu, Y., Chen, C., Naile, J.E., Khim, J.S. and Giesy, J.P. 2012. Perfluorinated compounds in a coastal industrial area of Tianjin, China. *Environ. Geochem. Health* **34**: 301–311, doi:10.1007/s10653-011-9422-2.

Wang, X.T., Zhang, Y., Miao, Y., Ma, L.L., Li, Y.C., Chang, Y.Y. and Wu, M.H. 2013. Short-chain chlorinated paraffins (SCCPs) in surface soil from a background area in China: occurrence, distribution, and congener profiles. *Environ. Sci. Pollut. Res. Int*. **20**: 4742–4749, doi:10.1007/s11356-012-1446-3.

Wang, Y. 2012. Polychlorinated naphthalenes and chlorinated paraffins in the atmosphere and soil in Dongjiang River catchment, South China. Guangzhou Institute of Geochemistry. PhD thesis (in Chinese), University of Chinese Academy of Sciences, Guangzhou, Guangdong.

Wang, Y., Luo, C., Li, J., Yin, H., Li, X. and Zhang, G. 2011. Characterization of PBDEs in soils and vegetations near an e-waste recycling site in South China. *Environ. Pollut*. **159**: 2443–2448, doi:10.1016/j.envpol.2011.06.030.

Wu, X.Y., Liu, R.H., Qin, J., Sun, P.Y., Gao, Z.W. and Jia, Y.G. 2007. Study on the variance character of heavy metals contents in sediments in Yellow River Estuary. *Trans. Oceanol. Limnol*. **33**: 69–74 (in Chinese).

Xia, C., Wu, X., Lam, J.C., Xie, Z. and Lam, P.K. 2013. Methylmercury and trace elements in the marine fish from coasts of East China. *J. Environ. Sci. Health A Tox. Hazard. Subst. Environ. Eng*. **48**: 1491–1501, doi:10.1080/10934529.2013.796820.

Xiao, C.L., Jian, H.M., Chen, L.F., Liu, C., Gao, H.Y., Zhang, C.S., Liang, S.K. and Li, Y.B. 2017. Toxic metal pollution in the Yellow Sea and Bohai Sea, China: distribution, controlling factors and potential risk. *Mar. Pollut. Bull*. **119**: 381–389, doi:10.1016/j.marpolbul.2017.03.027.

Xie, S., Wang, T., Liu, S., Jones, K.C., Sweetman, A.J. and Lu, Y. 2013. Industrial source identification and emission estimation of perfluorooctane sulfonate in China. *Environ. Int*. **52**: 1–8, doi:10.1016/j.envint.2012.11.004.

Xu, Y.Y., Bai, Y.C., Wang, Y.L., Yin, Y.E., Jiang, M., Yuan, Q. and Xu, Z.L. 2015. Variation characteristics and potential ecological risk assessment of Cd and Pb in the sediments of the East China Sea. *Ecol. Environ. Sci*. **24**: 650–657 (in Chinese).

Yan, Y.P. 1993. Heavy metals pollution and risk assessment in economic fish of China coastal seas. *Mar. Environ. Sci.* **12**: 99–103 (in Chinese).

Yang, H., Xue, B., Jin, L., Zhou, S. and Liu, W. 2011. Polychlorinated biphenyls in surface sediments of Yueqing Bay, Xiangshan Bay, and Sanmen Bay in East China Sea. *Chemosphere* **83**: 137–143, doi:10.1016/j.chemosphere.2010.12.070.

Yang, H., Zhuo, S., Xue, B., Zhang, C. and Liu, W. 2012. Distribution, historical trends and inventories of polychlorinated biphenyls in sediments from Yangtze River Estuary and adjacent East China Sea. *Environ. Pollut.* **169**: 20–26, doi:10.1016/j.envpol.2012.05.003.

Yang, L., Zhu, L. and Liu, Z. 2011. Occurrence and partition of perfluorinated compounds in water and sediment from Liao River and Taihu Lake, China. *Chemosphere* **83**: 806–814, doi:10.1016/j.chemosphere.2011.02.075.

Yang, R.-Q., Lv, A.-H., Shi, J.-B. and Jiang, G.-B. 2005a. The levels and distribution of organochlorine pesticides (OCPs) in sediments from the Haihe River, China. *Chemosphere* **61**: 347–354, doi: 10.1016/j.chemosphere.2005.02.091.

Yang, R.Q., Jiang, G.B., Zhou, Q.F., Yuan, C.G. and Shi, J.B. 2005b. Occurrence and distribution of organochlorine pesticides (HCH and DDT) in sediments collected from East China Sea. *Environ. Int.* **31**: 799–804, doi:10.1016/j.envint.2005.05.027.

Yang, Z., Shen, Z., Gao, F., Tang, Z. and Niu, J. 2009. Occurrence and possible sources of polychlorinated biphenyls in surface sediments from the Wuhan reach of the Yangtze River, China. *Chemosphere* **74**: 1522–1530, doi:10.1016/j.chemosphere.2008.11.024.

Ye, S.Y. and Du, Y.S. 2007. The distribution and compare study of surface sediment in eastern Jiaozhou Bay and Qingdao adjacent coastal sea. *Trans. Oceanol. Limnol*. **4**: 80–86 (in Chinese).

Yi, Y.J. and Zhang, S.H. 2012. Heavy metal (Cd, Cr, Cu, Hg, Pb, Zn) concentrations in seven fish species in relation to fish size and location along the Yangtze River. *Environ. Sci. Pollut. Res*. **19**: 3989–3996, doi:10.1007/s11356-012-0840-1.

Yu, G.L. 2012. Study on method and application for analysis of short chain chlorinated paraffins in marine environment. Master's thesis (in Chinese), Dalian Maritime University, Dalian.

Yu, Y., Song, J.M., Li, X.G., Yuan, H.M. and Li, N. 2013. Fractionation, sources and budgets of potential harmful elements in surface sediments of the East China Sea. *Mar. Pollut. Bull*. **68**: 157–167, doi: 10.1016/j.marpolbul.2012.11.043.

Yuan, H.M., Song, J.M., Li, X.G., Li, N. and Duan, L. 2012. Distribution and contamination of heavy metals in surface sediments of the South Yellow Sea. *Mar. Pollut. Bull*. **64**: 2151–2159, doi:10.1016/j.marpolbul.2012.07.040.

Yuan, Z., Liu, G., Lam, M.H.W., Liu, H. and Da, C. 2016. Occurrence and levels of polybrominated diphenyl ethers in surface sediments from the Yellow River Estuary, China. *Environ. Pollut*. **212**: 147–154, doi:10.1016/j.envpol.2016.01.058.

Zegers, B.N., Lewis, W.E., Booij, K., Smittenberg, R.H., Boer, W., De Boer, J. and Boon, J.P. 2003. Levels of polybrominated diphenyl ether flame retardants in sediment cores from Western Europe. *Environ. Sci. Technol*. **37**: 3803–3807, doi:10.1021/es034226o.

Zeng, L., Zhao, Z., Li, H., Wang, T., Liu, Q., Xiao, K., Du, Y., Wang, Y. and Jiang, G. 2012. Distribution of short chain chlorinated paraffins in marine sediments of the East China Sea: influencing factors, transport and implications. *Environ. Sci. Technol*. **46**: 9898–9906, doi:10.1021/es302463h.

Zeng, L., Chen, R., Zhao, Z., Wang, T., Gao, Y., Li, A., Wang, Y., Jiang, G. and Sun, L. 2013. Spatial distributions and deposition chronology of short chain chlorinated paraffins in marine sediments across the Chinese Bohai and Yellow Seas. *Environ. Sci. Technol*. **47**: 11,449–11,456, doi:10.1021/es402950q.

Zeng, L., Wang, T., Wang, P., Liu, Q., Han, S., Yuan, B., Zhu, N., Wang, Y. and Jiang, G. 2014. Distribution and trophic transfer of short-chain chlorinated paraffins in an aquatic ecosystem receiving effluents from a sewage treatment plant. *Environ. Sci. Technol*. **45**: 5529–5535, doi:10.1021/es200895b.

Zhang, G.S., Liu, D.Y., Wu, H.F., Chen, L.L. and Han, Q.X. 2012. Heavy metal contamination in the marine organisms in Yantai coast, northern Yellow Sea of China. *Ecotoxicology* **21**: 1726–1733, doi:10.1007/s10646-012-0958-4.

Zhang, H., Luo, Y. and Li, Q. 2009. Burden and depth distribution of organochlorine pesticides in the soil profiles of Yangtze River Delta Region, China: Implication for sources and vertical transportation. *Geoderma* **153**: 69–75, doi:10.1016/j.geoderma.2009.07.016.

Zhang, J. 1995. Geochemistry of trace metals from Chinese river/estuary systems: An overview. *Estuar. Coast. Shelf Sci*. **41**: 631–658, doi:10.1006/ecss.1995.0082.

Zhang, L. and Zhang, L. 2015. Contribution of shellfish consumption to lower mercury health risk for residents in northern Jiaozhou Bay, China. *Bioinorg. Chem. Appl*. **2015**: doi:10.1155/2015/159521.

Zhang, P., Song, J., Liu, Z., Zheng, G., Zhang, N. and He, Z. 2007. PCBs and its coupling with eco-environments in Southern Yellow Sea surface sediments. *Mar. Pollut. Bull*. **54**: 1105–1115, doi:10.1016/j.marpolbul.2007.05.005.

Zhang, P., Song, J., Jie, F., Liu, Z., Li, X. and Yuan, H. 2009. One century record of contamination by polycyclic aromatic hydrocarbons and polychlorinated biphenyls in core sediments from the southern Yellow Sea. *J. Environ. Sci*. **21**: 1080–1088, doi:10.1016/S1001-0742(08)62385-2.

Zhang, R., Zhang, F., Zhang, T., Yan, H., Shao, W., Zhou, L. and Tong, H. 2014. Historical sediment record and distribution of polychlorinated biphenyls (PCBs) in sediments from tidal flats of Haizhou Bay, China. *Mar. Pollut. Bull*. **89**: 487–493, doi:10.1016/j.marpolbul.2014.09.001.

Zhang, W.G., Feng, H., Chang, J.N., Qu, J.G., Xie, H.X. and Yu, L.Z. 2009. Heavy metal contamination in surface sediments of Yangtze River intertidal zone: an assessment from different indexes. *Environ. Pollut*. **157**: 1533–1543, doi:10.1016/j.envpol.2009.01.007.

Zhang, Y.B. and Lin, H. 2004. Concentrations and distributions of DDTs, HCHs and PCBs in surface sediments of Xiamen sea areas. *Oceanogr. Taiwan Strait* **23**: 423–428.

Zhao, B.G., Shao, M.H. and Bao, Y. 2008. The features of concentration and dispersion of the heavy meals and their changing pattern in surface sediment of East Chian Sea. *Chin. J. Dalian Marit. Univ*. **3**: 13–16 (in Chinese).

Zhao, S. 2012. Environmental characteristics of metals and accumulation in shellfish in Rongcheng Bay. Master's thesis (in Chinese), Ocean University of China, Qingdao.

Zhao, Z., Li, H., Wang, Y., Li, G., Cao, Y., Zeng, L., Lan, J., Wang, T. and Jiang, G. 2013a. Source and migration of short-chain chlorinated paraffins in the coastal East China Sea using multiproxies of marine organic geochemistry. *Environ. Sci. Technol*. **47**: 5013–5022, doi:10.1021/es304899j.

Zhao, Z., Tang, J., Xie, Z., Chen, Y., Pan, X., Zhong, G., Sturm, R., Zhang, G. and Ebinghaus, R. 2013b. Perfluoroalkyl acids (PFAAs) in riverine and coastal sediments of Laizhou Bay, North China. *Sci. Total Environ*. **447**: 415–423, doi:10.1016/j.scitotenv.2012.12.095.

Zhen, X., Tang, J., Xie, Z., Wang, R., Huang, G., Zheng, Q., Zhang, K., Sun, Y., Tian, C. and Pan, X. 2016. Polybrominated diphenyl ethers (PBDEs) and alternative brominated flame retardants (aBFRs) in sediments from four bays of the Yellow Sea, North China. *Environ. Pollut*. **213**: 386–394, doi:10.1016/j.envpol.2016.02.042.

Zhou, S., Yang, H., Zhang, A., Li, Y.-F. and Liu, W. 2014. Distribution of organochlorine pesticides in sediments from Yangtze River Estuary and the adjacent East China Sea: implication of transport, sources and trends. *Chemosphere* **114**: 26–34, doi:10.1016/j.chemosphere.2014.03.100.

Zhu, L.Y. and Hites, R.A., 2005. Brominated flame retardants in sediment cores from Lakes Michigan and Erie. *Environ. Sci. Technol*. **39**: 3488–3494, doi:10.1021/es048240s.

Zhu, Z., Wang, T., Wang, P., Lu, Y. and Giesy, J.P. 2014. Perfluoroalkyl and polyfluoroalkyl substances in sediments from South Bohai coastal watersheds, China. *Mar. Pollut. Bull*. **85**: 619–627, doi: 10.1016/j.marpolbul.2013.12.042.

2.6 Atmospheric Deposition

Sai-Chun Tan[1,2] and Chun-Ok Jo[3]

[1] Institute of Atmospheric Physics, Chinese Academy of Sciences, China
[2] Nanjing University of Information Science and Technology, China
[3] Reseach Institute of Oceanography, Anyang University, Korea

2.6.1 Introduction

The impacts of atmospheric deposition, especially dust aerosols, on oceans have received much attention since the "iron (Fe) hypothesis" (Martin and Fitzwater, 1988; Martin and Gordon, 1988). The iron hypothesis postulated that Fe deficiency limits phytoplankton growth in high nutrient low chlorophyll (HNLC) waters (such as the Northeast subarctic Pacific and the southern oceans) and thus the enhanced supply of Fe to the ocean from the atmosphere stimulates photosynthesis, which leads to the reduction in atmospheric CO_2 concentrations during glacial maxima (Martin and Fitzwater, 1988). Biological productivity in some marine ecosystems may be limited by nitrogen (N), phosphorus (P), or Fe, or co-limited by those nutrients (Wu *et al*., 2000; Zou *et al*., 2000, 2001; Liu *et al*., 2003; Wang *et al*., 2003; Shi *et al*., 2012; Mahowald *et al*., 2017). For example, based on field observation data, high N:P ratio was found in the south and southwest of the Yellow Sea, the inshore area of the East China Sea, and the area east of the Changjiang estuary, which implies that primary production in a considerable portion of the Yellow Sea and East China Sea may be limited by P (Liu *et al*., 2003; Wang *et al*., 2003) while there are potential N limitations off the southwestern Korean Peninsula and west of Jeju Island in the Yellow Sea (Liu *et al*., 2003). *In situ* incubation experiments show that N and Fe could obviously stimulate phytoplankton growth even in the P limiting area of the Yellow Sea (Zou *et al*., 2000; 2001). Productivity in the ocean would respond to the enhanced supply of these nutrients from aeolian dust or anthropogenic nitrogen deposition, affecting ocean biogeochemistry and hence having feedback effects on climate (Jickells *et al*., 2005; Duce *et al*., 2008). Thus, the scientific issues on atmospheric aerosols, atmospheric deposition, the marine ecosystem, marine biogeochemical cycles, and their interconnections were focused by many international projects, such as the Integrated Marine Biosphere Research project (IMBeR), the International Study of Marine Biogeochemical Cycles of Trace Elements and their Isotopes (GEOTRACES), the International Global Atmospheric Chemistry (IGAC), and particularly the Surface Ocean Lower Atmosphere Study (SOLAS; Brévière *et al*., 2016).

The deserts in Mongolia, western China and northern China are three major sources of Asian dust aerosols, accounting for 70% of the total dust production (Zhang *et al*., 2003; Wang *et al*., 2005). When dust is transported to the ocean, it provides macronutrients (such as N and P) and micronutrients (such as Fe) to surface ecosystems of the oceans (Jickells *et al*., 2005; Duce *et al*., 2008; Furutani *et al*., 2010; Qi *et al*., 2013; Shi *et al*., 2013; Tan *et al*., 2017). Bishop *et al*. (2002) observed a doubling of biomass in the mixed layer in the subarctic North Pacific near Station PAPA (145°W, 50°N) after the passage of a dust storm in April 2001, and provided evidence of biotic response to natural iron fertilization caused by the dust particles. After that, many studies found that the deposition of nutrients associated with the intrusion of Asian dust in the marginal seas of the

Asian continent and the Pacific Ocean could enhance phytoplankton growth (Yuan and Zhang, 2006; Jo *et al*., 2007; Han *et al*., 2011; Tan *et al*., 2011, 2016; Shi *et al*., 2012; Tan and Shi, 2012b; Wang *et al*., 2012; Tan and Wang, 2014; Yoon *et al*., 2017; Luo *et al*., 2020; Wang *et al*., 2021).

2.6.2 Atmospheric deposition in the Yellow Sea

Since the 1990s, studies have investigated the possibility that atmospheric aerosol deposition may play an important role in the ecosystem in the Yellow Sea, as one of the downwind seas influenced by Asian dust and anthropogenic aerosols. Table 2.6.1 shows the deposition of dust or nutrients into the Yellow Sea and the comparison with its riverine influx or sediment. Previous studies reported great variability in the dust deposition flux into the Yellow Sea (0.13–0.9 g m^{-2} d^{-1}, 9–76 g m^{-2} a^{-1}), and the flux is very large, being one order of magnitude higher than the open Pacific Ocean (Table 2.6.1). Gao *et al*. (1992b) suggested that the total suspended particulate load during one event in a high dust year is nearly 18 times higher than the highest concentration observed in a low dust year. Even in a low dust year, the estimated atmospheric deposition of mineral aerosols to the Yellow Sea based on the representative crustal elements is 9–76 g m^{-2} a^{-1}, and it can account for 20–70% of the total input of mineral material to the Yellow Sea (Gao *et al*., 1992a). It was estimated that annual dust flux was 53.7 g m^{-2} a^{-1} from a two-year observation in the northern Yellow Sea during the period from December 1989 to May 1991, which is one order of magnitude higher than that over the central North Pacific Ocean (Zhang *et al*., 1993).

Analyses of rainwater and total atmospheric deposition samples at Qingdao from October 1988 to May 1990 suggest that the concentrations of Fe and Mn from atmospheric deposition and marine sediment in the southern Yellow Sea are close to each other, while the concentrations of atmospheric deposition of Co, Pb, Zn, Cu, Ni and Cr is 2 to 25 times that in marine sediment, thereby showing that atmospheric deposition may have an important role in trace elements input to the surface ocean in the Yellow Sea (Liu *et al*., 1991). In addition, the dissolved trace elements in rainwater collected at Qingdao is about one to three orders of magnitude higher than that in the open ocean of the tropical Pacific Ocean (Enewetak Atoll, 11°N, 162°E), suggesting the important effects of city pollutants on atmospheric trace elements (Liu *et al*., 1991). Based on observations at two land-base stations in the Yellow Sea, Zhang and Liu (1994) indicated that atmospheric deposition of nutrient elements (*e.g*., nitrate, phosphate, *etc*.) may be equal to or even more important than input from rivers. This has been supported by recent model simulations and field measurements. Model simulations indicate that annual deposition of atmospheric ammonia nitrogen (NH_4^+–N) to the Yellow Sea (171 GgN a^{-1}) can account for 87% of the total external input (terrestrial + atmospheric), which is 16 times the riverine input (10.6 GgN a^{-1}) (Zhang *et al*., 2010, Table 2.6.1). Recently, analyses of rainwater samples collected at Qianliyan Island in the Yellow Sea from 2009 to 2010 showed that atmospheric deposition of NH_4^+–N and phosphate phosphorus (PO_4^{3-}—P) is 6.6 times and 1.1 times the riverine influx, respectively; nitrate nitrite (NO_3^- + NO_2^-) from atmospheric deposition accounted for 47% of total terrestrial input (*i.e*., atmospheric deposition and riverine influx), which is slightly less than and comparable to that from riverine influx (Han *et al*., 2013). In addition, Qi *et al*. (2013) indicated that annual atmospheric deposition of total dissolved nitrogen (TDN) in the coastal region of the Yellow Sea (494 GgN a^{-1}) was greater than that from riverine input (88.0 GgN a^{-1}) — the former is 5.6 times the latter (Table 2.6.1).

Table 2.6.1 The deposition of dust or nutrients into the Yellow Sea and comparison with its riverine influx or sediment.

Atmospheric deposition	Flux / Concentration / Total amount	Times the riverine influx or sediment	Reference
Dust aerosol	360–3300 × 10^{10} g a^{-1} (9–76 g m^{-2} a^{-1})	0.24–2.2 times the input of sandy sediment from all rivers	Gao *et al*. (1992a)
Dust aerosol	53.7 g m^{-2} a^{-1}	one order of magnitude higher than that over the central North Pacific Ocean	Zhang *et al*. (1993)
Dust aerosol	9.27 g m^{-2} a^{-1}		Liu and Zhou (1999)
Dust aerosol	13.3 g m^{-2} a^{-1}	one order of magnitude higher than the Northwest Pacific (east to 165°E, 0–30°N)	Uematsu *et al*. (2003)
Dust aerosol	0.44 g m^{-2} d^{-1} (5.05 ± 2.49 μg m^{-2} s^{-1})		Yang *et al*. (2010)
Dust aerosol	0.56 g m^{-2} d^{-1}		Tan and Shi (2012b)
Dust aerosol	0.33 g m^{-2} d^{-1} (30 g m^{-2} in spring)		Tan *et al*. (2012)
Dust aerosol	0.13 g m^{-2} d^{-1} for annual 0.2 g m^{-2} d^{-1} in spring		Zhang and Gao (2007)
Dust aerosol	0.9 g m^{-2} d^{-1}		Shi *et al*. (2013)
Soluble Fe	0.48 ± 0.29 mg m^{-2} d^{-1}		
Atmospheric dry deposition of Fe	31,582.9 μg/g	0.99 times the concentration in sediment in the southern Yellow Sea (31,900 μg/g)	Liu *et al*. (1991)
Atmospheric wet deposition of Fe	49,641.2 μg/g	1.6 times the concentration in sediment	
Ammonium (NH_4^+ and NH_3)	171 GgN a^{-1}	16 times	Zhang *et al*. (2010
NH_4^+–N	29.3 mol a^{-1}	6.6 times	Han *et al*. (2013)
PO_4^{3-}–P	0.35 mol a^{-1}	1.1 times	
SiO_3^{2-}–Si	0.66 mol a^{-1}	0.03 times	
NO_3^- + NO_2^-	23.4 mol a^{-1}	0.9 times	
TDN	494 GgN a^{-1}	5.6 times	Qi *et al*. (2013)

TDN = total dissolved nitrogen

2.6.3 Atmospheric deposition in the East China Sea

Besides the Yellow Sea, atmospheric aerosols may exert an important role in the ecosystem in the East China Sea. Previous studies showed that atmospheric deposition flux of aerosol into the East China Sea ranged from several to hundred mg m^{-2} d^{-1} for different dust events (Table 2.6.2), suggesting considerable variability. Hsu *et al*. (2010) showed that the fluxes were 39 ± 50 μg m^{-2} d^{-1} for soluble Fe and 41 ± 74 μg m^{-2} d^{-1} for the combination of some bioavailable elements (*e.g*., Zn, Cu, Mn, Ba, Co, V, Ni, and Cd) during the northeasterly monsoons of 2005–2007. Tan *et al*. (2016) estimated a similar mean soluble Fe of 37.5 μg m^{-2} d^{-1} for spring dust storms in 2010. Although the deposition flux of aerosol in the East China Sea is smaller than that in the Yellow Sea, the atmospheric deposition of nutrient species is still important compared with the riverine input in the East China Sea. Based on observations at Shengsi Archipelago in the East China Sea, the estimated deposition flux of NO_3^- + NO_2^- and NH_4^+ was 28,690 and 39,720 μmol m^{-2} a^{-1},

respectively (Table 2.6.2). The total inputs of dissolved inorganic nitrogen, DIN (= NO_3^- + NO_2^- + NH_4^+) to the East China Sea were 52.7 mol a^{-1}, which is comparable to the riverine input (58.6 mol a^{-1}). Organic nitrogen, which is also adsorbed into fine and coarse particles, is reported to account for 10–25% of total nitrogen in aerosols over the East China Sea (Nakamura *et al*., 2005). Atmospheric PO_4^{3-} input to the East China Sea contributes 11.8% of the total of atmospheric and riverine inputs. The atmospheric deposition of SiO_3^{2-} has less importance compared with riverine input (Zhang *et al*., 2007). Model results show that the atmospheric deposition of NH_4^+ and NH_3 to the East China Sea is up to 166 GgN a^{-1}, which is 1.1 times of the riverine input to the East China Sea (Zhang *et al*., 2010).

Table 2.6.2 The deposition of dust or nutrients into the East China Sea.

Atmospheric deposition	Flux / Concentration / Total amount	Reference
PM_{10}	8–43.6 mg m^{-2} d^{-1}	Yan *et al*. (2012)
Dust deposition	8–178 mg m^{-2} d^{-1}	Hsu *et al*. (2013)
Dust aerosol	76 mg m^{-2} d^{-1} (7 g m^{-2} for the whole spring)	Tan *et al*. (2012)
Dust aerosol Soluble Fe	13.0–145.6 (mean 64.7) mg m^{-2} d^{-1} 7.5–84.3 (mean 37.5) μg m^{-2} d^{-1}	Tan *et al*. (2016)
Soluble Fe Other elements (*e.g*., Zn, Cu, Mn, Ba, Co, V, Ni, and Cd)	39 ± 50 μg m^{-2} d^{-1} 41 ± 74 μg m^{-2} d^{-1}	Hsu *et al*. (2010)
NO_3^- + NO_2^- NH_4^+ PO_4^{3-} SiO_3^{2-}	28,690 μmol m^{-2} a^{-1} 39,720 μmol m^{-2} a^{-1} 114 μmol m^{-2} a^{-1} 1973 μmol m^{-2} a^{-1}	Zhang *et al*. (2007)
Ammonium (NH_4^+ + NH_3)	166 GgN a^{-1}	Zhang *et al*. (2010)

In summary, in the Yellow Sea, atmospheric ammonium input is significantly greater than riverine input, atmospheric phosphate input is slightly higher than riverine input, and atmospheric nitrate input is slightly less than and comparable to riverine input. In the East China Sea, atmospheric ammonium input is slightly higher than the riverine input, the inputs of DIN (NO_3^- + NO_2^- + NH_4^+) are comparable to the riverine input, while atmospheric phosphate and silicate inputs are less than the riverine input. Based on observations of rain and aerosols at Qianliyan Island in the Yellow Sea and Shengsi Archipelago in the East China Sea over the 1999–2003 period, nutrient species in both wet and dry deposition events show clear seasonal signatures, with high values during the dry season and low values during the rainy season. Nutrient concentrations are higher at Qianliyan Island than from Shengsi because of relatively low rainfall and a greater influence of continental dust storms at Qianliyan Island (Zhang *et al*., 2007). In the Yellow Sea and East China Sea wet depositions are higher than dry depositions for all nutrient species. Moreover, the atmospheric deposition of trace elements is very important in both the Yellow Sea and the East China Sea.

2.6.4 Relationship between atmospheric deposition and biological production in the Yellow Sea and the East China Sea

During the transport pathway to the ocean, atmospheric aerosol particles sometimes react or mix with atmospheric anthropogenic pollutants when they cross over industrial cities, altering the bioavailability of Fe and adding more nutrients, such as N and P. Zhuang *et al*. (1992) reported that a significant portion of the iron in remote marine aerosols is in the form of Fe(II) (soluble) and they may come from the coupling and feedback between Fe and S in the atmosphere and in the ocean. Zhuang *et al*. (2003) further detected a considerable amount of Fe(II) in the aerosols collected during dust storms in Beijing and found that Fe and S concentrations in the dust storm aerosol samples represent a very positive relationship. During the transport pathway of dust from East Asia to the North Pacific Ocean, acid mobilization is thought as one of the possible mechanisms for the solubilization of Fe in aeolian dust, and SO_2 pollutant emissions are thought as a potential source of acidity (Meskhidze *et al*., 2003, 2005). Field measurements over the South China Sea, the Yellow Sea and at a coastal site in Qingdao in spring 2005 and 2006 indicated that during dust storm events, the concentration of particulate water soluble organic nitrogen in the coarse particles (>2.1 μm) increased, which led to an increase of that in total suspended particulates (Shi *et al*., 2010).

Recently, some studies proposed a link between aerosol deposition and phytoplankton growth in the Yellow Sea. They not only suggested that a statistical relationship existed between biological productivity in the Yellow Sea and the inputs of dust aerosols, but also implied that dust deposition could promote the phytoplankton bloom. Tan *et al*. (2011) showed that a significant positive correlation occurred between annual average chlorophyll *a* concentration/primary production in the southern Yellow Sea and the East China Sea and the frequencies of severe and very severe dust storms (FDS) in China during 1998–2008 (Fig. 2.6.1), suggesting that biological productivity in the those seas might be associated with dust storms. Figure 2.6.1 also shows that the algae bloom frequencies are significantly correlated with the annually averaged occurrence days with the aerosol index AI ≥ 2 in the coastal seas of China, including the Bohai Sea, Yellow Sea and East China Sea (correlation coefficient = 0.62), indicating the occurrence of algae blooms might be associated with

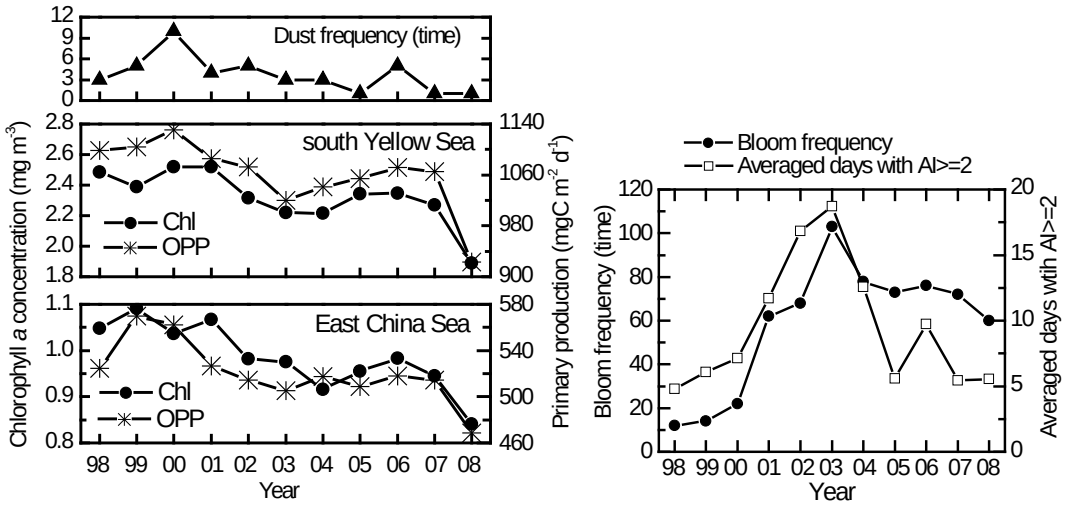

Fig. 2.6.1 (Left panel) Yearly variations of frequencies of dust storms (FDS) in China during 1998–2008, and annual average chlorophyll *a* concentration and primary production in the southern Yellow Sea and the East China Sea. From Tan *et al*. (2011); (right panel) Annual variations of bloom frequency and average days with aerosol index (AI) ≥ 2. From Tan *et al*. (2011). Reproduced with permission of Wiley & Sons.

atmospheric aerosol deposition, especially dust storms. Besides the annual correlation, the possible link between dust storms at different Asian dust source areas and phytoplankton growth in the Yellow Sea was further investigated. Based on dust storm observations at 222 meteorological stations in China during 1997–2007, significant correlation (Fig. 2.6.2) was found between dust events and chlorophyll *a* concentration in the Yellow Sea (Tan and Shi, 2012a). High correlation regions included the southeastern Xinjiang–Qinghai–Xizang region, the Hexi Corridor–western Inner Mongolia–Hetao regions, and the Hunshandake Desert.

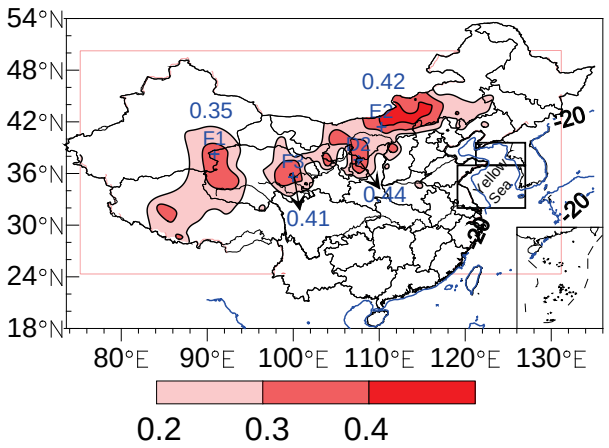

Fig. 2.6.2 Correlation coefficient between monthly occurrence frequency of dust storms (days month^{-1}) at 222 meteorological stations and monthly area-averaged chlorophyll *a* concentration (mg m^{-3}) in the Yellow Sea between September 1997 and December 2007. Minimum contour is 0.2. D2, E2, F1, and F3 are the stations of Dingbian, Damaoqi, Mangya, and Xinghai. Rectangles show the location of the Yellow Sea. Isobaths in the sea are 20 m. From Tan and Shi (2012a).

The importance of nutrient-containing aerosol deposition, especially dust aerosol, on the Yellow Sea was confirmed by recent satellite remote sensing analyses, aerosol field measurements, and onboard incubation experiments. Satellite observation analyses showed that algae blooms were detected in about 73% dust storm events in the southern central Yellow Sea (Tan *et al*., 2011). Satellite remote sensing (Fig. 2.6.3) further revealed that the initial timing of the spring bloom in dust years in the southern central Yellow Sea was about 11–18 days earlier than that in 2005 (non-dust year) and peak chlorophyll *a* concentration in dust years was about 1.4–2.6 times that in 2005 (Tan and Shi, 2012b). Cruise measurements in the southern Yellow Sea during the period from March 31 to April 24, 2007 indicate that the calculated dust-derived N and Fe supplies can satisfy the phytoplankton needs at the initiation of the bloom (Shi *et al*., 2012, 2013). Results of onboard incubation experiments performed in the southern Yellow Sea in the spring of 2011 showed that the addition of a large amount of Asian dust (20 mg L^{-1}) could increase both the maximum concentration of chlorophyll *a* and the conversion efficiency index of N into chlorophyll *a* concentration by ~40% and ~30%, respectively, which is indicative of promoting the growth of phytoplankton (Liu *et al*., 2013). The dry and wet nitrogen deposition estimated by Qi *et al*. (2013) could be converted to a new primary biological productivity of 1.5–30.0 gC m^{-2} a^{-1}, which accounts for 0.3% to 6.7% of the new productivity in the Yellow Sea.

Recent studies also show the contribution of nitrogen, phosphorus, and iron to phytoplankton bloom in the East China Sea. Tan *et al*. (2016) estimated that iron deposition from five dust storm events in the East China Sea in 2010 accounted for 20% to 227% of the new springtime production and 5% to 115% of the mean increase in chlorophyll *a* concentration in spring 2010. The total inorganic nitrogen deposition from five dust storm events may have supported 0.4% to 4.0% of the new

springtime production. Zhang *et al.* (2010) estimated that annual total nitrogen deposited to the eastern China seas can support 1.1% to 3.9% of the new production in the East China Sea. The contribution ratio of total inorganic nitrogen and soluble phosphorus supported by the five dust storms to the mean increase in chlorophyll *a* concentration varied from 0.1% to 2.0% and 0.01% to 0.2%, respectively (Tan *et al.*, 2016). As a result, the atmospheric deposition of iron is seen to be the most important factor in phytoplankton growth in the East China Sea; nitrogen also plays an important part, whereas phosphorus has less impact.

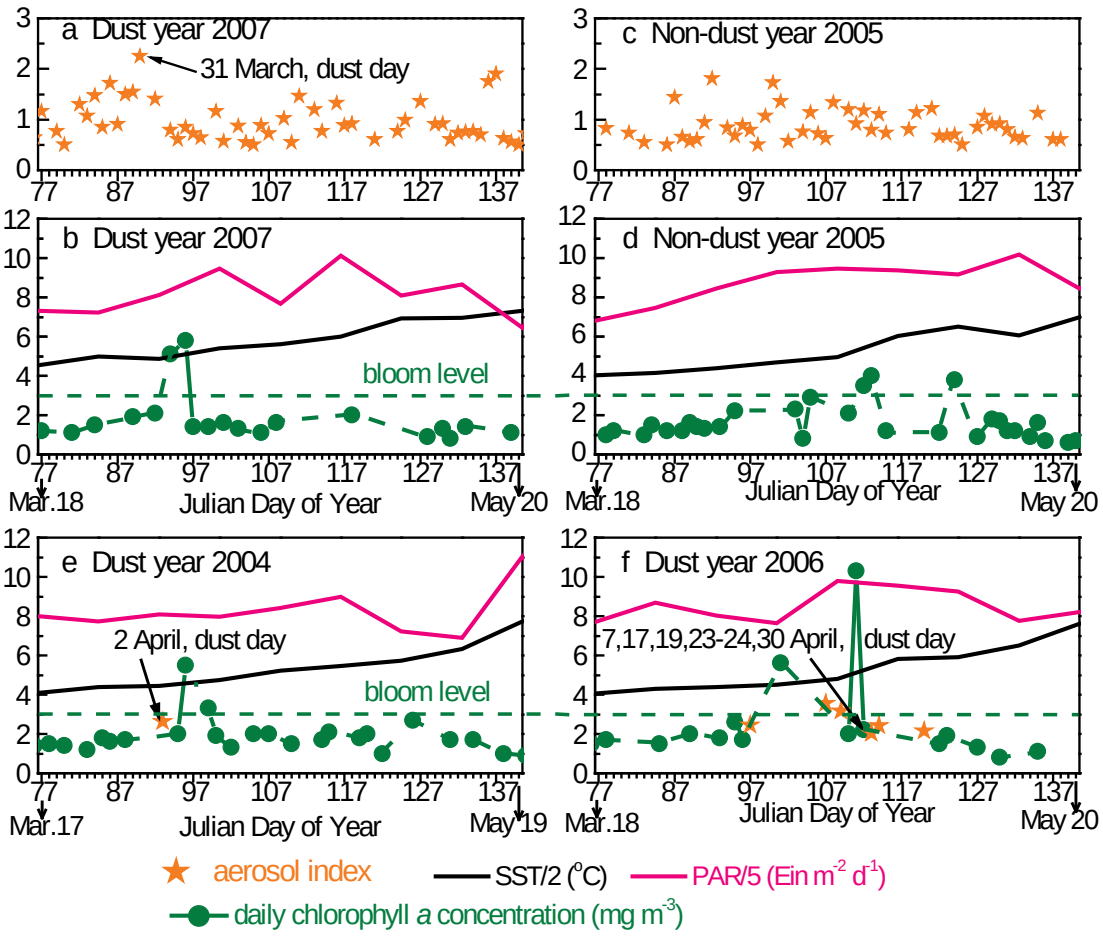

Fig. 2.6.3 Variations in daily aerosol index, daily chlorophyll *a* concentration, and 8-day surface photosynthetically available radiation (PAR) and sea surface temperature (SST) in the central southern Yellow Sea from March 17 through May 20 in 2007, 2005, 2004, and 2006. Green dashed line shows the bloom level defined as chlorophyll *a* concentration is 3 mg m^{-3} (twice as large as winter average). From Tan and Shi (2012b).

Note that not all dust depositions could stimulate phytoplankton blooms. Case studies illustrated that 6 out of 22 dust episodes did not induce any algae blooms in the southern central Yellow Sea (Tan *et al.*, 2011). Onboard incubation experiments performed in the southern Yellow Sea in the spring of 2011 found no promotion in phytoplankton growth when a small amount of Asian dust (2 mg L^{-1}) was added (Liu *et al.*, 2013). Incubation experiments in the northern Red Sea showed that toxic effects were observed with some aerosols, where the toxicity affected picoeukaryotes and *Synechococcus* but not *Prochlorococcus* (Paytan *et al.*, 2009). The toxic effects could be due to higher copper concentrations in these aerosols, and/or other elements present in the aerosols or unknown synergistic effects between these elements (Paytan *et al.*, 2009). *In situ* mesocosm

experiments at Huaniao island in the East China Sea found that phytoplankton growth was suppressed under high aerosol copper but was increased when high copper was accompanied by high iron in aerosols, suggesting the combined effects of iron and copper from atmospheric dry deposition (Wang *et al*., 2017). Those studies suggest the complex effect of atmospheric deposition on marine productivity.

2.6.5 Future perspective

The complexity of the impacts of atmospheric aerosols on marine ecosystems is due to the change in physical and chemical properties of aerosols during the transport pathway from the source regions to the oceans, the uncertainty in the estimate of atmospheric deposition flux, the bioavailability affected by atmospheric processing and environmental condition in surface water, the variation of N and P ratios, and the complicated effects of deposition on the ocean ecosystem. For example, global climate change and human activities could lead to more atmospheric pollution events, which will influence both the supply and impact of atmospheric material deposited into the surface ocean (Baker and Croot, 2010; Boyd *et al*., 2010; Li *et al*., 2012). In addition, atmospheric deposition may change the nutrient structure in the ocean. Kim *et al*. (2011) found that the abundance of N relative to P in northeastern Asian marginal seas has increased since 1980 due to atmospheric N deposition. Anthropogenic nitrogen deposition has even resulted in surplus of N in the marginal seas around China, Korea, Japan and Russia, commencing in the mid-1990s (Kim *et al*., 2011). Kodama *et al*. (2016) showed that phosphate concentrations has declined in the surface layers in summer and winter over the last 40 years (1964–2010), while no significant linear trend was observed for nitrate concentrations in the Tsushima Current area. They further concluded that the declining trend in the phosphate concentrations is caused by horizontal advection of East China Sea water. The increase in N:P due to larger increases in N than P in many regions of the globe can cause shifts from N to P limitation (Moore *et al*., 2013; Mahowald *et al*., 2017).

More systematic and accurate measurements of atmospheric chemistry, atmospheric deposition, nutrients, and ecosystem response are required to resolve variability in both atmospheric deposition and ecosystem response, particularly in regions where atmospheric supply plays an important role, including the Yellow Sea and the East China Sea.

Linkage between atmospheric deposition and marine ecosystem is related to atmospheric pollution, marine health, marine fertilization, fishery and carbon sequestration, *etc*., and is one of the hot topics in atmospheric and marine sciences. Thus, understanding how atmospheric aerosols impact the marine ecosystem in the Yellow Sea and the East China Sea is worth further investigation.

2.6.6 References

Baker, A.R. and Croot, P.L. 2010. Atmospheric and marine controls on aerosol iron solubility in seawater. *Mar. Chem*. **120**: 4–13, doi:10.1016/j.marchem.2008.09.003.

Bishop, J.K.B., Davis, R.E. and Sherman, J.T. 2002. Robotic observations of dust storm enhancement of carbon biomass in the North Pacific. *Science* **298**: 817–821, doi:10.1126/science.1074961.

Boyd, P.W., Mackie, D.S. and Hunter, K.A. 2010. Aerosol iron deposition to the surface ocean - Modes of iron supply and biological responses. *Mar. Chem*. **120**: 128–143, doi:10.1016/j.marchem.2009.01.008.

Brévière, E. 2016. SOLAS 2015-2025 Science Plan and Organisation, SOLAS International Project Office, GEOMAR Helmholtz Centre for Ocean Research Kiel, https://dev.solas-int.org/science/science-plan.html.

Duce, R.A., LaRoche, J., Altieri, K., Arrigo, K.R., Baker, A.R., Capone, D.G., Cornell, S., Dentener, F., Galloway, J., Ganeshram, R.S., Geider, R.J., Jickells, T., Kuypers, M.M., Langlois, R., Liss, P.S., Liu, S.M., Middelburg, J.J., Moore, C.M., Nickovic, S., Oschlies, A., Pedersen, T., Prospero, J., Schlitzer, R., Seitzinger, S., Sorensen, L.L., Uematsu, M., Ulloa, O., Voss, M., Ward, B. and Zamora, L. 2008. Impacts of atmospheric anthropogenic nitrogen on the open ocean. *Science* **320**: 893–897, doi: 10.1126/science.1150369.

Furutani, H., Meguro, A., Iguchi, H. and Uematsu, M. 2010. Geographical distribution and sources of phosphorus in atmospheric aerosol over the North Pacific Ocean. *Geophys. Res. Lett*. **37**: L03805, doi:03810.01029/02009GL041367.

Gao, Y., Arimoto, R., Duce, R.A., Lee, D.S. and Zhou, M.Y. 1992a. Input of atmospheric trace elements and mineral matter to the Yellow Sea during the spring of a low-dust year. *J. Geophys. Res*. **97**: 3767–3777, doi:10.1029/91JD02686.

Gao, Y., Arimoto, R., Zhou, M.Y., Merrill, J.T. and Duce, R.A. 1992b. Relationships between the dust concentrations over eastern Asia and the remote North Pacific. *J. Geophys. Res*. **97**: 9867–9872, doi:10.1029/92JD00714.

Han, L.-J., Zhu, Y.-M., Liu, S.-M., Zhang, J. and Li, R.-H. 2013. Nutrients of atmospheric wet deposition from the Qianliyan Island of the Yellow Sea. *Chin. Environ. Sci.* **33**: 1174–1184 (in Chinese).

Han, Y., Zhao, T., Song, L., Fang, X., Yin, Y., Deng, Z., Wang, S. and Fan, S. 2011. A linkage between Asian dust, dissolved iron and marine export production in the deep ocean. *Atmos. Environ*. **45**: 4291–4298, doi:10.1016/j.atmosenv.2011.04.078.

Hsu, S.-C., Wong, G.T.F., Gong, G.-C., Shiah, F.-K., Huang, Y.-T., Kao, S.-J., Tsai, F., Lung, S.-C.C., Lin, F.-J., Lin, I.I., Hung, C.-C. and Tseng, C.-M. 2010. Sources, solubility, and dry deposition of aerosol trace elements over the East China Sea. *Mar. Chem*. **120**: 116–127, doi:10.1016/j.marchem.2008.10.003.

Hsu, S.-C., Tsai, F., Lin, F.-J., Chen, W.-N., Shiah, F.-K., Huang, J.-C., Chan, C.-Y., Chen, C.-C., Liu, T.-H., Chen, H.-Y., Tseng, C.-M., Hung, G.-W., Huang, C.-H., Lin, S.-H. and Huang, Y.-T. 2013. A super Asian dust storm over the East and South China Seas: Disproportionate dust deposition. *J. Geophys. Res. Atmos*. **118**: 7169–7181, doi:10.1002/jgrd.50405.

Jickells, T.D., An, Z.S., Andersen, K.K., Baker, A.R., Bergametti, G., Brooks, N., Cao, J.J., Boyd, P.W., Duce, R.A., Hunter, K.A., Kawahata, H., Kubilay, N., laRoche, J., Liss, P.S., Mahowald, N., Prospero, J.M., Ridgwell, A.J., Tegen, I. and Torres, R. 2005. Global iron connections between desert dust, ocean biogeochemistry, and climate. *Science* **308**: 67–71, doi:10.1126/science.1105959.

Jo, C.-O., Lee, J.-Y., Park, K.-A., Kim, Y.-H. and Kim, K.-R. 2007. Asian dust initiated early spring bloom in the northern East/Japan Sea. *Geophys. Res. Lett*. **34**: L05602, doi:05610.01029/02006GL027395.

Kim, T.-W., Lee, K., Najjar, R.G., Jeong, H.-D. and Jeong, H.J. 2011. Increasing N abundance in the northwestern Pacific Ocean due to atmospheric nitrogen deposition. *Science* **334**: 505–509, doi: 10.1126/science.1206583.

Kodama, T., Igeta, Y., Kuga, M. and Abe, S. 2016. Long-term decrease in phosphate concentrations in the surface layer of the southern Japan Sea. *J. Geophys. Res. Oceans* **121**: 7845–7856, doi:10.1002/2016JC012168.

Li, J., Wang, Z., Zhuang, G., Luo, G., Sun, Y. and Wang, Q. 2012. Mixing of Asian mineral dust with anthropogenic pollutants over East Asia: a model case study of a super-duststorm in March 2010. *Atmos. Chem. Phys*. **12**: 7591–7607, doi:10.5194/acp-12-7591-2012.

Liu, S.M., Huang, W.-W., Zhang, J., Wang, J.-Y. and Ji, X.-W. 1991. Chemical composition analysis of atmospheric deposition at Qingdao—I. trace elements. *Mar. Environ. Sci*. **10**: 21–28 (in Chinese).

Liu, S.M., Zhang, J., Chen, S.Z., Chen, H.T., Hong, G.H., Wei, H. and Wu, Q.M. 2003. Inventory of nutrient compounds in the Yellow Sea. *Cont. Shelf Res*. **23**: 1161–1174, doi:10.1016/S0278-4343(03)00089-X.

Liu, Y. and Zhou, M. 1999. Atmospheric input of aerosols to the eastern seas of China. *Acta Oceanol. Sin.* **21**: 38–45 (in Chinese).

Liu, Y., Zhang, T.R., Shi, J.H., Gao, H.W. and Yao, X.H. 2013. Responses of chlorophyll a to added nutrients, Asian dust, and rainwater in an oligotrophic zone of the Yellow Sea: Implications for promotion and inhibition effects in an incubation experiment. *J. Geophys. Res. Biogeosci.* **118**: 1763–1772, doi:10.1002/2013JG002329.

Luo, C., Wang, W., Sheng, L., Zhou, Y., Hu, Z., Qu, W., Li, X. and Hai, S. 2020. Influence of polluted dust on chlorophyll-a concentration and particulate organic carbon in the subarctic North Pacific Ocean based on satellite observation and the WRF-Chem simulation. *Atmos. Res*. **236**: 104812, doi:10.1016/j.atmosres.2019.104812.

Mahowald, N.M., Scanza, R., Brahney, J., Goodale, C.L., Hess, P.G., Moore, J.K. and Neff, J. 2017. Aerosol deposition impacts on land and ocean carbon cycles. *Curr. Clim. Change Rep*. **3**: 16–31, doi:10.1007/s40641-017-0056-z.

Martin, J.H. and Fitzwater, S.E. 1988. Iron deficiency limits phytoplankton growth in the north-east Pacific subarctic. *Nature* **331**: 341–343, doi:10.1038/331341a0.

Martin, J.H. and Gordon, R.M. 1988. Northeast Pacific iron distributions in relation to phytoplankton productivity. *Deep Sea Res. Part A* **35**: 177–196, doi:10.1016/0198-0149(88)90035-0.

Meskhidze, N., Chameides, W.L., Nenes, A. and Chen, G. 2003. Iron mobilization in mineral dust: Can anthropogenic SO_2 emissions affect ocean productivity? *Geophys. Res. Lett*. **30**: 2085, doi:10.1029/2003GL018035.

Meskhidze, N., Chameides, W.L. and Nenes, A. 2005. Dust and pollution: A recipe for enhanced ocean fertilization. *J. Geophys. Res*. **110**: D03301, doi:03310.01029/02004JD005082.

Moore, C.M., Mills, M.M., Arrigo, K.R., Berman-Frank, I., Bopp, L., Boyd, P.W., Galbraith, E.D., Geider, R.J., Guieu, C., Jaccard, S.L., Jickells, T.D., La Roche, J., Lenton, T.M., Mahowald, N.M., Marañón, E., Marinov, I., Moore, J.K., Nakatsuka, T., Oschlies, A., Saito, M.A., Thingstad, T.F., Tsuda, A. and Ulloa, O. 2013. Processes and patterns of oceanic nutrient limitation. *Nature Geosci*. **6**: 701, doi:10.1038/ngeo1765.

Nakamura, T., Ogawa, H., Maripi, D.K. and Uematsu, M. 2006. Contribution of water soluble organic nitrogen to total nitrogen in marine aerosols over the East China Sea and western North Pacific. *Atmos. Environ*. **40**: 7259–7264, doi:10.1016/j.atmosenv.2006.06.026.

Paytan, A., Mackey, K.R.M., Chen, Y., Lima, I.D., Doney, S.C., Mahowald, N., Labiosa, R. and Post, A.F. 2009. Toxicity of atmospheric aerosols on marine phytoplankton. *Proc. Natl. Acad. Sci. USA* **106**: 4601–4605, doi:10.1073/pnas.0811486106.

Qi, J.H., Shi, J.H., Gao, H.W. and Sun, Z. 2013. Atmospheric dry and wet deposition of nitrogen species and its implication for primary productivity in coastal region of the Yellow Sea, China. *Atmos. Environ*. **81**: 600–608, doi:10.1016/j.atmosenv.2013.08.022.

Shi, J.-H., Gao, H., Qi, J., Zhang, J. and Yao, X. 2010. Sources, compositions, and distributions of water-soluble organic nitrogen in aerosols over the China Sea. *J. Geophys. Res*. **115**: D17303, doi:17310.11029/12009JD013238.

Shi, J.-H., Gao, H.-W., Zhang, J., Tan, S.-C., Ren, J.-L., Liu, C.-G., Liu, Y. and Yao, X. 2012. Examination of causative link between a spring bloom and dry/wet deposition of Asian dust in the Yellow Sea, China. *J. Geophys. Res*. **117**: D17304, doi:10.1029/2012JD017983.

Shi, J.-H., Zhang, J., Gao, H.-W., Tan, S.-C., Yao, X.-H. and Ren, J.-L. 2013. Concentration, solubility and deposition flux of atmospheric particulate nutrients over the Yellow Sea. *Deep Sea Res. II* **97**: 43–50, doi:10.1016/j.dsr2.2013.05.004.

Tan, S.-C. and Shi, G.-Y. 2012a. Correlation of dust storms in China with chlorophyll a concentration in the Yellow Sea between 1997–2007. *Atmos. Ocean. Sci. Lett.* **5**: 1–5, doi:10.1080/16742834.2012.11446980.

Tan, S.-C. and Wang, H. 2014. The transport and deposition of dust and its impact on phytoplankton growth in the Yellow Sea. *Atmos. Environ.* **99**: 491–499, doi:10.1016/j.atmosenv.2014.10.016.

Tan, S.-C. and Shi, G.-Y. 2012b. Transport of a severe dust storm in March 2007 and impacts on chlorophyll a concentration in the Yellow Sea. *SOLA* **8**: 85–89, doi:10.2151/sola.2012-022.

Tan, S.-C., Shi, G.-Y., Shi, J.-H., Gao, H.-W. and Yao, X. 2011. Correlation of Asian dust with chlorophyll and primary productivity in the coastal seas of China during the period from 1998 to 2008. *J. Geophys. Res.* **116**: G02029, doi:10.1029/2010JG001456.

Tan, S.-C., Shi, G.-Y. and Wang, H. 2012. Long-range transport of spring dust storms in Inner Mongolia and impact on the China seas. *Atmos. Environ*. **46**: 299–308, doi:10.1016/j.atmosenv.2011.09.058.

Tan, S.-C., Li, J., Gao, H., Wang, H., Che, H. and Chen, B. 2016. Satellite-observed transport of dust to the East China Sea and the North Pacific Subtropical Gyre: Contribution of dust to the increase in chlorophyll during spring 2010. *Atmosphere* **7**: 152, doi:10.3390/atmos7110152.

Tan, S.-C., Li, J., Che, H., Chen, B. and Wang, H. 2017. Transport of East Asian dust storms to the marginal seas of China and the southern North Pacific in spring 2010. *Atmos. Environ*. **148**: 316–328, doi:10.1016/j.atmosenv.2016.10.054.

Uematsu, M., Wang, Z. and Uno I. 2003. Atmospheric input of mineral dust to the western North Pacific region based on direct measurements and a regional chemical transport model. *Geophys. Res. Lett*. **30**: 1342, doi:1310.1029/2002GL016645.

Wang, B.-D., Wang, X.-L. and Zhan, R. 2003. Nutrient conditions in the Yellow Sea and the East China Sea. *Estuar. Coast. Shelf Sci*. **58**: 127–136, doi:10.1016/S0272-7714(03)00067-2.

Wang, F.J., Chen, Y., Guo, Z.G., Gao, H.W., Mackey, K.R., Yao, X.H., Zhuang, G.S. and Paytan, A. 2017. Combined effects of iron and copper from atmospheric dry deposition on ocean productivity. *Geophys. Res. Lett*. **44**: 2546–2555, doi:10.1002/2016GL072349.

Wang, S.-G., Wang, J.-Y., Zhou, Z.-J. and Shang, K.-Z. 2005. Regional characteristics of three kinds of dust storm events in China. *Atmos. Environ*. **39**: 509–520, doi:10.1016/j.atmosenv.2004.09.033.

Wang, S.-H., Hsu, N.C., Tsay, S.-C., Lin, N.-H., Sayer, A.M., Huang, S.-J. and Lau, W.K.M. 2012. Can Asian dust trigger phytoplankton blooms in the oligotrophic northern South China Sea? *Geophys. Res. Lett*. **39**: L05811, doi:10.1029/2011GL050415.

Wang, W., Luo, C., Sheng, L., Zhao, C., Zhou, Y. and Chen, Y. 2021. Effects of biomass burning on chlorophyll-a concentration and particulate organic carbon in the subarctic North Pacific Ocean based on satellite observations and WRF-Chem model simulations: A case study. *Atmos. Res*. **254**: 105526, doi:10.1016/j.atmosres.2021.105526.

Wu, J., Sunda, W., Boyle, E.A. and Karl, D.M. 2000. Phosphate depletion in the western North Atlantic Ocean. *Science* **289**: 759–762, doi:10.1126/science.289.5480.759.

Yan, H., Gao, H., Yao, X. and Wang, Z. 2012. Simulating dry deposition fluxes of PM10 and particulate inorganic nitrogen over the eastern China seas during a severe Asian dust event using WRF-Chem model. *J. Ocean Univ. China* **11**: 301–314, doi:10.1007/s11802-012-1857-2.

Yang, D.-X., Liu, Y. and Chen, W.-Z. 2010. Estimation of the total dust column and dry deposition flux over the Yellow Sea, China based on shipboard sun photometer measurements: Case study. *Atmos. Ocean. Sci. Lett.* **3**: 64–69, doi:10.1080/16742834.2010.11446846.

Yoon, J.-E., Kim, K., Macdonald, A.M., Park, K.-T., Kim, H.-C., Yoo, K.-C., Yoon, H.-I., Yang, E.J., Jung, J., Lim, J.-H., Kim, J.-H., Lee, J., Choi, T.-J., Song, J.-M. and Kim, I.-N. 2017. Spatial and temporal variabilities of spring Asian dust events and their impacts on chlorophyll-a concentrations in the western North Pacific Ocean. *Geophys. Res. Lett*. **44**: 1474–1482, doi:10.1002/2016GL072124.

Yuan, W. and Zhang, J. 2006. High correlations between Asian dust events and biological productivity in the western North Pacific. *Geophys. Res. Lett*. **33**: L07603, doi:07610.01029/02005GL025174.

Zhang, G., Zhang, J. and Liu, S. 2007. Characterization of nutrients in the atmospheric wet and dry deposition observed at the two monitoring sites over Yellow Sea and East China Sea. *J. Atmos. Chem*. **57**: 41–57, doi:10.1007/s10874-007-9060-3.

Zhang, J. and Liu, M. 1994. Observations on nutrient elements and sulphate in atmospheric wet depositions over the Northwest Pacific coastal oceans — Yellow Sea. *Mar. Chem*. **47**: 173–189.

Zhang, J., Liu, S.M., Lü, X. and Huang, W.W. 1993. Characterizing Asian wind-dust transport to the Northwest Pacific Ocean. Direct measurements of the dust flux for two years. *Tellus B* **45**: 335–345, doi:10.3402/tellusb.v45i4.15734.

Zhang, K. and Gao, H.-W. 2007. The characteristics of Asian-dust storms during 2000-2002: From the source to the sea. *Atmos. Environ*. **41**: 9136–9145, doi:10.1016/j.atmosenv.2007.08.007.

Zhang, X.Y., Gong, S.-L., Zhao, T.-L. and Arimoto, R. 2003. Sources of Asian dust and role of climate change versus desertification in Asian dust emission. *Geophys. Res. Lett*. **30**: 2272, doi:10.1029/2003GL018206.

Zhang, Y., Yu, Q., Ma, W. and Chen, L. 2010. Atmospheric deposition of inorganic nitrogen to the eastern China seas and its implications to marine biogeochemistry. *J. Geophys. Res. Atmos*. **115**: D00K10, doi:10.1029/2009JD012814.

Zhuang, G.-S., Yi, Z., Duce, R.A. and Brown, P.R. 1992. Link between iron and sulphur cycles suggested by detection of Fe(n) in remote marine aerosols. *Nature* **355**: 537–539, doi:10.1038/355537a0.

Zhuang, G.-S., Guo, J., Yuan, H. and Zhang, X. 2003. Coupling and feedback between iron and sulphur in air-sea exchange. *Chin. Sci. Bull*. **48**: 1080–1086, doi:10.1007/BF03185756.

Zou, L., Chen, H.T. and Zhang, J. 2000. Experimental examination of the effects of atmospheric wet deposition on primary production in the Yellow Sea. *J. Exper. Mar. Biol. Ecol*. **249**: 111–121, doi: 10.1016/s0022-0981(00)00186-6.

Zou, L., Zhang, J., Pan, W.-X. and Zhan, Y.-P. 2001. In situ nutrient enrichment experiment in the Bohai and Yellow Sea. *J. Plankt. Res*. **23**: 1111–1119, doi:10.1093/plankt/23.10.1111.

Biological Oceanography

Preface

This chapter summarizes the general understanding of biological oceanography in the Bohai, Yellow and East China seas based on published literature. The chapter consists of five sections: the pelagic microbial food web, phytoplankton, zooplankton, macrobenthos, and fish and invertebrate fisheries.

There is a large amount of observations and studies in this area; however, the information is still scattered, and was not easy to fully synthesize. The authors of each section have tried hard to synthesize within their limitations. Section 3.1 covers studies of abundances of virioplankton, heterotrophic bacteria, picophyoplankton, flagellates, ciliates, and tintinnids, as well as their interaction and community respiration. Section 3.2 deals with studies of chlorophyll-a and primary production from satellite observation, new production and nitrogen fixation, and pigment-based community structure, as well as the interannual variation caused by the Three Gorge Dam and typhoons. Section 3.3 considers studies of adaptation to distinct habitats, responses to climate change and anthropogenic impacts focusing on physical–biological coupling. Section 3.4 describes studies of macrobenthos taxonomic groups, dominant species, community structure, abundance, biomass and diversity, as well as secondary productivity for the Yellow Sea and East China Sea separately. Section 3.5 reports on the fish community, invertebrate community and 10 key species, mostly in the Yangtze River estuary.

At present, the ecosystem of this region is facing serious multiple pressures based on climate change, as well as anthropogenic stresses due to global warming, acidification, pollution, and fishing activity. However, it is noted that information on organisms for the whole area during the entire season is still limited. Understanding of ecosystem dynamics, including the end-to-end food web with energy transfer and material cycling coupled with physical and chemical processes, is required. Development of ecological models to understand and predict future conditions is also necessary to protect the natural resources and to recover ecological services. Long-term observations of large spatial coverage is necessary, and the development of molecular methods as well as other new technologies are expected. Finally, international collaboration between the countries surrounding these seas under an international body such as PICES is very important.

Joji Ishizaka

3.1 Pelagic Microbial Food Web

Wuchang Zhang[1], Chung Yeon Hwang[2], Hiroshi Koshikawa[3], Jae Hoon Noh[4] and Yuan Zhao[1]

[1] Institute of Oceanology, Chinese Academy of Sciences, China
[2] Seoul National University, Korea
[3] National Institute for Environmental Studies, Japan
[4] Korea Institute of Ocean Science and Technology, Korea

3.1.1 Introduction

The microbial food web includes small organisms such as viruses, heterotrophic bacteria and autotrophic bacteria (*Synechococcus* and *Prochlorococcus*), picoeukaryotes, and heterotrophic flagellates and ciliates (Fig. 3.1.1). In the 1990s, researchers in Asia began to pay attention to those organisms due to the notion of the "microbial loop" (Azam *et al*., 1983) and "microbial food web". Methodological developments and field studies on marine viruses and bacteria were conducted in Japan during that same period (Hara *et al*., 1991; Fukuda *et al*., 1998). Korean scientists took bacteria and bacterivores into consideration in understanding microbial ecology (Cho *et al*., 1994; Shim *et al*., 1995), and later added viruses as a member of the microbial loop in domestic studies (Hwang and Cho, 2002a,b). Microbial food web research was initiated in the scope of Chinese GLOBEC project in the Bohai Sea, Yellow Sea and East China Sea (Tang *et al*., 1996).

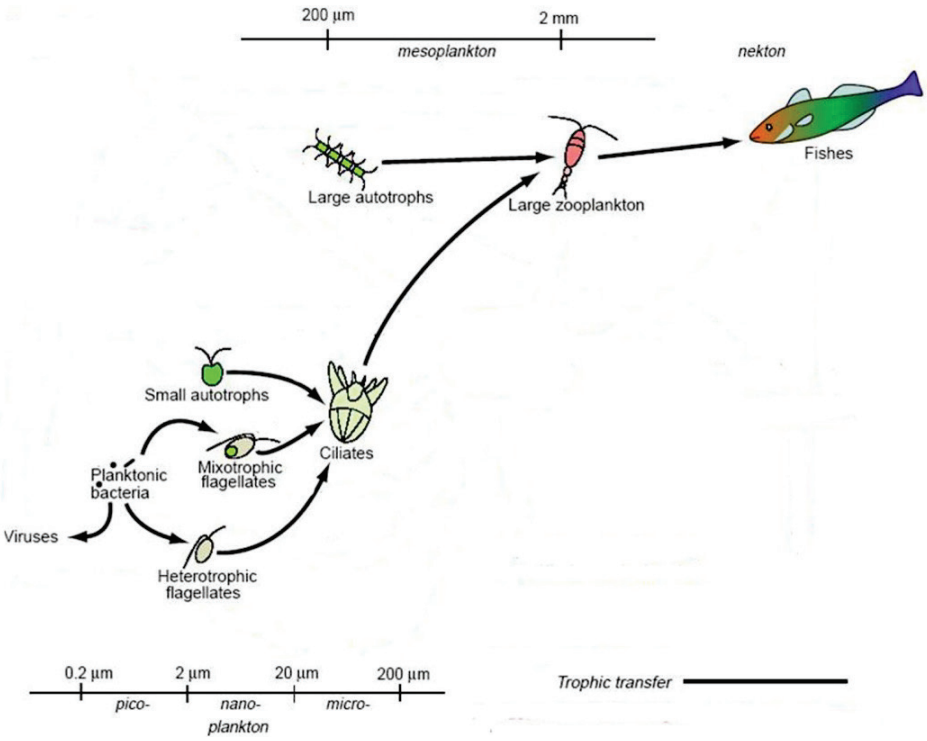

Fig. 3.1.1 Microbial food web and classical food chain. Adapted from Stenseth *et al*., (2004).

There are studies on the abundance and biomass distribution, growth or grazing rates of microbial organisms in the Yellow Sea and East China Sea, but seasonal or annual variation has been scarcely reported. In this section, we present a synoptic review on these topics. It is hard to synthesize the general characteristics of microbial distributions and the dominant factors influencing them. Making comparisons between the different seas is almost impossible because we do not even know the seasonal variation in each area. As a result, we could not identity whether the difference is a spatial difference or simply a result of phenology.

3.1.2 Virioplankton

In Bohai Sea, the virioplankton abundance was investigated by flow cytometry. The abundance of virioplankton ranged from 6.40 × 10^5 to 3.59 × 10^7 particles/mL in the four seasons under investigation (Wang *et al.*, 2013). In summer, the abundance of virioplankton was significantly higher than in the other seasons. In summer, there was a significant abundance difference between the surface and bottom layer. However, no vertical abundance difference was found in the other three seasons. Diel abundance fluctuation was obvious in summer. Virioplankton abundance was closely correlated with heterotrophic bacteria, picophytoplankton, and temperature.

In the northern Yellow Sea, the distribution and daily variation of virioplankton was determined by epifluorescence microscopy in summer (Bai *et al.*, 2008). The abundance of virioplankton ranged from 1.58 × 10^6 to 1.38 × 10^7 particles/mL, with a mean abundance of 5.86 × 10^6 particles/mL. Virioplankton was more abundant in the offshore than in other areas (Fig. 3.1.2). High virioplankton abundance was found at the surface, 30 m and bottom layers near Liaodong Peninsula. Vertically, virioplankton abundance was higher at surface than at the 30 m layer and bottom. The diel abundance fluctuation was more significant at surface layer than at the 10 m and 30 m layers. According to multi-correlation analysis, virioplankton abundance was negatively correlated with depth and salinity. No significant correlation was found between virioplankton abundance and water temperature.

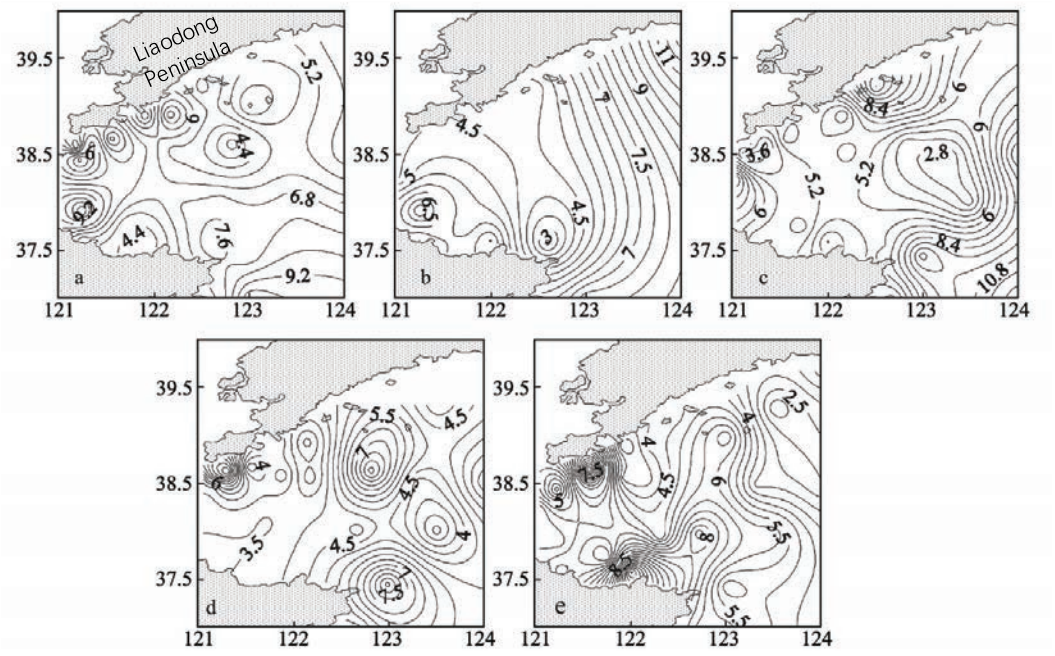

Fig. 3.1.2 Virioplankton abundance (×10^6 particles/mL) in summer in the northern Yellow Sea; a. surface layer; b. 5 m layer; c. 10 m layer; d. 30 m layer; e. bottom layer. From Bai *et al*. (2008).

In the northwestern part of the Yellow Sea, the abundance of virioplankton was (0.67 ± 0.95) × 10^6 particles/mL, ranging from 0.03 to 4.41 × 10^6 particles/mL in spring. In autumn, the abundance of virioplankton was (0.31 ± 0.28) × 10^6 particles/mL, ranging from 0.02 to 1.58 × 10^6 particles/mL (Shi *et al*., 2009). Virioplankton was more abundant inshore and gradually declined toward the offshore. In both spring and autumn, the abundance of virioplankton was higher at the surface layer than at the bottom. In spring, virioplankton abundance was negatively correlated with salinity. No correlation was found between virioplankton abundance and environmental factors in autumn.

Viral production and bacterial mortality due to viral lysis (BMVL) are important parameters in understanding biogeochemical cycles in marine microbial ecology (Fuhrman, 1999). Viruses are generally produced by rupturing host cells, which leads to the conversion of particulate organic matter into dissolved organic matter. However, information on viral activity is still rare in the Yellow Sea. Measurements of BMVL for surface samples obtained from a coastal site on the Korean Peninsula indicate that approximately 30% of bacterial populations in summer are subjected to viral lysis during a turnover time of the bacterial populations (Hwang and Cho, 2008). Spatial and seasonal changes of viral impacts on bacterial mortality need to be investigated further to enhance an understanding of the ecological roles of viruses.

In the Changjiang (Yangtze River) Estuary and adjacent coastal waters, virioplankton abundance was investigated with flow cytometry (Jiao *et al*., 2006; Pan *et al*., 2007; Li and Li, 2012) and epifluorescence microscopy (Bai *et al*., 2007; Liu *et al*., 2011) in different seasons. The dynamics of viruses in the Changjiang Estuary is characterized by distinct seasonal and spatial variations due to natural forcing and anthropogenic impacts (Jiao *et al*., 2006). Total viral abundance over various investigations fluctuated between 0.49 to 99.7 × 10^6 particles/mL. Seasonally, the abundance peak values were recorded in the summer and winter. The summer viral abundance peak was coupled with the development of bacterial hosts which were controlled largely by temperature year-round and by trophic state occasionally. The high winter viral abundance was mostly contributed to by high virus-containing freshwater discharge in winter due to a higher proportion of anthropogenic sewage relative to low natural flooding in winter run-off (Jiao *et al*., 2006).

In the East China Sea, the abundance of virioplankton was also investigated along the Kuroshio Current and adjacent area. The abundance of virioplankton ranged from 0.34 to 2.3 × 10^6 particles/mL (Yang and Jiao, 2002). In the Kuroshio Current water, virioplankton exhibited lower abundance than in the shelf water. Virioplankton abundance was positively correlated to heterotrophic bacteria, *Synechococcus*, and picoeukaryotes, but negatively correlated with *Prochlorococcus*. There was no significant correlation with chlorophyll *a* (Chl-*a*) concentration.

3.1.3 Heterotrophic bacteria

In the Bohai Sea, the abundance of heterotrophic bacteria enumerated with DAPI (4',6-diamidino-2-phenylindole) staining and epifluorescence microscopy varied from 5.57 × 10^3 cells/mL to 1.78 × 10^5 cells/mL from April to May. The abundance of bacteria was higher on the bottom than at the surface, with average abundance of 5.54 × 10^4 cells/mL and 3.47 × 10^4 cells/mL, respectively (Bai *et al*., 2003). Enumerated with flow cytometry, the abundance of bacteria ranged from 3.51 × 10^5 to 5.15 × 10^6 cells/mL in winter, and from 5.09 × 10^5 to 3.44 × 10^7 cells/mL in summer. The average bacteria abundance was markedly lower in winter (1.84 × 10^6 cells/mL) than in summer (5.05 × 10^6 cells/mL). High abundance of bacteria was observed around the Yellow River Estuary, and decreased towards the Bohai Strait (Bai *et al*., 2003). Vertically, bacteria abundance was slightly higher (~1.17 times) in the bottom than in the surface waters in winter. Conversely, in summer the surface bacteria abundance was higher (~1.14 times) than in the bottom layer (Fig. 3.1.3).

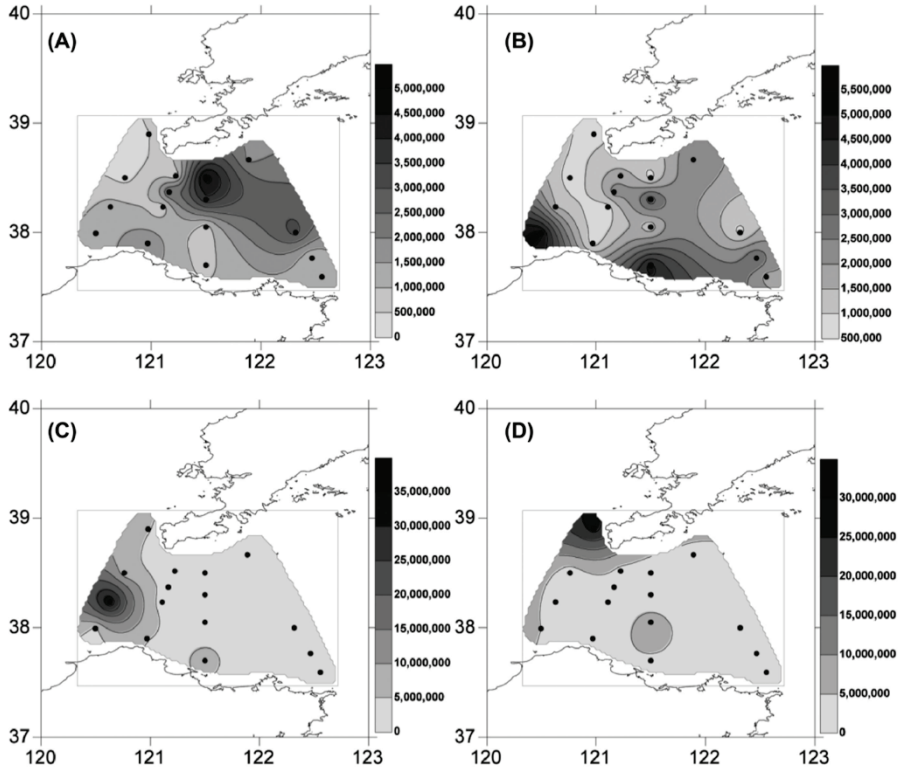

Fig. 3.1.3 Horizontal distribution of heterotrophic bacteria abundance (cells/mL) in the Bohai Strait in winter 2013 and summer 2014. (A) surface, winter; (B) bottom, winter; (C) surface, summer; (D) bottom, summer. From Wang *et al*. (2016). Reproduced with permission of Oxford University Press.

In the Bohai Strait, the abundance of bacteria was closely correlated with the concentration of dissolved organic carbon (DOC), water temperature and dissolved oxygen. In the bottom layer, bacteria abundance was also closely correlated with the concentrations of particulate organic carbon (POC). The main limiting factors to the number of bacterioplankton were the contents of DOC and POC, as well as the water temperature in the Bohai Strait in spring (Bai *et al*., 2003). Bacterial production (BP) is higher in autumn [125.5 mg/(m^2·d)] than spring [115 mg/(m^2·d)]. In autumn, the vertical distribution of BP was higher in the bottom layer, while in spring BP was greater in the surface layer (Xiao and Wang, 2003).

In the northern Yellow Sea, the abundance of bacteria ranged from 1.91×10^5 cells/mL to 5.33×10^6 cells/mL, with average abundance of $1.64 \pm 0.32 \times 10^6$ cells/mL in summer. High abundance of bacteria was observed in the near-shore regions off Liaodong Peninsula. Vertically, high abundance of bacteria mostly occurred in the 10 m layer, and the minimum values occurred mainly at the bottom (Bai *et al*., 2012). In southern Yellow Sea, bacteria abundance was at lower level in winter, with minimum average abundance of 4.1×10^5 cells/mL. From spring to summer, the abundance of bacteria increased along with the water temperature. The highest bacteria abundance was recorded in autumn, with average abundance of 8.9×10^5 cells/mL. High abundance of bacteria was observed around the central area of the southern Yellow Sea (Fig. 3.1.4). Seasonally, high concentrations of heterotrophic bacteria (>7×10^5 cells/mL) were found from late spring (May) to autumn (September, October). During the cold season (from winter to mid-spring, *i.e*., December to April), when the water temperature was lower, relatively few heterotrophic bacteria were present in the water column (Fig. 3.1.5). A positive relationship between average sea surface temperature and log average bacteria abundance was found in the southern Yellow Sea, suggesting a positive influence of temperature on the bacteria abundance (Zhao *et al*., 2011).

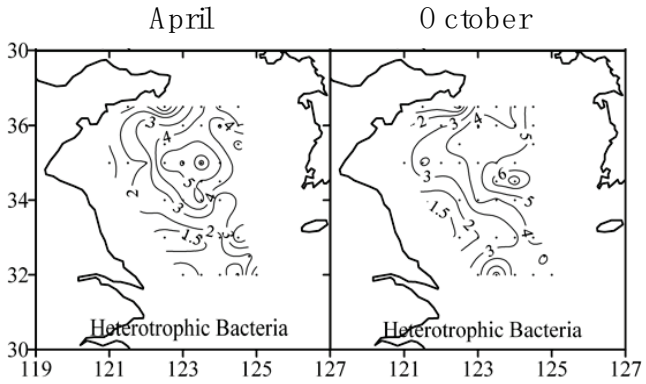

Fig. 3.1.4 Integrated cell abundance for heterotrophic bacteria ($\times 10^{13}$ cells/m^2) in April and October 2006 in the southern Yellow Sea. From Zhao *et al*. (2011). Reproduced with permission of Springer Nature.

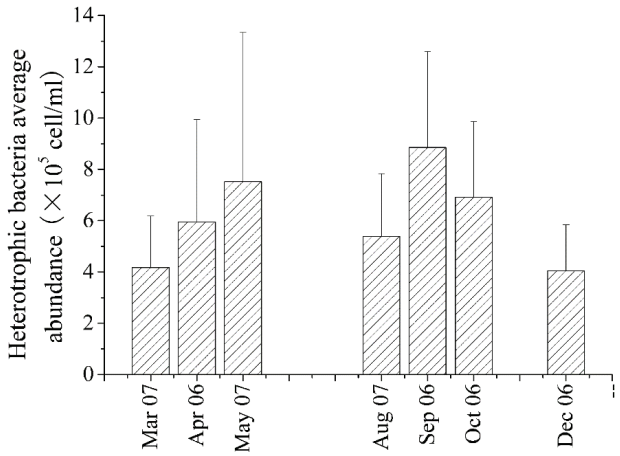

Fig. 3.1.5 Average abundance of heterotrophic bacteria ($\times 10^5$ cells/mL) in different seasons in the southern Yellow Sea. From Zhao *et al*. (2011). Reproduced with permission of Springer Nature.

The Yellow Sea Cold Water Mass (YSCWM) forms locally during the previous winter owing to surface cooling and strong vertical mixing. The distribution of heterotrophic bacteria is correlated with temperature and salinity, and the minimum distribution of heterotrophic bacteria occurs in the YSCWM waters (Li *et al*., 2006; Zhao *et al*., 2011; Bai *et al*., 2012). A tidal front is a significant physical phenomenon in the coastal waters of the Yellow Sea. Seasonally thermal stratification forms at the end of spring. The maximal abundance of bacteria occurs in both stratified and mixed zone. High abundance of bacteria does not necessarily couple with the front- associated Chl-*a* maximum, suggesting that the bacteria depend mainly on particles and dissolved organic matter brought into the sea by water run-off from land (Li *et al*., 2007).

Another study in the tidal front region in the Yellow Sea found notably that physical properties such as turbulent mixing and water temperature are important in regulating major energy pathways associated with bacteria and phytoplankton (Cho *et al*., 2001). The ratios of BP to primary production (PP), a parameter for estimating energy pathways on microbial food webs, revealed a significantly positive relationship with sea surface temperature (SST), but a significantly negative relationship with *f*-ratio (*i.e*., a fraction of total PP fueled by nitrate). These relationships are attributed to different hydrographic regimes in a euphotic zone, subsequently changing a dependency of the nitrogen source for phytoplankton. The new finding that SST may largely explain

the variations of BP/PP ratios is not a unique phenomenon in a local sea, but also was confirmed in an ocean-scale study in the Atlantic Ocean (Hoppe *et al*., 2002). In addition, the microbial ecological relationship between SST and BP/PP ratio has been successfully applied to evaluate environmental disturbance in dumping areas in the east of Korea (Choi *et al*., 2005).

During phytoplankton blooms in the southern Yellow Sea, enhanced bacterial abundance, biomass, production, and turnover rates were observed in the bloom area. The variation of abundance followed that of Chl-*a* concentration, but not with temperature (Hyun and Kim, 2003; Zhao, Y. *et al*., 2013). These results indicate that resource supply from phytoplankton primarily stimulates bacterial growth. Higher bacterial growth but smaller increases in bacterial biomass indicates that bacterial growth and biomass are independently controlled during the spring bloom in the central Yellow Sea, in which bacterial growth is primarily stimulated by organic material produced from the phytoplankton bloom, but the enhanced biomass is more tightly controlled by grazing (Hyun and Kim, 2003). In another study, diatom blooms were observed in the mouth of the Yellow Sea. The blooms occurred in the inner bay and in waters outside of a tidally induced turbidity maximum. Bacterial and phytoplankton variables were not correlated significantly with each other. The uncoupling appeared to be unrelated to phytoplankton community structure. Strong tidal mixing seemed to cause low substrates level and unbalanced growth for bacteria in the euphotic zone and thereby the observed uncoupling of bacteria from phytoplankton (Cho *et al*., 1994).

In the East China Sea, heterotrophic bacteria were ubiquitous, with average abundances of about 1.00–1.39 × 10^6 cells/mL (Pan *et al*., 2007a; Li and Li, 2012). The abundance and biomass of bacteria decreased distinctly in offshore directions (Fig. 3.1.6). Bacteria were most abundant in the plume area where nutrients were replete and DOC resources were rich although light availability was low, with depth-weighted average cell abundance reaching a level of 1.2 × 10^6 cells/mL (Jiao *et al*., 2002). The biomass of bacteria was positively correlated with the sum of that of *Synechococcus* and picoeukaryotes in the study area out of the estuary (Jiao *et al*., 2002; Li and Li 2012), while it was negatively correlated with that of *Prochlorococcus* (Jiao *et al*., 2002). The inverse relationship between the two seems to be a feature of the transitional zones between oligotrophic and eutrophic regimes (Jiao *et al*., 2002).

In an East China Sea survey, the cruises crossed three major water masses: the coastal water mass (CWM), the mixed water mass (MWM), which forms on the continental shelf, and the Kuroshio water mass (KWM). Depth-averaged integrated abundance of heterotrophic bacteria exhibited a small seasonal variation with respect to water mass (Zhao, L. *et al*., 2013). In autumn, the maximum abundance of heterotrophic bacteria in surface waters and the maximum concentration of surface Chl-*a* were observed in the MWM, but they did not overlap. In winter, both distributions showed maximum levels that overlap close to the central region of the study area (encompassing the intrusion of the CWM inside MWM) and the KWM, which expanded westward. The difference in non-overlapping and overlapping situations could be linked to differences in phytoplankton development dynamics; a lower rate in winter would help bacteria development catch up with phytoplankton development (Zhao, L. *et al*., 2013).

In the southern East China Sea during spring and fall, integrated bacterial biomass (IBB; 350–1200 mgC/m^2), integrated bacterial production [IBP; 28–329 mgC/(m^2·d)] and averaged turnover rates (μ = IBP/IBB; 0.09–0.22 /d) in the coastal and upwelling areas were at least 2-fold of those in the Kuroshio waters. IBB, IBP and μ were positively correlated with PP and POC, but showed a negative trend with temperature in the outer shelf area. The spatial patterns of IBB, IBP and μ were more likely to be controlled by substrate supply and temperature interactively. Under the assumption of a growth efficiency of 20%, shelf bacteria might consume carbon equivalent to almost 100% of the *in situ* daily particulate primary production. DOC from non-phytoplankton and allochthonous sources might play a significant role in supporting bacterial carbon demand in the shelf area of the East China Sea (Shiah *et al*., 2000).

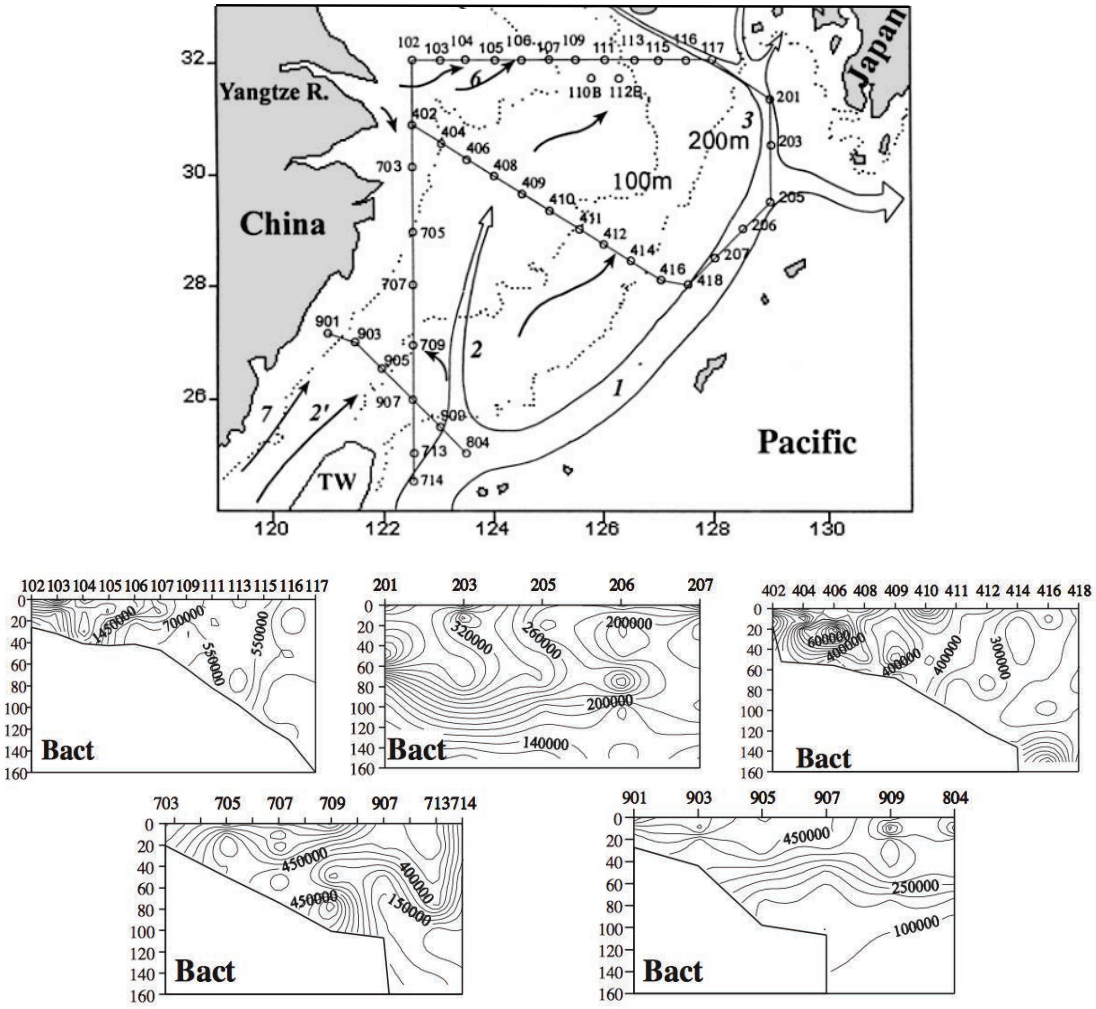

Fig. 3.1.6 Vertical distribution of heterotrophic bacteria (Bact, cells/mL) along transects in the East China Sea. From Jiao *et al*. (2002). Reproduced with permission of Inter-Research Science.

The bacteria distribution in the East China Sea was investigated during bloom (Chl-*a* concentration of >10 μg/L) events occurring in spring (June) and summer (August) 2011. In spring, there was no significant difference in bacteria abundances between areas where bloom conditions were or were not established. In the bloom area, bacteria exhibited higher abundance than in the non-bloom area at only some stations. Among the picoplankton components, heterotrophic prokaryotes represented the highest carbon biomass. Factors that most influenced bacteria distribution under bloom conditions varied with season. In spring, ciliates tended to be the main factor, whereas in summer, this role was played by Chl-*a* concentration as revealed by multiple stepwise regression analyses (Zhao *et al*., 2016).

3.1.4 Picophytoplankton

Cyanobacteria *Synechococcus* in the Bohai Sea were measured by epifluorescence microscopy in autumn (September to October 1998) and spring (April to May 1999). *Synechococcus* biomass was higher in autumn than in spring, with average biomass of 3.27 mgC/m^3 and 0.13 mgC/m^3, respectively. In spring, high *Synechococcus* biomass was found near Laizhou Bay and Dalian City, and the vertical distribution patterns were 10 m > surface > bottom. In autumn, *Synechococcus* biomass was minimum in the central Bohai Sea. Sea water temperature was an important factor

affecting the seasonal variations of *Synechococcus*. The cyanobacterial population was grazed by microzooplankton (Xiao and Wang, 2002).

From July 2006 to October 2007, the picophytoplankton (0.2–2 μm) abundance were enumerated seasonally in coastal area of the Bohai Sea. The average abundance of cyanobacteria *Synechococcus* was 4.46 × 10^3 cells/mL (0.79–16.19 × 10^3 cells/mL); the average biomass was 1.31 mgC/m^3 (0.84–17.47 mgC/m^3). The seasonal variation of *Synechococcus* was autumn > winter > summer > spring. Picoeukaryotes abundance ranged from 0.84–17.47 × 10^2 cells/mL (on average 4.43 × 10^2 cells/mL), and biomass was 0.21–4.37 mgC/m^3 (on average 1.11 mgC/m^3). The seasonal variation of picoeukaryotes was autumn > winter > spring > summer. The contribution of picophytplankton to total phytoplankton biomass was from 1.84–8.91% (average 5.32%), which was lower than in offshore and oligotrophic water. In the colder season, low temperature was an important factor limiting the growth and distribution of picophytoplankton (Li *et al*., 2012).

In the northern Yellow Sea, flow cytometry analysis revealed spatial heterogeneity in picophytoplankton populations in the offshore and near-shore waters during the summer. Total abundance of picophytoplankton varied greatly among stations, which ranged from 1.03 × 10^3 to 2.95 × 10^5 cells/mL, with a mean of 5.59 ± 1.04 × 10^4 cells/mL. *Synechococcus* abundance 49.4 ± 14.3 × 10^3 cells/mL was about one order of magnitude higher than picoeukaryotes abundance 6.49 ± 1.46 × 10^3 cells/mL, which accounted for the overwhelming majority of picophytoplankton in summer in the northern Yellow Sea (Fig. 3.1.7). The abundance of *Synechococcus* in surface waters was high in the offshore water and low in the near-shore water (Fig. 3.1.7). In contrast, high numbers of picoeukaryotes were found in the near-shore water, but they were less abundant in the offshore water (Fig. 3.1.7; Bai *et al*., 2012).

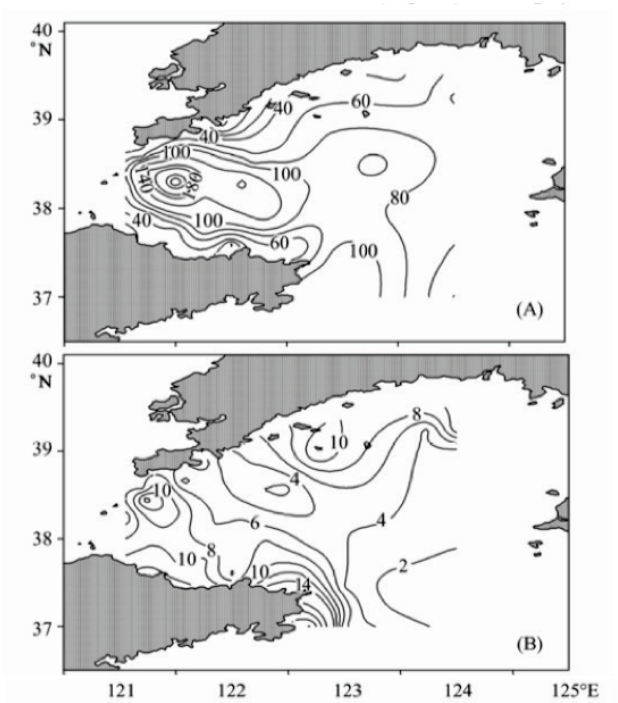

Fig. 3.1.7 Picophytoplankton abundance (×10^3 cells/mL) in the surface water of the northern Yellow Sea in summer. (A) *Synechococcus*; (B) Picoeukaryotes. From Bai *et al*. (2012). Reproduced with permission of Springer Nature.

In the southern Yellow Sea, *Synechococcus* abundance was minimum in spring, with an average of 4.0 × 10^3 cells/mL (range 0.3–25.2 × 10^3 cells/mL) in April. From summer to autumn, *Synechococcus* had high average abundance of 32.9–54.2 × 10^3 cells/mL, with a maximum value occurring in October. In winter, *Synechococcus* abundance dropped to 9.2 × 10^3 cells/mL. The seasonal variation of picoeukaryotes was quite different from *Synechococcus*. Picoeukaryotes average abundance was high in spring (2.9–8.0 × 10^3 cells/mL), with maximum abundance occurring in May. From summer to winter, picoeukaryotes abundance was at a low level (1.4–2.7 × 10^3 cells/mL), with little seasonal variation (Fig. 3.1.8). Spatially, a high value of *Synechococcus* was observed in the northeastern area, while in coastal waters near the Chinese mainland, relatively few *Synechococcus* were present in the water column. Picoeukaryotes were homogeneously distributed over the entire study area except in a small frontal zone in the coastal area on the western (in spring) and central Yellow Sea (in autumn) (Fig. 3.1.9). A positive relationship between average SST and log average *Synechococcus* abundance was found, suggesting a positive influence of temperature. However, population abundance of picoeukaryotes was negatively affected by temperature, indicating a different control mechanism (Zhao *et al*., 2011).

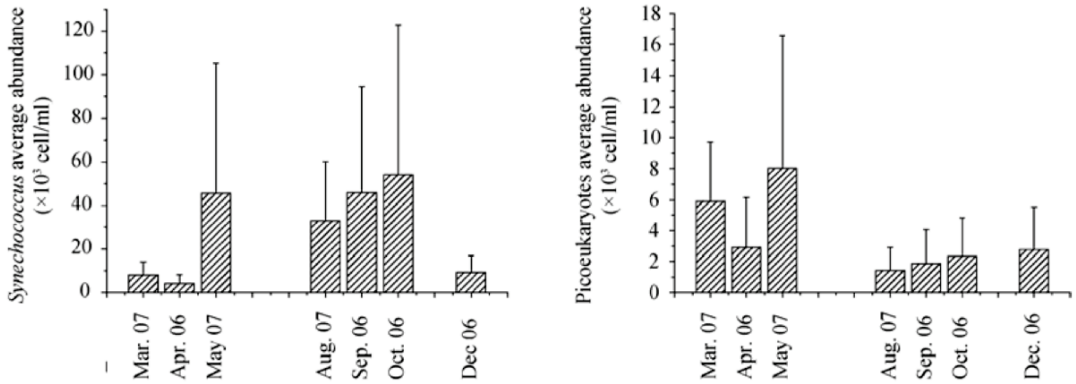

Fig. 3.1.8 Averaged cell abundance for *Synechococcus* and picoeukaryotes (×10^3 cells/mL) in different seasons. From Zhao *et al*. (2011). Reproduced with permission of Springer Nature.

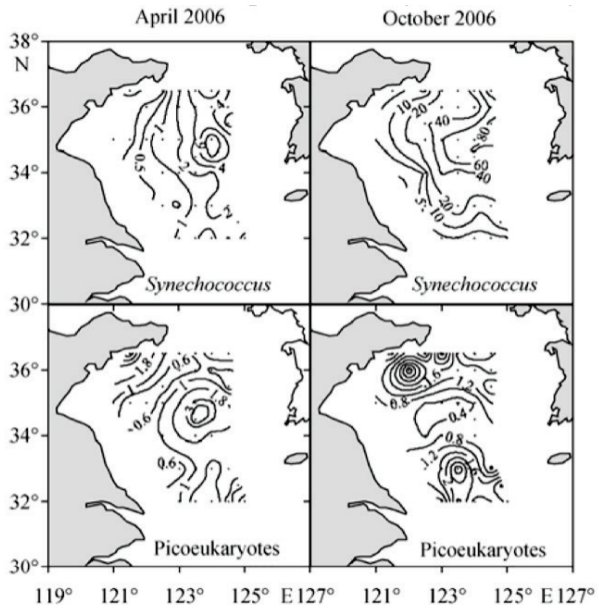

Fig. 3.1.9 Integrated cell abundance (×10^{11} cells/m^2) for *Synechococcus* and picoeukaryotes in April and October 2006. From Zhao *et al*. (2011). Reproduced with permission of Springer Nature.

In the offshore waters of the northern Yellow Sea, *Synechococcus* and picoeukaryote abundance in the upper layer was significantly higher than in the 30 m and bottom layers. It decreased sharply (up to one to two orders of magnitude) in the water columns deeper than 30 m at the offshore stations, which were located in the YSCWM. In contrast, in near-shore waters, picophytoplankton abundance showed no vertical variation (Bai *et al*., 2012). In the southern Yellow Sea, along the vertical direction, the main distribution order of *Synechococcus* abundance was surface > mid-layer > bottom zone, whether inside or out of the YSCWM. Picoeukaryote biomass was also lower in the YSCWM, but the vertical distribution pattern was mid-layer > surface > bottom zone (Zhao *et al*., 2011).These results showed picophytoplankton were sensitive to environmental changes. In the Yellow Sea, tidal fronts have steep horizontal gradients of density caused by turbulent mixing driven by tidal currents over shallow areas. High *Synechococcus* abundance distributed more often in the frontal area and middle-surface layer of a stratified zone (Li *et al*., 2007).

Temporal variation of *Synechococcus* and picoeukaryote abundance and depth-integrated biomass during three spring blooms in 2007 and 2009 were investigated in the Yellow Sea. *Synechococcus* and picoeukaryotes responded differently to different types and courses of spring blooms. During the diatom blooms of 2007 and at Station B20 (35.9°N, 123.0°E) in 2009, *Synechococcus* and picoeukaryote abundance decreased sharply during the bloom period. However, during a mixed dinoflagellate and diatom bloom at Station B23 (35.5°N, 124.0°E) in 2009, *Synechococcus* and picoeukaryotes increased in abundance and biomass with the development of the bloom. Ciliates and heterotrophic nanoflagellates grazing could be responsible for the *Synechococcus* and picoeukaryote abundance and biomass decrease during bloom periods (Zhao, Y. *et al*., 2013).

Prochlorococcus distributed ubiquitously from the surface to the bottom of the euphotic zone in the ocean between 40°N and 40°S. *Prochlorococcus* is present in most of the East China Sea. The coastward distribution boundary in the East China Sea is around the 50-m isobath in summer (Fig. 3.1.10, dashed line a), but back to the Kuroshio Current and adjacent waters in winter (Fig. 3.1.10, dashed line b). Abundance of *Prochlorococcus* changed significantly in different regions of the East China Sea with a general pattern of increasing in the offshore directions. In the shelf waters of the East China Sea, vertical distribution of *Prochlorococcus* could reach 50–100 m depth, whereas in the Kuroshio Current, *Prochlorococcus* was observed down to 150 m (Jiao and Yang, 2002).

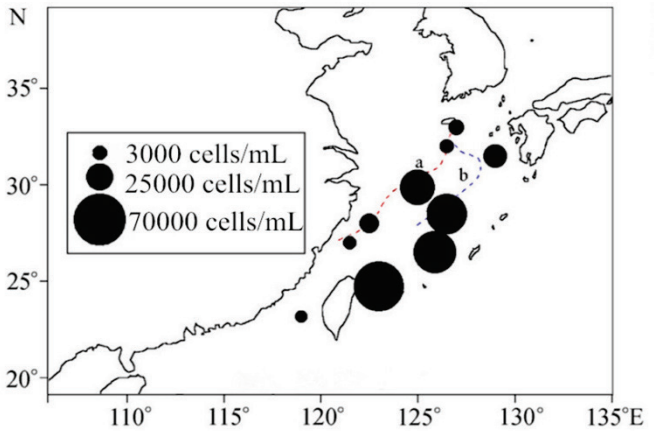

Fig. 3.1.10 Distribution of *Prochlorococcus* in the China seas (averaged depth-integrated cell abundance). Red dashed line a, summer distribution boundary; blue dashed line b, winter distribution boundary. Adapted from Jiao and Yang (2002).

In the northern East China Sea, temporal and spatial distribution of picophytoplankton abundance was investigated using flow cytometry with environmental factors in all seasons of May, August, and November 2010 and February 2012 (Fig 3.1.11; Lee *et al*., 2014). *Synechococcus* was the predominant group in the picophytoplankton abundance in all seasons, indicating its ecological importance as a primary producer in the northern East China Sea. In winter, *Synechococcus* abundance was low at 2.4 ± 1.0 × 10^3 cells/mL, but high in summer at 209.4 ± 163.9 × 10^3 cells/mL (Fig. 3.1.12a). Picoeukaryote abundance was relatively lower than *Synechococcus* abundance, ranging from 0.4 ± 0.4 × 10^3cells/mL in summer to 7.6 ± 8.9 × 10^3 cells/mL in spring (Fig. 3.1.12b). However, picoeukaryotes contributed significantly to the total picophytoplankton carbon biomass in spring and winter due to their larger size among picophytoplankton groups. *Prochlorococcus* was detected in the eastern side of the study area during autumn and winter but not during spring and summer, indicating the possible effect of the low Kuroshio intrusion on the northern East China Sea in late spring and intrusion of Changjiang diluted water in summer (Fig. 12c). This study showed that the distributions of these picophytoplanktons are strongly influenced by the seasonal fluctuations of the Changjiang discharges and Kuroshio intrusion in the northern East China Sea.

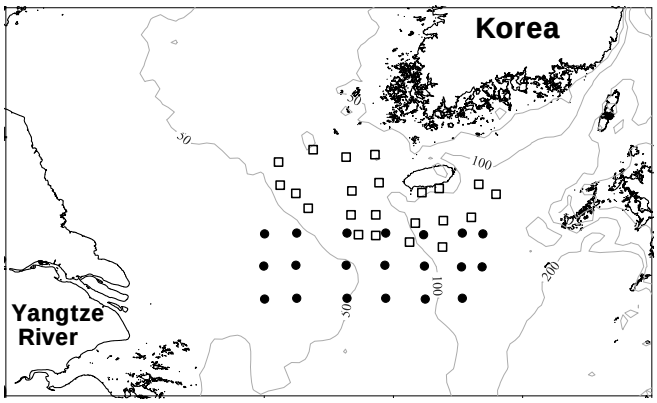

Fig. 3.1.11 Sampling stations in the East China Sea (● stations from May, August, and February cruises, □ stations from November cruise). From Lee *et al*. (2014).

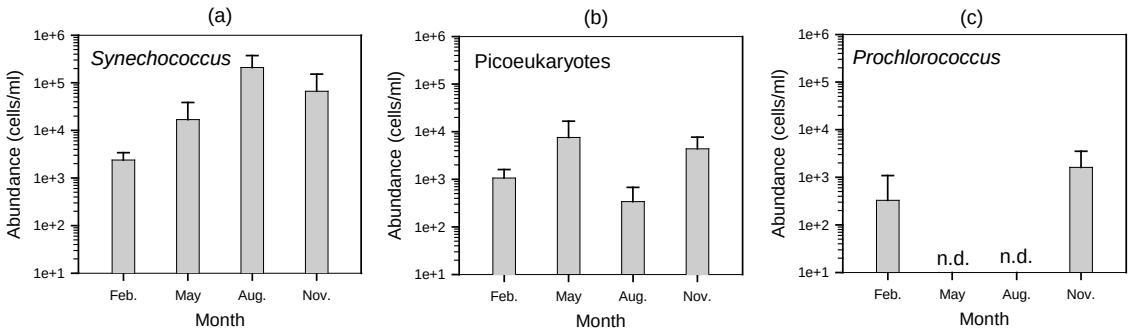

Fig. 3.1.12 Seasonal variation of picophytoplankton abundances. (a) *Synechococcus*; (b) Picoeukaryote; (c) *Prochlorococcus*. Figures were drawn from the data in Lee *et al*. (2014) provided by the main author. Note that stations in November are different from stations in other months. n.d. denotes no data (no studies in May and August).

In the continental shelf region of the northern East China Sea (125.10°E, 32.07°N), *Synechococcus* abundance varied by up to three orders of magnitude across seasons (Fig 3.1.13a). In February, *Synechococcus* abundance was extremely low, 0.07×10^4 cells/mL; the abundance then showed a sharp increase and peaked between late spring and autumn. *Synechococcus* diversity also showed seasonal variations. The coastal and cold water-adapted *Synechococcus* Clades 5.1-I and 5.1-IV were dominant during winter and spring, whereas the warm water-adapted *Synechococcus* Clade 5.1-II was dominant during summer and autumn (Fig. 3.1.13b). *Prochlorococcus* was not detected in this region, suggesting that their growth appears to be inhibited in shallow shelf waters and/or inhibited by the low salinity effect of Changjiang diluted waters.

Temperature is a good predictor for the relative seasonal change in *Synechococcus* abundance (Tsai *et al*., 2013b). The horizontal distribution of *Synechococcus* abundance showed pronounced seasonal changes with the effect of different water masses. From winter to early spring when temperature is low, few *Synechococcus* ($1–5 \times 10^{11}$ cells/m^2) existed in the water column, and the population distributed homogeneously over the entire continental shelf, except for a high front located to the north side of East China Sea in winter (Fig. 3.1.14A), which may have been driven by intrusions of the YSCWM. *Synechococcus* abundance increased in late spring (Fig. 3.1.14B). When the average temperature was over 20°C, more than 10×10^{11} cells/m^2 were observed at the Shelf Mixing Water (Fig. 3.1.14C). This represents an approximately 10-fold increase over the winter low abundance. In summer, *Synechococcus* abundance increased further to over 25×10^{11} cells/m^2, with a high-density area ($>25 \times 10^{11}$ cells/m^2) in the center of the East China Sea and lower densities ($<10 \times 10^{11}$ cells/m^2) in the coastal and Kuroshio waters. In autumn, *Synechococcus* abundance remained high, with a maximum of 70×10^{11} cells/m^2, and increased from the inner shelf to the outer shelf (Fig. 3.1.14E). The average carbon biomass of *Synechococcus* in the East China Sea ranged from 0.09 (early spring) to 0.90 C/m^2 (autumn). *Synechococcus* is a major contributor to the seasonal variation of phytoplankton in the East China Sea, accounting for less than 25% of the total photosynthetic plankton in the cold season and about 50% in the warm season (Chiang *et al*., 2002).

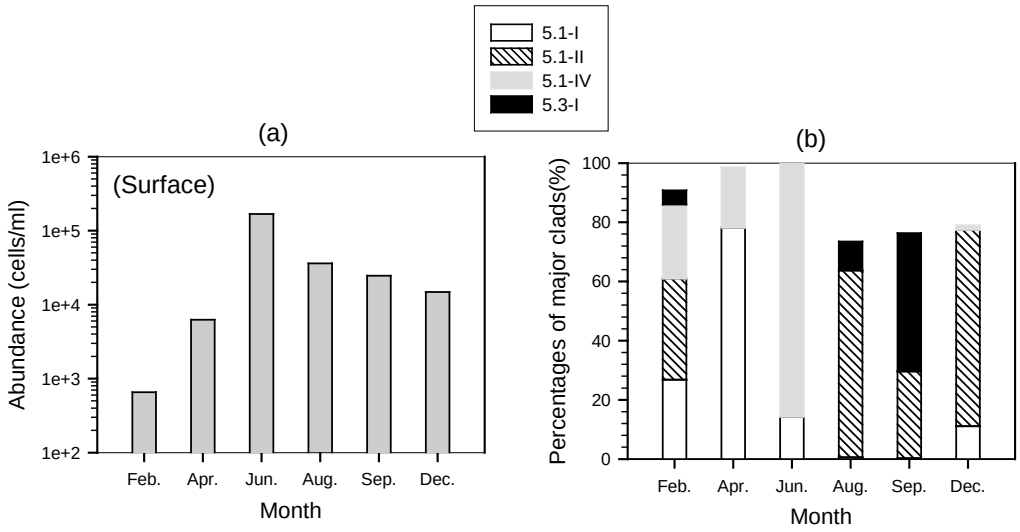

Fig. 3.1.13 (a) Seasonal variation of *Synechococcus* abundance at the surface and (b) relative percentage of clades in each sample. Figures redrawn using the data from station H6 from Tables 1 and 2 from Choi *et al*. (2013). Data are from 6 research cruises conducted between 2008–2011.

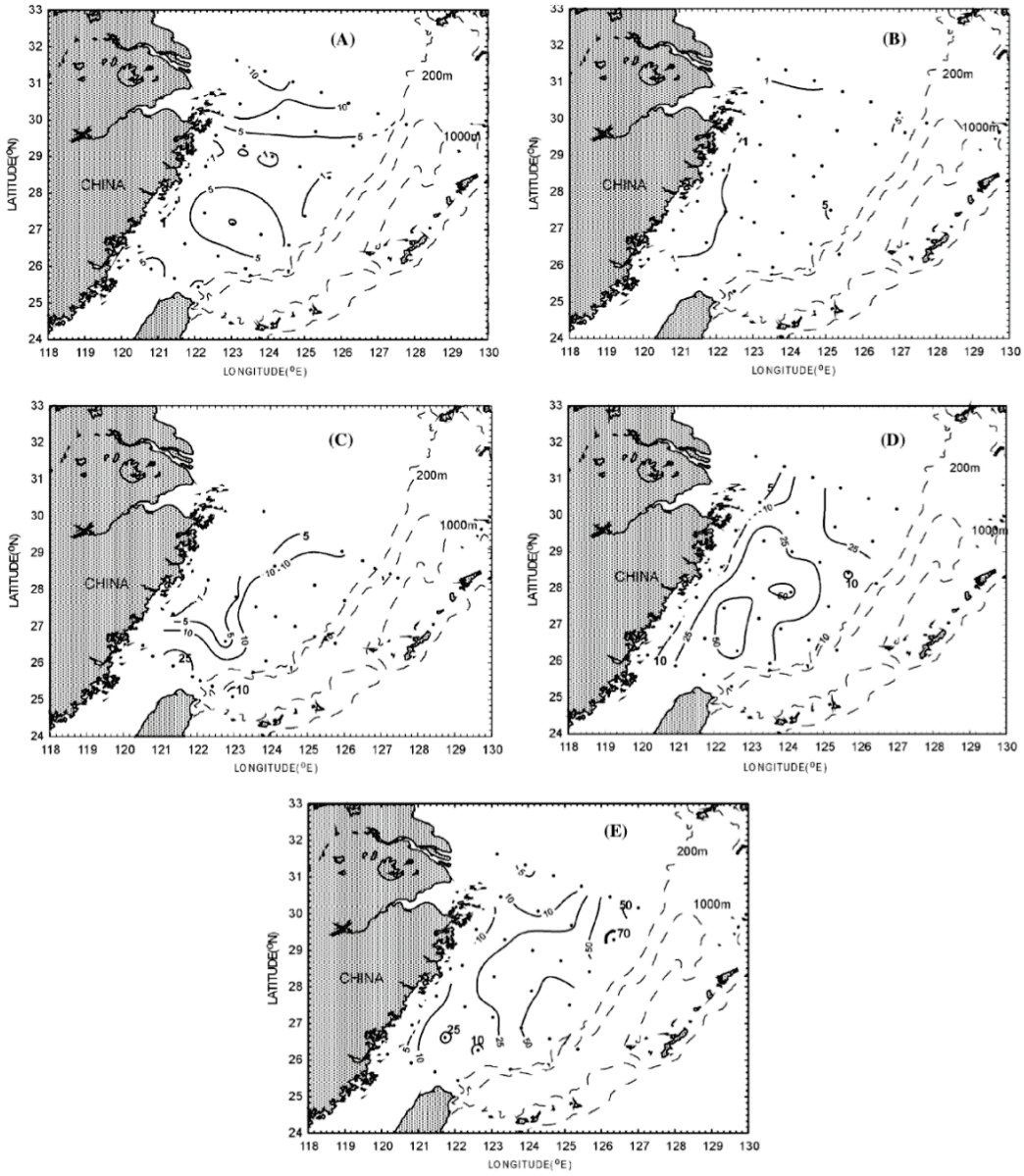

Fig. 3.1.14 Horizontal distribution of integrated *Synechococcus* abundance ($\times 10^{11}$ cells/m^2) in the East China Sea. (A) winter (December 1997); (B) early spring (March 1998); (C) late spring (May 1996); (D) summer (June 1998) and (E) autumn (October 1998). From Chiang *et al*. (2002). Reproduced with permission of Elsevier.

The influences of sudden environmental changes on *Synechococcus* assemblage composition were also investigated. The injection of abundant anthropogenic pollutants, and the enhancement of transparency within the Changjiang River diluted water expansion area after flooding appear to alter the ecology of *Synechococcus*. During the non-flooding summer of 2009, phycoerythrin-rich (PE-rich) *Synechococcus* thrived near the outer boundary of the Changjiang River diluted water coverage, while phycocyanin-rich (PC-rich) *Synechococcus* predominated inside the turbid diluted water with a transparency of <80%. During the 2010 summer, flooding expanded the Changjiang River diluted water coverage area to over half of the East China Sea. PE-rich cells showed a homogeneous distribution and a decline in abundance, while the spatial pattern of the PC-rich *Synechococcus* resembled the pattern from 2009 (Chung *et al*., 2014).

In summer and winter, the abundance of picoeukaryotes was about 4 $\times 10^3$ cells/mL. Though picoeukaryotes were less abundant compared with *Prochlorococcus* and *Synechococcus*, they still

contributed significantly to picophytoplankton biomass. Picoeukaryotes exhibited very different distribution patterns in different seasons. In summer, the average picoeukaryote abundance decreased from the plume region to the transitional and Kuroshio regions, showing a tendency to distribute in regions with lower salinity and higher nutrient and Chl-*a* concentrations. In winter, average picoeukaryote abundance increased dramatically from the plume region to the transitional and Kuroshio region, which was positively correlated with temperature, salinity and Chl-*a* concentrations, but negatively correlated with nutrient concentrations. The highest abundances of picoeukaryotes occurred at around 10 to 20 m depths in the inshore region and 40 m depth in the offshore the region in summer, while they were highest in the surface in winter (Guo *et al*., 2014).

Picophytoplankton distribution in the East China Sea was investigated during bloom events occurring in spring (June) and summer (August) 2011. In spring, *Synechococcus* and picoeukaryote abundance resolved by flow cytometry exhibited similar vertical distribution patterns along the study transect. No significant difference in *Synechococcus* and picoeukaryote abundance was found between the non-bloom (<10 μg/L) and bloom stations (>10 μg/L). However, during the summer bloom, abundances of *Synechococcus* and picoeukaryotes were significantly higher under bloom than non-bloom conditions. Ciliate grazing and salinity could be the controlling factors of picophytoplankton population variation in spring. In summer, temperature was the most important variable that controlled the abundances and distribution of picophytoplankton (Zhao *et al*., 2016).

3.1.5 Flagellates

In early summer, flagellate abundance in surface waters was higher in the coastal area than in the central part in the Yellow Sea (Huang *et al*., 2003; Ding and Xu, 2012). The vertical distribution pattern varied in different studies. Flagellate abundance in the YSCWM was very high in early summer (Huang *et al*., 2003). However, this phenomenon was not found in October (Lin *et al*., 2014). High abundance of flagellates was also found to occur in both surface and bottom waters in spring and summer (Ding and Xu, 2012). As to the seasonal change, there was a higher percentage of heterotrophic flagellates in summer than in spring (Ding and Xu, 2012).

Abundance, biomass, cell size composition and trophic structure of flagellates dramatically changed with the succession of the spring bloom. Compared with that in the pre-bloom phase, the cell abundance and biomass of flagellates in the water column and deep Chl-*a* maximum increased more than 2-fold in the bloom phase and the post-bloom phase. Flagellates were composed mainly of 2- to 5-μm pigmented nanoflagellates (PNF) whose rapid growth in response to the bloom outbreak characterized the flagellate dynamics in the bloom phase. Heterotrophic nanoflagellates (HNF) showed a rather mild response during the bloom. The 2- to 5-μm fraction decreased during the bloom despite a significant increase of both pigmented and heterotrophic flagellates. In the post-bloom phase, HNF increased while PNF declined. Larger flagellates (5–20 μm) constituted <20% of flagellate abundance in most of the samples. However, their biomass occupied a larger percentage in total biomass (Lin *et al*., 2013).

Water mass had a significant impact on the distribution of flagellates. Either in autumn or in winter, the highest abundance and biomass of flagellates were recorded in the East China Sea Shelf Mixing Water (ECSSMW), and the lowest in the Kuroshio Subsurface Water (KSSW). While in the East China Sea Coastal Water (ECSCW), the abundance and biomass of both HNF and PNF were only slightly higher than that in Taiwan Strait Water (TSW) and Kuroshio Surface Water (KSW). In respect to the seasonal variation, the abundance and biomass of nanoflagellates in TSW declined in winter, while in other four water masses they showed an increasing trend from autumn to winter, mainly due to the decrease (in TSW) or increase (in ECSCW, ECSSMW, KSW and KSSW) of HNF.

The distribution pattern of abundance- or biomass-based PNF/HNF ratio was found to be correlated to the nutrient level of the water mass. Results of Pearson correlation analysis and principal component analysis indicates that PNF was mainly constrained by nutrient supply, and HNF was controlled by food availability (Lin *et al*., 2016).

Changjiang Diluted Water (CDW) could also affect the nanoflagellates distribution. Tsai *et al*. (2010) divided CDW into two different periods: large plume period and small plume period. Nanoflagellate abundance was higher in the large plume period than in the small plume period. During large plume period, high total nanoflagellates abundance occurred in the CDW. The abundance variation was closely related to changes in salinity.

3.1.6 Ciliates

Planktonic ciliate data in the Bohai Sea is very scarce. Typhoons have a significant impact on planktonic ciliates. In the period from 23 September to 7 October, 1998, planktonic ciliates were sampled during two grid station investigations which were six days apart during which time a typhoon swept through the Bohai Sea between the two cruises. Surface ciliate biomass decreased from 0.2–12.3 mg C/m^3 in the first cruise to 0.02–2.8 mg C/m^3 in the second cruise. Water column ciliate biomass also decreased from 2–136 mg C/m^2 to 0.01–47 mg C/m^2. The ratio between ciliate biomass to Chl-*a* concentration decreased from 0.07–4.7 (on average 1.41) to 0.01–1.18 (on average 0.26) (Fig. 3.1.15; Zhang and Wang, 2000a).

In the southern Yellow Sea, ciliates exhibited a seasonal cycle, with two peaks in abundance (May and August) but only one biomass peak (May). Larger ciliates were more prevalent in spring, while smaller ones dominated in the summer. Abundance and biomass of total ciliates were associated with different water masses, which then influenced the entire seasonal pattern in the basin. The YSCWM had an important influence on the distribution of ciliates. High ciliate abundance mainly occurred around a thermal front from December to April. In August through October, low ciliate abundance was observed inside the YSCWM (Yu *et al*., 2014).

In spring, ciliate distribution pattern along the coast of the Shandong Peninsula was coincident with that of the anchovy larva (Zhang *et al*., 2002). Ding and Xu (2012) attributed the low ciliate abundance in some transects in summer to the possible grazing effects by jellyfish, which has been an emerging ecological nuisance recently. During the spring phytoplankton bloom in the central Yellow Sea, high ciliate abundance occurred in the bloom area. In October, there was very low abundance in the central deep area (Zhang *et al*., 2017).

The mixotrophic ciliate *Laboea strobila* also occurred in the Yellow Sea (Zhang *et al*., 2002; Zhang *et al*., 2017). With large size (body length 80–145 μm) and unique spiral body, this species was easily identified. Possibly due to the need of light to photosynthesize, it mainly occurred in the upper 20 m. Abundance as high as 10,000 ind./L was found in the Yellow Sea in spring. Its abundance dropped in autumn (Zhang *et al*., 2017).

In the East China Sea, planktonic ciliate populations had a distinct seasonal cycle. The abundance of ciliates increased by 3- to 5-fold in summer compared to the other seasons. The high abundance area was in the Changjiang River Plume with salinity <31. The Three Gorges Dam appears to have an important influence on ciliates in the river plume. Before the completion of the Three Gorges Dam, heterotrophic ciliates were more abundant (1000–2000 ind./L) in the river plume (salinity <32) than in the waters outside of the plume (salinity >32) in Junes of 1998 and 2003. After the completion of the Three Gorges Dam, the abundance of ciliates in the river plume became comparable with that outside of the plume in summer (2003–2007) (Tsai *et al*., 2011a). However, in 2011 the Changjiang

River plume had higher ciliate abundance than in waters outside of the plume (Yu *et al*., 2016). In cruises during 2006–2009, higher ciliate biomass was found in areas affected by the Changjiang River discharge (Choi *et al*., 2012).

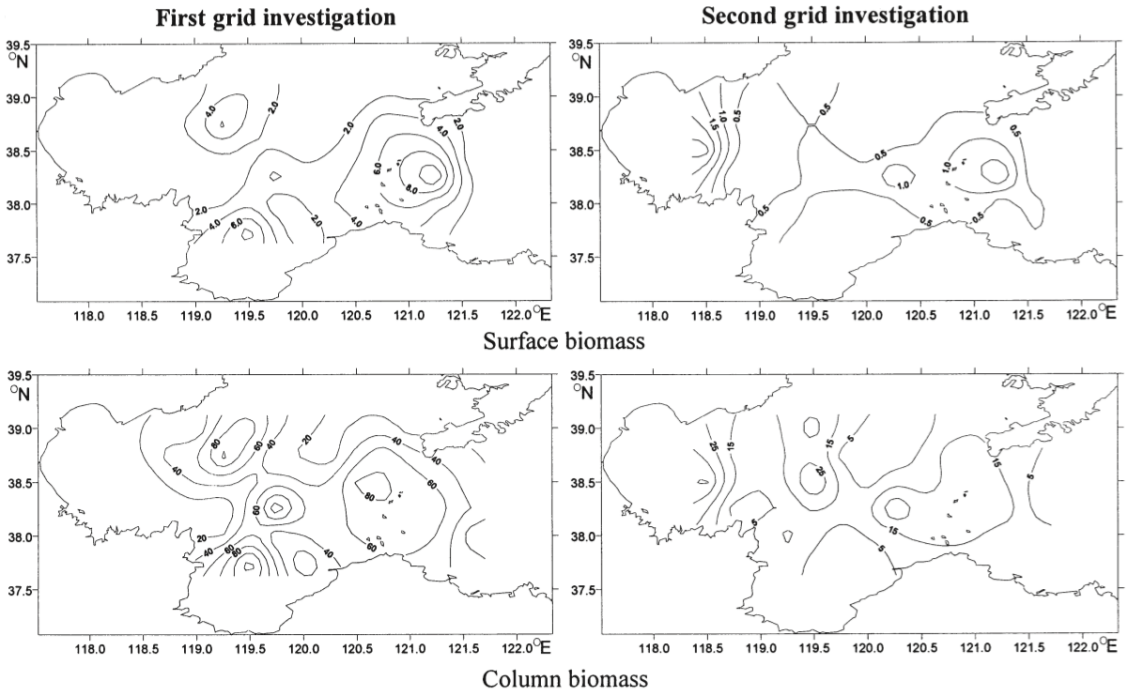

Fig. 3.1.15 Surface biomass (mg C/m^3) and column biomass (mg C/m^2) of planktonic ciliates in the Bohai Sea during two grid investigations. From Zhang and Wang (2000a). Reproduced with permission of Inter-Research Science.

Mixotrophic ciliate abundance using the epifluorescence microscope was also investigated. In summer, abundance (>1200 ind./L) was higher in the Changjiang plume than in waters outside of the plume. Correspondingly, mixotrophic ciliate abundance occupied >50% of total ciliate abundance in the plume compared with <30% outside of the plume (Chiang *et al*., 2003). The size of the ciliates had a regional trend: ciliates in the coastal shallow waters were larger than those in the deeper waters. This trend in summer was not as obvious as in other seasons (Chiang *et al*., 2003).

Ciliate abundance in the shelf region of the East China Sea was high in the upper 50 m water column. In waters deeper than 50 m, ciliate abundance decreased sharply. There usually was a subsurface abundance peak around 25 m depth (Ota and Taniguchi, 2003; Tsai *et al*., 2011a) but ciliate abundance showed surface peaks in some stations (Zhang *et al*., 2001; Ota and Taniguchi, 2003). The vertical peak of ciliate abundance was not coincident with the Chl-*a* concentration peak in most of the stations. Although both ciliate biomass and pico-/nano-plankton biomass decreased with depth, ciliate biomass decreased more rapidly. As a result, the ratio between ciliate biomass and pico-/nano-plankton biomass decreased with depth (Suzuki and Miyabe, 2007).

3.1.7 Tintinnids

In spring, *Codonellopsis mobilis* (Fig. 3.1.16) was the dominant tintinnid species in the Bohai Sea. In a cruise in 1–15 June 1997, tintinnid abundance was investigated at five stations in the Bohai Sea. *C. mobilis* was the dominant tintinnid species with 981, 200 and 30 ind./L in surface waters of Stn. 1,

Stn. 5 and Stn. 3, respectively. Tintinnid abundance was lower in deep waters than in surface waters (Zhang and Wang, 2000b). From 28 April to 1 May, 1999, tintinnids were sampled using a vertical net (mesh size 76 μm) towed from bottom to surface in 30 stations in Bohai Sea. Almost all the tintinnids were *C. mobilis*. Other species were rarely found. *C. mobilis* occurred in 27 out of the 30 occupied stations with maximum abundance of 10,731 ind./m^3 (Zhang *et al*., 2004).

C. mobilis was also dominant in Laizhou Bay. Large-sized tintinnids were collected by vertical towing a shallow sea type III plankton net (open area 0.1 m^2, mesh size 76 μm) during 9 cruises between May and November of 2011 and from March to April 2012. The abundance of *C. mobilis* was more than 50 ind./L. *C. mobilis* was a dominant species during all time periods and significantly influenced the pattern of total ciliate abundance. The highest abundance of *C. mobilis* (489 ind./L) occurred in May (Chen *et al*., 2014).

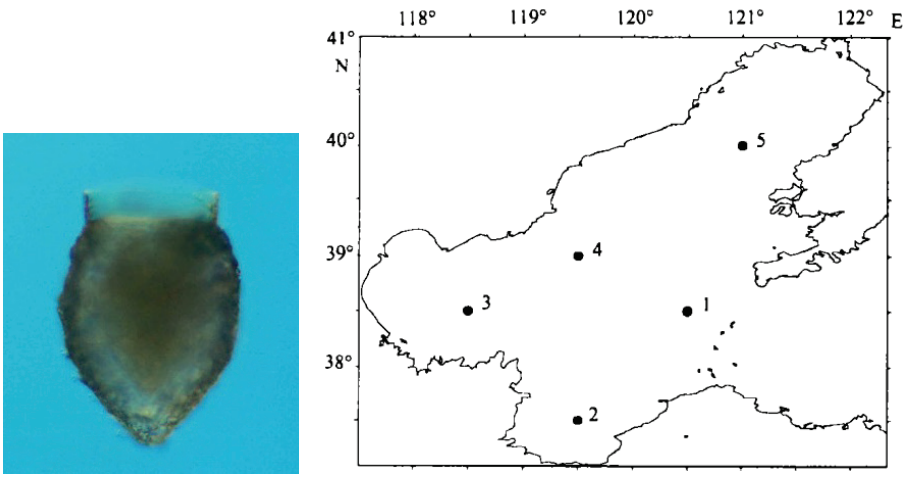

Fig. 3.1.16 (Left) Tintinnid species *Codonellopsis mobilis*. Photo from Wuchang Zhang and (right) stations in the Bohai Sea. From Zhang and Wang (2000b).

Tintinnids in the Yellow Sea were composed of boreal genera *Parafavella* spp. (Fig. 3.1.17a) and *Ptychocyli obtusa* (Fig. 3.1.17b). *Parafavella elongata* and *C. mobilis* were reported only in the Bohai Sea and Yellow Sea (Zhang *et al*., 2008; Yu *et al*., 2013). *Parafavella* spp. occurred in waters north of 36°N in June (Zhang *et al*., 2009) and in waters north of 34.5°N in November and January (Zhang *et al*., 2008; Fig. 3.1.18). *Ptychocyli obtusa* occurred in deep waters (>50 m) north of 35°N in high abundance (503 ± 874 ind./L) in April (Zhang *et al*., 2018).

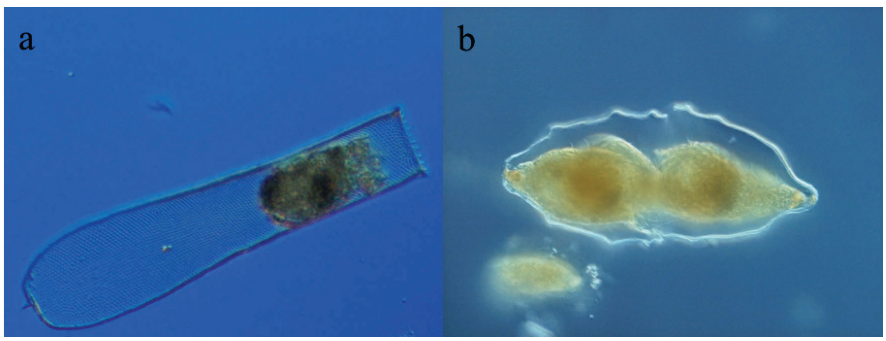

Fig. 3.1.17 Tintinnid species *Parafavella elongata* (a) and *Ptychocyli obtusa* (b). Photos from Wuchang Zhang.

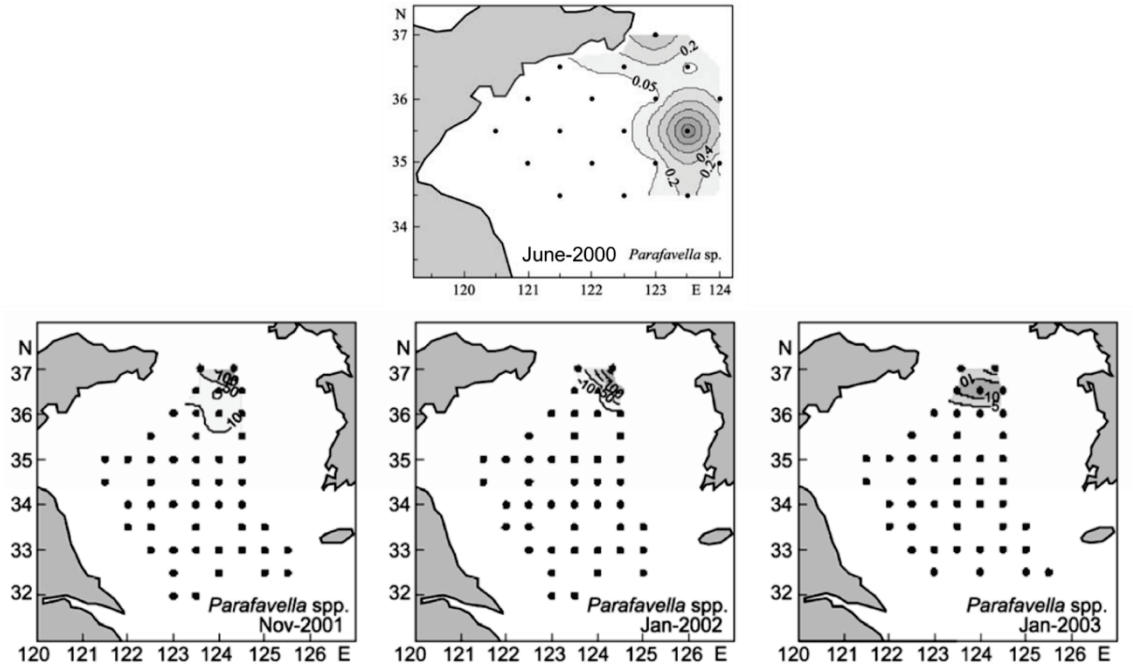

Fig. 3.1.18 Distributions of *Parafavella* spp. (ind./L in the upper panel and ind./m^3 in the bottom panels) in the Yellow Sea. Solid circles indicate the positions of sampling stations. From Zhang *et al*. (2008, 2009). Reproduced with permission of Springer Nature.

Tintinnids and aloricate ciliates had different vertical distributions in the East China Sea. Tintinnids were distributed mainly near the bottom waters, while a higher abundance of aloricate ciliates was found in waters 30–70 m above the bottom. The contribution of tintinnids to the total ciliate abundance decreased with increasing distance from the bottom. In waters with distance from the bottom >80 m, tintinnids accounted for <10% of the total ciliate abundance. The Changjiang River discharge in summer enhanced aloricate ciliate abundance compared with spring and autumn, although tintinnid abundance did not change significantly. *Tintinnidium primitivum* (Fig. 3.1.19a) was the dominant tintinnid near the bottom waters. Aloricate ciliates and tintinnids had different vertical distributions and responses to freshwater discharge in the East China Sea (Yu *et al*., 2016).

A total of 94 species in 36 genera of tintinnids were found in the East China Sea in three cruises in May, August and October, respectively (Li *et al*., 2016). The tintinnid assemblage was the result of the interaction between neritic and warm water tintinnids. Factors influencing neritic tintinnid species richness and abundance were water depth while salinity influenced species richness and abundance of warm water tintinnids. Most neritic genera are agglutinated species with particles on the loricae, which add additional weight to the cell. These genera settled down faster than hyaline genera. Therefore, the neritic genera had lower mobility compared with warm water genera. Thus, neritic genera were adapted to a turbulent environment in order to stay in the water column. Neritic genera stayed in shallow waters which had a higher turbulence due to tidal mixing. According to the difference in their expansion ability, neritic and warm water genera could be divided into core genera (with smallest expansion range from its distribution center) and pioneer genera (with larger expansion range than that of the core genera). In the case of neritic genera, core and pioneer neritic genera stayed together in May and August while pioneer neritic genera expanded into oceanic water in October. In the case of warm water genera, the pioneer genera always expanded toward the coast in all three cruises. In May and August, the pioneers of neritic and warm water genera did not meet. Thus, there was a low species richness area in the middle of the East China Sea. However, in October, the cores of neritic and warm water genera collided. The Changjiang River freshwater

plume is not suitable for both neritic and warm-water genera tintinnids. Warm-water genera cannot live in diluted water because of its low salinity (<32), but neritic genera lived well in the diluted waters quite near river mouth because of its high turbulence. However, at some distance from the river mouth, where water became stratified because of the low salinity of the diluted water, neritic genera could not thrive due to low turbulence (Zhang *et al*., 2015; Li *et al*., 2016).

However, there was neritic genera tintinnid species adapted to live in the estuarine low salinity waters. A new tintinnid ciliate, *Tintinnopsis estuariensis* (Fig. 3.1.19b) was found recently in the estuary of the Changjiang River. It was most abundant in September. Its arenaceous lorica is cylindro-conical in shape, (120–180) μm × (50–75) μm in size, agglutinated with mineral particles, and open at both ends. Two characters distinguish it from others: the unique lateral flattened posterior portion with a vertical aboral opening and wider oral diameter. It occurred in water with surface temperature of 14–27°C and surface salinity of 3.9–29.8. This species was also found in Yellow River Estuarine (Zhang Wuchang, unpublished data).

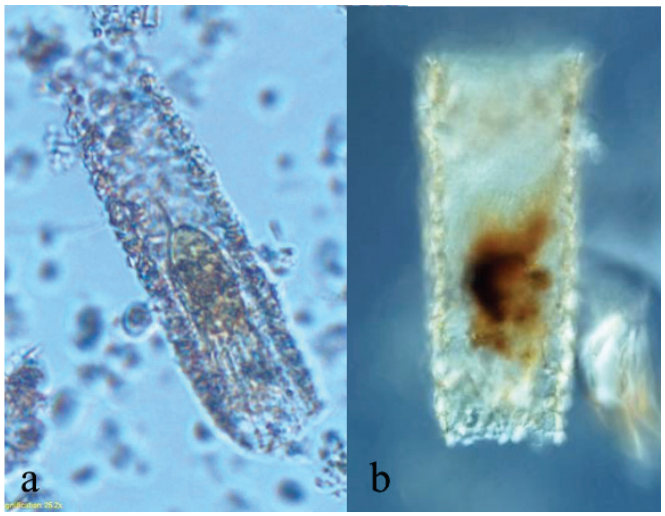

Fig. 3.1.19 Tintinnid species *Tintinnidium primitivum* (a) and *Tintinnopsis estuariensis* (b). Photos from Wuchang Zhang.

3.1.8 Trophodynamics

In addition to the distribution patterns of the component organisms in the microbial food webs, some authors have made a probe into the trophodynamics of the microbial food web. This probe focused on two aspects: one is the numerical relationships between (among) abundances (or biomass) of the organisms; another one is the grazing impact of the grazers on their prey.

Huang *et al*. (2003) reported the abundance ratio of heterotrophic bacteria : *Synechococcus* : flagellates : dinoflagellates : ciliates = 10^5:10^3:10^2:10:1 in the southern Yellow Sea (Fig. 3.1.20). Therefore, the numerical relationship among these organisms was comparatively stable. However, there was weak coupling between heterotrophic nanoflagellates and bacteria in the YSCWM area (Lin *et al*., 2014).

Suzuki and Miyabe (2007) provided a different view. In the deep eastern part of the East China Sea, the ratio of ciliates:prey candidates tend to increase with the increase of prey candidates. That means when prey candidates decrease, ciliates decrease more rapidly. As a result, the ratio of ciliates : prey candidates decreased with depth to 400 m (Fig. 3.1.21; Suzuki and Miyabe, 2007).

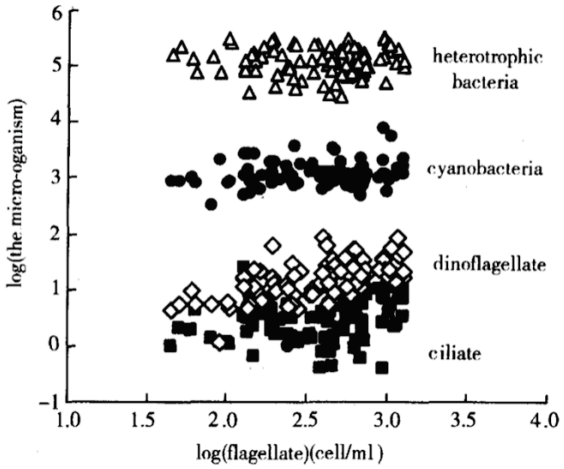

Fig. 3.1.20 Relationship of marine flagellate abundance with that of heterotrophic bacteria, cyanobacteria, dinoflagellates and ciliates in the southern Yellow Sea. From Huang *et al*. (2003).

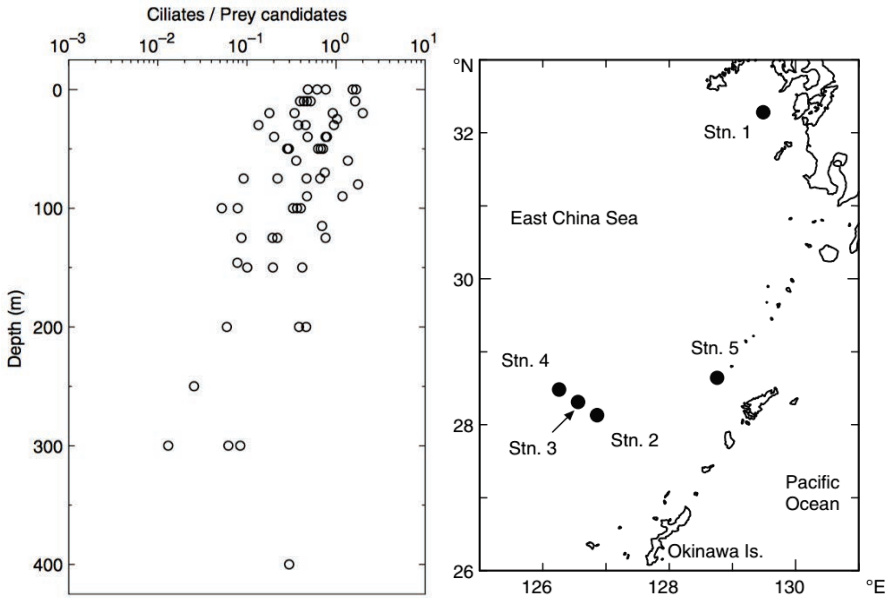

Fig. 3.1.21 Biovolume ratio (left) of planktonic ciliates to prey candidates (picoplankton + nanoplankton) on vertical profile at Stns. 1–5 in the East China Sea (right) in May 1999. From Suzuki and Miyabe (2007). Reproduced with permission of Springer Nature.

A number of dilution incubation experiments were carried out in the Yellow Sea (Zhang *et al*., 2002c; Yu *et al*., 2010; Sun *et al*., 2013) and East China Sea (Zhang *et al*., 2001; Zhang *et al*., 2006; Sun and Song, 2009) to study microzooplankton grazing on phytoplankton. These studies showed that microzooplankton was the major grazer of phytoplankton and had a higher grazing pressure on phytoplankton than mesozooplankton did. However, mesozooplankton might enhance phytoplankton growth by removing microzooplankton (Zhang *et al*., 2006; Yu *et al*., 2010).

Dilution incubations also were used to estimate microzooplankton grazing rates (0.02–0.19 h^{-1}) on bacteria and *Synechococcus* (0.01–0.13 h^{-1}) in the East China Sea. Nanoflagellates largely depend on heterotrophic bacteria as an important energy source contributing 76% and 59% of carbon consumed by nanoflagellates within the Changjiang River Plume (salinity <31) and outside of the plume (salinity >31), respectively (Tsai *et al*., 2012).

Paralleled dilution incubations (dilution with 0.2-μm filtered seawater and 30-dDa filtered seawater, respectively) estimated the contribution of microzooplankton and viruses to bacteria mortality. In summer, flagellate grazing was responsible for most of the bacterial mortality, accounting for 59% and 66% of total mortality within the plume (salinity <31) and outside of the plume (salinity >31), respectively (Tsai *et al*., 2013a,c).

In another study, fluorescently labeled bacteria was used to determine the grazing rates of heterotrophic flagellates on bacteria (Lin *et al*., 2014). In the Yellow Sea, the grazing rate fell to a range of 3.92–15.57 bacteria HNF^{-1} h^{-1}. The grazing rate was high in the surface waters and decreased with depth. Heterotrophic flagellates grazed 9.27–33.80% of bacteria standing stock and 8.12–16.09% of bacteria production per day in autumn. Therefore, heterotrophic flagellate grazing might not have a major impact on planktonic bacteria (Lin *et al*., 2014).

In the East China Sea from May to September, PNF had a larger grazing rate (0.9–15.5 bacteria PNF^{-1} h^{-1}) than that of HNF (0.3–5.8 bacteria HNF^{-1} h^{-1}). The 3–6 μm PNF, 2–3 μm HNF, and 3–6 μm HNF were major consumers in the nanoflagellate community and were responsible for an average of 52, 28 and 16% of the total consumption of bacteria, respectively (Tsai *et al*., 2011b).

3.1.9 Planktonic community respiration

Planktonic community respiration (CR) rates were measured using the oxygen methods in autumn 1998 (Chen *et al*., 2003), June and August 2003 (Chen *et al*., 2006, 2009), June and July 2004, June 2005 (Chen *et al*., 2009) in the euphotic zone of East China Sea. Seawater samples were incubated in the dark for 12 h or 24 h. CR rate was 127.6–4728.6 mg C m^{-2} d^{-1} in autumn (Chen *et al*., 2003). CR was higher in June (~114 mg C m^{-3} d^{-1}) than in August (~40 mg C m^{-3} d^{-1}) (Chen *et al*., 2006). CR in surface waters was higher in June (128.4 in 2003, 91.4 in 2004, 103.8 in 2005) than in July (89.5 in 2004) and August (52.2 in 2003) (Chen *et al*., 2009). Spatially, CR was higher in the inner shelf and Changjiang Diluted Water than in the middle and outer shelf area. Changjiang River discharge governed the CR pattern. Phytoplankton and bacteria were the main contributors, which accounted for >96% of CR. CR occupied about 35–42% of primary production. Therefore, CR was supported more by riverine organic carbon input than *in situ* autotrophic production. Changjiang River discharge may also stimulate high primary autotrophic production by providing nutrients, which in turn, enhance the CR.

3.1.10 Synthesis and perspectives

The microbial food web and its function in Yellow Sea and East China Sea have been studied for about 40 years. However, this information is fragmented and there are a lot of unknowns about the microbial food web in this area. It is very difficult to make a synthesis in order to compare the differences among the Bohai Sea, Yellow Sea and East China Sea. There are no taxonomic data for most of the organisms. Their abundance, biomass and production has the largest dataset. However, we could not compare their abundance because (1) they are not from the same season, (2) we do not yet know the annual evolution of these organisms, and (3) viruses, bacteria, flagellates and ciliates occurred everywhere (whenever you sampled, you get a value larger than 0). The only group we could compare is the present/absent of *Prochlorococcus* and some tintinnids. Some topics were rarely studied, and we could not find corresponding data in other study areas. As a result, we could not make a synthesis about these topics such as biovolume ratio of planktonic ciliates to prey candidates (Fig. 3.1.21).

In response to the above-mentioned knowledge gap, some topics are proposed as future research priorities. The taxonomic compositions of these groups need more study, perhaps with the help of molecular methods. The coupling between microbial organisms and water mass and currents is still obscure. The seasonal variation of the microbial food web in different parts of the research area is not clear. Different groups of the organisms in the microbial food web were studied separately in most of the reports, And end-to-end food web research was absent. The influence of dust storms on microbial organisms was not yet studied in these marginal seas right after facing the famous East Asian Dust Storm. The energy transfer between different compartments still need to be clarified. Finally, determining how the microbial food web will change facing global warming and other forcings (acidification, pollution) is the most significant challenge.

3.1.11 References

Azam, F., Fenchel, T., Field, J.G., Gray, J.S., Meyer-Reil, L.A. and Thingstad, F. 1983. The ecological role of water-column microbes in the sea. *Estuaries* **50**: 257–263.

Bai, J., Li, K., Li, Z., Sun, J., Wei, H., Liu, S. and Wu, Z. 2003. Relationship between the environmental factors and distribution of bacterioplankton in the Bohai Sea. *J. Ocean Univ. Qingdao* **33**: 841–846 (in Chinese with English abstract).

Bai, X.-G., Wang, M., Ma, J., Sun, J., Liang, Y.-T. and Qiao, Q. 2007. Virioplankton abundance in winter and spring in Changjiang River Estuary by fluorescence microscope counting. *Oceanol. Limnol. Sin.* **38**: 367–372 (in Chinese with English abstract).

Bai, X.-G., Wang, M., Liang, Y.-T., Jiang, X.-J., Wang, F. and Yang, L. 2008. Spatial Distribution of Virioplankton in the Northern Yellow Sea in Summer. *Period. Ocean Univ. China* **38**: 609–613 (in Chinese with English abstract).

Bai, X., Wang, M., Liang, Y., Zhang, Z., Wang, F. and Jiang, X. 2012. Distribution of microbial populations and their relationship with environmental variables in the North Yellow Sea, China. *J. Ocean Univ. China* **11**: 75–85.

Chen, C.-C., Shiah, F.-K., Gong, G.-C. and Chiang, K.-P. 2003. Planktonic community respiration in the East China Sea: importance of microbial consumption of organic carbon. *Deep Sea Res. II* **50**: 1311–1325, doi:10.1016/S0967-0645(03)00025-0.

Chen, C.-C., Chiang, K.-P., Gong, G.-C., Shiah, F.-K., Tseng, C.-M. and Liu, K.-K. 2006. Importance of planktonic community respiration on the carbon balance of the East China Sea in summer. Global *Biogeochem. Cycles* **20**: GB4001, doi:10.1029/2005GB002647.

Chen, C.-C, Shiah, F.-K., Chiang, K.-P., Gong, G.-C. and Kemp, W.M. 2009. Effects of the Changjiang (Yangtze) River discharge on planktonic community respiration in the East China Sea. *J. Geophys. Res. Oceans* **114**: C03005, doi:10.1029/2008JC004891.

Chen, X., Wu, Q., Luan, Q., Zhang, W. and Xiao, T. 2014. Seasonal change of the community of large-sized tintinnids (Ciliophora, Tintinnida) in Laizhou Bay. *Biodivers. Sci*. **22**: 649–657 (in Chinese with English abstract), doi:10.3724/SP.J.1003.2014.13257.

Chiang, K.-P., Kuo, M.-C., Chang, J., Wang, R.-H. and Gong, G.-C. 2002. Spatial and temporal variation of the *Synechococcus* population in the East China Sea and its contribution to phytoplankton biomass. *Cont. Shelf Res*. **22**: 3–13, doi:10.1016/S0278-4343(01)00067-X.

Cho, B.C., Choi, J.-K., Chung, C.-S. and Hong, G.H. 1994. Uncoupling of bacteria and phytoplankton during a spring diatom bloom in the mouth of the Yellow Sea. *Mar. Ecol. Prog. Ser.* **115**: 181–190.

Cho, B.C., Park, M.G., Shim, J.H. and Choi, D.H. 2001. Sea-surface temperature and f-ratio explain large variability in the ratio of bacterial production to primary production in the Yellow Sea. *Mar. Ecol. Prog. Ser.* **216**: 31–34, doi:10.3354/meps216031.

Choi, D.H., Yang, S.R., Hong, G.H., Chung, C.S., Kim, S.H., Park, J.S. and Cho, B.C. 2005. Different interrelationships among phytoplankton, bacterial and environmental variables in dumping and reference areas in the East Sea. *Aquat. Microb. Ecol*. **41**: 171–180, doi:10.3354/ame041171.

Choi, D.H., Noh, J.H. and Shim, J.S. 2013. Seasonal changes in picocyanobacterial diversity as revealed by pyrosequencing in temperate waters of the East China Sea and the East Sea. *Aquat. Microb. Ecol.* **71**: 75–90, doi:10.3354/AME01669.

Choi, K.-H., Yang, E.J., Kim, D., Kang, H.-K., Noh, J.H. and Kim, C.-H. 2012. The influence of coastal waters on distributions of heterotrophic protists in the northern East China Sea, and the impact of protist grazing on phytoplankton. *J. Plankt. Res*. **34**: 886–904, doi:10.1093/plankt/fbs046.

Chung, C.-C., Huang, C.-Y., Gong, G.-C. and Lin, Y.-C. 2014. Influence of the Changjiang River Flood on *Synechococcus* Ecology on the Surface Waters of the East China Sea. *Microb. Ecol*. **67**: 273–285, doi:10.1007/s00248-013-0299-8.

Ding, J.-J. and Xu, K.-D. 2012. Community structure and distribution of pelagic nanoflagellates and ciliates and their relationship with jellyfish occurrence in southern Yellow Sea. *Oceanol. Limnol. Sin.* **43**: 527–538 (in Chinese with English abstract).

Fuhrman, J.A. 1999. Marine viruses and their biogeochemical and ecological effects. *Nature* **399**: 541–548, doi:10.1038/21119.

Fukuda, R., Ogawa H., Nagata, T. and Koike, I. 1998. Direct determination of carbon and nitrogen contents of natural bacterial assemblages in marine environments. *Appl. Environ. Microbiol*. **64**: 3352–3358, doi:10.1128/AEM.64.9.3352-3358.1998.

Guo, C., Liu, H., Zheng, L., Song, S., Chen, B. and Huang, B. 2014. Seasonal and spatial patterns of picophytoplankton growth, grazing and distribution in the East China Sea. *Biogeosciences* **11**: 1847–1862, doi:10.5194/bg-11-1847-2014.

Hara, S., Terauchi, K. and Koike, I. 1991. Abundance of viruses in marine waters: assessment by epifluorescence and transmission electron microscopy. *Appl. Environ. Microbiol*. **57**: 2731–2734, doi:10.1128/aem.57.9.2731-2734.1991.

Hoppe, H.-G., Gocke, K., Koppe, R. and Begler, C. Bacterial growth and primary production along a north-south transect of the Atlantic Ocean. *Nature* **416**: 168–171, doi:10.1038/416168a.

Huang, L., Guo, F., Huang, B. and Xiao, T. 2003. Distribution pattern of marine flagellate and its controlling factors in the central and north part of the Huanghai Sea in early summer. *Acta Oceanol. Sin*. **22**: 273–280.

Hwang, C.Y. and Cho, B.C. 2002a. Uneven growth and different susceptibility to viruses among bacteria increase estimates of virus production in the East Sea based on TEM observations. *Aquat. Microb. Ecol.* **27**: 211–218.

Hwang, C.Y. and Cho, B.C. 2002b.Virus-infected bacteria in oligotrophic open waters of the East Sea, Korea. *Aquat. Microb. Ecol.* **30**: 1–9, doi:10.3354/ame030001.

Hwang, C.Y. and Cho, B.C. 2008. Effects of storage on the estimates of virus-mediated bacterial mortality based on observation of preserved seawater samples with TEM. *Aquat. Microb. Ecol.* **52**: 263–271, doi:10.3354/ame01234.

Hyun, J.-H. and Kim, K.-H. 2003. Bacterial abundance and production during the unique spring phytoplankton bloom in the central Yellow Sea. *Mar. Ecol. Prog. Ser.* **252**: 77–88, doi:10.3354/meps252077.

Jiao, N. and Yang, Y. 2002. Ecological studies on *Prochlorococcus* in China seas. *Chin. Sci. Bull*. **47**: 1243–1250, doi:10.1360/02tb9276.

Jiao, N., Yang, Y., Koshikawa, H. and Watanabe, M. 2002. Influence of hydrographic conditions on picoplankton distribution in the East China Sea. *Aquat. Microb. Ecol*. **30**: 37–48, doi:10.3354/AME030037.

Jiao, N., Zhao, Y., Luo, T. and Wang, X. 2006. Natural and anthropogenic forcing on the dynamics of virioplankton in the Yangtze river estuary. *J. Mar. Biol. Assoc. UK* **86**: 543–550, doi:10.1017/S0025315406013452.

Lee, Y., Choi, J.K, Youn, S. and Roh, S. 2014. Influence of the physical forcing of different water masses on the spatial and temporal distributions of picophytoplankton in the northern East China Sea. *Cont. Shelf Res*. **88**: 216–227, doi:10.1016/j.csr.2014.08.001.

Li, H., Xiao, T., Ding, T. and Lü, R. 2006. Effect of the Yellow Sea Cold Water Mass (YSCWM) on distribution of bacterioplankton. *Acta Ecol. Sin*. **26**: 1012–1019.

Li, H., Zhao, Y., Chen, X., Zhang, W., Xu, J., Li, J. and Xiao, T. 2016. Interaction between neritic and warm water tintinnids in surface waters of East China Sea. *Deep Sea Res. II* **124**: 84–92, doi: 10.1016/j.dsr2.2015.06.008.

Li, H.-B., Lv, R.-H., Ding, T. and Lin, Y.-A. 2007. Impact of tidal front on the distribution of bacterioplankton in the southern Yellow Sea, China. *J. Mar. Syst*. **67**: 263–271.

Li, H.-B., Liu, S.-X., Lin, F.-A. and Feng, Z.-Q. 2012. Distribution characteristics of picophyplankton in coastal area of Hebei. *Mar. Sci.* **36**: 49–55 (in Chinese with English abstract).

Li, Y. and Li, D. 2012. Spatial distributions of picoplankton and viruses in the Changjiang Estuary and its adjacent sea area during summer. *J. Mar. Biol*. **2012**: 1–11, doi:10.1155/2012/465168.

Lin, S., Huang, L., Zhu, Z. and Jia, X. 2013. Changes in size and trophic structure of the nanoflagellate assemblage in response to a spring phytoplankton bloom in the central Yellow Sea. *Deep Sea Res. II* **97**: 93–100, doi:10.1016/j.dsr2.2013.05.017.

Lin, S., Huang, L. and Lu, J. 2014. Weak coupling between heterotrophic nanoflagellates and bacteria in the Yellow Sea Cold Water Mass area. *Acta Oceanol. Sin*. **33**: 125–132, doi:10.1007/s13131-014-0523-5.

Lin, S., Huang, L., Zhu, Z., Xiong, Y. and Lu, J. 2016. Distribution of nanoflagellates in five water masses of the East China Sea in autumn and winter. *Deep Sea Res. II* **124**: 93–99, doi:10.1016/j.dsr2.2015.02.017.

Liu, J.-J., Zeng, J.-N., Du, P. and Chen, Q.-Z. 2011. Abundance distribution of virioplankton in Yangtze River estuary and its adjacent East China Sea in summer and winter. *Chin. J. Appl. Ecol*. **22**: 793–799 (in Chinese with English abstract).

Ota, T. and Taniguchi, A. 2003. Standing crop of planktonic ciliates in the East China Sea and their potential grazing impact and contribution to nutrient regeneration. *Deep Sea Res. II* **50**: 423–442, doi:10.1016/S0967-0645(02)00461-7.

Pan, L.A., Zhang, J. and Zhang, L.H. 2007. Picophytoplankton, nanophytoplankton, heterotrohpic bacteria and viruses in the Changjiang Estuary and adjacent coastal waters. *J. Plankt. Res*. **29**: 187–197, doi:10.1093/plankt/fbm006.

Shi, Y., Bai, J., Li, H.-Y. and Li, Z.-Y. 2009. Ecological distribution character of virioplankton in the Northwest of the Yellow Sea in spring and autumn. *Period. Ocean Univ. China* **39**(Suppl.): 165–170 (in Chinese with English abstract).

Shiah, F.-K., Liu, K.-K., Kao, S.-J. and Gong, G.-C. 2000. The coupling of bacterial production and hydrography in the southern East China Sea: Spatial patterns in spring and fall. *Cont. Shelf Res.* **20**: 459–477, doi:10.1016/S0278-4343(99)00081-3.

Shim, J.H., Yoon, S.H., Yoon, S.S., Choi, D.H. and Cho, B.C. 1995. Abundances and bacterivory of heterotrophic and mixotrophic nanoflagellates in and estuarine system of the Mankyung and Dongjin rivers, Korea. *J. Korean Soc. Oceanogr*. **30**: 413–425 (in Korean with English abstract).

Stenseth, N.C., Ottersen, G., Hurrell, J.W. and Belgrano, A. (Eds.) 2004. Marine Ecosystems and Climate Variation: The North Atlantic. A Comparative Perspective. Oxford University Press, New York.

Sun, J. and Song, S. 2009. Phytoplankton growth and micro-zooplankton herbivory during the spring phytoplankton bloom period in the East China Sea. *Acta Oceanol. Sin*. **29**: 6429–6438 (in Chinese with English abstract).

Sun, J., Feng, Y., Zhou, F., Song, S., Jiang, Y. and Ding, C. 2013. Top-down control of spring surface phytoplankton blooms by microzooplankton in the Central Yellow Sea, China. *Deep Sea Res. II* **97**: 51–60, doi:10.1016/j.dsr2.2013.05.005.

Suzuki, T. and Miyabe, C. 2007. Ecological balance between ciliate plankton and its prey candidates, pico-and nanoplankton, in the East China Sea. *Hydrobiologia* **586**: 403–410, doi:10.1007/s10750-007-0715-5.

Tang, Q., Fan, Y. and Lin, H. 1996. Initial inquiring into the developmental strategy of Chinese ocean ecosystem dynamics research. *Adv. Earth Sci*. **11**: 160–168 (in Chinese with English abstract).

Tsai, A.-Y., Gong, G.-C., Sanders, R.W., Wang, C.-J. and Chiang, K.-P. 2010. The impact of the Changjiang River plume extension on the nanoflagellate community in the East China Sea. *Estuar. Coast. Shelf Sci*. **89**: 21–30, doi:10.1016/j.ecss.2010.05.005.

Tsai, A.-Y., Gong, G.-C., Chiang, K.-P., Chao, C.-F. and Guo, H.-R. 2011a. Long-term (1998–2007) trends on the spatial distribution of heterotrophic ciliates in the East China Sea in summer: effect of the Three Gorges Dam construction. *J. Oceanogr*. **67**: 725–737.

Tsai, A.-Y., Gong, G.-C., Sanders, R.W., Chen, W.-H., Chao, C.-F. and Chiang, K.-P. 2011b. Importance of bacterivory by pigmented and heterotrophic nanoflagellates during the warm season in a subtropical western Pacific coastal ecosystem. *Aquat. Microb. Ecol*. **63**: 9–18, doi:10.3354/AME01470.

Tsai, A.-Y., Gong, G.-C., Sanders, R.W., Chiang, K.-P. and Chao, C.-F. 2012. Heterotrophic bacterial and *Synechococcus* spp. Growth and mortality along the inshore-offshore in the East China Sea in summer. *J. Oceanogr*. **68**: 151–162, doi:10.1007/s10872-011-0076-6.

Tsai, A.-Y., Gong, G.-C., Huang, J.-K. and Lin, Y.-C. 2013a. Viral and nanoflagellate control of bacterial production in the East China Sea summer 2011. *Estuar. Coast. Shelf Sci*. **120**: 33–41, doi:10.1016/j.ecss.2013.01.012.

Tsai, A.-Y., Gong, G.-C., Sanders, R.W. and Chiang, K.-P. 2013b. Relationship of *Synechococcus* abundance to seasonal ocean temperature ranges. *Terr. Atmos. Ocean. Sci*. **24**: 925–932, doi:10.3319/TAO.2013.06.17.01(Oc).

Tsai, A.-Y., Gong, G.-C., Sanders, R.W. and Huang, J.-K. 2013c. Contribution of viral lysis and nanoflagellate grazing to bacterial mortality in the inner and outer regions of the Changjiang River plume during summer. *J. Plankt. Res*. **35**: 1283–1293, doi:10.1093/plankt/fbt074.

Wang, C., Wang, Y., Paterson, J.S., Mitchell, J.G., Hu, X., Zhang, H. and Sheng, Y. 2016. Macroscale distribution of virioplankton and heterotrophic bacteria in the Bohai Sea. *FEMS Microbiol. Ecol*. **92**: fiw017, doi:10.1093/femsec/fiw017.

Wang, J., Wang, M., Liu, Z., Liu, D., Yang, L., Lu, L., Wang, Y. and Sun, H. 2013. The spatial and temporal distribution of virioplankton in the Bohai Sea. *Oceanol. Limnol. Sin*. **44**: 1597–1603 (in Chinese with English abstract).

Xiao, T. and Wang, R. 2002. Distribution of *Synechococcus* in the Bohai Sea in autumn and spring. *Acta Oceanol. Sin*. **22**: 2071–2078 (in Chinese with English abstract).

Xiao, T. and Wang, R. 2003. Distribution of heterotrophic bacterial production in the Bohai Sea. *Acta Oceanol. Sin*. **25**: 58–65 (in Chinese with English abstract).

Yang, Y.-H. and Jiao, N. 2002. Distribution of virioplankton in the Kuroshio Current and the adjacent area in the East China Sea as determined by flow cytometry. *Chin. J. Oceanol. Limnol*. **20**: 1–7.

Yu, Y., Zhang, W., Xiao, T., Li, H., Li, C. and Sun, S. 2010. Impact of microzooplankton and *Calanus sinicus* (Brodsky, 1962) on phytoplankton in the Yellow Sea during early summer. *Chin. J. Oceanol. Limnol.* **28**: 881–886, doi:10.1007/s00343-010-9916-0.

Yu, Y., Zhang, W., Wang, S. and Xiao, T. 2013. Abundance and biomass of planktonic ciliates in the sea area around Zhangzi Island, Northern Yellow Sea. *Acta Ecol. Sin*. **33**: 45–51, doi:10.1016/j.chnaes.2012.12.007.

Yu, Y., Zhang, W., Zhang, C., Zhou, F., Zhao, N. and Xiao, T. 2014. Basin-scale variation in planktonic ciliate distribution: A detailed temporal and spatial study of the Yellow Sea. *Mar. Biol. Res*. **10**: 641–654, doi:10.1080/17451000.2013.852683.

Yu, Y., Zhang, W., Feng, M., Zhao, Y., Zhang, C., Zhou, F. and Xiao, T. 2016. Differences in the vertical distribution and response to freshwater discharge between aloricate ciliates and tintinnids in the East China Sea. *J. Mar. Syst*. **154**: 103–109, doi:10.1016/j.jmarsys.2015.02.005.

Zhang, C., Zhang, W., Xiao, T., Lü, R., Sun, S. and Song, W. 2008. Meso-scale spatial distribution of large tintinnids in early summer in southern Yellow Sea. *Chin. J. Oceanol. Limnol.* **26**: 81–90, doi:10.1007/s00343-008-0081-9.

Zhang, C., Zhang, W., Xiao, T., Lü, R., Sun, S. and Song, W. 2009. Wintertime meso-scale horizontal distribution of large tintinnids in the southern Yellow Sea. *Chin. J. Oceanol. Limnol.* **27**: 31–37, doi:10.1007/s00343-009-0031-1.

Zhang, C., Zhang, W., Ni, X., Zhao, Y., Huang, L. and Xiao, T. 2015. Influence of different water masses on planktonic ciliate distribution on the East China Sea shelf. *J. Mar. Syst.* **141**: 98–111, doi:10.1016/j.jmarsys.2014.09.003.

Zhang, S., Chen, X., Zhang, W., Zhang, F. and Xiao, T. 2018. Differences in planktonic ciliate spatial distribution in spring and autumn in the southern Yellow Sea. *Acta Oceanol. Sin.* **37**: 48–57, doi:10.1007/s13131-018-1147-y.

Zhang, W. and Wang, R. 2000a. Rapid changes in stocks of ciliate microzooplankton associated with a hurricane in the Bohai Sea (China). *Aquat. Microb. Ecol*. **23**: 97–101.

Zhang, W. and Wang, R. 2000b. Summertime ciliate and copepod nauplii distributions and micro-zooplankton herbivorous activity in the Laizhou Bay, Bohai Sea, China. *Estuar. Coast. Shelf Sci*. **51**: 103–114, doi:10.1006/ecss.2000.0644.

Zhang, W., Xiao, T. and Wang, R. 2001. Abundance and biomass of copepod nauplii and ciliates and herbivorous activity of microzooplankton in the East China Sea. *Plankt. Biol. Ecol*. (Japan) **48**: 28–34.

Zhang, W., Xu, K., Wan, R., Zhang, G., Meng, T., Xiao, T., Wang, R., Sun, S. and Choi, J.K. 2002c. Spatial distribution of ciliates, copepod nauplii and eggs, *Engraulis japonicus* post-larvae and microzooplankton herbivorous activity in the Yellow Sea, China. *Aquat. Microb. Ecol*. **27**: 249–259, doi:10.3354/AME027249.

Zhang, W., Sun, J. and Sun, S. 2004. Spatial distribution of tintinnidous ciliate *Codonellopsis mobilis* (Protozoa, Ciliophora) in April, 1999 in Bohai Sea, China. *Mar. Sci*. **28**: 67–69 (in Chinese with English abstract).

Zhang, W., Li, H., Xiao, T., Zhang, J., Li, C. and Sun, S. 2006. Impact of microzooplankton and copepods on the growth of phytoplankton in the Yellow Sea and East China Sea. *Hydrobiol*. **553**: 357–366, doi:10.1007/s10750-005-0857-2.

Zhao, L., Zhao, Y., Zhang, W., Zhou, F., Zhang, C., Ren, J., Ni, X., Denis, M. and Xiao, T. 2013. Picoplankton distribution in different water masses of the East China Sea in autumn and winter. *Chin. J. Oceanol. Limnol.* **31**: 247–266, doi:10.1007/s00343-013-2085-3.

Zhao, Y., Zhao, L., Xiao, T., Zhao, S., Xuan, J., Li, C. and Ning, X. 2011. Spatial and temporal variation of picoplankton distribution in the Yellow Sea, China. *Chin. J. Oceanol. Limnol.* **29**: 150–162, doi:10.1007/s00343-011-9086-x.

Zhao, Y., Zhao, L, Xiao, T., Liu, C., Sun, J., Zhou, F., Liu, S. and Huang, L. 2013. Temporal variation of picoplankton in the spring bloom of Yellow Sea, China. *Deep Sea Res. II* **97**: 72–84, doi:10.1016/j.dsr2.2013.05.015.

Zhao, Y., Zhao, L., Zhang, W., Sun, J., Huang, L., Li, J., Zhai, H., Liu, S. and Xiao, T. 2016. Variations of picoplankton abundances during blooms in the East China Sea. *Deep Sea Res. II* **124**: 100–108, doi:10.1016/j.dsr2.2015.03.010.

3.2 Phytoplankton

Joji Ishizaka

Institute for Space-Earth Environmental Research, Nagoya University, Japan

3.2.1 Introduction

Recently, as many red tide events are happening in the East China Sea and Yellow Sea (Fig. 3.2.1), more attention is being paid to the ecosystem and phytoplankton in this area and their relationship to human activities and climate change. This area is a region of complex current systems, and it is known that discharge from the Changjiang River and Kuroshio Intermediate Water are major sources of nutrients (see Section 2.2). More recently, atmospheric input is also recognized as an important contributor (also see Section 2.6). Ning *et al*. (1988) described the chlorophyll-a and primary production in the Changjiang Estuary extending to offshore of the East China Sea in January and July 1986. They found smaller phytoplankton (<10 μm) dominated in the estuary and nearshore in winter whereas diatoms dominated at 100 km offshore where chlorophyll-a and primary production was maximum and salinity was 25–30. They concluded that turbidity limits the light for primary producers in the coastal area, and nutrients are poor in the offshore area. A large amount of data was accumulated after this study describing more complex temporal and spatial variability of phytoplankton, including the influence of strong anthropogenic and climatic forcing in this area. In this section, our present understanding of phytoplankton abundance, primary production, and phytoplankton community in the East China Sea and Yellow Sea are summarized, as well as the influence of the Three Gorge Dam and typhoons as sources of interannual variation.

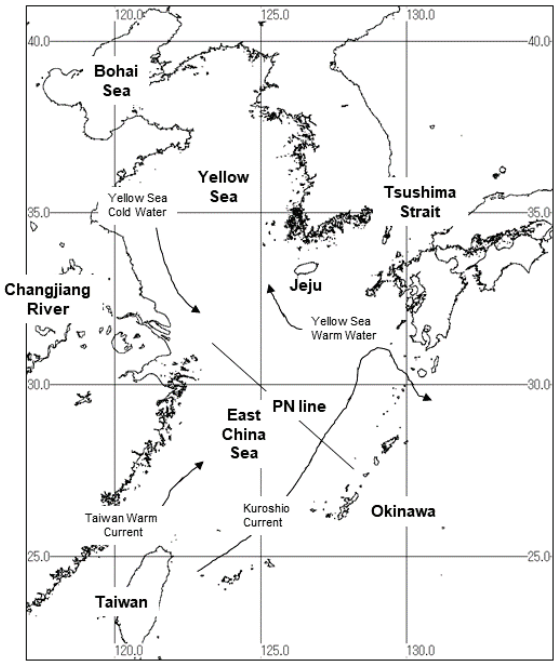

Fig. 3.2.1 Map of the East China Sea, Yellow Sea, and Bohai Sea, with names of location and currents used in the text.

3.2.2 Chlorophyll-a

Phytoplankton abundance is often expressed by the photosynthetic pigment, chlorophyll-a (Chl-*a*). Because of the complex and large variability of Chl-*a* in the East China Sea and Yellow Sea, recently, satellite ocean color data are often used to understand the over-all structures. Ning *et al*. (1998) and Tang *et al*. (1998) are the pioneers to describe satellite-derived phytoplankton abundance in this area in combination with satellite-derived sea surface temperature (SST). Using Coastal Zone Color Scanner (CZCS) phytoplankton pigments (Chl-*a* and pheopigments) data from 1978 to 1986, they clearly showed various water mass structures and associated phytoplankton distributions, especially the extension of high phytoplankton-rich water from the Changjiang Estuary to the offshore. However, ocean color remote sensing data overestimate Chl-*a* near the coastal area because of the high amount of suspended matter near the coast (Kiyomoto *et al*., 2001) and high amount of colored dissolved organic matter from river discharge (Gong, 2004), as well as the problem of atmospheric correction (Shi and Wang, 2009). Many attempts have been made to reduce the error of satellite-derived Chl-*a* in this area. For example, Siswanto *et al*. (2011) developed local algorithms under the Yellow Sea Large Marine Ecosystem Project (YOC algorithm), specifically for high turbidity areas identified with bright (high remote sensing reflectance) water, to reduce the influence of high suspended matter.

Knowing the presence of errors in ocean color data, Yamaguchi *et al*. (2012, 2013) described seasonal variation of NASA ocean color sensor SeaWiFS Chl-*a* in the East China Sea and Yellow Sea from January 1997 to December 2006 with standard product and locally tuned product by YOC algorithm, respectively. (Figs. 3.2.2 and 3.2.3). They recognized the overestimation of the satellite

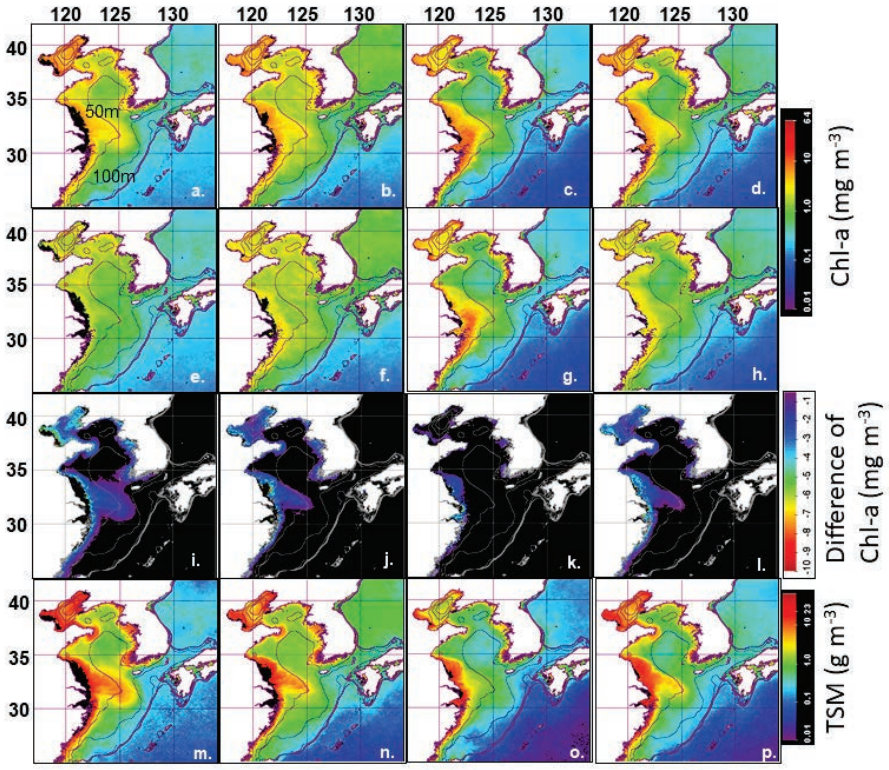

Fig. 3.2.2 Distribution of 10-year (1997– 2006) average of monthly chlorophyll-a (Chl-*a*, mg m^{-3}) from (a–d) standard MODIS algorithm and from (e–h) YOC algorithm, (i–l) the difference between the two (Chl-*a*, mg m^{-3}), and (m–p) total suspended matter (TSM, g m^{-3}) with bathymetry. (a, e, i, m) January, (b, f, j, n) April, (c, g, k, o) July, and (d, h, l, p) October. Redrawn from Yamaguchi *et al*. (2013). Reproduced with permission of Elsevier.

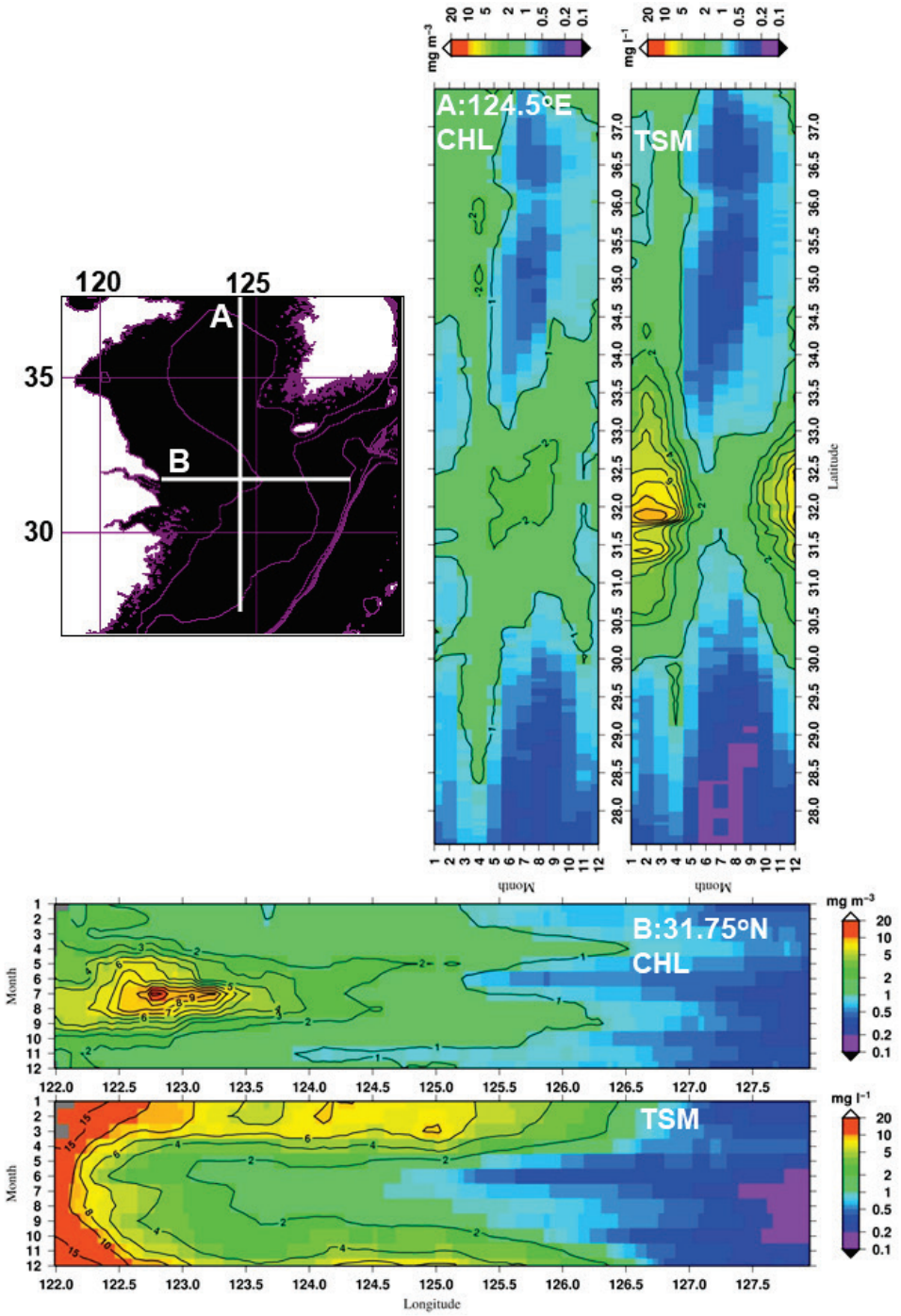

Fig. 3.2.3 Seasonal variation in 10-year (1997–2006) averaged monthly chlorophyll-a (Chl-*a*, mg m^{-3}) and total suspended matter (TSM, g m^{-3}) along (A) 124.5°E and (B) 31.75°N lines. Gray color in bottom plots indicates no data. From Yamaguchi *et al*. (2013). Reproduced with permission of Elsevier.

Chl-*a* data caused by suspended matter near coastal areas as well as on the Changiiang Bank during winter. They reported a spring bloom in large parts of these areas; however, the summer maximum of Chl-*a* was also seen from the Changjiang Estuary to near the east of Jeju Island from July to September. The summer maximum shifts eastward, coinciding with the movement of the Changjiang Diluted Water (CDW), taking approximately 2 months to move from the Changjiang River mouth to around Jeju Island. Yamaguchi *et al*. (2012) also reported that the summer Chl-*a* was positively correlated with Changjiang River discharge with a time lag of 0 to 2 months between 1998 and 2006, and they showed that Changjiang River Discharge is one of the most important

factors for the interannual variation of Chl-*a* in the middle East China Sea. Yamaguchi *et al*. (2013) found relatively low Chl-*a* with high suspended matter near the coast and Changjiang Bank in winter (Fig. 3.2.4). The high suspended matter decreases in spring to summer in the offshore area, and phytoplankton increase with the decrease; a spring bloom can be seen covering a large area, indicating suspended matter is important for phytoplankton dynamics in the shallow area.

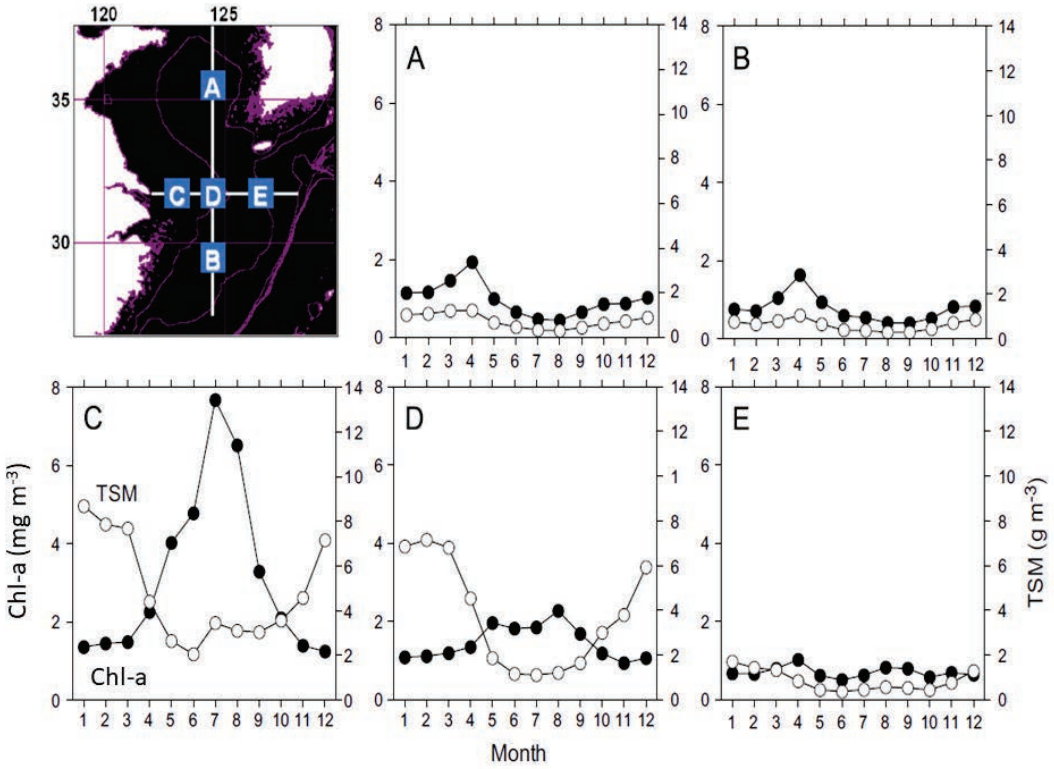

Fig. 3.2.4 Seasonal variation in 10-year (1998–2007) averaged monthly satellite chlorophyll (Chl-*a*, mg m^{-3}) and total suspended matter (TSM, g m^{-3}) from January to December in the middle of the Yellow Sea (A), south of the Changjiang Bank (B), offshore of the Changjiang River mouth (C), around the Changjiang Bank (D), and east of the Changjiang Bank (E). Black and white symbols indicate Chl-*a* and TSM, respectively. From Yamaguchi *et al*. (2013). Reproduced with permission of Elsevier.

Yamaguchi *et al*. (2013) further suggested that the increase in summer Chl-*a* in the Yellow Sea over the last 10 years is possibly caused by eutrophication. In addition, Xu *et al*. (2013) analyzed bloom conditions in this area with a consistent 13-year (1998 to 2010) time series from SeaWiFS to MODIS to understand the relation of phytoplankton blooms to the giant jellyfish blooms, and found that the phytoplankton bloom magnitude increased in the Yellow Sea and Bohai Sea. The Northwest Pacific Action Plan (NOWPAP) of the United Nations Environment Programme (UNEP) has used changes of Chl-*a* concentrations over time to monitor eutrophication of this area. They found an increasing trend of Chl-*a* during 1998 to 2016 in the Yellow Sea and Bohai Sea (Fig. 3.2.5; Terauchi *et al*., 2018). However, an increasing trend in the Chinese coastal area was not persistent, maybe because of high turbidity.

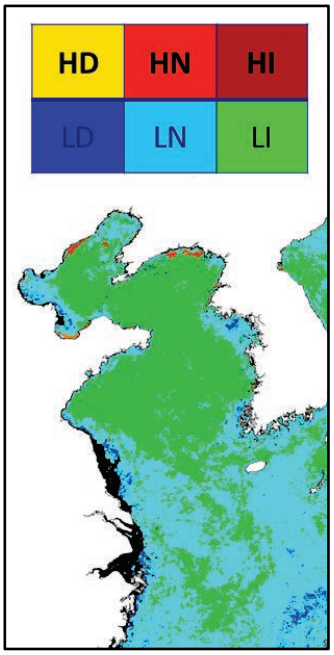

Fig. 3.2.5 Results of a preliminary assessment of eutrophication status conducted by NOWPAP for the Bohai, Yellow and East China seas, by ocean color data (Terauchi *et al*., 2018). H (high) and L (low) indicate that average chlorophyll-a during 2014–2016 was more and less than 5 mg m^{-3}, respectively. D, N, and I indicate decreasing, no, and increasing trend during 1998–2016.

3.2.3 Primary production

Primary production in the Yellow Sea and East China Sea has been measured since the 1970s with the ^{14}C method (Guo *et al*., 1991), and later with the ^{13}C method (Hama *et al*., 1997). Ning *et al*. (1988) described very low primary production of 5 to 40 mgC m^{-2} d^{-1} on the shelf and higher offshore (mid-shelf) during winter. On the other hand, it was higher (50–2000 mg C m^{-2} d^{-1}) during summer, with the low and high production observed in the offshore and nearshore, respectively. Hama *et al*. (1997) reported 220 to 350 mgC m^{-2} d^{-1} at the Kuroshio, with little seasonal variability whereas high primary productivity (above 570 mgC m^{-2} d^{-1}) at the center of the continental shelf and nearest to the Changjiang Estuary exhibited a distinctive seasonal change from 68 to 1,500 mgC m^{-2} d^{-1}. Depth-integrated primary productivity was 2.7 times higher in the shelf area than the rates at the Kuroshio, and high Chl-*a* specific productivity (mgC mgChl-a^{-1} d^{-1}) throughout the euphotic zone was found mainly in the shelf area. Gong *et al*. (1997) reported high primary production of 1540 and 1900 mgC m^{-2} d^{-1} in the upwelling region north of Taiwan and in a dinoflagellate bloom in the coastal waters off China, respectively, whereas the Kuroshio water had a low value of 420 mgC m^{-2} d^{-1}.

Because of the importance of annual euphotic zone averaged primary production, Gong *et al*. (1999, 2000, 2003) conducted extensive estimations of seasonal primary production with photosynthesis–irradiance relationships. Gong *et al*. (1999) first estimated 104 gC m^{-2} y^{-1} in Kuroshio water near Taiwan with little seasonal variation. Next, Gong *et al*. (2000) observed the west–east section north of Taiwan and found the annual average in the shelf waters to be quite uniform 549 ± 84 mgC m^{-2} d^{-1} (200 gC m^{-2} y^{-1}). The offshore Kuroshio water showed a weak seasonal variation of 292 ± 15 mgC m^{-2} d^{-1} (107 gC m^{-2} y^{-1}). Then, Gong *et al*. (2003) covered the large area of the southwestern East China Sea from Taiwan to the mouth of the Changjiang River. They found seasonal variation with high primary production with annual primary production of 155 gC m^{-2} y^{-1} in the northwestern area (Changjiang Estuary), where nutrients are high year-round. In the southeastern area, the seasonal variation in production was small and the annual value was 144 gC m^{-2} y^{-1}, although nutrients varied seasonally. They estimated 145 gC m^{-2} y^{-1} for annual primary production of the entire area. They also reported the controlling factors of the primary production were temperature, phosphate, and turbidity in the inner shelf.

Although extensive measurements have been made, it is difficult to cover the large variation of primary production in space and time. Thus, it is natural to use satellite Chl-*a* data to estimate euphotic zone integrated primary production. Gong and Liu (2003) first suggested a simple empirical algorithm for satellite data with specific parameters on the continental shelf of the East China Sea, taking into account the high turbidity in the Changjiang Estuary. Son *et al*. (2005) used satellite Chl-*a* data derived by a local algorithm with an approach using local photosynthesis-irradiance (P-E) parameters and vertical profile models to estimate the primary production in May and September. They pointed out that the primary production is lower in the coastal area than the middle of the Yellow Sea where the turbidity was low and Chl-*a* was higher. They also estimated the daily total primary production for the entire Yellow Sea: 19.7×10^4 tC d^{-1} in May and 15.8×10^4 tC d^{-1} in September.

Siswanto *et al*. (2005) used a vertically resolved primary production model and found the subsurface Chl-*a* maximum contribution to be 20% and 30% for the Kuroshio and Kuroshio frontal area, respectively, although the difference was not easily distinguished. Then, Siswanto *et al*. (2006) tested several different satellite primary production algorithms, including that of Gong and Liu (2003), the vertically resolving model of Siswanto *et al*. (2005) and the Vertically Generalized Production Model (VGPM) of Behrenfeld and Falkowski (1997) with the data of southeastern East China Sea. They concluded the VGPM is the most effective after local tuning of one parameter, and they used it to study the influence of typhoons, as described in subsection 3.2.7. Around the Korean Peninsula, including the Yellow Sea, Yoon *et al*. (2012) tested several primary production models with *in situ* Chl-*a* and euphotic zone depth and found the VGPM modified by Kameda and Ishizaka (2005) works better than with the parameter modified by Siswanto *et al*. (2006) for net primary production. The Kameda and Ishizaka (2005) model was also used by Tan *et al*. (2011) and Tan and Shi (2012) for their study of influence of atmospheric input described later in the middle of the Yellow Sea and in the entire Bohai Sea, Yellow Sea and East China Sea, respectively. Even though Tan *et al*. (2011) and Tan and Shi (2012) verified the satellite Chl-*a* and primary production data with few *in situ* data, as described in the previous section, it is known that there are large errors for the Chl-*a* and euphotic zone depth from the standard algorithm in coastal turbid water, and the results need to be further verified.

There are still few observations of primary production of different phytoplankton groups. Chen, Y.L.L. (2000) measure size fractionated primary production in the Kuroshio and upwelling off Taiwan and shelf area. They found picoplankton (<3 μm) dominated primary productivity (54–83%) as well as Chl-*a* concentration (67–89%) in the Kuroshio water. They also reported that although the picoplankton contribution was less in the Kuroshio, they made important contributions in shelf and upwelling areas, accounting for 29–86% of the Chl-*a* contribution and 19–72% of the primary production. Microplankton was the dominant contributor in the upwelling.

Recently, the use of fluorescence to understand the photophysiology of phytoplankton is becoming popular. Wang, Z. *et al*. (2014) used a phyto-PAM (Pulse Amplitude Modulation) fluorometer to observe the change of maximum photochemical efficiency of photosystem II (Fv/Fm) during spring blooms of *Skeletomema* spp. and *Prorocentrum donghaiense* in the Changjiang Estuary. They found Fv/Fm varied with temperature, turbidity and nutrients with a strong diel cycle, and reported it increased to more than 0.6 before the Chl-*a* increase and start of the bloom, and declined after the bloom. Li *et al*. (2016) also used the phyto-PAM fluorometer to derive various photophysiological parameters of the summer phytoplankton population in the Yellow Sea and East China Sea. They found the Fv/Fm was generally less than 0.5 and photosynthesis activity was relatively low. Recently, Zhu *et al*. (2017) used the Fast Repetitive Rate Fluorometer (FRRF) to derive the Electron Transfer Rate (ETR) of phytoplankton in the East China Sea to compare with carbon uptake, and they found that the electron requirement for carbon uptake is linearly correlated to the light intensity,

and that the slope was different with phytoplankton size structure. They also suggested using the FRRF method to estimate carbon uptake.

3.2.4 New production and nitrogen fixation

Nutrient sources to support primary production are important to understand the ecosystem. The amount of the production supported by external nutrients, such as upwelling, mixing, and river discharge from outside of the euphotic zone is called new production, and the ratio to the total production is the *f*-ratio. Chen *et al*. (1999, 2001, 2004), Chen and Chen (2003) and Kanda *et al*. (2003) intensively studied this subject in the south of the East China Sea by measuring nitrate uptake rate with addition of $^{15}NO_3$. They found that the *f*-ratio, compared to the total primary production measured by carbon isotope incubations after converting with the Redfield ratio, was about 0.3 in a large part of the mid-shelf area. This indicates that two thirds of the production was supported by nitrogen other than nitrate, and regenerated production was dominant. Exceptions were upwelling areas of north of Taiwan and at the mouth of the Changjiang River in winter and summer, respectively, where the *f*-ratio can be higher, and production supported by nitrate can be dominant. Depending on the season and region, there are several different causes for the low *f*-ratio. In the mouth of the Changjiang, phosphate limitation is probably the reason for the low *f*-ratio during summer because the production is supported mostly by the regeneration of both nitrogen and phosphate even when the nitrate iss high. Phosphate supply by wind-induced upwelling produces a higher *f*-ratio with use of abundant nitrate. Light limitation caused by turbidity is also an important factor. Low nitrate is the major factor for the low *f*-ratio in the area not influenced by high nitrate Changjiang discharge, high nitrate and phosphate upwelling, and low-light turbid water.

Shiozaki *et al*. (2011) compared nitrate assimilation with diapycnal nitrate flux in the eastern East China Sea, and found a large discrepancy. The nitrate assimilation was more than 10 times higher than the diapycnal nitrate flux. They also detected a significant amount of archaeal amoA gene at 10 to 1% light depth, and concluded that the nitrification in the euphotic zone may be an important process to keep high nitrate assimilation in this area.

Nitrogen (N_2) fixation is another important biological activity to introduce new nitrogen into the ecosystem. Marumo and Asaoka (1974) reported the importance of the *Trichodesmium* spp. in the East China Sea, which was later reported as a major N_2 fixer in this area by Minagawa and Wada (1986) using nitrogen isotope ratio, in the Kuroshio area of the East China Sea. Shiozaki *et al*. (2010) recently confirmed N_2 fixation in the Kuroshio and eastern East China Sea was 10 times higher than the western and central oligotrophic North Pacific, and mainly associated with *Trichodesimum* spp. Zhang *et al*. (2012a) also measured N_2 fixation in the Yellow Sea and northwest of the East China Sea. They found the maximum N_2 fixation rate in the stratified Kuroshio in the northeastern East China Sea, and very little N_2 fixation in the low salinity water on the shelf. The rate covers 4.6% for Kuroshio and 0.01 to 0.78% of the nitrogen demand for primary production, and the nitrogen flux in this area in summer is equivalent to the atmospheric input and much less than Kuroshio upwelling and Changjiang River input.

Liu *et al*. (2013) compared upward turbulent nitrate flux across the pycnocline, nitrate assimilation, N_2 fixation and primary production to compare the nitrogen sources for new production in summer at the shelf edge of the East China Sea across the Kuroshio. They found high turbulent nitrate flux at the coastal side of the Kuroshio jet which supports high nitrate assimilation and primary production. Although N_2 fixation was low near the jet, it is more important off the shelf and around islands where there is less nitrate flux. They concluded that the source for new production in this area was highly variable.

3.2.5 Community structure

Phytoplankton community structure has been studied by microscope for a long time (*cf*. Ning *et al*., 1988). More recently, epifluorescence microscopy and flow cytometry have been used to discriminate non-photosynthetic microorganisms with photosynthetic organisms, and to determine small phytoplankton efficiently, respectively (see Section 3.1). However, phytoplankton contain various taxonomic groups and determining the whole community structure has not been easy. It is now possible to determine the concentrations of phytoplankton pigments with High Performance Liquid Chlromatography (HPLC), and thus phytoplankton pigments can be used an indicator of each phytoplankton group. CHEMTAX software (Mackey *et al*., 1996) can statistically estimate the percentage of each phytoplankton group of total Chl-*a* concentration. Some studies have been conducted in this area (Table 3.2.1).

Furuya *et al*. (2003) first reported the phytoplankton community measured by HPLC and analyzed by CHEMTAX in an early spring bloom and in well-stratified summer water along the PN line (the Changjiang mouth to the northeast of Okinawa Island, Fig. 3.2.1). During spring, they found a diatom spring bloom on the shelf, and in the contrast, abundant prochlorophytes, chrysophytes, prymnesiophytes and chlorophytes and only patchy diatoms in off-shelf Kuroshio water. During summer, they found a two-layer distribution with cyanobacteria and prochlorophytes in the surface and prochlorophytes, chrysophytes, prymnesiophytes in the subsurface chlorophyll maximum both off and on the shelf.

Lee *et al*. (2009) reported the difference in phytoplankton communities in the northern and southern coastal waters of Jeju Island in May 2005: a predominance (>50%) of diatoms followed by prasinophytes (~14%) and fewer diatoms (<30%) with cryptophytes, prymnesiophytes and cyanobacteria (10–15%) in the higher Chl-*a* northern and lower Chl-*a* southern waters, respectively. They concluded that the discrepancy was caused by the slight difference in source waters. Liu *et al*. (2015a) studied the influence of the Yellow Sea Warm Water from the southeast to the phytoplankton community of the western Yellow Sea in early spring. They found a high concentration of diatoms and dinoflagellates in the Yellow Sea Cold Water to the west and more prasinophytes and cyanobacteria in the Yellow Sea Warm Current to the east. They also found high nutrient content in the Yellow Sea Warm Current compared to the Yellow Sea Cold Water, and remarked about the complexity of the coastal water.

Zhu *et al*. (2009) studied surface phytoplankton pigments of the Changjiang Estuary and adjacent area in spring and summer. They reported that diatoms (34%) and chlorophytes (33%) accounted for equal amounts followed by cryptophytes, prasinophytes, dinoflagellates, chrysophytes and cyanobacteria in spring, and offshore in summer the community was mainly composed by diatoms (74.6%) and dinoflagellates (11.3%) with minor amount of prasinophytes, cryptophytes, cyanobacteria, prochlorophytes and chlorophytes.

Recently, Liu *et al*. (2015b, 2016) extensively studied the seasonal change of phytoplankton pigments in the Yellow Sea and East China Sea. In the southwestern Yellow Sea, Liu *et al*. (2015b) found generally high abundance of diatoms with similar variation with Chl-*a*. In April, a spring bloom was observed with a maximum and average of 98% and 76% of diatom dominances, respectively, with *Thalassiosira pacific*, specifically in the central part of the Yellow Sea influenced by the Yellow Sea Warm Current from the southwest. In August, when stratification was strong and the Yellow Sea Cold Water Mass prevailed, Chl-*a* and diatoms (30%) decreased and cyanobacteria (36%) increased. In October, with the decaying of the Yellow Sea Cold Water Mass, chrysophytes (38%) and pracinophyte (18%) increased. In March, pracinophytes (29%) increased along with diatoms (50%), such as *Paralia sulcata* and *Coscinodiscus* spp. Therefore, the strong seasonality of phytoplankton variability is clear in the central part of the Yellow Sea.

Table 3.2.1 Dominant phytoplankton groups in the Yellow Sea and East China Sea.

Yellow Sea

		Spring				Summer				Fall	Winter	
Water mass	**Reference**	**March**	**April**	**May**	**May–early Jun.**	**late Jun.–Aug.**	**Jul.**	**Jul.–Aug.**	**Aug.**	**Oct.**	**late Nov.–early Dec.**	**late Dec.–early Jan.**
YSCC	Liu *et al.*, 2015a	Diatom (68%)										
YSCWM	Liu *et al.*, 2015b							Diatom (30%) Cyano (20%)		Chryso (40%) Diatom (30%) Prasino (20%)		
Spring bloom YSCWM, YSWC	Liu *et al.*, 2015b		Diatom (80%)									
Frontal area of YCC and YSWC	Liu *et al.*, 2015a	Diatom (60%) Cyano (40%) Chloro (12%)										
YSWC	Liu *et al.*, 2015a	Diatom (35%) Cyano (35%) Chloro (30%)										
	Liu *et al.*, 2015b	Diatom (50%) Pracino (30%)										
North of Jeju	Lee *et al.*, 2009			Diatom (45%) Prasino (20%)								
South of Jeju				Prasino (30%) Diatom (20%) Crypto (15%) Pelago (15%) Cyano (15%)								

Table 3.2.1 Continued.

East China Sea

		Spring				Summer				Fall	Winter	
Water mass	**Reference**	**March**	**April**	**May**	**May–early Jun.**	**late Jun.–Aug**	**Jul.**	**Jul.–Aug.**	**Aug.**	**Oct.**	**late Nov.–early Dec.**	**late Dec.–early Jan.**
Changjiang Estuarine	Zhu *et al.*, 2009		Diatom (34%) Chloro (33%) Crypto (12%)						Diatom (75%) Dino (11%)			
	Furuya *et al.*, 2003		Diatom (50%) Chloro (25%)					Diatom (90%)				
CDW 2009	Xu *et al.*, 2018						Diatom (44%) Dino (18%)					
CDW 2013							Diatom (50%) Dino (14%) Prymnesio (26%)					
CDW 2010							Cyano (47%) Chloro (16%)					
CDW 2011							Cyano (21%) Chloro (17%)					
Mid-shelf water	Liu *et al.*, 2016				Diatom (40%) Dino (40%)	Diatom (60%)					Diatom (60%) Crypto (15%)	Diatom (60%) Crypto (15%)
	Furuya *et al.*, 2003		Diatom (50%) Chloro (15%)					Diatom (15%) Cyano (25%) Prochloro (25%)				
SW 2009	Xu *et al.*, 2018						Datom (54%) Dino (14%)					
SW 2011							Cyano (32%) Prymnesio (29%)					
SW 2013							Prymnesio (43%)					

Table 3.2.1 Continued.

East China Sea

		Spring				Summer				Fall	Winter	
Water mass	**Reference**	**March**	**April**	**May**	**May–early Jun.**	**late Jun.–Aug**	**Jul.**	**Jul.–Aug.**	**Aug.**	**Oct.**	**late Nov.–early Dec.**	**late Dec.–early Jan.**
Kuroshio Water	Liu *et al.*, 2016				Diatom (55%)	Diatom (35%) Synecho (30%) Prochloro (10%)					Diatom (40%) Prasino (18%) Chryso (15%) Chrypto (12%)	Diatom (42%) Prasinos (20%) Chryso (15%) Chrypto (12%)
	Furuya *et al.*, 2003		Chryso (25%) Prymnesio (20%) Chloro (20%) Prochloro (15%)					Cyano (20%) Prochloro (30%) Chryso (15%) Prymnesio (15%)				
	Xu *et al.*, 2018						Cyano (51%) Prochloro (28%)					

Percentages are approximated from the description in the references.

YSCC: Yellow Sea Cold Current, YSCWM: Yellow Sea Cold Water Mass, YSWC: Yellow Sea Warm Current, CDW: Changjiang Diluted Water, SW: Shelf Water. Diatom (orange), Dino (Dinoflagellate, red), Crypoto (Crypotophyte, yellow), Chloro (Chlorophyte, green), Pracino (Pracinophyte, green), Cyano (Cyanobacteria, blue), Synecho (*Synechococcus*, blue), Prochloro (Prochlorophyte, light green), Chryso (Chrysophyte), Prymnesio (Prymnesiophyte), Pelago (Pelagophyte), Chryso (Chrysophyte), Cyanobacteria may include *Synechococcus* but not *Prochlorococcus*.

Liu *et al*. (2016) studied the seasonal and spatial patterns of phytoplankton variability in the East China Sea. They found three patterns of seasonal variability: (i) blooms in the Changjiang River plume with high biomass of dinoflagellates and diatoms in spring; (ii) significant spatial differences, including high biomass of diatoms in the river plume and low biomass and picophytoplankton, such as *Prochlorococcus* dominance in the Kuroshio water during summer and early autumn; and (iii) relatively low biomass and uniform distributions but higher contributions of cryptophytes, prasinophytes, and chrysophytes during late autumn and winter.

With the large dataset, Liu *et al*. (2016) used the Generalized Additive Model (GAM) to elucidate the specific environmental factors related to the phytoplankton community structure. Diatoms dominated, especially during the summer months, influenced by the Changjiang River plume. Dinoflagellates, a important group during spring blooms, showed a clear salinity optimum of around 31, and were also affected by temperature. *Prochlorococcus* and *Synechococcus* abundance increased strongly with higher temperature; while *Prochlorococcus* was abundant in the Kuroshio, *Synechococcus* was abundant in the Changjiang River plume during summer, with sensitivity to nutrient variability and with broader tolerance to low-salinity conditions. Chrysophytes (~17%) and prasinophytes (~15%) were abundant in the Kuroshio during autumn and winter, whereas cryptophytes (~20%) were higher in winter in the plume and at mid-shelf.

More recently, Xu *et al*. (2018) reported the interannual variation of the summer phytoplankton community south of Jeju Island where Changjiang Diluted Water can be seen. In general, the spatial distribution was similar to the previous reports, with more diatoms in the west and *Prochlorococcus* and other cyanobacteria abundant in Kuroshio-originated water in the east. However, there was significant interannaual differences, where diatoms were more abundant in 2009 and 2013 while a mixed population of cyanobacteria, chlorophytes and other groups were observed in 2010 and 2011. They also found a significant difference in inorganic phosphate amounts between those different years: high inorganic phosphate in diatom-dominated years and low inorganic phosphate in other phytoplankton-dominated years. They further discussed the possibility that mixing of high N:P ratio Changjiang River waters with low N:P ratio coastal upwelling water along the Chinese coast may influence the N:P ratio and consequently the variability of the phytoplankton community in the south of Jeju Island.

Using HPLC phytoplankton pigment information, Wang, S.Q. *et al*. (2014) calculated the phytoplankton community by size, separating micro- (diatoms and dinoflagellates), nano- (cryptophytes, chromophytes, green flagellates), and pico- (cyanobacteria including *Prochlorococcus*) sized phytoplankton. They compared the relation between size fraction to Chl-*a* concentration between waters from the south of Jeju to Tsushima Strait. It is known that in the global ocean large phytoplankton dominate when the Chl-*a* concentration is increased. However, they found the relationship was consistent in the water in Tsushima Strait, but not in the East China Sea. This finding agrees with the report of Xu *et al*. (2018) who found diatoms were less abundant in phosphate-limited Changjiang Diluted Water. Wang, S.Q. *et al*. (2014) further found that the difference in the size structure was also noticeable from the optical properties. Wang, S.Q. *et al*. (2015) and Wang, S. (2016) and Zhang *et al*. (2018) further indicated that the phytoplankton size structure can be observable by multi-spectral fluorescence as well as from ocean color satellite data. In the near future, it is expected that those methods will be used to understand the variability of the phytoplankton community structure.

3.2.6 Influence of the Three Gorge Dam

As we described earlier, Changjiang River Discharge is known as one of the most important factors for phytoplankton variability in the East China Sea. Much attention has been paid to the impact the construction of the Three Gorges Dam has had on the East China Sea ecosystem because it has drastically changed the nutrient supply, including upwelling, and sediment input as well as freshwater discharge (Chen, C.T.A. 2000). Gong *et al*. (2006) suggested a reduction of the Si:N ratio from 1.5 to 0.4 with sediment loading of 55% at the Datong station from 1998 to 2004, specifically after the first filling phase of June 2003. Comparing results of six cruises during June 1998 and July 2003 in the traditionally high nutrient Changjiang Estuary, they also showed an 86% reduction in primary production as well as a reduction of nutrients and diatoms associated with the increase of salinity. Jiao *et al*. (2007) suggested significant differences in ecological parameters between September 2003, two months after the first filling of the dam in June 2003, and September 2002, before the filling. They found higher salinity, expected from low freshwater discharge and possible expansion of the Taiwan Warm Current in 2003, and higher Chl-*a*, particulate organic carbon and transparency estimated by satellite. They also found high Chl-*a* with larger size fraction (>20 μm), including *Chaetoceros* spp. and *Pseudo-nitzschia* spp. in the estuary, whereas smaller size *Synechococcus* was abundant offshore, and this result seems to contradict the earlier observation of Gong *et al*. (2006). They also reported more *Prochlorococcus* on the shelf, more heterotrophic bacteria both in the estuary and on the shelf in 2003, and lower diversity of microbial community by the 16s rDNA analysis in 2003.

On the other hand, Yuan *et al*. (2007) argued that the change in June 2003 was within the large variation shown by satellite Chl-*a* from 1997 September to June 2006, although Gong *et al*. (2007) denied the objection because of the inaccurate satellite data with a non-focused studied area. Yamaguchi *et al*. (2012) carefully analyzed the satellite Chl-*a* data, specifically focusing on a relatively accurate mid-shelf region and showed that Chl-*a* in 2003 was within the 10-year variation and that Chl-*a* was lower in 2006, when the second filling phase of the dam took place. However, they concluded that even the change in 2006 was mostly not caused by the filling because Dai *et al*. (2008) indicated that the reduction of Changjiang freshwater discharge from 2005 to 2006 was mostly caused by a severe drought in 2006 and that the influence of the filling of the dam was only 1/5 that of the drought.

More recently, Chen *et al*. (2017) analyzed the satellite Chl-*a* of the Changjiang Estuary and where hypoxia frequently occurs, and they concluded that the reduction of suspended matter caused by the construction of Three Gorges Dam was what caused the shift of high Chl-*a* and hypoxia area to a more shoreward direction. It is necessary to do a long-term study on the influence of the construction of the Three Gorge Dam not only by the change in freshwater discharge, but also changes in the amount of sediment and nutrients, as well as the composition of nutrients.

3.2.7 Influence of typhoons

It has been suggested that global warming may enhance the intensity of tropical cyclones, such as typhoons in the western Pacific. It is also suggested that the strong disturbance of the tropical cyclone may influence the marine ecosystem, specifically by increasing primary production because of strong mixing and/or upwelling caused by the strong wind. The East China Sea is one of the locations where several typhoons often pass and turn in a year, and the influence of the typhoon is expected to be large. Studying the influence of typhoons on the marine ecosystem is not particularly easy because of its unpredictability and destructive capabilities. It is becoming popular to study the influence of typhoons on primary production by ocean color satellite; however,

scientists from Chinese Taipei are fairly active in investigating typhoons, even by ship, in the East China Sea.

Chang *et al*. (1996) is a pioneer in studying the influence of typhoons in the region northeast of Taiwan. They conducted four cruises before and after the typhoon in 1994 and reported the initial decrease in phytoplankton and increase in nutrients following the increase of larger (>5 μm) phytoplankton. Shiah *et al*. (2000) also noted an increase in Chl-*a*, nitrate, particulate organic carbon, primary production, bacteria production and bacteria biomass by ship observation northwest of Taiwan before and after typhoons Gloria and Herb in 1996, and suggested wind mixing, resuspension and terrestrial runoff are the important factors. Chen*et al*. (2003) suggested upwelling enhanced by buoyancy effects as well as the coastward movement of the Kuroshio for the same typhoons in 1996. The shelfward movement of the Kuroshio caused by the long-lasting southerly wind by typhoon was confirmed by Morimoto *et al*. (2009) through high frequency (HF) radar observation and a coupled atmospheric–ocean model, and Chang *et al*. (2008) confirmed the phytoplankton responses to the upwelling by satellite observations. Siswanto *et al*. (2009) used satellite observations of 16 typhoons from 2003 to 2007 in the upwelling region northeast of Taiwan and estimated enhancement of the upwelling of nutrients promoted new productivity, which consists 0.6 to 11.8% of the East China Sea summer–fall new production.

Further observations were conducted in the southern East China Sea to verify the increase of particulate organic carbon flux by typhons in 2008 (Hung *et al*., 2010, 2013, 2014; Hung and Gong, 2011; Shih *et al*., 2013). Chung *et al*. (2012) and Jang *et al*. (2013) observed that upwelling and floodwater enhanced by typhoon Morakot in 2009 produced a low N:P ratio and an increase in chain-forming centric diatoms (*Chaetoceros* spp.) instead of the cyanobacteria, *Trichodesmium*, and dinoflagellates, *Gymnodinium* spp. Furthermore, they suggested copepod grazing terminated the diatom bloom. He *et al*. (2014) also showed, by transparency images from ocean color satellite, transport of terrestrial material to the northeast of Taiwan from east and west of Taiwan Island coasts and Mainland China coast, and a bloom of phytoplankton by typhoon Morakot in 2009.

Zhao *et al*. (2015) observed the influence of typhoon Marat in 2005 and compared the offshore east of Taiwan Island and nearshore of Mainland China and showed a decrease in satellite Chl-*a* in the nearshore area. Wang, T. *et al*. (2016) also observed the influence of typhoon Haikui in 2012 in the Changjiang River Estuary and found vertical mixing was strong during the passing of the typhoon, and that both terrestrial runoff and intrusion of offshore water were important for the nutrients and phytoplankton dynamics after the typhoon.

Although the ship observations were conducted in the coastal area to the north of Taiwan, satellite is the still the only tool for most of the other areas, including outer shelf. In the outer shelf of the East China Sea, Siswanto *et al*. (2008) conducted a detailed observation of upwelling/mixing caused by typhoon Meari in 2004. They were lucky to find Argo float data on time, as well as the satellite microwave SST and ocean color Chl-a/primary production data. They estimated nitrate concentration from the temperature change and 3.8% of annual carbon export caused by this one strong typhoon. Siswanto *et al*. (2007) analyzed 13 typhoons from 1998 to 2004 using ocean color Chl-*a* and primary production and information of the typhoon passing through the outer shelf of East China Sea. They formulated a simple equation of estimation of primary production enhancement from maximum wind speed, typhoon transit speed, and bottom depth and reconstructed the enhancement from 1980 to 2004. They estimated the enhancement was 0.4 to 39.7% of new production in the East China Sea. They found that the enhancement was much higher for El Niño years because of the occurrence of strong winds, and that the enhancement increased during the 1990s because of more typhoons passing over the East China Sea.

One interesting style of observations was conducted on the northwestern coast of Okinawa Island, Japan, in which Grossmann *et al*. (2015) set a camera mounted on an underwater observatory system and reported the change of 20-m near-bottom mesoplankton compositions after a series of typhoons in 2013. They observed an increase in *Trichodesmium*, diatom, and radiolarian abundances after a series of September typhoons although Chl-*a* concentrations were not increased.

3.2.8 Future perspective

Development of ocean color satellite data is helping us to understand large-scale seasonal-to-decadal variations and some event-scale variations in chlorophyll-a in the Yellow Sea and East China Sea. Associated variations in primary production and phytoplankton size structure are also promising to be understood. However, ocean color satellite information is only limited to the surface. Subsurface chlorophyll-a maximum is often reported in this area and detailed behavior of this phenomena is still not well studied. HPLC pigment analysis gives a clearer view of the phytoplankton community structure, although the dynamics of this complicated physical and chemical regime is far from being understood. Recent improvement of sensors, to measure the physiological parameters, and of molecular biological techniques are definitely opening new paradigms of phytoplankton studies. It is obvious that phytoplankton and primary production is the key process onnecting physical oceanographic research on variabilities, including climate change, and ecosystem dynamics, including carbon cycles. Those processes should be studied simultaneously to understand the close coupling between physics, chemistry and biology.

3.2.9 References

Behrenfeld, M.J. and Falkowski, P.G. 1997. Photosynthetic rates derived from satellite-based chlorophyll concentration. *Limnol. Oceanogr*. **42**: 1–20, doi:10.4319/lo.1997.42.1.0001.

Chang, J., Chung, C.C. and Gong, G.C. 1996. Influences of cyclones on chlorophyll a concentration and *Synechococcus* abundance in a subtropical western Pacific coastal ecosystem. *Mar. Ecol. Prog. Ser.* **140**: 199–205, doi:10.3354/meps140199.

Chang, Y., Liao, H.-T., Lee, M.-A., Chan, J.-W., Shieh, W.-J., Lee, K.-T., Wang, G.-H. and Lan, Y.-C. 2008. Multisatellite observation on upwelling after the passage of Typhoon Hai-Tang in the southern East China Sea. *Geophys. Res. Lett*. **35**: L03612, doi:10.1029/2007GL032858.

Chen, C.-T.A. 2000. The Three Gorges Dam: Reducing the upwelling and thus productivity in the East China Sea. *Geophys. Res. Lett*. **27**: 381–383, doi:10.1029/1999GL002373.

Chen, C.T.A., Liu, C.T., Chuang, W.S., Yang, Y.J., Shiah, F.-K., Tang, T.Y. and Chung, S.W. 2003. Enhanced buoyancy and hence upwelling of subsurface Kuroshio waters after a typhoon in the southern East China Sea. *J. Mar. Syst.* **42**: 65–79, doi:10.1016/S0924-7963(03)00065-4.

Chen, J., Pan, D., Liu, M., Mao, Z., Zhu, Q., Chen, N., Zhang, X. and Tao, B. 2017. Relationships between long-term trend of satellite-derived chlorophyll-a and hypoxia off the Changjiang Estuary. *Estuar. Coasts* **40**: 1055–1065, doi:10.1007/s12237-016-0203-0.

Chen, Y.L.L. 2000. Comparisons of primary productivity and phytoplankton size structure in the marginal regions of southern East China Sea. *Cont. Shelf Res*. **20**: 437–458, doi:10.1016/S0278-4343(99)00080-1.

Chen, Y.L.L., Lu, H.B., Shiah, F.K., Gong, G.C., Liu, K.K. and Kanda, J. 1999. New production and F-ratio on the continental shelf of the East China Sea: Comparisons between nitrate inputs from the subsurface Kuroshio current and the Changjiang River. *Estuar. Coast. Shelf Sci*. **48**: 59–75, doi:10.1006/ecss.1999.0404.

Chen, Y.L.L., Chen, H.Y., Lee, W.H., Hung, C.C., Wong, G.T.F. and Kanda, J. 2001. New production in the East China Sea, comparison between well-mixed winter and stratified summer conditions. *Cont. Shelf Res*. **21**: 751–764, doi:10.1016/S0278-4343(00)00108-4.

Chen, Y.L.L. and Chen, H.Y. 2003. Nitrate-based new production and its relationship to primary production and chemical hydrography in spring and fall in the East China Sea. *Deep Sea Res. II* **50**: 1249–1264, doi:10.1016/S0967-0645(03)00021-3.

Chen, Y.L.L., Chen, H.Y., Gong, G.C., Lin, Y.H., Jan, S. and Takahashi, M. 2004. Phytoplankton production during a summer coastal upwelling in the East China Sea. *Cont. Shelf Res*. **24**: 1321–1338, doi:10.1016/j.csr.2004.04.002.

Chung, C.C., Gong, G.C. and Hung, C.-C. 2012. Effect of Typhoon Morakot on microphytoplankton population dynamics in the subtropical Northwest Pacific. *Mar. Ecol. Prog. Ser.* **448**: 39–49, doi:10.3354/meps09490.

Dai, Z., Du, J., Li, J., Li, W. and Chen, J. 2008. Runoff characteristics of the Changjiang River during 2006: effect of extreme drought and the impounding of the Three Gorges Dam. *Geophys. Res. Lett*. **35**: L07406, doi:10.1029/2008GL033456.

Furuya, K., Hayashi, M., Yabushita, Y. and Ishikawa, A. 2003. Phytoplankton dynamics in the East China Sea in spring and summer as revealed by HPLC-derived pigment signatures. *Deep Sea Res. II* **50**: 367–387, doi:10.1016/S0967-0645(02)00460-5.

Gong, G.C. 2004. Absorption coefficients of colored dissolved organic matter in the surface waters of the East China Sea. *Terr. Atmos. Ocean. Sci*. **15**: 75–87, doi:10.3319/TAO.2004.15.1.75(O).

Gong, G.C. and Liu, G.J. 2003. An empirical primary production model for the East China Sea. *Cont. Shelf Res*. **23**: 213–224, doi:0.1016/S0278-4343(02)00166-8.

Gong, G.C., Shiah, F.K., Liu, K.K., Chuang, W.S. and Chang, J. 1997. Effect of the Kuroshio intrusion on the chlorophyll distribution in the southern East China Sea during spring 1993. *Cont. Shelf Res*. **17**: 79–94, doi:10.1016/0278-4343(96)00022-2.

Gong, G.-C., Chang, J. and Wen, Y.-H. 1999. Estimation of annual primary production in the Kuroshio waters northeast of Taiwan using a photosynthesis-irradiance model. *Deep Sea Res*. **46**: 93–108, doi:10.1016/S0967-0637(98)00057-0.

Gong, G.-C., Shiah, F.-K., Liu, K.-K., Wen, Y.-H. and Liang, M.-H. 2000. Spatial and temporal variation of chlorophyll *a*, primary productivity and chemical hydrography in the southern East China Sea. *Cont. Shelf Res*. **20**: 411–436, doi:10.1016/S0278-4343(99)00079-5.

Gong, G.C., Wen, Y.H., Wang, B.W. and Liu, G.J. 2003. Seasonal variation of chlorophyll a concentration, primary production and environmental conditions in the subtropical East China Sea. *Deep Sea Res. II* **50**: 1219–1236, doi:10.1016/S0967-0645(03)00019-5.

Gong, G.C., Chang, J., Chiang, K.-P., Hsiung, T.-M., Hung, C.-C., Duan, S.-W. and Codispoti, L.A. 2006. Reduction of primary production and changing of nutrient ratio in the East China Sea: Effect of the Three Gorges Dam? *Geophys. Res. Lett*. **33**: doi:10.1029/2006GL025800.

Gong, G.C., Hung, C.C. and Chang, J. 2007. Reply to Comment by Jinchun Yuan et Al. on 'Reduction of primary production and changing of nutrient ratio in the East China Sea: Effect of the Three Gorges Dam?' *Geophys. Res. Lett*. **34**: 2–4, doi:10.1029/2006GL029036.

Grossmann, M.M., Gallager, S.M. and Mitarai, S. 2015. Continuous monitoring of near-bottom mesoplankton communities in the East China Sea during a series of typhoons. *J. Oceanogr.* **71**: 115–124.

Guo, Y.J. 1991. The Kuroshio. 2. Primary productivity and phytoplankton. *Oceanogr. Mar. Biol*. **29**: 155–189.

Hama, T., Shin, K.H. and Handa, N. 1997. Spatial variability in the primary production in the East China Sea and adjacent waters. *J. Oceanogr*. **53**: 41–51, doi:10.1007/BF02700748.

He, X., Bai, Y., Chen, C.-T.A, Hsin, Y.-C., Wu, C.-R., Zhai, W., Liu, Z. and Gong, F. 2014. Satellite views of the episodic terrestrial material transport to the southern Okinawa Trough driven by typhoon. *J. Geophys. Res. Oceans* **119**: 4490–4504, doi:10.1002/2014JC009872.

Hung, C.C. and Gong, G.C. 2011. Biogeochemical responses in the southern East China Sea after typhoons. *Oceanography* **24**: 42–51, doi:10.5670/oceanog.2011.93.

Hung, C.C., Gong, G.C., Chou, W.-C., Chung, C.-C., Lee, M.-A., Chang, Y., Chen, H.-Y., Huang, S.-J., Yang, Y., Yang, W.-R., Chung, W.-C., Li, S.-L. and Laws, E. 2010. The effect of typhoon on particulate organic carbon flux in the southern East China Sea. *Biogeosciences* **7**: 3007–3018, doi:10.5194/bg-7-3007-2010.

Hung, C.C., Chung, C.C., Gong, G.C., Jan, S., Tsai, Y., Chen, K.-S., Chou, W.C., Lee, M.-A., Chang, Y., Chen, M.H., Yang, W.R., Tseng, C.-J. and Gawarkiewicz, G. 2013. Nutrient supply in the southern East China Sea after Typhoon Morakot. *J. Mar. Res*. **71**: 133–149, doi:10.1357/002224013807343425.

Hung, C.C., Gong, G.C., Lee, M.-A., Liao, C.-H., Chang, Y., Shih, Y.-Y., Chen, K.-S., Chen, M.-H. and Santschi, P.H. 2014. Impacts of typhoons on nutrient supply and potential fish production in the southern East China Sea, pp. 267–282 *in:* Typhoon Impact and Crisis Management *edited by* G. Sui, Springer, Berlin.

Jang, P.G., Shin, H.H., Jang, P.-G., Shin, H.H., Baek, S.H., Jang, M.C., Lee, T.S. and Shin, K. 2013. Nutrient distribution and effects on phytoplankton assemblages in the western Korea/Tsushima Strait. *N.Z. J. Mar. Fresh. Res*. **47**: 21–37, doi:10.1080/00288330.2012.718284.

Jiao, N., Zhang, Y., Zeng, Y., Gardner, W.D., Mishonov, A.V., Richardson, M.J., Hong, N., Pand, D., Yane, X.-H., Joe, Y.-H., Chen, C.-T.A., Wang, P., Chen, Y., Hong, H., Bai, Y., Chen, X., Huang, B., Deng, H., Shi, Y. and Yang, D. 2007. Ecological anomalies in the East China Sea: impacts of the Three Gorges Dam? *Water Res*. **41**: 1287–1293, doi:10.1016/j.watres.2006.11.053.

Kameda, T. and Ishizaka, J. 2005. Size-fractionated primary production estimated by a two-phytoplankton community model applicable to ocean color remote sensing. *J. Oceanogr.* **61**: 663–672, doi:10.1007/s10872-005-0074-7.

Kanda, J., Itoh, T., Ishikawa, D. and Watanabe, Y. 2003. Environmental control of nitrate uptake in the East China Sea. *Deep Sea Res. II* **50**: 403–422, doi:10.1016/S0967-0645(02)00464-2.

Kiyomoto, Y., Iseki, K. and Okamura, K. 2001. Ocean color satellite imagery and shipboard measurements of chlorophyll a and suspended particulate matter distribution in the East China Sea. *J. Oceanogr.* **57**: 37–45, doi:10.1023/A:1011170619482.

Lee, Y.-W., Lee, J.-M. and Kim, G. 2009. Identifying sharp hydrographical changes in phytoplankton community structure using HPLC pigment signatures in coastal waters along Jeju Island, Korea. *Ocean Sci. J.* **44**: 1–10, doi:10.1007/s12601-009-0001-8.

Li, J.L., Sun, X.X. and Zheng, S. 2016. In situ study on photosynthetic characteristics of phytoplankton in the Yellow Sea and East China Sea in summer 2013. *J. Mar. Syst.* **160**: 94–106, doi:10.1016/j.jmarsys.2016.03.016.

Liu, X., Furuya, K., Shiozaki, T., Masuda, T., Kodama, T., Sato, M., Kaneko, H., Nagasawa, M. and Yasuda, I. 2013. Variability in nitrogen sources for new production in the vicinity of the shelf edge of the East China Sea in summer. *Cont. Shelf Res.* **61–62**: 23–30, doi:10.1016/j.csr.2013.04.014.

Liu, X., Chiang, K.P., Liu, S.M., Wei, H., Zhao, Y. and Huang, B.Q. 2015a. Influence of the Yellow Sea Warm Current on phytoplankton community in the central Yellow Sea. *Deep Sea Res.* **106**: 17–29, doi:10.1016/j.dsr.2015.09.008.

Liu, X., Huang, B.Q., Huang, Q., Wang, L., Ni, X.B., Tang, Q.S., Sun, S., Wei, H., Liu, S.M., Li, C.L. and Sun, J. 2015b. Seasonal phytoplankton response to physical processes in the southern Yellow Sea. *J. Sea Res*. **95**: 45–55, doi:10.1016/j.seares.2014.10.017.

Liu, X., Xiao, W.P., Landry, M.R., Chiang, K.P., Wang, L. and Huang, B.Q. 2016. Responses of phytoplankton communities to environmental variability in the East China Sea. *Ecosystems* **19**: 832–849, doi:10.1007/s10021-016-9970-5.

Mackey, M.D., Mackey, D.J., Higgins, H.W. and Wright, S.W. 1996. CHEMTAX – a program for estimating class abundances from chemical markers: application to HPLC measurements of phytoplankton. *Mar. Ecol. Prog. Ser.* **144**: 265–283, doi:10.3354/meps144265.

Marumo, R. and Asaoka, O. 1974. *Trichodesmium* in the East China Sea: 1. Distribution of *Trichodesmium thiebautii* Gomont during 1961–1967. *J. Oceanogr. Soc. Japan* **30**: 298–303, doi: 10.1007/BF02109673.

Minagawa, M. and Wada, E. 1986. Nitrogen isotope rations of red tide organisms in the East China Sea: A characterization of biological nitrogen fixation. *Mar. Chem*. **19**: 245–259, doi:10.1016/0304-4203(86)90026-5.

Morimoto, A., Kojima, S., Jan, S. and Takahashi, D. 2009. Movement of the Kuroshio axis to the northeast shelf of Taiwan during typhoon events. *Estuar. Coast. Shelf Sci*. **82**: 547–552, doi:10.1016/j.ecss.2009.02.022.

Ning, X., Vaulot, D., Zhensheng, L. and Zilin, L. 1988. Standing stock and production of phytoplankton in the estuary of the Changjiang (Yangtse River) and the adjacent East China Sea. *Mar. Ecol. Prog. Ser.* **49**: 141–150.

Ning, X., Liu, Z., Cai, Y. and Fang, M. 1998. Physicobiological oceanographic remote sensing of the East China Sea: Satellite and in situ observations. *J. Geophys. Res. Oceans* **103**: 21,623–21,635, doi:10.1029/98JC01612.

Shi, W. and Wang, M. 2009. An assessment of the black ocean pixel assumption for MODIS SWIR bands. *Remote Sens. Environ*. **113**: 1587–1597.

Shiah, F.K., Chung, S.W., Kao, S.-J., Gong, G.-C. and Liu, K.-K. 2000. Biological and hydrographical responses to tropical cyclones (typhoons) in the continental shelf of the Taiwan Strait. *Cont. Shelf Res.* **20**: 2029–2044, doi:10.1016/S0278-4343(00)00055-8.

Shih, Y.Y., Hsieh, J.S., Gong, G.-C., Hung, C.-C., Chou, W.-C., Lee, M.-A., Chen, K.-S., Chen, M.-H. and Wu, C.-R. 2013. Field observations of changes in SST, chlorophyll and POC flux in the southern East China Sea before and after the passage of Typhoon Jangmi. *Terr. Atmos. Ocean. Sci*. **24**: 899–910, doi:10.3319/TAO.2013.05.23.01.

Shiozaki, T., Furuya, K., Kodama, T., Kitajima, S., Takeda, S., Takemura, T. and Kanda, J. 2010. New estimation of N_2 fixation in the western and central Pacific Ocean and its marginal seas. *Global Biogeochem. Cycles* **24**: doi:10.1029/2009GB003620.

Shiozaki, T., Furuya, K., Kurotori, H., Kodama, T., Takeda, S., Endoh, T., Yoshikawa, Y., Ishizaka, J. and Matsuno, T. 2011. Imbalance between vertical nitrate flux and nitrate assimilation on a continental shelf: Implications of nitrification. *J. Geophys. Res. Oceans* **116**: C10031, doi:10.1029/2010JC006934.

Siswanto, E., Ishizaka, J. and Yokouchi, K. 2005. Estimating chlorophyll-a vertical profiles from satellite data and the implication for primary production in the Kuroshio front of the East China Sea. *J. Oceanogr.* **61**: 575–589, doi:10.1007/s10872-005-0066-7.

Siswanto, E., Ishizaka, J. and Yokouchi, K. 2006. Optimal primary production model and parameterization in the eastern East China Sea. *J. Oceanogr.* **62**: 361–372, doi:10.1007/s10872-006-0061-7.

Siswanto, E., Ishizaka, J., Yokouchi, K., Tanaka, K. and Tan, C.K. 2007. Estimation of interannual and interdecadal variations of typhoon-induced primary production: A case study for the outer shelf of the East China Sea. *Geophys. Res. Lett*. **34**: L03604, doi:10.1029/2006GL028368.

Siswanto, E., Ishizaka, J., Morimoto, A., Tanaka, K., Okamura, K., Kristijono, A. and Saino, T. 2008. Ocean physical and biogeochemical responses to the passage of Typhoon Meari in the East China Sea observed from Argo float and multiplatform satellites. *Geophys. Res. Lett*. **35**: L15604, doi:10.1029/2008GL035040.

Siswanto, E., Morimoto, A. and Kojima, S. 2009. Enhancement of phytoplankton primary productivity in the southern East China Sea following episodic typhoon passage. *Geophys. Res. Lett*. **36**: doi:10.1029/2009GL037883.

Siswanto, E., Tang, J., Yamaguchi, H., Ahn, Y.-H., Ishizaka, J., Yoo, S., Kim, S.-W., Kiyomoto, Y., Yamada, K., Chiang, C. and Kawamura, H. 2011. Empirical ocean-color algorithms to retrieve chlorophyll-a, total suspended matter, and colored dissolved organic matter absorption coefficient in the Yellow and East China Seas. *J. Oceanogr.* **67**: 627–650, doi:10.1007/s10872-011-0062-z.

Son, S., Campbell, J., Dowell, M., Yoo, S. and Noh, J. 2005. Primary production in the Yellow Sea determined by ocean color remote sensing. *Mar. Ecol. Prog. Ser.* **303**: 91–103, doi:10.3354/meps303091.

Tan, S.C. and Shi, G.Y. 2012. The relationship between satellite-derived primary production and vertical mixing and atmospheric inputs in the Yellow Sea cold water mass. *Cont. Shelf Res*. **48**: 138–145, doi:10.1016/J.CSR.2012.07.015.

Tang, D.L., Ni, I.H., Muller-Karger, F.E. and Liu, Z.J. 1998. Analysis of annual and spatial patterns of CZCS-derived pigment concentration on the continental shelf of China. *Cont. Shelf Res*. **18**: 1493–1515, doi:10.1016/S0278-4343(98)00039-9.

Terauchi, G., Yu, Z., Wu, Z., Maure, E., Kachur, V., Lee, C. and Ishizaka, J. 2018. Assessment of Eutrophication Using Remotely Sensed Chlorophyll-a in the Northwest Pacific Region. Proc. of the SPIE, Vol. 10778, p. 107780H–4, doi:10.1117/12.2324641.

Wang, S., Xiao, C., Ishizaka, J., Qiu, Z., Sun, D., Xu, Q., Zhu, Y., Huan, Y. and Watanabe, Y. 2016. Statistical approach for the retrieval of phytoplankton community structures from in situ fluorescence measurements. *Optics Express* **24**: 23,635–23,653, doi:10.1364/OE.24.023635.

Wang, S.Q., Ishizaka, J., Yamaguchi, H., Tripathy, S.C., Hayashi, M., Xu, Y.J., Mino, Y., Matsuno, T., Watanabe, Y. and Yoo, S.J. 2014. Influence of the Changjiang River on the light absorption properties of phytoplankton from the East China Sea. *Biogeosciences* **11**: 1759–1773, doi:10.5194/bg-11-1759-2014.

Wang, S.Q., Ishizaka, J., Hirawake, T., Watanabe, Y., Zhu, Y., Hayashi, M. and Yoo, S. 2015. Remote estimation of phytoplankton size fractions using the spectral shape of light absorption. *Optics Express* **23**: 10,301–10,318, doi:10.1364/OE.23.010301.

Wang, T., Liu, G.P., Gao, L., Zhu, L., Fu, Q. and Li, D. 2016. Biological and nutrient responses to a typhoon in the Yangtze estuary and the adjacent sea. *J. Coast. Res*. **32**: 323–332, doi:10.2112/JCOASTRES-D-15-00006.1.

Wang, Z., Wang, J. and Tan, L. 2014. Variation in photosynthetic activity of phytoplankton during the spring algal blooms in the adjacent area of Changjiang River estuary. *Ecol. Indicat*. **45**: 465–473.

Xu, Q., Sukigara, C., Goes, J.I., do Rosario Gomes, H., Zhu, Y., Wang, S., Shen, A., de Raús Maúre, E., Matsuno, T., Watanabe, Y., Yoo, S. and Ishizaka, J. 2018. Interannual changes in summer phytoplankton community composition in relation to water mass variability in the East China Sea. *J. Oceanogr*. **75**: 61–79, doi:10.1007/s10872-018-0484-y.

Xu, Y.J., Ishizaka, J., Yamaguchi, H., Siswanto, E. and Wang, S.Q. 2013. Relationships of interannual variability in SST and phytoplankton blooms with giant jellyfish (*Nemopilema nomurai*) outbreaks in the Yellow Sea and East China Sea. *J. Oceanogr.* **69**: 511–526, doi:10.1007/s10872-013-0189-1.

Yamaguchi, H., Kim, H.-C., Son, Y.B., Kim, S.W., Okamura, K., Kiyomoto, Y. and Ishizaka, J. 2012. Seasonal and summer interannual variations of SeaWiFS chlorophyll alpha in the Yellow Sea and East China Sea. *Prog. Oceanogr*. **105**: 22–29, doi:10.1016/j.pocean.2012.04.004.

Yamaguchi, H., Ishizaka, J., Siswanto, E., Son, Y.B., Yoo, S. and Kiyomoto, Y. 2013. Seasonal and spring interannual variations in satellite-observed chlorophyll-a in the Yellow and East China Seas: New datasets with reduced interference from high concentration of resuspended sediment. *Cont. Shelf Res*. **59**: 1–9, doi:10.1016/j.csr.2013.03.009.

Yoon, J.E., Park, J. and Yoo, S. 2012. Comparison of primary productivity algorithms for Korean waters. *Ocean Sci. J.* **47**: 473–487, doi:10.1007/s12601-012-0043-1.

Yuan, J., Hayden, L. and Dagg, M. 2007. Comment on "Reduction of primary production and changing of nutrient ratio in the East China Sea: Effect of the Three Gorges Dam?" by Gwo-Ching Gong et al. *Geophys. Res. Lett*. **34**: L14609, doi:10.1029/2006GL029036.

Zhang, H., Wang, S., Qiu, Z., Sun, D., Ishizaka, J., Sun, S. and He, Y. 2018. Phytoplankton size class in the East China Sea derived from MODIS satellite data. *Biogeosciences* **15**: 4271–4289 doi: 10.5194/bg-15-4271-2018.

Zhang, R., Chen, M., Cao, J.P., Ma, Q., Yang, J.H. and Qiu, Y.S. 2012. Nitrogen fixation in the East China Sea and southern Yellow Sea during summer 2006. *Mar. Ecol. Prog. Ser*. **447**: 77–86, doi: 10.3354/MEPS09509.

Zhao, H., Shao, J., Han, G, Yan, D. and Lv, J. 2015. Influence of Typhoon Matsa on phytoplankton chlorophyll-a off East China. *PLOS One* **10**: doi:10.1371/journal.pone.0137863.

Zhu, Z.Y., Ng, W.M., Liu, S.M., Zhang, J., Chen, J.C. and Wu, Y. 2009. Estuarine phytoplankton dynamics and shift of limiting factors: A study in the Changjiang (Yangtze River) Estuary and adjacent area. *Estuar. Coast. Shelf Sci*. **84**: 393–401, doi:10.1016/j.ecss.2009.07.005.

Zhu, Y., Ishizaka, J., Tripathy, S.C., Wang, S., Sukigara, C., Goes, J., Matsuno, T. and Suggett, D.J. 2017. Relationship between light, community composition and the electron requirement for carbon fixation in natural phytoplankton. *Mar. Ecol. Prog.Ser*. **580**: 83–100, doi:10.3354/meps12310.

3.3 Zooplankton

Guang-Tao Zhang

Institute of Oceaonology, Chinese Academy of Sciences, China

3.3.1 Introduction

Zooplankton refer to metazoa that swim weakly or drift passively in the water column. Owing to their linking role in the marine food web, their diversity and biomass are commonly used in the 5-module (productivity, fish and fisheries, pollution and ecosystem health, socioeconomics and governance) strategy for measuring the changing states of the Large Marine Ecosystem, aiming at taking remedial actions toward the recovery and sustainability of degraded goods and services (Sherman, 1994). As an ecological rather than strict taxonomic categorization, zooplankton cover a large size range from single-cell heterotrophic flagellates to giant jellyfish, and a broad evolution echelon from protozoan to chordate, with complex inter-specific interactions among those sharing the same water column through competition and predation. Meanwhile, owing to lack of or weak swimming ability, their distribution pattern and life strategies are mostly determined by physical oceanographic characteristics. These are the main obstacles preventing a full evaluation of the zooplankton contribution in marine ecological dynamics.

As two of the 64 Large Marine Ecosystems around the world coastal seas, zooplankton diversity is lower in the Yellow Sea (YS) compared to that in the East China Sea (ECS) where it is significantly influenced by the Kuroshio Current. Among 1140 metazoan species recorded in the YS, approximately 300 species are planktonic (Huang, 1994). During investigations with limited spatial and temporal coverage, species sampled in the YS by traditional conical net (mesh size 500 μm and diameter 0.8 m) methods were approximately 100. Total zooplankton biomass varied between 5 and 1000 mg m^{-3}, commonly dominated by *Calanus sinicus*, *Sagitta crassa*, *Euphausia pacifica* and *Themisto gracilipes* (Tang, 2003). However, a total of 611 zooplankton species (excluding meroplankton and protozoa) were recorded in the ECS during a two-year investigation, and dominant species also varied seasonally.

Therefore, we focus this section on distinguishing features of zooplankton communities in the context of physical–biological coupling rather than species composition. Impacts of climate change and human activities are also discussed, based on existing reports, with anomalies at both species and community levels.

3.3.2 Adaptation to distinct habitats

Yellow Sea Cold Water Mass

The Yellow Sea Cold Water Mass (YSCWM) is formed in winter by vertical mixing under strong winds. It remains in a bottom layer under the thermocline at 15–30 m depth from May to November

(Lee and Beardsley, 1999). The low-temperature conditions of the YSCWM protect cold water fauna, with *C. sinicus* as the most prominent representative (Fig. 3.3.1). When sea surface temperature (SST) was over 20ºC in summer and autumn, *E. pacifica* could be found mainly in the Yellow Sea Bottom Cold Water (YSBCW) area too.

As a common adaptation behavior in most zooplankton species, diel vertical migration patterns can be influenced by strong stratification in YSCWM. According to the amplitude of diel vertical migration (DVM) in relation to depth of the thermocline, four DVM patterns were defined (Zuo *et al*., 2004). DVM of *Doliolum denticulatum*, *Penilia avirostris*, *Lucifer intermedius* and *Sagitta enflata* was limited to above the thermocline, with *S. enflata* reaching the deepest of 26 m depth. The second group distributed inside the thermocline, including *Sagitta crassa*, *Paracalanus parvus* and *Oithona similis*. Preference to cold bottom water was detected in *Themisto gracilipes*, *C. sinicus* and *E. pacifica*, which were completely absent above the thermocline. Reversed DVM was observed only in the hydrozoan *Muggiaea atlantica*, which presented in the surface layer during daytime and descended to the bottom layer at night.

Echo sounding also detected a different DVM pattern in the YSBCW area in spring and summer. In the spring of 2010 and 2011, the sound-scattering layer (SSL) clearly showed vertical migration throughout the entire water column, with zooplankton moving from the surface layer at night to near the bottom during the day. However, in the summer of 2010, when SST increased to 28°C, the SSL migrated to near the bottom during the day, but two SSLs occurred above and below the thermocline at a depth of 10–30 m at night (Lee *et al*., 2013).

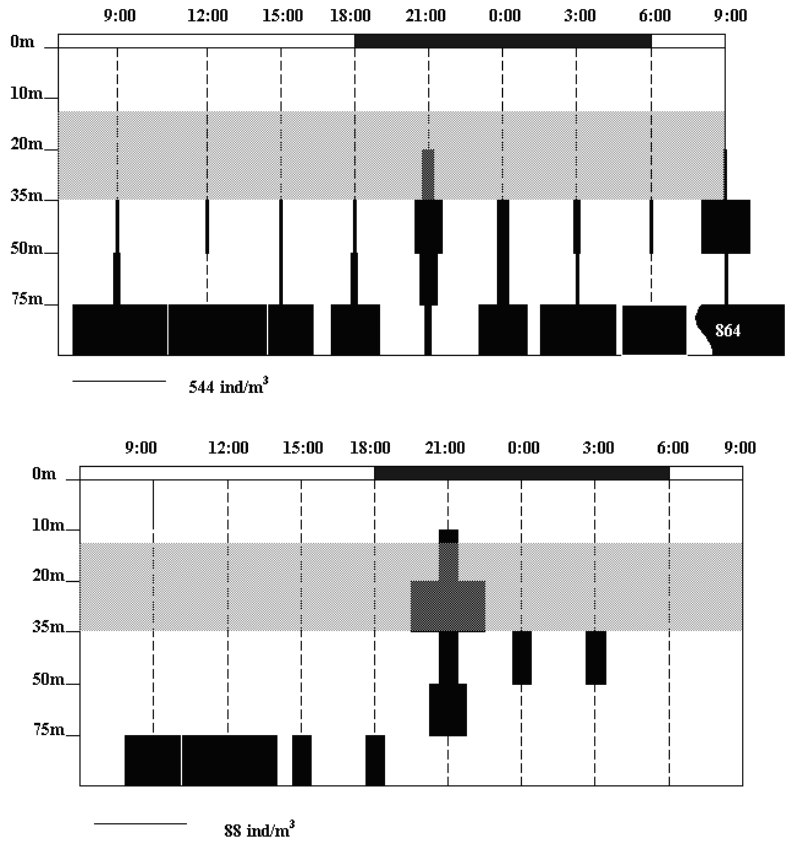

Fig. 3.3.1 Diel vertical migration of copepodite stage 5 and females of *Calanus sinicus* inside (upper panel) and outside (lower panel) of the Yellow Sea Cold Water Mass. Line at the bottom of each figure indicates the scale, and shaded areas represent the thermocline. From Zhang *et al*. (2007). Reproduced with permission of Oxford University Press.

Physiological adaptations were also detected in association with the YSCWM, but evidence exists overwhelmingly in *C. sinicus*. Over-summering in the YSCWM is actually a tradeoff between thermal fitness and food limitation. Along with a retreat from coastal waters and a concentration in the YSCWM, the dominance of copepodite stage 5 suggests a diapause state for the over-summering population (Zhang *et al*., 2007). Meanwhile, unfavorable food conditions were confirmed by decreased egg production and feeding rate (Zhang *et al*., 2005). Over-summering of *C. sinicus* is often compared with the seasonal descent to deep waters of *C. finmarchicus* in the North Atlantic, but instead of real dormancy, quiescence that can be awoken rapidly by environmental amelioration was proposed for C. *sinicus* (Yin *et al*., 2013; Zhou *et al*., 2016).

Besides affording an over-summering site, the YSCWM can also influence the seasonal pattern of zooplankton through cascading effects. As vertical mixing is prevented by strong thermal stratification, nutrients are exhausted in the upper layer (0–30 m) and accumulate in the bottom layer. With the disappearance of the YSCWM in late autumn, strengthened vertical mixing carries the enriched bottom nutrients into the surface layer and further to coastal waters, intensifying the phytoplankton bloom in autumn and even next spring. This process was extremely evident in a sea ranching area in the northern YS (Yin *et al*., 2013). Though the cascading effects to zooplankton were not as significant as for phytoplankton, the egg production rate of the dominant *C. sinicus* peaked in spring and autumn (Zhang *et al*., 2005).

Yellow Sea Warm Current

The Yellow Sea Warm Current (YSWC) is an asymmetric upwind flow that intrudes into the central YS along the western side of the Yellow Sea Trough from winter to early spring (Lin *et al*., 2011). The most attractive issue to address is the simultaneous invasion of organisms and nutrients. Remotely sensed SST has revealed that the YSWC can reach the Bohai Sea in the surface in winter, but for warm water species, mostly pelagic tunicates, remote sensing indicated a northward extension only to the northern YS (Franco *et al*., 2014; Yin *et al*., 2017). To date, however, little is known concerning biogeochemical behavior of the YSWC (Liu *et al*., 2015). Chen (2009) revealed that the YSWC originates from the Kuroshio and Taiwan Warm Current and thus it is relatively warmer, saltier, and nutrient-poor. Recent studies have revealed that the nitrate concentrations in the YSWC can reach up to 8 μM (Fu *et al*., 2009; He *et al*., 2013; Jin *et al*., 2013). It has been established that cyanobacteria and eukaryotic picoplankton, dominated mostly by prasinophytes, is significantly more abundant in the YSWC (Lü *et al*., 2013). Meanwhile, low zooplankton biomass was observed in the YSWC area, especially at stations along the axis of the warm saline water tongue (Liu *et al*., 2015). However, the DVM weakened markedly while warm water prevailed at the mooring sites. The DVM change was believed to result from the YSWC, rather than from sunlight (Lü *et al*., 2013).

Changjiang River diluted water

Changjiang River diluted water (CDW) forms a typical estuarine zooplankton community in this region (Zhang *et al*., 2005). Freshwater species, represented by *Brachionus falcatus, B. calyciflorus, Sinocalanus dorrii, Mesocyclops leuckarti* and *Thermocyctops taihokuensis*, occupy regions with salinity lower than 2. Between 122–122.5ºE, where salinity ranges from 2 to 10, the zooplankton community was dominated by *Tortanus vermiculus, Schmackeria poplesis* and *Monoculodes limnophilus*. In the plume region with salinity of 10–25, common coastal species were dominant, including *Labidocera euchaeta, Sagitta nagae, Pseudeuphausia sinica* and *Acanthomysis sinensis*. Oceanic species were comparatively scarce in the estuary area, and the occurrence of *Sagitta enflata* and *C. sincus* was proposed, as a result of their exchange with open waters.

As transportation of estuarine species into the oceanic environment is difficult to detect, the ecological impacts of CDW on zooplankton has been recorded mainly as cascading effects through increased nutrient input and thereafter primary production. Another influence of CDW on the configuration of the zooplankton community in the Yellow Sea is that the northward invasion of warm water species is prevented on the coastal side.

Kuroshio Current

The Kuroshio Current (KC) is a warm current (24°C in annual average SST) carrying nutrient-rich waters. Confirmation of the Nearshore Kuroshio Branch Current has stimulated much research interest in China, as it can at least partially explain the observed phosphate-rich bottom water off the coast of Zhejiang province (Yang *et al*., 2012). Phosphate limitation has been proposed as the main reason for the massive dinoflagellate bloom in this region (Li *et al*., 2009).

However, KC-driven changes in zooplankton assemblage were detected mostly in the south of the ECS. Both copepods and jellyfish are used as indicator species of the KC. Meanwhile, the KC has been known to transport tropical or subtropical species to water bodies on both the eastern and western sides of Taiwan Island, as it can flow northward through the continental shelf break northeast of Taiwan and the Luzon Strait into the Taiwan Strait.

The intrusion of warm water into the central ECS and north of it has been shown by the interaction between neritic and warm water tintinnids in the surface waters (Li *et al*., 2016). Warm water genera can reach the coast of Zhejiang province. Consistent with the seasonal change in KC strength, the largest coverage of warm water genera was observed in August and October, compared to May (Fig. 3.3.2). In May and August, neritic and warm-water genera were completely separated in geographical distribution, whereas in October pioneer genera that overlapped geographical coverage was also observed (Li *et al*., 2016).

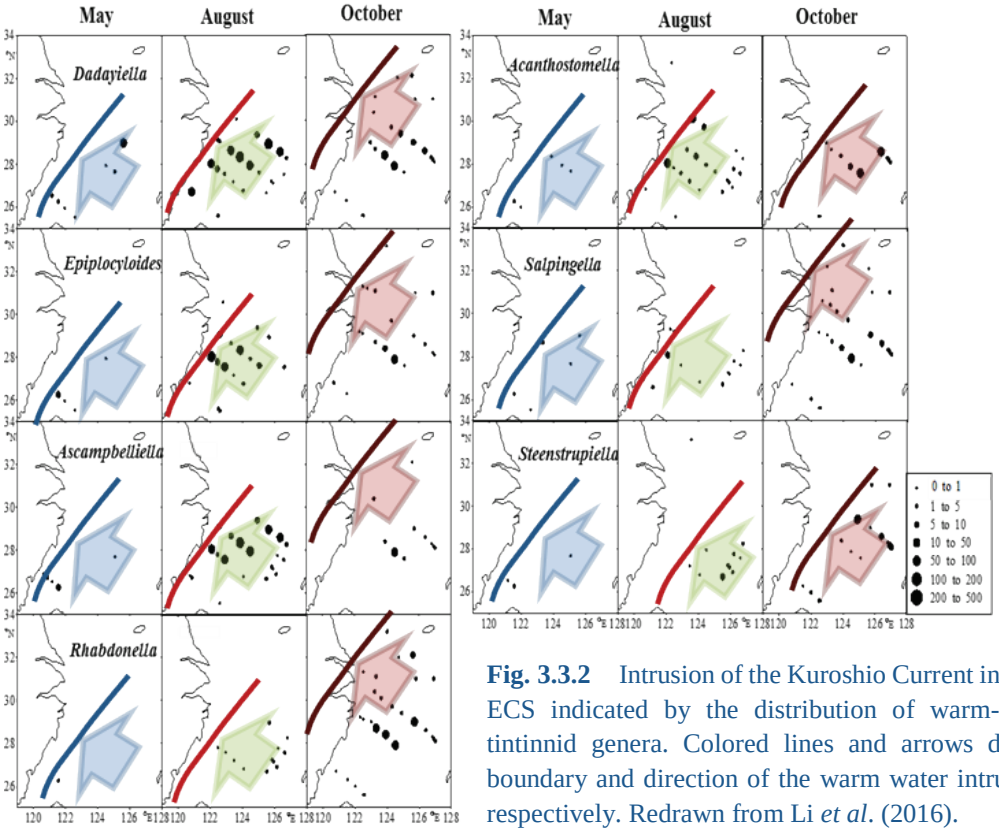

Fig. 3.3.2 Intrusion of the Kuroshio Current into the ECS indicated by the distribution of warm-water tintinnid genera. Colored lines and arrows denote boundary and direction of the warm water intrusion, respectively. Redrawn from Li *et al*. (2016).

3.3.3 Responses to climate change

According to report of the Scientific Committee on Oceanic Research (SCOR) Working Group 125 (Global Comparisons of Zooplankton Time Series, https://scor-int.org/group/125/), long-term zooplankton time series in the YS and ECS exist only near the Korean coast, where sampling has been conducted bimonthly by Korea's National Institute of Fisheries Science (formerly known as the National Fisheries Research and Development Institute) since 1965. Biomass of mesozooplankton in the eastern YS and northern ECS began to increase after the early 1990s, with sharp increases after the late 1990s, indicating a regime shift triggered by the increased SST (Fig. 3.3.3). Unusually higher biomass was also occasionally observed in April, June or October after the late 1990s. Abundances of the four major zooplankton groups (copepods, amphipods, chaetognaths and euphausiids) have generally increased since the late 1990s (Kang *et al*., 2012).

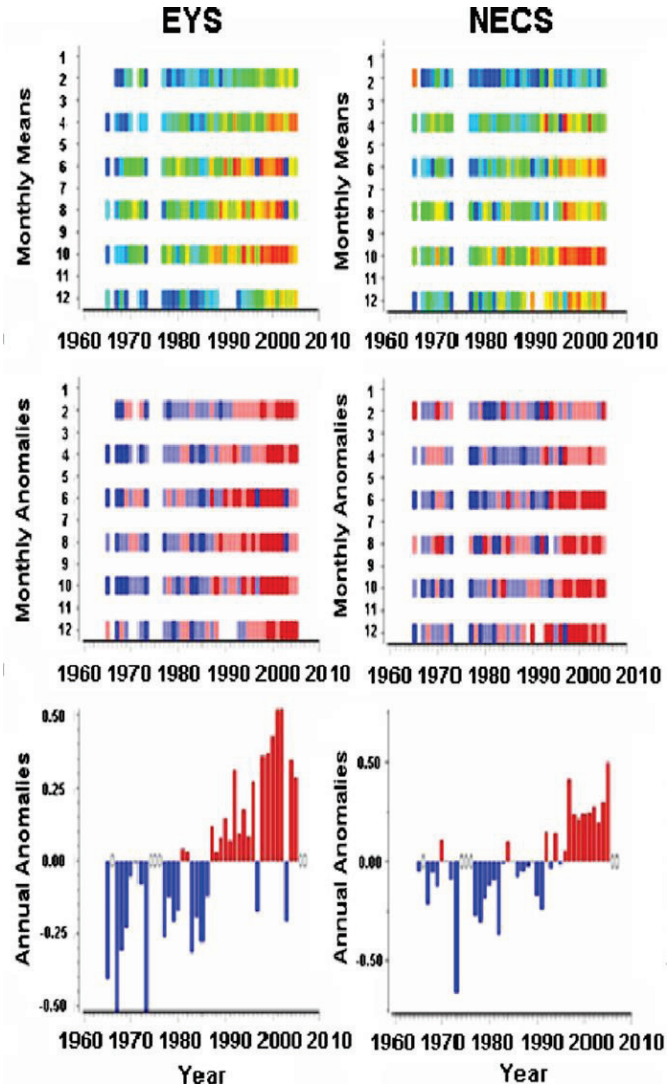

Fig. 3.3.3 Standardized (SCOR WG 125) time-series plots of monthly anomalies and annual anomalies for zooplankton biomass from 1967 to 2006 in the eastern Yellow Sea (EYS) and the northern East China Sea (NECS). From Kang *et al*. (2012). Reproduced with permission of Elsevier.

On the Chinese side, detection of zooplankton responses to climate change has been impeded by a lack of time series. However, the comprehensive marine investigation from 1958–1959 provides a baseline for zooplankton change, as this monthly sampling covered a large area from the Bohai Sea to South China Sea. Through comparisons, a decline was observed in *Euphausia pacifica* and *Euchaeta plana* in the coastal waters of ECS (Xu *et al*., 2013, 2014).

The northward extension of warm-water species and changed seasonality were also reported in this region. A subtropical estuarine copepod, *Temora turbinata*, was found to be the most abundant zooplankton species in this area for the first time in August 2004 (Zhang *et al*., 2010), the first year after the Three Gorges Reservoir was impounded to a water level of 135 m. *Temora turbinata*'s unexpected dominance suggests a northward extension of warm-water species resulting from global warming, although it appeared immediately following water control at the Three Gorges Reservoir. The changes in peaked abundance of *C. sinicus* in the Changjiang River (Yangtze River) Estuary were compared between 1959 and 2002. In spring 2005, the time for occurrence and decrease of the peak in *C. sinicus* abundance advanced about one month, accompanied by an increase in SST. Abundance peaked in June and decreased in July in 1959; however, in 2005, it peaked in May and attenuated sharply in early June (Xu *et al*., 2011).

3.3.4 Anthropogenic impacts

Commercial harvesting of zooplankton species is scarce. In the YS and ECS, fishing target species include euphausiids, shrimps, and giant jellyfish. However, zooplankton can still be severely impacted by human activities through decreased top-down control (overfishing) and increased bottom-up control (eutrophication).

Considering decreased top-down control (overfishing) and increased bottom-up control (eutrophication), an increase in zooplankton abundance is expected. However, despite the well-documented overfishing and eutrophication studies, the increase in zooplankton biomass has not observed. It may be attributed to the change in community composition, notably giant jellyfish blooms.

Among the four giant jellyfish species, *Nemopilema nomurai*, *Cyanea nozakii*, *Aurelia aurita* and *Rhopilema esculentum*, commonly observed in the YS and ECS, the edible *R. esculentum* is overfished, and the fishing population is supported mostly by artificial release. Blooms of *N. nomurai*, *C. nozakii* and *A. aurita*, reported frequently since this century, have had negative effects on fishing, tourism and coastal industries. However, polyps, the benthic larvae of jellyfish, are found in the natural environment only for *A. aurita*. It is quite certain that artificial constructions in coastal regions have contributed significantly to its bloom.

The damming of major rivers can have a broad impact on ecological processes in adjacent marine ecosystems. Evidence shows that the recent impounding of water by the Three Gorges Dam on the Changjiang River can have a dramatic impact on the mesozooplankton community. The operation of the reservoir has significantly altered the fluctuation of freshwater discharge. Reduction of riverine nutrients, especially dissolved silicate loads into the Changjiang River Estuary could contribute to the decline in Bacillariophyta species. Consequently, decreased zooplankton and increased benthos biomass has been observed (Fig. 3.3.4; Chen *et al*., 2015).

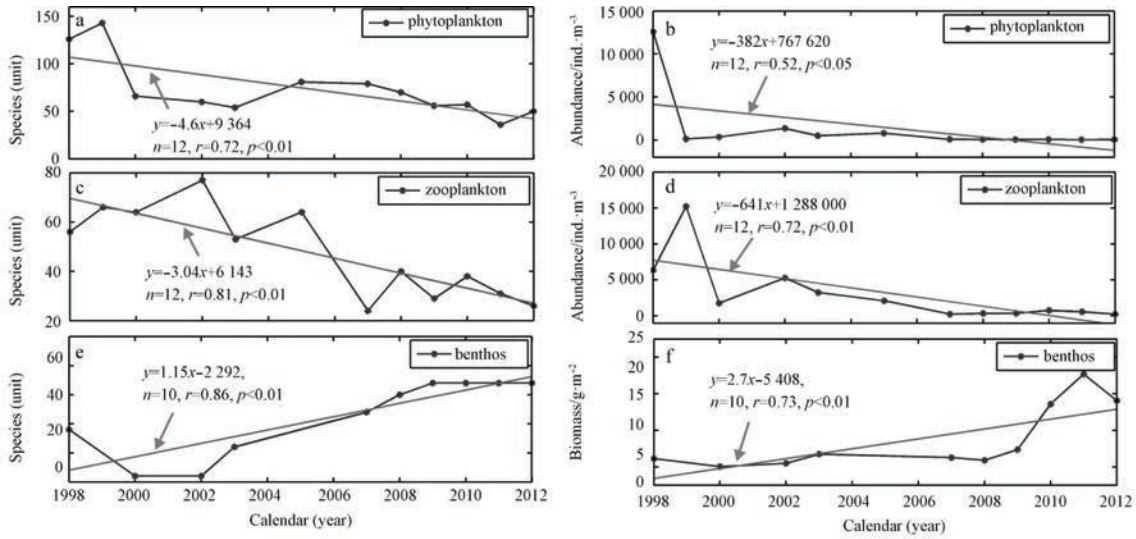

Fig. 3.3.4 Changes in (a) number of phytoplankton species and (b) their abundance, (c) number of zooplankton species and (d) their abundance, and (e) number of benthos species and (f) their biomass in the Changjiang (Yangtze) estuarine ecosystem. From Chen *et al*. (2015). Reproduced with permission of Elsevier.

In another study in the northern YS, the reduction in freshwater discharge and subsequent increases in phytoplankton biomass have resulted in a substantial increase in total mesozooplankton wet weight but sharp declines in the abundance of all of the crustacean components (Hwang *et al*., 2013). The increase in mesozooplankton biomass is probably associated with an increase in small, gelatinous zooplankton. Together with an increase in SST in the region, the reduced freshwater and sediment discharge might have led to the proliferation of gelatinous mesozooplankton in this historically overfished region, generating significantly increased grazing pressure on planktonic crustaceans (Hwang *et al*., 2013).

Human activities are also responsible for introducing persistent organic pollutants into the ocean. For instance, total concentrations of polycyclic aromatic hydrocarbons (PAHs) in zooplankton from surface waters of ECS were measured (Fig. 3.3.5; Hung *et al*., 2014). Values of PAHs ranged from 2 to 3500 ng m^{-3} in the ECS, with highest PAH levels located at the salinity front between the CDW and mid-shelf waters. In contrast, concentrations of zooplankton PAHs in the mid-shelf and outer-shelf waters were significantly lower (2–23 ng m^{-3}) than those in the CDW. These results demonstrate that PAHs are conspicuously accumulated in zooplankton at the salinity front between the CDW and the mid-shelf waters. As both large and tiny non-zooplankton particles were removed by visual check and high-speed centrifugation, there is convincing evidence that these higher levels of PAHs in zooplankton at the salinity front may be further biomagnified in marine organisms of higher trophic levels through their feeding activities (Hung *et al*., 2014).

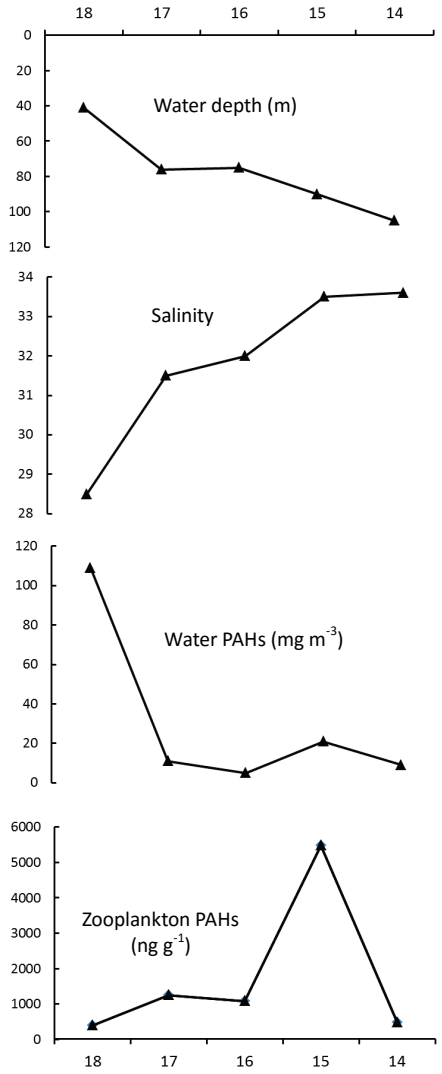

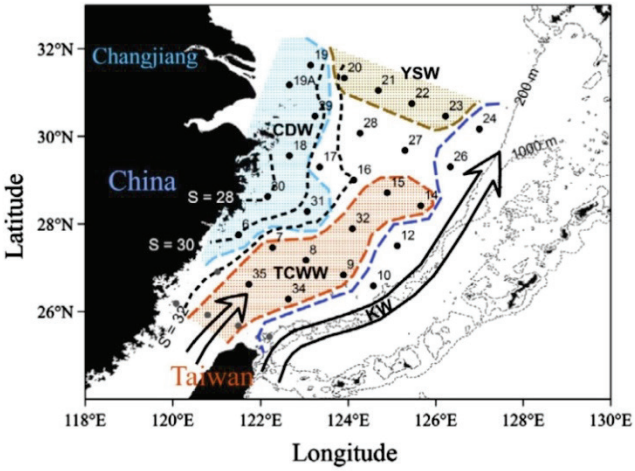

Fig. 3.3.5 Water depth, salinity (S) and total polycyclic aromatic hydrocarbons (PAHs) in surface water and zooplankton along a transect in the ECS, with the inlet map showing the location of sampling stations. CDW = Changjiang Diluted Water, YSW = Yellow Sea Water, TCWW = Taiwan Current Warm Water, KW = Kuroshio Water. Redrawn from Hung *et al*. (2014).

3.3.5 Attractive issues and future perspective

The most attractive issue in zooplankton study is blooms of unwanted species, such as jellyfish. Another jelly-like species, *Salpa fusiformis*, is a pelagic tunicate. A massive aggregation of this tunicate was recorded in the YS in 1965 and 2007 (Chen, 1978; Liu *et al*., 2012). In coastal Korean waters, a dense swarm was observed in 2003, clogging the screen system of a nuclear power plant (Lee *et al*., 2005). The negative impacts are obvious, but the reasons for jellyfish blooms are poorly understood.

The function of zooplankton in the marine ecosystem is well understood, but it is still hard to integrate them into a numerical ecological model. The obstacles lie mostly in quantification of critical parameters, such as feeding pressure on phytoplankton and mortality caused by predation and natural death.

Potential responses to climate change and anthropogenic stresses depend critically on time series. To establish long-term observation plans and free access to the existing plans are important steps towards resolution of such scientific questions.

Introduction of new technology and methods for measuring zooplankton production is also important. The Continuous Plankton Recorder (CPR), equipped on commercial ships, has been used in the North Atlantic for many years, and has been introduced in North Pacific in the recent decades. According to the existing literature, most of the long-term zooplankton time series was obtained by CPR, showing very attractive results on climate change impacts. The application of molecular methods in zooplankton research can also help in many aspects other than biodiversity.

3.3.6 References

Chen, D., Dai, Z., Xu, R., Li, D. and Mei, X. 2015. Impacts of anthropogenic activities on the Changjiang (Yangtze) estuarine ecosystem (1998–2012). *Acta Oceanol. Sin.* **34**: 86–93, doi:10.1007/s13131-015-0679-7.

Chen C.T.A. 2009. Chemical and physical fronts in the Bohai, Yellow and East China seas. *J. Mar. Syst.* **78**: 394–410, doi:10.1016/j.jmarsys.2008.11.016.

Chen, J.K. 1978. Two salps observed in the northern Yellow Sea. *Chin. J. Zool.* **2**: 13–16 (in Chinese).

Franco, P., Chen, H.J. and Liu, G,X. 2014. Distribution and abundance of pelagic tunicates in the North Yellow Sea. *J. Ocean Univ. China* **13**: 782–790.

Fu, M., Wang, Z., Li., Sun, P., Li, Y. and Li, R. 2009. Spatial distribution characteristics and the environmental regulation mechanisms of phytoplankton chlorophyll a in Southern Yellow Sea during summer 2006. *Acta Ecol. Sin.* **29**: 5366–5375 (in Chinese with English abstract).

He, X., Bai, Y. and Gong, F. 2013. Satellite views of the seasonal and interannual variability of phytoplankton blooms in the eastern China seas over the past 14 yr (1998–2011). *Biogeosciences* **10**: 4721-4739, doi:10.5194/bg-10-4721-2013.

Huang, Z.G. 1994. General characteristics of the species in China seas. *Chinese Biodiv.* **2**: 63–67 (in Chinese).

Hung, C.C., Ko, F.C., Gong, G.C., Chen, K.S., Wu, J.M., Chiang, H.L., Peng, S.C. and Santschi, P.H. 2014. Increased zooplankton PAH concentrations across hydrographic fronts in the East China Sea. *Mar. Pollut. Bull.* **83**: 248–257, doi:10.1016/j.marpolbul.2014.03.045.

Hwang, S.-W., Kang, H.-K., Son, Y.-B., Jang, M.-C. and Choi, K.-H. 2013. Collapse of the crustacean mesozooplankton in the northern East China Sea: effects of Three Gorges Dam? *J. Coast. Res.* **29**: 1464–1469, doi:10.2112/JCOASTRES-D-13-00011.1.

Jin, J., Liu, S.M., Ren, J.L., Liu, C.G., Zhang, J., Zhang, G.L. and Huang, D.J. 2013. Nutrient dynamics and coupling with phytoplankton species composition during the spring blooms in the Yellow Sea. *Deep Sea Res. II* **97**: 16–32, doi:10.1016/j.dsr2.2013.05.002.

Kang, Y.S., Jung, S., Zuenko, Y., Choi, I. and Dolganov, N. 2012. Regional differences in the response of mesozooplankton to oceanographic regime shifts in the northeast Asian marginal seas. *Prog. Oceanogr.* **97–100**: 120–134, doi:10.1016/j.pocean.2011.11.012.

Lee, S.H. and Beardsley R.C., 1999. Influence of stratification on residual tidal currents in the Yellow Sea. *J. Geophys. Res. Oceans* **104**: 679–701, doi:10.1029/1999JC900108.

Lee, J.H., Kim, D., Shin, K.S., Choi H.W. and Chae, J. 2005. Prevention of bio-impingement against power plant intake. KORDI Report BSPN52700-1716-3.

Lee, H., Cho, S., Kim, W. and Kang, D. 2013. The diel vertical migration of the sound-scattering layer in the Yellow Sea Bottom Cold Water of the southeastern Yellow sea: focus on its relationship with a temperature structure. *Acta Oceanol. Sin.* **32**: 44–49, doi:10.1007/s13131-013-0351-z.

Li, H., Zhao, Y., Chen, X., Zhang, W., Xua, J., Li, J. and Xiao, T. 2016. Interaction between neritic and warm water tintinnids in surface waters of East China Sea. *Deep Sea Res. II* **124**: 84–92, doi: 10.1016/j.dsr2.2015.06.008.

Li, J., Glibert, P.M., Zhou, M., Lu, S. and Lu, D. 2009. Relationships between nitrogen and phosphorus forms and ratios and the development of dinoflagellate blooms in the East China Sea. *Mar. Ecol. Prog. Ser*. **383**: 11–26, doi:10.3354/meps07975.

Lin, X., Yang, J., Guo, J., Zhang, Z., Yin, Y. Song, X. and Zhang, X. 2011. An asymmetric upwind flow, Yellow Sea Warm Current: 1. New observations in the western Yellow Sea. *J. Geophys. Res. Oceans* **116**: doi:10.1029/2010JC006513.

Liu, Y., Sun, S. and Zhang, G. 2012. Seasonal variation in abundance, diel vertical migration and body size of pelagic tunicate *Salpa fusiformis* in the Southern Yellow Sea. *Chin. J. Ocean. Limnol*. **30**: 92–104, doi:10.1007/s00343-012-1048-4.

Liu, X, Chiang, K.-P., Liu, S.-M., Wei, H., Zhao, Y. and Huang, B.-Q. 2015. Influence of the Yellow Sea Warm Current on phytoplankton community in the central Yellow Sea. *Deep Sea Res*. **106**: 17–29, doi:10.1016/j.dsr.2015.09.008.

Lü, L.-G., Wang, X., Wang, H., Li, L. and Yang, G. 2013. The variations of zooplankton biomass and their migration associated with the Yellow Sea Warm Current. *Cont. Shelf Res*. **64**: 10–19, doi: 10.1016/j.csr.2013.05.007.

Sherman, K. 1994. Sustainability, biomass yields, and health of coastal ecosystems: an ecological perspective. *Mar. Ecol. Prog. Ser.* **112**: 277–301.

Tang, Q. 2003. The Yellow Sea LME and mitigation action, pp. 121–144 *in:* Large Marine Ecosystems of the World – Trends in Exploitation, Protection and Research, *edited by* G. Hempel and K. Sherman, Elsevier, Amsterdam, the Netherlands.

Wang, B. 2000. Characteristics of variations and interrelations of biogenic elements in the Huanghai Sea Cold Water Mass. *Acta Oceanol. Sin*. **22**: 47–54.

Xu, Z.-L. and Zhang, D. 2014. Dramatic declines in *Euphausia pacifica* abundance in the East China Sea: Response to recent regional climate change. *Zool. Sci*. **31**: 135–142, doi:10.2108/zsj.31.135.

Xu, Z.L., Ma Z.L. and Wu Y.M. 2011. Peaked abundance of *Calanus sinicus* earlier shifted in the Changjiang River (Yangtze River) Estuary: a comparable study between 1959, 2002 and 2005. *Acta Oceanol. Sin*. **30**: 84–91.

Xu, Z.-L., Gao, Q., Kang, W. and Zhou, J. 2013. Regional warming and decline in abundance of *Euchaeta plana* (Copepoda, Calanoida) in the nearshore waters of the East China Sea. *J. Crust. Biol*. **33**: 323–331, doi:10.1163/1937240X-00002140.

Yang, D., Yin, B., Liu, Z., Bai, T., Qi, J. and Chen, H. 2012. Numerical study on the pattern and origins of Kuroshio branches in the bottom water of southern East China Sea in summer. *J. Geophys. Res. Oceans* **117**: C02014, doi:10.1029/2011JC007528.

Yin, J., Zhang, G., Zhao, Z., Wang, S. and Wan, A. 2013. Annual variation in *Calanus sinicus* abundance and population structure in the northern boundary area of the Yellow Sea Cold Water Mass. *Chin. J. Oceanol. Limnol*. **31**: 1284–1294, doi:10.1007/s00343-013-3004-3.

Yin, J., Zhang, G., Li, C., Wang, S., Zhao, Z. and Wan, A. 2017. Community composition, abundance and biomass of zooplankton in Zhangzi Island waters, Northern Yellow Sea. *Chin. J. Oceanol. Limnol*. **35**: 1144–1151, doi:10.1007/s00343-017-6135-0.

Zhang, G.T., Sun, S. and Zhang, F. 2005. Seasonal variation of reproduction rates and body size of *Calanus sinicus* in the Southern Yellow Sea, China. *J. Plankt. Res.* **27**: 135–143, doi:10.1093/plankt/fbh164.

Zhang, G.T., Sun, S. and Yang, B. 2007. Summer reproduction of the planktonic copepod *Calanus sinicus* in the Yellow Sea: influences of high surface temperature and cold bottom water. *J. Plankt. Res.* **29**: 179–186, doi:10.1093/plankt/fbm005.

Zhang, G.T., Sun, S., Xu, Z.L. and Zhang Q.L. 2010. Unexpected dominance of the subtropical copepod *Temora turbinata* in the temperate Changjiang River Estuary and its possible causes. *Zool. Stud*. **49**: 492–503.

Zhou, K.L., Sun, S., Wang, M.X., Wang, S.W. and Li, C.L. 2016. Differences in the physiological processes of *Calanus sinicus* inside and outside the Yellow Sea Cold Water Mass. *J. Plankt. Res.* **38**: 551–563, doi:10.1093/plankt/fbw011.

Zuo, T., Wang R., Wang, K. and Gao, S.-W. 2004. Vertical distribution and migration of zooplankton in the southern Yellow Sea in summer. *Acta Ecol. Sin*. **24**: 524-530 (in Chinese).

3.4 Macrobenthos

Xinzheng Li and Yong Xu

Institute of Oceanology, Chinese Academy of Sciences, China

3.4.1 Introduction

Marine benthos are those organisms living on, in, or near the seabed. They are widely distributed from the intertidal zone to the abyss and compose the most abundant group of marine organisms. Marine benthos play important roles in energy flow and material circulation in marine ecosystems. They make full use of the organic detritus settled on the seafloor from the water column and facilitate the decomposition of nutrients.

According to body size, benthos is classified into macrobenthos, meiobenthos and microbenthos. Macrobenthos are defined as benthos which cannot pass through 0.5 mm mesh sieve (Shen *et al*., 2010). Other literature defines the macrobenthos with body size not passing through a 1 mm mesh size (Lalli and Parsons, 2000). The main taxonomic groups of macrobenthos are Polychaeta, Mollusca, Crustacea and Echinodermata. Other taxonomic groups such as Porifera, Cnidaria, Sipuncula, Echiura, Nemertea and Pisces are also common in the benthic habitat. Activities of macrobenthic fauna, such as burrowing, crawling, feeding and avoiding enemies can change the sediment structure and result in the deformation or fracture of the seabed. The mobility of most macrobenthos is limited and some of them are sessile, the lifestyle of which is significantly different from plankton and nekton. Because of limited mobility, macrobenthos cannot escape from environmental stresses immediately and are impacted particularly profoundly when the environment deteriorates. So, the long-term variation of species composition, community structure and secondary productivity of macrobenthos can reflect the long-term variation of the environment.

The study of the macrobenthos in the Yellow Sea and East China Sea dates back to the 1930s and 40s. Researchers investigated the macrobenthos in the adjacent waters of Shandong Province (Tchang, 1935; Tchang and Ma, 1936, 1949). However, large spatial-scale investigations of macrobenthos started in the late 1950s. These large spatial-scale investigations carried out in the Yellow Sea and East China Sea are the Marine Comprehensive Scientific Survey from Coast of China (National Ocean Census) (1958–1959), the Continental Shelf Marine Comprehensive Survey from the East China Sea (1975–1976), the National Survey of Coastal Resource (1980–1985), the National Insular Comprehensive Survey (1989–1993), the National Basic Research Program of China–The Ecosystem Dynamics and Sustainable Use of Marine Biological Resources from the East China Sea and the Yellow Sea (1999–2004), the Marine Comprehensive Scientific Survey and Assessment from Coast of China (also called “the second National Ocean Census”) (2004–2009), the National Basic Research Program of China–The Key Process, Mechanism and Effect of Ecological Environment of the Jellyfish Bloom from the Coast of China (2011–2015), and the ongoing “Strategic Priority Research Program” of the Chinese Academy of Sciences–Western Pacific Ocean System: Structure, Dynamics and Consequences (2013–2018). Large amounts of macrobenthic samples were collected in these investigations and data have been accumulated from

the Yellow Sea and East China Sea. According to these samples and data, many researchers have reported the phased investigation results of macrobenthos, including macrobenthic community structure (Gurjanova and Wu, 1963; Liu *et al*., 1986; Zhang *et al*., 1990; Sui *et al*., 2010), species composition and distribution pattern (Liu *et al*., 1986; Qi *et al*., 1989; Liu and Li, 2002, 2003; Li *et al*., 2007; Liu *et al*., 2008; Gao *et al*., 2009), species diversity (Li *et al*., 2006; Liu *et al*., 2009), secondary productivity (Li *et al*., 2005,b,c,d), biomass and stock (Liu, 1992; Han *et al*., 2001; Han *et al*., 2004), the relationship between macrobenthos and environmental factors such as sediment, temperature, salinity, heavy metal, current, and marine disasters (Li, B.Q. *et al*., 2005; Wang *et al*., 2006; Li *et al*., 2010; Wang, *et al*., 2011), thus achieving much knowledge.

However, there are also some issues that need to be addressed urgently in the study of macrobenthic ecology and diversity in the Yellow Sea and East China Sea. The first problem is the systematical analysis and arrangement of the historical materials, that is, exploring the dynamic regularity of the macrobenthic community structure, diversity and secondary productivity using the data obtained since the 1950s, predicting the direction of changes in the future, and assessing the influence of climate change and human activities. The second problem is the coupling between macrobenthos and plankton, meiobenthos, hydrologic and sedimentary characteristics, especially the analysis of the effects of physical and chemical variables on the ecology of macrobenthos. The objective of this section is to show the status of the macrobenthic community in different decades. The area surveyed in the Yellow Sea and East China Sea covered most of the sub-tidal area. The gear used to sample macrobenthos was grab or box corer unless specifically stated otherwise.

3.4.2 Yellow Sea

Taxonomic groups

From October 1997 to December 2000, macrobenthos in the Yellow Sea were investigated in a large spatial scale. A total of 414 species were collected. Polychaeta, Crustacea and Mollusca were the predominant groups and accounted for 89.37% of all species, with 194 species of Polychaeta, 90 Crustacea, 86 Mollusca, 21 Echinodermata and 23 species in other groups (Li, 2003). Species numbers showed a decreasing trend from spring to winter, with 247 species in spring, 206 in summer, 181 in autumn, and 178 in winter (Table 3.4.1).

Table 3.4.1 Seasonal variation in species numbers for marcrobenthos in the Yellow Sea from 1998 to 2000. From Li (2003).

Season	Polychaeta	Mollusca	Crustacea	Echinodermata	Others	Total
Spring	125	47	52	13	10	247
Summer	103	46	41	9	7	206
Autumn	88	19	54	9	11	181
Winter	92	30	34	13	9	178
Full year	194	86	90	21	23	414

During 2006 and 2007 in the project “the second National Ocean Census”, 853 macrobenthic species were recorded in the Yellow Sea. Seasonal variation in species numbers is shown in Table 3.4.2, with higher values in autumn and winter and lower values in spring and summer (Sun, 2012).

Table 3.4.2 Seasonal variation in species numbers for macrobenthos in the Yellow Sea during 2006 and 2007. From Sun (2012).

Season	Polychaeta	Mollusca	Crustacea	Echinodermata	Others	Total
Spring	184	104	114	27	44	473
Summer	201	97	101	23	54	476
Autumn	218	121	137	24	61	561
Winter	207	102	104	30	48	491
Full year	313	206	198	39	97	853

Table 3.4.3 Number and percentage (%) of species in the northern and southern Yellow Sea during 2006 and 2007. From Sun (2012).

Area	Polychaeta		Mollusca		Crustacea		Echinodermata		Others		Total
	S	P	S	P	S	P	S	P	S	P	
Northern Yellow Sea	261	39.67	124	18.84	178	27.05	33	5.02	62	9.42	658
Southern Yellow Sea	199	47.84	81	19.47	78	18.75	25	6.01	33	7.93	416

S: Number of species; P: Percentage of species

In the northern Yellow Sea, 658 species were collected. Polychaeta (261 species) was the dominant group, followed by Crustacea (178), Mollusca (124), Echinodermata (33) and other groups (62) (Table 3.4.3). In the southern Yellow Sea, 416 species were collected. Polychaeta (199 species) was the dominant group, followed by Mollusca (81), Crustacea (78), Echinodermata (25) and other groups (33) (Table 3.4.3).

In spring, a higher number of species were located in the southern area and northern area of the Yellow Sea, while a lower number were found in the middle area (Li, 2003, Fig. 3.4.1). In summer, the species number was higher in southwestern and northern area and lower in middle area. In autumn, a higher species number occurred in the southwestern and northeastern area, and a lower number occurred in the middle and eastern area. In winter, the number was higher in the southern area of the Yellow Sea.

It may be difficult to understand the seasonal variation in species number for macrobenthos, especially for those non-migrating polychaetes. It is true that some species are non-migrating species, but there are some polychaetes that could still migrate within a limited spatial area. Because the sampling area for each station was only 0.2 m^2 for the quantitative sampling methods (grab or box corer, 0.1 m^2 for each sample and two samples collected for each station), the limited sampling area might also contribute to the seasonal variation if there was spatial heterogeneity in a limited area.

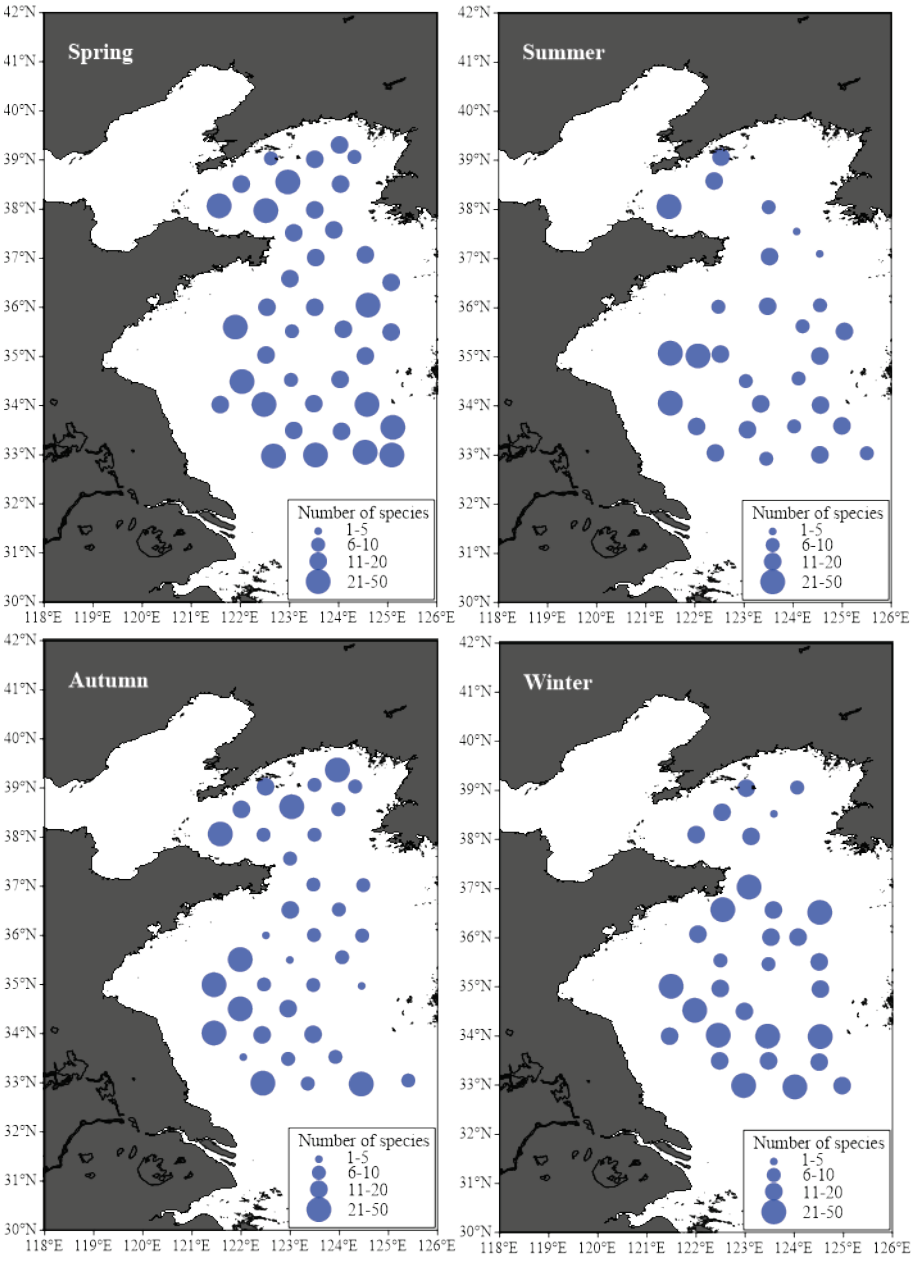

Fig. 3.4.1 The distribution of macrobenthic species numbers in the Yellow Sea in each season from 1998 to 2000. From Li (2003).

The species number for taxonomic groups of macrobenthos from eight cruises (March 2001 (Li *et al*., 2014), June–August 2006 (Xu *et al*., 2009), September–October 2008 (Jia *et al*., 2010), April and August 2011 (Li *et al*., 2014), June, August and October 2012 (Xu *et al*., 2016)) in the southern Yellow Sea are shown in Figure 3.4.2. Polychaeta showed the highest proportion of species number in each cruise, while Echinodermata showed the lowest proportion. There were no obvious changes in species numbers for Mollusca among cruises compared to other taxonomic groups.

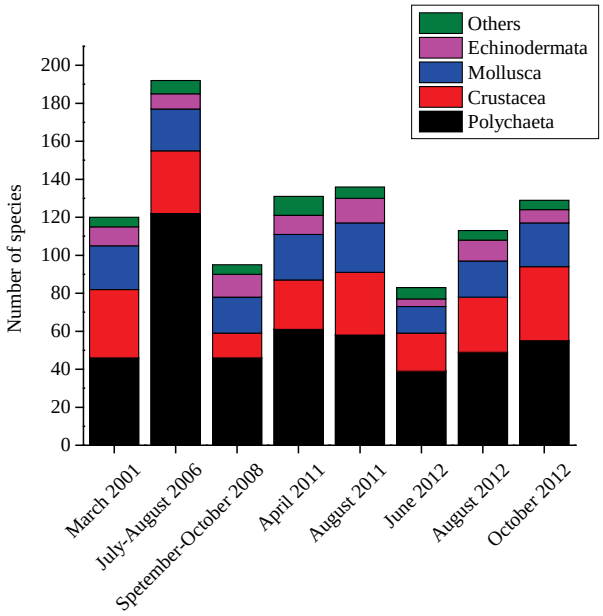

Fig. 3.4.2 Number of species of the main taxonomic groups in the southern Yellow Sea collected during eight cruises.

Dominant species

The dominant species in the Yellow Sea were stenohaline northern temperate species, including *Goniada maculata*, *Aricidea fragilis*, *Ninoe palmata*, *Terebellides stroemii*, *Thyasira tokunagaii*, *Eudorella pacifica*, *Callianassa japonica*, *Ophiura sarsii vadicola*, *etc*. (Table 3.4.4, Sun, 2012).

In the survey for macrobenthos carried out during 1997–1998 in the coastal area of the Yellow Sea, the species compositions and distribution patterns in the southern and northern areas showed obvious differences (Hu *et al*., 2000). In the coastal area of the northern Yellow Sea, because of the influence of the Yellow Sea Cold Water Mass (YSCWM), the bottom temperature was low and the cold water species such as *Crangon affinis*, *Heptacarpus geniculatus*, *Palaemon ortmanni*, *Ophiura sarsii vadicola*, *Amphipholis kochii*, *Thyasira* sp., *Volutharpa ampullaceal perryi*, *Yoldia notabilis*, *etc*. increased in abundance. The temperate species of the North Pacific Ocean, such as *Ophiopholis mirabilis*, *Acila mirabilis*, *etc*. dominated in number and abundance. In the coastal area of the southern Yellow Sea, the marine environment was characterized by complex composition of sediment and low salinity, so the macrobenthos in this area were dominated by eurythermal and low saline species. Because of the influence of warm currents in summer, some species in the East China Sea or South China Sea, such as *Nephtys ciliata* (Polychaeta) and *Temnopleurus hardwickii* (Echinodermata) appeared in this area.

During 2006 and 2007, in the project “the second National Ocean Census”, the dominant macrobenthos in the northern Yellow Sea included *Sternaspis scutata*, *Melinna cristata*, *Thyasira tokunagai*, *Laternula anatina*, *Pagurus ochotensis*, *Alpheus japonicus*, *Echinocardium cordatum*, *Ophiura sarsii vadicola*, Actiniaria, *Urechis unicinctus*, *etc*. (Table 3.4.5, Sun, 2012). The dominant species in the southern Yellow Sea were *Notomastus latericeus*, *Lumbrineris latreilli*, *Cadella narutoensis*, *Theora fragilis*, *Alpheus japonicus*, *Callianassa harmandi*, *Stegophiura sladeni*, *Ophiura sarsii vadicola*, *Antillesoma antillarum*, *etc*. (Sun, 2012).

Table 3.4.4 Dominant species in the Yellow Sea. From Sun (2012).

Taxonomic group	Dominant species	Taxonomic group	Dominant species
Polychaeta	*Sigambra hanaokai*	Crustacea	*Eudorella pacifica*
	Nereis longior		*Harpinopsis* sp.
	Goniada maculata		*Ampelisca brevicornis*
	Aricidea fragilis		*Ampelisca miharaensis*
	Ophelia acuminata		*Byblis japonicus*
	Ninoe palmata		*Eriopisella sechellensis*
	Terebellides stroemii		*Photis hawaiensis*
	Lumbrineris sp.		*Caprella equilibra*
Mollusca	*Thyasira tokunagaii*		*Callianassa japonica*
	Raetellops pulchella	Echinodermata	*Ophiura sarsii vadicola*
	Calliodentalium crocinum		
	Episiphon kiaochowwanensis		
	Cryptonatica andoi		
	Natica janthostomoides		
	Philine orientalis		
	Philine japonica		

Table 3.4.5 Dominant species in the Yellow Sea during 2006 and 2007. From Sun (2012).

Taxonomic group	Northern Yellow Sea	Southern Yellow Sea
Polychaeta	*Sternaspis scutata*	*Notomastus latericeus*
	Melinna cristata	*Lumbrineris latreilli*
	Laonice cirrata	*Ophelina acuminata*
	Glycera chirori	*Euclymene lombricoides*
	Aphrodita australis	*Terebellides stroemii*
		Ninoe palmata
Mollusca	*Thyasira tokunagai*	*Cadella narutoensis*
	Laternula anatina	*Theora fragilis*
	Raetellops pulchella	*Nucula nipponica*
Crustacea	*Pagurus ochotensis*	*Alpheus japonicus*
	Alpheus japonicus	*Callianassa harmandi*
	Eudorella pacifica	*Ampelisca bocki*
	Ampelisca brevicornis	
	Crangon affinis	
Echinodermata	*Echinocardium cordatum*	*Stegophiura sladeni*
	Ophiura sarsii vadicola	*Ophiura sarsii vadicola*
	Ophiopholis mirabilis	*Ophiopholis mirabilis*
Others	Actiniaria	*Antillesoma antillarum*
	Urechis unicinctus	
	Nemertinea	

The long-term variations of dominant species in the southern Yellow Sea were described by Xu *et al*. (2016). The dominant species in the western region (WR, depth < 40 m, Figure 3.4.3) changed from *Scapharca* and *Nassarius* (Mollusca) and sea urchin (Echinodermata) in the 1950s (Liu *et al*., 1986), and *Praxillella praetermissa*, *Sternaspis scutata*, *Praxillella pacifica*, and *Glycera chirori* (Polychaeta with big body size) in 1992 (Zhang *et al*., 2012) to *Ninoe palmata* and *Notomastus latericeus* (Polychaeta with small body size) in 2012. Small species with short life cycles (small Polychaeta) had replaced big species with long life cycles (Mollusca, Echinodermata and large Polychaeta) in the WR from the 1950s to 2012. The inshore WR area of the southern Yellow Sea is also experiencing environmental disturbances, and short-life species with high competitiveness and adaptability can adapt to the increasingly unstable environment. Thus, we predict that macrobenthos living in the WR of the southern Yellow Sea will become smaller and have short life cycles. In the middle region (MR, 40 ≤ depth < 70 m, Figure 3.4.3), dominant species in 2012 (*e.g*., *Ophiura sarsii vadicola, O. acuminate* and *Ninoe palmata*) were also different from those in 1950s (*e.g*., *Ditrupa arientina*, *Travisia pupa* and *Eunephythya* sp.) (Liu *et al*., 1986) and those in 1992 (*e.g*., *Terebellides stroemii* and *Thyasira tokunagai*) (Zhang *et al*., 2012). However, they were not significantly different in body size from the 1950s to 2012. The species dominated in eastern region (ER, depth > 70 m, Figure 3.4.3) (*e.g*., *Ophiura sarsii vadicola* and *Thyasira tokunagai*) remained unchanged from the 1950s to 2012 (Liu *et al*., 1986; Zhang *et al*., 2012). The YSCWM in the ER remained stable all the year round and had a low bottom temperature in areas deeper than 40–50 m (Liu and Hsu, 1963; Weng *et al*., 1988). Cold water species like *Ophiura sarsii vadicola* and *Thyasira tokunagai* were typical species of YSCWM in the southern Yellow Sea. Furthermore, the ER is the farthest offshore area of the southern Yellow Sea, and had the least human influence. As a result, the environment of the ER remains stable for a typical macrobenthic community to inhabit. Thus, we predict that the stability of the ER environment will continue and cold water species like *Ophiura sarsii vadicola* and *Thyasira tokunagai* will dominate the macrobenthic community in the next 50 years, unless heavy pollution or other devastating events occur at the bottom of the southern Yellow Sea.

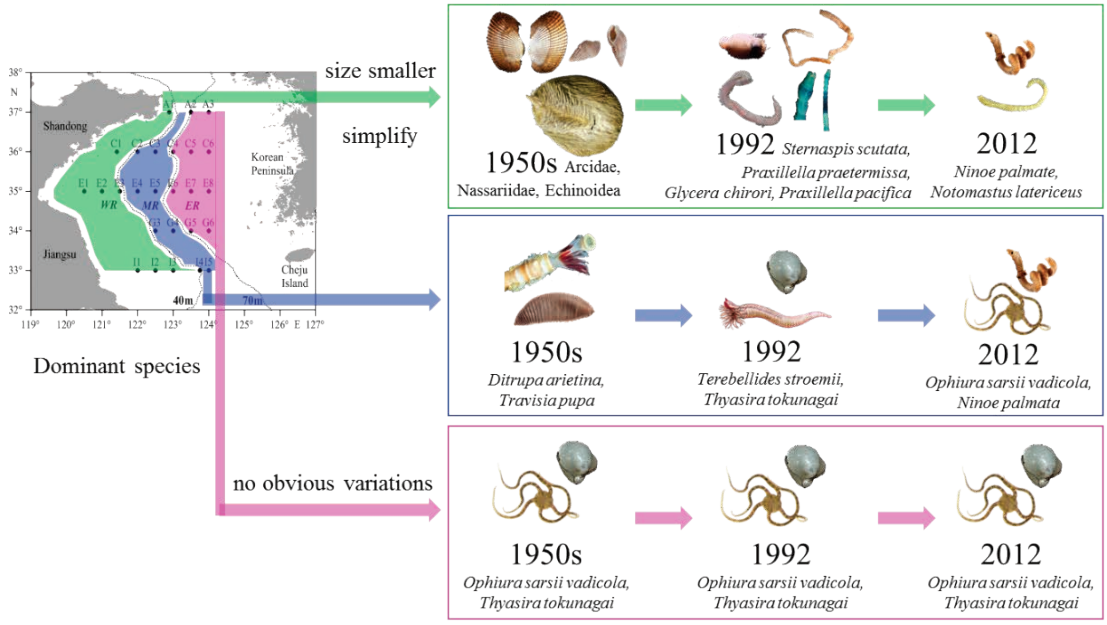

Fig. 3.4.3 Long-term variations of dominant species in the three regions in the southern Yellow Sea.

Community structure

The macrobenthic species in the coastal area of the Yellow Sea were classified into 4 communities according to the species collected by box corer and Agassiz trawl (Fig. 3.4.4, Hu *et al*., 2000).

1) *Crangon affinis*-Ophiuroidea community

This community was located in the northern area of the northern Yellow Sea and was mainly composed of cold water species. The representative species included *Crangon affinis*, *Amphioplus japonicus*, *Stegophiura sladeni*, *Ophiopholis mirabilis*, *Ophiura sarsii vadicola*, *etc*.

2) *Echinocardium cordatum*-Ophiuroidea community

This community was situated in the southern area of the northern Yellow Sea, north of Shandong Province and the representative species were *Echinocardium cordatum*, *Temnopleurus hardwickii*, *Distolasterias nipon*, *Bullacta exarata*, *Stegophiura sladeni*, *etc*.

3) *Alpheus japonicas-Nassarius* spp. community

This community was located in the northern area of the southern Yellow Sea and from Weihai (on the northern coast of Shandong peninsula) south to Lianyungang. The representative species were composed of *Alpheus japonicus*, *Odontamblyopus rubicundus*, *Nassarius succinctus*, *Nassarius variciferus*, *etc*.

4) *Palaemon gravieri-Collichthys* spp. community

This community was situated along the coast in the southern area of the southern Yellow Sea from Sheyang to Shanghai. The representative species were *Collichthys lucidus*, *Palaemon gravieri*, *Sternaspis scutata*, *Metapenaeopsis dalei*, *etc*., with the obvious component of subtropical flora.

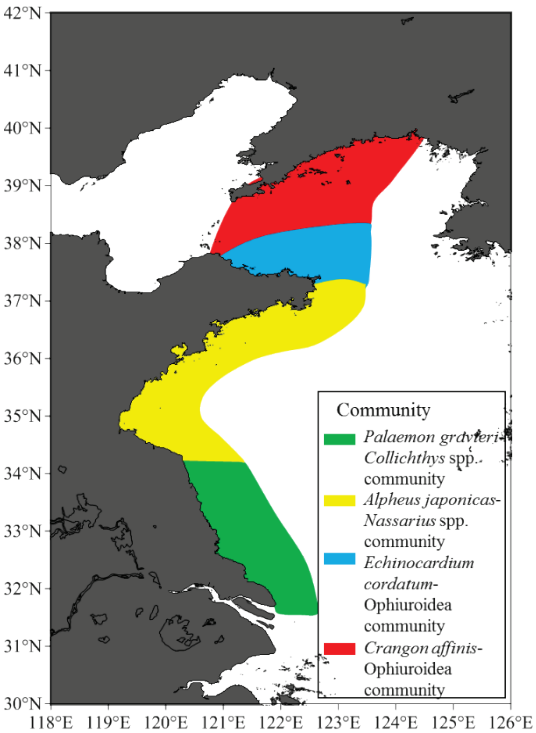

Fig. 3.4.4 The distribution of macrobenthic communities in the coastal area of the Yellow Sea, as sampled by box corer and Agassiz trawl net from 1997 to 1998. From Hu *et al*. (2000).

Li (2003) classified the macrobenthos into 7 communities according to the species collected by box corer, and these communities distributed in the northern, middle, and southern areas in the Yellow Sea (Fig. 3.4.5; Li, 2003).

There were two communities in the northern area of the Yellow Sea, named as *Spiophanes bombyx –Mactra chinensis–Ampelisca brevicornis–Echinocardium cordatum* community (Community I) and *Goniada maculata–Thyasira tokunagai–Ophiura sarsii vadicola* community (Community II).

Four communities were located in the middle area of the Yellow Sea, including *Mediomastus californiensis–Thyasira tokunagai–Metridium* sp. community (Community I), *Praxillella praetermissa–Thyasira tokunagai–Leptochela aculeocaudata* community (Community II), *Onuphis geophiliformis–Raeta pulchella–Cerianthus filiformis* community (Community III), and *Lumbrineris japonica–Thyasira tokunagai–Molgula manhattensis* community (Community IV).

In the southern area of the Yellow Sea, the macrobenthic community was *Terebellides stroemii–Raeta pulchella–Eudorella pacifica–Amphioplus depressus–Listriolobus brevirostris* community.

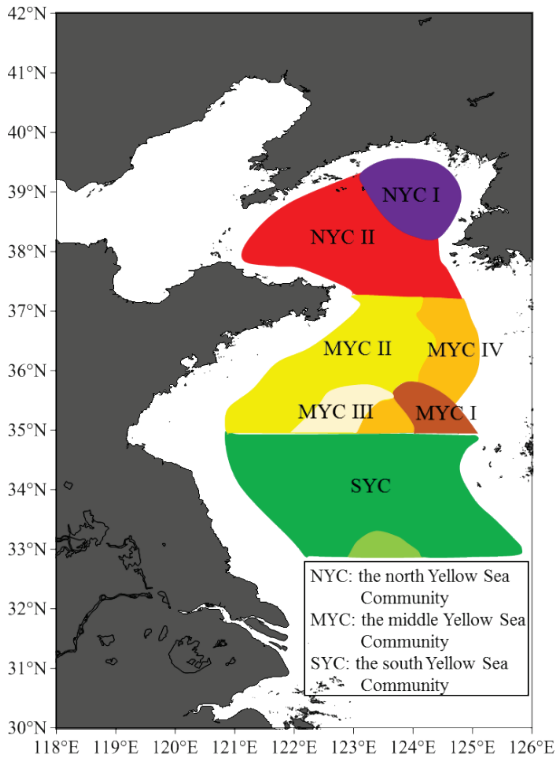

Fig. 3.4.5 The distribution pattern of macrobenthic communities in the Yellow Sea, as sampled by box corer from 1998 to 2000. From Li (2003).

The long-term variations in the macrofaunal community structure at the species, genus and family levels in three regions (WR, MR, ER; Fig. 3.4.3) in the southern Yellow Sea were described by Xu *et al*. (2017, Fig. 2.4.6). Two groups were at the species level (Fig. 3.4.6a). One group was composed of the samples collected during 1958 and 1959, and the other consisted of the samples collected from 2000 to 2014. A regional difference in the community structure was observed in two groups (1958–1959 and 2000–2014), while a seasonal difference was not obvious.

At the genus level, two groups (1958–1959 and 2000–2014) were also identified and regional differences were also detected in each group, while seasonal variations were not visually identifiable (Fig. 3.4.6b).

The community structure at the family level was slightly different from that at the species and genus levels, for which regional differences were the most obvious (Fig. 3.4.6c). Two groups were identified at the family level. One group was composed of the samples collected in the WR, and the other contained the samples collected in the MR and ER. Two subgroups (1958–1959 and 2000–2014) showing temporal differences in each group were observed.

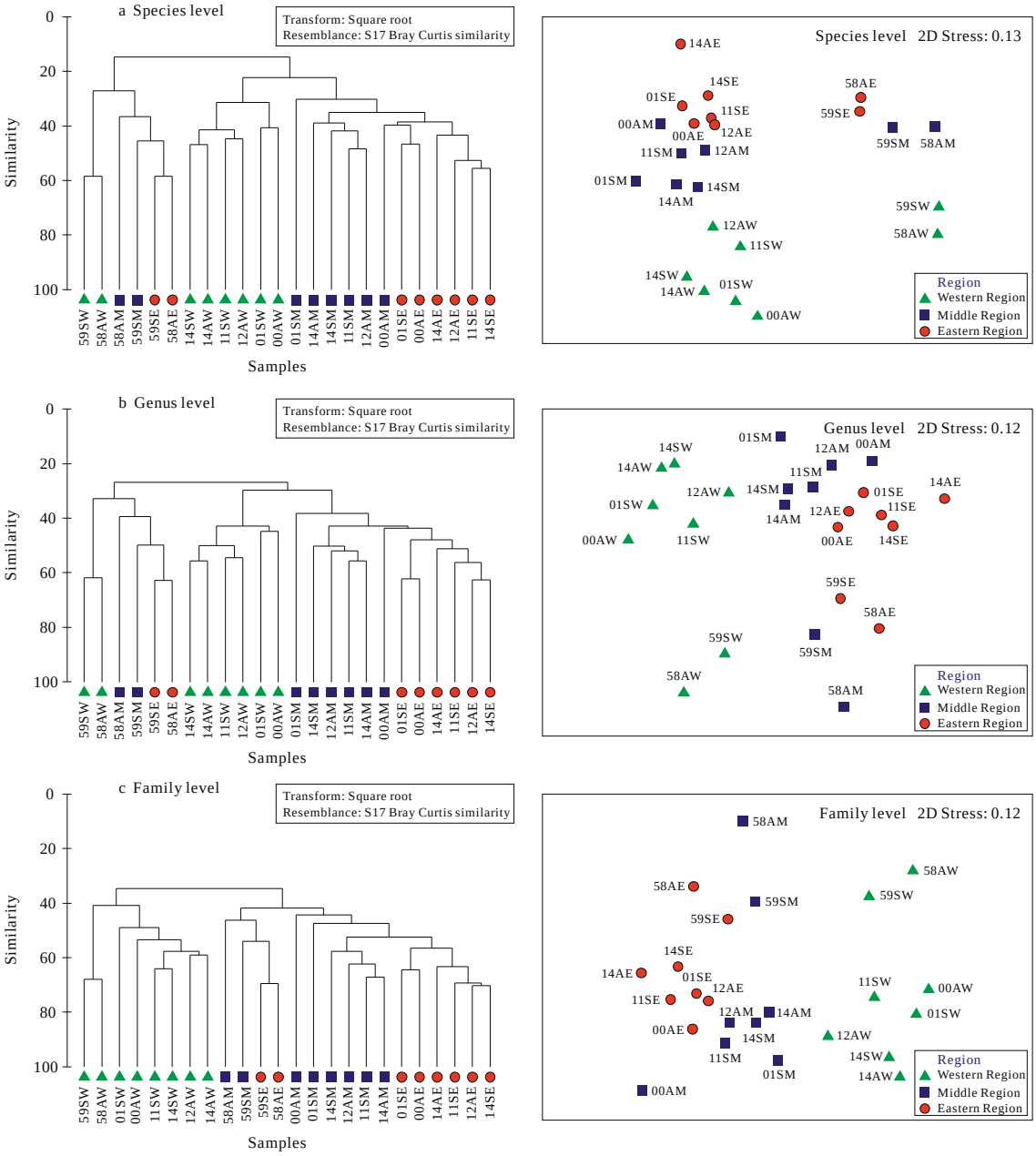

Fig. 3.4.6 Cluster analysis (left) and non-metric multidimensional scaling (nMDS) ordination (right) of macrofaunal community structure based on pooled abundance data for each region in the southern Yellow Sea at the (a) species level, (b) genus level and (c) family level. From Xu *et al*. (2017). 58: 1958; 59: 1959; 00: 2000; 01: 2001; 11: 2011; 12: 2012; 14: 2014; S: spring; A: autumn; W: western region; M: middle region; E: eastern region. Reproduced with permission of Elsevier.

Abundance, biomass and diversity

Abundance

The mean abundance of macrobenthos in the Yellow Sea was 250 ind./m^2. Polychaeta was the most abundant taxonomic group, followed by Crustacea and Mollusca. The seasonal variations of macrobenthic abundance was spring (358 ind./m^2) > winter (289 ind./m^2) > summer (187 ind./m^2) > autumn (164 ind./m^2) (Table 3.4.6, Li, 2003).

Macrobenthic abundance showed an obvious spatial variation in the coastal area of the Yellow Sea (Fig. 3.4.7, Hu *et al.*, 2000), with a decreasing trend from the northern area to the southern area, which was in accordance with the spatial distribution of organic matter in the sediment. The mean abundance in the northern Yellow Sea was 511.0 ind./m^2, and in the southern Yellow Sea was 129.4 ind./m^2.

Table 3.4.6 Seasonal variation of macrobenthic abundance (ind./m^2) in the Yellow Sea from 1998 to 2000. From Li (2003).

Season	Polychaeta	Mollusca	Crustacea	Echinodermata	Others	Total
Spring	202	57	70	24	5	358
Summer	109	15	55	5	2	187
Autumn	130	7	13	11	3	164
Winter	131	72	37	11	38	289
Average	143	38	44	13	12	249

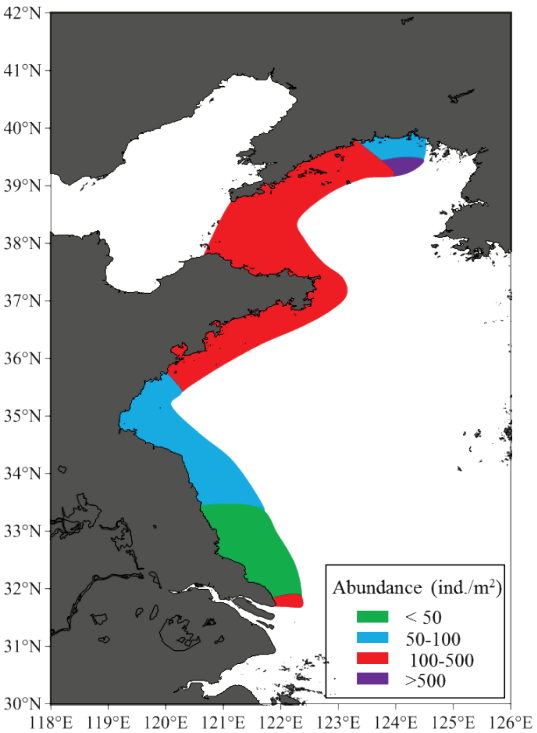

Fig. 3.4.7 The distribution of macrobenthic abundance in the coastal area of the Yellow Sea from June 1997 to July 1998. From Hu *et al.* (2000).

During 2006 and 2007 in the project "the second National Ocean Census", the mean abundance was 2017.41 ind./m^2 in the northern Yellow Sea. Polychaeta was the most abundant taxonomic group, followed by Crustacea and Mollusca. Echinodermata and others groups showed low abundance (Table 3.4.8, Sun, 2012). Compared with the northern Yellow Sea, the abundance in the southern Yellow Sea was lower, with a mean abundance of 88.67 ind./m^2. Polychaeta accounted for more than half of the total abundance and Mollusca, Crustacea, Echinodermata and other groups showed low abundance. The seasonal variation of mean abundance is shown in Table 3.4.9.

The abundance of macrobenthos taxonomic groups from eight cruises (March 2001 (Li *et al*., 2014), June–August 2006 (Xu *et al*., 2009), September–October 2008 (Jia *et al*., 2010), April and August 2011 (Li *et al*., 2014), June, August and October 2012 (Xu *et al*., 2016)) in the southern Yellow Sea is shown in Figure 3.4.8. Polychaeta had the highest abundance in each cruise, while Echinodermata had the lowest proportion, except during August 2012. There were no obvious changes in abundance of Mollusca among cruises compared to other taxonomic groups.

Table 3.4.8 Mean abundance (ind./m^2) and its percentage (%) in the northern and southern Yellow Sea during 2006 and 2007. From Sun (2012).

Area	Polychaeta		Mollusca		Crustacea		Echinodermata		Others		Total
	Ab	P	Ab	P	Ab	P	Ab	P	Ab	P	
Northern Yellow Sea	865.92	42.92	415.04	20.57	568.61	28.19	112.30	5.57	55.54	2.75	2017.40
Southern Yellow Sea	51.79	58.41	13.95	15.73	10.89	12.28	6.64	7.49	5.40	6.09	88.67

Ab: Abundance; P: Percentage of abundance

Table 3.4.9 Seasonal variation of macrobenthic abundance (ind./m^2) in the Yellow Sea during 2006 and 2007. From Sun (2012).

Season	Polychaeta	Mollusca	Crustacea	Echinodermata	Others	Total
Spring	218	80	145	28	4	476
Summer	250	173	178	44	11	655
Autumn	217	88	123	29	18	476
Winter	468	164	283	39	26	979

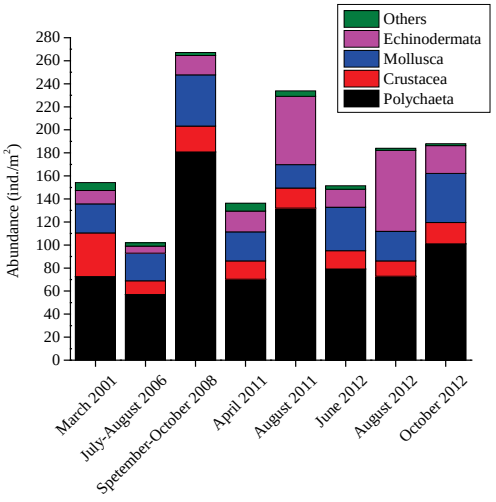

Fig. 3.4.8 Abundance of the main taxonomic groups in the southern Yellow Sea.

Biomass

The mean biomass of macrobenthos in the Yellow Sea was 37.09 g/m^2. Echinodermata showed the highest biomass, followed by Polychaeta. The seasonal variations of macrobenthic biomass was spring (51.01 g/m^2) > autumn (35.34 g/m^2) > summer (32.06 g/m^2) > winter (29.94 g/m^2) (Table 3.4.10; Li, 2003).

The macrobenthic biomass also showed an obvious spatial variation in the coastal area of the Yellow Sea (Fig. 3.4.9) (Hu *et al*., 2000). A decreasing trend from the northern area to the southern area was detected, in accordance with the spatial distribution of organic matter in the sediment and abundance. The mean biomass in the northern Yellow Sea was 106.1 g/m^2, dominated by Echinodermata (55.0% of total biomass), and in the southern Yellow Sea was 13.36 g/m^2, dominated by Polychaeta (44.3% of total biomass).

Table 3.4.10 Seasonal variation of macrobenthic biomass (g/m^2) in the Yellow Sea from 1998 to 2000. From Li (2003).

Season	Polychaeta	Mollusca	Crustacea	Echinodermata	Others	Total
Spring	11.07	8.54	3.81	18.99	8.60	51.01
Summer	10.39	3.11	6.36	6.25	5.94	32.06
Autumn	10.75	1.78	2.56	11.56	8.69	35.34
Winter	7.89	3.69	1.56	9.48	7.33	29.94
Average	10.03	4.28	3.57	11.57	7.64	37.09

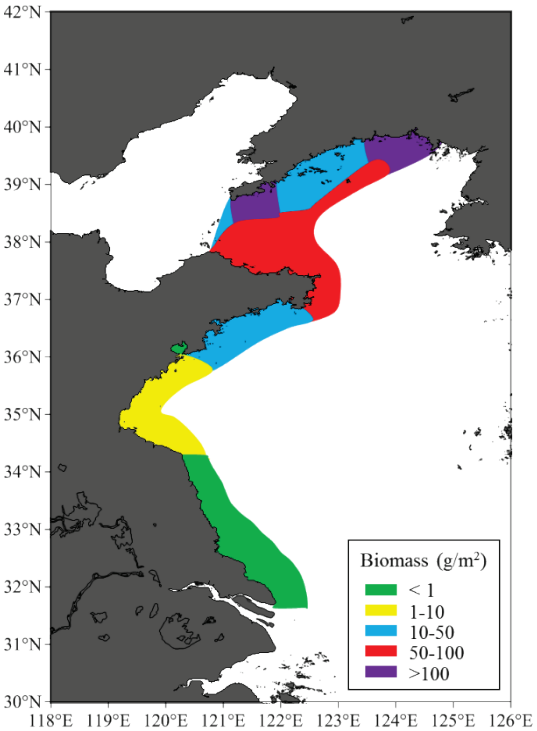

Fig. 3.4.9 The distribution of macrobenthic biomass in the coastal area of the Yellow Sea from June 1997 to July 1998. From Hu *et al*. (2000).

During 2006 and 2007 in the project "the second National Ocean Census", the mean biomass was 99.66 g/m^2 in the northern Yellow Sea (Sun, 2012). Echinodermata was the taxonomic group showing highest biomass, followed by Polychaeta and other groups. Crustacea and Mollusca showed low biomass (Table 3.4.11). The mean biomass in the southern Yellow Sea was 27.67 g/m^2 (Sun, 2012). The rank of the biomass for each taxonomic group was Polychaeta > Echinodermata > Mollusca > other groups > Crustacea. The seasonal variation of mean biomass is shown in Table 3.4.12.

Table 3.4.11 Mean biomass (g/m^2) and its percentage (%) in the northern and southern Yellow Sea during 2006 and 2007. From Sun (2012).

Area	Polychaeta		Mollusca		Crustacea		Echinodermata		Others		Total
	Bio	P	Bio	P	Bio	P	Bio	P	Bio	P	
Northern Yellow Sea	20.41	20.48	12.99	13.03	7.70	7.73	36.42	36.55	22.14	22.21	99.66
Southern Yellow Sea	9.25	33.40	5.64	20.38	2.18	7.86	7.64	27.61	2.98	10.76	27.69

Bio: biomass; P: Percentage of biomass

Table 3.4.12 Seasonal variation of macrobenthic biomass (g/m^2) in the Yellow Sea during 2006 and 2007. From Sun (2012).

Season	Polychaeta	Mollusca	Crustacea	Echinodermata	Others	Total
Spring	7.50	4.44	3.45	11.88	5.36	32.63
Summer	11.37	5.85	2.26	10.09	5.67	35.23
Autumn	7.55	7.02	2.90	12.63	8.46	38.55
Winter	8.94	8.95	2.34	11.01	8.07	39.32

The biomass of macrobenthos taxonomic groups from eight cruises (March 2001 (Li *et al*., 2014), June–August 2006 (Xu *et al*., 2009), September–October 2008 (Jia *et al*., 2010), April and August 2011 (Li *et al*., 2014), June, August and October 2012 (Xu *et al*., 2012)) in the southern Yellow Sea is shown in Fig. 3.4.10. Echinodermata and Mollusca had the highest abundance in most cruises. During August 2012, the biomass of Echinodermata showed an overwhelming advantage in biomass compared to other taxonomic groups.

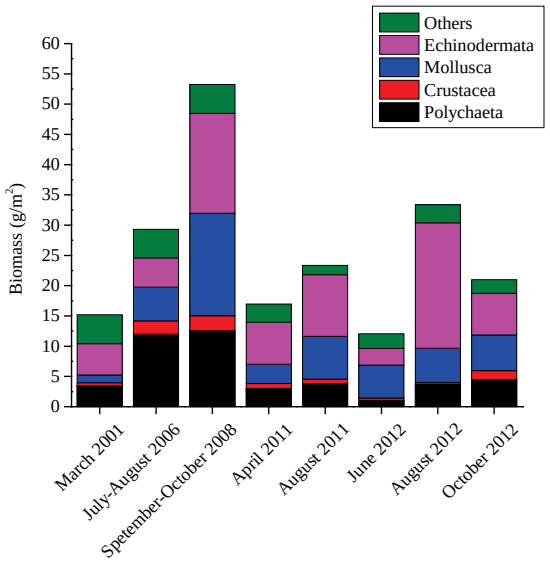

Fig. 3.4.10 Biomass of the main taxonomic groups in the southern Yellow Sea.

Diversity

According to the Shannon-Wiener diversity index (*H'*), Margalef richness index (*d*), and Pielou evenness index (*J'*), the offshore area of Dalian–Dandong and the coastal area of Qiangdao–Rushan, the Qidong–Yangtze River estuary showed high macrobenthic diversity and richness (*H'* >3; *d*: 2.07–4.36), with a relatively homogeneous (*J'*: 0.71–0.97) distribution of species (Fig. 3.4.11) (Hu *et al*., 2000). This phenomenon was related to the richness in types of species, high organic matter content and less pollution in the sediment (Hu *et al*., 2000). The coastal area in Dandong, Yantai–Weihai, Rizhao–Sheyang showed the lowest species diversity and richness (*H'*: 0.48–1.87; *d*: 0.37–1.75), with a heterogeneous (*J'*: 0.12–0.57) distribution of species. This phenomenon was related to heavy pollution and instability of the sediment (Hu *et al*., 2000).

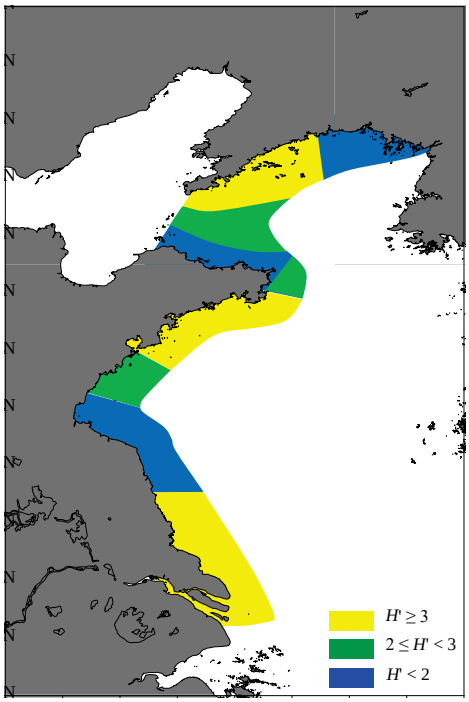

Fig. 3.4.11 Distribution of the Shannon-Wiener diversity index (*H'*) in the coastal area of the Yellow Sea during June 1997 and July 1998. From Hu *et al*. (2000).

The diversity indexes (Margalef richness index, Shannon-Wiener index and Pielou's evenness index) from six cruises (March 2001, April and August 2011, June, August and October 2012 (Xu *et al*., 2016)) in the southern Yellow Sea are shown in Figure 3.4.12.

The mean value of Margalef richness index (*d*) was highest (3.72) in October 2012 and lowest (3.12) in June 2012, with values fluctuating from 2001 to 2012. The mean value of Shannon-Wiener index (*H'*) showed the same trend with *d*, having the highest value in October 2012 (3.23) and the lowest value (2.85) in June 2012. The mean value of Pielou's evenness index (*J'*) was relative stable during the six cruises, with the highest mean value (0.86) occurring in October 2012 and the lowest mean value (0.83) in August 2011.

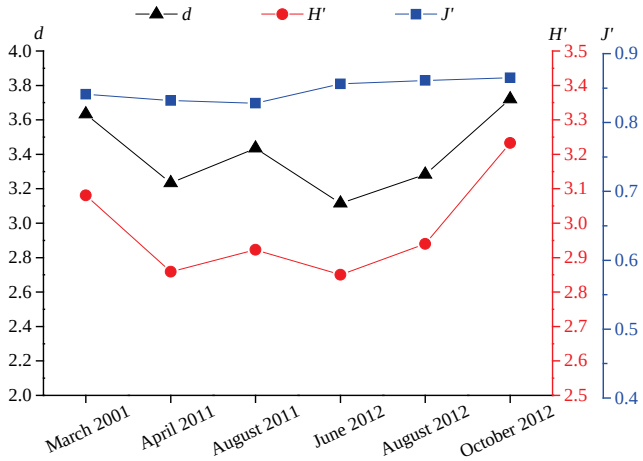

Fig. 3.4.12 Diversity indexes (Margalef richness index (*d*), Shannon-Wiener index (*H'*) and Pielou's evenness index (*J'*)) in the southern Yellow Sea.

Secondary productivity

Secondary production is the conversion of energy from primary producers by consumers to produce new biomass (Blomberg and Montagna, 2014). In this section, all productivity occurring higher than at the primary level is referred to as secondary productivity of macrobenthos. Secondary productivity (g(AFDW)/(m^2·a)) is calculated using the formula (Li *et al.*, 2005d): Secondary productivity = $Abundance^{0.27} \times Biomass^{0.737}/10^{0.4}$, which was transformed from Brey's empirical formula (Brey, 1990): log(Secondary productivity) = –0.4 + 1.007log(Biomass) – 0.27log(Biomass/Abundance).

As shown in Fig. 3.4.13, the mean secondary productivity in the southern Yellow Sea was 3.00 g(AFDW)/(m^2·a) in April 2011. In August 2011, the mean value increased to 4.77 g(AFDW)/(m^2·a). The mean of the secondary productivity in June, August and October, 2012 was 2.53, 5.74 and 4.12 g(AFDW)/(m^2·a), respectively. It can be concluded that in summer (August), the macrobenthos in the southern Yellow Sea had the highest secondary productivity.

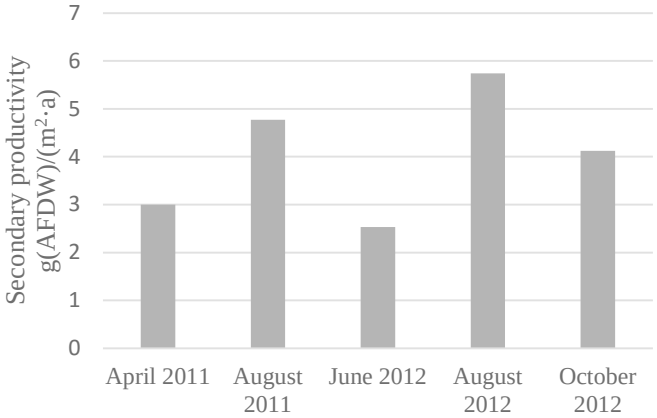

Fig. 3.4.13 Secondary productivity (g(AFDW)/(m^2·a)) of macrobenthos during five cruises in the southern Yellow Sea.

3.4.3 East China Sea

Taxonomic groups

From October 1997 to March 2000, a total of 855 macrobenthic species were collected in the East China Sea. Polychaeta, Mollusca and Crustacea were the predominant groups which accounted for 85.94% of all species, with 268 species of Polychaeta, 283 Mollusca, 171 Crustacea, 68 Echinodermata and 65 species in other groups (Li, 2003).

Compared to the species composition in the Bohai Sea and the Yellow Sea, the species composition in the East China Sea was more diverse. The East China Sea shared 209 species with the Yellow Sea, among which were 139 species of Polychaeta, 31 Mollusca, 18 Crustacea, 16 Echinodermata and 5 species in other groups (Li, 2003).

The species composition of macrobenthos in the East China Sea had obvious seasonal variations, with the rank of species number being spring (452 species) > autumn (435) > summer (380) > winter (288) (Table 3.4.13, Li, 2003).

Table 3.4.13 Seasonal variation in species numbers for macrobenthos in the East China Sea from 1997 to 2000. From Li (2003).

Season	Polychaeta	Mollusca	Crustacea	Echinodermata	Others	Total
Spring	155	147	92	37	21	452
Summer	139	92	86	36	27	380
Autumn	153	126	100	25	31	435
Winter	129	66	48	24	21	288
Full year	268	283	171	68	65	855

Figure 3.4.13 shows the seasonal distribution pattern of macrobenthic species numbers in the East China Sea. In spring, a high number of species was found in the southern area and the northern area of the East China Sea and the northern area of the Taiwan Strait, but in the middle area of the East China Sea, the species number was low (Li, 2003). In summer, a high number of species was found in the middle and northern area of the East China Sea and the northern area of the Taiwan Strait. In autumn, the middle and northeastern area showed high species number, but the number in the southern area was low. In winter, the distribution of species numbers was relatively homogenous.

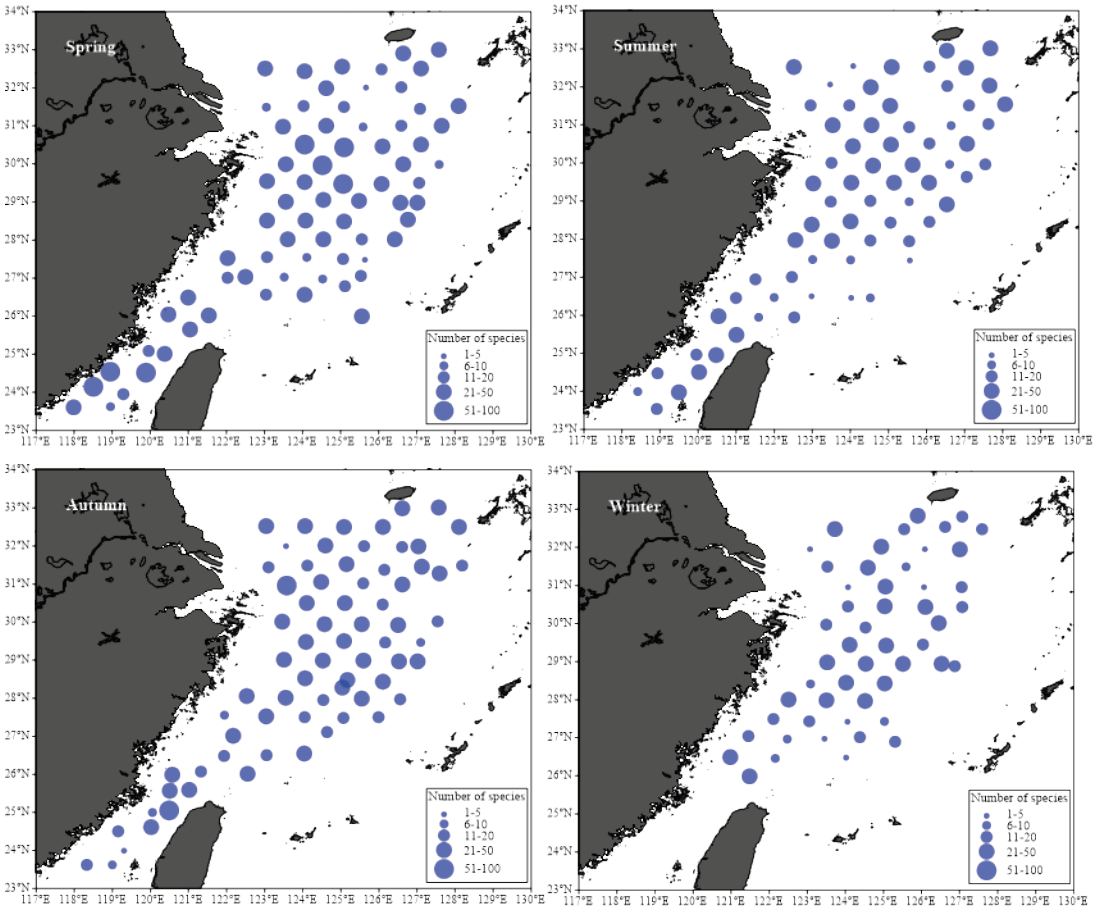

Fig. 3.4.13 The distribution pattern of macrobenthic species numbers in the East China Sea. From Li (2003).

During 2006 and 2007 in the project “the second National Ocean Census”, 1300 macrobenthic species were recorded in the East China Sea, including 428 species of Polychaeta, 291 of Mollusca, 283 of Crustacea, 80 of Echinodermata, and 218 species in other groups (Sun, 2012). Seasonal variation in species numbers is shown in Table 3.4.14, with higher values in summer and winter and lower values in spring and autumn.

In the sea area adjacent to the Yangtze River estuary, the area off the Zhejiang coast and the Taiwan Strait, the number of species was 418, 327 and 492, respectively, with Polychaeta being the dominant taxonomic group (Table 3.4.15).

Table 3.4.14 Seasonal variation of the species number of macrobenthos in the East China Sea during 2006 and 2007 (Sun, 2012).

Season	Polychaeta	Mollusca	Crustacea	Echinodermata	Others	Total
Spring	239	108	157	41	86	631
Summer	274	169	170	43	117	773
Autumn	256	102	133	46	82	619
Winter	260	121	156	44	76	657
Full year	428	291	283	80	218	1300

Table 3.4.15 Number and percentage (%) of species in the sea adjacent to the Yangtze River estuary, the area off the Zhejiang coast, and the Taiwan Strait during 2006 and 2007. From Sun (2012).

Area	Polychaeta		Mollusca		Crustacea		Echinodermata		Others		Total
	S	P	S	P	S	P	S	P	S	P	
Sea adjacent to Yangtze River estuary	148	35.41	135	32.30	69	16.51	27	6.46	39	9.33	418
Area off Zhejiang coast	187	57.19	46	14.07	49	14.98	29	8.87	16	4.89	327
Taiwan Strait	249	50.61	50	10.16	135	27.44	31	6.30	27	5.49	492

S: Number of species; P: Percentage of species

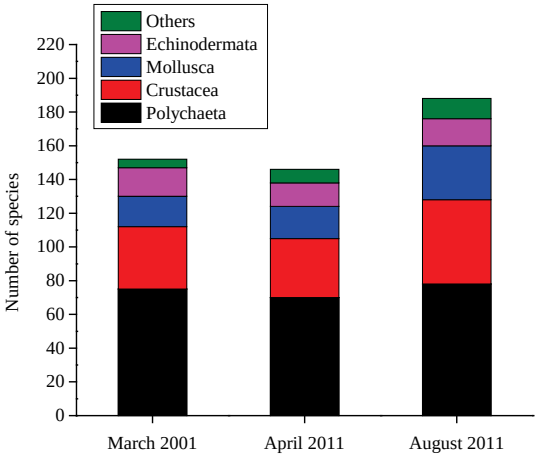

Fig. 3.4.14 Number of species of the main taxonomic groups in the East China Sea.

The main taxonomic groups of macrobenthos from three cruises (March 2001, April and August 2011) in the East China Sea are shown in Figure 3.4.14. The proportion of species number of each taxonomic group was relative stable among cruises.

Dominant species

The dominant, and most common, macrobenthic species are listed in Table 3.4.16. The spatial distributions of different dominant species were also different.

During 2006 and 2007, in the project “the second National Ocean Census”, researchers found that some dominant species in the sea adjacent to the Yangtze River estuary, the area off the Zhejiang coast and the Taiwan Strait had similar distributions, while species in the other group had different distributions. *Sternaspis scutata* and Nemertinea had high dominance in all three areas (Table 3.4.17, Sun, 2012).

Table 3.4.16 Dominant species in the East China Sea from 1997 to 2000 (Li, 2003).

Taxonomic group	Dominant species	Taxonomic group	Dominant species
Polychaeta	*Paralacydonia paradoxa*	Mollusca	*Dentalium octangulatum*
	Sigambra hanaokai		*Bursa rana*
	Goniada maculata		*Mitrella burchardi*
	Glycera sp.		*Nassarius siquijorensis*
	Glycera chirori		*Zeuxis* sp.
	Prionospio malmgreni		*Inquisitor flavidula*
	Prionospio pygmaea		*Lophiotoma leucotropis*
	Paraprionospio pinnata	Crustacea	*Ampelisca cyclops*
	Paraprionospio sp.		*Ampelisca miharaensis*
	Lumbrineris latreilli		*Eriopisella sechellensis*
	Magelona sp.		*Leptochela acculeocaudata*
	Notomastus aberans		*Alpheus distinguendus*
	Onuphis eremita		*Callianassa japonica*
	Aglaophamus dibranchis		*Jassa falcata*
	Aricidea fragilis		*Byblis japonicus*
Mollusca	*Angulus lanceolatus*		*Grandidierella japonica*
	Spiniplicatula muricata	Echinodermata	*Amphioplus laevis*
	Episiphon kiaochowwanensis		*Amphioplus depressus*
	Graptacme buccinulum		*Amphioplus ancistrotus*
	Calliodentalium crocinum		*Amphiura vadicola*
	Solen canaliculatus		*Amphiura digitula*
	Olivella sp.		*Ophiura kinbergi*

Table 3.4.17 Dominant species in the sea adjacent to the Yangtze River estuary, the area off the Zhejiang coast and the Taiwan Strait during 2006 and 2007. From Sun (2012).

Sea adjacent to Yangtze River estuary	Area off the Zhejiang coast	Taiwan Strait
	Polychaeta	
Paraprionospio pinnata	*Sternaspis scutata*	*Sternaspis scutata*
Cossurella dimorpha	*Notomastus latericeus*	*Paralacydonia paradoxa*
Capitella capitata	*Laonice cirrata*	*Paralacydonia ehlersi*
Sternaspis scutata	*Cossurella dimorpha*	*Mediomastus californiensis*
Laonice cirrata	*Magelona cincta*	*Notomastus aberans*
	Mollusca	
Nassarius variciferus	*Eocylichna braunsi*	*Modiolus comptus*
Nassarius succinctus	*Nassarius siquijorensis*	*Moerella culter*
Moerella jedoensis		*Angulus vestalis*
	Crustacea	
Hemigrapsus peniciillatus	Gammaridea	*Eriopisella sechellensis*
Alpheus distinguendus	*Xenophthalmus pinnotheroides*	*Urothoe grimaldii*
Ampelisca cyclops	Diogenidae	*Harpiniopsis* sp.
Leptochela gracilis		*Byblis japonicus*

Table 3.4.17 Contined.

Sea adjacent to Yangtze River estuary	Area off the Zhejiang coast	Taiwan Strait
	Echinodermata	
Amphiura vadicola	*Protankyra bidentata*	*Amphiura* sp.
Amphioplus depressus	*Amphiura vadicola*	*Ophiactis affinis*
		Amphioplus depressus
	Others	
Nemertinea	Nemertinea	*Apionsoma trichocephala*
Odontamblyopus rubicundus	Actiniaria	Nemertinea
Actiniaria		*Branchiostoma belcheri*

Community structure

Li (2003) classified the macrobenthos in the East China Sea into 5 communities named as north inshore community, north offshore community, south inshore community, south offshore community and Taiwan Strait community (Fig. 3.4.15).

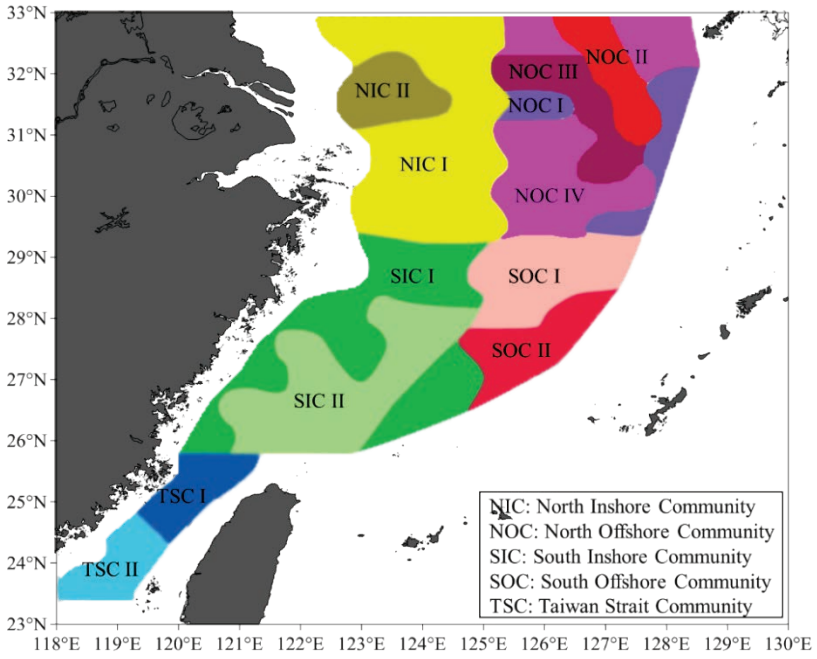

Fig. 3.4.15 The distribution pattern of macrobenthic communities in the East China Sea from 1997 to 2000. From Li (2003).

1) North inshore community, including 2 sub-communities

Sub-community I, *Aricidea fragilis–Calliodentalium crocinum–Raetellops pulchella–Callianassa japonica –Amphioplus depressus* community.

Sub-community II, *Micronephtys sphaerocirrata–Eulima bifascialis–Scapharca inaequivalvis–Ogyrides orientalis* community.

2) South inshore community, including 2 sub-communities

Sub-community I, *Onuphis eremita–Calliodentalium crocinum–Callianassa japonica–Amphioplus ancistrotus* community.

Sub-community II, *Aricidea fragilis–Calliodentalium crocinum–Grandidierella japonica–Amphioplus ancistrotus* community.

3) North offshore community, including 4 sub-communities

Sub-community I, *Mediomastus californiensis–Byblis japonicus–Golfingia* sp. community.

Sub-community II, *Amphictene* sp.*–Calliodentalium crocinum–Leptochelia aculeocauclata–Placophiothrix striolata* community.

Sub-community III, *Sigambra hanaokai–Calliodentalium crocinum–Callianassa japonica–Amphiura digitula* community.

Sub-community IV, *Aricidea fragilis–Calliodentalium crocinum–Callianassa japonica–Amphioplus* sp. community.

4) South offshore community, including 2 sub-communities

Sub-community I, *Aglaophamus dicirris–Turritella fascialis–Callianassa japonica–Placophiothrix striolata* community.

Sub-community II, *Paraprionospio pinnata–Spiniplicatula muricata–Solenocera pectinulata–Ophionephthys difficilis* community.

5) Taiwan Strait community, including 2 sub-communities

Sub-community I, *Tharyx acutus–Calliodentalium crocinum–Ampelisca cyclops–Amphioplus depressus* community.

Sub-community II, *Haploscoloplos elongatus–Nucula convexa–Ampelisca brevicornis* community.

Abundance, biomass and diversity

Abundance

The mean abundance of macrobenthos in the East China Sea was 280 ind./m^2, among which Polychaeta showed the highest abundance, followed by Crustacea and Mollusca. The seasonal variation of macrobenthic abundance was autumn (461 ind./m^2) > spring (336 ind./m^2) > summer (178 ind./m^2) > winter (146 ind./m^2). The seasonal variations of the abundance of five taxonomic groups are shown in Table 3.4.18 (Li, 2003).

Table 3.4.18 Seasonal variations of the macrobenthic abundance (ind./m^2) in the East China Sea from 1997 to 2000. From Li (2003).

Season	Polychaeta	Mollusca	Crustacea	Echinodermata	Others	Total
Spring	151	69	69	13	34	336
Summer	99	6	50	12	11	178
Autumn	134	108	203	6	10	461
Winter	81	3	47	5	10	146
Average	116	47	92	9	16	280

The spatial distribution pattern of macrobenthic abundance showed that high abundance existed in the inshore area and low abundance in the offshore area. There were also obvious seasonal and latitudinal patterns for abundance. In spring, the abundance was high in the middle area of the East China Sea, the inshore area of the Yangtze River estuary, and the north of the Taiwan Strait, with the highest value of 1000 ind./m^2, showing a decreasing trend from inshore to offshore. In summer, there were two high abundance areas. One was located in the inshore area of the Yangtze River estuary and the other was situated from the Yangtze River estuary to the north of the Taiwan Strait, both of which had the highest value of 250 ind./m^2. In autumn, the abundance in the inshore area (highest abundance was up to 1500 ind./m^2) was higher than that in the offshore area. In winter, high abundance occurred in the coastal area of Zhejiang province and in the offshore area of Hangzhou Bay, with the high abundance of 250 ind./m^2 (Li, 2003).

During 2006 and 2007 in the project “the second National Ocean Census”, the mean abundance was 164 ind./m^2 in the East China Sea (Sun, 2012). The seasonal variation of mean abundance is shown in Table 3.4.19.

The macrobenthic abundance in the sea adjacent to the Yangtze River estuary, the area off the Zhejiang coast and the Taiwan Strait had its own characteristics, with the total abundance showing an increasing trend from the north to the south. The mean abundance was 92.06 ind./m^2 in the sea adjacent to the Yangtze River estuary, 140.87 ind./m^2 in the area off the Zhejiang coast, and 330.52 ind./m^2 in the Taiwan Strait (Sun, 2012). The main contributor for abundance in the three areas was Polychaeta, corresponding to its small size and centralized distribution. The reason for the high abundance in the Taiwan Strait was the existence of large amounts of small Crustacea, such as Gammaridea, Cumacea, Limnoria, *etc*. In winter, these small Crustacea accounted for more than half of the total abundance (Table 3.4.20).

Table 3.4.19 Seasonal variation of macrobenthic abundance (ind./m^2) in the East China Sea during 2006 and 2007. From Sun (2012).

Season	Polychaeta	Mollusca	Crustacea	Echinodermata	Others	Total
Spring	61	8	29	12	10	120
Summer	123	11	47	10	9	200
Autumn	65	8	16	9	10	108
Winter	122	8	65	14	15	224

Table 3.4.20 Mean abundance (ind./m^2) and its percentage (%) in the adjacent sea area of the Yangtze River estuary, the area off the Zhejiang coast and the Taiwan Strait during 2006 and 2007.

Area	Polychaeta		Mollusca		Crustacea		Echinodermata		Others		Total
	Ab	P	Ab	P	Ab	P	Ab	P	Ab	P	
Sea adjacemt to Yangtze River estuary	53.60	58.23	11.78	12.79	19.48	21.16	4.32	4.69	2.88	3.13	92.06
Area off Zhejiang coast	92.81	65.88	6.58	4.67	20.50	14.55	9.88	7.01	11.10	7.88	140.87
Taiwan Strait	148.13	44.82	2.88	0.87	128.21	38.79	26.70	8.08	24.61	7.44	330.51

Ab: Abundance; P: Percentage of abundance

The abundance of each taxonomic group from three cruises (March 2001, April and August 2011) in the East China Sea is shown in Figure 3.4.16. All taxonomic groups had obviously higher abundance values in summer than in spring, while almost no long-term variation of abundance in spring was detected.

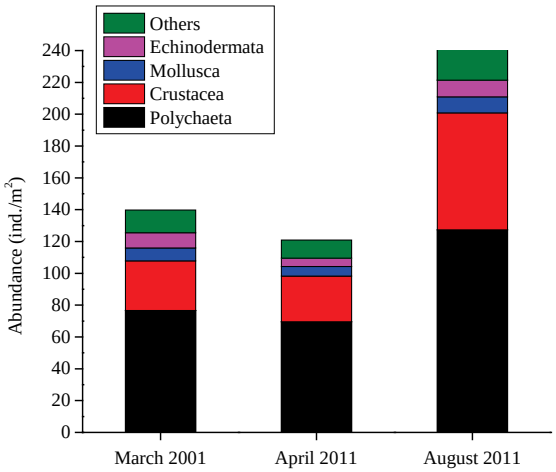

Fig. 3.4.16 Abundance of the main taxonomic groups in the East China Sea.

Biomass

The mean biomass of macrobenthos in the East China Sea was 20.84 g/m^2, among which Mollusca showed the highest biomass, followed by Echinodermata and species in other groups (Li, 2003). The seasonal variation of macrobenthic biomass was spring (41.24 g/m^2) > autumn (19.10 g/m^2) > summer (12.45 g/m^2) > winter (10.58 g/m^2). The seasonal variations of the biomass for different taxonomic groups were shown in Table 3.4.21.

Table 3.4.21 Seasonal variation of macrobenthic biomass (g/m^2) in the East China Sea from 1997 to 2000. From Li (2003).

Season	Polychaeta	Mollusca	Crustacea	Echinodermata	Others	Total
Spring	3.27	29.3	2.14	2.91	3.62	41.24
Summer	3.49	1.29	1.53	3.65	2.48	12.45
Autumn	3.32	5.74	1.55	3.51	4.98	19.10
Winter	2.42	1.69	1.17	3.75	1.55	10.58
Average	3.13	9.51	1.60	3.46	3.16	20.84

The spatial distribution of macrobenthic biomass also showed obvious seasonal and latitudinal patterns. In spring, the biomass was high in the inshore area of the East China Sea, showing a decreasing trend from inshore to offshore; the biomass had highest values (250 g/m^2) in the coastal area of Zhejiang province and formed high value areas in the north and middle of the Taiwan Strait. In summer, the biomass was lower than that in spring; high biomass areas were located in the middle area of the Yangtze River estuary and the offshore area of Hangzhou Bay, and low biomass area in the north of the Taiwan Strait. In autumn, high biomass areas were formed in the coastal areas of the Yangtze River estuary and Hangzhou Bay with the highest value being 150 g/m^2, and low biomass area in the north of the Taiwan Strait. In winter, high biomass areas were the middle area of the Yangtze River estuary and the inshore area of Hangzhou Bay, with the highest value being 90 g/m^2 (Li, 2003).

During 2006 and 2007 in the project “the second National Ocean Census”, detailed investigations of macrobenthos were made in the East China Sea. The seasonal variation of mean biomass is shown in Table 3.4.22 (Sun, 2012).

The macrobenthic biomass in the sea adjacent to the Yangtze River estuary, the area off the Zhejiang coast and the Taiwan Strait were different (Table 3.4.23). The mean biomass was highest in the area off the Zhejiang coast, and lowest in the Taiwan Strait (Sun, 2012). The biomass of each taxonomic group in the three areas was also different. Mollusca and Echinodermata accounted for the highest proportion of biomass for its comparatively large size. Polychaeta only accounted for a small proportion of biomass for its small size though its abundance was high.

Table 3.4.22 Seasonal variation of macrobenthic biomass (g/m^2) in the East China Sea during 2006 and 2007. From Sun (2012).

Season	Polychaeta	Mollusca	Crustacea	Echinodermata	Others	Total
Spring	2.06	3.31	1.17	11.26	1.59	19.39
Summer	2.84	3.20	2.06	3.92	2.05	14.07
Autumn	1.81	3.08	1.96	3.53	1.32	11.71
Winter	2.69	2.74	1.20	6.43	2.00	15.06

Table 3.4.23 Mean biomass (g/m^2) and its percentage (%) in the sea adjacent to the Yangtze River estuary, the area off the Zhejiang coast and the Taiwan Strait during 2006 and 2007. From Sun (2012).

Area	Polychaeta		Mollusca		Crustacea		Echinodermata		Others		Total
	Bio	P	Bio	P	Bio	P	Bio	P	Bio	P	
Sea adjacent to Yangtze River estuary	2.85	18.33	4.78	30.74	2.75	17.72	3.53	22.71	1.63	10.50	15.55
Area off Zhejiang coast	1.49	5.28	2.77	9.81	1.36	4.82	19.73	69.92	2.87	10.16	28.22
Taiwan Strait	1.46	16.26	2.01	22.42	1.01	11.20	3.27	36.46	1.23	13.66	8.98

Bio: biomass; P: Percentage of biomass

The biomass of each taxonomic group from three cruises (March 2001, April and August 2011) in the East China Sea are shown in Figure 3.4.17. The biomass showed high difference among cruises for each taxonomic group, especially for Mollusca, Echinodermata, and others (species not belonging to Polychaeta, Crustacea, Mollusca and Echinodermata).

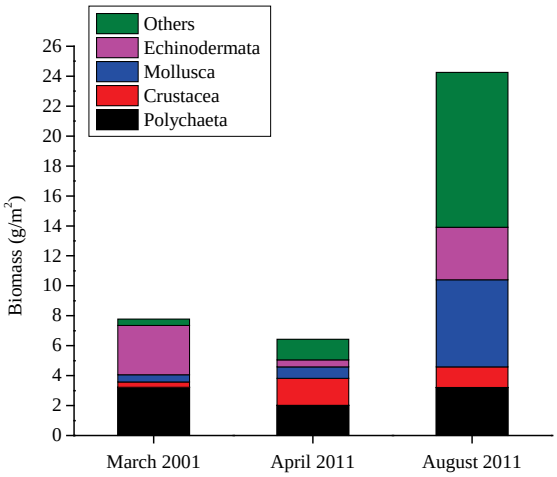

Fig. 3.4.17 Biomass of the main taxonomic groups in the East China Sea.

Diversity

The diversity indexes (Margalef richness index (*d*), Shannon-Wiener index (*H'*) and Pielou's evenness index (*J'*)) from three cruises (March 2001, April and August 2011) in the East China Sea are shown in Figure 3.4.18.

The mean value of Margalef richness index (*d*) was highest (3.81) in March 2001 and lowest (3.05) in April 2011 (Li *et al.*, 2014). The mean value of the Shannon-Wiener index (*H'*) also had the highest value (3.06) in March 2001, but the lowest value (2.36) in August 2011. The mean value of Pielou's evenness index (*J'*) was highest (0.88) in March 2001 and lowest (0.65) in August 2011.

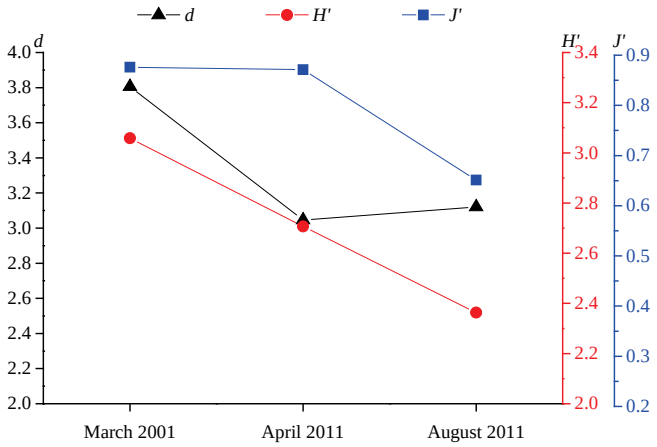

Fig. 3.4.18 Diversity indexes (Margalef richness index (*d*), Shannon-Wiener index (*H'*) and Pielou's evenness index (*J'*)) in the East China Sea.

Secondary productivity

The mean secondary productivity in the East China Sea was 1.37 g(AFDW)/(m^2·a) in April 2011 (Li *et al.*, 2014). In August 2011, the mean value of secondary productivity increased to 4.11 g(AFDW)/(m^2·a).

3.4.4 Summary and prospects

In this section, we discussed the number of species, dominant species, community structure, abundance, biomass, diversity and secondary productivity of macrobenthos in the Yellow Sea and East China Sea. The macrobenthic community changed through time and areas, together with these community parameters. However, there were still some things that did not change. For example, in both the southern Yellow Sea and the East China Sea, the macrobenthos had the highest secondary productivity in summer.

Up to now, we still lack the long-term, large spatial scale investigations of macrobenthos in the Yellow Sea and East China Sea. The forming mechanism and the variation regularity of the macrobenthic community are still short of macroscopic analysis. However, many studies have been conducted on macrobenthic ecology and biodiversity in the Yellow Sea and East China Sea. A geographic information system (GIS) database has also been established. We think that in the future it is essential to conduct research in the following directions (Li, 2011).

1) First, data from macrobenthos investigations collected since 1956 should be collected and integrated, and a new ecological theory and new data analyzing method should be applied to analyze the temporal and spatial variations of macrobenthic community structure of more than half a century, combined with environmental variables such as primary productivity, hydrology, and sediment characters. The relationship between macrobenthic variation and global climate variation also requires on-going research. Second, the bio-indicating function of the macrobenthic community to marine environmental pollution needs to be studied; the indicator species, dominant species and their variations over time also need to be clarified. Third, ecological models should be developed to predict the variation trends of the macrobenthic community; the role and status of the macrobenthos in nutrient flow and material flow in the ecosystem and their relationship with plankton and nekton as well as hydrology also requires explanation.

Specific researches for future investigation are as follows:

1) Drawing the diagrams to depict the distribution pattern of macrobenthic abundance, biomass, diversity indices and other ecological indices in the Yellow Sea and East China Sea and illustrate their temporal and spatial variations. The main indices include species composition, the abundance and distribution of dominant species, biodiversity indices, secondary productivity, the contribution of the four main taxonomic groups of macrobenthos to community structure and quantity distribution. As we know, the species composition of macrobenthos has changed a lot since the 1950s.

2) Data standardization. The mesh size used in most macrobenthic investigations was 1.0 mm before 1995 and 0.5 mm after 1995. The difference in mesh size may cause variations in species number, abundance, biomass and other indices. So the data should be standardized when using the historical data to analyze the temporal variation trend. Li *et al*. (2005) compared the macrobenthic investigation results with the 1.0 mm mesh size and the 0.5 mm mesh size in Jiaozhou Bay, which could be used as a reference (Li *et al*., 2005a).

3) Collecting the historical data on: water masses, currents, sediment characteristics, temperature, salinity, planktons, meiobenthos and other environmental and biological variables; analyzing the relationship between these variables and macrobenthos; coupling the regularities of environmental variation and the macrobenthic community variation; exploring the relationship between these regularities, and establishing a GIS database.

4) Conducting macrobenthic investigations, collecting samples, and clarifying the current status of macrobenthos in the Yellow Sea and East China Sea. The sampling methods should focus on quantitative grabbing, quantitative and qualitative trawling, and diving in special marine habitats. The status of macrobenthic community structure, biodiversity and secondary productivity and their relationship with environmental variables need to be studied.

Through research of the above, we hope to clarify the regularity of macrobenthic ecological variations in the Yellow Sea and East China Sea, confirm the relationship between macrobenthic community variations and the environmental variables, establish a GIS database of macrobenthos in the Yellow Sea and East China Sea, explore the mechanism of variation of the macrobenthic community and predict variation trends, and study the ecological services of the macrobenthos and put forward advice for natural resource protection to management and policy makers.

3.4.5 References

Blomberg, B.N. and Montagna, P.A. 2014. Meta-analysis of Ecopath models reveals secondary productivity patterns across the Gulf of Mexico. *Ocean Coast. Mgmt.* **100**: 32–40, doi:10.1016/j.ocecoaman.2014.07.014.

Brey, T. 1990. Estimating productivity of macrobenthos invertebrates from biomass and mean individual weight. *Meeresforschung* **32**: 329–343.

Gao, A.G., Yang, J.Y., Zeng, J.N., Shou, L., Liao, Y.B., Xu, X.Q., Chen, Q.Z. and Hu, X.G. 2009. Distribution of the intertidal macrobenthos in the Haizhouwan Bay. *J. Mar. Sci*. **27**: 22–29.

Gurjanova, P.V. and Wu, B.L. 1963. Benthic community from Jiaozhou Bay. *Studia Mar. Sin*. **3**: 51–57.

Han, J., Zhang, Z.N. and Yu, Z.S. 2001. Study on the macrobenthic abundance and biomass in Bohai Sea. *J. Ocean Univ. Qingdao* **31**: 889–896.

Han, Q.X., Gao, W.F., Li, B.Q. and Li, X.Z. 2004. Evaluation on the biomass and resource of *Ruditapes philippinarum* from Jiaozhou Bay. *Chin. J. Zool*. **39**: 60–62 (in Chinese).

Hu, H.Y., Huang, B., Tang, J.L., Ren, S.J. and Shao, X.W. 2000. Studies on benthic ecology in coastal waters of Bohai and Yellow Sea. *Donghai Mar. Sci*. **18**: 39–46.

Jia, H.B., Hu, H.Y., Tang, J.L., Huang, B., Mao, H.Y., Wang, J.Y. and Wei, N. 2010. The macrobenthos ecology of the southern Yellow Sea. *Oceanol. Limnol. Sin*. **41**: 842–849.

Lalli, C.M. and Parsons, T.R. 2000. Biological Oceanography: An Introduction. Publishing House of Qingdao Ocean University, Qingdao.

Li, B.Q., Li, X.Z., Yu, H.Y., Wang, H.F., Wang, J.B., Xu, F.S. and Zhang, B.L. 2005. Macrobenthic mollusca fauna and its relations to environmental factors in Jiaozhou Bay. *Oceanol. Limnol. Sin*. **36**: 193–198 (in Chinese with English abstract).

Li, B.Q., Li, X.Z., Wang, H.F. and Zhang, B.L. 2006. Species diversity of macrobenthic mollusk fauna in Jiaozhou Bay, Shandong. *Biodiv. Sci*. **14**: 136–144, doi:10.1360/biodiv.050100.

Li, B.Q., Li, X.Z., Wang, H.F. and Jiang, Y.X. 2010. Situation and assessment on heavy metal contents in five important marine animal species in sea area near Rushan, Shandong Peninsula. *Mar. Environ. Sci*. **29**: 392–395.

Li, R.G. 2003. Macrobenthos on the Continental Shelves and Adjacent Waters, China Sea. Ocean Press, Beijing.

Li X.Z. 2011. An overview of studies on marine macrobenthic biodiversity from Chinese waters: principally from the Yellow Sea. *Biodiv. Sci*. **19**: 676–684, doi:10.3724/SP.J.1003.2011.09126.

Li, X.Z., Wang, H.F., Wang, J.B., Zhang, B.L. and Li, B.Q. 2005a. Comparison of sampling results of macrobenthos using different apertures of sampling sieve in Jiaozhou Bay. *Mar. Sci. Beijing* **29**: 68–74.

Li, X.Z., Wang, H.F. and Zhang, B.L. 2005b. The secondary production of macrobenthos in Jiaozhou Bay, Shandong. *Oceanol. Limnol. Sin*. **36**: 527–533.

Li, X.Z., Wang, J.B., Wang, H.F. and Zhang, B.L. 2005c. Secondary production of macrobenthos from the East China Sea. *Chin. J. Appl. Environ. Biol*. **11**: 459–462.

Li, X.Z., Yu, Z.S., Wang, J.B. and Wang, H.F. 2005d. Secondary production of macrobenthos in southern Yellow Sea. *Chin. J. Appl. Environ. Biol*. **11**: 702–705.

Li, X.Z., Zhang, B.L. and Wang, H.F. 2005e. Secondary production of macrobenthos from the anchovy spawning ground in the southern Yellow Sea. *Chin. J. Appl. Environ. Biol*. **11**: 324–327.

Li, X.Z., Zhang, B.L., Li, B.Q., Li, S.L., Wang, H.F. and Wang, J.B. 2007. Changes of body length and weight of *Branchiostoma belcheri tsingtauense* outside of Jiaozhou Bay and the environmental factors causing the changes. *Mar. Sci*. **31**: 55–59.

Li, X.Z., Wang, H.F., Wang, J.B., Dong, D., Ma, L., Kou, Q., Sui, J.X., Gan, Z.B. and Zhang, B.L. 2014. Biodiversity variability of macrobenthic in the Yellow Sea and East China Sea between 2001 and 2011. *Zool. Systemat*. **39**: 459–484.

Liu, J.Y. and Hsu, F.S. 1963. Preliminary studies on the benthic fauna of the Yellow Sea and the East China Sea. *Oceanol. Limnol. Sin*. **5**: 306–321.

Liu, L.S. and Li, X.Z. 2002. Distribution of macrobenthos in spring and autumn in the East China Sea. *Biodiv. Sci*. **10**: 351–358, doi:10.17520/biods.2002049.

Liu, L.S. and Li, X.Z. 2003. Distribution of macrobenthos in spring and autumn in the southern Yellow Sea. *Oceanol. Limnol. Sin*. **34**: 26–32.

Liu, L.S., Meng, W., Tian, Z.Q. and Cai, Y.L. 2008. Distribution and variation of macrobenthos from the Changjiang Estuary and its adjacent waters. *Acta Ecol. Sin*. **28**: 3027–3034.

Liu, L.S., Meng, W., Li, X.Z., Li, Z.C., Zheng, B.H., Lei, K. and Li, Z.Y. 2009. Studies on macrobenthos in the northern waters of Liaodong Bay. II. Biodiversity and community structure. *Res. Environ. Sci*. **22**: 155–161 (in Chinese).

Liu, R.Y. 1992. Ecology and Living Resources of Jiaozhou Bay. Science Press, Beijing.

Liu, R.Y., Cui, Y.H., Xu, F.S. and Tang, Z.C. 1986. Ecological characteristics of macrobenthos of the Yellow Sea and the East China Sea. *Studia Mar. Sin*. **27**: 153–173.

Margalef, R. 1968. Perspective in Ecological Theory. University of Chicago Press.

Pielou, E.C. 1975. Ecological Diversity. Wiley, New York.

Qi, Z.Y., Ma, X.T., Wang, Z.R., Lin, G.Y., Xu, F.S., Dong, Z.Z., Li, F.L. and Lv, D.H. 1989. Mollusca of Huanghai and Bohai. Science Press, Beijing.

Shannon, C.E. and Weaver W. 1949. The Mathematical Theory of Communication. University of Illinois Press, Urbanna.

Shen, G.Y., Shi, B.Z., Guo, F. and Shi, B.Z. 2010. Marine Ecology. Science Press, Beijing.

Sui, J.X., Yu, Z.S., Qu, F.Y. and Liu, W.X. 2010. Preliminary ecological study of the macrobenthos in the middle part of the Jiaozhou Bay. *Mar. Sci*. **34**: 1–6.

Sun S. 2012. Regional Oceanography of China Seas - Biological Oceanography. Ocean Press, Beijing.

Tchang, S. 1935. Report on the first collection in the Kiaochow Bay and its vicinity. *Bull. Inst. Zool. Nat. Acad. Peiping* **11**: 195–262.

Tchang, S. and Ma, S.T. 1936. Report on the second and third collections in the Kiaochow Bay and its vicinity. *Bull. Inst. Zool. Nat. Acad. Peiping* **17**: 1176–1210.

Tchang, S. and Ma, S.T. 1949. Report on the fourth collection in the Kiaochow Bay and its vicinity. *Bull. Inst. Zool. Nat. Acad. Peiping* **23**: 1113–1180.

Wang, H.F., Li, X.Z., Wang, J.B. and Li, B.Q. 2011. The ecological research of the macrobenthic community from sea areas around Qingdao during the upsurge of green seaweed *Enteromorpha prolifera* in summer of 2008. *Mar. Sci*. **35**: 10–18.

Wang, J.B., Li, X.Z. and Wang, H.F. 2006. Ecological characteristics of dominant polychaete species from the Jiaozhou Bay. *Acta Zool. Sin*. **52**: 63–69.

Weng, X.C., Zhang, Y.K., Wang, C.M. and Zhang, Q.L. 1988. The variational characteristics of the Huanghai (Yellow Sea) cold water mass. *Oceanol. Limnol. Sin*. **19**: 368–379.

Xu, Q.Z., Li, R.X., Wang, Z.L., Fan, S.L. and Wang, Z.X. 2009. Macrobenthos distribution of the South Yellow Sea in summer. *Adv. Mar. Sci*. **27**: 393–399.

Xu, Y., Li, X.Z., Wang, H.F. and Zhang, B.L. 2016. Seasonal and spatial variations of macrobenthic community structure and diversity in the South Yellow Sea. *Aquat. Ecosyst. Health Mgmt.* **19**: 92–100, doi:10.1080/14634988.2016.1139429.

Xu, Y., Sui, J., Yang, M., Sun, Y., Li, X., Wang, H. and Zhang, B. 2017. Variation in the macrofaunal community over large temporal and spatial scales in the southern Yellow Sea. *J. Mar. Syst*. **173**: 9–220, doi:10.1016/j.jmarsys.2016.11.006.

Zhang, J.L., Xu, F.S. and Liu, R.Y. 2012. Community structure changes of macrobenthos in the South Yellow Sea. *Chin. J. Oceanol. Limnol*. **30**: 248–255, doi:10.1007/s00343-012-1076-0.

Zhang, Z.N., Tu, L.H. and Yu, Z.S. 1990. Preliminary study on the macrofauna in the Huanghe River Estuary and its adjacent waters (I) The Biomass. *J. Ocean Univ. Qingdao* **20**: 37–45.

3.5 Fish and Invertebrate Fisheries

Weiwei Xian and Cui Liang

Institute of Oceanology, Chinese Academy of Sciences, China

3.5.1 Introduction

A large amount of freshwater and terrigenous materials are injected into the Yangtze River estuary annually, which sustain the productive fishery grounds, Zhoushan and Lüsi fisheries, in the adjacent seas (Zhuang, 2006), and provide a changeable environmental condition for estuarine organisms. In the offshore area of Yangtze River estuary, 16 stations were set to examine the fish and invertebrate community composition and variation from 1985 to 2004 (Fig. 3.5.1). This section provides specific information of seasonal variation of fish and invertebrate communities in the offshore area of the Yangtze River estuary based on data obtained in 2004. In addition, information and interannual variation of the key species in this area were also described based on information from FishBase and the co-author's unpublished data.

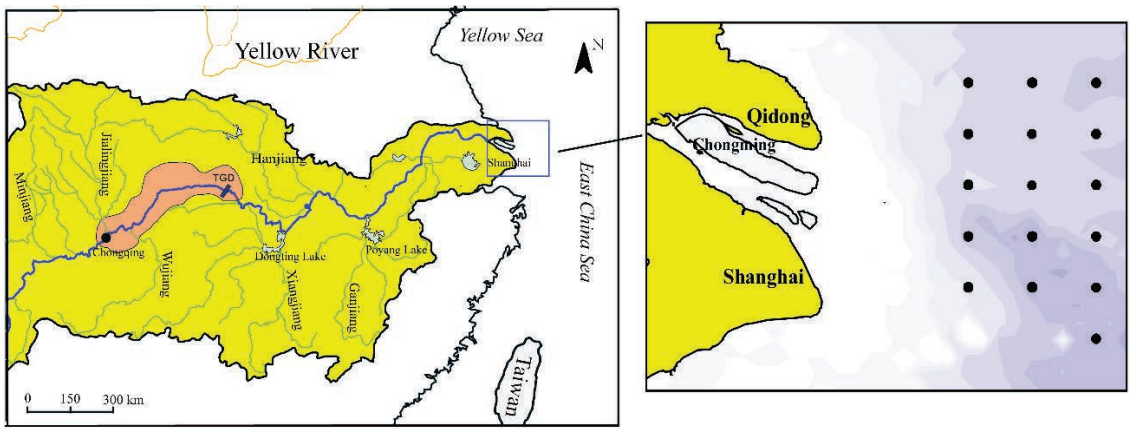

Fig. 3.5.1 Map of the Changjiang River basin and estuary, with the sampling stations (solid black circles).

3.5.2 Methods

From 1985 to 2004 (autumn in 1985; spring in 1986; autumn in 1998; spring in 1999; autumn in 2000; spring in 2001; spring, summer, autumn and winter in 2004), 16 stations in the offshore area of Yangtze River estuary were sampled by trawl survey. At each station, a trawl survey was conducted by two vessels with the vessel speed of approximately 3 knots (5.5 kph) for 1 hour. The fish and invertebrate samples were weighed, counted and sorted to the species level according to their morphological features.

The ecological density of marine fishery species can be measured by two indexes: number ecological density (NED, $\times 10^3$ ind./km^2) and biomass ecological density (BED, kg/km^2) as follows:

$$NED = Y_N/[(A)(q)],$$

$$BED = Y_W/[(A)(q)]$$

where A is the swept area per hour, Y_N is the mean trawl fish capture number per hour, Y_W is the mean trawl fish capture weight per hour, and q is the catchability coefficient, assumed to be 0.6.

3.5.3 Nekton assemblages in the Yangtze River estuary

Fish community

The particular geographical position generates a unique environment in the offshore area of the Yangtze River estuary, and also results in distinguishing fish and invertebrate communities in this area. The fish community in the offshore area of the Yangtze River estuary includes both warm-water pelagic and cold-water demersal species, and includes both coastal species and offshore migratory species. According to the fishery investigation in 2004, the fish community in the offshore area of Yangtze River estuary included 47 species, representing 42 genera and 31 families, among which Perciformes occupied the most, including 23 species, 21 genera and 15 families (Fig. 3.5.2). Fish community composition showed seasonal variation in the estuary, with the common feature that the community was comprised mainly by Perciformes (Fig. 3.5.3). All fish species and their occurrence in different months are listed in Table 3.5.1.

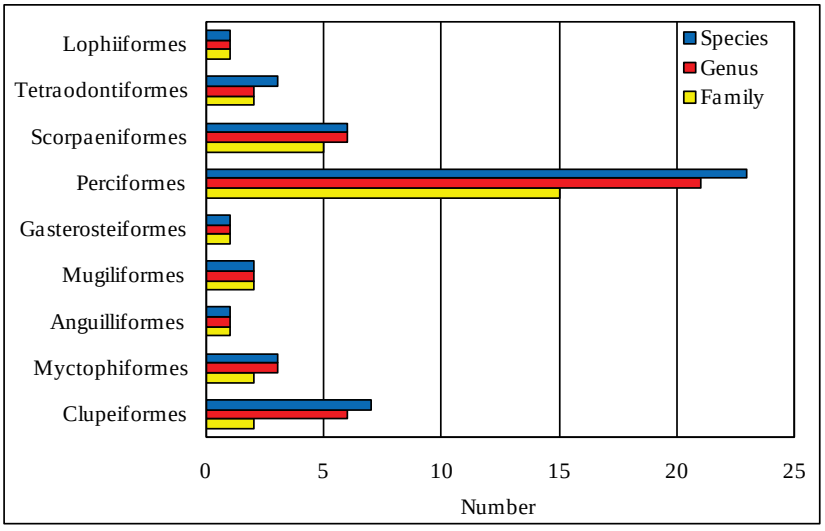

Fig. 3.5.2 Fish catches composition in the offshore area of the Yangtze River estuary in 2004.

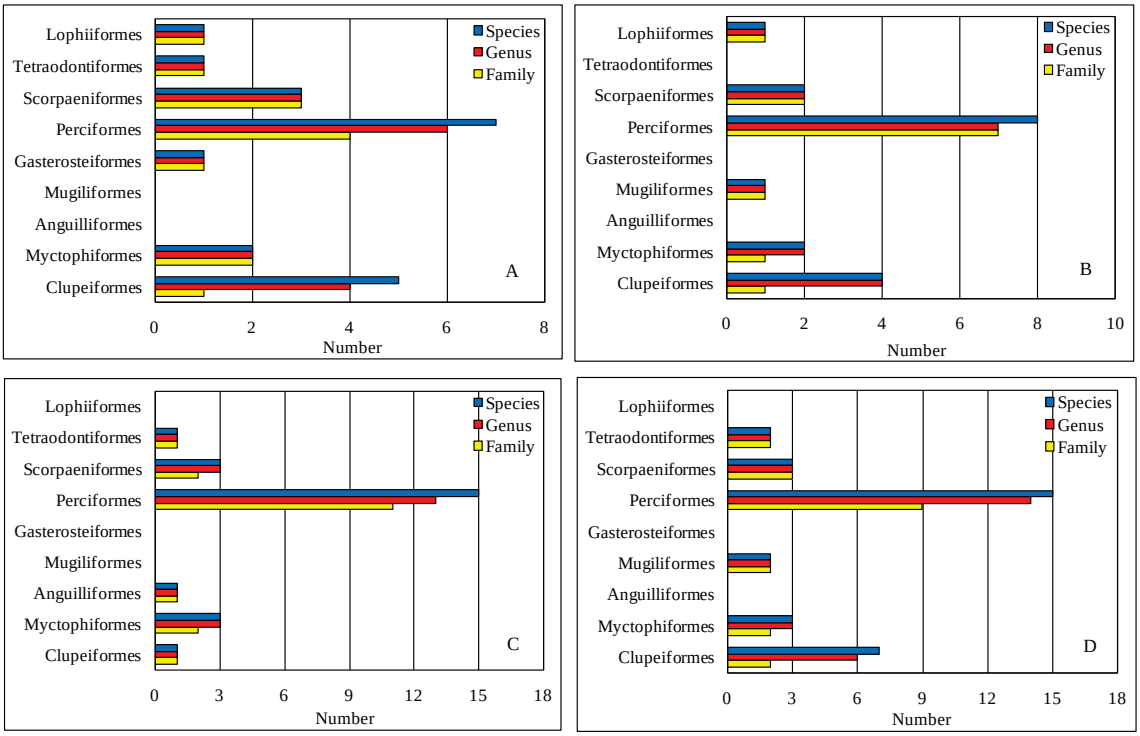

Fig. 3.5.3 Fish community composition and monthly variation in the offshore area of the Yangtze River estuary in 2004 (A: spring, B: summer, C: autumn, D: winter).

Table 3.5.1 Fish species in the offshore area of Yangtze River estuary in 2004.

Scientific name	February	May	August	November
Clupeiformes				
Clupeidae				
Ilisha elongata				+
Engraulidae				
Engraulis japonicus	+	+	+	+
Thrissa kammalensis	+			+
Coilia ectenes	+			+
Coilia mystus	+	+		+
Setipinna taty	+	+		+
Anchoviella commersonii		+		+
Myctophiformes				
Synpdidae				
Saurida elongata		+	+	+
Harpadon nehereus	+	+	+	+
Myctophidae				
Benthosema pterotum	+		+	+
Anguilliformes				
Muraenesocidae				
Muraenesox cinereus			+	

Table 3.5.1 Continued.

Scientific name	February	May	August	November
Mugiliformes				
Sphyraenidae				
Sphyraena pinguis		+		+
Polynemidae				
Polynemus sextarius				+
Gasterosteiformes				
Syngnathidae				
Syngnathus acus	+			
Kurtiformes				
Apogonidae				
Apogonichthys lineatus			+	+
Perciformes				
Pomadasyidae				
Hapalogenys mucronatus			+	
Priacanthidae				
Priacanthus macracanthus			+	
Acropomatidae				
Acropoma japonicum				+
Sillaginidae				
Sillago japonica				+
Carangiformes				
Carangidae				
Selar crumenophthalmus			+	
Decapterus maruadsi				+
Trachurus japonicus		+		+
Sciaenidae				
Argyrosomus argentatus (			+	+
Nibea albiflora	+		+	+
Collichthys lucidus	+			+
Johnius belengeri				+
Pseudosciaena polyactis	+	+	+	+
Trichiuridae				
Trichiurus japonicus	+	+	+	+
Scombridae				
Pneumatophorus japonicus		+	+	
Scomberomorus niphonius			+	
Theraponidae				
Therapon jarbua				+
Stromateidae				
Pampus nozawae		+	+	+
Pampus argenteus	+	+	+	+
Centrolophidae				
Psenopsis anomala		+	+	+
Gobiidae				
Chaeturichthys stigmatias	+		+	
Chaeturichthys hexanema	+		+	
Odontamblyopus rubicundus		+		

Table 3.5.1 Continued.

Scientific name	February	May	August	November
Scorpaeniformes				
Triglidae				
Lepidotrigla punctipectoralis		+	+	+
Aploactidae				
Erisphex potti	+	+		
Synanceiidae				
Minous monodactylus			+	
Vespicula sinensis			+	+
Platycephlidae				
Platycephalus indicus	+			+
Liparidae				
Liparis tanakae	+			
Tetraodontiformes				
Aluteridae				
Navodon septentrionalis				+
Tetraodontidae				
Fugu obscurus			+	+
Fugu alboplumbeus	+			
Lophiiformes				
Lophiidae				
Lophius litulon	+	+		

+ indicates occurrence.

Invertebrate community

In 2004, 27 species were sampled in the offshore area of the Yangtze River estuary, representing 19 Crustacea, 6 Mollusca and 2 Coelenterata (Fig. 3.5.4). Crustacea was the predominant category in all four months, and no Coelenterates were observed during the survey conducted in February. All invertebrate species and their occurrence in different months are listed in Table 3.5.2.

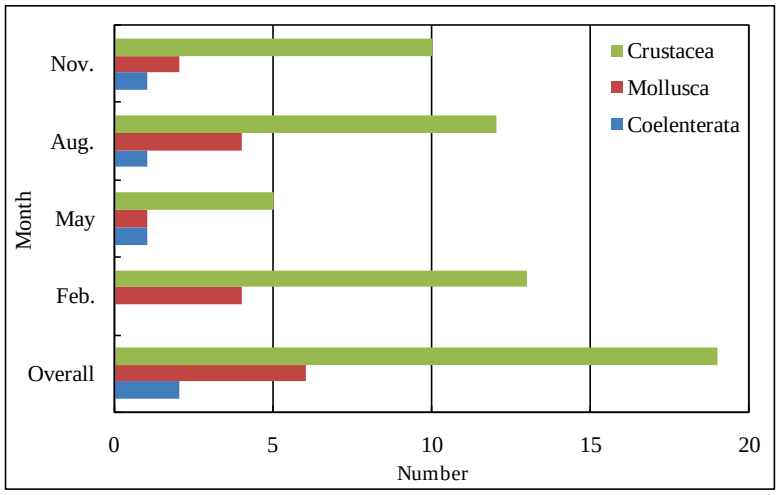

Fig. 3.5.4 Invertebrate catches composition and monthly variation in the offshore area of the Yangtze River estuary in 2004 (Xian, unpub.).

Table 3.5.2 Invertebrate species in the offshore area of Yangtze River estuary in 2004.

Scientific name	February	May	August	November
Crustacea				
Oratosquilla oratoria	+	+	+	+
Charybdis bimaculata	+		+	+
Charybdis japonica	+		+	+
Portunus sanguinolentus	+		+	+
Portunus trituberculatus	+	+	+	+
Matuta planipes			+	
Neodorippe japonicum			+	
Calappidae		+		
Eucrate crenata				+
Crangon affinis	+			
Palaemon gravieri	+	+	+	+
Exopalaemon carinicauda	+			
Alpheus distinguendus	+			
Acetes chinensis	+			+
Penaeus spp.			+	
Penaeus orientalis			+	
Metapenaeopsis dalei	+		+	+
Trachypenaeus curvirostris	+	+	+	+
Leptochela gracilis	+			
Mollusca				
Loligo japonica	+	+	+	+
Euprymna spp.	+			
Sepiola birostrata	+			
Sepiola spp.	+		+	+
Octopus variabilis			+	
Hyriopsis cumingii			+	
Coelenterata				
Sanderia malayensis		+		
Rhopilema esculenta			+	+

+ indicates occurrence.

3.5.4 Key species

Sliver pomfret

Pampus argenteus

Sliver pomfret *Pampus argenteus* is a coastal species, inhabiting in areas with slow flow, and its preferable water layer range is 30–70 m. In spring, sliver pomfret head north from the northern part of Taiwan waters to the north East China Sea, and move into the Yangtze River estuary to spawn in early May. After spawning, they disperse for feeding and migrate to the south after autumn. Sliver pomfret feed on small fishes and shrimps, as well as plankton, *i.e.*, jellyfish, copepods and diatoms.

In spring, the resource of sliver pomfret in the offshore area of the Yangtze River estuary, assessed both by NED and BED, showed an increasing trend, and reached its peak value in 2001; while the resource decreased remarkably in 2004, and the NED and BED occupied only 0.01% and 0.69%, respectively, of the corresponding values in 2001 (Fig. 3.5.5A).

Sliver pomfret resource in the offshore area of the Yangtze River estuary witnessed larger variation in autumn from 1985 to 2004, with its peak value in 1998 and the lowest value in 2000. The BED in 2004 was only 4.28% of that in 2001, and NED was 1.00% (Fig 3.5.5B).

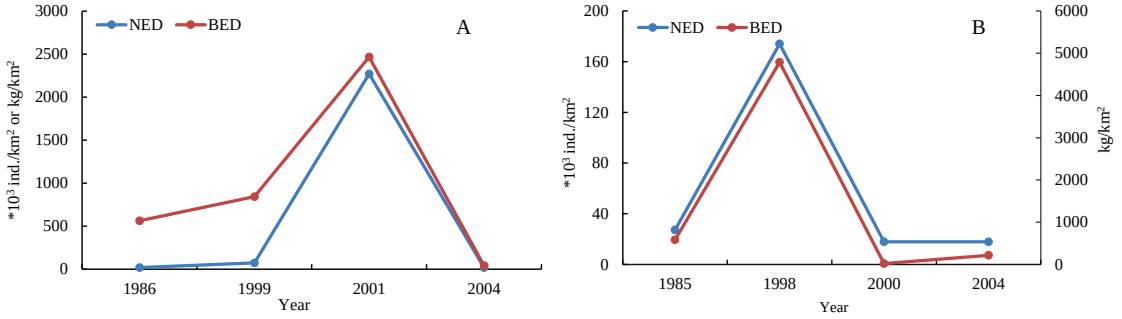

Fig. 3.5.5 Number ecological density (NED) and biomass ecological density (BED) variation of sliver pomfret in the offshore area of the Yangtze River estuary in (A) spring and (B) autumn (Xian, unpub.).

Small yellow croaker

Larimichthys polyactis

Small yellow croaker *Larimichthys polyactis* was regarded as one of the four most important commercial fishery resources in China and was the main target fish of the bottom trawl fishery before the 1970s, while, with the repid increase of fishing intensity, their resources have greatly declined in the last few decades (Cheng *et al.*, 2003). Because of the significant role of *Larimichthys polyactis* in Chinese fisheries, a number of studies have focused on their status and indicated a tendency of smaller size and faster growth (Liang and Pauly, 2017). *Larimichthys polyactis* is always found in the sublittoral zone above 120 m sandy mud bottoms, and has vertical movement habit. Every year in April or May, when the water temperature starts to rise, the small yellow croaker community migrates north from the junction of the Yellow Sea and the East China Sea to Jiangsu–Shandong coast for spawning, after which they disperse and prey near shore; when the autumn comes, water temperature declines, and the community migrates back for overwintering. Small yellow croaker feed mainly on shrimps and small fishes.

In spring, small yellow croaker BED in 1986 was quite low, only 134 kg/km^2, then it increased abruptly to 1993 kg/km^2 in 1999. Afterwards, it decreased again in 2001, and further down in 2004; the same variation trend was detected in NED in spring (Fig. 3.5.6A). In autumn, the resource varied in the same way as spring (Fig. 3.5.6B).

The resource of small yellow croaker was low in the 1980s, which could be attributed to intensive fishing activities, while, with the establishment of no-fishing zones, the resource started to rebuild in the late 1990s, although it declined again afterwards.

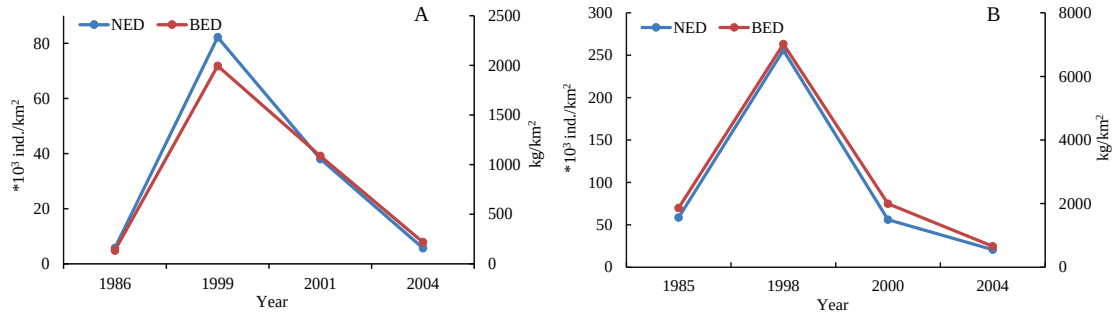

Fig. 3.5.6 Number ecological density (NED) and biomass ecological density (BED) variation of small yellow croaker in the offshore area of the Yangtze River estuary in (A) spring and (B) autumn (Xian unpub.).

Largehead hairtail

Trichiurus lepturus

Largehead hairtail *Trichiurus lepturus* is a migratory species, which is widespread in China's seas, especially in the East China Sea. Largehead hairtail has its main fishing grounds in the East China, Yellow and Bohai seas, is the fish species with the highest national catch in China (Wu and Zhu 1979). In recent years, *T. japonicus* has produced high yields in Chinese waters, attributed to intense fishing pressure, offshore expansion of the fisheries and high proportion of larvae (Zhang *et al.* 2006). In May–July, the largehead hairtail community spawns and feeds in the Yangtze River estuary, after which the community migrates northward to develop the summer fishing season. Then, in the late autumn and early winter, the community moves southward and forms the winter fishing season in Zhoushan waters and its adjacent area. Largehead hairtail feed mainly on shrimps, squids and other fishes, and is the most important commercial fish in China's coastal area.

In spring, BED and NED of largehead hairtail were both stable at low levels, compared to autumn, in the offshore area of the Yangtze River estuary (Fig. 3.5.7A). In November, BED and NED had the similar trends, with the highest value in 2004 and lowest in 1985 (Fig. 3.5.7B).

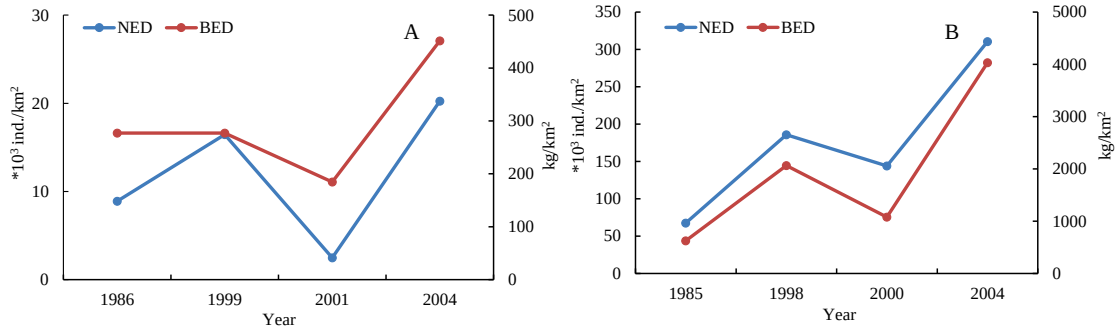

Fig. 3.5.7 Number ecological density (NED) and biomass ecological density (BED) variation of largehead hairtail in the Yangtze River estuary in (A) spring and (B) autumn (Xian unpub.).

Japanese grenadier anchovy

Coilia nasus

Japanese grenadier anchovy *Coilia nasus* is an estuarine migratory species, and spends its whole life in the estuary area. In the early spring, the fish community gathers in the estuary and forms the spring fishing season in March–April. In the late April, Japanese grenadier anchovy migrate to the freshwater area inside the estuary to spawn, with the main spawning season during early May to early July. The main prey of Japanese grenadier anchovy are shrimps, copepods and juvenile fishes. The maximum output of Japanese grenadier anchovy once reached 281.8 tonnes in 1973, but its yield reduced in 1980s because of the intensive fishing pressure, and further sharply decreased in 1990s (Li and Huang, 2009). The output of Japanese grenadier anchovy was only 5 tonnes in 1994 and could barely form a fishing season, which suggests that it was in severe recession (Chen *et al*., 2002).

In May, the NED of Japanese grenadier anchovy had its highest value in 2001, while the peak value of BED occurred in 1999, which indicates that its catches had larger individual size in 1999 compared to 2001; in 2004, both NED and BED experienced their lowest levels in spring investigations (Fig. 3.5.8A).

In autumn, NED was highest in 1998 in the offshore area of Yangtze River estuary, while BED decreased significantly from 1985 to 2004, which resulted in the conclusion that the catches in 1998 had smaller body size (Fig. 3.5.8B).

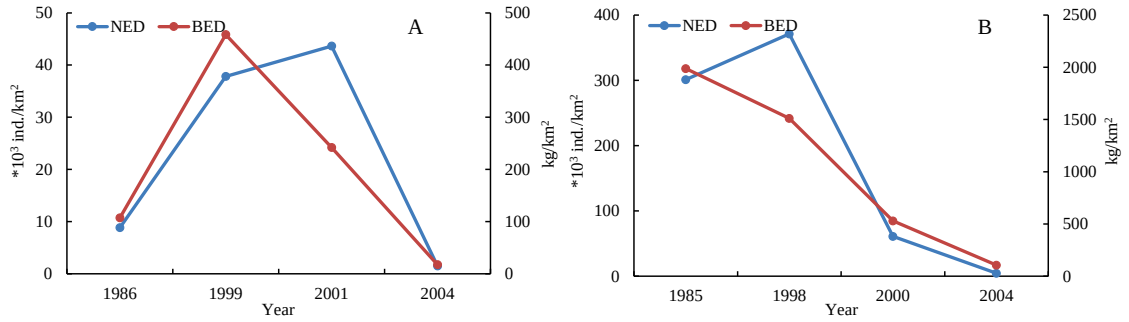

Fig. 3.5.8 Number ecological density (NED) and biomass ecological density (BED) variation of Japanese grenadier anchovy in the offshore area of the Yangtze River estuary in (A) spring and (B) autumn (Xian, unpub.).

Scaly hairfin anchovy

Setipinna taty

Scaly hairfin anchovy *Setipinna taty* is a warm water marine species which has a wide distribution; it can be caught during the whole year in the Yangtze River estuary, with its fishing season occurring in spring and autumn. Scaly hairfin anchovy feed mainly on plankton, and it can also be the prey of carnivorous fishes in the estuary. With intense fishing activities, the spawning stock of scaly hairfin anchovy has been experiencing an earlier sexual maturity and smaller individual size (Xiong *et al*., 2009).

In May, both NED and BED showed slight ascendant trends from 1986 to 2001, and had the lowest values in 2004 while, in autumn, NED appeared a more fluctuate trend, with its highest and lowest values occurred in 1998 and 2004, respectively (Fig. 3.5.9). BED shared the similar tendency with NED, which implied that no significant change was observed in body size catches.

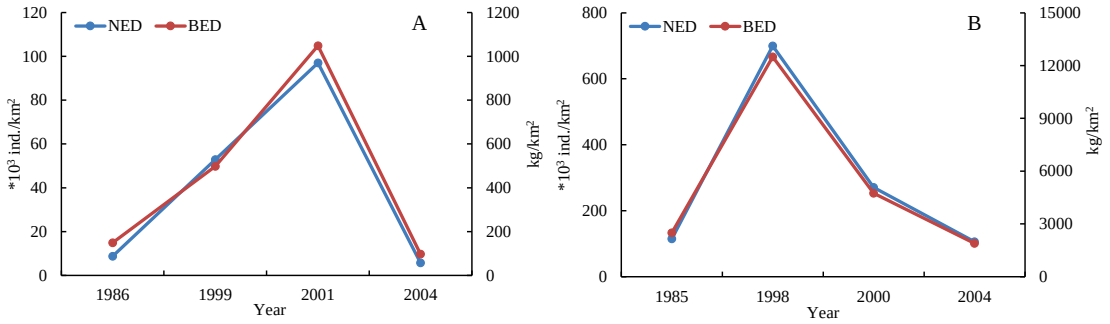

Fig. 3.5.9 Number ecological density (NED) and biomass ecological density (BED) variation of scaly hairfin anchovy in the offshore area of Yangtze River estuary in (A) spring and (B) autumn (Xian, unpub.).

Bombay-duck

Harpadon nehereus

Bombay-duck *Harpadon nehereu* is a benthopelagic species living in warm oceans. It usually inhabits deep water offshore on sandy mud bottom for most of the year, but also gathers in large shoals in deltas of rivers to feed during monsoons. In China, Bombay-duck distributes in the South China Sea, East China Sea and the southern Yellow Sea and their estuaries; in the investigation area, it can be caught in both spring and autumn, with a large number occurring in autumn. It feeds mainly on benthic shrimps and small fishes. As the catches of Bombay-duck has increased significantly since the mid-1990s, its fishery resource value has been noticed (Li *et al.*, 2004). The catch of Bombay-duck has been stable, and capture size has not changed significantly, which means that there is a certain potential for its resource exploitation (Chen *et al.*, 2012; Luo *et al.*, 2012). On the other hand, the proportion of the low-age groups of Bombay-duck has increased in the capture, so attention should be paid to its resource management to guarantee its sustainable use (Chen *et al.*, 2012).

The Bombay-duck resource in spring, measured by BED, remained stable at a low level; however, the NED reached a high value in 2001, which indicated that the catch during this time was characterized by small body size (Fig. 3.5.10A).

Bombay-duck played a relatively important role in fishery resources in the offshore area of the Yangtze River estuary in autumn. NED and BED shared similar trends, except in 1985, when BED had lower proportion compared with NED, implying a smaller body size in catches in autumn (Fig. 3.5.10B).

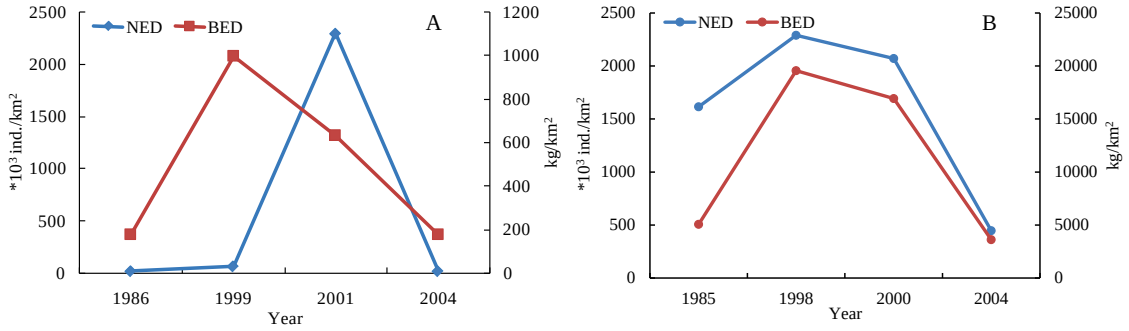

Fig. 3.5.10 Number ecological density (NED) and biomass ecological density (BED) variation of bombay-duck in the offshore area of Yangtze River estuary in (A) spring and (B) autumn (Xian unpub.).

Horse crab

Portunus trituberculatus

Horse crab *Portunus trituberculatus* is distributed only in coastal areas of China, Japan and Democratic People's Republic of Korea, and inhabits sandy to sandy-muddy substrates with depths of 7–100 m (Ng, 1998). Horse crab has become one of the most important commercial resources in the Yangtze River and its adjacent area since the 1970s, and can form two commercial aggregations annually, with spawning stock in spring and feeding stock in autumn.

For both spring and autumn, the maximum resource of horse crab occurred in the 1980s. After that, the resource decreased abruptly and stayed stable at a low level compared to the 1980s. NED and BED had the similar trend, indicating that no significant change in size (Fig. 3.5.11).

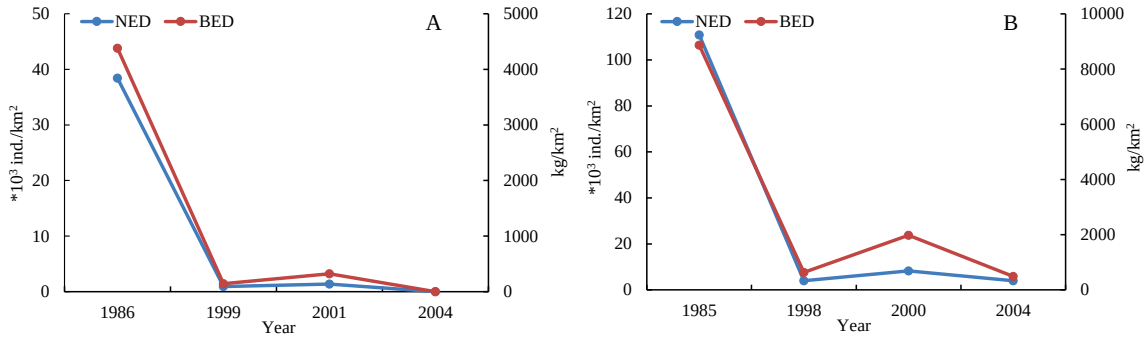

Fig. 3.5.11 Number ecological density (NED) and biomass ecological density (BED) variation of horse crab in the offshore area of Yangtze River estuary in (A) spring and (B) autumn (Xian, unpub.).

Japanese squillid mantis shrimp

Oratosquilla oratoria

Japanese squillid mantis shrimp *Oratosquilla oratoria*has has become an important invertebrate resource in the Yangtze River estuary since the traditional commercial invertebrate species declined. It burrows in near-shore bottom substrates (Manning, 1998) in sheltered embayment or estuaries (Ahyong, 2001), and occurs in muddy bottoms of bays and inlets (Hamano *et al.*, 1987). Japanese squillid mantis shrimp feeds mainly on crustaceans, mollusks, polychaetes, and fishes.

The stock of Japanese squillid mantis shrimp in the offshore area of the Yangtze River estuary showed a stable increasing trend from 1998 to 2001, except for mean individual biomass in autumn (Table 3.5.3).

Table 3.5.3 Resource estimation of Japanese squillid mantis shrimp in autumn and spring during 1998–2001.

Parameter	Nov. 1998	Nov. 2000	May 1999	May 2001
NED	5.28	11.64	0.17	1.34
BED	44.08	66.05	3.05	22.94
Mean individual biomass	9.52	9.50	13.74	19.23
Resource ($\times 10^4$ kg)	62.6	93.8	4.33	32.6

NED: Number ecological density; BED: biomass ecological density

Chinese ditch prawn

Palaemon gravieri

Chinese ditch prawn *Palaemon graviera* is a pelagic species, and is distributed in subtropical waters, mainly in China and Korea (www.sealifebase.org).

The resource of Chinese ditch prawn fluctuated during 1998 to 2001. In autumn, NED, BED and resource increased from 1998 to 2000; however, the individual size shrunk. In spring, NED, BED and resource decreased significantly from 1999 to 2001, whereas the mean individual size increased (Table 3.5.4).

Table 3.5.4 Resource estimation of Chinese ditch prawn in autumn and spring during 1998–2001.

Parameter	Nov. 1998	Nov. 2000	May 1999	May 2001
NED	3.50	5.39	17.77	3.53
BED	5.80	8.52	24.51	10.86
Mean individual biomass	2.32	1.58	1.37	3.08
Resource ($\times 10^4$ kg)	8.24	12.10	34.80	15.42

Japanese squid

Loliolus japonica

Japanese squid *Loliolus japonica* is one of the most important marine cephalopods in the Yangtze River estuary. Its male and female adults usually die shortly after spawning and brooding, respectively. Embryos hatch into planktonic stage and live for some time before they grow larger and take up a benthic existence as adults (Ruppert *et al*., 2004).

In autumn, NED, BED, mean individual size and resource of Japanese squid in the offshore area of the Yangtze River estuary decreased in 2000 compared to 1998, indicating declining stock in autumn. In spring, these parameters in 2001 were all higher than in 1999, except for mean individual size, which was slightly lower than that in 1999 (Table 3.5.5).

Table 3.5.5 Resource estimation of Japanese squid in autumn and spring during 1998–2001.

Parameter	Nov. 1998	Nov. 2000	May 1999	May 2001
NED	12.37	5.44	0.70	1.54
BED	26.39	9.40	9.49	20.33
Mean individual biomass	2.13	1.73	13.56	13.20
Resource ($\times 10^4$ kg)	37.47	13.35	13.47	28.87

3.5.5 Summary and future perspective

The offshore area of the Yangtze River estuary, as the prime spawning and feeding ground for fish and invertebrates, is one of the highest fishery production areas in China. On account of the complexity of terrain and water mass conditions, as well as fishing activities, fish and invertebrate community structure have always been under a great variation.

Located in the junction of the Yellow Sea and East China Sea, the Yangtze River estuary provides spawning ground, nursing ground, feeding ground and migratory passage for important commercial species. Although studies focusing on fish and invertebrates in the Yangtze River estuary started in the mid-1980s, there are still some unknowns need to be further explored. Multiple pressures, *i.e*., human activities, global warming and environmental pollution, are occurring in the Yangtze River estuary, but the adaptive mechanism of fish and invertebrates to them is still obscure. The number of fish stocks is mainly driven by the amount of recruitment, and the recruitment mechanism of population directly determines the sustainable yield of biological resources, while recruitment process and mechanism of key resources still need to be clarified. Moreover, to explore the theoretical basis of habitat restoration and resource conservation for inshore fishery stocks, resource dynamic model analysis and comprehensive evaluation of resource effects are also necessary.

3.5.6 References

Ahyong, S.T. 2001. Revision of the Australian stomatopod Crustacea. *Rec. Austral. Museum* **26**(Suppl.): 1–326, doi:10.3853/j.0812-7387.26.2001.1333.

Chen, D.Q., Duan, X.B. and Liu, S.P. 2002. On the dynamics of fishery resources of the Yangtze River and its management. *Acta Hydrobiol. Sin*. **26**: 685–690 (in Chinese with English abstract).

Chen, L., Shui, B. and Dong, W. 2012. The growth characteristics and sustainable resource use of *Harpadon nehereus*. *Technol. Mgmt*. **3**: 68–70 (in Chinese).

Cheng, J., Lin, L., Ling, J., Li, J. and Ding, F. 2003. Effects of summer close season and rational utilization on redlip croaker (*Larimichthys polyactis* Bleeker) resource in the East China Sea Region. *J. Fish. Sci. China* **11**: 554–560.

Hamano, T., Morrissy, N.M. and Matsuura, S. 1987. Ecological information on *Oratosquilla oratoria* (Stomatopoda, Crustacea) with an attempt to estimate the annual settlement date from growth parameters (Hakata bay, Japan). *J. Shimonoseki Univ. Fish.* **36**: 9–27 (in Japanese with English abstract).

Li, J., Li, S. and Cheng, J. 2004. Structure analysis on the utilization of trawl fishery resources on the fishing grounds of the Changjiang estuary. *Mar. Fish*. **26**: 24–28 (in Chinese with English abstract).

Li, M. and Huang, S. 2009. Management of fishery resources in Yangtze River Estuary. *Asian Agri. Res*. **1**: 31–35, 40.

Liang, C. and Pauly, D. 2017. Fisheries impacts on China's coastal ecosystems: Unmasking a pervasive 'fishing down' effect. *PLOS One* **12**: e0173296, doi:10.1371/journal.pone.0173296.

Luo, H., Zhang, H., Li, P. and Zhou, Y. 2012. Analysis of the current situation of fishery biology of *Harpadon nehereus* in the East China Sea. *J. Zhejiang Ocean Univ*. (Natural Science) **31**: 202–205, 233 (in Chinese with English abstract).

Manning, R.B. 1998. Stromatopods, pp. 827–849 *in*: The Living Marine Resources of the Western Central Pacific. Vol. 2. Cephalopods, Crustaceans, Holothurians and Sharks *edited by* K.E. Carpenter and V.H. Niem, FAO Species Identification Guide for Fishery Purposes, FAO, Rome.

Ng, P.K.L. 1998. Crabs, pp. 1045–1155 *in*: The Living Marine Resources of the Western Central Pacific. Vol. 2. Cephalopods, Crustaceans, Holothurians and Sharks *edited by* K.E. Carpenter and V.H. Niem, FAO Species Identification Guide for Fishery Purposes, FAO, Rome.

Ruppert, E.E., Fox, R.S. and Barnes, R.D. 2004. Invertebrate Zoology. A Functional Evolutionary Approach. 7th Ed. Brooks/Cole, Thomson Learning, Inc. 990 pp.

Wu, J.Z. and Zhu, D.L. 1979. Study on the change and rational utilization of fish resources in Zhejiang offshore and adjacent sea areas. *Mar. Fish*. **3**: 6–10 (in Chinese with English abstract).

Xiong, Y., Tang, J., Liu, P., Zhong, X., Yan, L., Gao, Y., Wu, L. and Mao, H. 2009. Resource estimate on *Setipinna taty* in the Southern Yellow Sea. *Oceanol. Limnol. Sin.* **40**: 500–505 (in Chinese with English abstract).

Zhang, Q.H., Cheng, J.H., Xu, H.X., Shen, X.Q., Yu, G.P. and Zhen, Y.J. 2006. Fishery Resources and Their Sustainable Utilization in the East China Sea. Fudan University Press.

Zhuang, P. 2006. Fishes of the Yangtze Estuary. Shanghai Scientific and Technical Publishers.